Mission-Oriented Seismic Research Program

Annual Report

2008

M-OSRP

University of Houston

Sponsors and Advisory Board representatives

Corporate Sponsors

Amerada Hess ..... Scott Morton, Jacques Leveille
Anadarko ..... Roger Reagan
BP ..... Uwe Albertin
BHP ..... Michael Richardson
ChevronTexaco ..... Debbie Bones
ConocoPhillips ..... Douglas Foster, Robert Stolt
Devon Energy ..... Kenneth Beeney
Encana ..... William Goodway, David Mackidd
ENI-Agip ..... Michele Buia
ExxonMobil ..... Peter Traynin
Geotrace Technologies ..... Jaime Stein
GX Technology ..... Nick Bernitsas, Robert Bloor
IBM ..... Tom McClure
Landmark ..... Dave Diller
Petrochina Company Limited ..... Jixiang Xu
Petrobras ..... Neiva Zago
PGS ..... Martin Widmaier, Steve Kelly
Repsol ..... Francisco Ortigosa Fernandez
Saudi Aramco ..... Yi Luo
Shell ..... Jonathan Sheiman
Statoil-Hydro ..... Lasse Amundsen
WesternGeco ..... William Dragoset

Federal Support

DOE Basic Energy Sciences ..... Nick Woodward
NSF CMG ..... Henry A. Warchall

M-OSRP Personnel

Faculty

Lasse Amundsen (Statoil) ..... Adjunct Professor (Physics)
Douglas J. Foster[1] (ConocoPhillips) ..... Adjunct Professor (Physics)
Kristopher A. Innanen ..... Assistant Professor (Physics)
Robert G. Keys (ConocoPhillips) ..... Adjunct Professor (Physics)
Jacques Leveille (Amerada Hess) ..... Adjunct Professor (Physics)
Fang Liu ..... Research Assistant Professor (Physics)
Ken H. Matson (BP) ..... Adjunct Associate Professor (Physics)
Bogdan Nita (Assistant Professor, Montclair State U.) .... Adjunct Assistant Professor (Physics)
Partha Routh ..... Adjunct Professor (Physics)
Jon Sheiman (Shell) ..... Adjunct Professor (Physics)
Robert H. Stolt (ConocoPhillips) ..... Adjunct Professor (Physics)
T. Hing Tan (Shell) ..... Adjunct Professor (Physics)
Arthur B. Weglein ..... Cullen Professor (Physics)
Daniel Whitmore (PGS) ..... Adjunct Professor (Physics)

Ph.D. Students

Walter Kessinger ..... Geosciences
Shansong Jiang ..... Physics
Jose Eduardo Lira ..... Geosciences[2]
Xu Li ..... Physics
Zhiqiang Wang ..... Physics
Jim Mayhan ..... Physics
Shih-Ying Hsu ..... Physics
Min Wang ..... Physics
Tao Jiang ..... Geosciences
Hong Liang ..... Physics
Mehdi Eftekhari ..... Geosciences

Recent Alumni

Adriana Citlali Ramirez ..... Physics
Haiyan Zhang ..... Physics
Jingfeng Zhang ..... Physics
Fang Liu ..... Physics
Zhiqiang Guo ..... Geosciences
Francisco Miranda ..... Physics
Simon A. Shaw ..... Geosciences

Administrative Support

Jennifer Chin-Davis ..... Business Administrator
Nguyen Tran ..... Program Accountant
Angela Cowan ..... Program Coordinator
Joseph Ghobrial, Marco Moncada ..... Computer/IT Support
Jesse Weglein ..... Webmaster

[1]Chair, M-OSRP Advisory Board
[2]Petrobras, Brazil

Table of Contents

M-OSRP 2008 Introduction and Preface

This Annual Report describes the progress, status and plans of the Mission-Oriented Seismic Research Program for the Fall 2008-Spring 2009 Academic Year. The Introduction provides a perspective and program overview that includes: (1) code release to sponsors and (2) technical highlights from the projects within the program; and the latter technical highlights are detailed in individual reports within this Annual Report.

Release of code: 3D inverse scattering free surface multiple elimination

The successful testing of the M-OSRP inverse scattering 3D free surface multiple elimination code was carried out in conjunction with ConocoPhillips, and the release to sponsors is scheduled for June, 2009. This code is a research prototype code, and it will be available to the M-OSRP HPC committee, chaired by Nicola Bienati of ENI, working with the IBM team directed by Tom McClure and Michael Perrone -for compute architecture comparisons and benchmark purposes.

We describe here the differential added-value of this particular algorithm and code, both within the overall multiple removal toolbox, and relative to other free surface multiple removal codes available from other sources and consortia.

The method is in principle able to eliminate free surface multiples given its prerequisites of: (1) the source signature, (2) deghosted data and (3) the input data for the algorithm needs to include the sub-events of the multiples to be eliminated – either through data acquisition or data reconstruction. Independent synthetic data tests of e.g., P.M. Carvalho, Jingfeng Zhang and Bill Dragoset, indicate that the inverse scattering series free surface multiple elimination code with its obliquity factor, and using de-ghosted and wavelet removed data, precisely predicts and subtracts free surface multiples of all orders, with equally effectiveness at all offsets, and without the need for adaptive subtraction.

The 3D free surface multiple removal method fits within our M-OSRP strategy that turns the typical prediction and subtraction two-step sequence into a more competent prediction, and, in practice, a reduced dependence and reliance on subtraction.

Absent of the source signature removal and deghosting, the method still provides multiple predictive value and usefulness- but has diminished fidelity of amplitude and can suffer timing errors, as well. The ConocoPhillips tests did not involve wavelet removal or deghosting. Adaptive subtraction methods could be called upon to then adjust the amplitude and phase of the prediction to match (and subtract) the multiple. In the case where the prerequisite wavelet and ghosts are not removed the inclusion of the frequency and wave-number dependent obliquity factor in the M-OSRP inverse scattering series algorithm provides important differential added predictive value of the multiple, at all offsets, in comparison to free surface multiple elimination methods and codes available from other consortia and vendors.

In contrast with other traditional multiple removal methods, this algorithm requires no subsurface information, no velocity model, nor assumptions on statistics of primaries and periodicity of multiples. The method and code are completely unchanged for any type of earth model, e.g., no line of code changes for acoustic, elastic, anisotropic and anelastic earth models.

The method in principle predicts the amplitude and phase of the multiple, and allows for surgical removal without damaging proximal or interfering primaries. In practice, the method could call upon a mild and judicious use of an adaptive subtraction, to only deal with real data issues outside of its maximal physics and deterministic and inclusive predictive competence. The reduced dependence on the adaptive subtraction step reduces the mischief and harm the adaptive can cause with, e.g., proximal and destructively interfering events. The M-OSRP strategy is to maximize the deterministic physics of prediction to increase the competence of the prediction so the difference between prediction and subtraction is minimized, and thus reduce the burden on the adaptive step. Reducing its burden reduces its opportunity for harmful and injurious effect. Interfering events do not cause problems in the surgical amplitude and phase prediction of the underlying physics of the inverse scattering free surface removal method. The latter positive quality can be compromised by energy minimizing adaptive subtraction, which can fail at precisely the point where the underlying physics of the inverse scattering free surface multiple elimination method has one of its greatest strengths.

In contrast to the capability provided by other consortia, this free surface elimination algorithm and code: (1) is equally effective at all offsets, and includes the obliquity factor; (2) multiples don't reappear in the stack, that seemed to be gone in the pre-stack domain, and (3) a Radon de-multiple is not called upon for long offset residuals, with the potential to harm primaries. All orders of free surface multiples are able to be eliminated by computing the appropriate number of terms in the series, and that capability is part of this code delivery. The method demonstrates its mettle in highly complex rapidly varying heterogeneous media.

Acknowledgements

The inverse scattering free surface de-multiple theory was pioneered, developed and tested in the thesis of Paulo M. Carvalho, (of Petrobras while a student at UFBa, in Salvador, Brazil) and documented in SEG and EAGE Abstracts and papers that followed. The 3D M-OSRP free surface code was produced and documented by Sam Kaplan, as a special case of the 2D internal multiple code also produced by Sam Kaplan for M-OSRP. Einar Otnes and Kris Innanen provided valuable suggestions, insights and assistance.

The 3D synthetic data used for the test was arranged by Bill Dragoset for M-OSRP from a data set owned by WesternGeco, Statoil-Hydro and Lawrence Livermore National Lab. We thank WesternGeco, Statoil-Hydro and Lawrence Livermore National Lab for permission to use their data.

The testing of the 3D free surface code at ConocoPhillips was managed and guided in technical detail by Simon Shaw. Kris Innanen was the connection and technical link on the M-OSRP side during the ConocoPhillips tests. Haiyan Zhang provided significant and extensive debugging and test evaluation, and careful error location and analysis. Recently the M-OSRP intern Zhiqiang Wang working with Haiyan, provided further debugging progress and contribution. Among others at ConocoPhillips that contributed to the data management and testing are Paul Valasek and Doug

Foster. Sam Kaplan kept a helpful eye on the code testing and was always available with useful insights and invaluable suggestions.

M-OSRP thanks all mentioned in this acknowledgement for helping this high watermark of capability for free surface multiple removal to become available to our students and faculty and to our sponsors.

Technical highlights

Depth imaging and AVO

In our direct depth imaging (without subsurface information) project we are pursuing a fundamental new concept and capability to add to the seismic imaging toolbox. In our past, we researched and developed capability for removing free surface and internal multiples as distinct subseries of the inverse scattering series. Those developments were first examined and tested in simple acoustic models before being extended and ultimately applied in their current model-type independent forms. The M-OSRP fundamental research projects on depth imaging, target identification and Q compensation each pass through the same stages that we went through in the earlier work on multiples. At some point, we decide that the new formalism has passed tests with sufficient synthetic data model realism to warrant a field data test. At this moment, we have not developed a model-type independent inverse scattering series depth imaging algorithm. It is therefore reasonable to ask what specific type of model test success would point to a test with field data.

In seismic exploration, we want a minimally complicated model adequate to achieve our predictive purposes, but not too simple to be unrealistic, and misleading or harmful , nor too complicated to be more than necessary to reach E & P goals. How to determine model adequacy? In our view, a model is too simple if its output recommends drilling decisions that a more complicated and complete model would improve upon, and is too complicated if a simpler model would not change the efficacy of drilling prediction, e.g., changing a drill to no-drill or a no-drill to a drill decision. Model adequacy depends on the exploration region, the data quality and type of play, structural or stratigraphic, among other factors. Model-type independent processing algorithms have a tremendous conceptual and practical advantage.

Among the basic assumptions behind all traditional and currently applied seismic depth imaging methods are: (1) the ability to determine an adequate velocity model, and (2) that an imaging algorithm is available to adequately back-propagate waves through that medium, where only the velocity is changing. If the velocity configuration is achievable, and your goal is a structure map, then thinking about (and then worrying about) additional subsurface properties such as e.g., density is completely unnecessary and a more complicated model than needed for the goal of structure. Although the structure determination only cares about velocity and only uses the phase in seismic events for that purpose, the migrated images themselves are interpreted by their location, and (at the very least) qualitatively interpreted using their amplitudes. The latter image location and amplitude character cares about all properties of the seismic event and all of the properties of the subsurface that the event has experienced. Furthermore, if your goal is reflector location and inversion at depth , i.e., migration-inversion, then all overburden properties are relevant and required.

Since the goal of our M-OSRP imaging project was to use the inverse scattering series for locating structure (without concern for the amplitude of the image) and without knowing any subsurface properties it was reasonable to begin with an earth model that only allowed variation in velocity, and that the velocity would be unknown, and never would be estimated or determined. In that thinking, no other physical property other than velocity needs to be considered. Our inverse scattering imaging subseries with different degrees of imaging capture and capability LOIS (Simon Shaw, Bob Keys *et al.*), HOIS (Fang Liu *et al.*) followed that path and reasoning of developing and testing direct depth imaging methods for an earth where the only variable and relevant unknown property was assumed to be velocity. The thinking went as follows: "if having the velocity was adequate to determine depth, then assuming you didn't know the velocity would be adequate for an inverse scattering series method to directly determine structure without subsurface information". If velocity was all you needed to know, not knowing the velocity was all you needed to assume that you didn't need to know.

The announced plan a year ago was to test Fang Liu's HOIS algorithm on 3D marine data. At that time, there were two initiatives: one was with Xu Li seen as inheriting the mantle of Haiyan Zhang to further progress and develop methods for non-linear direct target identification, and a second with Shansong Jiang , was to provide a second generation of field data capability to 3D imaging, where both velocity and density could vary.

However, following discussions with Michael Richardson of BHP and Scott Morton of Hess, and others, about the prevalence of rapid variations in density, and density and velocity in the subsurface, and following subsequent HOIS tests with models where both the velocity and density varied, caused a change in plans. In that process it became clear that in contrast to the velocity only need when you know the subsurface velocity configuration, the simplest realistic model for the inverse scattering series to produce a structural subsurface map (on field data) without subsurface information was a model that allowed both velocity and density to vary, and where both physical quantities would not be known or determined or needed in principle and practice.

The initial steps represented by LOIS and HOIS to develop a structure map from the inverse scattering series for a subsurface where only the velocity can vary still made sense, for the first stage of testing an embryonic concept. However an added step of inverse scattering imaging theory and algorithmic development and testing needed to take place where the earth can have rapid and unknown variation in both velocity and density, before going forward with the first field data tests. Why is the simplest model that the inverse scattering series requires for field data application pointing to a model where both velocity and density can vary, and why is a model with velocity and density both varying needed to only determine structure? Velocity and density both variable, for structure- how can that make any sense? The reason goes back to the way the inverse scattering series performs all of the tasks of seismic processing directly in terms of the data, and without knowing or determining or requiring subsurface properties. The inverse scattering series is the only method that performs all seismic processing tasks of multiple removal, depth imaging, non-linear direct AVO, and Q compensation in the same way that free surface multiples are removed, and with the same prerequisites, and the same single set of equations. Free surface multiples are removed without knowledge, need, determination or estimation of any subsurface properties, by using the amplitude and phase of events in multiplicative combinations, directly inputting data with free surface multiples and outputting data without free surface multiples. If you imagine a marine earth model where the velocity is homogeneous at water speed but the density has rapid

variations, and that those rapid variations in density cause reflections, then those reflections play no role in correcting the image with a water speed migration, which is perfect and not in need of help. A model of the subsurface that assumes all variations are only due to velocity would misinterpret all of the reflections in this last example as due to rapid velocity changes and would incorrectly seek to correct the already correct water speed image. A generalization of the velocity only imaging theories was extended to velocity and density varying media by Weglein in what is called the "imaging conjecture". The imaging conjecture uses the strength of a multi-parameter inverse series to exclude density only variations from the multiplicative conversations of event amplitudes and phases, towards a structure only map, while avoiding the new and daunting issues of multi-parameter inverse of seeking several separate images, one for each parameter, with new complications due, e.g., to linear inverse leakage, that don't exist in the earlier one parameter velocity only varying earth model and experience of LOIS and HOIS. A single collective image of a reflectivity like quantity is output as part of the imaging conjecture. Jingfeng Zhang confirmed the conjecture for the elastic case, and Shansong Jiang showed that the conjecture held to third order in a multi-parameter acoustic earth. Initial synthetic tests of the conjecture were carried out with distinct front end and imaging issues that need to be examined, tested and analyzed. That analysis and testing are provided in this Annual Report in separate reports of Xu Li *et al.* and Shansong Jiang *et al.*. The imaging conjecture has a multi-parameter front end that excludes density only reflections, and outputs reflectivity, sitting on top of a Fang Liu type of HOIS imaging algorithm engine. In the elastic world there is much to examine and progress: Xu Li will focus on front end issues while Shansong Jiang deals with imaging.

An unexpected potential AVO opportunity and significant tool developed from the imaging conjecture, for automatic flat common image gathers of a reflectivity like output without the need for ironing, and ironing away polarity reversals. We are following a good suggestion by Doug Foster to examine this imaging conjecture output for type 1 and type 2 AVO targets and application. Early tests of that possibility are encouraging and are presented in the two reports cited here by Shansong Jiang and Xu Li. The plan is now for the imaging conjecture to be used for our first field data imaging test, and we expect that test for this coming year.

On-shore project

M-OSRP's mandate is to address pressing petroleum industry challenges in seismic exploration and production. Those challenges occur in the marine and in the on-shore arenas and there are some shared problems/issues and others which are unique to those distinct types of plays. The daunting combination of technical and economic challenges in deep water sub-salt exploration has caused a shift in the investment portfolios of the petroleum industry, towards an increased interest in on-shore prospects and investment.

M-OSRP is responding to that shift by allocating resources to both our traditional marine and a newer on-shore specific project. This Annual Report contains a report by Shih-Ying Hsu and a note from Min Wang from the on-shore project. It is part of a campaign to address pressing issues specific to on-shore exploration; and specifically to allow the added-value methods developed within the group for removing multiples in a marine environment to be applied to on-shore exploration.

Among the key basic differences in on shore and offshore E & P activity is the nature of the medium immediately at and beneath the source and receiver measurement surface. In the methods based

on the inverse scattering series for removing multiples and processing primaries there is a a call for a reference medium and a wavelet. The inverse scattering series overall has conditions on the reference medium, conditions that are designed to keep the perturbation V, the difference between the actual and reference medium, beneath the measurement surface. That condition translates into the reference and actual medium agreeing above and on the measurement surface. Satisfying that condition on the reference medium in the marine towed streamer case is not much of an issue, but it is an issue for the on-shore and ocean bottom cases. In the Ken Matson thesis, he develops the theory and evaluates inverse scattering series de-multiple methods for ocean bottom and on-shore application. There is an assumption on the properties of the reference medium consistent with the latter arguments, that places a stringent requirement on knowledge of the on shore near measurement surface properties (or subsea floor properties) that one could imagine becoming a practical obstacle for field data application. There is also a need for reference medium properties in transforming multi-component data to P and S wave types. A report by Shih-Ying Hsu *et al.* demonstrates that while the overall inverse scattering series has the above mentioned reference medium condition, the internal multiple subseries is insensitive to the choice of reference property for both acoustic and elastic media where the near surface is assumed to be homogeneous. Once again, we find that certain task specific subseries have more favorable and forgiving attitudes and less sensitivity than the overall inverse scattering series. That is an initial look and encouraging note for on-shore application of the internal multiple algorithm. Min Wang is looking at applying a Green's theorem like approach to determining the source signature, for on-shore application, and has written a note in this report describing the background, formulation and plan. In current on-shore application of internal multiple algorithms there is a tremendous over-reliance and dependence of the adaptive step due to the typical on shore data complexity. That great weight on the adaptive often allows the interpreter to choose any event as an internal multiple, and to remove it. The on-shore wavelet project seeks to increase the predictive competence of the prediction in the prediction and subtraction sequence. There is a pressing need for deterministic improvement of internal multiple prediction in the on-shore arena.

These activities, e.g., reference medium choice issues (under more complex near surface properties), and limited data tests, and wavelet estimation, will progress within the on-shore project and are interdependent, and will be first developed and/or examined separately and tested and then linked for overall testing and evaluation.

Important advances and plans that support and/or enhance our de-multiple and imaging efforts

In the M-OSRP program we have a portfolio of projects that manage risk, and deliver different types of benefits from code delivery, on the one end, to synthetic data tests that exemplify progress of fundamental new concepts, on the other end.

In developing a fundamental new seismic capability from thought-experiment and concept to field data applications- there is a very long list of theoretical and practical issues to be concerned about and address. If you look at them all at once you have little or no chance of addressing any one issue let alone the entire collection. The strategy we adopt is to bring the new concept along examining and then hopefully addressing different challenges in isolation and in order. Sometimes

issues within the program are progressed in series and sometimes in parallel, and sometimes in series and parallel. We describe briefly below a few of the initiatives and advances that support and/or advance different aspects or issues of projects within the program.

Fang Liu developed a much more accurate water speed FK Stolt migration, due to including large vertical wave numbers in the inverse Fourier transforms of the algorithm. This has resulted in an improved velocity independent direct depth imaging algorithm, HOIS (higher order imaging subseries). It was tested on a synthetic salt model, and showed improvement, especially in locating the salt vertical wall, and mitigating the impact of diffractions. This is a significant and fundamental computational mathematics breakthrough with implications for all methods both within M-OSRP, and outside, that require and use a Fourier inverse transform to depth.

Zhiqiang Wang developed a fundamentally new migration method that is wave theoretic in line and aperture compensated asymptotic cross line. It gives the data the wave theory imaging where the data can support that method, and simultaneously provides an asymptotic migration that is less complete and less data demanding, but anticipates and understands data limitations. The use of an asymptotic aperture compensated migration was examined as the input for the inverse scattering imaging series HOIS. Initial tests indicate an improvement for HOIS with a wave theory migration front end, over asymptotic migration, for large aperture data, and the opposite judgment for limited aperture data.

Adriana C. Ramirez and A. B. Weglein have written an invited tutorial for Geophysics on Green's theorem for seismic exploration and interferometry: "Green's theorem as a comprehensive framework for data reconstruction, regularization, wavefield separation, seismic interferometry and wavelet estimation: A tutorial". The purpose and scope of this document is to provide a tutorial on various Green' s theorem derived methods in seismic exploration, with an emphasis on seismic data reconstruction and its relationship to interferometry and discusses related subjects such as wavelet estimation and wavefield separation. The tutorial provides a perspective of the interferometry field, and uses Green's theorem as both a platform to understand current capability and to develop improvements and new methods for data reconstruction. Examples that illustrate those comparisons and improvements are presented.

There is a report within the Annual Report by Jim Mayhan that presents an overview plan to code and test a 3D Greens theorem based deghosting, wavelet estimation and data reconstruction all based upon and extending Jingfeng Zhang and Adriana C. Ramirez thesis research and testing results in those areas. That will complement and enhance the code delivery described in the first item of this introduction. Development and testing of these prerequisite and data reconstruction codes will take place this summer.

Weglein *et al.* have written a paper providing a clearer and unambiguous meaning of linear inversion. This paper and its incontrovertible but apparently radical message, provides both a platform and guide to inversion theory, and reason for pause and careful scrutiny for many methods which are indirect, model-matching and "full wave form", but represent something less than an inverse solution. Solving a forward problem in an inverse sense is not the same as solving an inverse problem. The direct inversion for target elastic properties is in principle not achievable with PP data. There are important implications for our research projects within M-OSRP and for those pursuing inversion methods in general.

The anelastic inverse scattering project

In the anelastic inverse scattering series project two major advances took place: (1) the understanding of how the inverse scattering internal multiple algorithm operates in an anelastic earth (Jose Eduardo Lira *et al.*) and the subsequent use of that knowledge to estimate and remove the impact of absorption experienced in the overburden on a given primary reflection and (2) Kris Innanen *et al.* researched and provide a deeper understanding of the particular way that the amplitudes and phases of events are used in an inverse scattering series method that inputs recorded data, that has experienced a subsurface with absorption, and outputs data as though there was no absorption, without knowing or determining or requiring the values of Q.

Jose Eduardo Lira *et al.* have provided a new way to enhance traditional migration-inversion, with the promise of removal of the overburden transmission loss experienced by a primary, by using the difference between a proximal internal multiple and its approximate amplitude predicted by the inverse scattering internal multiple algorithm. He turns a deficit of the internal multiple attenuation algorithm into an information bearing asset to enhance the traditional information extraction of primaries.

This Introduction has presented an overview of projects and highlights that have progressed within this past academic year. It was an exciting year with an important code delivery, and much new directed fundamental science and some surprises, revised timetables for field data imaging tests as unforeseen issues arose, and new imaging theory then responded, and a positive and unanticipated potential AVO exploration product arrived before we expected that to happen. It was a good, and busy and productive year. Thank you for your encouragement and support.

Best regards,
Art

Arthur B. Weglein

A short note about elastic wavelet estimation

M. Wang and A. B. Weglein, M-OSRP, University of Houston

Abstract

In this short note, we present a review of the elastic wavelet estimation method which has been developed by Weglein and Secrest (1990). A direct prediction of the wavelet for on-shore application is offered which requires an surface integral over the measurement surface. We will also discuss the boundary conditions for vibrators and explosives in land surveys and give a future plan for testing this method.

1 Introduction

Wavelet estimation is one of the classic and central issues in seismic data processing. In order to extract information about the subsurface from the reflection data recorded on the measurement surface, it is important to identify and remove the effects of the source characteristics from the reflected energy. Furthermore, inverse scattering subseries methods for removing multiples, imaging and inverting primaries without knowledge of the subsurface, have placed a high-bar on the pre-processing steps including the source signature estimation.

Recently, ConocoPhillips has successfully tested the inverse scattering 3D free surface multiple elimination code. Given its prerequisites, the method is in principle able to eliminate free surface multiple no matter what type of earth model it is, i.e., it can be used for acoustic, elastic, anisotropic and anelastic earth models without changing any line of the code. Among these prerequisites, the first one is the source signature/wavelet.

Unfortunately, the source wavelet is practically never known. We need to estimate or record it. To obtain the wavelet, both statistical and deterministic (matching surface seismic to well-log data) methods are generally used. In the marine case, common practice to date is to estimate wavelets directly from the data by direct measurement with hydrophones. Weglein and Secrest (1990) presented a method of calculating the wavelet by measuring the pressure and its normal derivative along the cable, which is in principle exact and yet no information about the properties of the earth is required. Osen et al. (1998) and Tan (1999) showed that the wavelet due to an isotropic source can be determined from the pressure on the measurement surface and an extra hydrophone between the measurement surface and the free surface. Recently, the simultaneous measurement of the pressure and the vertical component of particle velocity (simply related to the normal derivative of pressure in the space and temporal frequency domain) in a single towed streamer cable becomes possible which means the wavelet estimation method proposed by Weglein and Secrest (1990) will be the most direct one. Now, Jim Mayhan is trying to use this robust method to estimate acoustic wavelet.

In offshore case, the reference medium is water and only compressional wave (P wave) can propagate. In on-shore case, sources and receivers are located on or in an elastic medium where both

compressional wave (P wave) and shear wave (S wave) can propagate inside. The recorded data are far more complex and the nature of the near surface medium is always unknown. The difficulties associated with noise, statics, resolution and the dynamic range of a seismic recording system also make the construction of a seismic reflection profile far more complex than the marine case. In this circumstance, accurate wavelet estimation becomes more important in order to distinguish the primaries from the multiples. The current method for estimating the wavelet in offshore case, the energy minimizing adaptive subtraction, is also applicable to the land case. The idea is that the data contain less energy without the multiples than with them. Using this method, the wavelet is then found which best removes the multiples from the data (Verschuur, 1991). The problem is, when multiples interfere with primaries and weak internal multiples are proximal to weak primaries, this energy minimization criterion tends to fail. In order to give a better prediction and reduce the overburden of adaptive subtraction, M-OSRP has started two on-shore projects to apply the relevant methods developed within the group for estimating wavelet and removing multiples in a marine setting to the on-shore arena. The latter project is shown by Shih-Ying Hsu regarding the reference velocity sensitivity for the elastic internal multiple attenuation algorithm. The former one will be addressed in this note.

2 Elastic wavelet estimation method

Weglein and Secrest (1990) outlined the generalization of the elastic wavelet estimation method which is similar as that in the acoustic case. They showed that a comparison of the Lippmann-Schwinger equation and the Green's theorem can be used to determine the elastic wavelet. In fact, the Green's theorem result for elastic waves has been given by Pao and Varatharajulu (1976). Next, we will show the derivation given by them.

2.1 The Lippmann-Schwinger equation

For isotropic elastic solids with Lamé's constants λ and μ, the equation of wave motion is

$$[(\lambda+\mu)\nabla\nabla\cdot+\mu\nabla^2]\vec{u}(\vec{x},\omega)+\rho\omega^2\vec{u}(\vec{x},\omega)=-\rho\vec{f}(\vec{x},\omega) \tag{1}$$

where $\vec{u}(\vec{x},\omega)$ is the displacement vector and $\vec{f}(\vec{x},\omega)$ is the body force per unit mass in the frequency domain. ρ is the mass density and ω is the circular frequency.

Let the Green's displacement tensor G be the response in a homogeneous medium, the equation of motion is

$$[(\lambda+\mu)\nabla\nabla\cdot+\mu\nabla^2]G(\vec{x},\vec{x}',\omega)+\rho\omega^2G(\vec{x},\vec{x}',\omega)=-\delta(\vec{x}-\vec{x}')I \tag{2}$$

where $\vec{x}$ and $\vec{x}'$ are the positions of the observation point and the source point, I is the unit dyadic and $\delta(\vec{x}-\vec{x}')$ is the three-dimensional delta function.

By inverting the operator

$$(\lambda+\mu)\nabla\nabla\cdot+\mu\nabla^2+\rho\omega^2=G^{-1} \tag{3}$$

we have the operator relationship

$$\tilde{u} = \rho \tilde{f} G \tag{4}$$

or, equivalently, the L-S equation:

$$\begin{aligned} \vec{u}(\vec{x},\omega) &= \int_{-\infty}^{\infty} \rho \vec{f}(\vec{x'},\omega) \cdot G(\vec{x},\vec{x}',\omega) d\vec{x}' \\ &= \int_{-\infty}^{\infty} [\rho \vec{f_p}(\vec{x}',\omega) + A(\omega)\delta(\vec{x}' - \vec{x}_s)I] \cdot G(\vec{x},\vec{x}',\omega) d\vec{x}' \\ &= A(\omega) I \cdot G(\vec{x},\vec{x}_s,\omega) + \int_V \rho \vec{f_p}(\vec{x}',\omega) \cdot G(\vec{x},\vec{x}',\omega) d\vec{x}' \end{aligned} \tag{5}$$

where $\vec{f_p}(\vec{x},\omega)$ are the passive sources (the scattering centers) of the scattered displacement field originating from the inhomogeneities in the medium and the physical sources $A(\omega)\delta(\vec{x} - \vec{x}_s)I$ are outside the volume V. This Lippmann-Schwinger integral equation is valid for all the observation points $\vec{x}$.

2.2 The Green's theorem

To derive the Green's theorem for the isotropic elastic solids, a rank three Green's stress tensor Σ is defined as the following

$$\Sigma = \lambda I \nabla \cdot G + \mu(\nabla G + G\nabla) \tag{6}$$

Physically, Σ represents the stress field at $\vec{x}$ generated by three mutually perpendicular concentrated forces at $\vec{x}'$. Then we can rewrite equation (2) as the following

$$\nabla \cdot \Sigma(\vec{x},\vec{x}',\omega) + \rho\omega^2 G(\vec{x},\vec{x}',\omega) = -\delta(\vec{x} - \vec{x}')I \tag{7}$$

Similarly, a rank two stress tensor $T(\vec{x},\omega)$ is related to the displacement vector $\vec{u}(\vec{x},\omega)$ by

$$T = \lambda I \nabla \cdot \vec{u} + \mu(\nabla \vec{u} + \vec{u}\nabla) \tag{8}$$

And we can rewrite equation (1) as the following

$$\nabla \cdot T(\vec{x},\omega) + \rho\omega^2 \vec{u}(\vec{x},\omega) = -\rho \vec{f}(\vec{x},\omega) \tag{9}$$

Taking the scalar product of equation (7) on the left by $\vec{u}(\vec{x},\omega)$ and of equation (9) on the right by $G(\vec{x},\vec{x}',\omega)$, we have

$$\vec{u} \cdot (\nabla \cdot \Sigma) + \vec{u} \cdot \rho\omega^2 G = -\vec{u}\delta(x - x') \tag{10}$$

$$(\nabla \cdot T) \cdot G + \rho\omega^2 \vec{u} \cdot G = -\rho \vec{f} \cdot G \tag{11}$$

Subtracting equation (10) from (11), we obtain

$$(\nabla \cdot T) \cdot G - \vec{u} \cdot (\nabla \cdot \Sigma) = -\rho \vec{f} \cdot G + \vec{u}\delta(x - x') \tag{12}$$

Considering that we have

$$\nabla \cdot (T \cdot G) = (\nabla \cdot T) \cdot G + T : \nabla G \tag{13}$$

$$\nabla \cdot (\vec{u} \cdot \Sigma) = \vec{u} \cdot (\nabla \cdot \Sigma) + \nabla \vec{u} : \Sigma \tag{14}$$

and

$$[T : \nabla G - \nabla \vec{u} : \Sigma]_l = T_{jk}(\partial_j G_{kl}) - (\partial_j u_k)\Sigma_{jkl} = 0 \tag{15}$$

The left-hand side of equation (12) can be rewritten as

$$(\nabla \cdot T) \cdot G - \vec{u} \cdot (\nabla \cdot \Sigma) = \nabla \cdot (T \cdot G) - \nabla \cdot (\vec{u} \cdot \Sigma) \tag{16}$$

Then we can obtain

$$\nabla \cdot (T \cdot G - \vec{u} \cdot \Sigma) = -\rho \vec{f} \cdot G + \vec{u}\delta(\vec{x} - \vec{x}') \tag{17}$$

Integrating equation (17) over a region V which is bounded by the surface S and using the divergence theorem to the left-hand side, we obtain the following result:

$$\begin{aligned}
&\int_V \nabla \cdot (T \cdot G - \vec{u} \cdot \Sigma) dV = \oint_S (T \cdot G - \vec{u} \cdot \Sigma) \cdot \hat{n}' dS' \\
&= \oint_S \left\{ \vec{t}(\vec{x}') \cdot G(\vec{x}, \vec{x}') - \vec{u}(\vec{x}') \cdot \left[\hat{n}' \cdot \Sigma(\vec{x}, \vec{x}') \right] \right\} dS' \\
&= \int_V \left[-\rho \vec{f}(\vec{x}') \cdot G(\vec{x}, \vec{x}') \right] dV + \int_V \vec{u}(\vec{x}')\delta(\vec{x} - \vec{x}') dV \\
&= \int_V [-\rho \vec{f}_p(\vec{x}', \omega) - A(\omega)\delta(\vec{x}' - \vec{x}_s) I] \cdot G(\vec{x}, \vec{x}', \omega) d\vec{x}' + \int_V \vec{u}(\vec{x}')\delta(\vec{x} - \vec{x}') dV \\
&= \int_V \left[-\rho \vec{f}_p(\vec{x}') \cdot G(\vec{x}, \vec{x}') \right] dV + \int_V \vec{u}(\vec{x}')\delta(\vec{x} - \vec{x}') dV
\end{aligned} \tag{18}$$

where $\vec{t}$ is the traction at the surface which is related to the displacement tensor T by $t = \hat{n}' \cdot T$. We still consider the body force $\vec{f}$ as two parts: (1) the physical sources outside the volume V which make the integral equal zero; (2) the passive sources of the scattered displacement field inside the volume. Then equation (18) can be rewritten as the following

$$\begin{aligned}
&\oint_S \left\{ t(\vec{x}') \cdot G(\vec{x}, \vec{x}') - \vec{u}(\vec{x}') \cdot \left[\hat{n}' \cdot \Sigma(\vec{x}, \vec{x}') \right] \right\} dS' + \int_V \left[\rho \vec{f}_p(x') \cdot G(\vec{x}, \vec{x}') \right] dV \\
&= \begin{cases} \vec{u}(\vec{x}), & \vec{x} \text{ in } V \\ 0, & \vec{x} \text{ not in } V \end{cases}
\end{aligned} \tag{19}$$

When the observation point $\vec{x}$ is exactly on the boundary S, we can assume that this discontinuous function is $\vec{u}(\vec{x})$ within *and on* S and is zero outside S (Morse and Feshbach, 1953). This is to some extent a matter of convention, though once we decide on the convention, we must be consistent about it.

Let $u_{mn}(\vec{x},\vec{x}')$ be the displacement at $\vec{x}$ in the n-axis direction due to a source at $\vec{x}'$ in the m-axis direction and G_{mn} be the mnth component of the Green's displacement tensor. The source is $A_m(\omega)\delta(\vec{x}-\vec{x}')I$. Comparing equations (5) and (19), for $\vec{x}$ in the volume V, we can determine the wavelet $A_m(\omega)$ by dividing the surface term by G_{mn} as the following

$$A_m(\omega) = \frac{\left\{ \oint\!\!\!\!\!\!\diagup_S \left[t \cdot G - \vec{u} \cdot (\hat{n}' \cdot \Sigma)\right] dS' \right\}_{mn}}{G_{mn}} \tag{20}$$

If we use the integral formula given by Morse & Feshbash (Morse and Feshbach, 1953), then

$$\begin{aligned} A_m(\omega) = & \Big\{ \rho c_p^2 \oint_S \left[\left(G \cdot \hat{n}'\right) \left(\nabla' \cdot \vec{u}\right) - \left(\nabla' \cdot G\right) \left(\vec{u} \cdot \hat{n}'\right) \right] dS' \\ & - \rho c_s^2 \oint_S \left[G \cdot \left(\hat{n}' \times \nabla' \times \vec{u}\right) + \left(\nabla' \times G\right) \cdot \left(\hat{n}' \times \vec{u}\right) \right] dS' \Big\}_{mn} / G_{mn} \end{aligned} \tag{21}$$

where c_p and c_s are the reference values of the compressional velocity and shear velocity.

3 Discussion

In order to use equation (20) or equation (21) to determine the elastic wavelet, we need to measure the following quantities: $\vec{u} \cdot \hat{n}'$ and $\hat{n}' \times \vec{u}$ are the normal components and tangential components of the field at the surface, while $\nabla' \cdot \vec{u}$ and $\hat{n}' \times \nabla' \times \vec{u}$ represent the pressure and tangential stress at the surface, respectively.

For land surveys, there are two kinds of seismic sources: vibrators and explosives. The vibrators are on the earth while the explosive charges are usually deployed in shot holes which are drilled to depths ranging between ten to hundreds of feet. The seismic receivers (i.e., the geophones) are always placed at near surface. If we define a volume V enclosed by the physical surface (i.e., the land) and a hemisphere under the surface, then the vibrators and the geophones are just on the boundary while the explosives such as dynamite are under the measurement surface and inside the volume.

As numerically shown in the second section, the Green's theorem needs the sources and receivers to be inside and outside the volume, respectively. However, for vibrators, the physical sources $A_m(\omega)\delta(\vec{x}-\vec{x}')I$ and the receivers are both on the boundary, not specifically inside or outside the volume V, except that the sources are a little bit higher than the receivers. In the near future, we plan to design some numerical tests where we assume the vibrators are "in" the air and extremely close to the land and the receivers are under the physical boundary with a very small distance. We will consider the continuity of the measurements and find out whether we can obtain an approximate wavelet by this method.

For explosives, mathematically speaking, the physical sources $A_m(\omega)\delta(\vec{x}-\vec{x}')I$ (such as dynamite) and the receivers are both inside the volume V, so the surface integral term in equation (19) will be zero. Then we can not determine the wavelet $A_m(\omega)$ by comparing the Lippmann-Schwinger equation and the Green's theorem any more. This is another open question we need to study in future.

4 Conclusion and future plan

In this short note, we have presented the elastic wavelet estimation method which has been proposed by Weglein and Secrest (1990). By comparing the Lippmann-Schwinger equation and the Green's theorem, two final equations are derived to determine the elastic wavelet which require an integral over the measurement surface. The normal components and tangential components of the displacement, the pressure and the tangential stress at the surface need to be measured. To use this method in practice, we need to pay attention to the boundary conditions in case that the surface integral becomes zero. In the near future, we will design some numerical tests for vibrators as described in the discussion section. We will also try to find a solution to determine the wavelet of dynamites.

Acknowledgments

Min Wang would like to thank Shansong Jiang for his great help in editing this note and Shih-Ying Hsu for her valuable discussions during this research review. All members in M-OSRP are thanked for their help in finishing this note and valuable discussions in this research program. The authors would also like to acknowledge all sponsors of M-OSRP for the encouragement and financial support for this research program.

References

Amundsen, L., L. T. Ikelle, and L. E. Berg. "Multidimensional signature deconvolution and free-surface multiple elimination of marine multicomponent ocean-bottom seismic data." *Geophysics* 66 (2001): 1594–1604.

Morse, P. M. and H. Feshbach. *Methods of theoretical physics.* McGraw-Hill Book Co., 1953.

Osen, Are, Bruce G. Secrest, and Lasse Amundsen. "Wavelet estimation from marine pressure measurements." *Geophysics* 63 (November-December 1998): 2108–2119.

Pao, Y. H. and V. Varatharajulu. "Huygens' principle, radiation conditions, and integral formulas for the scattering of elastic waves." *J. Acoust. Soc. Am.* 59 (1976): 1361–1371.

Tan, T. H. "Wavelet spectrum estimation." *Geophysics* 64 (November-December 1999): 1836–1846.

Verschuur, D. J. *Surface-related multiple elimination: an inversion approach.* PhD thesis, Delft University of Technology, 1991.

Weglein, Arthur B. and Bruce G. Secrest. "Wavelet estimation for a multidimensional acoustic earth model." *Geophysics* 55 (July 1990): 902–913.

Preprocessing 3D data

J. D. Mayhan and A. B. Weglein, M-OSRP, University of Houston

Abstract

In this report, we present a plan for designing, coding, and testing an application for preprocessing 3D seismic data: source signature estimation, deghosting, and data extrapolation and interpolation. We are targeting the code to be ready August 1, 2009.

1 Introduction

M-OSRP is generating code to accomplish three pre-processing goals based on Green's theorem: wavelet estimation, deghosting, and data reconstruction. These methods are critically important to the success of the inverse scattering series methods, which has a higher bar for these requirements than do traditional methods. Green's theorem provides a wave theoretic approach to providing these prerequisites that is consistent with the inverse scattering series methods they are meant to serve. For reference, Figure 1 distinguishes events and their processing, whether involving the inverse scattering series or Green's theorem. This code development is especially timely because (1) M-OSRP code to remove free surface multiples from 3D seismic data has been tested at ConocoPhillips and will shortly be distributed, and this code would use the output of these pre-processing codes as input, and (2) PGS is in the process of collecting 2D and 3D seismic data using their proprietary GeoStreamer® cable, which is designed to provide input data as expected by many Green's theorem applications.

The research project outlined in this report consists of developing code (in C) to estimate the source signature from measured 3D data, deghost 3D data, and perform near offset data extrapolation. The output of this code will be the input to the 3D free surface multiple removal code. This report outlines the basic theory and plan to produce Green's theorem based processing code for 3D. It is organized as follows. The theory underpinning the code is discussed, with theoretical details included in appendices. We then discuss the targeted timing of code delivery.

2 Green's theorem and inverse scattering series processing chain

Each single algorithm or subseries operates on data; the output of that algorithm or subseries is the input to the next algorithm or subseries. (1) Measured data is input to data interpolation, whose output is the input to (2) source signature estimation, whose output is the input to (3) deghosting, whose output is the input to (4) free surface multiple removal, whose output is the input to (5) internal multiple removal, whose output is the input to (6)–(8) imaging, inversion, and

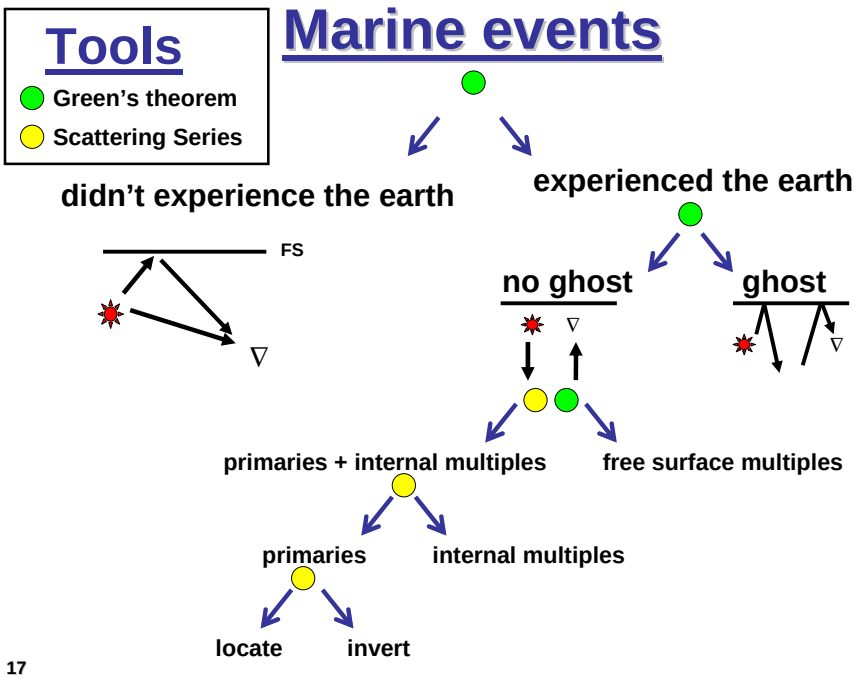

Figure 1: *Classification of marine events and how they are processed.*

Q compensation. The success of any inverse scattering series task-separated algorithm hinges on the success of all the steps done before it.

This paper involves a plan to code source signature estimation, deghosting, and data extrapolation and interpolation as variants of the same Green's theorem template. (Within extrapolation and interpolation, another important issue is near offset extrapolation in various water depths.) The application will be tested on 3D data (reflectivity data and/or data from ConocoPhillips).

3 Green's theorem processing theory

3.1 Source signature estimation

This section outlines the theory to be used in the source signature estimation code. Weglein and Secrest (1990) derive two equations containing the source signature: the Lippmann-Schwinger equation and a second equation derived from Green's theorem. Comparing the two equations gives an equation for the source signature as a function of measured 3D data and a reference medium Green function.

The Lippmann-Schwinger part begins with the constant density acoustic wave equation for the pressure field P created by a source $A(t)$ at position $\mathbf{r}_s$, restates wave speed $c(\mathbf{r})$ as a function of

reference medium speed c_0 and a perturbation $\alpha(\mathbf{r})$, and converts the partial differential equation into an integral equation (the Lippmann-Schwinger equation) involving a causal Green function (to get a causal solution for P). The result is

$$\tilde{P}(\mathbf{r},\mathbf{r}_s,\omega) = \tilde{A}(\omega)G_0^+(\mathbf{r},\mathbf{r}_s,\omega) + \int_\infty d\mathbf{r}' G_0^+(\mathbf{r},\mathbf{r}',\omega)\frac{\omega^2}{c_0^2}\alpha(\mathbf{r}')\tilde{P}(\mathbf{r}',\mathbf{r}_s,\omega). \quad (1)$$

The Green's theorem part begins with (1) a reference medium consisting of a half space of air overlaying a half space of water, (2) a perturbation $\alpha(\mathbf{r})$ which converts the lower part of the half space of water into earth, (3) an integration volume V consisting of a hemisphere bounded from above by the measurement surface, (4) a free surface (air-water interface) above the measurement surface (*i.e.*, outside V), and (5) a source $\mathbf{r}_s$ on or above the measurement surface (*i.e.*, outside V). Substituting the above, the partial differential equation for the pressure field P, and the corresponding reference medium Green function differential equation into Green's theorem, and for consistency with Eq. (1) choosing a causal Green function give

$$\begin{aligned}\tilde{P}(\mathbf{r},\mathbf{r}_s,\omega) &= \int_\infty d\mathbf{r}' G_0^+(\mathbf{r}',\mathbf{r},\omega)\frac{\omega^2}{c_0^2}\alpha(\mathbf{r}')\tilde{P}(\mathbf{r}',\mathbf{r}_s,\omega) \\ &\quad + \oint_S \mathbf{n}\, ds' \cdot [\tilde{P}(\mathbf{r}',\mathbf{r}_s,\omega)\nabla' G_0^+(\mathbf{r}',\mathbf{r},\omega) - G_0^+(\mathbf{r}',\mathbf{r},\omega)\nabla'\tilde{P}(\mathbf{r}',\mathbf{r}_s,\omega)]. \quad (2)\end{aligned}$$

Comparing Eqs. (1) and (2) gives an equation for the source signature:

$$\begin{aligned}\tilde{A}(\omega) &= \frac{1}{G_0^+(\mathbf{r},\mathbf{r}_s,\omega)}\oint_S \mathbf{n}\, ds' \cdot [\tilde{P}(\mathbf{r}',\mathbf{r}_s,\omega)\nabla' G_0^+(\mathbf{r}',\mathbf{r},\omega) \\ &\quad - G_0^+(\mathbf{r}',\mathbf{r},\omega)\nabla'\tilde{P}(\mathbf{r}',\mathbf{r}_s,\omega)]. \quad (3)\end{aligned}$$

Note that Eq. (3) is computing more than a traditional wavelet, *i.e.*, instrument response is included.

The details of the above derivation can be found in Appendix A.

3.2 Deghosting

This section outlines the theory to be used in the deghosting code. The theory of deghosting based on Green's theorem is covered in Zhang (2007) (pp. 19–23). The procedure begins with (1) a reference medium consisting of a whole space of water, (2) a perturbation $\alpha_{air}(\mathbf{r}')$ which converts the upper part of the whole space into air, (3) a perturbation $\alpha_{earth}(\mathbf{r}')$ which converts the lower part of the whole space into earth, (4) an integration volume V consisting of a hemisphere bounded below by the measurement surface, (5) a free surface (air-water interface) above the measurement surface (*i.e.*, inside V), and (6) a source $\mathbf{r}_s$ on or above the measurement surface (*i.e.*, inside V). Substituting the above into Green's theorem and invoking the Sommerfeld radiation condition give the receiver side deghosting equation:

$$\tilde{P}^{deghosted}(\mathbf{r},\mathbf{r}_s,\omega) = \int_{MS} \mathbf{n}\, ds \cdot [\tilde{P}(\mathbf{r}',\mathbf{r}_s,\omega)\nabla' G_0^+(\mathbf{r}',\mathbf{r},\omega)$$

$$-G_0^+(\mathbf{r}',\mathbf{r},\omega)\nabla'\tilde{P}(\mathbf{r}',\mathbf{r}_s,\omega)]. \tag{4}$$

where $\tilde{P}^{deghosted}(\mathbf{r},\mathbf{r}_s,\omega)$ is the deghosted wavefield, and $\tilde{P}(\mathbf{r}';\mathbf{r}_s;\omega)$ and $\nabla'\tilde{P}(\mathbf{r}';\mathbf{r}_s;\omega)$ are the hydrophone measurements and their spatial derivatives (in the frequency domain). Using reciprocity, a similar integration on the source side will remove source ghosts.

In 2D Eq. (4) can be written in the form

$$\begin{aligned} & \oint_S \mathbf{n}\, ds' \cdot [\tilde{P}(\mathbf{r}',\mathbf{r}_s,\omega)\nabla' G_0^+(\mathbf{r}',\mathbf{r},\omega) - G_0^+(\mathbf{r}',\mathbf{r},\omega)\nabla'\tilde{P}(\mathbf{r}',\mathbf{r}_s,\omega)] \\ = \;& \tilde{P}(\mathbf{r},\mathbf{r}_s,\omega) - \int_V d\mathbf{r}' G_0^+(\mathbf{r}',\mathbf{r},\omega) k_0^2 \alpha_{air}(\mathbf{r}')\tilde{P}(\mathbf{r}',\mathbf{r}_s,\omega) \\ & -\tilde{A}(\omega)G_0^+(\mathbf{r},\mathbf{r}_s,\omega). \end{aligned} \tag{5}$$

The physical meaning of Eq. (5) is that the total wavefield at $\mathbf{r}$ can be separated into three parts: (1) the direct wave which travels from the source at $\mathbf{r}_s$ to $\mathbf{r}$ (third term on the right hand side), (2) the pressure field whose last motion is downward from the free surface (second term on the right hand side), and (3) the pressure field whose last motion is upward from the earth (the entire right hand side).

In practice, the derivative of the pressure is usually not measured. The procedure uses a "double Dirichlet" Green function $G_0^{DD}(\mathbf{r}',\mathbf{r},\omega)$ which vanishes on the measurement surface as well as the free surface to predicts the pressure and its vertical derivative on a "pseudo-measurement surface" located between the free surface and the measurement surface using pressure measurements on the cable plus the source signature. The predicted pressure and vertical derivative are then substituted into Eq. (4).

The details of the above derivation can be found in Appendix B.

3.3 Interpolation

This section outlines the theory to be used in the data interpolation code. The theory of extrapolating near offset data in a towed streamer marine experiment is derived in Ramírez (2007) (pp. 64–69), where near offset means the data not collected between the source and the receiver (on each towed streamer) nearest the source. The procedure begins with Green's theorem, a causal reference Green function, and the assumption that the velocity distributions for the pressure field and the Green function are equal only within the integration volume V (and on its surface S). V is chosen to be a right circular cylinder bounded above by the free surface and below by the measurement surface. The radius of the cylinder is assumed to be at infinity. Further assuming that the source and receiver are inside V gives an equation for data interpolation/extrapolation:

$$P_s(\mathbf{x}_a|\mathbf{x}_b;\omega) = \int_{Sm} [P(\mathbf{x}|\mathbf{x}_a;\omega)\nabla\mathcal{G}_0^+(\mathbf{x}|\mathbf{x}_b;\omega) - \mathcal{G}_0^+(\mathbf{x}|\mathbf{x}_b;\omega)\nabla P(\mathbf{x}|\mathbf{x}_a;\omega)] \cdot \mathbf{n} ds \tag{6}$$

where
$P_s(\mathbf{x}_a|\mathbf{x}_b;\omega)$ is the scattered wavefield,

$\mathcal{G}_0^+(\mathbf{x}|\mathbf{x}_b;\omega)$ is the causal reference Green function,
$\mathbf{x}_a$ and $\mathbf{x}_b$ are the locations of the source and receiver, respectively, and
the integration is performed over the measurement surface.

More on the above derivation can be found in Appendix C.

4 Results

The authors are targeting to have the application ready for testing GeoStreamer® data beginning August 1, 2009.

5 Acknowledgments

The first author is grateful to all M-OSRP sponsors for their support of this research; to Sam Kaplan (University of Alberta), Dr. Fang Liu (M-OSRP), Jeff Sarlo (UH Computing), and Dr. Jingfeng Zhang (BP) for their help when he was learning how to run Dr. Zhang's 2D deghosting code and 1.5D data generation code and Sam's 1.5D and 2D free surface multiple elimination code; to Eduardo Lira (M-OSRP and Petrobras) for translating parts of Dr. Paulo Carvalho's thesis (from Portuguese); to Dr. Kris Innanen, Shih-Ying Hsu, and Xu Li (M-OSRP) for their helpful feedback on this report; and especially to Dr. Arthur Weglein for his teaching, guidance, and patience.

References

Carvalho, P. M. *Free-surface multiple reflection elimination method based on nonlinear inversion of seismic data*. PhD thesis, Universidade Federal da Bahia, 1992.

Clayton, R. W. and R. H. Stolt. "A Born-WKBJ inversion method for acoustic reflection data." *Geophysics* 46 (1981): 1559–1567.

De Santo, J. A. *Scalar Wave Theory: Green's Functions and Applications*. Springer-Verlag, 1992.

Jackson, J. D. *Classical Electrodynamics*. Third edition. New York: John Wiley & Sons, Inc., 1999.

Morse, P. M. and H. Feshbach. *Methods of theoretical physics*. McGraw-Hill Book Co., 1953.

Ramírez, A. C. *I. - Inverse scattering subseries for removal of internal multiples and depth imaging primaries; II. - Green's theorem as the foundation of interferometry and guiding new practical methods and applications*. PhD thesis, University of Houston, 2007.

Weglein, A. B., F. V. Araújo, P. M. Carvalho, R. H. Stolt, K. H. Matson, R. T. Coates, D. Corrigan, D. J. Foster, S. A. Shaw, and H. Zhang. "Inverse Scattering Series and Seismic Exploration." *Inverse Problems* (2003): R27–R83.

Weglein, Arthur B. and Bruce G. Secrest. "Wavelet estimation for a multidimensional acoustic earth model." *Geophysics* 55 (July 1990): 902–913.

Zhang, Jingfeng. *Wave theory based data preparation for inverse scattering multiple removal, depth imaging and parameter estimation: analysis and numerical tests of Green's theorem deghosting theory.* PhD thesis, University of Houston, 2007.

Zhang, Jingfeng and Arthur B. Weglein. "Documentation for the M-OSRP Extinction Theorem Deghosting code." *M-OSRP Code Documentation* (2005).

Appendix A — Theory of source signature estimation

Weglein and Secrest (1990) derive two equations containing the source signature: the Lippmann-Schwinger equation and a second equation derived from Green's theorem. Comparing the two equations gives an equation for the source signature as a function of measured 3D data and a reference medium Green function.

Lippmann-Schwinger approach

The constant density acoustic wave equation for the pressure field P created by a source $A(t)$ at position $\mathbf{r}_s$ is

$$\left(\nabla^2 - \frac{1}{c^2(\mathbf{r})}\frac{\partial^2}{\partial t^2}\right) P(\mathbf{r}, \mathbf{r}_s, t) = A(t)\delta(\mathbf{r} - \mathbf{r}_s). \tag{7}$$

Fourier transforming from the time domain to the frequency domain gives

$$\left(\nabla^2 + \frac{\omega^2}{c^2(\mathbf{r})}\right) \tilde{P}(\mathbf{r}, \mathbf{r}_s, \omega) = \tilde{A}(\omega)\delta(\mathbf{r} - \mathbf{r}_s). \tag{8}$$

Restating wave speed $c(\mathbf{r})$ as a function of reference medium speed c_0 and an actual medium perturbation $\alpha(\mathbf{r})$ gives

$$\frac{1}{c^2(\mathbf{r})} = \frac{1}{c_0^2}(1 - \alpha(\mathbf{r})). \tag{9}$$

Substituting Eq. (9) into Eq. (8) gives

$$\left(\nabla^2 + \frac{\omega^2}{c_0^2}\right) \tilde{P}(\mathbf{r}, \mathbf{r}_s, \omega) = \tilde{A}(\omega)\delta(\mathbf{r} - \mathbf{r}_s) + \frac{\omega^2}{c_0^2}\alpha(\mathbf{r})\tilde{P}(\mathbf{r}, \mathbf{r}_s, \omega). \tag{10}$$

Converting Eq. (10) from a partial differential equation into an integral equation (the Lippmann-Schwinger equation) gives

$$\tilde{P}(\mathbf{r}, \mathbf{r}_s, \omega) = \tilde{A}(\omega)G_0(\mathbf{r}, \mathbf{r}_s, \omega) + \int_\infty d\mathbf{r}' G_0(\mathbf{r}, \mathbf{r}', \omega)\frac{\omega^2}{c_0^2}\alpha(\mathbf{r}')\tilde{P}(\mathbf{r}', \mathbf{r}_s, \omega). \tag{11}$$

Because the Lippmann-Schwinger equation covers all space, there is no boundary condition to impose a causal solution; therefore choose a causal Green function G_0^+ to get a causal solution $\tilde{P}(\mathbf{r}, \mathbf{r}_s, \omega)$:

$$\tilde{P}(\mathbf{r}, \mathbf{r}_s, \omega) = \tilde{A}(\omega) G_0^+(\mathbf{r}, \mathbf{r}_s, \omega) + \int_\infty d\mathbf{r}' G_0^+(\mathbf{r}, \mathbf{r}', \omega) \frac{\omega^2}{c_0^2} \alpha(\mathbf{r}') \tilde{P}(\mathbf{r}', \mathbf{r}_s, \omega). \tag{12}$$

Green's theorem approach

Weglein and Secrest (1990) define the following to isolate the source signature: (1) a reference medium consisting of a half space of air above a half space of water, (2) a perturbation $\alpha(\mathbf{r})$ which converts the lower part of the half space of water into earth, (3) an integration volume V consisting of a hemisphere bounded from above by the measurement surface (the plane $z = 0$), (4) a free surface (air-water interface) above the measurement surface (*i.e.*, outside V), and (5) a source $\mathbf{r}_s$ on or above the measurement surface (again outside V).

Substituting $\tilde{P}$ and G_0 into Green's theorem gives

$$\begin{aligned} &\int_V d\mathbf{r}' [\tilde{P}(\mathbf{r}', \mathbf{r}_s, \omega) \nabla'^2 G_0(\mathbf{r}', \mathbf{r}, \omega) - G_0(\mathbf{r}', \mathbf{r}, \omega) \nabla'^2 \tilde{P}(\mathbf{r}', \mathbf{r}_s, \omega)] = \\ &\oint_S \mathbf{n}\, ds' \cdot [\tilde{P}(\mathbf{r}', \mathbf{r}_s, \omega) \nabla' G_0(\mathbf{r}', \mathbf{r}, \omega) - G_0(\mathbf{r}', \mathbf{r}, \omega) \nabla' \tilde{P}(\mathbf{r}', \mathbf{r}_s, \omega)], \end{aligned} \tag{13}$$

where V is the hemispheric volume defined above, and S is the hemisphere's surface. Substituting Eq. (10) and its corresponding reference medium Green function differential equation into Eq. (13) gives

$$\begin{aligned} &\oint_S \mathbf{n}\, ds' \cdot [\tilde{P}(\mathbf{r}', \mathbf{r}_s, \omega) \nabla' G_0(\mathbf{r}', \mathbf{r}, \omega) - G_0(\mathbf{r}', \mathbf{r}, \omega) \nabla' \tilde{P}(\mathbf{r}', \mathbf{r}_s, \omega)] \\ = &\int_V d\mathbf{r}' [\tilde{P}(\mathbf{r}', \mathbf{r}_s, \omega) \underbrace{\nabla'^2 G_0(\mathbf{r}', \mathbf{r}, \omega)}_{(-\omega^2/c_0^2) G_0(\mathbf{r}', \mathbf{r}, \omega) + \delta(\mathbf{r}' - \mathbf{r})} \\ &- G_0(\mathbf{r}', \mathbf{r}, \omega) \underbrace{\nabla'^2 \tilde{P}(\mathbf{r}', \mathbf{r}_s, \omega)}_{(-\omega^2/c_0^2) \tilde{P}(\mathbf{r}', \mathbf{r}_s, \omega) + \frac{\omega^2}{c_0^2} \alpha(\mathbf{r}') \tilde{P}(\mathbf{r}', \mathbf{r}_s, \omega) + \tilde{A}(\omega) \delta(\mathbf{r}' - \mathbf{r}_s)}] \\ = &\int_V d\mathbf{r}' [\underbrace{-\frac{\omega^2}{c_0^2} G_0(\mathbf{r}', \mathbf{r}, \omega) \tilde{P}(\mathbf{r}', \mathbf{r}_s, \omega)}_{cancel} + \delta(\mathbf{r}' - \mathbf{r}) \tilde{P}(\mathbf{r}', \mathbf{r}_s, \omega) \\ &+ \underbrace{\frac{\omega^2}{c_0^2} \tilde{P}(\mathbf{r}', \mathbf{r}_s, \omega) G_0(\mathbf{r}', \mathbf{r}, \omega)}_{cancel} - \frac{\omega^2}{c_0^2} \alpha(\mathbf{r}') \tilde{P}(\mathbf{r}', \mathbf{r}_s, \omega) G_0(\mathbf{r}', \mathbf{r}, \omega) \\ &- \tilde{A}(\omega) \delta(\mathbf{r}' - \mathbf{r}_s) G_0(\mathbf{r}', \mathbf{r}, \omega)] \\ = &\int_V d\mathbf{r}' [\tilde{P}(\mathbf{r}', \mathbf{r}_s, \omega) \delta(\mathbf{r}' - \mathbf{r}) - \frac{\omega^2}{c_0^2} \alpha(\mathbf{r}') \tilde{P}(\mathbf{r}', \mathbf{r}_s, \omega) G_0(\mathbf{r}', \mathbf{r}, \omega) \end{aligned}$$

$$-\tilde{A}(\omega)\delta(\mathbf{r}'-\mathbf{r}_s)G_0(\mathbf{r}',\mathbf{r},\omega)]. \tag{14}$$

Choosing $\mathbf{r}\in V$ gives

$$\begin{aligned}
&\oint_S \mathbf{n}\,ds'\cdot[\tilde{P}(\mathbf{r}',\mathbf{r}_s,\omega)\nabla' G_0(\mathbf{r}',\mathbf{r},\omega)-G_0(\mathbf{r}',\mathbf{r},\omega)\nabla'\tilde{P}(\mathbf{r}',\mathbf{r}_s,\omega)]\\
=&\int_V d\mathbf{r}'[\underbrace{\tilde{P}(\mathbf{r}',\mathbf{r}_s,\omega)\delta(\mathbf{r}'-\mathbf{r})}_{\tilde{P}(\mathbf{r},\mathbf{r}_s,\omega)}-\frac{\omega^2}{c_0^2}\alpha(\mathbf{r}')\tilde{P}(\mathbf{r}',\mathbf{r}_s,\omega)G_0(\mathbf{r}',\mathbf{r},\omega)\\
&-\tilde{A}(\omega)\underbrace{\delta(\mathbf{r}'-\mathbf{r}_s)}_{0}G_0(\mathbf{r}',\mathbf{r},\omega)]\\
=&\tilde{P}(\mathbf{r},\mathbf{r}_s,\omega)-\int_V d\mathbf{r}'\frac{\omega^2}{c_0^2}\alpha(\mathbf{r}')\tilde{P}(\mathbf{r}',\mathbf{r}_s,\omega)G_0(\mathbf{r}',\mathbf{r},\omega).
\end{aligned} \tag{15}$$

If the support for $\alpha\in V$, rearranging Eq. (15) gives

$$\begin{aligned}
&\tilde{P}(\mathbf{r},\mathbf{r}_s,\omega)\\
=&\int_V d\mathbf{r}'G_0(\mathbf{r}',\mathbf{r},\omega)\frac{\omega^2}{c_0^2}\alpha(\mathbf{r}')\tilde{P}(\mathbf{r}',\mathbf{r}_s,\omega)\\
&+\oint_S \mathbf{n}\,ds'\cdot[\tilde{P}(\mathbf{r}',\mathbf{r}_s,\omega)\nabla' G_0(\mathbf{r}',\mathbf{r},\omega)-G_0(\mathbf{r}',\mathbf{r},\omega)\nabla'\tilde{P}(\mathbf{r}',\mathbf{r}_s,\omega)]\\
=&\int_\infty d\mathbf{r}'G_0(\mathbf{r}',\mathbf{r},\omega)\frac{\omega^2}{c_0^2}\alpha(\mathbf{r}')\tilde{P}(\mathbf{r}',\mathbf{r}_s,\omega)\\
&+\oint_S \mathbf{n}\,ds'\cdot[\tilde{P}(\mathbf{r}',\mathbf{r}_s,\omega)\nabla' G_0(\mathbf{r}',\mathbf{r},\omega)-G_0(\mathbf{r}',\mathbf{r},\omega)\nabla'\tilde{P}(\mathbf{r}',\mathbf{r}_s,\omega)].
\end{aligned} \tag{16}$$

In Eq. (16) the surface integral involves actual pressure measurements and their vertical derivatives. Hence the surface integral will choose a causal solution. For consistency with Eq. (12) choose a causal Green function which gives

$$\begin{aligned}
\tilde{P}(\mathbf{r},\mathbf{r}_s,\omega)=&\int_\infty d\mathbf{r}'G_0^+(\mathbf{r}',\mathbf{r},\omega)\frac{\omega^2}{c_0^2}\alpha(\mathbf{r}')\tilde{P}(\mathbf{r}',\mathbf{r}_s,\omega)\\
&+\oint_S \mathbf{n}\,ds'\cdot[\tilde{P}(\mathbf{r}',\mathbf{r}_s,\omega)\nabla' G_0^+(\mathbf{r}',\mathbf{r},\omega)-G_0^+(\mathbf{r}',\mathbf{r},\omega)\nabla'\tilde{P}(\mathbf{r}',\mathbf{r}_s,\omega)]
\end{aligned} \tag{17}$$

Comparing approaches

Comparing Eqs. (12) and (17) gives an equation for the source signature:

$$\begin{aligned}
\tilde{A}(\omega)=&\frac{1}{G_0^+(\mathbf{r},\mathbf{r}_s,\omega)}\oint_S \mathbf{n}\,ds'\cdot[\tilde{P}(\mathbf{r}',\mathbf{r}_s,\omega)\nabla' G_0^+(\mathbf{r}',\mathbf{r},\omega)\\
&-G_0^+(\mathbf{r}',\mathbf{r},\omega)\nabla'\tilde{P}(\mathbf{r}',\mathbf{r}_s,\omega)].
\end{aligned} \tag{18}$$

A few comments about Eq. (18): (1) Eq. (18) is one form of the "triangle relation" relating the pressure wavefield $\tilde{P}(\mathbf{r}', \mathbf{r}_s, \omega)$, its vertical derivative $\nabla'\tilde{P}(\mathbf{r}', \mathbf{r}_s, \omega)$, and the source signature $\tilde{A}(\omega)$. In this instance the first two variables are used to calculate the third. (2) The numerator and denominator in Eq. (18) can be evaluated at any $\mathbf{r} \in V$. (3) The source signature estimation code will use the 3D form $G_0^+(\mathbf{r}, \mathbf{r}_s, \omega) = \exp(ikR)/R$ where $k = \omega/c_0$ and $R = |\mathbf{r} - \mathbf{r}_s|$ (Morse and Feshbach, 1953, p. 810).

Appendix B — Theory of deghosting

The theory of Green's theorem based deghosting is covered in Zhang (2007) (pp. 19–23).

The procedure defines the following to separate upward moving and downward moving waves: (1) a reference medium consisting of a whole space of water, (2) a perturbation $\alpha_{air}(\mathbf{r}')$ which converts the upper part of the whole space into air, (3) a perturbation $\alpha_{earth}(\mathbf{r}')$ which converts the lower part of the whole space into earth, (4) an integration volume V consisting of a hemisphere bounded from below by the measurement surface (the plane $z = 0$), (5) a free surface (air-water interface) above the measurement surface (*i.e.*, inside V), and (6) a source $\mathbf{r}_s$ on or above the measurement surface (again inside V). The procedure also defines the following: (7) a causal Green function $G_0^+(\mathbf{r}', \mathbf{r}, \omega)$ in the whole space reference medium, (8) $k_0 = \omega/c_0$, (9) $\mathbf{r} \in V$ and on or below the free surface, and (10) S as the hemisphere's surface.

Substituting the above into Green's theorem (Eq. (13)) gives

$$
\begin{aligned}
& \oint_S \mathbf{n}\, ds' \cdot [\tilde{P}(\mathbf{r}', \mathbf{r}_s, \omega)\nabla' G_0^+(\mathbf{r}', \mathbf{r}, \omega) - G_0^+(\mathbf{r}', \mathbf{r}, \omega)\nabla'\tilde{P}(\mathbf{r}', \mathbf{r}_s, \omega)] \\
= & \int_V d\mathbf{r}' [\underbrace{\tilde{P}(\mathbf{r}', \mathbf{r}_s, \omega)\delta(\mathbf{r}' - \mathbf{r})}_{\tilde{P}(\mathbf{r}, \mathbf{r}_s, \omega)} \\
& -k_0^2(\alpha_{air}(\mathbf{r}') + \underbrace{\alpha_{earth}(\mathbf{r}')}_{0})\tilde{P}(\mathbf{r}', \mathbf{r}_s, \omega)G_0^+(\mathbf{r}', \mathbf{r}, \omega) \\
& - \underbrace{\tilde{A}(\omega)\delta(\mathbf{r}' - \mathbf{r}_s)G_0^+(\mathbf{r}', \mathbf{r}, \omega)}_{\tilde{A}(\omega)G_0^+(\mathbf{r}_s, \mathbf{r}, \omega)}] \\
= & \tilde{P}(\mathbf{r}, \mathbf{r}_s, \omega) - \int_V d\mathbf{r}' k_0^2 \alpha_{air}(\mathbf{r}')\tilde{P}(\mathbf{r}', \mathbf{r}_s, \omega)G_0^+(\mathbf{r}', \mathbf{r}, \omega) \\
& -\tilde{A}(\omega)\underbrace{G_0^+(\mathbf{r}_s, \mathbf{r}, \omega)}_{G_0^+(\mathbf{r}, \mathbf{r}_s, \omega)} \\
= & \tilde{P}(\mathbf{r}, \mathbf{r}_s, \omega) - \int_V d\mathbf{r}' G_0^+(\mathbf{r}', \mathbf{r}, \omega)k_0^2\alpha_{air}(\mathbf{r}')\tilde{P}(\mathbf{r}', \mathbf{r}_s, \omega) \\
& -\tilde{A}(\omega)G_0^+(\mathbf{r}, \mathbf{r}_s, \omega). \qquad (19)
\end{aligned}
$$

The physical meaning of Eq. (19) is that the total wavefield at $\mathbf{r}$ can be separated into three parts: (1) the direct wave which travels from the source at $\mathbf{r}_s$ to $\mathbf{r}$ (third term on the right hand side), (2)

the pressure field whose last motion is downward from the free surface (second term on the right hand side), and (3) the pressure field whose last motion is upward from the earth (the entire right hand side). Hence, Eq. (19) is the receiver side deghosting algorithm.

Letting the radius of the hemisphere go to ∞, the Sommerfeld radiation condition gives

$$\begin{aligned}\tilde{P}^{deghosted}(\mathbf{r},\mathbf{r}_s,\omega) &= \int_{MS}\mathbf{n}\,ds\cdot[\tilde{P}(\mathbf{r}',\mathbf{r}_s,\omega)\nabla' G_0^+(\mathbf{r}',\mathbf{r},\omega)\\ &\quad -G_0^+(\mathbf{r}',\mathbf{r},\omega)\nabla'\tilde{P}(\mathbf{r}',\mathbf{r}_s,\omega)],\end{aligned}\tag{20}$$

where $\tilde{P}(\mathbf{r}';\mathbf{r}_s;\omega)$ and $\nabla'\tilde{P}(\mathbf{r}';\mathbf{r}_s;\omega)$ are respectively the hydrophone measurements and their spatial derivatives (in the frequency domain). Using reciprocity, a similar integration on the source side will remove source ghosts.

In practice, the derivative of the pressure is usually not measured. The procedure predicts the pressure and its vertical derivative on a "pseudo-measurement surface" located between the free surface and the measurement surface using pressure measurements on the cable plus the source signature. The procedure includes a "double Dirichlet" Green function $G_0^{DD}(\mathbf{r}',\mathbf{r},\omega)$ which vanishes on the measurement surface as well as the free surface. $G_0^{DD}(\mathbf{r}',\mathbf{r},\omega)$ is a solution of

$$\nabla'^{\,2}G_0^{DD}(\mathbf{r}',\mathbf{r},\omega)+k_0^2G_0^{DD}(\mathbf{r}',\mathbf{r},\omega)=\delta(\mathbf{r}'-\mathbf{r})+\sum_{n=1}^{\infty}a_i\delta(\mathbf{r}'-\mathbf{r}_i),\tag{21}$$

where $a_i=\pm1$, and $\mathbf{r}_i$ is the position of the ith mirror image of $\mathbf{r}$ as the wavefield reflects from the earth and free surface. Substituting Eq. (21) into Green's theorem (Eq. (13)) gives

$$\begin{aligned}&\oint_S\mathbf{n}\,ds'\cdot[\tilde{P}(\mathbf{r}',\mathbf{r}_s,\omega)\nabla'G_0^{DD}(\mathbf{r}',\mathbf{r},\omega)-G_0^{DD}(\mathbf{r}',\mathbf{r},\omega)\nabla'\tilde{P}(\mathbf{r}',\mathbf{r}_s,\omega)]\\
=&\int_V d\mathbf{r}'[\tilde{P}(\mathbf{r}',\mathbf{r}_s,\omega)\nabla'^{\,2}G_0^{DD}(\mathbf{r}',\mathbf{r},\omega)-G_0^{DD}(\mathbf{r}',\mathbf{r},\omega)\nabla'^{\,2}\tilde{P}(\mathbf{r}',\mathbf{r}_s,\omega)]\\
=&\int_V d\mathbf{r}'[\tilde{P}(\mathbf{r}',\mathbf{r}_s,\omega)\left(-\underbrace{k_0^2G_0^{DD}(\mathbf{r}',\mathbf{r},\omega)}_{cancel}+\delta(\mathbf{r}'-\mathbf{r})+\sum_{n=1}^{\infty}a_i\delta(\mathbf{r}'-\mathbf{r}_i)\right)\\
&-G_0^{DD}(\mathbf{r}',\mathbf{r},\omega)\left(-\underbrace{k_0^2\tilde{P}(\mathbf{r}',\mathbf{r}_s,\omega)}_{cancel}+A(\omega)\delta(\mathbf{r}'-\mathbf{r}_s)+k_0^2(\alpha_{air}(\mathbf{r}')+\alpha_{earth}(\mathbf{r}'))\tilde{P}(\mathbf{r}',\mathbf{r}_s,\omega)\right)]\\
=&\int_V d\mathbf{r}'\tilde{P}(\mathbf{r}',\mathbf{r}_s,\omega)\delta(\mathbf{r}'-\mathbf{r})+\int_V d\mathbf{r}'\tilde{P}(\mathbf{r}',\mathbf{r}_s,\omega)\sum_{n=1}^{\infty}a_i\delta(\mathbf{r}'-\mathbf{r}_i)\\
&-\int_V d\mathbf{r}'G_0^{DD}(\mathbf{r}',\mathbf{r},\omega)A(\omega)\delta(\mathbf{r}'-\mathbf{r}_s)\\
&-\int_V d\mathbf{r}'G_0^{DD}(\mathbf{r}',\mathbf{r},\omega)k_0^2\alpha_{air}(\mathbf{r}')\tilde{P}(\mathbf{r}',\mathbf{r}_s,\omega)\\
&-\int_V d\mathbf{r}'G_0^{DD}(\mathbf{r}',\mathbf{r},\omega)k_0^2\alpha_{earth}(\mathbf{r}')\tilde{P}(\mathbf{r}',\mathbf{r}_s,\omega).\end{aligned}\tag{22}$$

Choosing V to be the space sandwiched between the free surface and measurement surface and $\mathbf{r} \in V$ gives

$$\begin{aligned}
&\int_{MS} \mathbf{n}\, ds' \cdot [\tilde{P}(\mathbf{r}', \mathbf{r}_s, \omega) \nabla' G_0^{DD}(\mathbf{r}', \mathbf{r}, \omega) - \underbrace{G_0^{DD}(\mathbf{r}', \mathbf{r}, \omega)}_{=0} \nabla' \tilde{P}(\mathbf{r}', \mathbf{r}_s, \omega)] \\
= \; & \underbrace{\int_V d\mathbf{r}' \tilde{P}(\mathbf{r}', \mathbf{r}_s, \omega) \delta(\mathbf{r}' - \mathbf{r})}_{=\tilde{P}(\mathbf{r}, \mathbf{r}_s, \omega)} + \underbrace{\int_V d\mathbf{r}' \tilde{P}(\mathbf{r}', \mathbf{r}_s, \omega) \sum_{n=1}^{\infty} a_i \delta(\mathbf{r}' - \mathbf{r}_i)}_{=0} \\
& - \underbrace{\int_V d\mathbf{r}' G_0^{DD}(\mathbf{r}', \mathbf{r}, \omega) A(\omega) \delta(\mathbf{r}' - \mathbf{r}_s)}_{=G_0^{DD}(\mathbf{r}_s, \mathbf{r}, \omega) A(\omega)} \\
& - \int_V d\mathbf{r}' G_0^{DD}(\mathbf{r}', \mathbf{r}, \omega) k_0^2 \underbrace{\alpha_{air}(\mathbf{r}')}_{=0} \tilde{P}(\mathbf{r}', \mathbf{r}_s, \omega) - \int_V d\mathbf{r}' G_0^{DD}(\mathbf{r}', \mathbf{r}, \omega) k_0^2 \underbrace{\alpha_{earth}(\mathbf{r}')}_{=0} \tilde{P}(\mathbf{r}', \mathbf{r}_s, \omega) \\
= \; & \tilde{P}(\mathbf{r}, \mathbf{r}_s, \omega) - G_0^{DD}(\mathbf{r}_s, \mathbf{r}, \omega) A(\omega).
\end{aligned}$$

Hence

$$\tilde{P}(\mathbf{r}, \mathbf{r}_s, \omega) = A(\omega) G_0^{DD}(\mathbf{r}_s, \mathbf{r}, \omega) + \int_{MS} \mathbf{n}\, ds' \cdot \tilde{P}(\mathbf{r}', \mathbf{r}_s, \omega) \nabla' G_0^{DD}(\mathbf{r}', \mathbf{r}, \omega). \tag{23}$$

Taking the derivative of Eq. (23) gives

$$\frac{\partial}{\partial z} \tilde{P}(\mathbf{r}, \mathbf{r}_s, \omega) = A(\omega) \frac{\partial}{\partial z} G_0^{DD}(\mathbf{r}_s, \mathbf{r}, \omega) + \int_{MS} \mathbf{n}\, ds' \cdot \tilde{P}(\mathbf{r}', \mathbf{r}_s, \omega) \nabla' \frac{\partial}{\partial z} G_0^{DD}(\mathbf{r}', \mathbf{r}, \omega). \tag{24}$$

The procedure predicts the pressure and its vertical derivative on the pseudo measurement surface using Eqs. (23) and (24), respectively, and performs receiver side deghosting on the pseudo-measurement surface using Eq. (20) (Zhang and Weglein, 2005, p. 2).

After receiver side deghosting, using reciprocity the procedure predicts the pressure and its vertical derivative on the source side using

$$\tilde{P}(\mathbf{r}, \mathbf{r}_s, \omega) = \int_{MS} \mathbf{n}\, ds' \cdot \tilde{P}(\mathbf{r}', \mathbf{r}_s, \omega) \nabla' G_0^{DD}(\mathbf{r}', \mathbf{r}, \omega), \tag{25}$$

$$\frac{\partial}{\partial z} \tilde{P}(\mathbf{r}, \mathbf{r}_s, \omega) = \int_{MS} \mathbf{n}\, ds' \cdot \tilde{P}(\mathbf{r}', \mathbf{r}_s, \omega) \nabla' \frac{\partial}{\partial z} G_0^{DD}(\mathbf{r}', \mathbf{r}, \omega). \tag{26}$$

which are the same as Eqs. (23) and (24) with their first right hand side terms omitted. When the receivers are <u>below</u> the source, all field components (the direct wave, the downward moving pressure field reflected from the free surface, and the deghosted pressure field) are $\in V$. However, when the receiver is <u>above</u> the sources, only two components (the downward moving pressure field reflected from the free surface and the deghosted pressure field) are $\in V$; the direct wave is $\notin V$.

After predicting the pressure and its vertical derivative using Eqs. (25) and (26), the procedure performs source side deghosting on the pseudo-measurement surface using Eq. (20).

When coding the above, the authors will use the forms $G_0^+(\mathbf{r}, \mathbf{r}_s, \omega) = \exp(ikR)/R$ where $k = \omega/c_0$ and $R = |\mathbf{r} - \mathbf{r}_s|$ (Morse and Feshbach, 1953, p. 810), and $G_0^{DD}(\mathbf{r}, \mathbf{r}_s, \omega) = \exp(ikR_+)/R_+ - \exp(ikR_-)/R_-$ where $k = \omega/c_0$ and $R_\pm = \sqrt{(x - x_s)^2 + (y - y_s)^2 + (z \mp z_s)^2}$.

Appendix C — Theory of data interpolation

Numeric simulations showing the importance of near offset data extrapolation in accurately estimating the source signature are shown in Zhang (2007) (pp. 19–23).

The theory of extrapolating near offset data in a towed streamer marine experiment is derived in Ramírez (2007) (pp. 64–69), where near offset means the data not collected between the source and the receiver (on each towed streamer) nearest the source. The procedure begins with Green's theorem

$$\begin{aligned} & \int_V [P(\mathbf{x}|\mathbf{x}_a;\omega)\delta(\mathbf{x}-\mathbf{x}_b) - G^+(\mathbf{x}|\mathbf{x}_b;\omega)A(\omega)\delta(\mathbf{x}-\mathbf{x}_a)\, d\mathbf{x} \\ = & \oint_S [P(\mathbf{x}|\mathbf{x}_a;\omega)\nabla G^+(\mathbf{x}|\mathbf{x}_b;\omega) - G^+(\mathbf{x}|\mathbf{x}_b;\omega)\nabla P(\mathbf{x}|\mathbf{x}_a;\omega)] \cdot \mathbf{n} ds \end{aligned} \tag{27}$$

where
$P(\mathbf{x}|\mathbf{x}_a;\omega)$ is the pressure wavefield,
$G^+(\mathbf{x}|\mathbf{x}_b;\omega)$ is a causal Green function,
$A(\omega)\delta(\mathbf{x}-\mathbf{x}_a)$ is an impulsive source at $\mathbf{x}_a$) with signature $A(\omega)$, and
$\mathbf{x}_b$ is the location of the receiver.

Assuming that the velocity distributions for the pressure field and the Green function are equal only within the integration volume V (and on its surface S) gives the following:
if $\mathbf{x}_a, \mathbf{x}_b \in V$, then left hand side of (27) $= P(\mathbf{x}_b|\mathbf{x}_a;\omega) - A(\omega)G^+(\mathbf{x}_a|\mathbf{x}_b;\omega)$, else
if $\mathbf{x}_b \in V$, then left hand side of (27) $= P(\mathbf{x}_b|\mathbf{x}_a;\omega)$, else
if $\mathbf{x}_a \in V$, then left hand side of (27) $= -A(\omega)G^+(\mathbf{x}_a|\mathbf{x}_b;\omega)$.

Choosing the first case and noting that the left hand side is the total wavefield minus the direct wavefield, which is the scattered wavefield, gives the data interpolation/extrapolation equation:

$$P_s(\mathbf{x}_a|\mathbf{x}_b;\omega) = \int_{Sm} [P(\mathbf{x}|\mathbf{x}_a;\omega)\nabla \mathcal{G}_0^+(\mathbf{x}|\mathbf{x}_b;\omega) - \mathcal{G}_0^+(\mathbf{x}|\mathbf{x}_b;\omega)\nabla P(\mathbf{x}|\mathbf{x}_a;\omega)] \cdot \mathbf{n} ds \tag{28}$$

where
$P_s(\mathbf{x}_a|\mathbf{x}_b;\omega)$ is the scattered wavefield,
$\mathcal{G}_0^+(\mathbf{x}|\mathbf{x}_b;\omega)$ is the causal reference Green function,
$\mathbf{x}_a$ and $\mathbf{x}_b$ are the locations of the source and receiver, respectively, and
the integral is performed over the measurement surface.

Appendix D — Theory of free surface multiple elimination

The theory of free surface multiple elimination is derived in Carvalho (1992). This derivation has been included because the first author needs to understand the free surface multiple elimination code currently being tested by ConocoPhillips.

If a given term in the forward scattering series creates a certain type of data, that term in the inverse scattering series removes that type of data, *e.g.*, if there is no free surface, there are no

ghosts and free surface multiples in the data. Hence, G_0 must be of the form $G_0^d + G_0^{FS}$ where G_0^{FS} acts to create and remove ghosts and free surface multiples.

Deghosting is accomplished by multiplying each inverse scattering series equation from the left and right by G_0^{-1} then G_0^d; now the outer G_0's have been replaced by G_0^d (but the inner G_0's are still $G_0^d + G_0^{FS}$).

$$\begin{aligned} G_0^d V_1 G_0^d &= D && (29)\\ G_0^d V_2 G_0^d &= -G_0^d V_1 G_0 V_1 G_0^d && (30)\\ G_0^d V_3 G_0^d &= -G_0^d V_1 G_0 V_2 G_0^d - G_0^d V_2 G_0 V_1 G_0^d \\ &\quad -G_0^d V_1 G_0 V_1 G_0 V_1 G_0^d && (31)\\ &\vdots \end{aligned}$$

Reasoning by analogy, the subseries for free surface multiple elimination is developed by replacing the inner instances of G_0 in the above equations with G_0^{FS}.

$$\begin{aligned} G_0^d V_1 G_0^d &= D_1' && (32)\\ G_0^d V_2 G_0^d &= -G_0^d V_1 G_0^{FS} V_1 G_0^d && (33)\\ G_0^d V_3 G_0^d &= -G_0^d V_1 G_0^{FS} V_2 G_0^d - G_0^d V_2 G_0^{FS} V_1 G_0^d \\ &\quad -G_0^d V_1 G_0^{FS} V_1 G_0^{FS} V_1 G_0^d && (34)\\ &\vdots \end{aligned}$$

where D_1' is deghosted data.

Rewrite Eq. (34) in the suggestive form

$$\begin{aligned} G_0^d V_3 G_0^d &= -G_0^d V_1 G_0^{FS} V_2 G_0^d - G_0^d V_2 G_0^{FS} V_1 G_0^d \\ &\quad -G_0^d \underbrace{V_1 G_0^{FS} V_1}_{=-V_2} G_0^{FS} V_1 G_0^d \\ &= -G_0^d V_1 G_0^{FS} V_2 G_0^d \underbrace{-G_0^d V_2 G_0^{FS} V_1 G_0^d}_{cancel} \underbrace{+G_0^d V_2 G_0^{FS} V_1 G_0^d}_{cancel} \\ &= -G_0^d V_1 G_0^{FS} V_2 G_0^d && (35)\\ \Rightarrow G_0^d V_n G_0^d &= -G_0^d V_1 G_0^{FS} V_{n-1} G_0^d && (36)\\ \Rightarrow D' &= \sum_{n=1}^{\infty} D_n' = \sum_{n=1}^{\infty} G_0^d V_n G_0^d. && (37) \end{aligned}$$

Transform Eq. (36) into the (k_g, k_s, ω) domain:

$$\begin{aligned} D'(k_g, k_s, \omega) &= \sum_{n=1}^{\infty} D_n'(k_g, k_s, \omega), && (38)\\ where\ D_n'(k_g, k_s, \omega) &= \frac{1}{i\pi\rho_0 B(\omega)} \int_{-\infty}^{\infty} dk\, q \exp\left(iq(\epsilon_g + \epsilon_s)\right) \end{aligned}$$

$$\times D_1'(k_g, k, \omega) D_{n-1}'(k, k_s, \omega) \tag{39}$$

for $n = 2, 3, 4, \ldots$ Eqs. (39) and (38) are used in Sam Kaplan's 2D free surface multiple elimination code.

The procedure (Carvalho, 1992, pp. 12–14, 29–30) derives Eq. (39) from Eq. (29) and a causal Green function (Eq. (42) derived below). The procedure defines the following in 2D: $B(\omega)$ as the source signature, $c_0 = \sqrt{\kappa_0/\rho_0}$ as the speed of sound in the reference medium (water), $k = \sqrt{k_x^2 + k_z^2}$, k_g, k_s, and k_x as the Fourier conjugates of x_g, x_s, and x, respectively, $k_z = -(q_g + q_s)$, κ_0 as the bulk modulus of water, $q = sgn(\omega)\sqrt{(\omega/c_0)^2 - k_x^2}$, $q_g = sgn(\omega)\sqrt{(\omega/c_0)^2 - k_g^2}$, $q_s = sgn(\omega)\sqrt{(\omega/c_0)^2 - k_s^2}$, ρ_0 as the density of water, (x, z) as a point in 2D space, (x_g, ϵ_g) as the line receiver location, and $(x', z') = (x_s, \epsilon_s)$ as the line source location.

Derivation of the Green function

The procedure chooses a reference medium consisting of a half space of water with a free surface at $z = 0$. $L_0 G_0 = \delta$ takes the form

$$\left(\nabla^2 + \frac{\omega^2}{c_0^2}\right) G_0(x, z, x', z'; \omega) = -\rho_0 \delta(x - x')[\delta(z - z') - \delta(z + z')]. \tag{40}$$

$\delta(z - z')$ models an impulsive source at depth z', and $\delta(z + z')$ models an impulsive source that "looks like" it originates at height $-z'$ above the free surface because its pressure wave has reflected off the free surface (method of images). Fourier transforming Eq. (40) with respect to x gives

$$\begin{aligned}
& \left((-ik_x)^2 + \frac{d^2}{dz^2} + \frac{\omega^2}{c_0^2}\right) G_0(k_x, z, x', z'; \omega) \\
= & \left(\frac{d^2}{dz^2} + \underbrace{\frac{\omega^2}{c_0^2} - k_x^2}_{=q^2}\right) G_0(k_x, z, x', z'; \omega) \\
= & -\frac{\rho_0}{\sqrt{2\pi}} \exp(-ik_x x')[\delta(z - z') - \delta(z + z')].
\end{aligned} \tag{41}$$

The causal solution of Eq. (41) is

$$G_0^+(k_x, z, x', z'; \omega) = \frac{\rho_0}{\sqrt{2\pi}} \frac{\exp(-ik_x x')}{-2iq} (\exp(iq|z - z'|) - \exp(iq|z + z'|)) \tag{42}$$

$$= \underbrace{-\frac{\rho_0}{\sqrt{2\pi}} \frac{\exp(-ik_x x')}{2iq} \exp(iq|z - z'|)}_{=G_0^d} + \underbrace{\frac{\rho_0}{\sqrt{2\pi}} \frac{\exp(-ik_x x')}{2iq} \exp(iq|z + z'|)}_{=G_0^{FS}}. \tag{43}$$

(De Santo, 1992, Chapter 2), (Carvalho, 1992, (2.3) p. 12)

Derivation of Eq. (39)

Letting $D_0(k_g, k_s, \omega) = D(k_g, k_s, \omega)/B(\omega)$ gives

$$\begin{aligned}
D_0(k_g,k_s,\omega) &= G_0^d V_1 G_0^d \\
&= \int_{-\infty}^{\infty}\int_{-\infty}^{\infty} dx\,dz\,\frac{\rho_0}{\sqrt{2\pi}}\frac{\exp(-ik_g x)}{-2iq_g} \\
&\quad \times(\exp(iq_g|z-\epsilon_g|)-\exp(iq_g|z+\epsilon_g|))V_1(x,z,\omega) \\
&\quad \times\frac{\rho_0}{\sqrt{2\pi}}\frac{\exp(ik_s x)}{-2iq_s}(\exp(iq_s|z-\epsilon_s|)-\exp(iq_s|z+\epsilon_s|)) \\
&= \frac{\rho_0^2}{2\pi}\frac{1}{(2i)^2 q_g q_s}\int_{-\infty}^{\infty}\int_{-\infty}^{\infty} dx\,dz \\
&\quad \times\exp(-ik_g x)(\exp(iq_g(z-\epsilon_g))-\exp(iq_g(z+\epsilon_g)))V_1(x,z,\omega) \\
&\quad \times\exp(ik_s x)(\exp(iq_s(z-\epsilon_s))-\exp(iq_s(z+\epsilon_s))) \\
&= \frac{\rho_0^2}{2\pi}\frac{1}{(2i)^2 q_g q_s}\int_{-\infty}^{\infty}\int_{-\infty}^{\infty} dx\,dz \\
&\quad \times\exp(-ik_g x)\exp(iq_g z)\underbrace{(\exp(-iq_g\epsilon_g)-\exp(iq_g\epsilon_g))}_{=-2i\sin(q_g\epsilon_g)}V_1(x,z,\omega) \\
&\quad \times\exp(ik_s x)\exp(iq_s z)\underbrace{(\exp(-iq_s\epsilon_s)-\exp(iq_s\epsilon_s))}_{=-2i\sin(q_s\epsilon_s)} \\
&= \frac{\rho_0^2}{2\pi}\frac{\sin(q_g\epsilon_g)\sin(q_s\epsilon_s)}{q_g q_s}\int_{-\infty}^{\infty}\int_{-\infty}^{\infty} dx\,dz \\
&\quad \times\exp(-ik_g x)\exp(iq_g z)V_1(x,z,\omega)\exp(ik_s x)\exp(iq_s z). \qquad (44)
\end{aligned}$$

(Carvalho, 1992, (2.5) p. 12 and (2.6) p. 13)

Now we need V_1.

$$\begin{aligned}
V &= L_0 - L = \nabla\cdot\frac{1}{\rho_0}\nabla + \frac{\omega^2}{\kappa_0} - \nabla\cdot\frac{1}{\rho(\mathbf{r})}\nabla - \frac{\omega^2}{\kappa(\mathbf{r})} \\
&= \nabla\cdot\left(\frac{1}{\rho_0}-\frac{1}{\rho(\mathbf{r})}\right)\nabla + \omega^2\left(\frac{1}{\kappa_0}-\frac{1}{\kappa(\mathbf{r})}\right) \\
&= \nabla\cdot\frac{\beta(\mathbf{r})}{\rho_0}\nabla + \omega^2\frac{\alpha(\mathbf{r})}{\kappa_0} \qquad (45)
\end{aligned}$$

(Carvalho, 1992, (1.6) p. 6)

Combining Eqs. (44) and (45) gives

$$\begin{aligned}
D_0(k_g,k_s,\omega) &= \frac{\rho_0^2}{2\pi}\frac{\sin(q_g\epsilon_g)\sin(q_s\epsilon_s)}{q_g q_s}\int_{-\infty}^{\infty}\int_{-\infty}^{\infty} dx\,dz \\
&\quad \times\exp(-ik_g x)\exp(iq_g z)\left(\nabla\cdot\frac{\beta_1(\mathbf{r})}{\rho_0}\nabla + \omega^2\frac{\alpha_1(\mathbf{r})}{\kappa_0}\right)
\end{aligned}$$

$$
\begin{aligned}
& \times \exp(ik_s x)\exp(iq_s z) \\
= \; & \frac{\rho_0^2}{2\pi}\frac{\sin(q_g\epsilon_g)\sin(q_s\epsilon_s)}{q_g q_s}(I_1+I_2) \\
where\ I_1 \equiv \; & \int_{-\infty}^{\infty}\int_{-\infty}^{\infty} dx\,dz\ \exp(-ik_g x)\exp(iq_g z)\omega^2\frac{\alpha_1(\mathbf{r})}{\kappa_0} \\
& \times \exp(ik_s x)\exp(iq_s z) \qquad (46) \\
and\ I_2 \equiv \; & \int_{-\infty}^{\infty}\int_{-\infty}^{\infty} dx\,dz\ \exp(-ik_g x)\exp(iq_g z)\nabla\cdot\frac{\beta_1(\mathbf{r})}{\rho_0}\nabla \\
& \times \exp(ik_s x)\exp(iq_s z). \qquad (47)
\end{aligned}
$$

Rewriting Eq. (47) gives

$$
\begin{aligned}
I_2 = \; & \int_{-\infty}^{\infty}\int_{-\infty}^{\infty} dx\,dz\,\nabla\cdot\Big[\exp(-ik_g x)\exp(iq_g z)\frac{\beta_1(\mathbf{r})}{\rho_0} \\
& \times \nabla(\exp(ik_s x)\exp(iq_s z))\Big] \\
& -\int_{-\infty}^{\infty}\int_{-\infty}^{\infty} dx\,dz\,\frac{\beta_1(\mathbf{r})}{\rho_0}\nabla(\exp(ik_s x)\exp(iq_s z)) \\
& \cdot\nabla(\exp(-ik_g x)\exp(iq_g z)). \qquad (48)
\end{aligned}
$$

(Jackson, 1999, inside front cover, 7th Vector Formula)

The first integral in Eq. (48) vanishes (use the divergence theorem, then the expression inside the square brackets vanishes at ∞ by causality). The second integral in Eq. (48) gives

$$
\begin{aligned}
I_2 = \; & -\int_{-\infty}^{\infty}\int_{-\infty}^{\infty} dx\,dz\,\frac{\beta_1(\mathbf{r})}{\rho_0}(ik_s\hat{x}+iq_s\hat{z})(\exp(ik_s x)\exp(iq_s z)) \\
& \cdot(-ik_g\hat{x}+iq_g\hat{z})(\exp(-ik_g x)\exp(iq_g z)) \\
= \; & -\int_{-\infty}^{\infty}\int_{-\infty}^{\infty} dx\,dz\,\frac{\beta_1(\mathbf{r})}{\rho_0}(k_s k_g - q_s q_g) \\
& \times \exp(ik_s x)\exp(iq_s z)\exp(-ik_g x)\exp(iq_g z). \qquad (49)
\end{aligned}
$$

Substituting Eqs. (46) and (49) into Eq. (44) gives

$$
\begin{aligned}
D_0(k_g,k_s,\omega) = \; & \frac{\rho_0^2}{2\pi}\frac{\sin(q_g\epsilon_g)\sin(q_s\epsilon_s)}{q_g q_s}\int_{-\infty}^{\infty}\int_{-\infty}^{\infty} dx\,dz \\
& \exp(-i(k_g-k_s)x)\exp(-i(-q_g-q_s)z) \\
& \times\left[\omega^2\frac{\alpha_1(x,z)}{\kappa_0}+(q_g q_s - k_g k_s)\frac{\beta_1(x,z)}{\rho_0}\right]. \qquad (50)
\end{aligned}
$$

Performing the Fourier transforms gives

$$
D_0(k_g,k_s,\omega) = \frac{\rho_0^2}{2\pi}\frac{\sin(q_g\epsilon_g)\sin(q_s\epsilon_s)}{q_g q_s}\left[\omega^2\frac{\tilde{\tilde{\alpha}}_1(k_g-k_s,-q_g-q_s)}{\kappa_0}\right.
$$

$$+ (q_g q_s - k_g k_s) \frac{\tilde{\tilde{\beta}}_1(k_g - k_s, -q_g - q_s)}{\rho_0} \Bigg]. \tag{51}$$

where $[\ldots] = V_1(k_g, k_s, \omega)$. Therefore

$$\begin{aligned}
V_1(k_g, k_s, \omega) &= \frac{2\pi}{\rho_0^2} \frac{q_g q_s}{\sin(q_g \epsilon_g) \sin(q_s \epsilon_s)} D_0(k_g, k_s, \omega) \\
&= \frac{2\pi}{\rho_0^2} \frac{(2i)^2 q_g q_s D_0(k_g, k_s, \omega)}{(\exp(iq_g\epsilon_g) - \exp(-iq_g\epsilon_g))(\exp(iq_s\epsilon_s) - \exp(-iq_s\epsilon_s))} \\
&= \frac{2\pi}{\rho_0^2} \frac{-4 q_g q_s \exp(iq_g\epsilon_g) \exp(iq_s\epsilon_s)}{(\exp(2iq_g\epsilon_g) - 1)(\exp(2iq_s\epsilon_s) - 1)} \underbrace{D_0(k_g, k_s, \omega)}_{= D(k_g, k_s, \omega)/B(\omega)} \\
&= 2\pi \frac{-4}{B(\omega)} \frac{q_g q_s}{\rho_0^2} \exp(iq_g\epsilon_g) \exp(iq_s\epsilon_s) \\
&\quad \times \underbrace{\frac{D(k_g, k_s, \omega)}{(\exp(2iq_g\epsilon_g) - 1)(\exp(2iq_s\epsilon_s) - 1)}}_{= D_1'(k_g, k_s, \omega)}
\end{aligned} \tag{52}$$

Using Eq. (43) to transform Eq. (36) into the (k_g, k_s, ω) domain gives

$$V_n(k_g, k_s, \omega) = \frac{1}{2\pi} \int_{-\infty}^{\infty} dk \, \frac{\rho_0}{-2iq} V_1(k_g, k, \omega) V_{n-1}(k, k_s, \omega) \tag{53}$$

Substituting Eq. (52) into Eq. (53) (for all terms except the first) give the desired result

$$\begin{aligned}
V_n(k_g, k_s, \omega) &= \frac{1}{2\pi} \frac{\rho_0}{-2i} \int_{-\infty}^{\infty} \frac{dk}{q} \\
&\times \underbrace{2\pi \frac{-4}{B(\omega)} \frac{q_g q}{\rho_0^2} \exp(iq_g\epsilon_g) \exp(iq\epsilon_s)}_{drop} D_1'(k_g, k, \omega) \\
&\times \underbrace{2\pi \frac{-4}{B(\omega)} \frac{q q_s}{\rho_0^2} \exp(iq\epsilon_g) \exp(iq_s\epsilon_s)}_{modify} D_{n-1}'(k, k_s, \omega) \\
&= \frac{1}{2\pi} \frac{\rho_0}{-2i} \int_{-\infty}^{\infty} \frac{dk}{q} D_1'(k_g, k, \omega) \\
&\times 2\pi \frac{-4}{B(\omega)} \frac{q^2}{\rho_0^2} \exp(iq\epsilon_g) \exp(iq\epsilon_s) D_{n-1}'(k, k_s, \omega) \\
&= 2\pi \frac{1}{i\pi\rho_0 B(\omega)} \int_{-\infty}^{\infty} dk \, q \exp(iq(\epsilon_g + \epsilon_s)) \\
&\times D_1'(k_g, k, \omega) D_{n-1}'(k, k_s, \omega)
\end{aligned} \tag{54}$$

which is the desired form to within a factor of 2π.

An analytic example examining the reference velocity sensitivity of the elastic internal multiple attenuation algorithm

S.-Y. Hsu, S. Jiang and A. B. Weglein, M-OSRP, University of Houston

Abstract

Internal multiple attenuation is a pre-processing step for seismic imaging and amplitude analysis. Hsu and Weglein (2007) showed that the internal multiple algorithm from the inverse scattering series is independent of reference velocity for an 1D earth with acoustic background. In this study, we followed the analysis of Nita and Weglein (2005) and used the elastic internal multiple algorithm (Matson, 1997) to investigate velocity sensitivity for an 1D earth with elastic reference medium. The result suggests that the algorithm is also independent of reference velocity for an 1D earth with elastic background.

1 Introduction

Seismic processing is used to estimate subsurface properties from the reflected wave-fields. The seismic data are a set of reflected waves including primaries and multiples. Primaries are events that have only one upward reflection before arriving at the receiver. Multiply reflected events (multiples) are classified as free-surface or internal multiples depending on the location of their downward reflections. Free-surface multiples have at least one downward reflection at the air-water or air-land surface (free surface). Internal multiples have all downward reflections below the measurement surface (Weglein et al., 1997; Weglein and Matson, 1998).

Methods for seismic imaging and amplitude analysis usually assume that the reflection data are primaries-only. To accommodate this assumption, multiple removal/attenuation is a prerequisite for seismic processing. Conventional methods successfully attenuate multiples by assuming simple or known subsurface geology. However, in geologically complex areas those methods may become inadequate (Otnes et al., 2004). To overcome the limitations of conventional methods, the inverse scattering series (ISS) methods were proposed to perform multiple removal/suppression for acoustic data without subsurface information or assumptions (Carvalho, 1992; Araújo, 1994; Weglein et al., 1997). Following this framework, Matson (1997) extended the multiple attenuation algorithm from acoustic to elastic.

In order to keep the perturbation below the measurement surface, the ISS multiple removal/attenuation methods usually require a known source wavelet and information about the near surface (Matson, 1997). To obtain the source wavelet, Wang and Weglein (2008) has shown how Green's theorem is used to fulfill the requirement. The need of the near surface properties is a practical obstacle for on-shore/ocean bottom application. Here, we present an analytic example to show the inner workings of the elastic internal multiple algorithm. In particular, we demonstrate how this scattering-based algorithm can predict exact arrival times without the above assumption being true.

2 Theory

We start with the forward scattering series derived from the Lippmann-Schwinger equation

$$G = G_0 + G_0 V G, \tag{1}$$

which can be expanded in a forward series

$$G = G_0 + G_0 V G_0 + G_0 V G_0 V G_0 + \cdots, \tag{2}$$

where G and G_0 are the actual and reference Green's functions. The perturbation V can be written as $V = \sum_n V_n$ where V_n is n-th order in the data.

Define $D = G - G_0$ as the measurement of the scattered field. Substituting into the forward series gives the inverse scattering series in terms of data

$$\begin{aligned} D &= G_0 V_1 G_0, \\ 0 &= G_0 V_2 G_0 + G_0 V_1 G_0 V_1 G_0, \\ 0 &= G_0 V_3 G_0 + G_0 V_2 G_0 V_1 G_0 + G_0 V_1 G_0 V_2 G_0 + G_0 V_1 G_0 V_1 G_0 V_1 G_0, \\ &\vdots \end{aligned} \tag{3}$$

The term $G_0 V_1 G_0 V_1 G_0 V_1 G_0$ is the first term in the inverse series of first order internal multiples.

Following the method developed by Weglein et al. (1997) and Araújo (1994), the equation for first order internal multiples in 2-D acoustic data is

$$\begin{aligned} b_{3IM}(k_g, k_s, q_g + q_s) = \frac{1}{(2\pi)^2} &\int_{-\infty}^{\infty} dk_1 e^{-iq_1(z_g - z_s)} \int_{-\infty}^{\infty} dk_2 e^{iq_2(z_g - z_s)} \\ &\times \int_{-\infty}^{\infty} dz_1' b_1(k_g, k_1, z_1') e^{i(q_g + q_1) z_1'} \\ &\times \int_{-\infty}^{z_1' - \epsilon} dz_2' b_1(k_1, k_2, z_2') e^{-i(q_1 + q_2) z_2'} \\ &\times \int_{z_2' + \epsilon}^{\infty} dz_3' b_1(k_2, k_s, z_3') e^{i(q_2 + q_s) z_3'} \end{aligned} \tag{4}$$

The parameter $\epsilon > 0$ ensures $z_1' > z_2'$ and $z_3' > z_2'$ which satisfy the geometric relationship between reflections of internal multiples (lower-higher-lower). b_1 is defined in terms of the original pre-stack data without free surface multiples. The data can be written as

$$D(k_g, k_s, \omega) = (-2iq_s)^{-1} b_1(k_g, k_s, q_g + q_s), \tag{5}$$

where $b_1(k_g, k_s, q_g + q_s)$ represents the data result from a single-frequency incident plane wave.

The adapted elastic version of (4) given by Matson (1997) is

$$\begin{aligned} B_{ij}^{3IM}(k_g,k_s,q_g^i+q_s^j) = \frac{1}{(2\pi)^2}\int_{-\infty}^{\infty} dk_3 e^{-iq_1^l(z_g-z_s)} \int_{-\infty}^{\infty} dk_2 e^{iq_2^m(z_g-z_s)} \\ \times \int_{-\infty}^{\infty} dz_1' B_{il}(k_g,k_1,z_1') e^{i(q_g^i+q_1^l)z_1'} \\ \times \int_{-\infty}^{z_1'-\epsilon} dz_2' B_{lm}(k_1,k_2,z_2') e^{-i(q_1^l+q_2^m)z_2'} \\ \times \int_{z_2'+\epsilon}^{\infty} dz_3' B_{mj}(k_2,k_s,z_3') e^{i(q_2^m+q_s^j)z_3'} \end{aligned} \tag{6}$$

where q_1^i indicate P and S vertical wavenumbers for $i = P$ and S, respectively.

Similarly, B_{ij} is defined in terms of the original pre-stack data, that is

$$D_{ij}(k_1,k_2,\omega) = (-2iq_2^j)^{-1} B_{ij}(k_g,k_s,q_1^i+q_2^j). \tag{7}$$

Hence,

$$\begin{aligned} D_{PP}(k_1,k_2,\omega) =& (-2iq_2^P)^{-1} B_{PP}(k_g,k_s,q_1^P+q_2^P), \\ D_{PS}(k_1,k_2,\omega) =& (-2iq_2^S)^{-1} B_{PS}(k_g,k_s,q_1^P+q_2^S), \\ D_{SP}(k_1,k_2,\omega) =& (-2iq_2^P)^{-1} B_{SP}(k_g,k_s,q_1^S+q_2^P), \\ D_{SS}(k_1,k_2,\omega) =& (-2iq_2^S)^{-1} B_{SS}(k_g,k_s,q_1^S+q_2^S). \end{aligned} \tag{8}$$

One can see that if the converted waves do not exist, equation (6) becomes equation (4), which is the first order internal multiple attenuator in acoustic form.

3 Attenuation of elastic internal multiples : a 1.5D example

We consider a layering model given by Nita and Weglein (2005) (see Figure 1). The velocity changes across the interfaces located at $z = z_a$ and $z = z_b$ where the velocities are c_0, c_1, and c_2, respectively. The sources and receivers are located at the measurement surface where the depth $z = 0$. The reference vertical speeds are defined as

$$c_v^i = \begin{cases} \alpha_0/cos\theta_i, & \text{if } i = P \\ \beta_0/cos\theta_i, & \text{if } i = S \end{cases} \tag{9}$$

The reference horizontal speed is defined as

$$c_h^i = \begin{cases} \alpha_0/sin\theta_i, & \text{if } i = P \\ \beta_0/sin\theta_i, & \text{if } i = S \end{cases} \tag{10}$$

where α_0 and β_0 are P-wave and S-wave velocity in the reference medium, respectively.

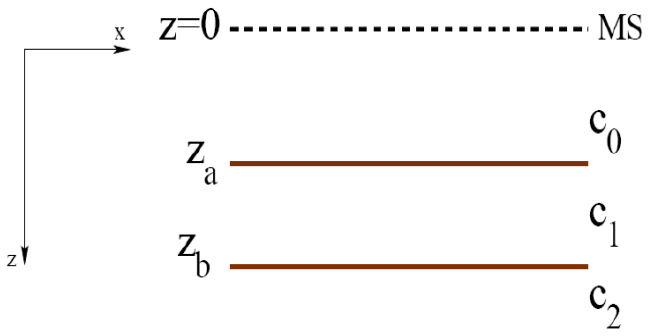

Figure 1: The model for the 1.5D example

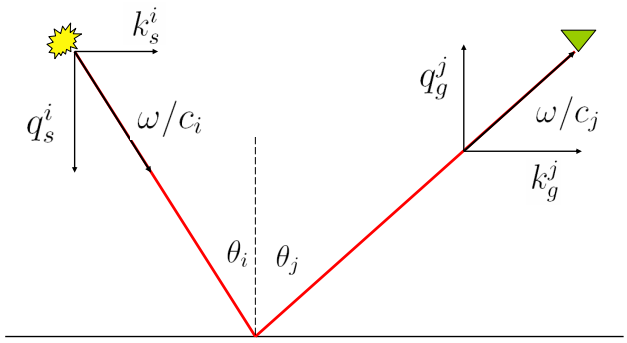

Figure 2: The geometry of the first primary in the data

The horizontal wave numbers are

$$\begin{aligned} k_s^i &= \omega/c_h^i, \\ k_g^j &= \omega/c_h^j. \end{aligned} \tag{11}$$

For media with depth-dependent velocity, the horizontal slowness ($sin\theta_i/c(z) \equiv p$) is constant along

a ray path whether or not converted waves are present (Aki and Richards, 2002). Therefore,

$$\begin{aligned} k_s^i &= k_g^j = \omega/c_h, \\ k_s^i + k_g^j &= 2\omega/c_h. \end{aligned} \tag{12}$$

The vertical wave numbers are

$$q_s^i = \begin{cases} \sqrt{(\frac{\omega}{\alpha_0})^2 - k_s^2}, & \text{if } i = P \\ \sqrt{(\frac{\omega}{\beta_0})^2 - k_s^2}, & \text{if} i = S \end{cases} \tag{13}$$

$$q_g^j = \begin{cases} \sqrt{(\frac{\omega}{\alpha_0})^2 - k_g^2}, & \text{if } j = P \\ \sqrt{(\frac{\omega}{\beta_0})^2 - k_g^2}, & \text{if} j = S \end{cases} \tag{14}$$

The total travel time for the n-th primary can be written as

$$T_n = \tau_n + t_h, \tag{15}$$

where τ_n and t_h are the vertical and horizontal travel times, respectively. The horizontal travel time is defined as

$$t_h = \frac{x_g - x_s}{c_h} = \frac{2x_h}{c_h}, \tag{16}$$

and the vertical travel time corresponding to the n-th event is

$$\tau_n = \frac{z_n}{c_v^i} + \frac{z_n}{c_v^j}, \tag{17}$$

where z_n is the pseudo depths for the n-th event. Therefore,

$$\begin{aligned} \omega\tau_n &= z_n(\frac{\omega}{c_v^i} + \frac{\omega}{c_v^j}) \\ &= z_n(q_s^i + q_g^j) = z_n k_z^{ij}, \\ \omega t_h &= \omega(\frac{2x_h}{c_h}) = k_h x_h. \end{aligned} \tag{18}$$

The data in the frequency ω domain can be written as

$$D_{ij}(x_h, 0; \omega) = \frac{1}{2\pi}\int_{-\infty}^{\infty} dk_h \sum_n \frac{R_n^{ij} e^{ik_z^{ij} z_n}}{2iq_s^i} e^{ik_h x_h}. \tag{19}$$

where $k_z^{ij} = q_s^i + q_g^j$, $k_h = k_g + k_s$,and $x_h = (x_g - x_s)/2$.

Fourier transform over x_g, x_s,

$$D_{ij}(k_h, 0, \omega) = \frac{2\pi}{2iq_s^i} \sum_n R_n^{ij} e^{iz_n k_z^{ij}} \delta(k_g - k_s). \tag{20}$$

The data is

$$\begin{aligned} B_{ij}(k_h,0,\omega) &= 2iq_s^i D_{ij}(k_h,0,\omega) \\ &= 2\pi \sum_n R_n^{ij} e^{ik_z^{ij} z_n} \delta(k_g - k_s). \end{aligned} \tag{21}$$

Inverse Fourier transforming into the pseudo depth domain gives

$$B_{ij}(k_h,z,\omega) = 2\pi \sum_n R_n^{ij} \delta(z - z_n)\delta(k_g - k_s). \tag{22}$$

Substituting equation (22) into equation (6), the integration over z_3 gives

$$\begin{aligned} \int_{z_2'+\epsilon}^{\infty} dz_3' e^{ik_z'^{mj} z_3'} B_{mj}(k_2',k_s',z_3') =& 2\pi \int_{z_2'+\epsilon}^{\infty} dz_3' e^{ik_z'^{mj} z_3'} \sum_p R_p^{mj} \delta(z_3' - z_p')\delta(k_2' - k_s') \\ =& 2\pi \sum_p R_p^{mj} e^{ik_z'^{mj} z_p'} H(z_p' - (z_2' + \epsilon))\delta(k_2' - k_s') \end{aligned}$$

The integration over z_2' is

$$\begin{aligned} &\int_{-\infty}^{z_1'-\epsilon} dz_2' e^{-ik_z'^{lm} z_2'} B_{lm}(k_1',k_2',z_2') \times 2\pi \sum_p R_p^{mj} e^{ik_z'^{mj} z_p'} H(z_p' - (z_2' + \epsilon))\delta(k_2' - k_s') \\ &= (2\pi)^2 \int_{-\infty}^{z_1'-\epsilon} dz_2' e^{-ik_z'^{lm} z_2'} \sum_q R_q^{lm} \delta(z_2' - z_q')\delta(k_1' - k_2') \sum_p R_p^{mj} e^{ik_z'^{mj} z_p'} H(z_p' - (z_2' + \epsilon))\delta(k_2' - k_s') \\ &= (2\pi)^2 \sum_{p,q} R_p^{mj} R_q^{lm} e^{ik_z'^{mj} z_p'} e^{-ik_z'^{lm} z_q'} H(z_p' - (z_q' + \epsilon)) H((z_1' - \epsilon) - z_q')\delta(k_2' - k_s')\delta(k_1' - k_2') \end{aligned}$$

The integration over z_1' is

$$\begin{aligned} &\int_{-\infty}^{\infty} dz_1' e^{ik_z'^{jl} z_1'} B_{jl}(k_g',k_1',z_1') \\ &\quad \times [(2\pi)^2 \sum_{p,q} R_p^{mj} R_q^{lm} e^{ik_z'^{mj} z_p'} e^{-ik_z'^{lm} z_q'} H(z_p' - (z_q' + \epsilon)) H((z_1' - \epsilon) - z_q')\delta(k_2' - k_s')\delta(k_1' - k_2')] \\ &\quad = (2\pi)^3 \int_{-\infty}^{\infty} dz_1' e^{ik_z'^{jl} z_1'} \sum_r R_r^{jl} \delta(z_1' - z_r')\delta(k_g' - k_1') \sum_{p,q} R_p^{mj} R_q^{lm} e^{ik_z'^{mj} z_p'} e^{-ik_z'^{lm} z_q'} \\ &\quad \times H(z_p' - (z_q' + \epsilon)) H((z_1' - \epsilon) - z_q')\delta(k_2' - k_s')\delta(k_1' - k_2') \\ &\quad = (2\pi)^3 \sum_{p,q,r} R_p^{mj} R_q^{lm} R_r^{jl} e^{i(k_z'^{mj} z_p - k_z'^{lm} z_q + k_z'^{jl} z_r)} H(z_p' - (z_q' + \epsilon)) H(z_r' - (z_q' + \epsilon)) \\ &\quad \times \delta(k_2' - k_s')\delta(k_1' - k_2')\delta(k_g' - k_1') \end{aligned} \tag{23}$$

Note that the parameter $\epsilon > 0$ ensures $z_p' > z_q'$ and $z_r' > z_q'$ which satisfy a lower-higher-lower relationship between the pseudo depths.

The result for B_{ij}^{3IM} is

$$B_{ij}^{3IM}(k_h, z, \omega) = 2\pi \sum_{\substack{p,q,r \\ z_p > z_q \\ z_r > z_q}} R_p^{mj} R_q^{lm} R_r^{jl} e^{i(k'^{mj}_z z_p - k'^{lm}_z z_q + k'^{jl}_z z'_r)} \delta(k'_g - k'_s) \tag{24}$$

Inverse Fourier transforming over k_m and k_h gives

$$B_{ij}^{3IM}(k'_h, k'_z, \omega) = \frac{1}{2\pi} \int dk'_h \sum_{p,q,r} R_p^{mj} R_q^{lm} R_r^{jl} e^{i(k'^{mj}_z z'_p - k'^{lm}_z z'_q + k'^{jl}_z z'_r)} e^{ik'_h x_h}. \tag{25}$$

The predicted first internal multiple in the space domain is

$$IM_{predicted}^{1st} = \frac{1}{2\pi} \int dk'_h \sum_{p,q,r} \frac{R_p^{mj} R_q^{lm} R_r^{jl} e^{i(k'^{mj}_z z'_p - k'^{lm}_z z'_q + k'^{jl}_z z'_r)} e^{ik'_h x_h}}{2iq_s^i}. \tag{26}$$

Note that

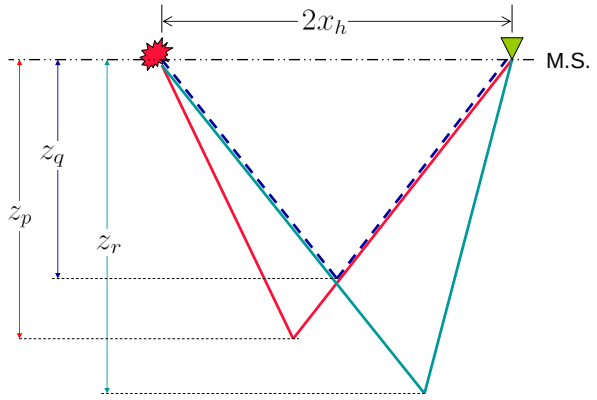

Figure 3: The geometry of pseudo depths

$$\begin{aligned} k'^{mj}_z z'_p &= \omega\tau'_p, \\ k'^{lm}_z z'_q &= \omega\tau'_q, \\ k'^{jl}_z z'_r &= \omega\tau'_r, \\ k'_h x_h &= \omega t'_h. \end{aligned} \tag{27}$$

Therefore,

$$k'^{mj}_z z'_p - k'^{lm}_z z'_q + k'^{jl}_z z'_r + k'_h x_h = \omega(\tau'_p - \tau'_q + \tau'_r + t'_h) \tag{28}$$

The travel time for the predicted first order internal multiple is

$$\begin{aligned} \tau'_p - \tau'_q + \tau'_r + t'_h &= (T_p - t'_h) - (T_q - t'_h) + (T_r - t'_h) + t'_h \\ &= T_p - T_q + T_r \end{aligned} \tag{29}$$

where T_p, T_q and T_r are travel times corresponding to the p-th, q-th, and r-th event, respectively. The travel time for the actual first order internal multiple is

$$\begin{aligned} T_{total} = \tau_p - \tau_q + \tau_r + t_h &= (T_p - t_h) - (T_q - t_h) + (T_r - t_h) + t_h \\ &= T_p - T_q + T_r. \end{aligned} \tag{30}$$

The result $T_{total} = T_p - T_q + T_r$ agrees with the actual arrival time for the first order internal multiple.

One can see that reference velocity errors give incorrect vertical and horizontal travel times for each event (see equation (16) and (17)). However, equation (29) shows that the errors due to wrong reference velocities can be canceled, and the predicted arrival times remain correct.

To attenuate an internal multiple for a single frequency requires data at all frequencies. This requirement comes from the integral over temporal frequency when transforming data from the frequency domain to the pseudo-depth domain. The integral transformation is truncated with band-limited data. The 1.5D example suggests that the algorithm is insensitive to reference velocities and hence has potential for spectral extrapolation if we choose reasonable reference velocities.

4 Conclusion

In this paper, we have presented an elastic internal multiple attenuation algorithm (Matson, 1997) following the analysis of Nita and Weglein (2005). Although the scattering-based methods usually require known near surface properties, our study has suggested that the internal multiple attenuation algorithm can tolerate errors in reference velocity for 1D earth. The capability of predicting exact travel time without known reference velocities is useful for land application, where the near surface properties are often complicated and ill-defined. Moreover, the freedom of choosing reference velocities has potential for the spectral extrapolation. The future direction of this study includes extending the algorithm to multi-dimensional elastic case and extrapolation of band-limited synthetic data.

Acknowledgments

We would like to thank all M-OSRP sponsors for constant support and encouragement. We especially thank all the members in M-OSRP for valuable suggestions.

References

Aki, K. and P. G. Richards. *Quantitative Seismology.* 2nd edition. University Science Books, 2002.

Araújo, F. V. *Linear and non-linear methods derived from scattering theory: backscattered tomography and internal multiple attenuation*. PhD thesis, Universidade Federal da Bahia, 1994.

Carvalho, P. M. *Free-surface multiple reflection elimination method based on nonlinear inversion of seismic data*. PhD thesis, Universidade Federal da Bahia, 1992.

Hsu, Shih-Ying and Arthur B. Weglein. On-shore project report I– Reference velocity sensitivity for the marine internal multiple attenuation algorithm: analytic examples. Technical report, Mission-Oriented Seismic Research Project, University of Houst on, 2007.

Matson, K. H. *An inverse-scattering series method for attenuating elastic multiples from multicomponent land and ocean bottom seismic data*. PhD thesis, University of British Columbia, 1997.

Nita, Bogdan G. and Arthur B. Weglein. Inverse scattering internal multiple attenuation algorithm in complex multi-d media. Technical report, Mission-Oriented Seismic Research Project, University of Houston, 2005.

Otnes, Einar, Ketil Hokstad, and Roger Sollie. "Attenuation of internal multiples for multicomponent- and towed streamer data.." *SEG Technical Program Expanded Abstracts* 23 (2004): 1297–1300.

Wang, Min and Arthur B. Weglein. A short note about elastic wavelet estimation. Technical report, Mission-Oriented Seismic Research Project, University of Houst on, 2008.

Weglein, A. B., F. A. Gasparotto, P. M. Carvalho, and R. H. Stolt. "An Inverse-Scattering Series Method for Attenuating Multiples in Seismic Reflection Data." *Geophysics* 62 (November-December 1997): 1975–1989.

Weglein, Arthur B. and Ken H. Matson. "Inverse scattering internal multiple attenuation: an analytic example and subevent interpretation." SPIE, 1998, 108–117.

Correcting primary amplitudes for plane-wave transmission loss using internal multiple attenuation I: an iterative procedure with 1D numerical examples

J. E. Lira, K. A. Innanen, A. C. Ramirez and A. B. Weglein, M-OSRP, University of Houston

Abstract

The objective of extracting the spatial location of a reflector, and its local angle-dependent reflection coefficient, from seismic data, depends on the ability to identify and to remove the effect on primary amplitudes of propagation down to and back from the reflector. All conventional methods that seek to correct for such transmission loss require estimates of the properties of the overburden. In this paper we describe a new approach that will in principle permit correction of primaries for such transmission loss without requiring overburden properties as input. The approach is based on the amplitude of the first term of the inverse scattering series internal multiple attenuation algorithm, which predicts the correct phase and approximate amplitude of first order internal multiples. The amplitude is estimated to within a factor determined by plane wave transmission loss down to and across the reflector producing the event's shallowest downward reflection. Hence, the amplitude difference between a given predicted and actual multiple, both of which are directly available from the data and the algorithm output, in principle contain all necessary information to correct specific primary reflections for their overburden transmission losses. Because of their strong influence on transmission loss absorptive overburdens/media require particular focus. As a first step, previous amplitude analysis of the internal multiple attenuation algorithm is here extended to include stratified absorptive media. Using this newly derived relationship between predicted and actual internal multiples, and existing results for acoustic elastic media, correction operators, to be applied to specific isolated primaries in both types of media, are then computed using combinations of multiples and their respective predictions. We illustrate the approach on synthetic data for the absorptive case with three Earth models with different Q profiles. Further research into the amplitudes of the plane wave internal multiple predictions in 2D and 3D media as a likely pre-requisite to field data application of this concept-level algorithm.

1 Introduction

In this paper we continue to report on progress towards use of inverse scattering series internal multiple attenuation to address an important issue in migration-inversion as it is carried out in the industry today. Namely, the correction of primary amplitudes for transmission through an unknown overburden, "laying bare" the reflection coefficient, and increasing the accuracy of, for instance, parameter inversion at the associated interface.

A primary is a recorded seismic event whose history (see Figure 1) can be roughly subdivided into: propagation down from the source through the overburden, reflection at a target, and propagation back through the overburden up to the receiver:

$$\text{Primary} \quad = \quad [\text{Transmission Down}] \times [\text{Reflection}] \times [\text{Transmission Up}]. \tag{1}$$

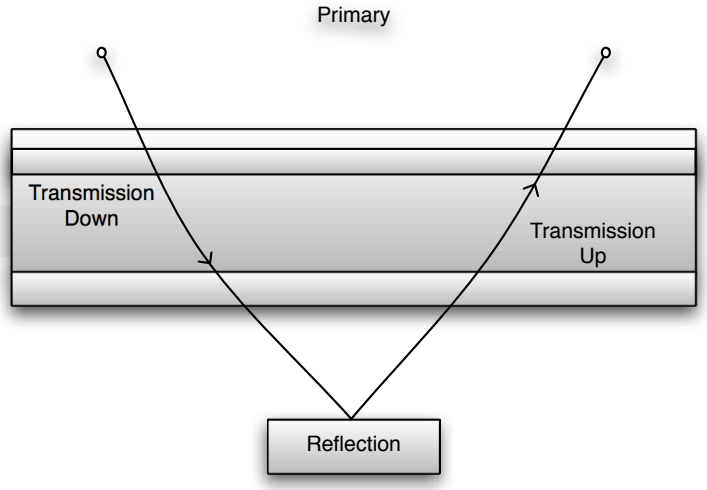

Figure 1: *Sketch of a primary. Amplitudes are determined by the material property contrast at the point of reflection, and propagation down and back through the overburden.*

In exploration seismology primaries are the main seismic source of subsurface information, and are used for structural mapping, parameter estimation, and, ultimately, petroleum delineation at the target. Techniques of *migration-inversion* (Weglein and Stolt, 1999) accomplish these goals by first generating maps of seismic reflectors at depth, typically positioning at these reflectors, reflection coefficients as functions of angle, and, second, by using this behavior to determine local contrasts in medium properties. Therefore, an important part of migration-inversion is the processing of primary amplitudes, which are themselves essentially described by equation (1), to remove the effects of transmission down to and back from the point of reflection, "laying bare" the reflection coefficient information so that it may be used in parameter estimation. This removal as it is conventionally accomplished requires an accurate estimate of all medium properties above the target.

In this paper we describe an approach for the correction of primary amplitudes for transmission loss through various types of overburdens, that avoids the requirement for prior characterization of overburden properties, thus aiding otherwise conventional migration-inversion methods. A corrective operator is sought, derivable directly from the data, of the form

$$\text{Corrective Operator} = (\text{[Transmission Down]} \times \text{[Transmission Up]})^{-1}, \tag{2}$$

which, when applied to a particular primary as modeled by equation (1), provides the reflection coefficient information required by the inversion component of migration-inversion:

$$\text{Corrected Primary} = \text{Primary} \times \text{Corrective Operator} = \text{[Reflection]}. \tag{3}$$

The approach derives from the inverse scattering series internal multiple attenuation algorithm (Araujo et al., 1994; Araújo, 1994; Weglein et al., 1997, 2003). Multiples are defined, herein,

as events which have experienced at least one downward reflection. When at least one of these downward reflections takes place at the free surface, the event is a *free-surface* multiple[1], otherwise the event is an *internal multiple*.

The *order* of a free-surface multiple refers to the number of downward reflections experienced by the event at the free surface, and the order of an internal multiple refers to the number of downward reflections experienced by the event anywhere in the subsurface (Weglein et al., 2003); e.g., first order internal multiples have one downward reflection, etc. The inverse scattering series has the ability to eliminate all multiples without *a priori* subsurface information (Weglein et al., 2003). The inverse series algorithm for free-surface multiples eliminates a single order of free-surface multiples with a single algorithm term (of the same order). In contrast, each order of internal multiples requires a series for its removal. For instance, the internal multiple attenuation algorithm is a series, whose first term predicts the correct time and approximate amplitude of all first order internal multiples, and prepares the higher order multiples for attenuation by higher order terms in the algorithm[2].

The primary correction approach proposed here derives from the properties of the first term of the internal multiple attenuation algorithm. The precise difference between the actual amplitude of an internal multiple and the amplitude predicted by the first term of the algorithm, for plane wave data in an acoustic medium (Weglein et al., 2003; Nita and Weglein, 2005), is a direct expression of plane wave transmission losses down to and across the reflector where the multiple's shallowest downward reflection has taken place (Weglein and Matson, 1998; Weglein et al., 2003; Ramirez and Weglein, 2005b,a). This means that the amplitude difference between a given multiple and its prediction, both of which are directly available from the data and the algorithm output, in principle contain all the information necessary to correct specific primary reflections for their overburden transmission losses[3]. The main goal of this study is to use this information to construct a corrective operator essentially of the form described in equation (2). We will assume that wavelet estimation and deconvolution, instrument response analysis, and de-ghosting have already been carried out, and that the requisite data events have been identified and can be separately studied. The next chapter deals with the case when this last assumption cannot be made.

The design of the operator depends on whether or not the overburden is absorptive. Hence, after briefly re-stating the properties of the internal multiple attenuation algorithm as studied for acoustic/elastic media (Araujo et al., 1994; Araújo, 1994; Weglein et al., 1997, 2003; Ramirez and Weglein, 2005b,a), we begin with the important preliminary step of deriving, for the first time, expressions for the difference between the internal multiple attenuation algorithm prediction and

[1]This definition is contingent on prior removal of ghosts.

[2]Research has additionally progressed towards an elimination algorithm. Ramirez and Weglein (2005a); Ramirez (2007) have provided a closed-form *elimination* algorithm for a subset of first-order internal multiples, which eliminates internal multiples generated at the shallowest reflector in the earth and improves the attenuation of internal multiples generated at deeper reflectors. Further aspects of the internal multiple attenuation algorithm have been reported in the literature by (Carvalho et al., 1991; Matson, 1997; Weglein et al., 1997; Weglein and Matson, 1998; Kaplan et al., 2005; Nita and Weglein, 2005; Weglein and Dragoset, 2005).

[3]The use of the discrepancy for correcting for overburden effects was first suggested by Dennis Corrigan following discussions on the analytic example presented by A. Weglein at CWP and ARCO, later published by Weglein and Matson (1998).

the actual amplitude of the multiple event for a layered anelastic medium. This allows operators appropriate for either medium type to be derived.

We next work with the formulas expressing the difference between actual and predicted multiples, demonstrating that, when combined recursively, they may be used to produce correction operators ready for multiplicative application (in the frequency domain) to specific primaries. The operators are built only from the data and the output of the internal multiple algorithm (which itself has required no overburden information). Different operators are made for the acoustic/elastic vs. absorptive cases. Following this, weillustrate the procedure on synthetic data for the absorptive case, examining the form and effect of the correction operators.

2 Review: amplitudes predicted by the multiple attenuation algorithm

The first term in the internal multiple attenuation algorithm acts non-linearly on reflection seismic data to calculate the exact phase and approximate amplitude of all orders of internal multiples:

$$\begin{aligned} b_{3IM}(k_g,k_s,q_g+q_s) &= \frac{1}{(2\pi)^2}\int_{-\infty}^{\infty}dk_1 e^{-iq_1(z_g-z_s)}\int_{-\infty}^{\infty}dk_2 e^{iq_2(z_g-z_s)} \\ &\times \left[\int_{-\infty}^{\infty}dz_1' b_1(k_g,k_1,z_1')e^{i(q_g+q_1)z_1'}\right. \\ &\times \int_{-\infty}^{z_1'-\epsilon}dz_2' b_1(k_1,k_2,z_2')e^{-i(q_1+q_2)z_2'} \\ &\times \left.\int_{z_2'+\epsilon}^{\infty}dz_3' b_1(k_2,k_s,z_3')e^{i(q_2+q_s)z_3'}\right], \end{aligned} \tag{4}$$

where $q_g=\mathrm{sgn}(\omega)\sqrt{(\frac{\omega}{c_0})^2-(k_g)^2}$, $q_s=\mathrm{sgn}(\omega)\sqrt{(\frac{\omega}{c_0})^2-(k_s)^2}$, k_g and k_s are the horizontal wavenumbers conjugate to receiver and source coordinates (x_g,x_s), respectivelly, and ϵ is a small positive quantity. The input for the internal multiple attenuation algorithm is b_1, which is created from the pre-stack reflection seismic data. It is constructed as follows: the surface recorded data, deghosted and without free surface multiples, $D(x_g,x_s,t)$, is Fourier transformed over all variables, to produce $D(k_g,k_s,\omega)$. A change of variables is made, to $D(k_g,k_s,q_g+q_s)$, after which b_1 is defined as $b_1(k_g,k_s,q_g+q_s)=D(k_g,k_s,q_g+q_s)(2iq_s)$; b_1 is then inverse Fourier transformed over q_g+q_s to pseudo-depth. The result, $b_1(k_g,k_s,z)$, is used as input in equation (4), and the output, b_{3IM}, is the predicted internal multiple data set, produced without knowledge of Earth material properties or structure and it accommodating all Earth model types that satisfy the convolutional model (Ramirez and Weglein, 2005b).

2.1 The relationship between the predicted and the actual multiple amplitude

Being the first term in a series that removes first order internal multiples without subsurface information, the internal multiple attenuation algorithm provides the capability to predict the

exact time of all first order internal multiples and it is the first term to predict the amplitudes of the first order internal multiples. Weglein and Matson (1998) and Ramirez and Weglein (2005b) examined the difference between the actual amplitudes of internal multiples and those of the internal multiple attenuation algorithm predictions. The latter authors called the difference the *amplitude factor*, and showed that it is related to the transmission coefficients down to and across the multiple generator interface (Weglein and Matson, 1998; Ramirez and Weglein, 2005b). The difference can be understood intuitively by considering the way the algorithm builds its prediction. Consider Figure 2. On the left panel is an internal multiple and the primaries that are used in the algorithm

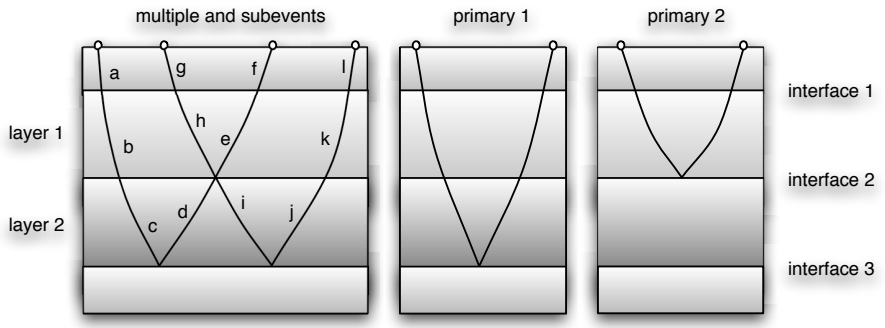

Figure 2: *Schematic diagram of primaries and internal multiples in a stratified medium. Left panel: an internal multiple and the primary subevents used to predict it. Middle and right panels: associated primaries whose amplitudes may be corrected using the discrepancy between the amplitudes of the predicted and actual multiple on the right.*

to predict it. The generator is the interface 2. The multiple has the path $abcdijkl$. The algorithm predicts the multiple by multiplying the amplitudes of the three primaries, adding the phases of the deeper two, $abcdef$ and $ghijkl$, and subtracting the phase of the shallower, $ghef$. The phase of the actual multiple and the predicted multiple are therefore identical. However, the amplitude of the actual multiple,

$$T_{ab}T_{bc}R_{cd}(-R_{he})R_{ij}T_{jk}T_{kl},$$

and the multiplied amplitudes of the primaries in the prediction,

$$[T_{ab}T_{bc}R_{cd}T_{de}T_{ef}] \times [T_{gh}R_{he}T_{ef}] \times [T_{gh}T_{hi}R_{ij}T_{jk}T_{kl}],$$

clearly differ in that the actual multiple does not experience the transmission history of the shallower primary. That is, the terms T_{de}, T_{ef}, T_{gh}, T_{hi} in the prediction are extraneous. This includes transmission across the generating interface (interface 2).

Let us next depart from schematics and consider the general accounting of this behavior for predicted multiples within an arbitrary stack of layers provided by Ramirez and Weglein (2005b). Figure 3 shows a 1-D acoustic model consisting of three reflectors, the lower two of which have associated reflection coefficients R_1 and R_2, and layer velocities c_0, c_1 and c_2. The transmission

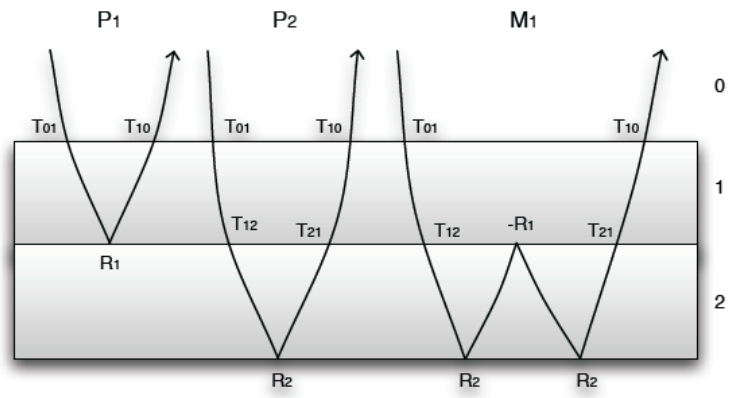

Figure 3: *Multilayered medium where the first layer,* 0*, is acoustic and the other two are anelastic. Three events are displayed and they were used to generate the data-set for testing the correction of the transmission losses of a primary in an absorptive medium. The parameters of the models are shown in Table* 1*.*

coefficient from layer i to layer j is T_{ij}. For example, a multiple generated at interface 2 in Figure 3 has an amplitude

$$M_1 = [T_{01}T_{12}R_2(-R_1)R_2T_{21}T_{10}]. \tag{5}$$

The predicted multiple amplitude is:

$$M_1^{\text{PRED}} = [T_{01}T_{12}R_2(-R_1)R_2T_{21}T_{10}][(T_{01}T_{10})^2(T_{12}T_{21})]. \tag{6}$$

Comparing equations (5) and (6) one sees that their ratio, as expected, carries information about the transmission coefficients down to and across the multiple generator interface. Ramirez and Weglein (2005b) refer to this ratio as the *amplitude factor* AF:

$$\text{AF}_2 = \frac{M_1^{\text{PRED}}}{M_1} = [T_{01}T_{10}]^2[T_{12}T_{21}]. \tag{7}$$

The index 2 anticipates our later use of this factor for corrective purposes, and signifies that the second interface is the generator. With this terminology the amplitude factor expressing the discrepancy between the predicted and actual amplitudes of an internal multiple generated at the j'th interface in a stack of layers is

$$\text{AF}_2 = \begin{cases} T_{01}T_{10} & \text{for j=1;} \\ \prod_{i=1}^{j-1}(T_{i,i-1}^2T_{i-1,i}^2)T_{j,j-1}T_{j-1,j} & \text{for } 1 < j < J, \end{cases} \tag{8}$$

where J is the total number of interfaces in the model. Presently we will manipulate this factor to become a correction operator for primary amplitudes.

2.2 Extension of the amplitude analysis to absorptive media

Ramirez and Weglein (2005b) assume an acoustic medium, in which plane-wave transmission losses are local, occurring at the point at which the wave crosses a contrast in material properties. For an absorptive stack of layers, in which transmission loss occurs over the entire course of propagation, an extension of their results is required. In later sections this minor theoretical alteration will be shown to lead to an important practical difference when the predicted-actual amplitude discrepancy is exploited.

In order to study the transmission coefficients in an anelastic medium we select an intrinsic attenuation model to describe amplitude and phase alterations in a wave due to friction. These alterations are modeled by a generalization of the wavefield phase velocity to a complex, frequency-dependent quantity parameterized in terms of Q. A reasonably well-accepted Q model (Aki and Richards, 2002) alters the scalar propagation constant of the j'th layer, $k_j = \omega/c_j(z)$, to

$$k_j = \frac{\omega}{c_j(z)}\left[1 + \frac{F(\omega)}{Q_j(z)}\right], \tag{9}$$

where $F(\omega) = \frac{i}{2} - \frac{1}{\pi}\log(\omega/\omega_0)$. The reference frequency ω_0 may be considered a parameter to be estimated, or assumed to be the largest frequency available to a given experiment. The model divides propagation into three parts: a propagation component, an attenuation component, and a dispersion component.

With this definition of k_j, and assuming that in Figure 3 the two bottom layers are anelastic, we again construct the prediction. It is convenient to re-define the transmission coefficient of a given interface to incorporate absorptive amplitude loss within the layer *above* that interface. For instance, the coefficients T_{12} and T_{21} of the previous section derived using the k_j of equation 9, become:

$$\mathcal{T}_{12} = \left[\frac{2c_2\left(1+\frac{F(\omega)}{Q_2}\right)^{-1}}{c_1\left(1+\frac{F(\omega)}{Q_1}\right)^{-1} + c_2\left(1+\frac{F(\omega)}{Q_2}\right)^{-1}}\right] \overbrace{e^{-\frac{\omega}{2Q_1c_1}(z_1-z_0)}}^{\text{attenuation component}} \; e^{\frac{i\omega}{\pi Q_1 c_1}\log(\frac{\omega}{\omega_0})(z_1-z_0)} \tag{10}$$

$$\mathcal{T}_{21} = \left[\frac{2c_1\left(1+\frac{F(\omega)}{Q_1}\right)^{-1}}{c_2\left(1+\frac{F(\omega)}{Q_2}\right)^{-1} + c_1\left(1+\frac{F(\omega)}{Q_1}\right)^{-1}}\right] \underbrace{e^{-\frac{\omega}{2Q_1c_1}(z_1-z_0)}}_{\text{attenuation component}} \; e^{\frac{i\omega}{\pi Q_1 c_1}\log(\frac{\omega}{\omega_0})(z_1-z_0)}. \tag{11}$$

We make particular note of the dependence (via the attenuation component) of this definition of transmission coefficients on the thickness of the layer *overlying* the interface in question. With this extension, the internal multiple attenuation can be expressed with essentially the same amplitude factor, used in the elastic case. For instance, by analogy with equation (7):

$$\mathrm{AF}_2 = [T_{01}T_{10}]^2\mathcal{T}_{12}\mathcal{T}_{21}. \tag{12}$$

Provided that this re-definition of the absorptive transmission coefficients is adopted, the amplitude factors and internal multiple attenuation error analysis for the general absorptive stack of layers at normal incidence is given again by equation (8).

3 Correction of primary amplitudes using internal multiples

We will make two comments about the amplitude error analysis above. First, the discrepancy between the predicted and the actual multiple for a given generator is directly related to the transmission losses experienced by a primary associated with that generator. Second, the discrepancy, characterized by the amplitude factor AF, is available directly from the data and the output of the internal multiple attenuation algorithm. In this section we use the information in the various AF factors as a direct means to correct the amplitude of the primary associated with the generator for transmission effects, in the sense put forward at the beginning of this chapter.

We define what will become the primary correction operator calling it PCO, to be built recursively from the data-determined AFs:

$$\mathrm{PCO}_n \equiv \frac{\mathrm{PCO}_{n-1}}{\mathrm{AF}_n}, \tag{13}$$

with the terminating definition

$$\mathrm{PCO}_0 = 1. \tag{14}$$

Expanding this operator over several orders n clarifies that it will indeed act as a correction operator when applied multiplicatively to a primary whose upward reflection has occurred at the n'th interface (or near; see bellow).

The precise primary to be corrected with the n'th operator depends on whether the medium is assumed to be absorptive or not. We next treat these cases in turn. It is useful to index primaries from 0 upward. In the scheme in Figure 2, the 0'th primary reflects upward at interface 1.

3.1 Correction of primaries in acoustic/elastic media

Consider once again the multiple sketched in Figure 2, whose generator is interface 2. Setting $n = 2$, expanding equation (13), and employing the alphabetical indices in the figure, the operator expands into

$$\mathrm{PCO}_2 = \frac{1}{T_{gh}T_{hi}T_{de}T_{ef}}. \tag{15}$$

If the medium is acoustic/elastic, for the primary depicted in the middle panel of Figure 2, the "last" overburden effect on the event before the reflection at interface 3 is the transmission through interface 2, and the "first" overburden effect on the event after the reflection is again transmission through interface 2. Consequently, PCO_2 is exactly appropriate as an operator to correct this (middle panel of Figure 2) primary. More generally, in the acoustic/elastic case, the operator PCO_n in equation (13) corrects the n'th primary, leaving the n'th reflection coefficient "bare" and suitable as input to other inverse procedures:

$$R_n = \mathrm{PCO}_n \times P_n. \tag{16}$$

3.2 Correction of primaries in absorptive media

Next, suppose that the medium in Figure 2 is absorptive, and again consider PCO_2. Recall that the same form for the amplitude discrepancy between predicted and actual multiples is maintained in absorptive media and so is this operator, PCO_2, provided we alter the transmission coefficients of a given interface to include absorptive propagation through the layer *above* that interface.

However, with this arrangement, PCO_2 is evidently no longer appropriate as an operator to correct primary 2, *i.e.*, the primary depicted in the middle panel of Figure 2, because it does not account for absorptive propagation through the layer between the reflection and the multiple generator.

To maintain the usefulness of the operator, we instead make an approximation. We assume that in an absorptive medium, the effect of the local transmission coefficient at a boundary on the amplitude of a primary is dwarfed by the effect of absorptive propagation. That is, the underbraced term in equation 11 is more important to the amplitude of the event than the term in square brackets. With that assumption we may simply change the primary being corrected by PCO_2 to the one depicted in the right panel of Figure 2. This statement is true to within the combined local transmission coefficient down and up across interface 2. More generally, in the absorptive case, the (now frequency-dependent) operator PCO_n in equation (13) corrects the $n-1$'th primary:

$$R_{n-1}(\omega) = \mathrm{PCO}_n(\omega) \times P_{n-1}(\omega). \tag{17}$$

4 Synthetic examples

In this section, we illustrate with simple synthetic examples the steps necessary to correct a primary for absorptive transmission losses, using a multiple and the internal multiple attenuation algorithm prediction. We generate zero-offset traces from plane waves normally incident on three layered models with the geometry of the model in Figure 2, assuming the waves behave in accordance with the propagation constant in equation (9), and using the layer parameter values in Table 1. We include the two primaries and the first order internal multiple. The traces are wavelet deconvolved, and bandlimited (3–50 Hz). Figure 4 shows the traces generated for each model, which differ in their Q values, ranging from relatively low attenuation to relatively high attenuation. The arrival times of the two primaries and the multiple are approximately 1.5s, 2.3s and 2.9s, respectively.

Depth (m)	c (m/s)	Q_1	Q_2	Q_3
000-500	1500	∞	∞	∞
500-1422	2200	200	100	50
1422-2422	2800	100	50	25
2422-∞	3300	50	25	10

Table 1. *Absorptive Earth models.*

With the knowledge that the medium is absorptive, and in accordance with the arguments in the previous section, we use the predicted multiples to correct the amplitude of the shallower primary. The prescription is:

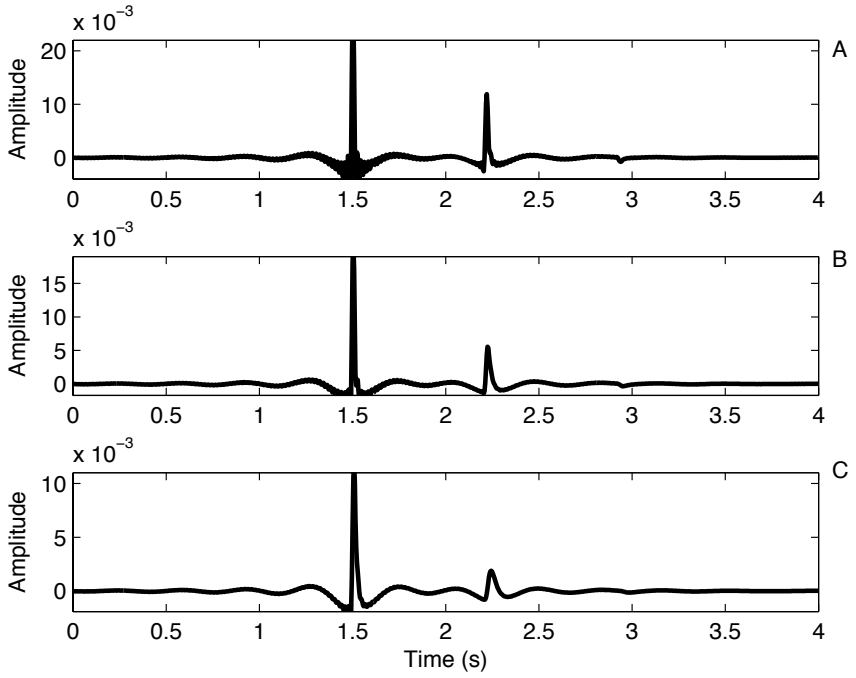

Figure 4: *Data generated for the numerical tests comprised of two primaries and one multiple for all models of Table 1:* (*A*) *The low absorptive Q-profile,* (*B*) *the intermediate Q-profile, and* (*C*) *the high absorptive Q-profile.*

1. Each trace is used as input to the internal multiple attenuation algorithm, generating predictions of the internal multiples.

2. Each internal multiple and its prediction are isolated and their spectra calculated.

3. The reciprocal of the ratio between the spectra of each internal multiple and its prediction is taken. By equation (13), this is the appropriate correction operator PCO.

4. The shallower primary is isolated, and the operator is applied to its spectrum.

We compare the result to an equivalent primary modeled in the absence of all effects of transmission through the overburden. Figure 5 illustrates the uncorrected, shallower primary from each of the three models. The multiple is predicted with the attenuation algorithm, the prediction and the original multiple are isolated from the trace, and their spectra are computed (Figure 6). The prediction evidently contains a greater level of attenuation then the actual multiple. This is in agreement with the extra transmission paths involved in the prediction, as discussed above. The frequency dependence of this discrepancy will form the basis for the correction of the shallower primary. This is effectively a data-driven Q-compensation algorithm. Figure 7 illustrates the spectra of the primary correction operators derived from these quantities, and Figure 8 illustrates the spectra of the shallower primaries for each model, before and after the correction. The

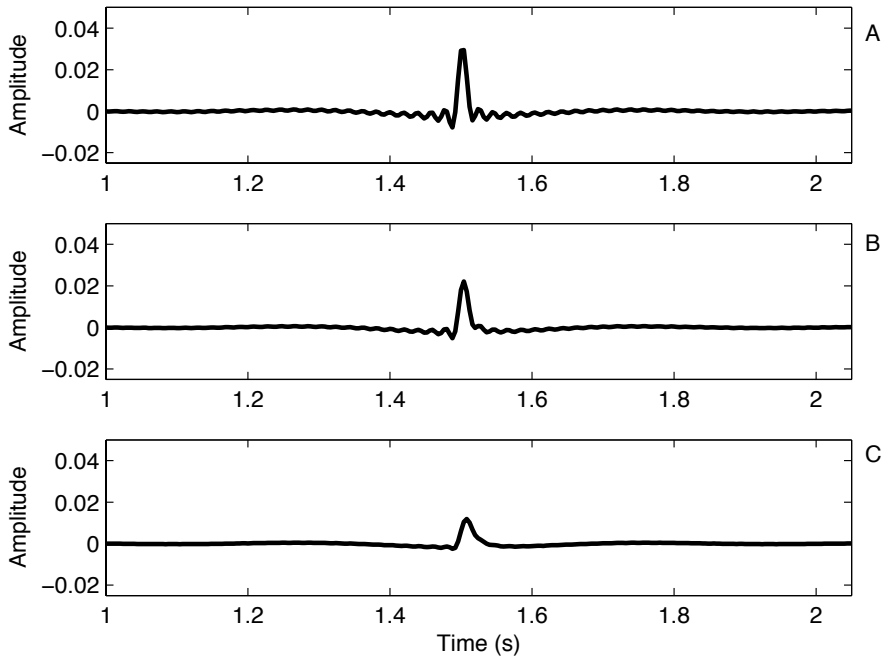

Figure 5: *Primary generated at interface* 1 *in Figure 3 for all models. These are the events I intend to compensate for transmission losses using the discrepancy between the actual multiple generated at interface* 1 *and the prediction of the internal multiple attenuation algorithm algorithm:* (A) *The low absorptive Q-profile,* (B) *the intermediate Q-profile, and* (C) *the high absorptive Q-profile.*

recovery of high frequencies is notable. In Figure 9, we illustrate the corrected primaries after inverse Fourier transforming to the time domain, and compare the results against their idealized counterparts constructed without transmission losses. Figures 10 to 12 illustrate in close succession the original primary in the data (top panel), the corrected primary (middle panel) and the idealized primary (bottom panel), for all models.

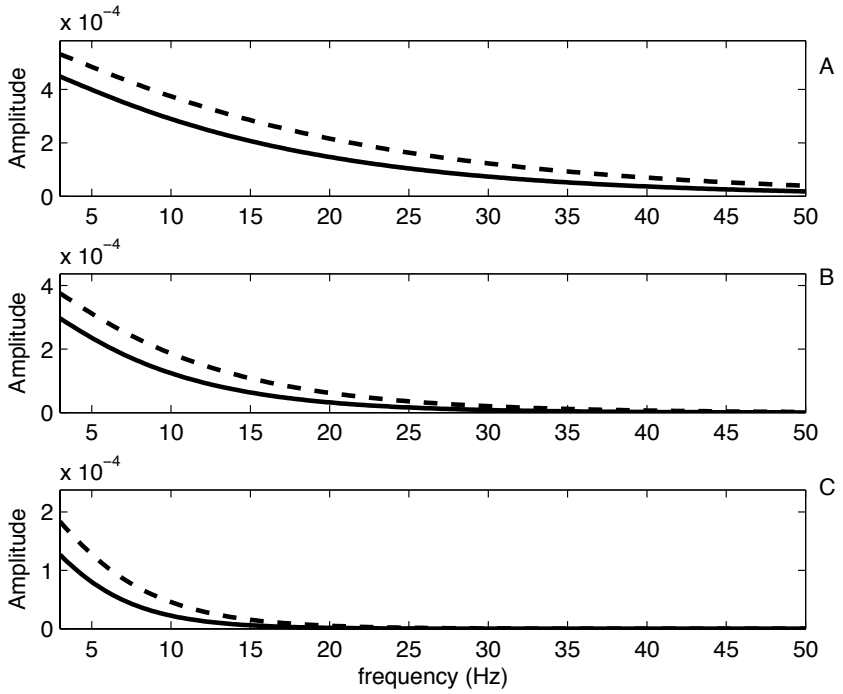

Figure 6: *The spectra of the multiple and its prediction from the internal multiple attenuation algorithm algorithm. The ratio between each pair of curves will be used for creating an operator for correcting the primaries of its transmission losses:* (A) *The low absorptive Q-profile,* (B) *the intermediate Q-profile, and* (C) *the high absorptive Q-profile.*

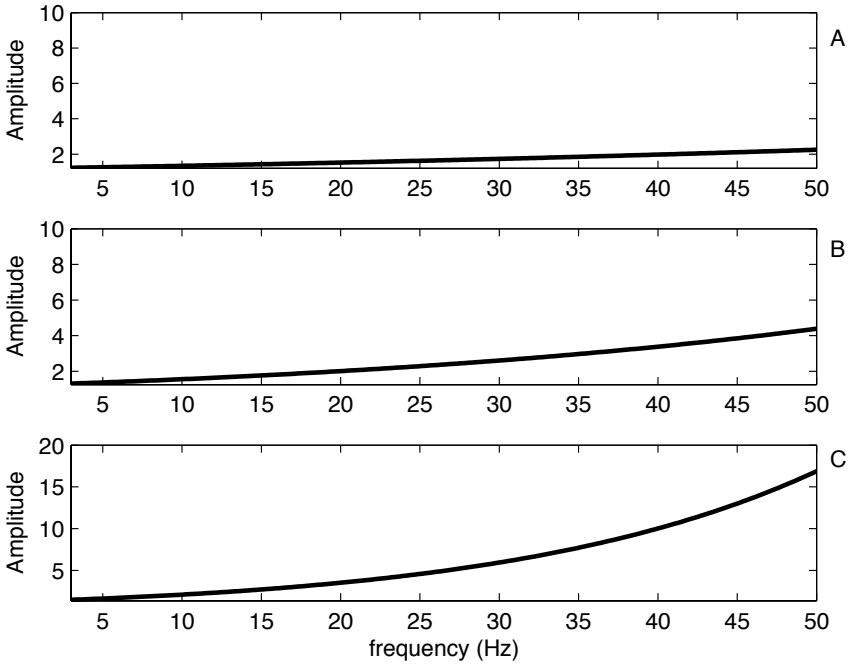

Figure 7: *Operators for correcting the primaries from transmission losses. They were generated by taking the ratio between the spectrum of the actual multiple and its prediction from the internal multiple attenuation algorithm algorithm in figure 6:* (A) *The low absorptive Q-profile,* (B) *the intermediate Q-profile, and* (C) *the high absorptive Q-profile.*

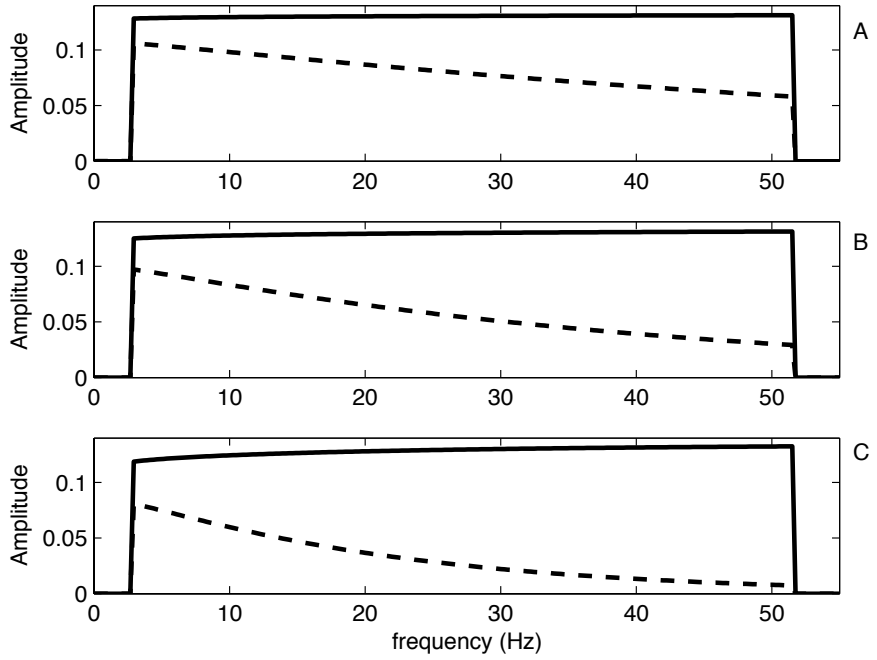

Figure 8: *Spectra of the original primaries and the corrected primaries for each model. These correction were performed by using the operator depicted in figure 7: (A) The low absorptive Q-profile, (B) the intermediate Q-profile, and (C) the high absorptive Q-profile.*

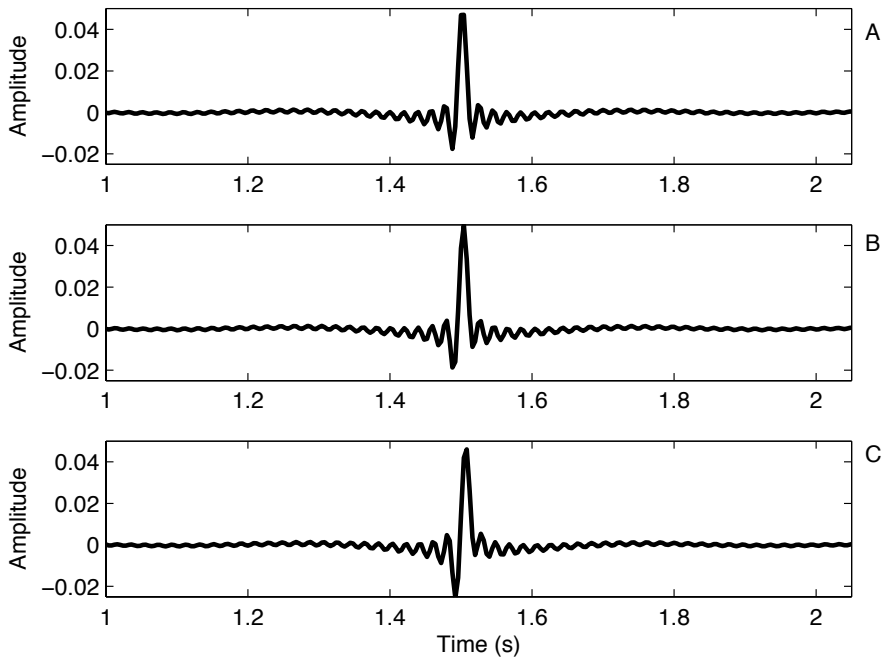

Figure 9: *The corrected primaries after the application of the operators in Figure 7 that were obtained by taking the ratio between the actual multiples and its prediction from the internal multiple attenuation algorithm algorithm: (A) The low absorptive Q-profile, (B) the intermediate Q-profile, and (C) the high absorptive Q-profile.*

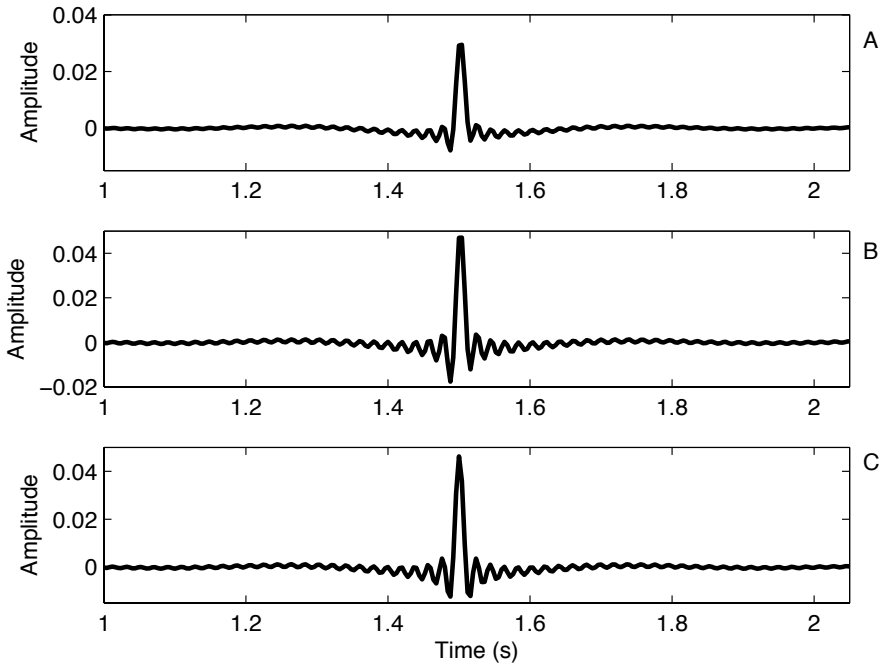

Figure 10: *The actual primary (A), the corrected primary (B) and the idealized primary (C), that was generated by dropping the transmission coefficients in the modeling, for the low attenuation case.*

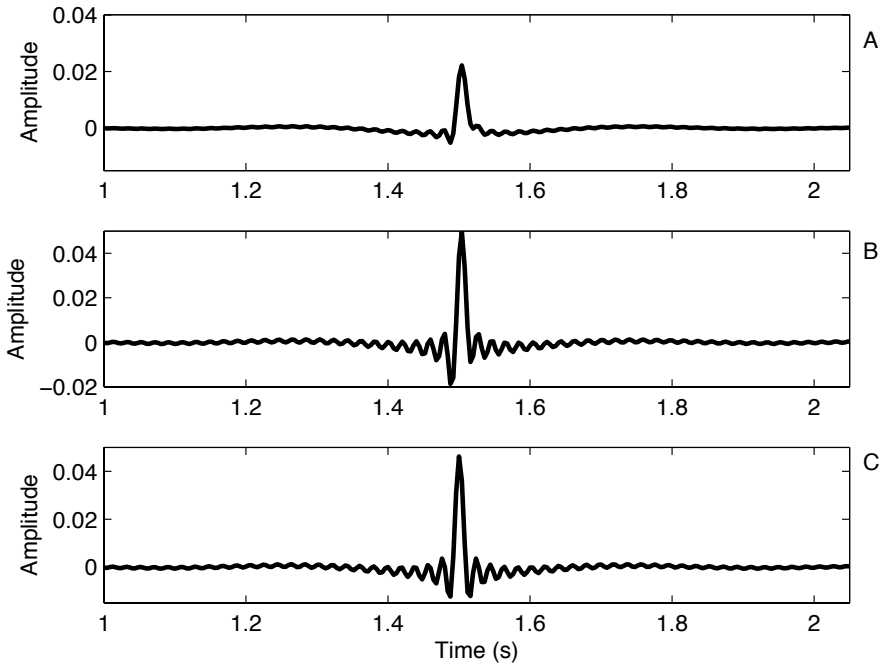

Figure 11: *The actual primary (A), the corrected primary (B) and the idealized primary (C), that was generated by dropping the transmission coefficients in the modeling for the medium attenuation case.*

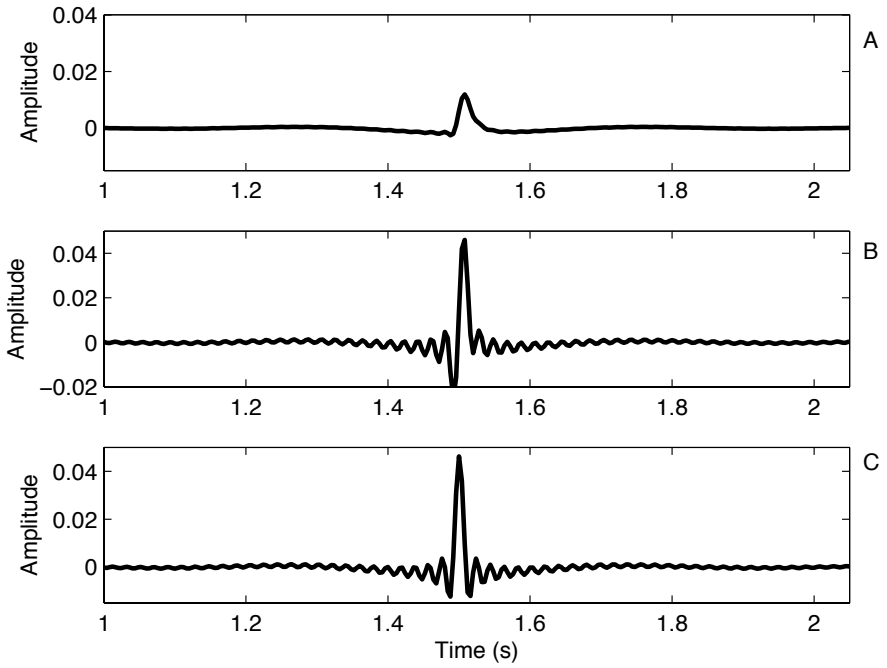

Figure 12: *The actual primary (A), the corrected primary (B) and the idealized primary (C), that was generated by dropping the transmission coefficients in the modeling, for the high attenuation case.*

The discrepancy between the corrected primaries and idealized primaries is of a form and magnitude expected given the absorptive correction approximation, which neglects the local transmission through the boundary nearest the primary's point of reflection.

5 Conclusions

In this paper we have presented a direct, data-driven procedure for correcting a primary for transmission losses using internal multiples and the output of the inverse scattering series internal multiple attenuation algorithm.

We have made particular mention and use of the distinction between situations involving significant absorption and situations that are largely acoustic or elastic. In spite of this broad categorization (that is found to be practically important), one of the strengths of the approach is that it will act to correct transmission losses *whatever* their physical origin or mechanism, without requiring a precise model. In this sense the approach is truly data-driven – the events in the data, in comparison to one another, "decide" what the transmission loss must be.

Simple numerical results are encouraging and motivate examination of the approach in the presence of more complex media, both absorptive and otherwise. The main tool in this approach, the internal multiple algorithm, is immediately applicable in multiple dimensions, and since the amplitude error is in terms of plane wave transmission coefficients, a plane wave decomposition of 2D and/or 3D data will likely suffice to extend the method. Nevertheless, detailed extension of the approach stands as ongoing and future research. For these reasons in particular, we identify field data testing as a medium-term to long-term goal, contingent on the fundamental study of the internal multiple attenuation amplitudes in multiple dimensions.

References

Aki, K. and P. G. Richards. *Quantitative Seismology.* 2nd edition. University Science Books, 2002.

Araújo, F. V. *Linear and non-linear methods derived from scattering theory: backscattered tomography and internal multiple attenuation.* PhD thesis, Universidade Federal da Bahia, 1994.

Araujo, F. V., A. B. Weglein, P. M. Carvalho, and R. H. Stolt. "Internal multiple attenuation." *56th Mtg., Assoc. Expl. Geophys. Session H036.* . 1994.

Carvalho, P. M., A. B. Weglein, and R. H. Stolt. "Examples of a non-linear inversion method based on the T-matrix of scattering theory: Application to multiple suppression." *61st Ann. Internat. Mtg: Soc. of Expl. Geophys., Expanded Abstracts.* . Soc. Expl. Geophys., 1991. 1319–1322.

Kaplan, Sam T., Billy Robinson, and Kristopher A. Innanen. "Optimizing internal multiple attenuation algorithms for large distributed computing systems." *Mission-Oriented Seismic Research Program (M-OSRP) Annual Report.* 2005.

Matson, K. H. *An inverse-scattering series method for attenuating elastic multiples from multi-component land and ocean bottom seismic data.* PhD thesis, University of British Columbia, 1997.

Nita, Bogdan G. and Arthur B. Weglein. Inverse scattering internal multiple attenuation algorithm in complex multi-d media. Technical report, Mission-Oriented Seismic Research Project, University of Houston, 2005.

Ramirez, A. C. *I - Inverse scattering subseries for 1:Removal of internal multiples and 2:Depth imaging primaries; II - Green's theorem as the foundation of interferomerty and guiding new practical methods and applications.* PhD thesis, University of Houston, 2007.

Ramirez, A. C. and A. B. Weglein. "An inverse scattering internal multiple elimination method: Beyond attenuation, a new algorithm and initial tests." *SEG Expanded Abstracts.* (2005): 2115–2118.

Ramirez, A. C. and A.B. Weglein. "Progressing the analysis of the phase and amplitude prediction properties of the inverse scattering internal multiple attenuation algorithm.." *J. of Seismic Expl.* 13 (2005): 283–301.

Weglein, A. B., F. A. Gasparotto, P. M. Carvalho, and R. H. Stolt. "An Inverse-Scattering Series Method for Attenuating Multiples in Seismic Reflection Data." *Geophysics* 62 (November-December 1997): 1975–1989.

Weglein, A. B. and K. H. Matson. "Inverse Scattering Internal Multiple Attenuation: An Analytic Example and Subevent interpretation." *SPIE Conference on Mathematical Methods in Geophysical Imaging.* 1998, 108–117.

Weglein, A. B. and R. H. Stolt. "Migration-Inversion Revisited." *The Leading Edge* Aug (1999): 950.

Weglein, A.B. and W.H. Dragoset. *Multiple Attenuation.* Geophysics reprint series. Soc. Expl. Geophys., 2005.

Weglein, Arthur B., Fernanda V. Araújo, Paulo M. Carvalho, Robert H. Stolt, Kenneth H. Matson, Richard T. Coats, Dennis Corrigan, Douglas J. Foster, Simon A. Shaw, and Haiyan Zhang. "Inverse Scattering Series and Seismic Exploration." *Inverse Problems* (2003): R27–R83.

Correcting primary amplitudes for plane wave transmission loss using internal multiple attenuation II: a direct procedure for the many-layers case

J. E. Lira, K. A. Innanen, A. C. Ramirez and A. B. Weglein, M-OSRP, University of Houston

Abstract

In the previous paper we described an iterative procedure for correcting reflected primary amplitudes for transmission losses through an unknown layered overburden. The correction operator is constructed using the inverse scattering series internal multiple attenuation algorithm, in particular making use of the discrepancy between its prediction and the actual amplitude of the multiples. The approach relies on the identification of events above the primary that is to be corrected. When the number of layers and events increases and/or the identification of individual events becomes more difficult, the procedure in this form may become inconvenient to apply. In this paper we specifically address this issue and present an approximation allowing the operator to be similarly calculated, but with the number of events to be identified, independent of the number of interfaces in a stratified overburden, reduced to one multiple and one primary. When the corrected primary is numerically compared to the idealized primary (with no transmission losses) it is verified that the approximation is incorrect only by the losses experienced in the lowest of the stack of many layers. Importantly, the correction procedure works correctly to correct either or both intrinsic and scattering attenuation, without knowing which mechanism is in place.

1 Introduction

In the previous paper we presented an iterative method for correcting the overburden effects on primary amplitudes without the need for such *a priori* information, using the inverse scattering series internal multiple attenuation algorithm (Araújo, 1994; Weglein et al., 1997, 2003). Synthetic testing of the methodology confirmed the potential practical value of the approach. However, one of the method's requirements, the need to isolate and analyze individual events reflecting from structures shallower than the primary to be corrected, will likely become burdensome when the number of contributing events and their proximity to one another grows. In this situation, *i.e.*, in a *many-layers* case, the procedure in its original form (Lira et al., 2008) may become inconvenient to apply.

In this paper we present an altered, approximate form for the procedure, which reduces the number of events to be identified to just the primary to be corrected and a single associated multiple. The approximation error of this new procedure is shown to be due only to the propagation losses within the bottom-most of a stack of layers, *i.e.*, the layer immediately above the reflector. The extension is therefore well-suited to the case when there are many layers overlying the bottom layer, in particular if they are thin enough to make isolation of the reflectors associated with them practically difficult. When the number of layers above a reflector to be corrected grows very large and the thickness of each layer falls below the dominant wavelength of the seismic wavefield, we point out that our procedure becomes, in effect, a correction of a component of the stratigraphic filtering effect.

2 A short review of the iterative procedure

The internal multiple attenuation algorithm is a series algorithm that attenuates sequentially higher orders of internal multiples in fully 3D pre-stack reflection data (Weglein et al., 2003). The first term of that algorithm in its 1D form for normal incidence data with a plane wave source (Araújo, 1994; Weglein et al., 1997) is:

$$b_{3IM}(k_z) = \int_{-\infty}^{\infty} dz_1' b_1(z_1') e^{ik_z z_1'} \times \int_{-\infty}^{z_1'-\epsilon} dz_2' b_1(z_2') e^{-ik_z z_2'} \int_{z_2'+\epsilon}^{\infty} dz_3' b_1(z_3') e^{ik_z z_3'}, \tag{1}$$

where ϵ is a small constant determined by the approximate length of the wavelet. The first term of the series provides the correct traveltime, and approximate amplitude, of the predicted multiples. The steps for producing the output are described in Weglein and Matson (1998), where $b_1(z)$ is the data in the pseudo-depth domain migrated with waterspeed. The term $b_1(z)$ is the input for equation 1. The algorithm can be understood in terms of sub-events, events that are combined to predict the internal multiple. In Figure 1 we schematically illustrate three events, two primaries, the shallower P_S and the deeper P_D, and one multiple, M_A. The algorithm combines the two primaries

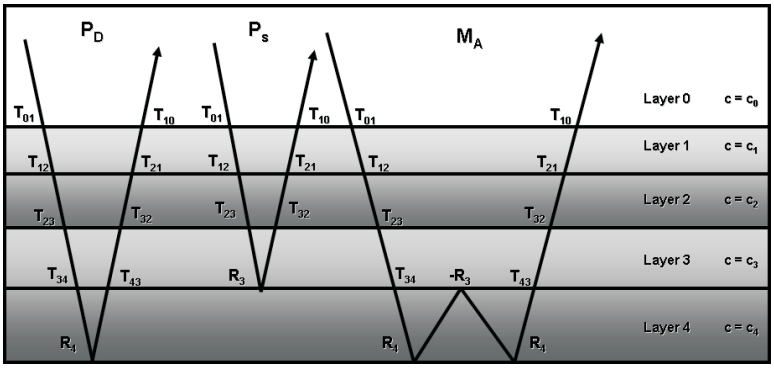

Figure 1: *A constant density 1-D model, comprised of a stack of five layers, where the velocities range from c_1 to c_4. Three events are displayed, two primaries P_S and P_D and one multiple M_A. The transmission and reflection coefficients are displayed above each interface, R_n signifying the reflection coefficient at the bottom of the n^{th} layer and T_{nm} signifying the coefficient of transmission from layer n to layer m.*

on the left to generate the multiple prediction, M_P. See Figure 2. In the previous chapter it was also pointed out that there is an excess of transmission coefficients in the prediction. In Figure 2, these excess transmission coefficients are circled. This excess of transmission coefficients within the prediction, which was discussed by Weglein and Matson (1998) and called the *amplitude factor* by Ramirez and Weglein (2005) is given by

$$\mathrm{AF}_n = \begin{cases} T_{01}T_{10} & \text{for n=1;} \\ \prod_{i=1}^{n-1}(T_{i,i-1}^2 T_{i-1,i}^2) T_{n,n-1}T_{n-1,n} & \text{for } 1 < n < J, \end{cases} \tag{2}$$

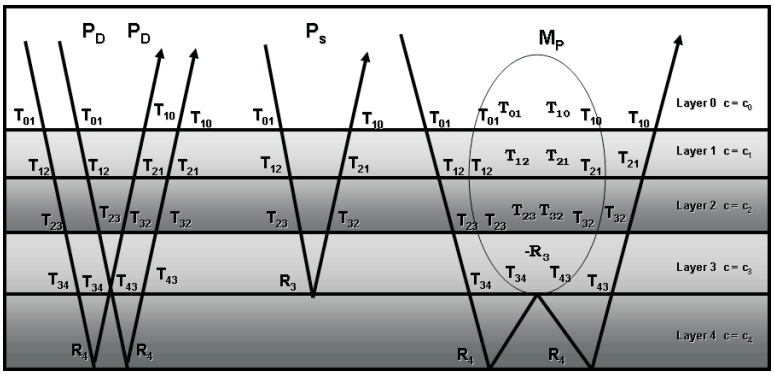

Figure 2: *A constant density 1-D model, comprised of a stack of five layers, where layers* 0 *to* 4 *with velocities ranging from* c_0 *to* c_4*, respectively. Three events are displayed, two primaries* P_S *and* P_D *and one multiple* M_A*. The transmission and reflection coefficients are displayed above each interface,* R_n *signifying the reflection coefficient at the]bottom of the nth layer and* T_{nm} *signifying the coefficient of transmission from layer* n *to layer* m*.*

where J is the total number of interfaces in the model. By comparing equation 2 and, for instance, Figure 2, AF can be seen to be related, but not equal, to the transmission losses experienced by a primary reflecting upward at the reflector where the multiple experienced its shallowest downward reflection.

We have used these relationships in the previous chapter to formulate a recursive procedure to correct the amplitudes of primaries for such overburden transmissions. The procedure involves iteratively calculating a primary correction operator (PCO) using the amplitude factor AF_n:

$$\begin{aligned} \mathrm{PCO}_n &\equiv \frac{\mathrm{PCO}_{n-1}}{AF_n}, \\ \mathrm{PCO}_0 &= 1, \end{aligned} \tag{3}$$

where n is the interface where the downward reflection of the multiple takes place; it is also proximal to where the upward reflection of the primary takes place. The operator PCO is defined in the frequency domain and is multiplicatively applied to the spectrum of the primary. After it has been applied, the amplitude of the primary was shown to be due solely to the reflection coefficient at the interface in question. The authors derived the amplitude factor for both elastic and absorptive media; the procedure for calculating the PCO is mathematically the same for both, but which primary is to be corrected with which multiple prediction was argued to depend on the medium model type.

3 Correction of primary amplitudes for transmission losses through an unknown, many-layered acoustic overburden

The recursive procedure showed potential practical value in numerical testing. However, one of the method's requirements, the need to isolate individual events reflecting from structures shallower

than the primary to be corrected, may become burdensome in a actual many-layers case. We begin by considering a few-layer case: the simple 1-D normal incidence acoustic/elastic layered medium displayed in Figure 3 showing two primaries P_1 and P_2, and two multiples, M_1 and M_2. A mathematical representation of primary P_1 is:

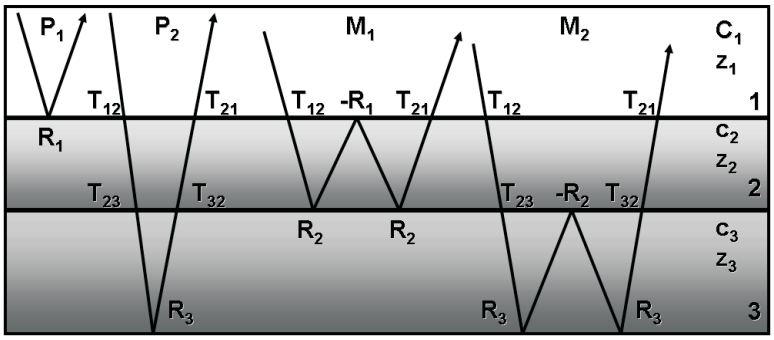

Figure 3: *A constant density 1-D model, comprised of a stack of three layers, where the velocities range from c_1 to c_3. Four events are displayed, two primaries P_1 and P_2 and two multiple M_1 and M_2. The transmission and reflection coefficients are displayed above each interface, R_n signifying the reflection coefficient at the bottom of the n^{th} layer and T_{nm} signifying the coefficient of transmission from layer n to layer m.*

$$P_1(t) = R_1\delta(t - t_1), \tag{4}$$

where $t_1 = \frac{2z_1}{c_0}$ is the arrival time and R_1 is the reflection coefficient at interface 1. In the frequency domain the same event can be described in terms of amplitude and phase as:

$$P_1(\omega) = e^{ik_1z_1}R_1e^{ik_1z_1}, \tag{5}$$

where z_1 is the depth of interface 1, $k_1 = \frac{\omega}{c_1}$, where ω is the angular frequency and c_1 is the velocity of layer 1. For the primary P_2 we write:

$$P_2(\omega) = e^{ik_1z_1}T_{12}e^{ik_2(z_2-z_1)}T_{23}e^{ik_2(z_3-z_2)}R_3e^{ik_2(z_3-z_2)}T_{32}e^{ik_2(z_2-z_1)}T_{21}e^{ik_1z_1}, \tag{6}$$

where T_{nm} represents the transmission coefficient from interface n to interface m, $k_2 = \frac{\omega}{c_2}$ and $k_3 = \frac{\omega}{c_3}$, and z_n represents the depth of interface n.

We next re-visit how the procedure of the last chapter would be carried out to correct the amplitude of P_2 for transmission losses (*i.e.*, $T_{12}T_{23}T_{32}T_{21}$). The iterative procedure requires the user to identify, first, P_1 and M_1, in order to calculate PCO_1 and then M_2, to calculate the AF_2 and from that the PCO_2, as in equation 3. At this point the issue is evident: the individual isolation of each contributing event becomes less straightforward the more layers there are in the overburden. The worst case scenario would be a many-layered medium where the thicknesses of the layers are below the resolving power of the data, e.g., where a train of short-period multiples below the seismic resolution can cause an absorption-like effect even in a fully elastic medium (O'Doherty and Anstey, 1971). The approximation we next introduce addresses this issue and allows the PCO calculation

to occur without an identification and isolated analysis of all events above the lowest layer in a multi-layer stack, leading to a correction operator able to correct even the stratigraphic filtering effect. To derive the approximation, I consider the multiple prediction M_P illustrated in Figure 2.

Since the time of the multiple prediction is exact, we omit the phase terms, and write the amplitude A_{M_P} for the predicted multiple M_P as:

$$A_{M_P} = \underbrace{[T_{01}T_{10}]^2[T_{12}T_{21}]^2[T_{23}T_{32}]^2[T_{34}T_{43}]}_{AF}.A_{M_A}, \tag{7}$$

where A_{M_A} is the amplitude of the actual multiple (M_A) in Figure 3, and AF is the amplitude factor. Comparing the transmission coefficients that conceal the reflection coefficient information, *i.e.*, R_3 in the primary P_S, in Figure 3, which is expressed by:

$$P_s(\omega) = e^{2ik_0z_0}e^{2ik_1(z_1-z_0)}e^{2ik_2(z_2-z_1)}e^{2ik_3(z_3-z_2)}[T_{01}T_{12}T_{23}]R_3[T_{10}T_{21}T_{32}], \tag{8}$$

with AF equation 7, they are seen to be differing only by an extra $[T_{34}T_{43}]$ in the latter. Recalling that AF is directly computable in terms of the data and the multiple prediction, suppose next the square root of AF were taken:

$$\left(\sqrt{AF}\right)^{-1} = \left([T_{01}T_{10}][T_{12}T_{21}][T_{23}T_{32}][\sqrt{T_{34}T_{43}}]\right)^{-1}. \tag{9}$$

Comparing this quantity with the transmission factors influencing the primary in equation 8, we argue that equation 9 can be made to act as an approximate multiplicative correction operator (*i.e.*, a new PCO):

$$PCO = (\sqrt{AF})^{-1} = \frac{1}{\left([T_{01}T_{10}][T_{12}T_{21}][T_{23}T_{32}][\sqrt{T_{34}T_{43}}]\right)}. \tag{10}$$

The missing $\sqrt{T_{34}T_{43}}$ produces an error due only to the last interface. In the many-layers case AF would be a function of the product of as many transmission coefficients as there are interfaces in the overburden. Since this number is large by definition in the many-layers case, we suggest that the approximation error of this procedure, applied in the right environment, to be small. Notice that in calculating this new, approximate operator PCO we have used as input only one multiple and its prediction, and have ignored all events reflecting above layer 3.

4 Correction of primary amplitudes for transmission losses through an unknown, many-layered absorptive overburden

We next extend the procedure to include the absorptive case. In the previous chapter, the absorption model of Aki and Richards (2002) is used:

$$k_n = \frac{\omega}{c_n}\left(1 + \frac{i}{2Q_n} - \frac{\log\left(\frac{\omega}{\omega_0}\right)}{\pi Q_n}\right), \tag{11}$$

where c_n is the velocity of the n-th layer, z_n is the depth, and $k_0 = \frac{\omega}{c_0}$. In the previous chapter the local transmission coefficients T_{nm} were re-written in a way that included absorption, which was assumed to dominate over "local" transmission through boundaries in an absorptive medium. The new transmission coefficients $\mathcal{T}_{nm}$ were written:

$$\mathcal{T}_{nm} = \underbrace{\left[\frac{2c_m\left(1+\frac{F(\omega)}{Q_m}\right)^{-1}}{c_n\left(1+\frac{F(\omega)}{Q_n}\right)^{-1}+c_m\left(1+\frac{F(\omega)}{Q_m}\right)^{-1}}\right]}_{T_{nm}} \overbrace{e^{-\frac{\omega}{2Q_nc_n}(z_n-z_{(n-1)})}}^{\text{Attenuation term}} e^{\frac{-i\omega}{\pi Q_nc_n}\log(\frac{\omega}{\omega_0})(z_n-z_{(n-1)})}, \quad (12)$$

where $F(\omega) = \frac{i}{2} - \frac{\log\frac{\omega}{\omega_0}}{\pi}$ and the term between the brackets is the local transmission coefficient T_{nm}. $\mathcal{T}_{nm}$ includes not only the local transmission coefficients T_{nm} but also the term, $e^{-\frac{\omega}{2Q_nc_n}(z_n-z_{(n-1)})}$, which represents attenuation in the n^{th} layer. The two primaries in Figure 5, P_S and P_D, can be expressed using the new transmission coefficients $\mathcal{T}_{nm}$:

$$\begin{aligned} P_s(\omega) &= e^{2ik_0z_0}T_{01}T_{10}e^{2ik_1'(z_1-z_0)}\mathcal{T}_{12}\mathcal{T}_{21}e^{2ik_2'(z_2-z_1)}\mathcal{T}_{23}\mathcal{T}_{32}e^{2ik_3'(z_3-z_2)} \quad (13)\\ &\quad \left[e^{-\frac{\omega}{Q_3c_3}(z_3-z_2)}e^{-\frac{2i\omega}{\pi Q_3c_3}\log(\frac{\omega}{\omega_0})(z_3-z_2)}\right]R_3,\\ P_d(\omega) &= e^{2ik_0z_0}T_{01}T_{10}e^{2ik_1'(z_1-z_0)}\mathcal{T}_{12}\mathcal{T}_{21}e^{2ik_2'(z_2-z_1)}\mathcal{T}_{23}\mathcal{T}_{32}e^{2ik_3'(z_3-z_2)} \quad (14)\\ &\quad \mathcal{T}_{34}\mathcal{T}_{43}e^{2ik_4'(z_4-z_3)}\left[e^{-\frac{\omega}{Q_4c_4}(z_4-z_3)}e^{-\frac{2i\omega}{\pi Q_4c_4}\log(\frac{\omega}{\omega_0})(z_4-z_3)}\right]R_4. \end{aligned}$$

where $k_n' = \frac{\omega}{c_n}$ is real. We again write the amplitude of the multiple prediction A_{M_P} (Figure 4) for the multiple M_A in Figure 5, now using absorptive coefficients:

$$A_{M_P} = [T_{01}T_{10}]^2[\mathcal{T}_{12}\mathcal{T}_{21}]^2[\mathcal{T}_{23}\mathcal{T}_{32}]^2[\mathcal{T}_{34}\mathcal{T}_{43}]A_{M_A}, \quad (15)$$

where A_{M_A} is the amplitude of the actual multiple M_A. That is, the amplitude factor for the absorptive medium case AF_a is:

$$AF_a = [T_{01}T_{10}]^2[\mathcal{T}_{12}\mathcal{T}_{21}]^2[\mathcal{T}_{23}\mathcal{T}_{32}]^2[\mathcal{T}_{34}\mathcal{T}_{43}]. \quad (16)$$

A comparison of AF_a in equation 16 to thetransmission coefficients concealing the reflection coefficient information in the primary P_S (equation 13), again reveals that they are equal but for the term $[\mathcal{T}_{34}\mathcal{T}_{43}]$. Following the same procedure for the acoustic/elastic case, we take the square root of AF and write an absorptive correction operator, the PCO_a as:

$$PCO_a = \left(\sqrt{AF_a}\right)^{-1} = \left([T_{01}T_{10}][\mathcal{T}_{12}\mathcal{T}_{21}][\mathcal{T}_{23}\mathcal{T}_{32}][\sqrt{\mathcal{T}_{34}\mathcal{T}_{43}}]\right)^{-1}. \quad (17)$$

To focus on its amplitude, I re-write equation 13 taking the absolute value of P_s:

$$|P_s(\omega)| = |T_{01}T_{10}||\mathcal{T}_{12}\mathcal{T}_{21}||\mathcal{T}_{23}\mathcal{T}_{32}||R_3|, \quad (18)$$

and, applying the PCO_a to $P_s(\omega)$, we generate the absorption-corrected primary P_{s_c}:

$$|P_{s_c}| = \left|\frac{1}{\sqrt{\mathcal{T}_{34}\mathcal{T}_{43}}}\right||R_3|. \quad (19)$$

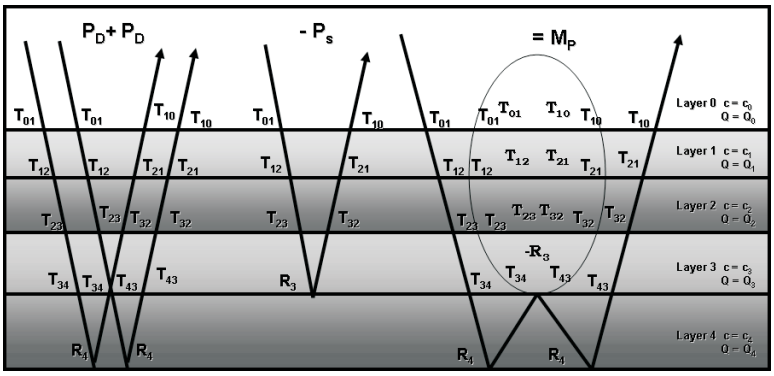

Figure 4: *How the inverse scattering series internal multiple attenuation algorithm combines the events P_S and P_D in Figure 5 to generate the multiple prediction M_P. The time of the multiple is predicted by summing the times of the deeper primaries (in this case, P_D and itself) and subtracting the time of the shallower primary (in this case P_S). The amplitude of the prediction is the product of the amplitudes of all events. The predicted time is exact, and the predicted amplitude has an excess of transmission coefficients (circled), when compared to the actual multiple.*

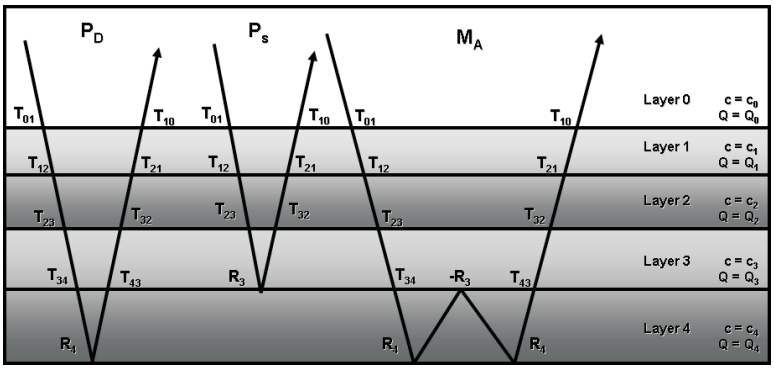

Figure 5: *A constant density 1-D model, comprised of a stack of five layers, where layers* 1 *to* 4 *are absorptive with the absorption parameters and velocities ranging from Q_1 to Q_4 and from c_1 to c_4, respectively, and layer* **0** *is non-absorptive,* i.e., *$Q_0 \to \infty$, and velocity $c = c_0$. Three events are displayed, two primaries P_S and P_D and one multiple M_A. The transmission and reflection coefficients are displayed above each interface, R_n signifying the reflection coefficient at the bottom of the n^{th} layer and T_{nm} signifying the coefficient of transmission from layer n to layer m.*

Using equation 12, the term in the denominator of equation 19 can be written as:

$$\sqrt{\mathcal{T}_{34}\mathcal{T}_{43}} = e^{-\frac{\omega}{2Q_3c_3}(z_3-z_2)}\left[\sqrt{T_{34}T_{43}}e^{\frac{-i\omega}{\pi Q_3c_3}\log(\frac{\omega}{\omega_0})(z_3-z_2)}\right]. \tag{20}$$

Equation 20 is again dominated by the real exponential $\left(e^{-\frac{\omega}{2Q_3c_3}(z_3-z_2)}\right)$, but, since in the many-layers case any individual layer's influence is expected to be small, it is true that:

$$|P_{s_c}| \approx |R_3|. \tag{21}$$

The operator PCO_a, which was built directly from data, is by this argument able to correct the transmission losses experienced by the primary P_S, to within an error that shrinks as the thickness of the lowest layer decreases. After the identification of the multiple whose downward reflection takes place at the same interface at which the primary to be corrected reflects - the main requirement of the approach - the procedure is fully data-driven. In the case of a many-layered medium, where the thickness of the layers may be below the seismic resolution, this direct approximate approach avoids the need for isolation of reflectors above the one generating P_S. This property suggests that the procedure is suitable for correcting absorptive effects generated by multiple reverberation in a thin, "many-layers" medium. The procedure is also independent of the physical mechanism causing the absorptive effects, and is specifically suitable for situations combining intrinsic and extrinsic ("scattering") attenuation. In the next section we present three numerical examples of the procedure in use.

5 Numerical examples

In this section we present three numerical examples of absorptive models, whose properties are described in Table 1. The models are comprised of a stack of horizontal layers. For the sake of clarity, we model only the four events shown in Figure 6. We then generate three zero-offset

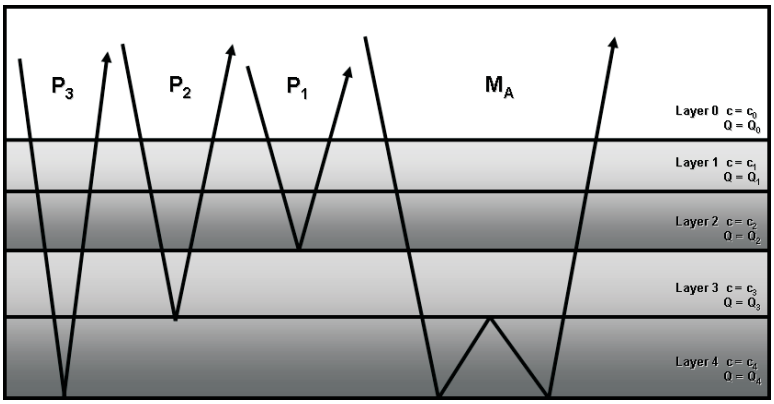

Figure 6: *A 1-D model comprised of a stack of horizontal absorptive layers, whose parameters are displayed in Table (1), and the four events, three primaries P_1, P_2 and P_3 and a multiple M_A illustrated in Figure 7.*

traces (Figure 7), run the internal multiple prediction algorithm, calculate the PCO with the direct procedure described in the previous section, and apply the operator to P_2 in Figure 8 to correct it for transmission losses.

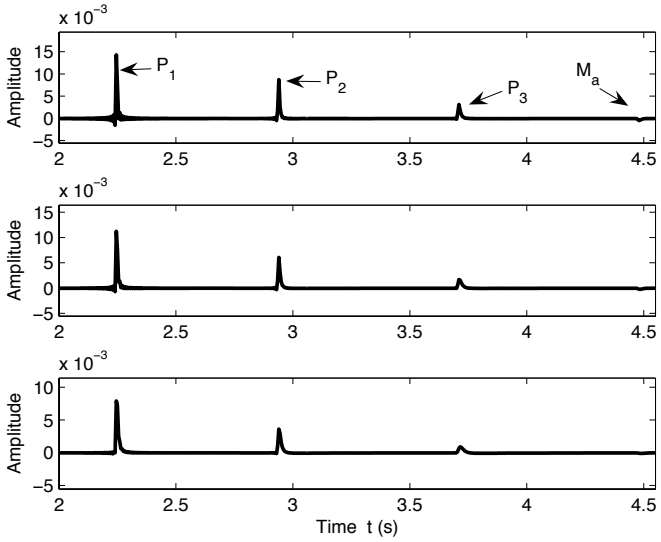

Figure 7: *An illustration of the three synthetic zero-offset traces generated using the parameters of Table* (1)*, showing four events, three primaries,* P_1*,* P_2*, and* P_3 *and one multiple* M_a*.* (A) *The low absorptive Q-profile,* (B) *the intermediate Q-profile, and* (C) *the high absorptive Q-profile.*

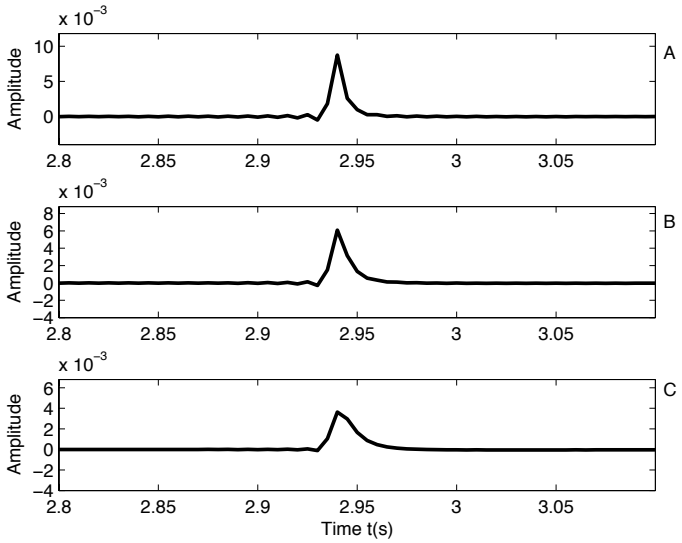

Figure 8: *An illustration showing in detail the primaries* P_2*, whose absorptive effects we want to correct with the direct procedure, for the Q-profiles listed in Table* 1*.* (A) *The low absorptive Q-profile,* (B) *the intermediate Q-profile, and* (C) *the high absorptive Q profile.*

Depth (m)	c (m/s)	A	B	C
000 - 600	1500	∞	∞	∞
600 - 1600	3300	650	400	250
1600 - 3100	3550	520	320	200
3100 - 4400	3750	390	240	150
4400 - 5900	3900	162.5	100	62.5
5900 - ∞	4000	97.5	60	37.5

Table 1. *Absorptive Earth models.*

The events to be corrected, P_2, are shown in Figure 8. The multiple M_A (Figure 7) that is to be used to correct P_2 is identified and isolated[1] for all three Q-profiles. The next step is to generate the multiple prediction, and this is done by using the data as the input for the internal multiple attenuation algorithm. With the multiple prediction and actual multiple available, both spectra are computed as shown in Figure 9.

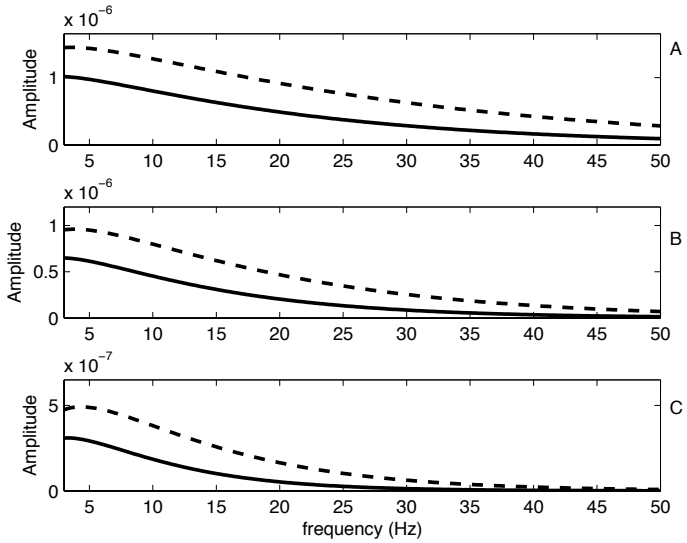

Figure 9: *An illustration showing the spectra of the actual multiple M_A(dashed curve), and the multiple prediction of the internal multiple attenuation algorithm (solid curve) for the three Q-profiles listed in Table* (1). (*A*) *The low absorptive Q-profile,* (*B*) *the intermediate Q profile, and* (*C*) *the high absorptive Q-profile. The ratio of each pair of spectra is used to construct the correction operator PCO.*

AF_a in equation 16 is calculated by taking the ratio of the spectra. Following equation 17 the square root of AF_a is next taken to calculate the PCO. The operator is illustrated in Figure 10.

[1]The internal multiple prediction algorithm itself acts as a useful tool for bootstrap identification of the needed multiples.

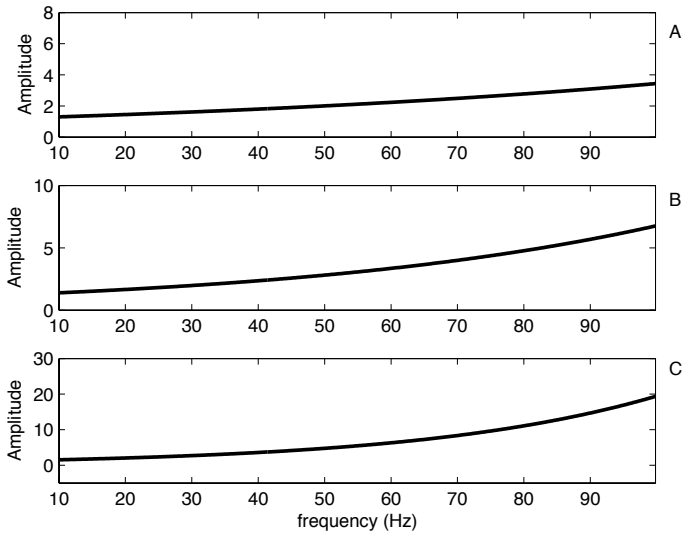

Figure 10: *An illustration showing the absolute value of the primary correction operators PCO, calculated using equation 17,* i.e.*, by taking the ratio of the spectra of the actual multiple and the internal multiple attenuation algorithm prediction, for the three Q-profiles listed in Table* 1. *(A) The low absorptive Q-profile, (B) the intermediate Q-profile, and (C) the high absorptive Q-profile.*

The final step is to apply the operator to the original primary, P_2, in order to correct it for the transmission losses along its path. Multiplying the spectrum of P_2 by the operator, PCO, the spectrum is corrected. In Figure 11 both spectra, the original spectrum of P_2 and the corrected spectrum, are shown. From the frequency domain, we go back to the time domain and display finally the corrected primary $P_{2C}(t)$, for all three Q-profiles of Table (1), Figure 12.

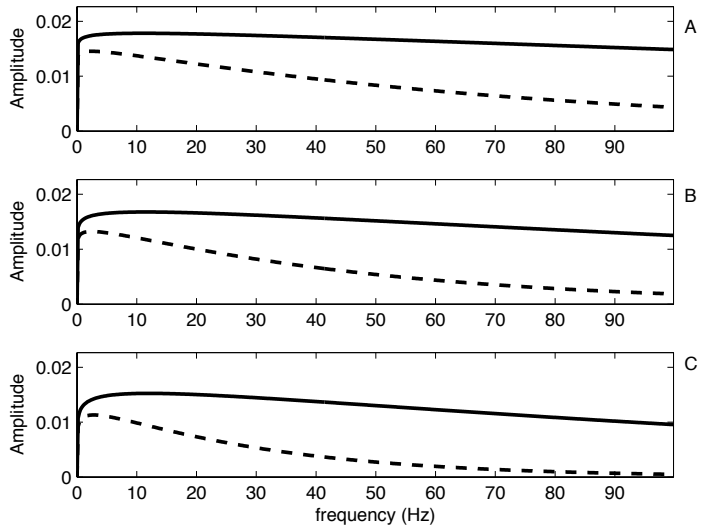

Figure 11: *An illustration comparing spectra of the original primary P_2 (dashed) and the corrected primary P_{2C} (solid), after the application of the primary correction operators PCO illustrated in Figure 10, for the three Q-profiles listed in Table* 1. *(A) The low absorptive Q-profile, (B) the intermediate Q-profile, and (C) the high absorptive Q-profile.*

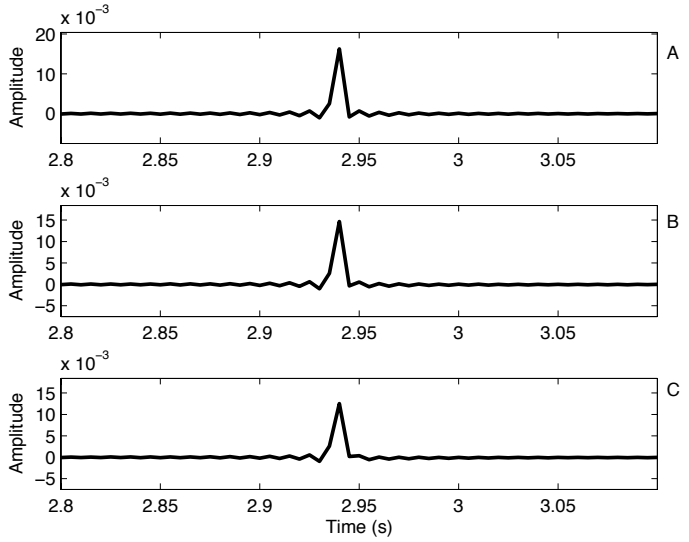

Figure 12: *An illustration of the corrected primaries P_{2C} in the time domain. (A) The low absorptive Q-profile, (B) the intermediate Q-profile, and (C) the high absorptive Q-profile.*

As this is a numerical exercise, and in order to evaluate the direct procedure, we numerically

generate an idealized primary P_{sId}, dropping all the transmission coefficients, and write it as follows:

$$P_{2Id}(\omega) = \underbrace{e^{2ik_0z_0}e^{2ik_1'(z_1-z_0)}e^{2ik_2'(z_2-z_1)}e^{2ik_3'(z_3-z_2)}}_{\Gamma} R_3. \tag{22}$$

We use equation 22 as a benchmark. The closer P_{2C} is to P_{2Id}, the more effective is the PCO and the direct procedure. Figures 13 to 15 display mosaics with the three primaries P_2, P_{2C} and P_{2Id} for all three Q-profiles of Table (1).

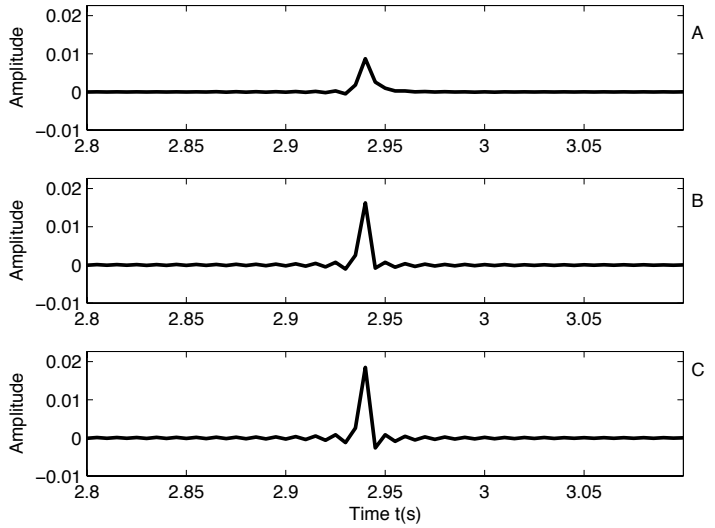

Figure 13: *An illustration* (A) *the original primary* P_2 *in the data,* (B) *the corrected primary* P_{2C}*, and* (C) *the idealized primary* P_{2Id} *without transmission losses for* Q*-profile* A *in Table* (1)*, the low attenuation case.*

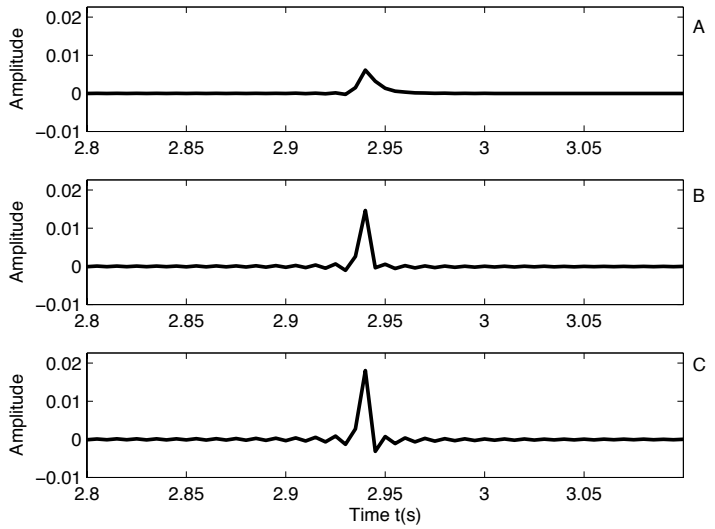

Figure 14: *An illustration* (A) *the original primary* P_2 *in the data,* (B) *the corrected primary* P_{2C}*, and* (C) *the idealized primary* P_{2Id} *without transmission losses for Q-profile B in Table* (1)*, the medium attenuation case.*

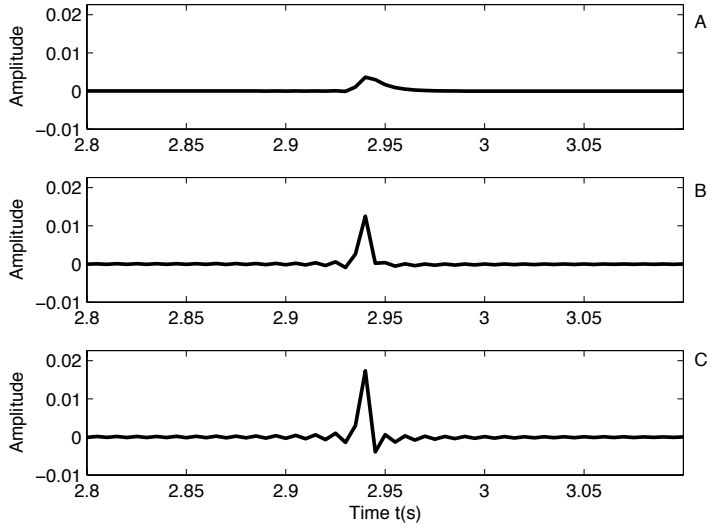

Figure 15: *An illustration* (A) *the original primary* P_2 *in the data,* (B) *the corrected primary,* P_{2C} *and* (C) *the idealized primary* P_{2Id} *without transmission losses for Q-profile C in Table* (1)*, the high attenuation case.*

Conclusions

We propose a direct method for compensating the losses experienced by the primaries in an absorptive medium using the inverse scattering series internal multiple attenuation algorithm (Araújo, 1994; Weglein et al., 1997). The direct procedure is based on our observations about the dependence of our iterative procedure (Lira et al., 2008) on event identification.

In the direct procedure the event identification requirement is reduced to the primary to be corrected and the associated multiple generated at the same interface. After the identification of the events all the procedure is data driven and the correction is determined solely by the characteristics of the data. All the losses above the bottom layer, layer 3 in Figure 6, are fully corrected. The number of layers above layer 3 does not affect or change the procedure, even if such layers are not resolvable by the seismic method. A good example of such situation is a thin layered medium with unresolvable short periods multiples causing an absorption-like effect. The losses in the last layer, layer 4 in Figure 6, were partially corrected; however, in a many-layered medium we expect such losses to be very small due to the small thicknesses of the layers. The procedure corrects the absorption independent of the mechanism that has generated such effects. Intrinsic attenuation and/or stratigraphic filtering effects are expected to be corrected in the same way.

References

Aki, K. and P. G. Richards. *Quantitative Seismology.* 2nd edition. University Science Books, 2002.

Araújo, F. V. *Linear and non-linear methods derived from scattering theory: backscattered tomography and internal multiple attenuation.* PhD thesis, Universidade Federal da Bahia, 1994.

Lira, J. E. M., K. A. Innanen, and A. B. Weglein. "Correction of primary amplitudes for plane-wave transmission loss through an acoustic or absorptive overburden with the inverse scattering series internal multiple attenuation algorithm: an initial study and 1D numerical examples." *Submitted to Geophysics* (2008).

O'Doherty, R. F. and N. A. Anstey. "Reflections on Amplitudes." *Geophysical Prospecting* 19 (1971): 430–458.

Ramirez, A. C. and A.B. Weglein. "Progressing the analysis of the phase and amplitude prediction properties of the inverse scattering internal multiple attenuation algorithm.." *J. of Seismic Expl.* 13 (2005): 283–301.

Weglein, A. B., F. A. Gasparotto, P. M. Carvalho, and R. H. Stolt. "An Inverse-Scattering Series Method for Attenuating Multiples in Seismic Reflection Data." *Geophysics* 62 (November-December 1997): 1975–1989.

Weglein, A. B. and K. H. Matson. "Inverse Scattering Internal Multiple Attenuation: An Analytic Example and Subevent interpretation." *SPIE Conference on Mathematical Methods in Geophysical Imaging.* 1998, 108–117.

Weglein, Arthur B., Fernanda V. Araújo, Paulo M. Carvalho, Robert H. Stolt, Kenneth H. Matson, Richard T. Coats, Dennis Corrigan, Douglas J. Foster, Simon A. Shaw, and Haiyan Zhang. "Inverse Scattering Series and Seismic Exploration." *Inverse Problems* (2003): R27–R83.

Aperture-compensated linear asymptotic imaging and testing as input for the nonlinear velocity independent depth imaging algorithms of the inverse scattering series: analysis and plans

Z. Wang, A. B. Weglein and F. Liu, M-OSRP, University of Houston

Abstract

Seismic imaging methods use seismic data measurements on the earth's surface to make inferences about the locations of subsurface reflectors. Any imaging method requires data on the measurement surface where the method's underlying theory predicts it will arrive. Full wave theory, like that underlying inverse scattering imaging methods, predicts wave energy everywhere on the measurement surface. When data collection is limited by economic and/or practical considerations, a compromise to wave theory using asymptotic analysis can be used to image limited data with a less complete theory. Wang et al. (2007) provides an in-line wave theoretic and cross-line asymptotic algorithm when the data is adequately sampled in the in-line direction but has a serious aperture limitation in the cross-line direction. In this note, we will continue to test this algorithm and use its result as the input for the nonlinear imaging algorithms of the inverse scattering series. The results show that this algorithm cannot provide accurate enough input, and one ad hoc approach is used to recover a more accurate value with some clear improvement.

1 Introduction

The inverse scattering series, a multidimensional direct inversion method, has been used to derive candidate direct nonlinear imaging algorithms that do not require the actual propagation velocity. In this series, α_1 is first order in the data, providing a linear approximation to the actual medium. Shaw and Weglein (2004) successfully isolated the leading order imaging subseries (LOIS) in the laterally invariant acoustic medium and Liu et al. (2005) derived the higher order imaging subseries (HOIS) in the laterally varying 2D and 3D acoustic media. These two algorithms are nonlinear and depend directly on the accuracy of α_1. Therefore, calculating α_1 accurately from the data D is an important step for the use of the algorithms.

Currently, data collection is often adequate in the in-line direction but has a serious aperture limitation in the cross-line direction because of economic and/or practical considerations. Based on the fundamentals of the wave theoretic algorithm (Liu et al., 2007) and the 2.5D finite-aperture migration (Stolt and Benson, 1986), we provided in Wang et al. (2007) an algorithm which is wave theory imaging in the direction that has adequate collection, and asymptotic migration in the aperture-limited cross-line direction. In this note, we test this algorithm in the 2D constant-density acoustic case, which has the aperture-limited cross-line direction, and input the result to the nonlinear imaging algorithms of the inverse scattering series to see how it satisfies the requirements of the nonlinear algorithms stated above. The results show that it cannot satisfy the requirement well. We address this by attempting to recover a more accurate value with an ad hoc approach, with some clear improvement.

2 Aperture compensated algorithm

Following the steps in Wang et al. (2007), we will provide the algorithm for the 2D case which just has the aperture-limited cross-line direction.

For a 2D constant-density acoustic medium, the wave equations for the actual and reference wave field are expressed by:

$$(\frac{\partial^2}{\partial x^2}+\frac{\partial^2}{\partial z^2}+\frac{\omega^2}{c^2(x,z)})G(x,z,x_s,z_s,\omega)=\delta(x-x_s)\delta(z-z_s),$$

$$(\frac{\partial^2}{\partial x^2}+\frac{\partial^2}{\partial z^2}+\frac{\omega^2}{c_0^2})G_0(x,z,x_s,z_s,\omega)=\delta(x-x_s)\delta(z-z_s).$$

Using ISS order-by-order logic, for the first order the equation is:

$$D(x_g,x_s,\omega)=G(x_g,z_g,x_s,z_s,\omega)-G_0(x_g,z_g,x_s,z_s,\omega)=G_0V_1G_0.$$

Fourier transform over x_g and x_s on both sides,

$$D(k_g,-k_s,\omega)=-\frac{\omega^2}{4q_gq_sc_0^2}\alpha_1(k_g-k_s,-(q_g+q_s))=-\frac{\omega^2}{4c_0^2q_gq_s}\alpha_1(k_m,-q_z). \tag{1}$$

The quantities $k_m,\ q_z$ used here and k_h to be used later are defined as following:

$$k_m=k_g-k_s,\ k_m=k_g+k_s,\ q_z=q_g+q_s.$$

The problem for solving for α_1 is overdetermined because D has one more degree of freedom than α_1. We will use that to compensate for the limited aperture.

In general, the inversion of α_1 can be written as a linear combination of the data:

$$\alpha_1(k_m,q_z)=\int_{-\infty}^{\infty}dk_hL(k_m,k_h,q_z)D(k_g,-k_s,\omega). \tag{2}$$

Using equation 1 and equation 2 together, we get the restriction function L:

$$1=-\int_{-\infty}^{\infty}dk_h\frac{k^2}{4q_gq_s}L(k_m,k_h,q_z). \tag{3}$$

If we define $\beta=\frac{k_m}{q_z}$ and $\gamma=\frac{k_h}{q_z}$, then q_g, q_s and q_z can be expressed as functions of β, γ and ω:

$$q_g=\frac{q_z}{2}(1-\beta\gamma),\qquad q_s=\frac{q_z}{2}(1+\beta\gamma),\qquad \frac{\omega}{c_0}=\frac{q_z}{2}\sqrt{(1+\beta^2)(1+\gamma^2)}.$$

Plugging into equation 3,

$$1=-\frac{\omega/c_0}{2}\int_{-\infty}^{\infty}d\gamma\frac{\sqrt{(1+\beta^2)(1+\gamma^2)}}{1-\beta^2\gamma^2}L(\omega,\beta,\gamma). \tag{4}$$

There are many choices, one of which is:

$$L(k_m, k_h, q_z) = -\frac{2c_0}{\omega}\frac{1-\beta^2\gamma^2}{\sqrt{(1+\beta^2)(1+\gamma^2)}}\cdot\frac{1}{\sqrt{2\pi}c}e^{-\frac{(\gamma-b)^2}{2c^2}}. \tag{5}$$

where b and c can take any value except $c \neq 0$. Here we use a Gaussian distribution instead of a boxcar function (Wang et al., 2007) to make L smoother at the boundary.

Inverse Fourier transforming equation 2 from the $k_m,\ q_z$ domain to the $x,\ z$ domain:

$$\alpha_1(x,z) = \int_{-\infty}^{\infty} dk_h \int_{-\infty}^{\infty} dk_m \int_{-\infty}^{\infty} dq_z e^{i(k_m x - q_z z)} L(k_m, k_h, q_z) \frac{1}{(2\pi)^2} \int_{-\infty}^{\infty} dx_g \int_{-\infty}^{\infty} dx_s e^{i(k_s x_s - k_g x_g)} D(x_g, x_s, \omega).$$

Changing the integration variables from (k_m, k_h, q_z) to (k_g, k_s, ω) and the order of integration:

$$dk_m dk_h = 2dk_g dk_s,\ dq_z = \frac{q_z \omega d\omega}{c^2 q_g q_s}.$$

$$\alpha_1(x,z) = \int_{-\infty}^{\infty} dx_g \int_{-\infty}^{\infty} dx_s \int_{-\infty}^{\infty} d\omega \frac{1}{c_0} D(x_g, x_s, \omega) I, \tag{6}$$

where

$$I = \frac{1}{(2\pi)^2} \int_{-\infty}^{\infty} dk_g \int_{-\infty}^{\infty} dk_s e^{-i[k_g(x_g - x) + q_g z]} e^{-i[k_s(x - x_s) + q_s z]} \frac{2\omega q_z}{c_0 q_g q_s} L(k_m, k_h, q_z).$$

Making the stationary phase approximation to k_g, (the quantities with hats are the values at the stationary points)

$$\int_{-\infty}^{\infty} dk_g A(k_g) e^{i h_g} \approx A(\hat{k}_g) \sqrt{\frac{2i\pi}{\hat{h}_g''}} e^{i\hat{h}_g},$$

we obtain :

$$h_g = -[k_g(x_g - x) + q_g z] \qquad h_g' = -[(x_g - x) - \frac{k_g z}{q_g}] \qquad h_g'' = \frac{z k^2}{q_g^3}$$

$$\hat{k}_g = \frac{x_g - x}{r_g} k \qquad \hat{h}_g = -r_g k \qquad \hat{h}_g'' = r_g^3/(z^2 k).$$

The same thing for k_s, and the final result for I is:

$$I = \frac{i\omega}{\pi c_0} e^{-iw(r_g + r_s)/c_0} \frac{(r_g + r_s) z}{(r_g r_s)^{3/2}} L(\hat{k}_m, \hat{k}_h, \hat{q}_z). \tag{7}$$

Plugging equation 5 and equation 7 into equation 6

$$\begin{aligned}\alpha_1(x,z) &= -\int_{-\infty}^{\infty} dx_s \int_{-\infty}^{\infty} dx_g \frac{2i}{\pi} \frac{rz}{(r_g r_s)^{3/2}} \frac{1-\beta^2\gamma^2}{\sqrt{(1+\beta^2)(1+\gamma^2)}} \cdot \frac{1}{\sqrt{2\pi}c} e^{-\frac{(\gamma-b)^2}{2c^2}} \int_{-\infty}^{\infty} d\omega \frac{1}{c_0} e^{-iwr/c_0} D(x_g, x_s, \omega) \\ &= -\frac{2i}{c_0 \pi} \int_{-\infty}^{\infty} dx_s \int_{-\infty}^{\infty} dx_g \frac{rz}{(r_g r_s)^{3/2}} \frac{1-\beta^2\gamma^2}{\sqrt{(1+\beta^2)(1+\gamma^2)}} \cdot \frac{1}{\sqrt{2\pi}c} e^{-\frac{(\gamma-b)^2}{2c^2}} D(x_g, x_s, r/c_0) \end{aligned} \tag{8}$$

If we choose some appropriate values for b and c, e.g. $b = \frac{\gamma_1+\gamma_2}{2}$ and $c = \frac{\gamma_2-\gamma_1}{4}$ where γ_1 and γ_2 are the values of γ on the boundary, the contribution of the data outside the aperture would be small,

$$\alpha_1(x,z) \approx -\frac{2i}{c_0 \pi} \int_{-\infty}^{\infty} dx_s \int_{x_s+h_1}^{x_s+h_2} dx_g \frac{rz}{(r_g r_s)^{3/2}} \frac{1-\beta^2\gamma^2}{\sqrt{(1+\beta^2)(1+\gamma^2)}} \cdot \frac{1}{\sqrt{2\pi}c} e^{-\frac{(\gamma-b)^2}{2c^2}} D(x_g, x_s, r/c_0) \tag{9}$$

3 Test of algorithm using a one-interface model

We start from the simplest case, a one-interface model, to test how this algorithm works. The model is shown in Figure 1. The location for the interface and the velocity for each layer are shown in the figure. Figure 2 is the shot gather we get using the finite-difference method. The receivers are spread on one side of the source. We have also tested the algorithm using split-spread data but there is little change, so we will use just the towed geophone data below.

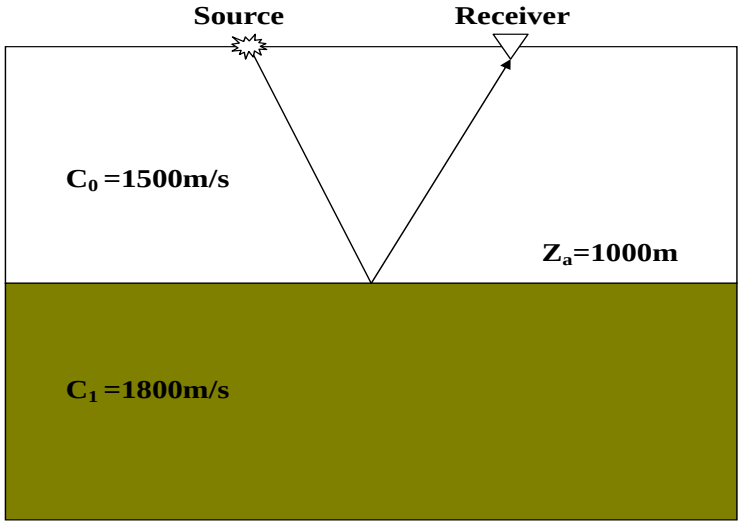

Figure 1: Model One: One-interface model

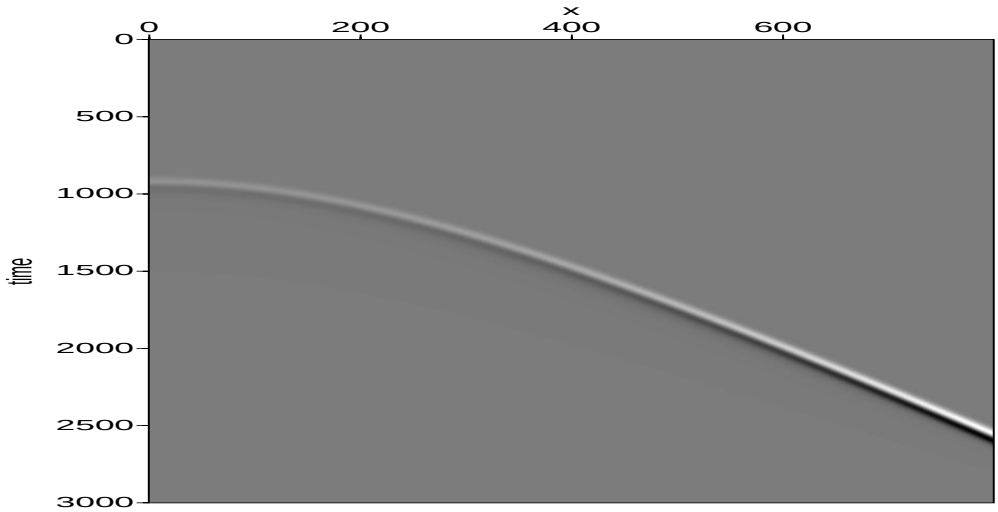

Figure 2: Shot gather

The reflection coefficient has the following form (Keys, 1989):

$$R(\theta) = \frac{(c_1/c_0)\sqrt{1-\sin^2\theta} - \sqrt{1-(c_1^2/c_0^2)\sin^2\theta}}{(c_1/c_0)\sqrt{1-\sin^2\theta} + \sqrt{1-(c_1^2/c_0^2)\sin^2\theta}},$$

here $tan\theta = \frac{|x_g - x_s|}{2z_a}$.

When $\theta = 0$, the ideal value of α_1 for the second layer is (Zhang, 2006):

$$\alpha_1(\theta) = 4R(\theta)\cos^2\theta H(z-a) \approx 0.3636. \tag{10}$$

Figure 3 is the result of α_1 using this aperture compensated linear asymptotic imaging algorithm. In order to see the amplitudes of α_1 more clearly, we pick the line at $x = 2000m$ in Figure 3 and draw their amplitudes in Figure 4.

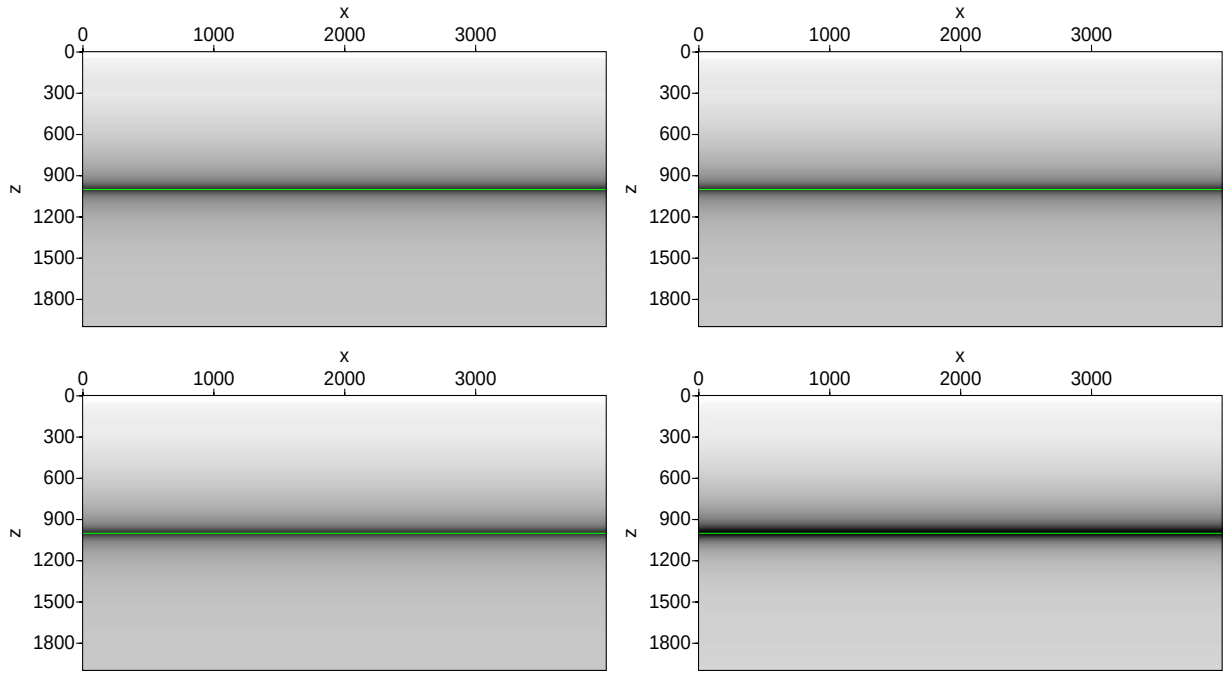

Figure 3: The imaging result of α_1 for Model 1 with *apertures* = $50m$(upper left), $250m$(upper right), $1000m$(lower left), $4000m$(lower right).

From Figure 3 and Figure 4, we see that the form of α_1 in a vertical line is a peak with long tails in both directions. The depth of the interface is correctly located by the peaks in all four different aperture cases. This is because we have just one interface, and knowing the water speed is enough to predict its location. But the form of α_1 differs from the case of fully collected data, which will be a Heaviside function (Zhang, 2006), and the amplitudes, even for the largest aperture, are much smaller than the value calculated in equation 10.

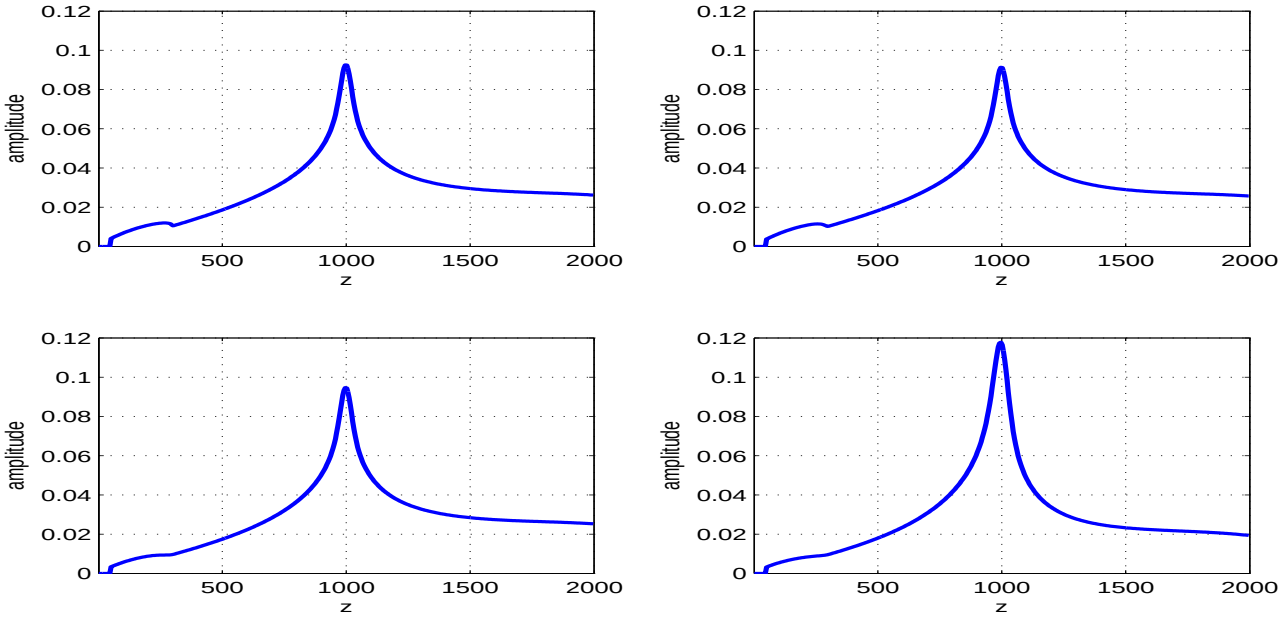

Figure 4: Amplitudes of α_1 at the line $x = 2000m$ with $apertures = 50m$(upper left), $250m$(upper right), $1000m$(lower left), $4000m$(lower right).

4 Test of algorithm using a two-interface model

We have seen that in the one-interface model case, although we can locate the interface correctly, the form and amplitudes of α_1 differ from what are analytically expected.

Next we consider a more complex model, the two-interface model shown in Figure 5, where the location for each interface and the velocity for each layer are labeled. Here we will not be able to migrate the second interface correctly, and would use the nonlinear imaging algorithms, (which only depend on α_1,) to improve the result.

The linear imaging result, α_1, is shown in Figure 6 for four different aperture cases and Figure 7 is also picking the line at $x = 2000m$ in Figure 6 and drawing their amplitudes. We see that the first interface is correctly located but the second interface is not, which is expected. The amplitude of α_1 is again different from its expected full-wave theoretic amplitude. Also, the second interface is dimmed by the tail of the first interface. Figure 8 is the result of using the higher order imaging subseries (HOIS) algorithm. We can see that it moves the second interface towards the desired location but not significantly. It also moves the first interface, an undesired result.

5 Linear imaging in the presence of a wavelet

In this algorithm each datum can be considered to be scattered back from any point on an ellipse, one of which is real. In the previous section, the data with a Gaussian wavelet, used to simulate the δ function, are always positive. The values contributing to the wrong place will be added up and

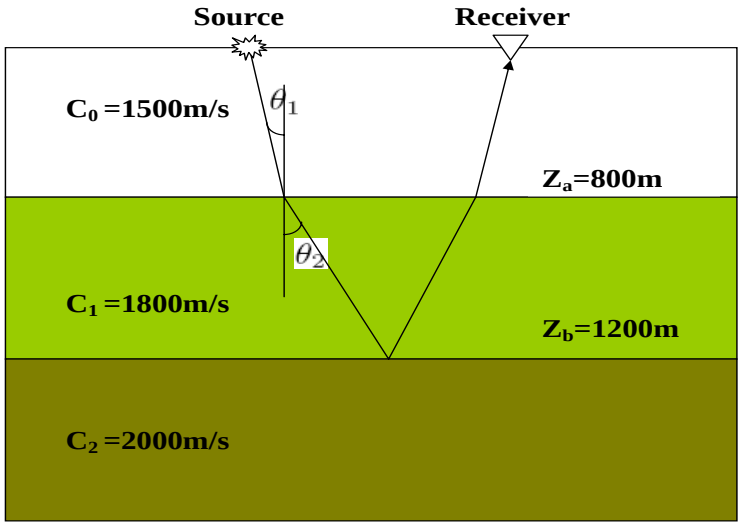

Figure 5: Model Two: Two-interface model

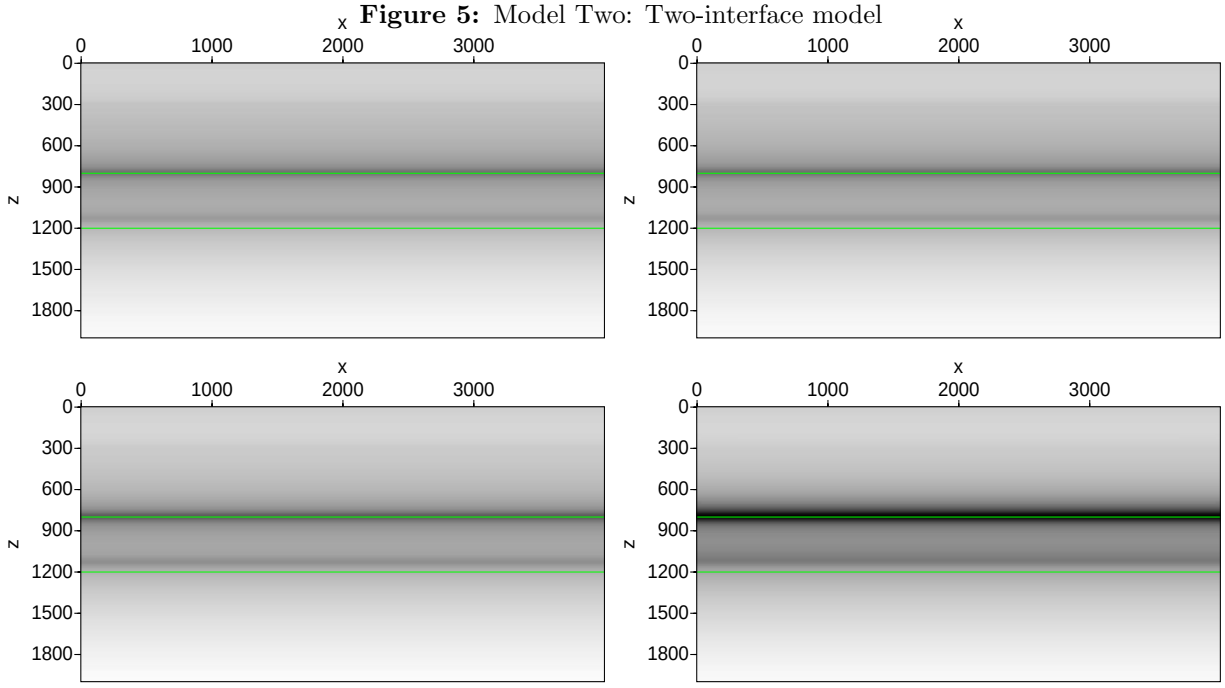

Figure 6: The imaging result of α_1 for Model 2 with *apertures* = $50m$(upper left), $250m$(upper right), $1000m$(lower left), $4000m$(lower right).

cannot be cancelled. That is why there are long tails around the peak at the interface. If we use a vibrating wavelet such as the derivative of a Gaussian function, the positive value (corresponding to the positive part in the wavelet) or the negative value (corresponding to the negative part in the wavelet) will be added up only at the correct locations, because at these locations the scatterers are real and the data show their properties. At the wrong locations, the scatterers are imaginary and different data show different properties. Some data contribute positively and the others contribute negatively, so they will cancel each other. The results are shown in Figure 9 and Figure 10.

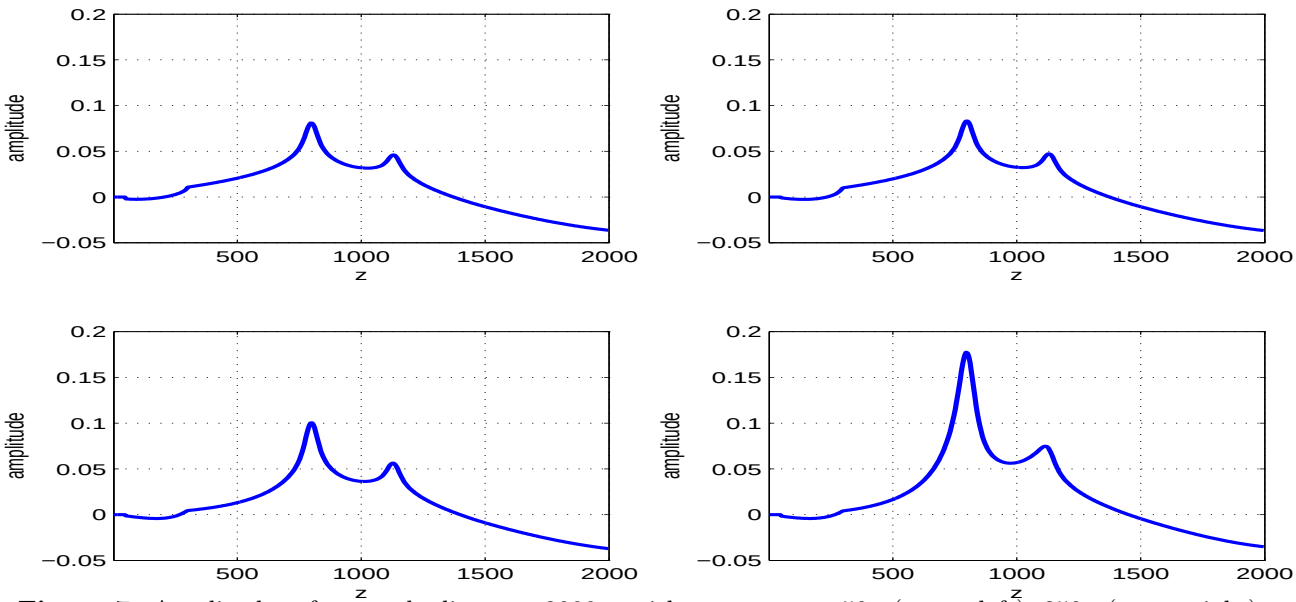

Figure 7: Amplitudes of α_1 at the line $x = 2000m$ with $apertures = 50m$(upper left), $250m$(upper right), $1000m$(lower left), $4000m$(lower right).

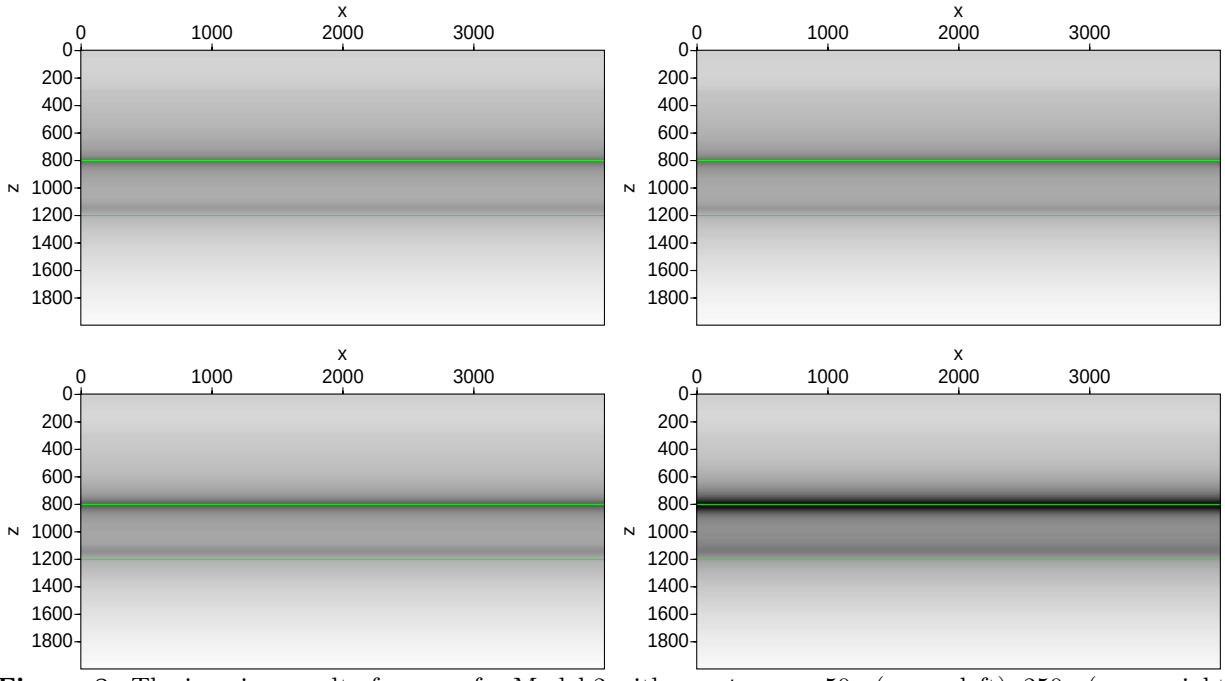

Figure 8: The imaging result of α_{HOIS} for Model 2 with $apertures = 50m$(upper left), $250m$(upper right), $1000m$(lower left), $4000m$(lower right).

Compared with Figure 6 and 7, the results are much clearer. But this result cannot be used as the input for the HOIS algorithm because at the interface it is almost symmetric and the integral of

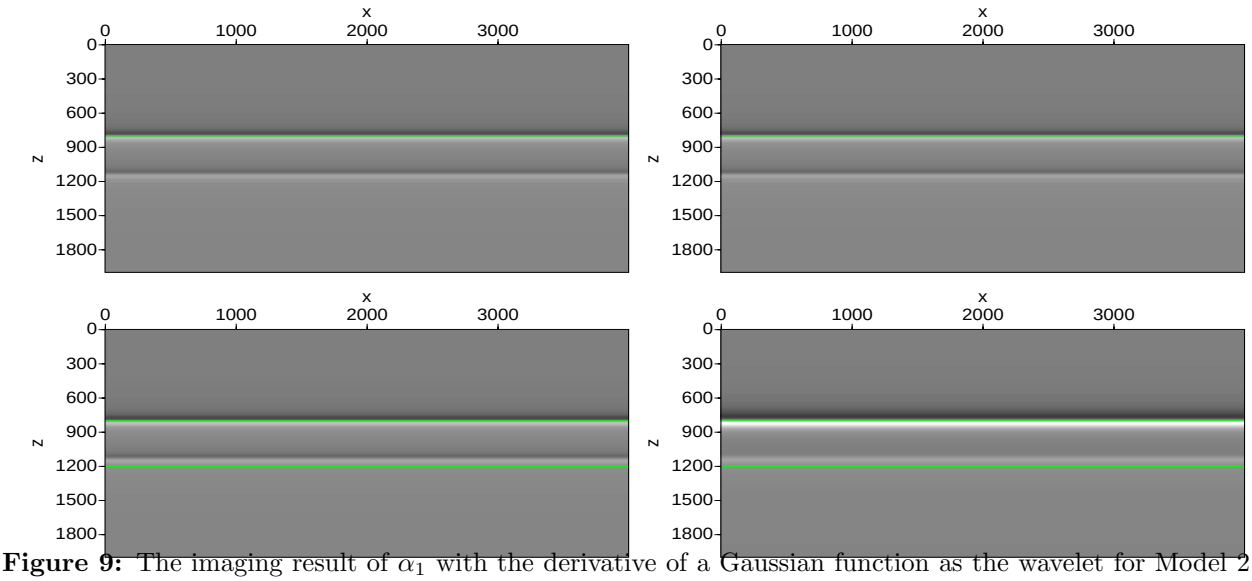

Figure 9: The imaging result of α_1 with the derivative of a Gaussian function as the wavelet for Model 2 with $apertures = 50m$(upper left), $250m$(upper right), $1000m$(lower left), $4000m$(lower right).

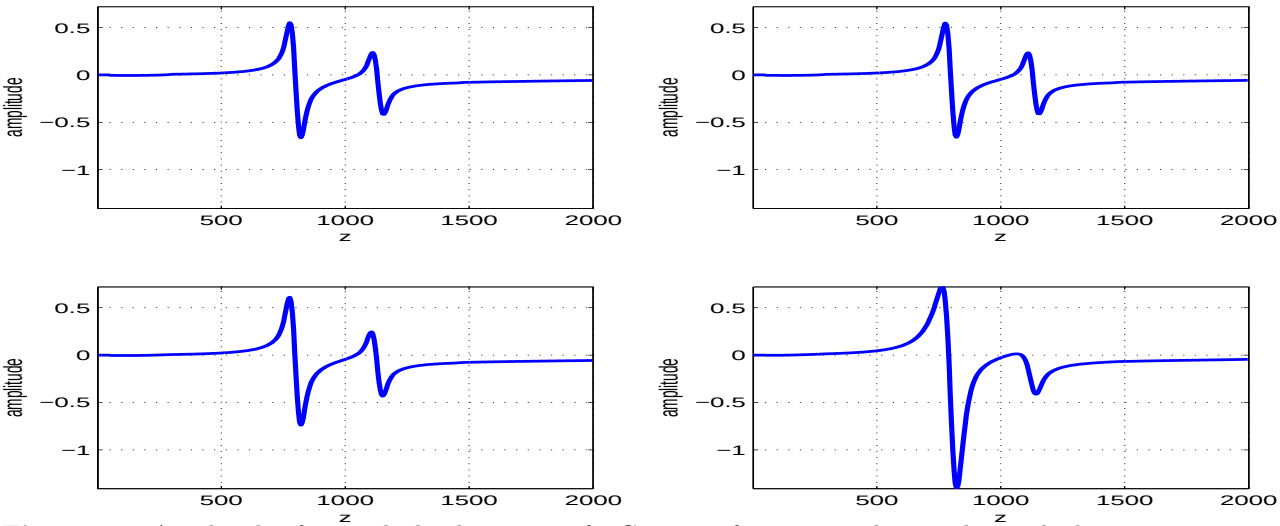

Figure 10: Amplitude of α_1 with the derivative of a Gaussian function as the wavelet at the line $x = 2000m$ with $apertures = 50m$(upper left), $250m$(upper right), $1000m$(lower left), $4000m$(lower right).

α_1 is very small.

6 Revised α_1

We have seen that this algorithm has changed the properties of α_1. HOIS, using α_1 as the input, can do little to improve the imaging in this case. Can we better or more accurately recover α_1? One method we have tried is as follows: For the imaging result of α_1, first find the interfaces. Then

calculate the root mean square (RMS) value near the interface and use it as the α_1 for the next layer. Here, for the range to do the RMS we have chosen three times the length from the trough to the peak. The revised α_1 is shown in Figure 11 and Figure 12, and the result of α_{HOIS} using the revised α_1 is shown in Figure 13.

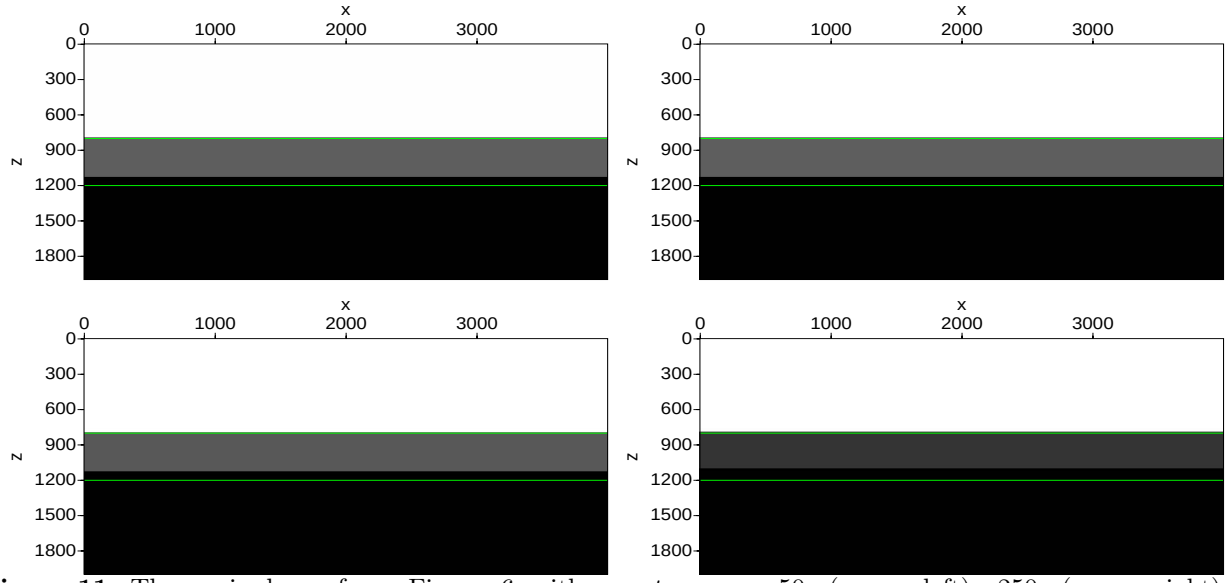

Figure 11: The revised α_1 from Figure 6 with $apertures = 50m$(upper left), $250m$(upper right), $1000m$(lower left), $4000m$(lower right).

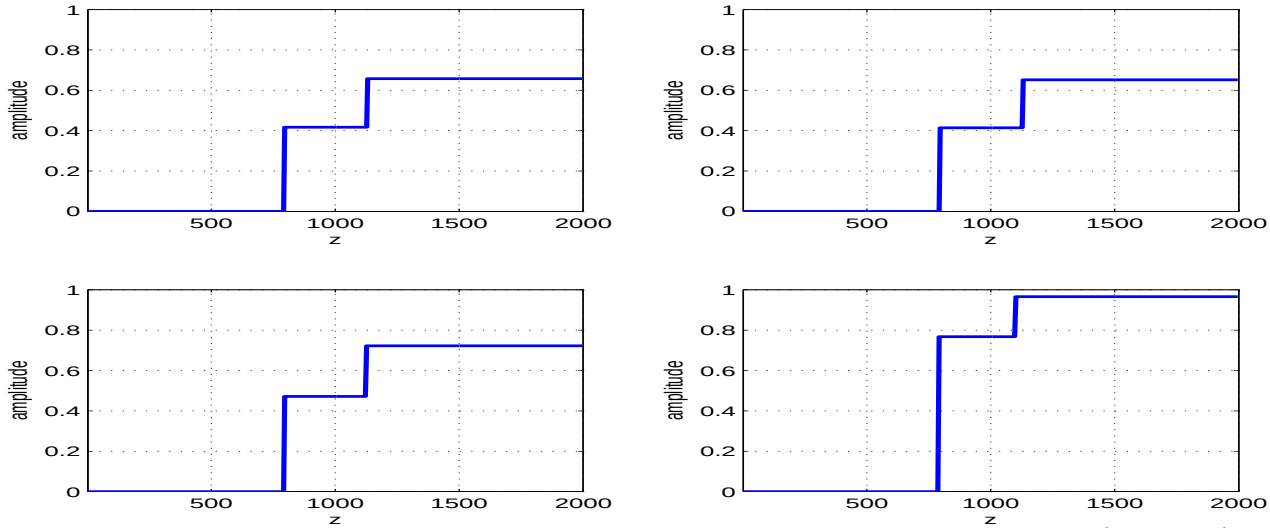

Figure 12: Amplitude of revised α_1 in Figure 11 at the line $x = 2000m$ with $apertures = 50m$(upper left), $250m$(upper right), $1000m$(lower left), $4000m$(lower right).

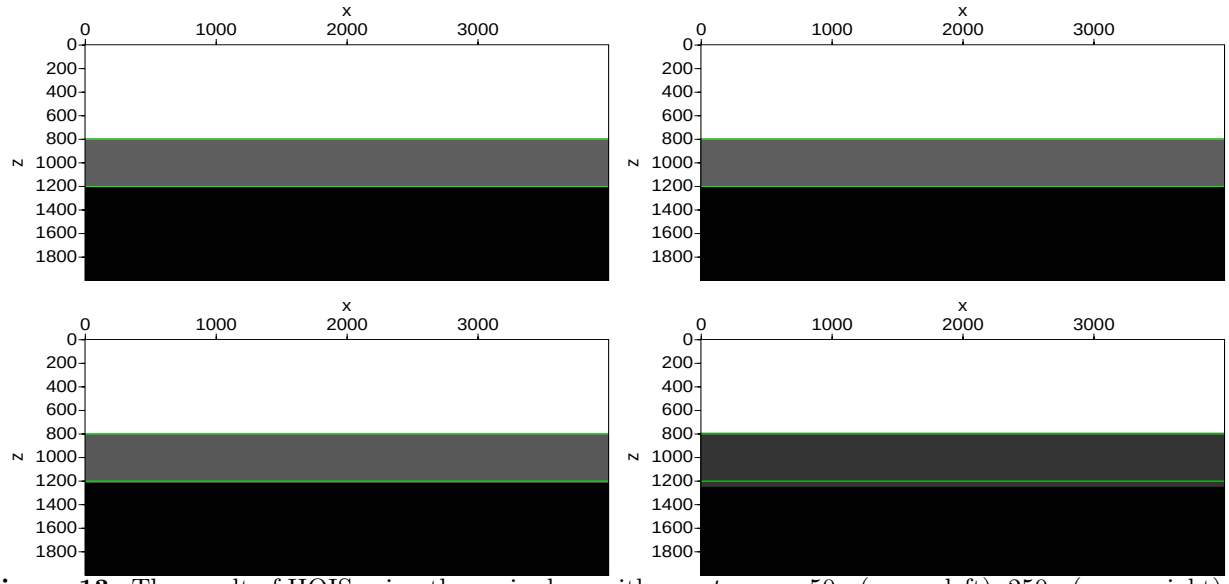

Figure 13: The result of HOIS using the revised α_1 with $apertures = 50m$(upper left), $250m$(upper right), $1000m$(lower left), $4000m$(lower right).

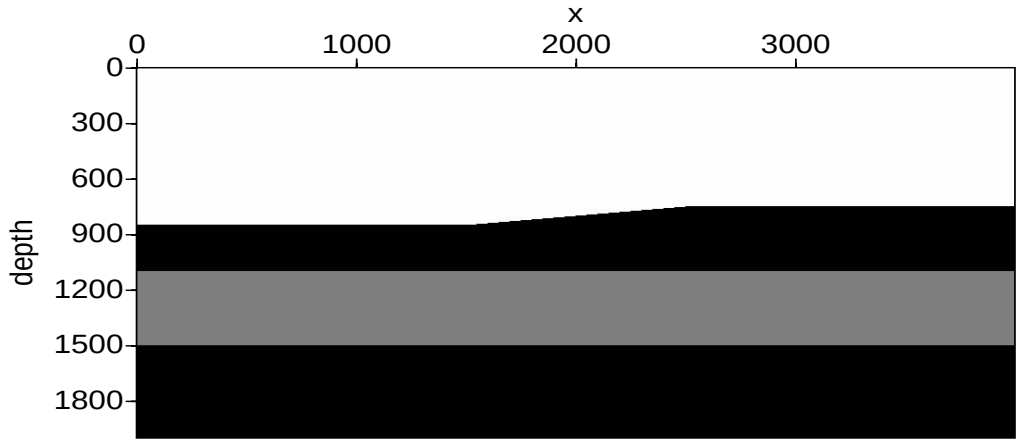

Figure 14: Model three: Three-interface model

7 Test of algorithm using a three-interface model

We also tested this using the three-interface model shown in Figure 14. Figure 15 and Figure 16 are the imaging result and the amplitudes of the result at the line $x = 2000m$. In the step of getting the revised α_1 with aperture=$4000m$, however, we cannot find the trough for the second interface because of the tail of the first interface. Therefore, the method used before cannot be used for the aperture=$4000m$ case here. But for the aperture=$50m$, $250m$ and $1000m$ cases, the results are still encouraging.

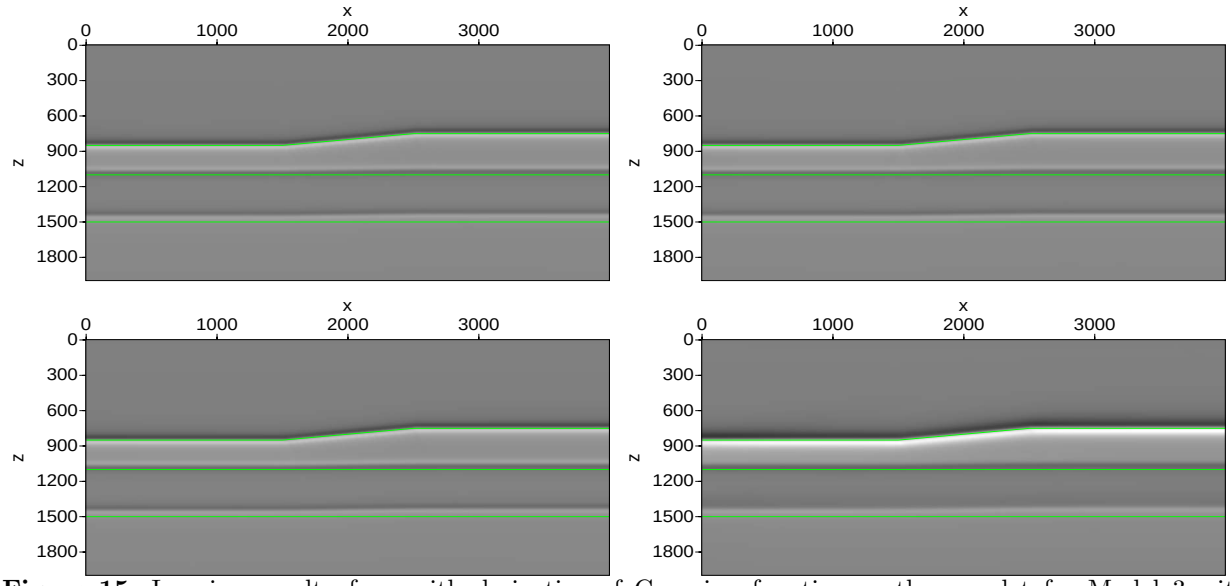

Figure 15: Imaging result of α_1 with derivative of Gaussian function as the wavelet for Model 3 with $apertures = 50m$(upper left), $250m$(upper right), $1000m$(lower left), $4000m$(lower right).

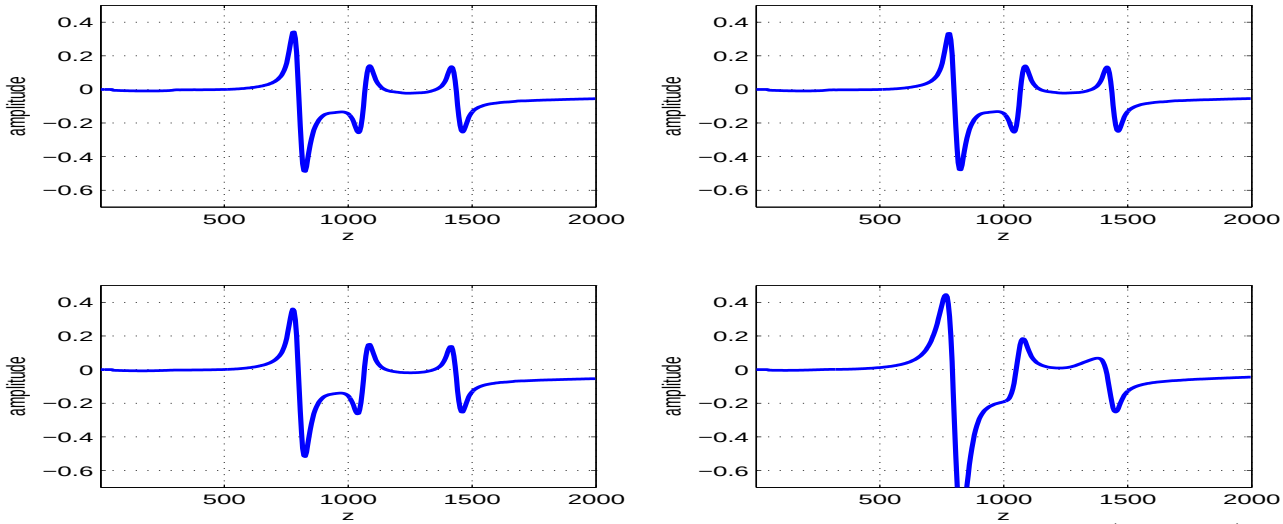

Figure 16: Amplitudes of α_1 at the line $x = 2000m$ in Figure 15 with $apertures = 50m$(upper left), $250m$(upper right), $1000m$(lower left), $4000m$(lower right).

8 Conclusions

We have used three different models to test the aperture-compensated linear asymptotic imaging algorithm. The results showed that this algorithm has changed the characteristics of α_1, making it less accurate as input to the nonlinear velocity-independent depth imaging algorithms of the inverse scattering series. We have addressed this by attempting an ad hoc approach to recover a

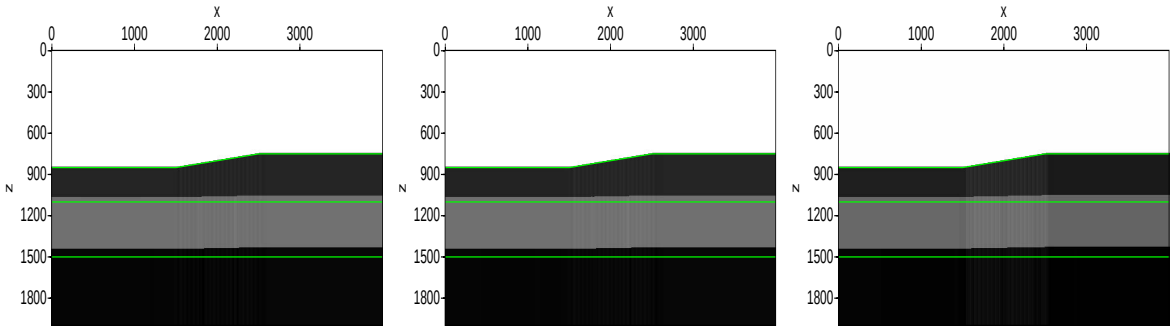

Figure 17: Revised α_1 using the α_1 from Figure 15 with $apertures = 50m$(upper left), $250m$(upper right), $1000m$(lower left), $4000m$(lower right).

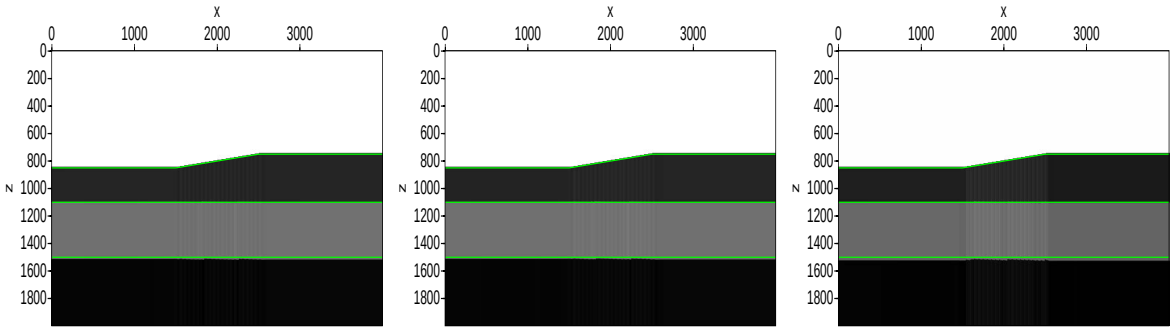

Figure 18: Result of α_{HOIS}, using the revised α_1 with $apertures = 50m$(upper left), $250m$(upper right), $1000m$(lower left), $4000m$(lower right).

more accurate α_1 value from the asymptotic result, with some clear improvement. More research is needed and is underway.

9 Acknowledgements

All M-OSRP sponsors are gratefully acknowledged for their support in the research. We thank Haiyan Zhang and Simon Shaw for invaluable discussions and suggestions. This work has been partially funded by NSF-CMG (award DMS-0327778) and U.S. DOE-BES (Grant No. DOE-De-FG02-05ER15697)

References

Liu, F., A. B. Weglein, and K. A. Innanen. "Inverse scattering series with lateral variations in 3D." *Mission-Oriented Seismic Research Program (M-OSRP) Annual Report*. 2007.

Liu, F., A. B. Weglein, B. G. Nita, and K. A. Innanen. "Investigating the Grouping of Inverse

Scattering Series Terms: Simultaneous Imaging and Inversion I(Theory)." *Mission-Oriented Seismic Research Program (M-OSRP) Annual Report*. 2005.

Shaw, S. A. and A. B. Weglein. "A leading order imaging series for prestack data acquired over a laterally invariant acoustic medium. Part I: Derivation and preliminary analysis." *M-OSRP Annual Report* 3 (2004).

Stolt, Robert H. and Alvin K. Benson. *Seismic Migration: Theory and Practice*. Ed. Klaus Helbig and Sven Treitel. Volume 5 of Seismic Exploration. Geophysical Press, 1986.

Wang, Z., A. Weglein, and F. Liu. "Preparing data with finite cross-line aperture for input to 3D non-linear imaging algorithms." *Mission-Oriented Seismic Research Program (M-OSRP) Annual Report*. 2007.

Zhang, H. *Direct non-linear aoustic and elastic inversion: Towards fundamentally new comprehensive and realistic target identification*. PhD thesis, University of Houston, 2006.

Progressing multiparameter imaging using the inverse scattering series: An initial analytic test of the leading order imaging subseries (LOIS) closed form and its extended higher order imaging subseries (HOIS) closed form for a laterally invariant two-parameter acoustic medium

S. Jiang[1], A. B. Weglein[1], and S. A. Shaw[2]
[1] M-OSRP, Department of Physics, University of Houston, 617 Science & Research Bldg. 1, Houston, TX 77204-5008
[2] Previously M-OSRP, University of Houston, currently ConocoPhillips, 600 N. Dairy Ashford, Houston, TX 77079

Abstract

A generalization of the single-parameter (velocity only) inverse scattering series (*ISS*) leading order and extended higher order imaging algorithms (*LOIS* and *HOIS*, respectively) to accommodate a multiparameter (parameters other than velocity can be varied) acoustic and elastic earth were presented in the 2007 M-OSRP annual report (Jiang and Weglein, 2008). In this report, as follow-up multiparameter imaging research, an initial 1D analytic example for a laterally invariant two-parameter (velocity and density) acoustic medium is presented where analytic analysis and some numerical examples are used to examine how effective the 1D acoustic two-parameter *LOIS* and *HOIS* imaging algorithms are working towards a satisfactory level in the multiparameter imaging toolbox. Results show that both *LOIS* and *HOIS* imaging algorithms are better at locating deeper reflectors than constant velocity migration, while the *HOIS* imaging algorithm can better image deeper reflectors than the *LOIS* algorithm, especially at big incident angles. The *HOIS* imaging algorithm has more tolerance than the *LOIS* algorithm for the magnitude and duration of velocity and density contrasts. As a further step to the multi-parameter imaging project, this initial analytic test of acoustic two-parameter imaging algorithm is very important to provide details of how the amplitude information of the acoustic data set is used in velocity-independent multi-parameter imaging algorithms. In future, the multi-component elastic datasets will be studied both analytically and numerically for providing a "proper" linear inversion of the imaging-related parameters.

1 Introduction

The one-dimensional leading-order imaging algorithm using inverse scattering theory and series developed in the M-OSRP group is a data-driven algorithm and can achieve the imaging objective to some satisfactory level (Weglein et al., 2000; Shaw et al., 2002; Shaw and Weglein, 2003; Shaw, 2005) without knowing any subsurface information but assuming only a constant reference velocity field. For a larger velocity contrast model, more imaging subseries terms need to be captured to form a higher order imaging algorithm (Liu et al., 2004, 2005; Liu, 2006) which can deal with

multidimensional variations in the model. However, all the imaging algorithms mentioned above make an assumption that velocity is the only medium parameter that varies, which is not true in a real earth where other parameters other than velocity can vary, such as density. Recently, Fang Liu tested the higher order imaging algorithm which was developed for velocity-only variation. The tested result showed that the algorithm can fail if applied to a medium with both velocity and density variation (discussed and shown within M-OSRP group). Therefore, based on an imaging conjecture proposed by Weglein in 2008 (discussed within M-OSRP group), an imaging algorithm was developed in the M-OSRP group in 2008 and reported in the 2007 M-OSRP annual meeting which can deal with the imaging problems for a medium with both density and velocity variations (Jiang and Weglein, 2008). A leading order imaging subseris (*LOIS*) and its closed form were first derived for a laterally invariant two-parameter (density and velocity) acoustic medium, and then were extended by Weglein to a higher order imaging closed form (*HOIS*) to accomodate multi-D multiparameter acoustic and elastic media (discussed within M-OSRP group and later shown in the 2007 M-OSRP annual meeting (Jiang and Weglein, 2008)).

This report is presented to demonstrate the effectiveness of the newly derived multi-parameter imaging algorithms and its imaging capability through an initial analytic example of a 1D three-layer acoustic medium with both velocity and density variations. The structure of this report is as follows: *Section 1* briefly introduces the history of the inverse scattering imaging algorithms; *Section 2* reviews the inverse scattering series which is the basis of the imaging algorithms to be tested in the later sections; *Section 3* briefly reviews the multiparameter *ISS LOIS* and extended *ISS HOIS* imaging algorithms, in which the two-parameter acoustic *ISS LOIS* and its extended *ISS HOIS* imaging algorithms will be tested in *Section 4*; An analytic dataset is prepared for a three-layer acoustic medium with both density and velocity variations in the beginning of *Section 4* and then is used to analytically calculate the *LOIS* algorithm. Numerical examples are presented at the end of *Section 4*; *Section 5* is the conclusion and discussion of the results reported in this paper.

2 Inverse scattering theory and series

Scattering theory is a form of perturbation analysis. Generally speaking, it describes how a perturbation in the properties of a medium relates to a wavefield that experiences that perturbed medium. Consider the two differential equations governing wave propagation in these media (Weglein et al., 2003):

$$LG = \delta(\mathbf{r} - \mathbf{r_s}), \tag{1}$$

$$L_0 G_0 = \delta(\mathbf{r} - \mathbf{r_s}). \tag{2}$$

where L, L_0 and G, G_0 are the actual and reference differential operators and Green's functions, respectively, for a single temporal frequency, ω, and $\delta(\mathbf{r} - \mathbf{r_s})$ is a Dirac delta function. $\mathbf{r}$ and $\mathbf{r_s}$ are the field point and source location, respectively.

2.1 Lippmann-Schwinger equation

The Lippmann-Schwinger equation is an integral solution to the wave equation (1) in terms of the reference wave equation (2) and a perturbation operator defined as $V = L_0 - L$:

$$\Psi_s = G - G_0 = G_0 V G. \tag{3}$$

where Ψ_s is the scattered field.

The total scattered field is related to the earth perturbation and the reference wave field (generally using water as reference background for marine seismic exploration) by the above recursive integral Lippmann-Schwinger equation. It is a direct solution to the real wave equation.

2.2 Forward scattering series

Expanding equation (3) by iteration (Taylor, 1972), a forward scattering series is obtained,

$$\begin{aligned} \Psi_s &= G_0 V G_0 + G_0 V G_0 V G_0 + \cdots & (4)\\ &= (\Psi_s)_1 + (\Psi_s)_2 + \cdots, & (5) \end{aligned}$$

where $(\Psi_s)_n$ is the portion of Ψ_s that is n^{th} order in V. The measured value of Ψ_s is the data, D, where $D = (\Psi_s)_{ms}$ and ms denotes "on the measurement surface".

The forward scattering series provides the ability to model the data since the perturbation V underneath the measurement surface is assumed known in the forward problem.

2.3 Inverse scattering series

Expanding the perturbation operator V in orders of data D yields,

$$V = V_1 + V_2 + V_3 + \cdots \tag{6}$$

where V_n is n^{th} order in the data D.

An inverse scattering series is obtained by setting the same order of the data equal on both sides of equation (4) at the measurement surface,

$$\begin{aligned} D &= [G_0 V_1 G_0]_{ms}, & (7)\\ 0 &= [G_0 V_2 G_0]_{ms} + [G_0 V_1 G_0 V_1 G_0]_{ms}, & (8)\\ 0 &= [G_0 V_3 G_0]_{ms} + [G_0 V_1 G_0 V_2 G_0]_{ms} \\ &+ [G_0 V_2 G_0 V_1 G_0]_{ms} + [G_0 V_1 G_0 V_1 G_0 V_1 G_0]_{ms}, & (9)\\ &\vdots \end{aligned}$$

The inverse scattering series provides a direct method for obtaining the subsurface information by inverting the series order by order to solve for the perturbation V, using only the measured data D and a reference wavefield G_0.

3 1D two-parameter acoustic medium

To study a 1D two-parameter acoustic medium where both velocity and density can vary, let us first consider the 3D acoustic wave equations in the actual and reference medium (Zhang and Weglein, 2005),

$$\begin{aligned}\left[\frac{\omega^2}{K(\vec{r})}+\nabla\cdot\frac{1}{\rho(\vec{r})}\nabla\right]G(\vec{r},\vec{r_s};\omega)&=\delta(\vec{r}-\vec{r_s}),\\ \left[\frac{\omega^2}{K_0(\vec{r})}+\nabla\cdot\frac{1}{\rho_0(\vec{r})}\nabla\right]G_0(\vec{r},\vec{r_s};\omega)&=\delta(\vec{r}-\vec{r_s}).\end{aligned}\tag{10}$$

where G and G_0 are the actual and reference Green's functions, or wavefields, respectively, for a single temporal frequency, ω. K is the bulk modulus and is equal to $c^2\rho$ where c is P-wave velocity and ρ is density. The quantities with subscript "0" are in the reference medium, otherwise, they are in the actual medium.

The perturbation operator is therefore defined as,

$$V=L_0-L=\frac{\omega^2\alpha}{K_0(\vec{r})}+\nabla\cdot\frac{\beta}{\rho_0(\vec{r})}\nabla,\tag{11}$$

where $\alpha=1-\frac{K_0}{K}$, $\beta=1-\frac{\rho_0}{\rho}$.

Similar to the operator V, we also expand α and β in orders of the data in considering a 1D acoustic medium,

$$\begin{aligned}\alpha(z)&=\alpha_1(z)+\alpha_2(z)+...\\ \beta(z)&=\beta_1(z)+\beta_2(z)+...\end{aligned}\tag{12}$$

3.1 Leading order imaging subseries and closed form

By analytically calculating higher order (up to the 3^{rd} order) *ISS* terms for the above 1D two-parameter acoustic media, a (*LOIS*) and its closed form were identified and reported in the 2007 M-OSRP annual report (Jiang and Weglein, 2008). The *LOIS* and its closed form are expressed here and will be tested in the following section.

$$\begin{aligned}&\sum_{n=0}^{\infty}\frac{\left(-\frac{1}{2}\frac{1}{\cos^2\theta}\right)^n}{n!}\frac{d^n\mathscr{D}^{LOIS}(z,\theta)}{dz^n}\left[\int_{-\infty}^{z}\left(\alpha_1(z')-\beta_1(z')\right)dz'\right]^n\\ &=\mathscr{D}^{LOIS}\left(z-\frac{1}{2}\frac{1}{\cos^2\theta}\int_{-\infty}^{z}\left(\alpha_1(z')-\beta_1(z')\right)dz'\right).\end{aligned}\tag{13}$$

Notice that the quantity $\mathscr{D}^{LOIS}$ is defined as,

$$\mathscr{D}^{LOIS}(z,\theta)\equiv\frac{1}{\cos^2\theta}\alpha_1(z)+\left(1-\tan^2\theta\right)\beta_1(z).\tag{14}$$

It is a rescaled PP dataset after a constant velocity migration indicated by the 1^{st} order *ISS* equation calculated in Zhang and Weglein (2005):

$$\mathscr{D}^{LOIS}(z,\theta) = -\frac{4}{\rho_0} D^{PP}(z,\theta) \tag{15}$$

3.2 Extended imaging algorithms based on imaging conjecture

As reported in the 2007 M-OSRP annual report (Jiang and Weglein, 2008), based on an imaging conjecture proposed by Weglein, the above 1D two-parameter (velocity and density) acoustic *LOIS* imaging closed form has been extended to a 1D three-parameter (density, bulk modulus and shear modulus) elastic case (for elastic PP data only), and then to higher order imaging algorithms (*HOIS*) for both acoustic and elastic media.

(1) Extended 1D three-parameter elastic PP data only *LOIS* algorithm:

$$\mathscr{D}^{LOIS}(z) = -4D^{PP}\left(z - \frac{1}{2}\frac{1}{\cos^2\theta}\int_{-\infty}^{z}\left(a_\gamma^1(z') - a_\rho^1(z')\right)dz'\right) \tag{16}$$

$D^{PP}(z,\theta)$ is a PP component dataset,

$$D^{PP}(z,\theta) = -\frac{1}{4}\left(1+\tan^2\theta\right)a_\gamma^1(z) - \frac{1}{4}\left(1-\tan^2\theta\right)a_\rho^1(z) + 2\frac{\beta_0^2\sin^2\theta}{\alpha_0^2}a_\mu^1(z). \tag{17}$$

where $a_\rho^1(z), a_\gamma^1(z), a_\mu^1(z)$ are the 1^{st} order approximations of density, bulk modulus and shear modulus variations, respectively. More details regarding the definitions of these parameters can be found in Zhang and Weglein (2006).

(2) Extended 1D *HOIS* algorithms:
(i) for a 1D two-parameter acoustic medium,

$$\mathscr{D}^{HOIS}\left(z + \frac{1}{2}\int_{-\infty}^{z}\frac{\alpha_1(z') - \beta_1(z')}{\cos^2\theta - 0.25\left(\alpha_1(z') - \beta_1(z')\right)}dz'\right) = D^{PP}(z,\theta) \tag{18}$$

where $D^{PP}(z,\theta)$ is expressed as,

$$D^{PP}(z,\theta) = -\frac{\rho_0}{4}\left(\frac{1}{\cos^2\theta}\alpha_1(z) + \left(1-\tan^2\theta\right)\beta_1(z)\right). \tag{19}$$

(ii) for a 1D three-parameter elastic PP data only case,

$$\mathscr{D}^{HOIS}\left(z + \frac{1}{2}\int_{-\infty}^{z}\frac{a_\gamma^1(z') - a_\rho^1(z')}{\cos^2\theta - 0.25\left(a_\gamma^1(z') - a_\rho^1(z')\right)}dz'\right) = D^{PP}(z,\theta) \tag{20}$$

where the PP dataset is defined in equation (17).

It is quite straightforward to extend the above 1D acoustic/elastic *HOIS* closed form to a multidimensional multi-parameter acoustic and elastic imaging closed form.
(3) For an acoustic medium,

$$\mathscr{D}^{HOIS}\left(x,y,z+\frac{1}{2}\int_{-\infty}^{z}\frac{\alpha_1(x,y,z')-\beta_1(x,y,z')}{\cos^2\theta-0.25\left(\alpha_1(x,y,z')-\beta_1(x,y,z')\right)}dz'\right)=D^{PP}(x,y,z,\theta) \tag{21}$$

(4) For PP data in an elastic medium,

$$\mathscr{D}^{HOIS}\left(x,y,z+\frac{1}{2}\int_{-\infty}^{z}\frac{a^1_\gamma(x,y,z')-a^1_\rho(x,y,z')}{\cos^2\theta-0.25\left(a^1_\gamma(x,y,z')-a^1_\rho(x,y,z')\right)}dz'\right)=D^{PP}(x,y,z,\theta) \tag{22}$$

The multidimensional dataset $D(x,y,z,\theta)$, for the acoustic case, is a PP only dataset; for ocean bottom measurements and an elastic medium, it can be a multi-component PP, PS, SP, or SS dataset.

4 1D analytic example

In this section, we will present a 1D analytic example to test the above *LOIS* and *HOIS* two-parameter imaging algorithms expressed in equation (13) and equation (18), respectively, for a laterally invariant three-layer acoustic medium where both velocity and density can be varied.

4.1 1D two-parameter acoustic model

The model to be tested is shown in Figure 1. We will consider only two primaries reflected from the 1^{st} interface and the 2^{nd} interface, since the *ISS* imaging task has assumed that all seismic events other than primaries have been removed already. Next we will analytically write out primaries data based on this model.

4.2 1D analytic data preparation

Since both the *LOIS* and *HOIS* multiparameter imaging algorithms are data-driven algorithms, we will first prepare analytic data for the above three-layered 1D acoustic model. The derivation of the imaging algorithms assumes an experiment with line sources and line receivers. But the data expressed at the end of this subsection is after plane wave decomposition, which is an immediate and proper input to the imaging algorithms to be tested.

We will first write down the analytic reflection and transmission coefficients according to the different impedance in the three layers. For plane wave at different incident angles, the impedance can be expressed as,

$$\begin{aligned} I_0 &= \frac{c_0\rho_0}{\cos\theta} \\ I_1 &= \frac{c_1\rho_1}{\cos i_1} \\ I_2 &= \frac{c_2\rho_2}{\cos i_2} \end{aligned} \tag{23}$$

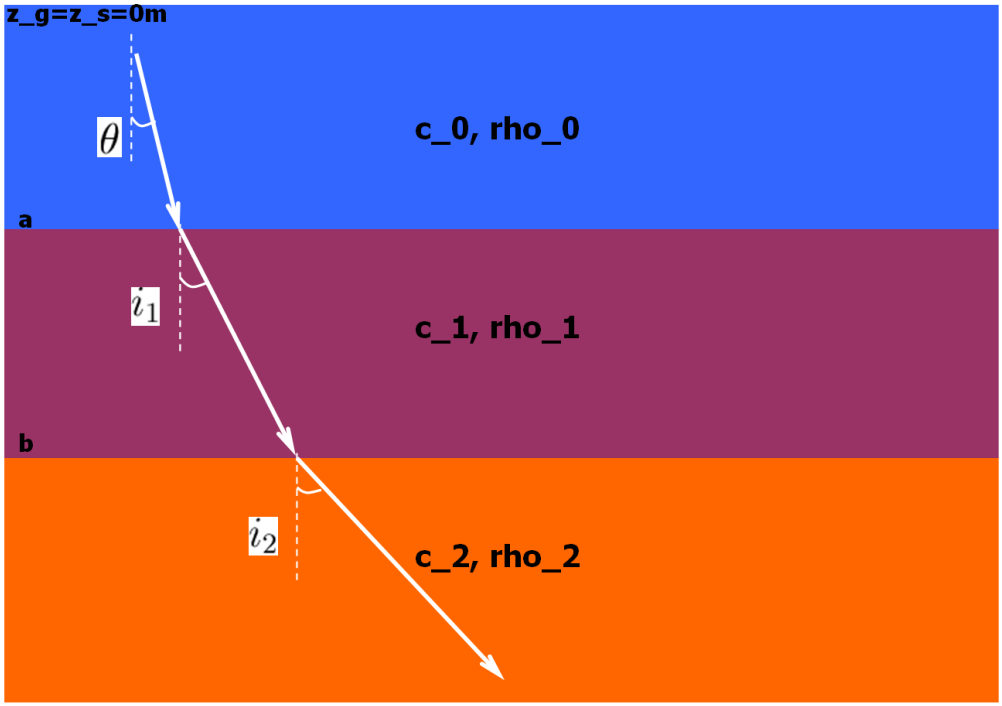

Figure 1: *A cartoon of a 1D acoustic model with both velocity (c_0, c_1, c_2) and density (ρ_0, ρ_1, ρ_2) variations in the three layers, where θ, i_1, i_2 are three incident angles in the layers, respectively; a and b are two constants to express the real depths of the two interfaces. For simplicity, both source depth z_s and receiver depth z_g are set to zero.*

For 1D layered media, Snell's law says that the value of the horizontal slowness p is constant through different layers, and hence provides the following relation among the three incident angles in the three layers of the media.

$$p = \frac{\sin\theta}{c_0} = \frac{\sin i_1}{c_1} = \frac{\sin i_2}{c_2} \tag{24}$$

Employing the above relation, we can rewrite the above impedances as,

$$\begin{aligned} I_0 &= \frac{c_0\rho_0}{\cos\theta} = \frac{c_0\rho_0}{\sqrt{1-c_0^2p^2}} = \frac{c_0\rho_0}{x_0} \\ I_1 &= \frac{c_1\rho_1}{\cos i_1} = \frac{c_1\rho_1}{\sqrt{1-c_1^2p^2}} = \frac{c_1\rho_1}{x_1} \\ I_2 &= \frac{c_2\rho_2}{\cos i_2} = \frac{c_2\rho_2}{\sqrt{1-c_2^2p^2}} = \frac{c_2\rho_2}{x_2} \end{aligned} \tag{25}$$

where $x_i = \sqrt{1-c_i^2p^2}, \quad i = 0, 1, 2.$

Now we can express the reflection and transmission coefficients as,

$$\begin{aligned} R_0(\theta) &= \frac{I_1 - I_0}{I_1 + I_0} \\ R_1(\theta) &= \frac{I_2 - I_1}{I_2 + I_1} \\ T_{01}(\theta) &= 1 - R_0 = \frac{2I_0}{I_1 + I_0} \\ T_{10}(\theta) &= 1 + R_0 = \frac{2I_1}{I_1 + I_0} \end{aligned} \tag{26}$$

We will write down the analytic data in the frequency domain.

$$\widetilde{D}^{PP}(\omega, \theta) = \rho_0 R_0(\theta) \frac{e^{2i\nu_g a}}{4\pi i \nu_g} + \rho_0 T_{01}(\theta) R_1(\theta) T_{10}(\theta) \frac{e^{2i\nu_g a + 2iq_g(b-a)}}{4\pi i \nu_g} \tag{27}$$

where the two vertical wave vectors in the first two layers are expressed as,

$$\nu_g = \frac{\omega \cos\theta}{c_0} = \frac{\omega}{c_0}\sqrt{1 - c_0^2 p^2} = \frac{\omega}{c_0} x_0 \tag{28}$$

and,

$$q_g = \frac{\omega \cos i_1}{c_1} = \frac{\omega}{c_1}\sqrt{1 - c_1^2 p^2} = \frac{\omega}{c_1} x_1 \tag{29}$$

Performing an inverse Fourier transformation w.r.t. ν_g, we can obtain the PP data in the pseudo-depth domain,

$$D^{PP}(z, \theta) = -\rho_0 R_0(\theta) H(z - a) - \rho_0 R_1'(\theta) H(z - b'(\theta)) \tag{30}$$

where the variable z is the Fourier conjugator of ν_g, and

$$\begin{aligned} b'(\theta) &= a + (b - a)\frac{c_0\sqrt{1 - c_1^2 p^2}}{c_1\sqrt{1 - c_0^2 p^2}} = a + (b - a)\frac{c_0 x_1}{c_1 x_0} \\ R_1'(\theta) &= T_{01}(\theta) R_1(\theta) T_{10}(\theta) \end{aligned} \tag{31}$$

Equation (30) is the analytic data we prepared for the purpose of the following tests on the two-parameter *LOIS* and *HOIS* imaging algorithms. The data in equation (30) is expressed in the pseudo-depth domain since it is migrated with a constant reference velocity c_0 which is in agreement with the velocity in the first layer. Generally the value of c_0 is water speed ($1500m/s$). After the constant velocity migration, the water bottom, i.e. the 1^{st} interface, is located exactly since we have correct migration velocity for the 1^{st} layer, but the 2^{nd} interface is wrongly located to $b'(\theta)$ instead of its real depth of b. It is understandable since we used a wrong migration velocity c_0 instead of its real velocity c_1. To understand whether $b'(\theta)$ is deeper or shallower than its real depth b, we need to do further analysis on this quantity.

Let us rewrite the expression of $b'(\theta)$ in equation (31) by using equation (24),

$$b'(\theta) = a + (b-a)\frac{c_0}{c_1}\sqrt{1 + \frac{c_0^2 - c_1^2}{c_0^2}\tan^2\theta} \tag{32}$$

We will discuss two cases:
(1) for $c_0 < c_1$, $c_0^2 - c_1^2 < 0$. Then, $b'(\theta) < b$ and $b'(\theta) \downarrow$ with $\theta \uparrow$;
(2) for $c_0 > c_1$, $c_0^2 - c_1^2 > 0$. Then, $b'(\theta) > b$ and $b'(\theta) \uparrow$ with $\theta \uparrow$.

In other words, the migrated depth of the 2^{nd} interface is shallower than its real depth when the migration velocity is slower than its real velocity, and deeper than its real depth when the migration velocity is faster than its real velocity. It is a reasonable result since constant velocity migration is a linear migration, i.e. rescaling the time axis of the data set to depth axis by a constant velocity. We emphasize this point here to show that there is a difference between the constant velocity migration and the *ISS LOIS* and *HOIS* imaging shown later where the relation between time domain and depth domain of the migration is no longer linear since the later imaging occurrs in a nonlinear world. More details on this point will be discussed in the following subsections.

4.3 Analytic calculation of *LOIS* closed form

Now we can use the data prepared in equation (30) as an input to the *LOIS* two-parameter imaging algorithm. Recall that in Zhang and Weglein (2005),

$$D^{PP}(z,\theta) = -\frac{\rho_0}{4}\left[\frac{1}{\cos^2\theta}\alpha_1(z) + \left(1-\tan^2\theta\right)\beta_1(z)\right] \tag{33}$$

Solve the above equation to obtain $\alpha_1(z) - \beta_1(z)$, using two separate incident angles,

$$\alpha_1(z) - \beta_1(z) = -\frac{4}{\rho_0}\frac{D^{PP}(z,\theta_1) - D^{PP}(z,\theta_2)}{\tan^2(\theta_1) - \tan^2(\theta_2)} \tag{34}$$

Insert the analytic expression of the data with different incident angles prepared in the previous subsection,

$$\begin{aligned}\alpha_1(z) - \beta_1(z) = \frac{4}{\tan^2(\theta_1) - \tan^2(\theta_2)}[&(R_0(\theta_1) - R_0(\theta_2))\,H(z-a) \\ &+ R_1'(\theta_1)H(z-b'(\theta_1)) \\ &- R_1'(\theta_2)H(z-b'(\theta_2))]\end{aligned} \tag{35}$$

Now we can calculate the integral with the above equation as the integrand, and hence get the shifted quantity,

$$\begin{aligned}\triangle z_{shift} &= \frac{1}{2\cos^2\theta}\int_{-\infty}^{z} dz'\left(\alpha_1(z') - \beta_1(z')\right) \\ &= \frac{2}{\tan^2(\theta_1) - \tan^2(\theta_2)}\frac{1}{\cos^2\theta}[(R_0(\theta_1) - R_0(\theta_2))\,(z-a)H(z-a) \\ &+ R_1'(\theta_1)(z-b'(\theta_1))H(z-b'(\theta_1)) - R_1'(\theta_2)(z-b'(\theta_2))H(z-b'(\theta_2))]\end{aligned} \tag{36}$$

Therefore, the migration result, i.e. the imaging composite equation (15), using the *LOIS* closed form is a constant velocity migration of the data set *shifted by a quantity as a function of* "z", i.e.

$$\begin{aligned}\mathscr{D}^{LOIS}(z,\theta) &= -\frac{4}{\rho_0}D^{PP}(z-\triangle z_{shift},\theta)\\ &= 4R_0(\theta)H(z-\triangle z_{shift}-a)+4R_1'(\theta)H(z-\triangle z_{shift}-b'(\theta))\end{aligned} \tag{37}$$

4.4 Analysis on the shifted quantity

Now we will perform some analysis on the above *LOIS* migration result.
(1) If $z \le a$, then

$$\triangle z_{shift} \equiv 0. \tag{38}$$

(2) If $a < z \le b'(\theta_1)$ *and* $z \le b'(\theta_2)$, then

$$\triangle z_{shift} = \frac{2}{\tan^2(\theta_1)-\tan^2(\theta_2)}\frac{1}{\cos^2\theta}\left[(z-a)\left(R_0(\theta_1)-R_0(\theta_2)\right)\right]. \tag{39}$$

(3) If $z > a$ *and* $b'(\theta_1) < z \le b'(\theta_2)$, then

$$\triangle z_{shift} = \frac{2}{\tan^2(\theta_1)-\tan^2(\theta_2)}\frac{1}{\cos^2\theta}\left[(z-a)\left(R_0(\theta_1)-R_0(\theta_2)\right)+(z-b'(\theta_1))R_1'(\theta_1)\right]. \tag{40}$$

(4) If $z > a$ *and* $b'(\theta_2) < z \le b'(\theta_1)$, then

$$\triangle z_{shift} = \frac{2}{\tan^2(\theta_1)-\tan^2(\theta_2)}\frac{1}{\cos^2\theta}\left[(z-a)\left(R_0(\theta_1)-R_0(\theta_2)\right)-(z-b'(\theta_2))R_1'(\theta_2)\right]. \tag{41}$$

(5) If $z > a$, $z > b'(\theta_1)$ *and* $z > b'(\theta_2)$, then

$$\begin{aligned}\triangle z_{shift} =& \frac{2}{\tan^2(\theta_1)-\tan^2(\theta_2)}\frac{1}{\cos^2\theta}[(z-a)\left(R_0(\theta_1)-R_0(\theta_2)\right)\\ &+(z-b'(\theta_1))R_1'(\theta_1)-(z-b'(\theta_2))R_1'(\theta_2)].\end{aligned} \tag{42}$$

Let us check the above shifted quantity for a simple 1D acoustic model with constant velocity, i.e. $c_0 = c_1 = c_2$, but varied density. For this model, the reflection and transmission coefficients, recalling expressions in equation (25) and equation (26), will be simplified ,

$$\begin{aligned}R_0 &= \frac{\rho_1-\rho_0}{\rho_1+\rho_0}\\ R_1 &= \frac{\rho_2-\rho_1}{\rho_2+\rho_1}\\ T_{01} &= 1-R_0\\ T_{10} &= 1+R_0\end{aligned} \tag{43}$$

Notice that the reflection and transmission coefficients are independent of θ. This leads to the following relation,

$$R_0(\theta_1) = R_0(\theta_2) \quad R_1'(\theta_1) = R_1'(\theta_2) \tag{44}$$

Similarly, the pseudo-depth expression of equation (32) becomes,

$$b'(\theta) = a + (b - a) = b \tag{45}$$

The pseudo-depth is also independent of θ, and it is equal to the real depth of the 2^{nd} interface, since the velocities for all three layers are the same in this case and equal to the reference velocity of the migration.

Therefore, the shifted quantities in the above five cases are all zero, i.e.

$$\triangle z_{shift} \equiv 0. \tag{46}$$

This means that for the 1D acoustic model with constant velocity but varied density, the data set migrated with constant c_0 velocity has exactly located all interfaces. This is to be expected, because all layers in this case have the same correct velocity c_0.

What about the case with three different velocities in three layers? From the mathematical expression of the shifted quantity shown in the above five cases, we can tell the value of the shifted quantity is actually dependent on the reflection and transmission coefficients at two different incident angles; in other words, when the reference velocity is different from the real velocity, the *ISS LOIS* imaging algorithm will *use velocity information* "buried" in the reflection and transmission coefficients through their *nonlinear communication* at two different incident angles, and this *nonlinear communication* will be carried on through a depth duration wherever its real velocity is different from the reference velocity. As discussed in the Appendix of Zhang and Weglein (2005), the integrand of the shifted quantity is a linear estimate of velocity changes in the media. Therefore, the more accurate the linear estimate of the velocity changes, the closer the migrated interfaces are to their real depths.

4.5 Numerical evaluations of the two-parameter *ISS LOIS* and *HOIS* imaging algorithms

For a 1D acoustic model with both density and velocity variation, it is not easy to "interpret" from the analytic expression of the shifted quantity how well it is locating the real depths. In this section, we will do some numerical evaluations on the above three-layer acoustic medium using the *ISS LOIS* imaging algorithm expressed in equation (13), and the extended acoustic *ISS HOIS* imaging algorithm expressed in equation (18) by varying the values of density and velocity in the models. First we will demonstrate how sensitive the *LOIS* imaging algorithm is to the changes of the velocity parameter, and then we will show the imaging improvement using the *HOIS* imaging algorithm by comparing its results with the *LOIS* results. Further, we will study how sensitive the *LOIS* and *HOIS* imaging algorithms to the changes in the density parameter. Finally, the effect of depth

duration in the model on the imaging capability of both imaging algorithms will be studied at the end of this section. We will first fix the two interface depths $a = 200m$ and $b = 400m$ in the models.

In Figure 2, we show a comparison of imaging results between constant velocity migration in the left most panel and the *ISS LOIS* imaging algorithm in the middle panel. For the model we tested, both methods exactly located the 1^{st} interface and mislocated the $2nd$ interface - the constant velocity migration method undermigrated the 2^{nd} interface since it assumed a constant velocity ($c_0 = 1500m/s$) which is less than its real velocity ($c_1 = 1600m/s$) in the 2^{nd} layer, while the *ISS LOIS* imaging algorithm overmigrated the 2^{nd} interface although the method also employs the same constant reference velocity ($c_0 = 1500m/s$) with the former method. Again, this result indicates that the *ISS LOIS* imaging algorithm developed from a *non-linear* series is conceptually different from the conventional migration method, the constant velocity migration for example, which originated from a *linear* imaging world. It is apparent that the *ISS LOIS* imaging algorithm pushed its imaged 2^{nd} interface much closer to its real depth than the constant velocity migration result, especially within the small incident angle range. To show the purposeful perturbation of the *ISS LOIS* imaging algorithm, we also present the imaging result of a model with no velocity changes but only density changes in the right most panel of Figure 2. The result shows that both interfaces are exactly located, since a correct velocity model ($c_0 = c_1 = c_2 = 1500m/s$) is provided in which case the *ISS LOIS* terms will be zero, and the dataset of constant velocity migration result has already exactly located the reflectors in the first term of the *ISS*.

In the following tests we will demonstrate the sensitivity of the *ISS LOIS* imaging algorithm to the changes of velocity parameter in the models. In Figure 3, the *LOIS* result comparison between the middle two panels shows that the *ISS LOIS* imaging algorithm used amplitude information from deeper layers, since the velocities are the same in the first two layers but different in the third layer - one is faster than the first layer velocity, the other is same with the first layer velocity. It seems the *ISS LOIS* imaging algorithm preferrs the latter velocity model. But both results of the *LOIS* are better than the constant velocity migration results for locating the 2^{nd} reflector, as can be seen from the direct comparison among the results in the four panels of Figure 3.

The imaging results in Figure 4 demonstrate that for a velocity model of "slow/faster/same as $1^{st}layer$", the *ISS LOIS* imaging algorithm preferrs a larger velocity contrast in the sense of locating the 2^{nd} reflector, especially within small incident angles. This observation further indicates that the *ISS LOIS* imaging algorithm used amplitude information of deeper events. For comparison purposes, the constant velocity migration result is also put in the Figure.

Figure 5 and Figure 6 show the imaging results for a velocity model of "faster/slower/same as $1^{st}layer$", in which case the *ISS LOIS* imaging algorithm shows a weaker imaging capability for a model with larger velocity contrast than smaller velocity contrast. Again, it demonstrates that the amplitude information of deeper events is involved in the imaging algorithm.

We mentioned in the previous section that $\alpha_1 - \beta_1$ is a linear estimate of the velocity changes between the real velocity model and the reference velocity. When there are no velocity changes, $\alpha_1 - \beta_1$ is zero, and the *ISS LOIS* imaging algorithm shuts down. The result in the right panel in Figure 7 demonstrates this key point. To verify this kind of linear estimate of velocity change, the results of $\alpha_1 - \beta_1$ are also plotted in Figure 7.

Because the *ISS LOIS* imaging algorithm partially captures the imaging terms in the two-parameter *ISS* formalism, it is to be expected that it has a limited imaging capability. The extended *ISS HOIS*

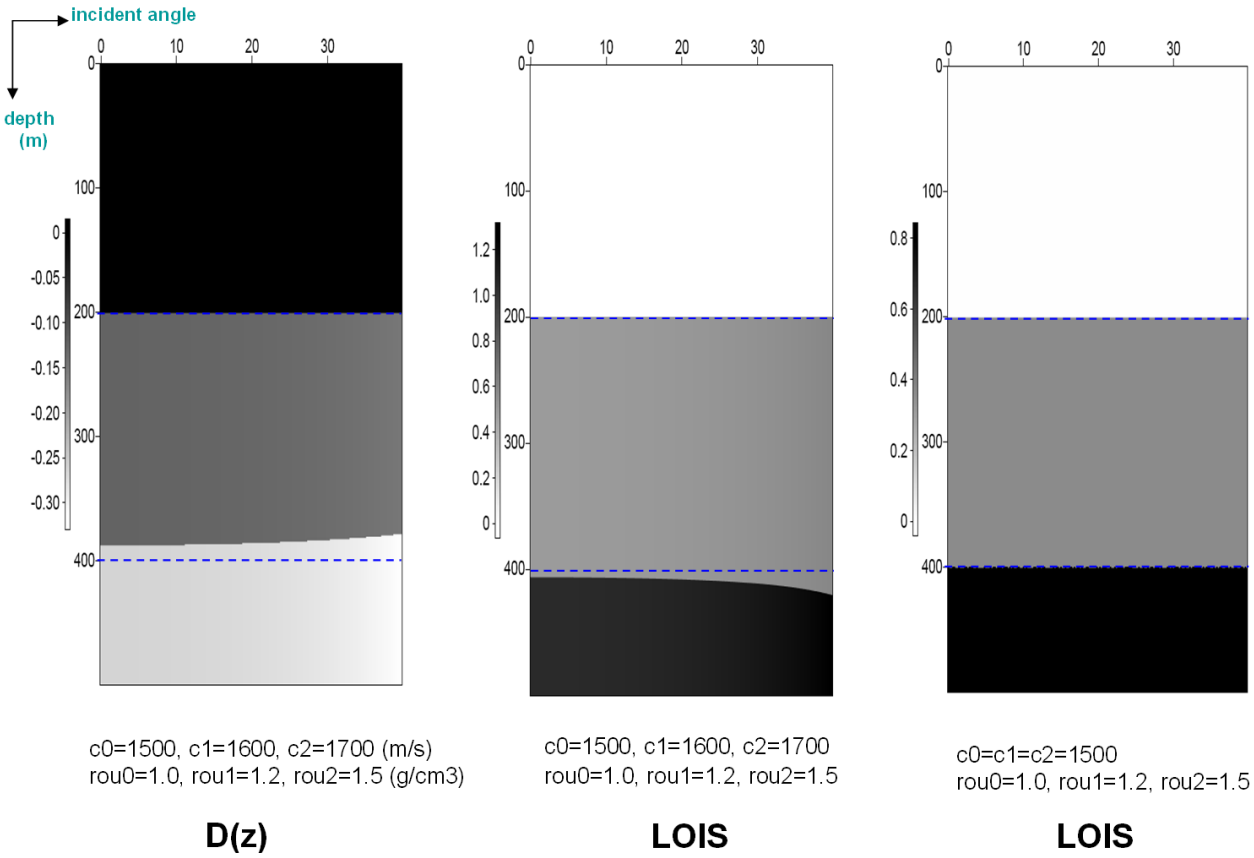

Figure 2: *Imaging comparison 1: left figure is a result of constant velocity ($c_0 = 1500m/s$) migration, middle and right figures are results using two-parameter ISS LOIS imaging algorithm, where the blue dashed lines are the real depths of the two interfaces in the model.*

imaging algorithm in equation (18) captures more imaging terms than the *LOIS*, and it should perform better imaging capability. To demonstrate this assumption, a numerical evaluation using the *ISS HOIS* imaging algorithm is a good starting point. Figure 8 and Figure 9 show the results of the *ISS HOIS*, *ISS LOIS* and constant velocity migration. For the smaller velocity contrast in Figure 8, the *ISS HOIS* algorithm almost exactly located the 2^{nd} interface, much better than the other two methods. For the larger velocity contrast in Figure 9, the *ISS HOIS* algorithm shows a better tolerance of velocity contrast than the *ISS LOIS* and constant velocity migration method.
To demonstrate how sensitive both *ISS LOIS* and *ISS HOIS* algorithms are to the changes in the density parameter, Figure 10 and Figure 11 show that the *ISS HOIS* imaging algorithm is much less affected by the density changes than the *ISS LOIS*, for the certain velocity model ("slower/faster/faster").
At the end of this section, we present a study to show how sensitive both *LOIS* and *HOIS* imaging algorithms will be to the depth duration in the model. The results are shown in Figure 12 where the 1^{st} interface depth is fixed at $a = 75m$, but the 2^{nd} interface is varied depth from $b = 150m$ to $b = 400m$. From the plotted results, we observe that the *ISS HOIS* imaging algorithm is more

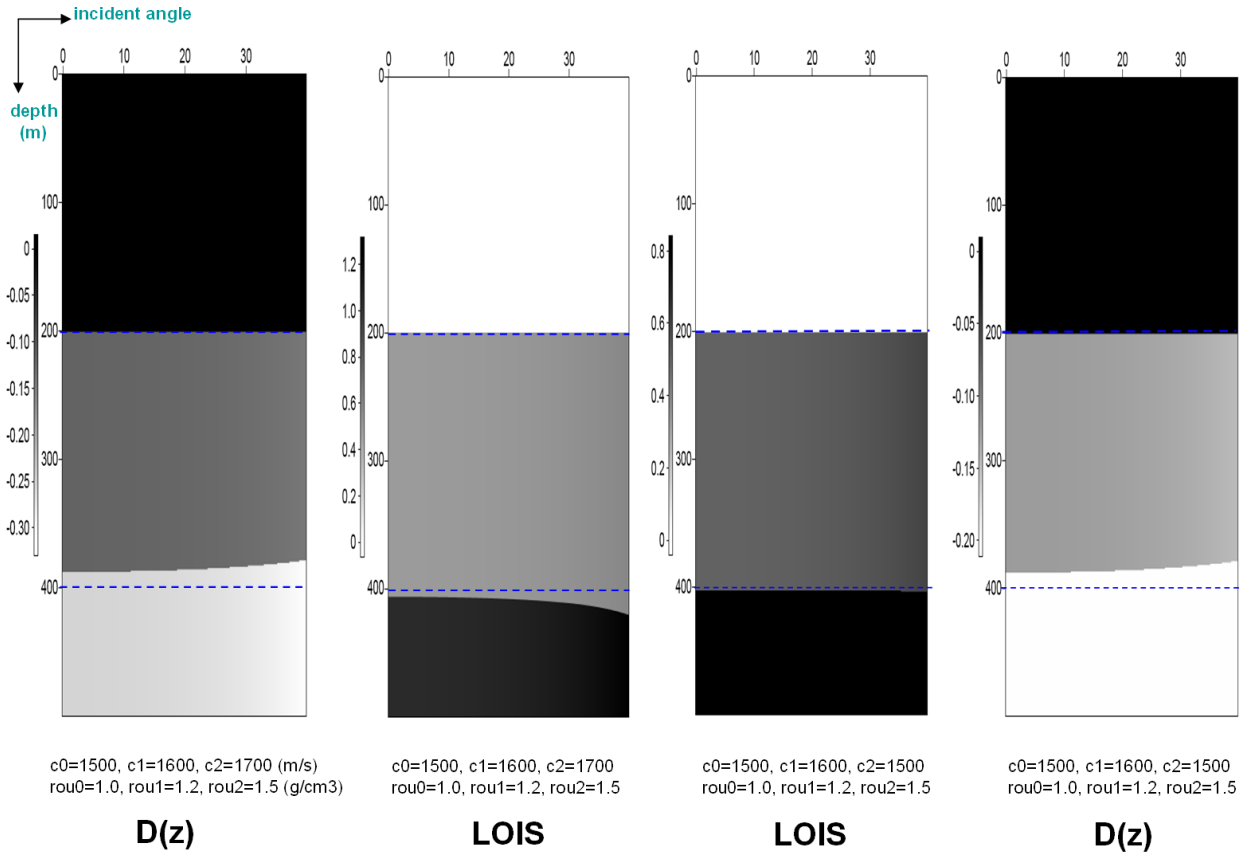

Figure 3: *Imaging comparison 2: the outer two figures are the results of constant velocity ($c_0 = 1500m/s$) migration, the inner two figures are the corresponding results using two-parameter ISS LOIS imaging algorithm, where the blue dashed lines are the real depths of the two interfaces in the model.*

robust to the bigger depth duration than the *ISS LOIS* imaging algorithm, for the considered velocity and density configuration.

5 Conclusion and discussion

In this report we first reviewed the *ISS LOIS* imaging algorithm for a two-paramter acoustic medium and some extended 1D and multi-D *ISS LOIS* and *ISS HOIS* imaging algorithms which were reported at the last M-OSRP's annual meeting. Secondly, we presented a 1D analytic example to test and demonstrate the effectiveness of the 1D acoustic two-parameter *ISS LOIS* and *ISS HOIS* imaging algorithms expressed in equation (13) and equation (18), respectively. Both analytic analysis and numerical evaluations show that both algorithms use amplitude information of seismic events through a nonlinear communication at different incident angles to estimate the real velocity information in the model. The *ISS LOIS* algorithm indicates a tendency to use amplitude information of deeper events, and shows weaker imaging capability than the *ISS HOIS* imaging algorithm

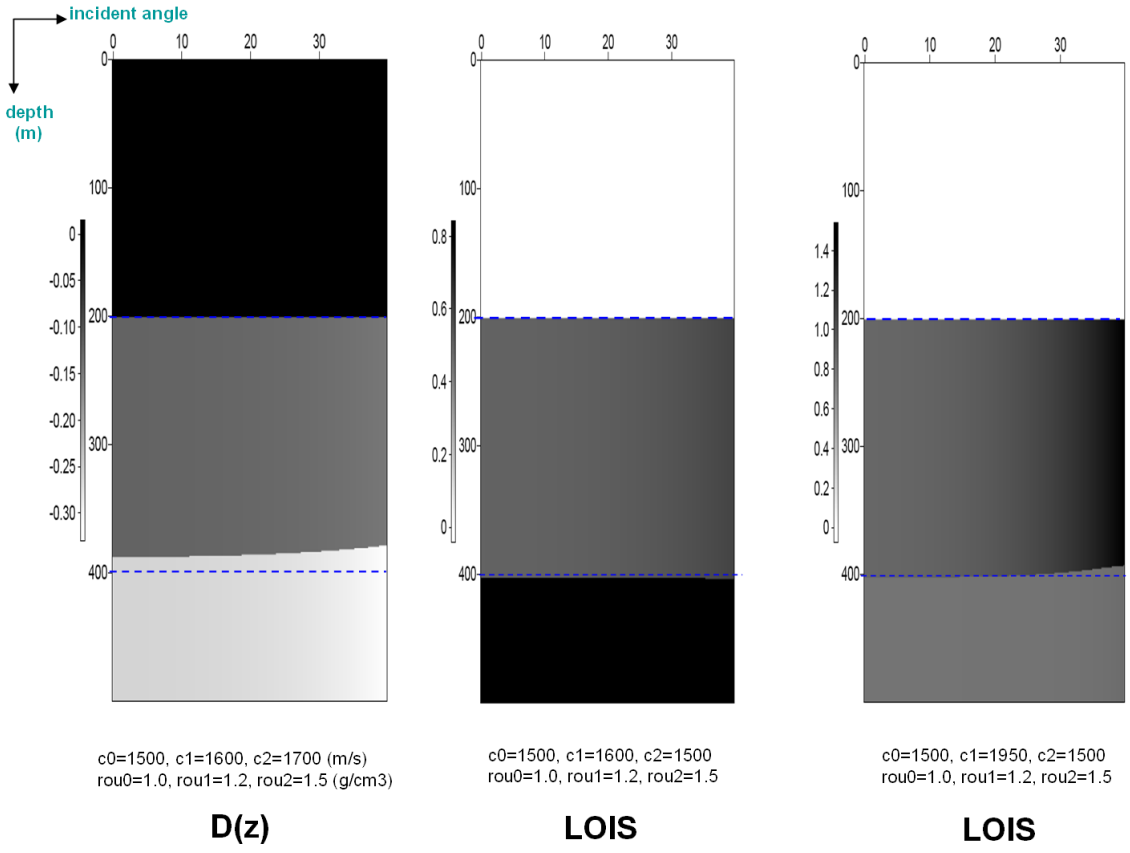

Figure 4: *Imaging comparison 3: left figure is a result of constant velocity ($c_0 = 1500m/s$) migration, middle and right figures are results using two-parameter ISS LOIS imaging algorithm, where the blue dashed lines are the real depths of the two interfaces in the model.*

in the situations of bigger velocity contrast, density changes and depth duration of the model. The *ISS HOIS* results for a bigger velocity contrast model show the necessity of capturing more imaging terms in the *ISS* formalism to correctly locate deeper reflectors. Density variation plays an important role in a model with velocity variation, especially for the *ISS LOIS* algorithm. Further work is needed to study density variation in the toolbox of multiparameter imaging algorithms.

Through the analytic calculation and tests presented in this report, we can observe that the amplitude information of dataset is used for linearly estimating the velocity change between the real velocity model and the reference velocity model which can be constant value. Since in a two-parameter acoustic medium, density is also an element which can affect amplitude, it is fair and important to conclude that density plays a very important role in multiparameter imaging using the ISS. We can expect that the extended multiparameter elastic imaging algorithms will use amplitude information from elastic datasets where more parameters can change and affect the amplitude information. Hence, linear inversion of the parameters in elastic medium is becoming extremely important for providing a "proper" input of the linear estimate of velocity change to the imaging depth correction term. In elastic medium, multi-component datasets will be studied for the linear

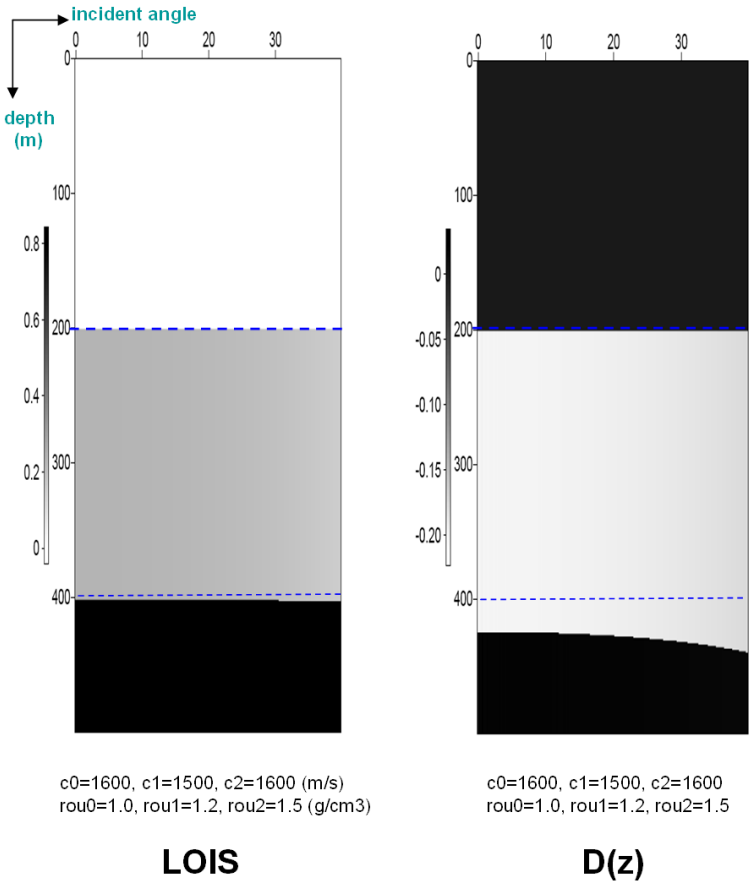

Figure 5: *Imaging comparison 4: right figure is a result of constant velocity ($c_0 = 1600m/s$) migration, left figure is the result using two-parameter ISS LOIS imaging algorithm, where the blue dashed lines are the real depths of the two interfaces in the model.*

inversion of the parameters.

Synthetic data tests of the 1D two-parameter acoustic *ISS LOIS* and *ISS HOIS* imaging algorithms are in progress. Future plans are: (1) synthetic tests of the extended multi-D multiparameter acoustic *ISS HOIS* imaging algorithm; (2) Analytic and synthetic tests of the extended 1D multiparameter elastic *ISS HOIS* using single PP dataset prepared in Jiang et al. (2007) and multi-component dataset; (3) multi-D multiparameter elastic *ISS HOIS*.

6 Acknowledgments

The research reported in this paper is financially supported by the sponsors of M-OSRP, NSF-CMG (award DMS-0327778) and U.S. DOE-BES (Grant No. DOE-De-FG02-05ER15697). Shansong Jiang would like to thank Simon Shaw and Arthur Weglein for their patient co-mentoring and insightful discussions on this work. Fang Liu and Kristopher Innanen are also thanked for their

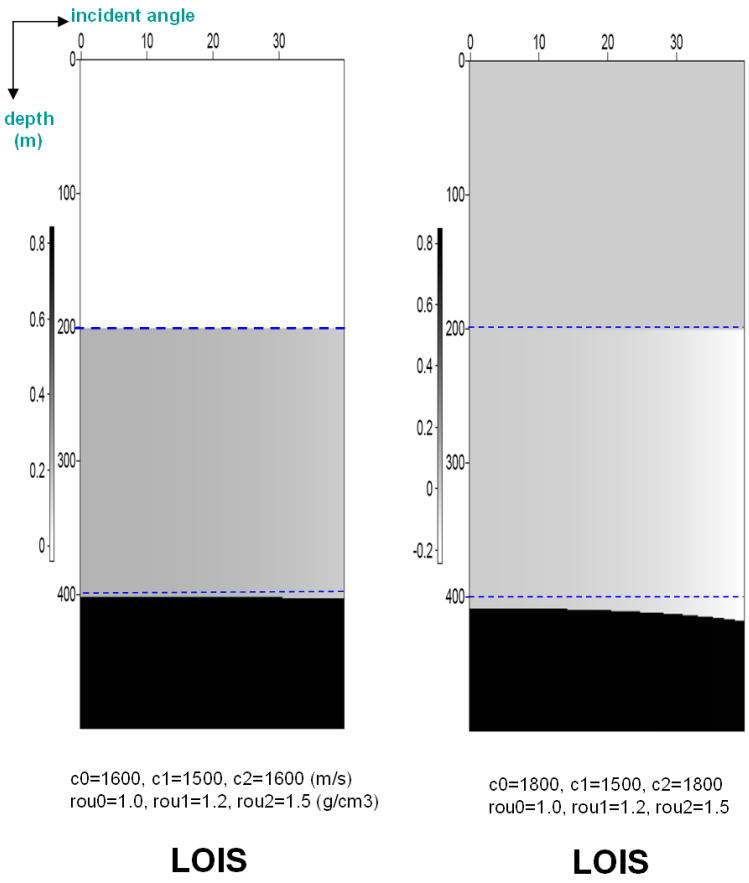

Figure 6: *Imaging comparison 5: both figures are results using two-parameter ISS LOIS imaging algorithm, where the blue dashed lines are the real depths of the two interfaces in the model.*

invaluable technical discussions during this research. Dolores Proubasta and Jim Mayhan are thanked for reviewing and revising this report.

References

Jiang, S., F. Liu, J. Zhang, and A. B. Weglein. "Progressing 1D elastic media imaging using inverse scattering series: analytic PP-data preparation and constant velocity migration." *M-OSRP 2006 Annual Meeting*. 2007, 253–268.

Jiang, S. and A. B. Weglein. "Deriving an imaging algorithm for a laterally invariant multi-parameter acoustic medium from the inverse scattering series." *M-OSRP 2007 Annual Meeting*. 2008, 125–141.

Liu, F., B. G. Nita, A. B. Weglein, and K. A. Innanen. "Inverse Scattering Series in the presence of lateral variations." *M-OSRP Annual Report* 3 (2004).

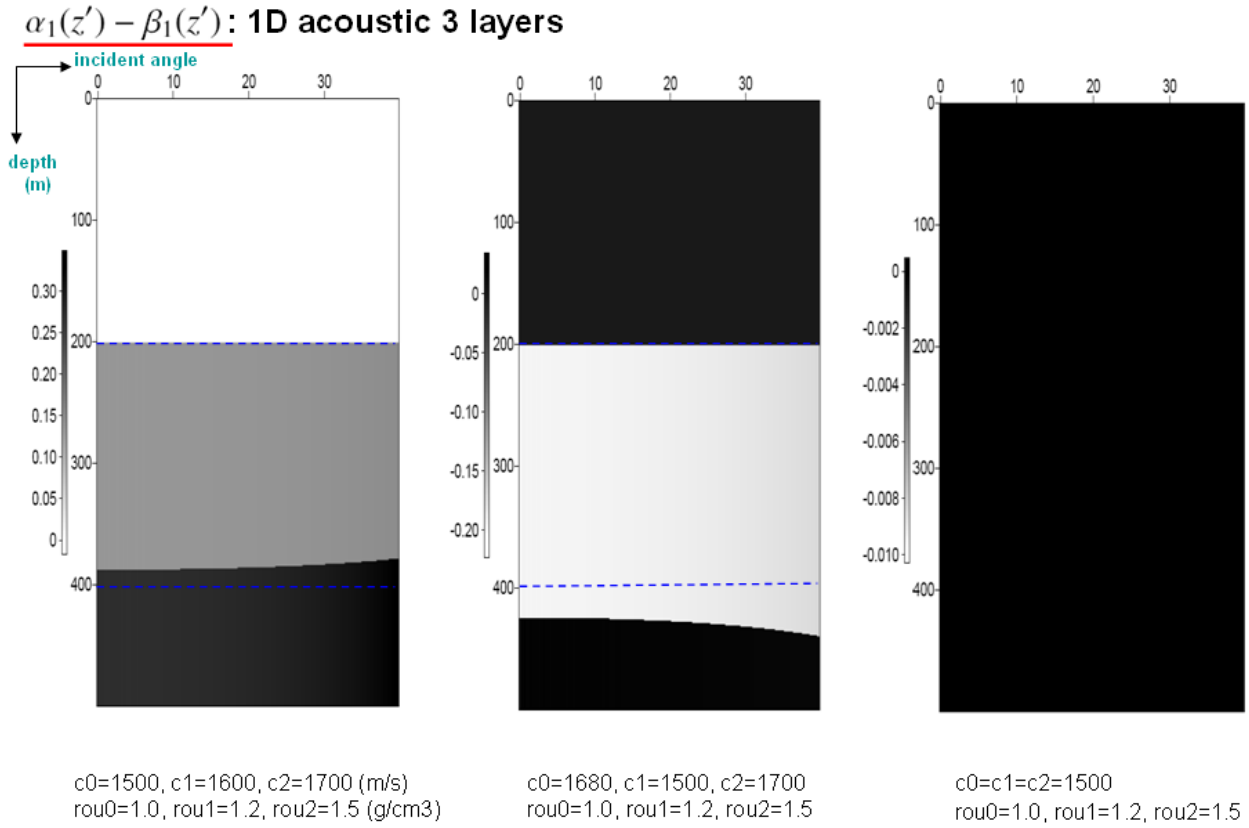

Figure 7: *Results of $\alpha_1(z,\theta) - \beta_1(z,\theta)$ for the three different models, where the blue dashed lines are the real depths of the two interfaces in the model.*

Liu, F., A.B. Weglein, K.A. Innanen, and B.G Nita. "Extension of the non-linear depth imaging capability of the inverse scattering series to multidimensional media: strategies and numerical results." 2005.

Liu, Fang. *Multi-Dimensional Depth Imaing without an Adequate Velocity model.* PhD thesis, University of Houston, 2006.

Shaw, S. A. *An inverse scattering series algorithm for depth imaging of reflection data from a layered acoustic medium with an unknown velocity model.* PhD thesis, University of Houston, 2005.

Shaw, S. A. and A. B. Weglein. "Imaging seismic reflection data at the correct depth without specifying an accurate velocity model: Initial examples of an inverse scattering subseries." *Frontiers of remote sensing information processing.* Ed. C. H. Chen. World Scientific Publishing Company, 2003. chapter 21, 469–484.

Shaw, Simon A., A. B. Weglein, K. H. Matson, and D. J. Foster. "Cooperation of the leading order terms in an inverse-scattering subseries for imaging: 1-D analysis and evaluation.." *SEG Technical Program Expanded Abstracts* (2002): 2277–2280.

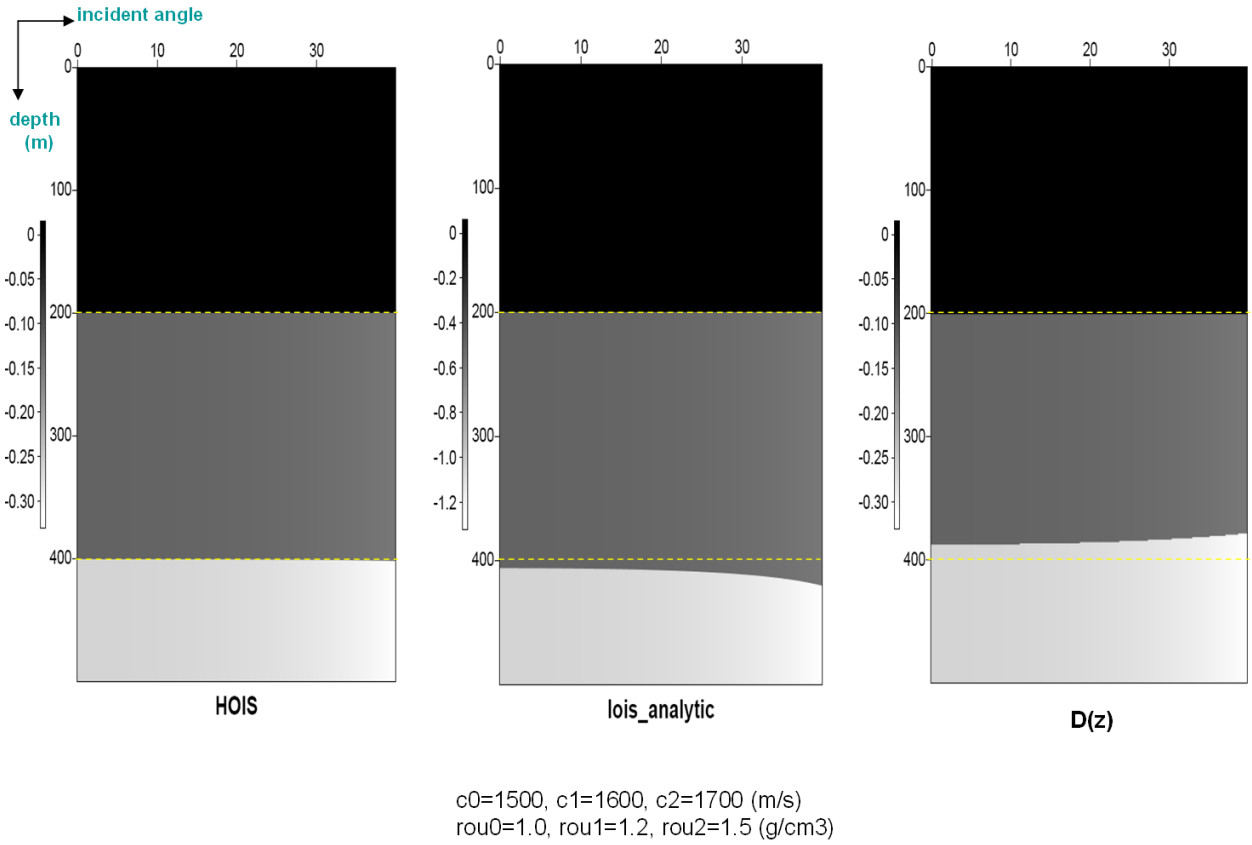

Figure 8: *Imaging comparison 6: right figure is a result of constant velocity ($c_0 = 1500m/s$) migration, middle and left figures are results using two-parameter ISS LOIS and HOIS imaging algorithms, respectively, where the yellow dashed lines are the real depths of the two interfaces in the model.*

Taylor, J. R. *Scattering theory: the quantum theory of nonrelativistic collisions.* John Wiley & Sons, Inc., 1972.

Weglein, A. B., F. V. Araújo, P. M. Carvalho, R. H. Stolt, K. H. Matson, R. T. Coates, D. Corrigan, D. J. Foster, S. A. Shaw, and H. Zhang. "Inverse Scattering Series and Seismic Exploration." *Inverse Problems* (2003): R27–R83.

Weglein, A. B., K. H. Matson, D. J. Foster, P. M. Carvalho, D. Corrigan, and S. A. Shaw. "Imaging and inversion at depth without a velocity model: Theory, concepts and initial evaluation." *70th Annual Internat. Mtg., Soc. Expl. Geophys., Expanded Abstracts.* . Soc. Expl. Geophys., 2000. 1016–1019.

Zhang, H. and A.B. Weglein. "The inverse scattering series for tasks associated with primaries: depth imaging and direct non-linear inversion of 1D variable velocity and density acoustic media." *SEG Technical Program Expanded Abstracts.* 2005, 1705–1708.

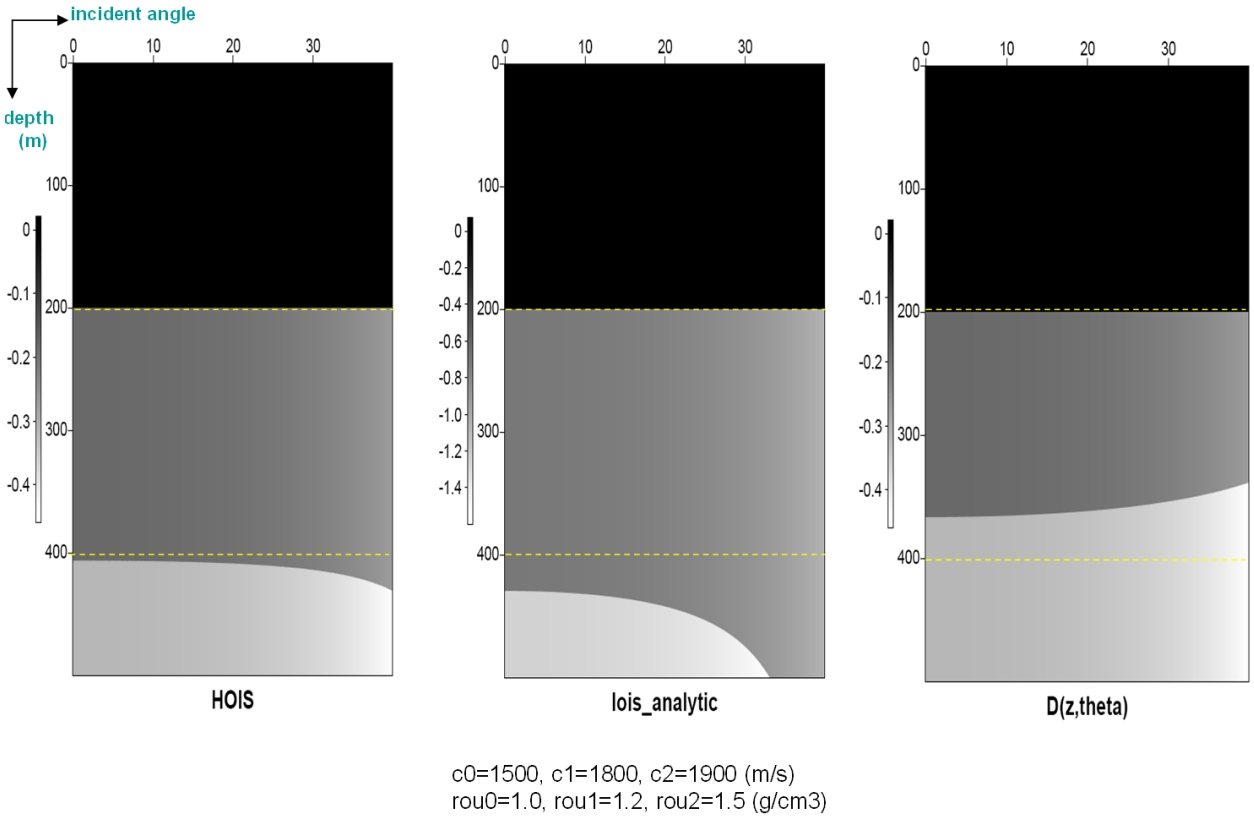

Figure 9: *Imaging comparison 7: right figure is a result of constant velocity ($c_0 = 1500m/s$) migration, middle and left figures are results using two-parameter ISS LOIS and HOIS imaging algorithms, respectively, where the yellow dashed lines are the real depths of the two interfaces in the model.*

Zhang, H. and A.B. Weglein. "Direct non-linear inversion of multi-parameter 1D elastic media using the inverse scattering series." *M-OSRP 2005 Annual Meeting*. 2006, 284–311.

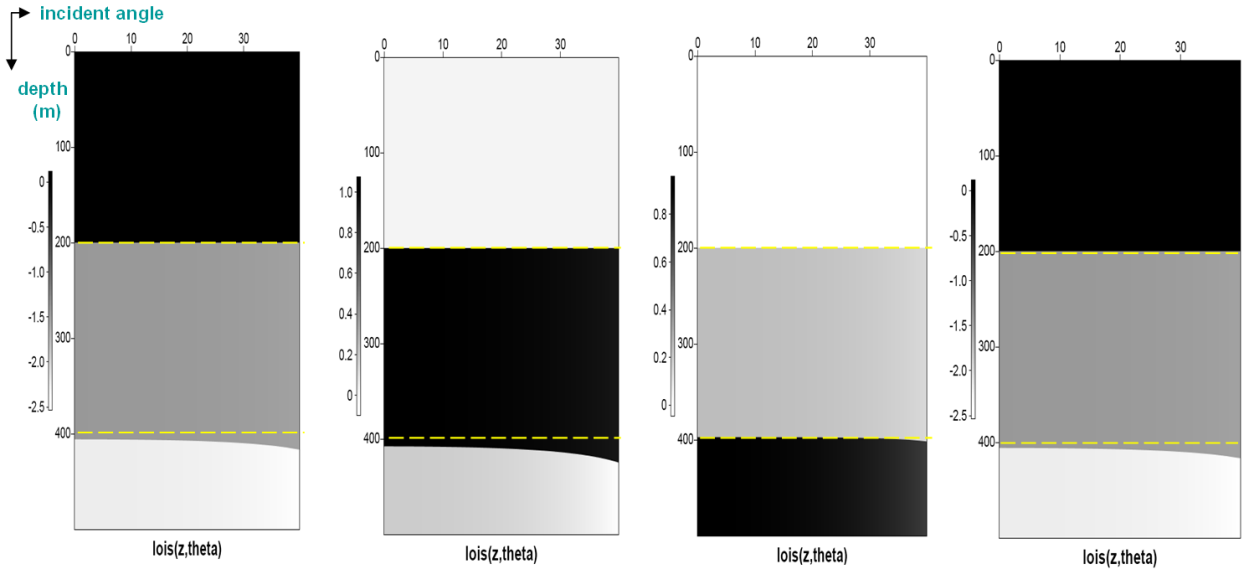

Figure 10: *The sensitivity of density changes to the result of the two-parameter ISS LOIS imaging algorithm: velocity model keeps same in all models. The yellow dashed lines are the real depths of the two interfaces in the model.*

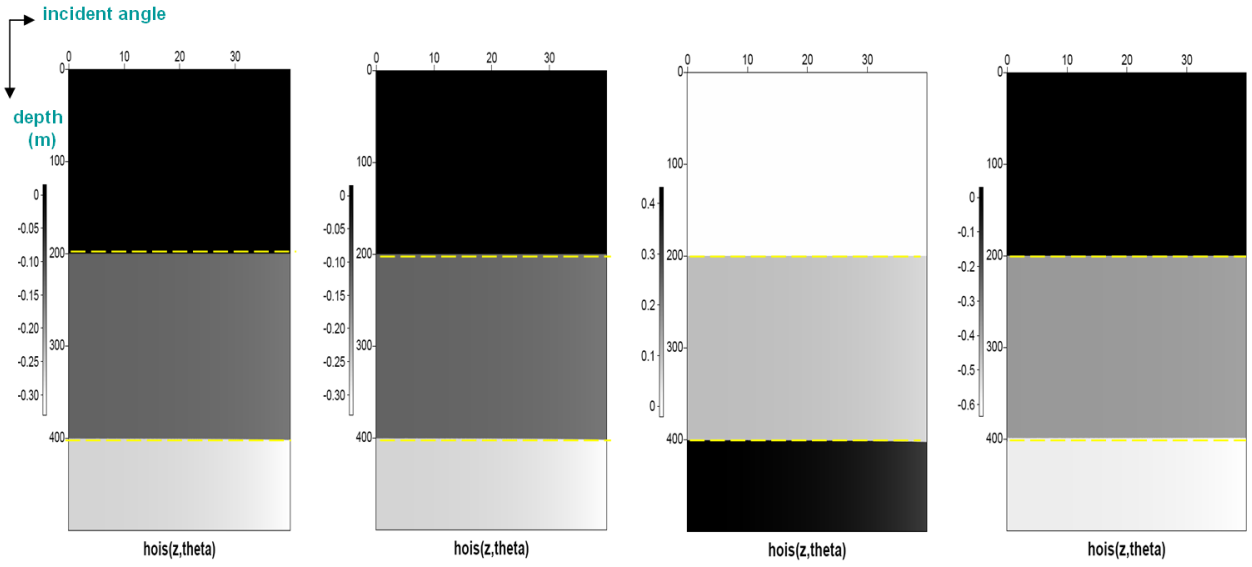

Figure 11: *The sensitivity of density changes to the result of the two-parameter ISS HOIS imaging algorithm: velocity model keeps same in all models. The yellow dashed lines are the real depths of the two interfaces in the model.*

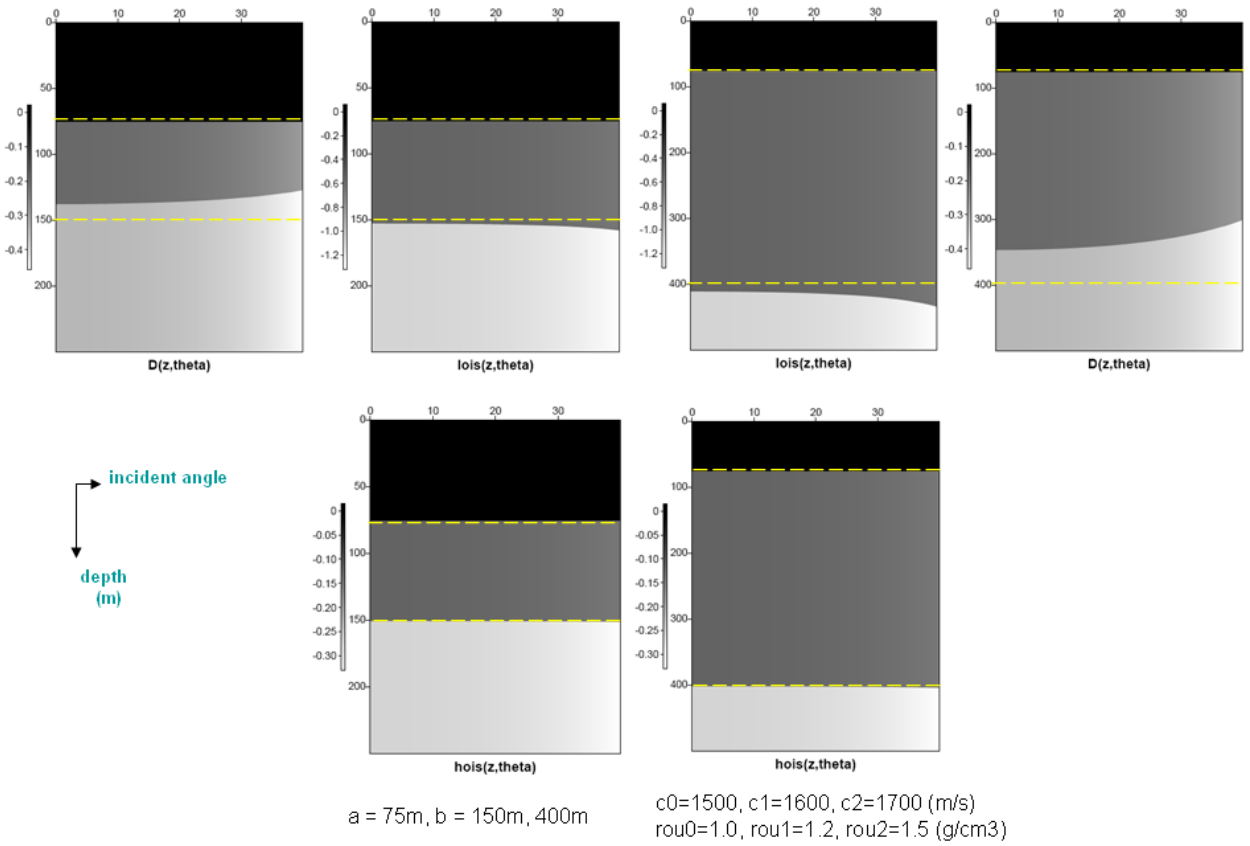

Figure 12: *Effect of depth duration changes to the results of constant velocity migration and the two-parameter ISS LOIS/HOIS imaging algorithms: for all models,density and velocity values are same in each layer. The yellow dashed lines are the real depths of the two interfaces.*

Depth imaging without the velocity cares about the phase and amplitude information of events: focusing on the use of the angle dependent amplitude information of events

X. Li, F. Liu, S. Jiang and A. B. Weglein, M-OSRP, University of Houston

Abstract

Depth imaging through a complicated geologic overburden is an important and long standing challenge in exploration seismology. Based on inverse scattering theory, the subseries for imaging without the velocity (Weglein et al., 2003) has the potential for directly producing an image of the earth using only the recorded data. A conjectured multiparameter imaging algorithm was proposed by Weglein in 2007, extending the single-parameter imaging series algorithms of Shaw et al. (2004) and Liu et al. (2005).

The input to inverse scattering series (ISS) depth imaging algorithms correctly pre-processed amplitudes of events and phases of events. In this report, we focus on the use of angle dependent event amplitudes. By combining amplitudes at appropriate incidence angles, we propose a framework to prepare the linear estimate of the velocity change, $(\alpha_1 - \beta_1)$, for the conjectured imaging algorithm for a 1D 2-parameter acoustic medium (velocity and density variation). Three analytic examples (layered medium with velocity variation only, with density variation only and with both velocity and density variation) were tested and analyzed. From the analytic results, we examined how density changes affect the linear estimate of the velocity change. Finally, also included are the initial imaging results for the reflection coefficient for analytic example, which, importantly preserves zero crossing and signs. Avoiding the loss of zero crossing information marks an improvement on current standard processing, which involves ironing common image gathers.

1 Introduction

In this report, I primarily focus on including certain reflections and excluding others which is one aspect within the project of the multi-parameter imaging effort. And in Shansong jiang's 2008 annual report, he focuses on another aspect of using the included reflections for the purpose of direct depth imaging without subsurface information. At this early stage, there are some expected overlap of activity and certain important distinct contributions in these two reports. When seeking goals within the elastic application and field data tests, these two aspects will require further serious concept development, and will be separately advanced and then coupled to address challenges.

For conventional imaging, people locate reflectors at depth using seismic reflection, taking advantage of both the arrival time of the events and the velocity field obtained from velocity analysis. With current data acquisitions which often miss small and cross-line offsets measurements and low frequency information, those imaging algorithms manage to provide satisfactory results for most cases. However, for cases like sub-salt imaging, where the velocity analysis has difficulties, the performance of those velocity dependent migration procedures will be affected.

The ISS has the potential to achieve all processing goals directly in terms of recorded data, and without any need, in principle or practice, to provide any subsurface information. Velocity independent imaging algorithm derived from the ISS is capable of using the amplitude information of the data as well as the arrival time. The inverse scattering series has given results which indicate that it is a good framework for doing imaging and inversion without a velocity model.

Since the announced goal of using the inverse scattering series for simply locating reflectors at their correct spatial location without knowing any subsurface properties including velocity, it was natural and reasonable to begin with an earth model that only allowed variation in velocity. Pioneering works (Weglein et al., 2000, 2001, 2002; Shaw et al., 2004, 2003; Shaw and Weglein, 2003; Innanen, 2005) have been done on a 1D one parameter medium (with only velocity varying) and seek to depth locate structure without knowing or determining the velocity model. The first step of performing imaging without the velocity is to obtain $\alpha_1(z)$ which is very close to the Stolt migration result using reference medium velocity (Stolt, 1978). More terms of the inverse scattering series have been identified to improve the locations of the reflectors in α_1. So far, there are two closed forms of the imaging sub-series known as the leading order imaging series (LOIS) (Shaw et al., 2003) and the higher order imaging series (HOIS)(Liu, 2006).

$$\alpha^{LOIS}(z) = \alpha_1(z - \frac{1}{2}\int_0^z \alpha_1(z')dz'); \tag{1}$$

$$\alpha^{HOIS}(z + \frac{1}{2}\int_0^z \frac{\alpha_1(z')}{1 - \frac{1}{4}\alpha(z')}dz') = \alpha_1(z). \tag{2}$$

Compared to α_1, these two functions provide better spatial locations. In the one parameter world, for an actual medium with changing velocity, there is an issue of mislocating the deeper reflectors. In the imaging-only terms, for example, $-\frac{1}{2}\frac{d\alpha_1(z)}{dz}\int_{-\infty}^z \alpha_1(z')dz'$, the attention needing term (the derivative part in imaging-only terms) lights up and the attention providing term (the integral part in imaging-only terms) acts to correct for the right location; for an actual medium with a constant velocity, if the reference velocity is selected to be the same as the waves in the background medium, the attention providing term will automatically shut down. That means the imaging algorithm is not attempting to correct for an issue that does not exist.

However, generally speaking, rapid changes in density is as common as rapid changes in velocity. In traditional seismic imaging the assumption is that we can determine an adequate velocity. If the velocity configuration is achievable, and the goal is a structure map, then thinking (and then worrying) about additional subsurface properties such as density are unnecessary unless you want location and inversion at depth, in which case all overburden properties are relevant and required. But what about the ISS? What will happen when velocity changes? Or density changes? Or both velocity and density change? LOIS and HOIS were challenged when there is not only density change. So we need a multi-parameter ISS to study how the depth imaging task is performed in this more realistic and much more complicated earth.

A conjectured imaging algorithm was proposed by Weglein, which has similar logic to that in the LOIS and HOIS algorithms. Further, for a 1D 2-parameter acoustic medium, higher order imaging-only terms has been calculated and captured to justify the conjectured imaging algorithm (Jiang and Weglein, 2007). For multiparameter imaging, the first step is to obtain $\alpha_1 - \beta_1$ as a composite

for the ISS imaging algorithm. In the following section, we will present how to find $\alpha_1 - \beta_1$ from the angle dependent amplitude information for a 1D 2-parameter acoustic medium. Further analysis about this framework will be shown as well.

In the last section, we will present the initial imaging results on polarity reversals in reflections from layered acoustic media, aimed towards type 1 and type 2 AVO applications.

2 Extended imaging algorithm

The ISS imaging algorithm has been extended to multiparameter case for both acoustic and elastic media. Let us consider a 1D 2-parameter acoustic earth model (e.g. bulk modulus and density or velocity and density). Starting with the 3D acoustic wave equations for reference and actual medium,

$$[\frac{\omega^2}{K_0(r)} + \nabla \cdot \frac{1}{\rho_0(r)}\nabla]G_0(\mathbf{r}, \mathbf{r_s}; \omega) = \delta(\mathbf{r} - \mathbf{r_s}), \tag{3}$$

$$[\frac{\omega^2}{K(r)} + \nabla \cdot \frac{1}{\rho(r)}\nabla]G(\mathbf{r}, \mathbf{r_s}; \omega) = \delta(\mathbf{r} - \mathbf{r_s}). \tag{4}$$

where G_0 and G are the reference and actual Green's functions respectively. $K = c^2\rho$, is P-bulk modulus, c is P-wave velocity and ρ is density. The subscript 0 represents those variables in the reference medium.

The perturbation is

$$V = L_0 - L = \frac{\omega^2\alpha}{K_0} + \nabla \cdot \frac{\beta}{\rho_0}\nabla, \tag{5}$$

where $\alpha = 1 - \frac{K_0}{K}$ and $\beta = 1 - \frac{\rho_0}{\rho}$ are the two parameters we are going to use. $V(z, \nabla)$, $\alpha(z)$ and $\beta(z)$ can be expanded in terms of recorded data (Weglein et al., 2003) respectively as

$$V(z, \nabla) = V_1(z, \nabla) + V_2(z, \nabla) + \cdots, \tag{6}$$

$$\alpha(z) = \alpha_1(z) + \alpha_2(z) + \cdots, \tag{7}$$

$$\beta(z) = \beta_1(z) + \beta_2(z) + \cdots. \tag{8}$$

Based on inverse scattering series, the second order approximation for the parameters was calculated in Zhang and Weglein 2005 for a layered acoustic media with both velocity and density changes, the imaging-only term in this 2^{nd} term was identified as:

$$-\frac{1}{2}\frac{1}{\cos^2\theta}[\frac{1}{\cos^2\theta}\alpha_1'(z) + (1 - \tan^2\theta)\beta_1'(z)]\int_{-\infty}^{z}[\alpha_1(z') - \beta_1(z')]dz', \tag{9}$$

Substituting $\alpha_1(z)$ of one parameter case shown in Eq.(2) with $\alpha_1(z) - \beta_1(z)$ of multiparameter case, we have the conjectured imaging algorithm for the latter one as

$$D^{HOIS}(z + \int_{-\infty}^{z}\frac{[\alpha_1(z') - \beta_1(z')]dz'}{\cos^2\theta - 0.25 \cdot [\alpha_1(z') - \beta_1(z')]}, \theta) = D(z, \theta).$$

In the conjectured imaging algorithm, the two parameters (velocity and density) will be imaged as a composite form, which means instead of distinguishing the details of the changed information (velocity change or density change), the imaging task recognizes them as a combined form linear in the recorded data. In other words, no matter what changes across the reflectors, the needing attention term will light up and the providing attention term will correct the depth structure if needed. The next step is to preprocess the amplitude information for $\alpha_1 - \beta_1$ that is needed.

3 Analytic examples

3.1 The use of angle dependent amplitude for $(\frac{\Delta v}{v})_1$

Considering a model that consists of two horizontal interfaces at depths a and b, with a discontinuous velocity profile c_0, c_1 and c_2. Above the first interface is the reference medium, and below is the actual medium.

The wavefield above the first interface consists of an incident field Ψ_i and a reflected field Ψ_r. The measured reflected wavefield can be derived by decomposing the incident field into a sum of plane waves (the Sommerfeld integral) and then matching boundary conditions at each interface. Suppose the source and receiver locate at $z = 0$, then

$$\Psi_r(r; q_g) = \int_0^\infty \frac{1}{4\pi i q_g}(R_{01}(\theta)e^{2iq_g a} + R'_{12}(\theta)e^{2iq_g b'})J_0(kr)kdk. \tag{10}$$

where $q_g = \sqrt{\frac{\omega^2}{c_0^2} - k^2}$. The reflection coefficients from the first and second reflectors are functions of angle and are respectively given by

$$R_{01}(\theta) = \frac{(c_1/c_0)\sqrt{1-\sin^2\theta} - \sqrt{1-(c_1^2/c_0^2)\sin^2\theta}}{(c_1/c_0)\sqrt{1-\sin^2\theta} + \sqrt{1-(c_1^2/c_0^2)\sin^2\theta}}. \tag{11}$$

and

$$R'_{12} = T_{01}R_{12}T_{10}$$

where $T_{01} = 1 + R_{01}$ and $T_{10} = 2 - T_{01}$ are also functions of angle. With these coefficients, data may be expressed analytically in the q_g domain as:

$$\tilde{D}(q_g, \theta) = R_{01}(\theta)\frac{e^{2iq_g a}}{4\pi i q_g} + R'_{12}(\theta)\frac{e^{2iq_g b'}}{4\pi i q_g}. \tag{12}$$

Fourier transforming over $2q_g$, we have

$$D(z, \theta) = R_{01}(\theta)H(z - a) + R'_{12}(\theta)H(z - b'). \tag{13}$$

At a fixed θ, we have (Zhang, 2006)

$$\frac{1}{\cos^2\theta}\alpha_1(z) + (1 - \tan^2\theta)\beta_1(z) = 4R_{01}(\theta)H(z - a) + 4R'_{12}(\theta)H(z - b'). \tag{14}$$

From Eq.(14), choosing two different angles to solve for $\alpha_1 - \beta_1$

$$\begin{aligned}(\alpha_1 - \beta_1)(z, \theta_1, \theta_2) &= \frac{4}{\tan^2\theta_2 - \tan^2\theta_1}[R_0(\theta_1) - R_0(\theta_2)]H(z-a) \\ &+\frac{4}{\tan^2\theta_2 - \tan^2\theta_1}[R_1'(\theta_1)H(z-b'(\theta_1)) - R_1'(\theta_2)H(z-b'(\theta_2))] \quad (15)\end{aligned}$$

where $b'(\theta) = a + (b-a)\frac{C_0\sqrt{1-C_1^2p^2}}{C_1\sqrt{1-C_0^2p^2}}$ and $\frac{\sin\theta}{C_0} = p$.

Now that we have $\alpha_1 - \beta_1$, we can do depth imaging through the conjectured imaging algorithm. But the problem is how should we use the angle dependent amplitude information to obtain $\alpha_1 - \beta_1$? Although α and β which are related to the medium properties, are not functions of angle, α_1, β_1 and $\alpha_1 - \beta_1$ should be functions of angle. In other words, different framework of using the amplitude information will in consequence produce different imaging results. So, what data combination do we need to find $\alpha_1 - \beta_1$? In this report, for each $(\alpha_1 - \beta_1)(z, \theta_1, \theta_2)$ in Eq.15, θ_1 and θ_2 were picked to be very close to each other. There are two reasons: 1) the deeper information should not contribute to correcting the location of the shallower reflector. If the angles we pick are close enough, we can avoid data from deeper depths talking to data from shallower depths; 2) the angle outside the integral will be easy to choose. Because the two angles are so close that no matter which one of them we choose will provide very close output.

3.2 Analytic Results

Here we study the simplest example of two reflectors for 1D acoustic medium, where the velocity and density for the reference are known.

In the following, three specific models were studied for the imaging conjecture. Figure 1 shows the constant velocity model, Figure 5 shows the constant density model and Figure 9 shows the model in which both velocity and density change. In each case, the water bottom is well located, and in all the pictures of $D(z)$ (which means water speed migration, the output is reflectivity), the blue lines represent the correct location of the second reflector, and the red lines in all the pictures of HOIS of $D(z)$ show the same thing.

4 Discussion

4.1 Density changes affect $(\frac{\Delta v}{v})_1$

Model 2 and model 3 have the same velocity change but different density changes, and the imaging results for model 3 is better, which lead us to question how does density change influence the linear estimation of velocity change? When we choose two different angles to solve for $\alpha_1 - \beta_1$:

$$\alpha_1 - \beta_1 = \frac{R(\theta_1) - R(\theta_2)}{\tan^2\theta_1 - \tan^2\theta_2}$$

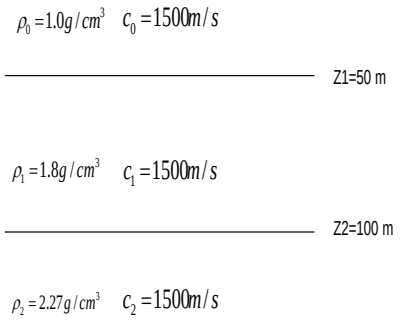

Figure 1: Model 1

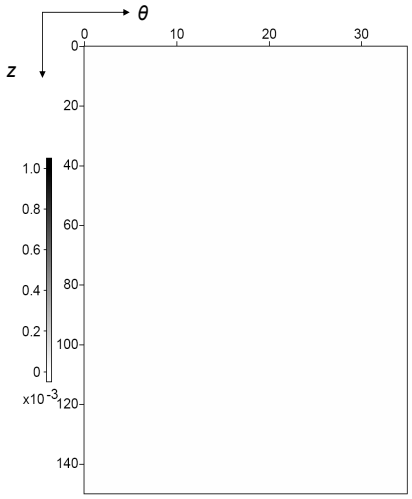

Figure 2: $\alpha_1 - \beta_1$ for model 1. θ_1 is fixed to 0, while θ_2 is changing. In this constant velocity case, $\alpha_1 - \beta_1$ is zero, which means the reflectors are well located, and the attention providing term shuts down.

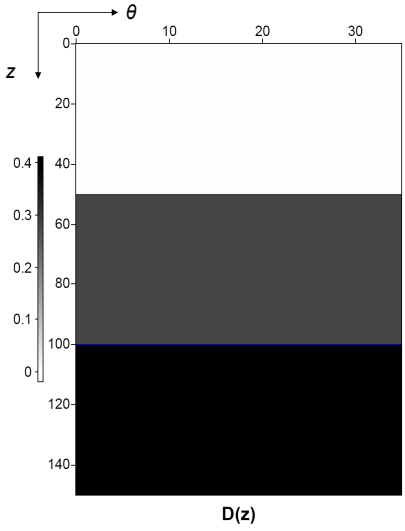

Figure 3: Data before HOIS

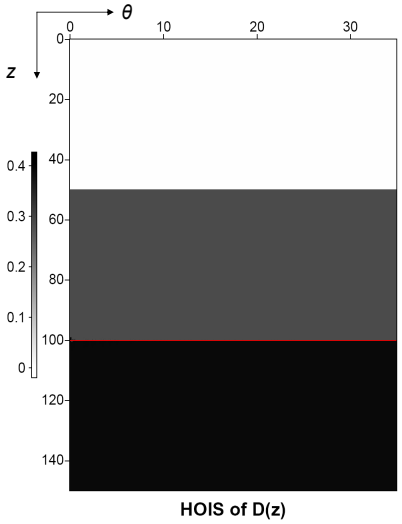

Figure 4: Data after HOIS

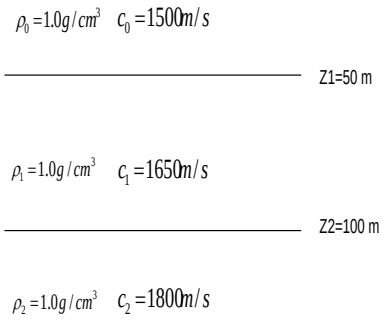

Figure 5: The second model

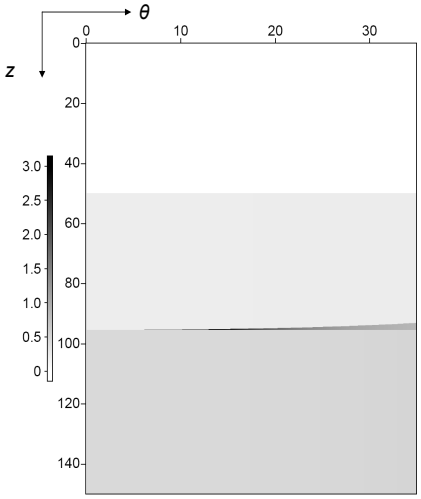

Figure 6: $\alpha_1 - \beta_1$ for model 2. θ_1 is fixed to 0, while θ_2 is changing.

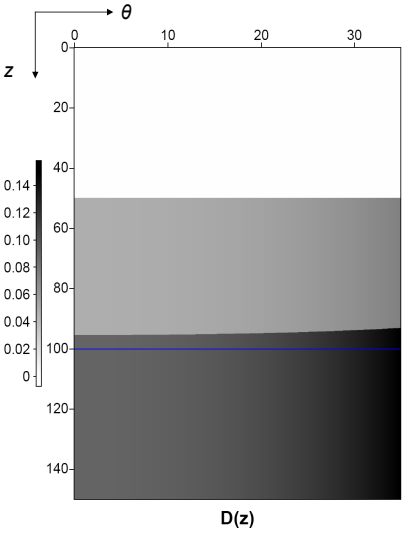

Figure 7: Data before HOIS

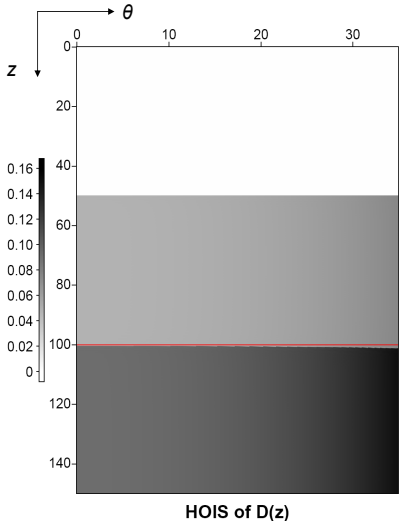

Figure 8: Data after HOIS

and,

$$R(\theta) = \frac{\rho_1 c_1(\theta) - \rho_0 c_0(\theta)}{\rho_1 c_1(\theta) + \rho_0 c_0(\theta)} = \frac{\frac{\rho_1}{\rho_0} c_1(\theta) - c_0(\theta)}{\frac{\rho_1}{\rho_0} c_1(\theta) + c_0(\theta)}$$

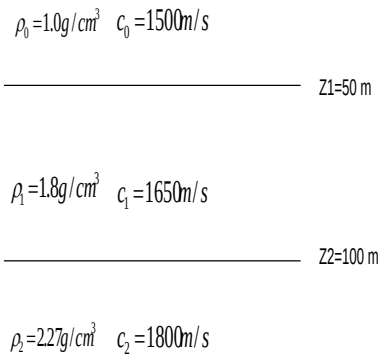

Figure 9: The third model

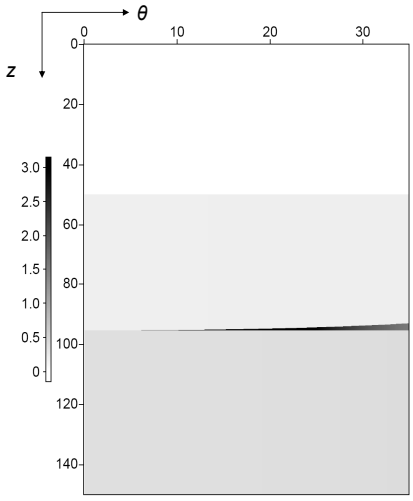

Figure 10: $\alpha_1 - \beta_1$ for model 3. θ_1 is fixed to 0, while θ_2 is changing.

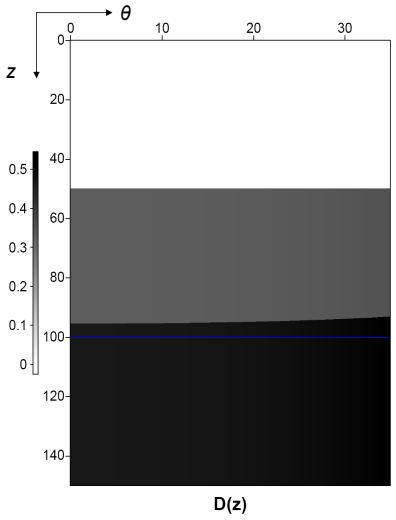

Figure 11: Data before HOIS

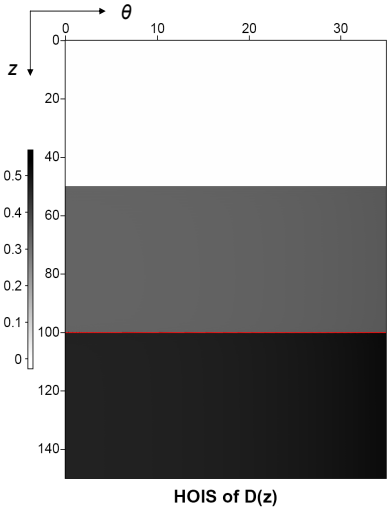

Figure 12: Data after HOIS

$$= 1 - \frac{2c_0(\theta)}{\frac{\rho_1}{\rho_0}c_1(\theta) + c_0(\theta)}$$

where $c_0(\theta) = c_0/\sqrt{1-\sin^2\theta}$, $\quad c_1(\theta) = c_1/\sqrt{1-\frac{c_1^2}{c_0^2}\sin^2\theta}$.

$$\begin{aligned}(\alpha_1-\beta_1) &= (2\frac{c_0(\theta_2)}{\frac{\rho_1}{\rho_0}c_1(\theta_2)+c_0(\theta_2)} - 2\frac{c_0(\theta_1)}{\frac{\rho_1}{\rho_0}c_1(\theta_1)+c_0(\theta_1)})/(\tan^2\theta_1-\tan^2\theta_2)\\ &= 2\frac{c_0(\theta_2)c_1(\theta_1)-c_0(\theta_1)c_1(\theta_2)}{\tan^2\theta_1-\tan^2\theta_2}\\ &\times \frac{1}{\frac{\rho_1}{\rho_0}c_1(\theta_1)c_1(\theta_2)+\frac{\rho_0}{\rho_1}c_0(\theta_1)c_0(\theta_2)+c_1(\theta_1)c_0(\theta_2)+c_0(\theta_1)c_1(\theta_2)}. \end{aligned} \tag{16}$$

In order to study how density changes affect $\alpha_1-\beta_1$ under a certain ratio of velocity changes, we should take a close look at the part of the above formula involving density:

$$\frac{\rho_1}{\rho_0}c_1(\theta_1)c_1(\theta_2)+\frac{\rho_0}{\rho_1}c_0(\theta_1)c_0(\theta_2).$$

Assuming the density of the medium in the second layer changes from ρ_1 to ρ_1', the change of the part involving density is as follows:

$$\begin{aligned}&\frac{\rho_1'}{\rho_0}c_1(\theta_1)c_1(\theta_2)+\frac{\rho_0}{\rho_1'}c_0(\theta_1)c_0(\theta_2)-(\frac{\rho_1}{\rho_0}c_1(\theta_1)c_1(\theta_2)+\frac{\rho_0}{\rho_1}c_0(\theta_1)c_0(\theta_2))\\ &=\frac{(\rho_1'-\rho_1)}{\rho_0}[c_1(\theta_1)c_1(\theta_2)-\frac{\rho_0^2}{\rho_1\rho_1'}c_0(\theta_1)c_0(\theta_2)].\end{aligned}$$

Let us go to some details:
1. When $c_1 > c_0$ and $\theta_2 > \theta_1$, the first term (please see Appendix A for details)

$$\frac{c_0(\theta_2)c_1(\theta_1)-c_0(\theta_1)c_1(\theta_2)}{\tan^2\theta_1-\tan^2\theta_2} > 0.$$

In the case of $\rho_1 > \rho_0$, the bigger the density contrast ($\rho_1' > \rho_1$), the smaller the second term. Then the value of $\alpha_1-\beta_1$ is smaller;
In the case of $\rho_1 < \rho_0$, when the density contrast is increasing ($\rho_1' < \rho_1$), and if $[c_1(\theta_1)c_1(\theta_2) - \frac{\rho_0^2}{\rho_1\rho_1'}c_0(\theta_1)c_0(\theta_2)] < 0$, the value of $\alpha_1-\beta_1$ will be also smaller, otherwise, it is larger.

2. When $c_1 < c_0$ and $\theta_2 > \theta_1$,

$$\frac{c_0(\theta_2)c_1(\theta_1)-c_0(\theta_1)c_1(\theta_2)}{\tan^2\theta_1-\tan^2\theta_2} < 0,$$

In the case of $\rho_1 > \rho_0$, when the contrast of the density is bigger ($\rho_1' > \rho_1$), and if $[c_1(\theta_1)c_1(\theta_2) - \frac{\rho_0^2}{\rho_1\rho_1'}c_0(\theta_1)c_0(\theta_2)] > 0$, the smaller the second term, thus, the value of $\alpha_1-\beta_1$ is smaller, otherwise, it is bigger.
In the case of $\rho_1 < \rho_0$, the bigger the contrast of the density ($\rho_1' < \rho_1$), the smaller the value of $\alpha_1-\beta_1$.

4.2 A clean separation of density contribution

In Eq.(14), when we find $\alpha_1 - \beta_1$ by combining amplitudes of two angles that are very close to each other, it is in some sense obtaining the derivative with respect to θ. Since $\alpha_1 - \beta_1$ is the linear estimation of the velocity change, it inspires us to think of separating the velocity and density contributions through data and its derivatives. For example, in the simplest one reflector case, starting from the shifting term of HOIS for one parameter, and $\alpha_1 = 4R$

$$shift = \frac{1}{2}\frac{\alpha_1}{\cos^2\theta - \frac{1}{4}\alpha_1} = \frac{2R}{\cos^2\theta - R}$$

where R is the reflection coefficient, and $R = \frac{I_1 - I_0}{I_1 + I_0}$, I_0 and I_1 are the impedances for the first and second medium respectively, we have

$$shift = \frac{2(I_1 - I_0)/(I_1 + I_0)}{\cos^2\theta - (I_1 - I_0)/(I_1 + I_0)} \tag{17}$$

Solving for $\frac{I_1}{I_0}$ and defining function $f \equiv \frac{I_1}{I_0}$, we have

$$f \equiv \frac{I_1}{I_0} = \frac{2 + (1 + \cos^2\theta)\cdot shift}{2 + \sin^2\theta \cdot shift} \tag{18}$$

where the function f is simply a function of the impedances. In the two parameter world, assuming f stays the same as in Eq.(18) which is a combination of data, and we also have

$$f = \frac{I_1}{I_0} = \frac{\rho_1}{\rho_0}\frac{c_1/\sqrt{1 - c_1^2 p^2}}{c_0/\sqrt{1 - c_0^2 p^2}}. \tag{19}$$

where $p = \frac{\sin\theta}{c_0}$.
Define $u = p^2$ and another function G,

$$\begin{aligned} G(u,v) &= \ln(\frac{f^2(u)}{f^2(v)}) = \ln(\frac{1 - c_0^2 u}{1 - c_1^2 u}\cdot\frac{1 - c_0^2 v}{1 - c_1^2 v}) &(20)\\ &= \ln(1 - c_0^2 u) - \ln(1 - c_1^2 u) + \ln(1 - c_1^2 v) - \ln(1 - c_0^2 v). &(21)\end{aligned}$$

we have $\frac{\partial G}{\partial u} = \frac{1}{c_1^{-2} - u} - \frac{1}{c_0^{-2} - u}$ and $\frac{\partial^2 G}{\partial u^2} = \frac{1}{(c_1^{-2} - u)^2} - \frac{1}{(c_0^{-2} - u)^2}$, then

$$(\frac{G''}{G'} - G')|_u = 2\frac{1}{c_0^{-2} - u};$$

$$(\frac{G''}{G'} + G')|_u = 2\frac{1}{c_1^{-2} - u};$$

So we can express the velocity related part as:

$$\frac{\sqrt{c_0^{-2} - u}}{\sqrt{c_1^{-2} - u}} = \sqrt{\frac{\frac{G''}{G'} + G'}{\frac{G''}{G'} - G'}}. \tag{22}$$

We would like to change the above expression in terms of the function $f(u)$ which is the data combination that corresponds to only one angle, as we can easily compute,

$$G'|_u = \frac{2f'}{f};$$

$$G''|u = 2\frac{f''f - (f')^2}{f^2};$$

It is obvious that we have

$$\frac{\sqrt{c_0^{-2} - u}}{\sqrt{c_1^{-2} - u}} = \sqrt{\frac{f''f + f'f'}{f''f - 3f'f'}}. \tag{23}$$

which indicates that if we can measure the derivative of the data with respect to angle, we can separate the contribution of the velocity and density.

5 Polarity reversal in a reflection from an acoustic interface

In this section, we study the polarity reversal in reflection from an acoustic interface in layered medium. Investigating polarity reversals in seismic reflection is a very important issue. Because they provide information of a very important type of AVO, and since multiplication by zero yields zero, they are insensitive to many of the extraneous factors that affect amplitude variations with offset.

As studied by Keys (1988), a polarity reversal in a reflection from an acoustic interface occurs when an increase in the acoustic impedance across the interface is accompanied by a decrease in the P-wave velocity. The imaging results are studied for the analytic model as follows: $c_0 = 1500m/s, \rho_0 = 1.0g/cm^3, c_1 = 1600m/s, \rho_1 = 1.1g/cm^3, c_2 = 1200m/s, \rho_2 = 1.5g/cm^3$. Figure 13 shows $\frac{\partial D}{\partial z}$ before HOIS. In this model, the amplitude is a function of angle and changes from positive to negative when the angle increases. The red line represents the correct location, and it is clear that the second reflector is mislocated. We have an enlarged picture on the right about the detailed information. (In all the pictures, we only keep the information for the second reflector in the picture to see better.)

Figure 14 shows $\frac{\partial D}{\partial z}$ after HOIS. Because the reflector is moved almost to the correct location, it is difficult to see the amplitude information in this picture. On the right hand side, there is an enlarged picture displaying the detail of the polarity reversal information. In Figure 15, we extract the information of amplitude changing with angle, from which we can see a small transmission difference between the real reflection coefficient and the $\frac{\partial D}{\partial z}$ output by imaging conjecture.

6 Conclusion and Future plan

In this report, we focused on the use of angle dependent amplitude information of events and let data from different angle talk to each other. The framework found analytically for $\alpha_1 - \beta_1$ for a

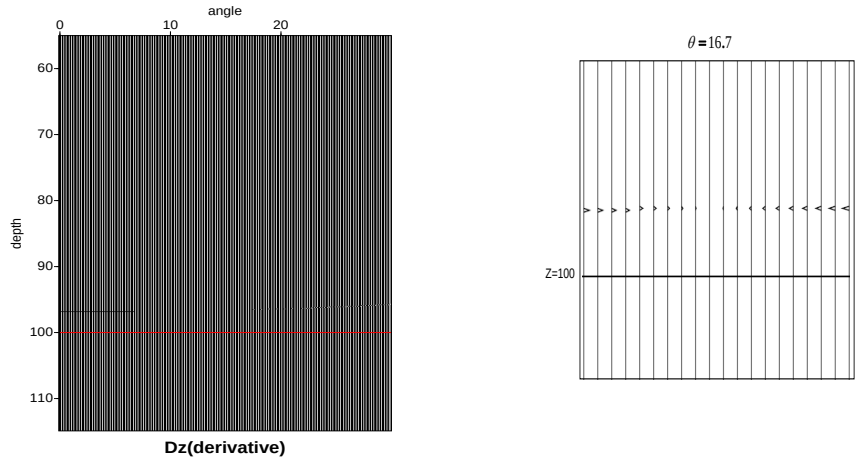

Figure 13: $\frac{\partial D}{\partial z}$ before HOIS. On the right side, there is an enlarged picture displaying in detail of the polarity reversal information. $z = 100$ is the correct location of the second reflector and zero crossing happens when $\theta = 16.7$

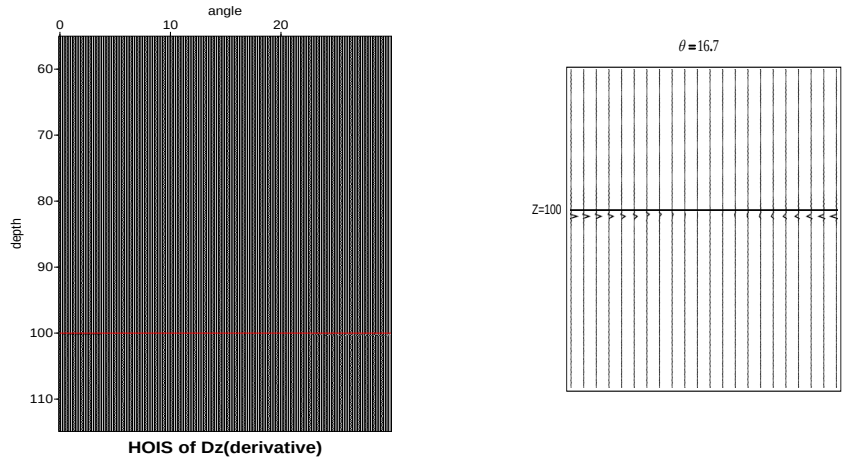

Figure 14: $\frac{\partial D}{\partial z}$ after HOIS. On the right side, is the enlarged picture as in Figure 13.

1D 2-parameter acoustic medium (velocity and density distribution) is very favorable. It provides an insightful analysis that can be applied to the concepts and algorithms of the inverse scattering series. A detailed explanation was provided on how density changes affect $\alpha_1 - \beta_1$ when other properties stay the same. In the end, a simple analytic study has been done on reflection coefficient preserving zero crossing and signs when going through an overburden, which has significant meaning in AVO. Next, we are going to find the framework for $\alpha_1 - \beta_1$ from PP data, and extend to PP plus synthesized PS and SS data in the elastic case. Meanwhile, polarity reversal tests will be extended

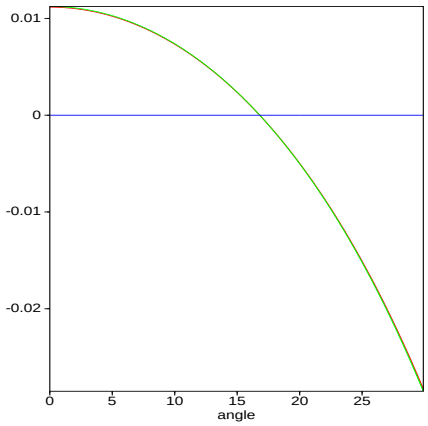

Figure 15: $\frac{\partial D}{\partial z}$ and real reflection coefficient vs. angle

to finite difference data and more complex models.

7 Acknowledgements

We are grateful to all M-OSRP sponsors for long-term encouragement and support in this research. All members in M-OSRP are thanked for the help of finishing this paper and valuable discussions in this research program.

References

Innanen, K. A. "Two non-linear forward and inverse approximations for wave fields in the presence of sustained medium perturbations." *Proceedings of the 75th Annual Meeting of the Society of Exploration Geophysicists, Houston, TX.* . Soc. Expl. Geophys., 2005.

Jiang, S. and Arthur B. Weglein. "Deriving an imaging algorithm for a laterally invariant multi-parameter acoustic medium from the inverse scattering series." (2007).

Keys, Rorbert G. "Polarity reversals in reflections from layered media." (1988).

Liu, F. *Multi-dimensional depth imaging without an adequte velocity model*. PhD thesis, University of Houston, 2006.

Liu, F., A.B. Weglein, K.A. Innanen, and B.G Nita. "Extension of the non-linear depth imaging capability of the inverse scattering series to multidimensional media: strategies and numerical results." 2005.

Shaw, S. A. and A. B. Weglein. "Imaging seismic reflection data at the correct depth without specifying an accurate velocity model: Initial examples of an inverse scattering subseries." *Frontiers of remote sensing information processing*. Ed. C. H. Chen. World Scientific Publishing Company, 2003. chapter 21, 469–484.

Shaw, S. A., A. B. Weglein, D. J. Foster, K. H. Matson, and R. G. Keys. "Convergence properties of a leading order depth imaging series." *73rd Annual Internat. Mtg., Soc. Expl. Geophys., Expanded Abstracts*. . Soc. Expl. Geophys., 2003. 937–940.

Shaw, S. A., A. B. Weglein, D. J. Foster, K. H. Matson, and R. G. Keys. "Isolation of a leading order depth imaging series and analysis of its convergence properties." *Journal of Seismic Exploration* 2 (November 2004): 157–195.

Stolt, R. H. "Migration by Fourier transform." *Geophysics* 43 (1978): 23–48.

Weglein, A. B., F. V. Araújo, P. M. Carvalho, R. H. Stolt, K. H. Matson, R. T. Coates, D. Corrigan, D. J. Foster, S. A. Shaw, and H. Zhang. "Inverse Scattering Series and Seismic Exploration." *Inverse Problems* (2003): R27–R83.

Weglein, A. B., D. J. Foster, K. H. Matson, S. A. Shaw, P. M. Carvalho, and D. Corrigan. "An inverse-scattering sub-series for predicting the spatial location of reflectors without the precise reference medium and wave velocity." *71st Annual Internat. Mtg., Soc. Expl. Geophys., Expanded Abstracts*. . Soc. Expl. Geophys., 2001. 2108–2111.

Weglein, A. B., D. J. Foster, K. H. Matson, S. A. Shaw, P. M. Carvalho, and D. Corrigan. "Predicting the correct spatial location of reflectors without knowing or determining the precise medium and wave velocity: initial concept, algorithm and analytic and numerical example." *Journal of Seismic Exploration* 10 (2002): 367–382.

Weglein, A. B., K. H. Matson, D. J. Foster, P. M. Carvalho, D. Corrigan, and S. A. Shaw. "Imaging and inversion at depth without a velocity model: Theory, concepts and initial evaluation." *70th Annual Internat. Mtg., Soc. Expl. Geophys., Expanded Abstracts*. . Soc. Expl. Geophys., 2000. 1016–1019.

Zhang, H. *Direct non-linear acoustic and elastic inversion: Towards fundamentally new comprehensive and realistic target identification*. PhD thesis, University of Houston, 2006.

Zhang, H. and A.B. Weglein. "The inverse scattering series for tasks associated with primaries: depth imaging and direct non-linear inversion of 1D variable velocity and density acoustic media." *SEG Technical Program Expanded Abstracts*. 2005, 1705–1708.

Appendix A

The detailed calculation of the first term in Eq. (16)

$$c_0(\theta_2)c_1(\theta_1) - c_0(\theta_1)c_1(\theta_2)$$

$$= \frac{c_0}{\sqrt{1-\sin^2\theta_2}}\frac{c_1}{\sqrt{1-\frac{c_1^2}{c_0^2}\sin^2\theta_1}} - \frac{c_0}{\sqrt{1-\sin^2\theta_1}}\frac{c_1}{\sqrt{1-\frac{c_1^2}{c_0^2}\sin^2\theta_1}}$$
$$= c_0c_1[\frac{1}{\sqrt{(1-\sin^2\theta_2)(1-\frac{c_1^2}{c_0^2}\sin^2\theta_1)}} - \frac{1}{\sqrt{(1-\sin^2\theta_1)(1-\frac{c_1^2}{c_0^2}\sin^2\theta_2)}}];$$

Since the two square root should be bigger than zero, we can just compare the terms inside, thus, we have

$$[1-\frac{c_1^2}{c_0^2}\sin^2\theta_1 - \sin^2\theta_2 + \frac{c_1^2}{c_0^2}\sin^2\theta_1\sin^2\theta_2] - [1-\frac{c_1^2}{c_0^2}\sin^2\theta_2 - \sin^2\theta_1 + \frac{c_1^2}{c_0^2}\sin^2\theta_1\sin^2\theta_2]$$
$$= -\frac{c_1^2}{c_0^2}\sin^2\theta_1 - \sin^2\theta_2 + \frac{c_1^2}{c_0^2}\sin^2\theta_2 + \sin^2\theta_1$$
$$= (\frac{c_1^2}{c_0^2}-1)(\sin^2\theta_2 - \sin^2\theta_1);$$

So, when $c_1 > c_0$ and $\theta_2 > \theta_1$, $c_0(\theta_2)c_1(\theta_1) - c_0(\theta_1)c_1(\theta_2) < 0$;
and when $c_1 < c_0$ and $\theta_2 > \theta_1$, $c_0(\theta_2)c_1(\theta_1) - c_0(\theta_1)c_1(\theta_2) > 0$.

Inverse scattering series velocity dependent imaging in laterally varying media: analysis of transcendental integrals in the mathematics of multidimensional imaging

F. Liu and A. B. Weglein, M-OSRP, University of Houston

Abstract

M-OSRP research is being conducted to prepare a field-data ready direct nonlinear depth imaging algorithm. In this volume, research is reported towards preparing the imaging algorithm for primaries reflecting from multiparameter, multidimensional media. Here we focus on issues related to the second of these aspects, i.e, imaging in multidimensional media, extending previous work on single-parameter leading- and higher-order imaging subseries of the inverse scattering series. In previously reported work, the analytically computable portion of the multidimensional imaging subseries had been separated and grouped into a closed form algorithm (the higher-order imaging subseries, HOIS), with encouraging numerical results. The remaining terms, which were not immediately analytically expressible, were examined through numerical approximations, but so far largely left out of our imaging algorithms. In this report, we focus on the mathematics of this part of the imaging subseries. The issue is that the integrals to be calculated in these terms are highly transcendental. To manage this, a systematic scheme capable of computing such integrals with arbitrary accuracy has been developed, as has a rapid means of calculating them based on Fast Fourier transforms. Further, in the course of our analysis we have (1) made new use of symmetries in the reference Green's operator, and (2) produced polynomial approximations for some of the transcendental functions that we expect to be of use for later incorporation in closed-form versions of multidimensional imaging. Numerical testing of these calculations show encouraging results, especially on diffraction artifacts associated with rapid lateral variations.

1 Introduction

In this paper we describe progress on the mathematics and numerics of multidimensional velocity independent imaging. The bulk of this report is devoted to deriving new analytic methods for calculating rapidly varying integrands in the non-linear parts of the imaging subseries. Following that, we provide numerical examples of a second aspect of this past year's research: a large k_z method for constructing the linear imaging result (i.e., the input to the velocity independent imaging algorithm). We demonstrate the improvement such results bring to our pre-existing imaging algorithm (HOIS) output.

First, some background. Rapid lateral variations are among the biggest challenges in seismic imaging, for example, sub-salt or sub-basalt targets, karstic formations, structures in foreland basins, etc. Rapid lateral variation is not only a significant impediment for many velocity analysis procedures to achieve a working velocity field, but also a formidable barrier for numerous leading-edge imaging algorithms to propagate through. In M-OSRP's coordinated efforts for the field data

application of velocity independent imaging algorithms, this article targets specifically the lateral variation aspect of the seismic imaging algorithm. Several closely related reports are also included in this volume, for example, Jiang et al. and Li et al. concentrate on the multiparameter aspect of the seismic imaging challenge; Lira et al. focus on the issues of absorption; Wang et al. consider the limited aperture in the real data; Mayhan et al., Hsu et al., and Wang et al. discuss many prerequisites to estimate the wavelet and remove direct waves, ghosts, and multiples from the input data.

After the pioneering work in Weglein et al. (2000, 2002), the seismic imaging subseries had been studied in many aspects; much fruitful research efforts had been subsequently presented to our sponsors, for example Shaw et al. (2003); Innanen (2003); Shaw (2005).

Targeting lateral variations specifically, this article is a direct continuation of the inverse scattering imaging work in Liu (2006); Liu and Weglein (2007). In our previous work, the portion of the seismic imaging operator which is analytically computable was separated and grouped into the higher-order imaging subseries (HOIS) with encouraging numerical results. However, the part that has no analytic expression was either approximated by discrete summation in a truncated manner, or left out entirely in the computational scheme. This article focuses on this aspect of the seismic imaging algorithm, or in the terminology of mathematics, the seismic imaging capability encapsulated in highly transcendental functions.

The complication of lateral variation on seismic imaging is significant in the inverse scattering series: If we assume a 1D earth, as demonstrated in section §2.5, the only horizontal wavenumber that matters is $k_m = 0$, and consequently the integral over the temporal frequency ω (or equivalently over the vertical wavenumber k_z) is always a Dirac δ-function (or its derivative). The integration over a δ-function is very easy to implement: it needs only a single isolated sample of data (or its derivative) at the exact grid point due to the sifting property of the δ-function. If the 1D earth assumption is removed, non-zero k_m will have to be considered. In this case, the integration over k_z will no longer result in a clean δ-function. Our approach is to decompose it into two parts: the first part leads to a linear combination of derivatives of the δ-function of various orders; the second part is a Riemann integral, which in the simplest scenario reduces to many formidable examples of "highly transcendental functions" in Arthur Erdélyi and Bateman (1954).

Every term in the first part, for example equation (90), is a Dirac δ-function (or its derivative); its integral over data is very easy to calculate, just like the 1D case. Partial derivatives over the lateral variable x (for example equation (2.25) from Liu (2006)) also appeared, but the overall algorithm shares the same simplicity and lightning speed with its 1D counterparts.

The Riemann integrals in the second part, e.g equation (93), however, turn out to be fast changing functions of depth z; both the magnitude and the frequency of the variation increase with z and k_m. Significant amount of research has been devoted to the calculation and interpolation of this type of integral, which we tackle with a two-interval scheme: (1) the first part $\int_0^{\Xi} dk_z$ is accurately implemented by interpolations with the help of various derivatives (with respect to k_z) of the integrand; a fast implementation of this interpolation using a discrete Fourier transform is derived and applied in the calculation; (2) the second part $\int_{\Xi}^{\infty}$ is accurately implemented with asymptotic

expansion to thousand of terms (each expansion by itself contains thousands of terms).

So far the seismic imaging operators have been coded for α_1 with very limited k_m range (about 10%). Encouraging numerical tests applied to the geological models with various degree of lateral variation have demonstrated the consistent benefit of an accurate seismic imaging operator, especially dealing with phenomena associated with lateral variations, e.g, diffractions.

1.1 Notation and conventions

It is worthwhile to provide a summary of the notations and conventions for Fourier transforms.

- The symbol $\mathbf{i}$ is reserved for the imaginary unit which satisfies $\mathbf{i}^2 = -1$. c_0 is reserved for the homogeneous reference (or migration) velocity.
- In this article, we use the symbol $\stackrel{\triangle}{=}$ to initiate a definition in an equation. For example, $a \stackrel{\triangle}{=} \sin(6)$ means that the definition of a is $\sin(6)$.
- In this article, the symbol "$\widetilde{\ }$" is extensively used above the name of a function to denote its Fourier transform.
- The superscript symbol $^{\mathsf{T}}$ is reserved for the transpose of a matrix or vector. All matrices are denoted by bold capitals, for examples $\mathbf{M}$ and Λ. The superscript symbol * is reserved for the conjugate of a complex number.

Square-roots are used extensively in this note, and it is well-known that the square-root of a number is not unique. For example, both 3 and -3 are valid square-root of 9. In summary,

- We use $\sqrt[?]{\ }$ to denote the square-root of a real number, which can be positive or negative. We use $\sqrt[?]{\ }$ to emphasize the fact that we have not decided which answer to choose. For example, $\sqrt[?]{9}$ can be 3 or -3, and $\sqrt[?]{-9}$ can be $3\mathbf{i}$ or $-3\mathbf{i}$.
- In this article, the symbol $\sqrt{\ }$ is reserved for the non-negative square-root of a non-negative real number. In these cases we force $\sqrt{\ }$ to be a single-valued function. For example, $\sqrt{9} = 3$, and $\sqrt{-9}$ is not defined.

We use t to denote time and ω to denote its Fourier conjugate (temporal frequency). The Fourier transform of a function $f(t)$ in the time domain into its spectrum in the frequency domain is defined as,

$$\widetilde{f}(\omega) = \int_{-\infty}^{\infty} f(t) e^{\mathbf{i}\omega t} dt. \tag{1}$$

The corresponding inverse Fourier transform is defined as,

$$f(t) = \frac{1}{2\pi} \int_{-\infty}^{\infty} \widetilde{f}(\omega) e^{-\mathbf{i}\omega t} d\omega. \tag{2}$$

We use z to denote depth (the vertical coordinate); its Fourier conjugate is denoted as vertical wavenumber k_z. The forward and inverse Fourier transform between z and k_z are respectively defined as,

$$\widetilde{f}(k_z) = \int_{-\infty}^{\infty} f(z) e^{\mathbf{i} k_z z} dz \quad , \quad f(z) = \frac{1}{2\pi} \int_{-\infty}^{\infty} \widetilde{f}(k_z) e^{-\mathbf{i} k_z z} dk_z. \tag{3}$$

On the other hand, the Fourier transform between $\vec{x}$ (the horizontal coordinate[1]) and $\vec{k}_m$ (the horizontal wavenumber[2]) is defined with a different sign convention,

$$\widetilde{f}(\vec{k}_m) \stackrel{\triangle}{=} \vec{\int} f(\vec{x}) e^{-\mathbf{i}\vec{k}_m \bullet \vec{x}} d\vec{x} \quad , \quad f(\vec{x}) \stackrel{\triangle}{=} \begin{cases} \frac{1}{2\pi} \vec{\int} \widetilde{f}(\vec{k}_m) e^{\mathbf{i}\vec{k}_m \bullet \vec{x}} d\vec{k}_m, & (\textbf{2D Seismic}) \\ \frac{1}{4\pi^2} \vec{\int} \widetilde{f}(\vec{k}_m) e^{\mathbf{i}\vec{k}_m \bullet \vec{x}} d\vec{k}_m, & (\textbf{3D Seismic}) \end{cases} . \tag{4}$$

In equation (4), we use $\vec{\int}$ to denote the integration over the entire vector space of all lateral variables (or lateral wavenumbers). Its definitions in 2D seismic and 3D seismic are listed below,

$$\begin{aligned} \vec{\int} d\vec{x} &= \int_{-\infty}^{\infty} dx && (\textbf{2D Seismic}), \\ \vec{\int} d\vec{x} &= \int_{-\infty}^{\infty} \int_{-\infty}^{\infty} dx dy && (\textbf{3D Seismic}). \end{aligned} \tag{5}$$

In this note a vector will be denoted by a symbol topped with $\vec{}$. To be consistent with our previous notations, the modulus of the vector will be denoted by the symbol without $\vec{}$,

$$k_m = \left| \vec{k}_m \right| \quad , \quad k_1 = \left| \vec{k}_1 \right| . \tag{6}$$

In this article, since the seismic imaging operators are the same in 2D and 3D, we describe both of them in the same context. The few differences between 2D and 3D will be mentioned explicitly.

1.2 Seismic imaging operators

In this article, the term "**seismic imaging operator**" is used extensively. It is worthwhile to clarify its meaning in the context. In the seismic imaging subseries, the output image for every term is calculated via an integral whose integrand is the product of the input data and a kernel function. We call this kernel function the seismic imaging operator of this term, as expressed in equation (7),

$$\textbf{Image} = \int \textbf{Data} * \textbf{Kernel}. \tag{7}$$

[1] In 2D seismic, $\vec{x}$ is defined as a single horizontal variable: x. In 3D seismic, $\vec{x}$ is defined as a vector with two components: x and y.

[2] In 2D seismic, $\vec{k}_m$ is defined as a single horizontal wavenumber: k_m. In 3D seismic, $\vec{k}_m$ is defined as a vector with two components: k_{mx} and k_{my}.

The useful integration operators in the inverse scattering series are usually not ordinary continuous functions; for example, the Dirac δ-function or various types of Green's functions are used in the inverse scattering series (Weglein et al., 2003, equations 1 and 2). They were chosen because they best describe the principle of superposition, and their behavior inside an integral has been rigorously defined, regardless of the difficulty in defining them in the ordinary sense.

1.3 Examples of seismic imaging operators

In the inverse scattering series, Green's function, for example, equation (64) from Weglein et al. (2003), equation (A-2) from Shaw et al. (2003), equation (2.9) from Liu (2006), or equation (17) from Liu and Weglein (2007), are all expressed in the ω (frequency) domain. Consequently, the corresponding imaging results, for example, equation (B-5) from Shaw et al. (2003), equation (A.25) from Liu (2006), and equation (66) from Liu and Weglein (2007), are all expressed in the ω (or equivalently, vertical wavenumber k_z) domain. An inverse Fourier transform needs to be applied to convert the result into the depth domain, for example, equation (B-6) from Shaw et al. (2003), equation (A.26) from Liu (2006), equation (67) from Liu and Weglein (2007). This inverse Fourier transform over k_z, if rearranged to be the innermost integral and applied first, will lead to a distribution independent of the data, for example, equation (A.29) from Liu (2006), equation (70) from Liu and Weglein (2007). These distributions are examples of seismic imaging operators.

Seismic imaging operators have several advantages: (1) They do not depend on measured data and hence only need to be calculated once, saving on computations. (2) They fully cover the "non-data" aspect of the seismic imaging algorithm, thus unambiguously pinpointing the portion of the seismic imaging algorithm where our efforts should be concentrated on[3]. (3) They always act in the form of an integration kernel, a heavily studied area in mathematics and scientific computation, and therefore lead us to many useful concepts and tools.

2 Seismic imaging operators for α_1 and α_2

2.1 Symmetry in Green's operator and the sign of the square-root

For any fixed horizontal wavenumber k and frequency ω, there are two different vertical wavenumbers q that satisfy the dispersion relation: $(\omega/c_0)^2 = k^2 + q^2$. Obviously q should be computed from k and ω through a square-root operation, and each answer differs from the other by a negative sign. Due to the fact that the vertical number q is present in the definition of Green's function used in the inverse scattering series, the choice of this sign for square-root has an immediate and significant impact on the inverse scattering series.

The requirement for the q information varies dramatically in the inverse scattering series:

[3]The other part is the input seismic data; in the framework of isolated task subseries, we assume the data satisfy our assumptions and by themself are not our concern for the seismic imaging subseries.

1. For models without lateral variation, as demonstrated in equation (42), q differs from ω by a constant factor, and the square-root in the entire inverse series always reduces to a much simpler linear relation.

2. To calculate a laterally varying α_1 with the restriction $k_h = 0$, although the nonlinear (q, ω)-relation will be encountered, only $(\omega/c_0)^2 - k^2 \geq 0$ are needed[4], and in this situation, the sign had been specified by equation (19) from Clayton and Stolt (1981)

3. To calculate laterally varying α_2, α_3, $\cdots$, for example in equation (34), we have to face not only the nonlinear (q, ω)-relation, but also the situation of $(\omega/c_0)^2 - k^2 < 0$.

This subsection is devoted to the issue. It is surprising that this choice can be simply and unambiguously derived from the symmetry of Green's function itself; nothing else is required. It is clear that in the space and time domain Green's function of a homogeneous medium in any dimension can be written as,

$$G_0\left(\vec{x}_g, \vec{x}_s, t, z_g, z_s\right) \overset{\texttt{denote as}}{\Longrightarrow\Longrightarrow} \phi\left(\vec{x}_g - \vec{x}_s, t, z_g - z_s\right).$$

The newly defined function ϕ is real[5]. If we switch the horizontal coordinate of the source and receiver, the phone should record the same data because the source-receiver distance has not changed. Consequently, the newly defined function ϕ must have the following symmetry,

$$\phi\left(\vec{x}, t, z\right) = \phi\left(-\vec{x}, t, z\right). \tag{8}$$

The well known $(\vec{k}, \omega)$-domain Green's function for wave propagation in a multi-D homogeneous medium, for example, equation (64) from Weglein et al. (2003), is $\frac{e^{\mathbf{i}q|z|}}{2\mathbf{i}q}$. By definition, it is also the double Fourier transform of equation (8) over space and time,

$$\frac{e^{\mathbf{i}q|z|}}{2\mathbf{i}q} = \tilde{\tilde{\phi}}(\vec{k}, \omega, z) = \vec{\int} d\vec{x} \int_{-\infty}^{\infty} dt \;\; \phi(\vec{x}, t, z) e^{\mathbf{i}(\omega t - \vec{k}\cdot\vec{x})}. \tag{9}$$

where $q = \sqrt[?]{(\omega/c_0)^2 - k^2}$; we use $\sqrt[?]{\;}$ to emphasize the fact that we haven't yet committed to any choice for the sign of q. It should satisfy the following symmetry relation,

$$\begin{aligned}
\tilde{\tilde{\phi}}(-\vec{k}, \omega, z) &= \vec{\int} d\vec{x} \int_{-\infty}^{\infty} dt \;\; \phi(\vec{x}, t, z) e^{\mathbf{i}(\omega t - (-\vec{k})\cdot\vec{x})} = \vec{\int} d\vec{x} \int_{-\infty}^{\infty} dt \;\; \phi(\vec{x}, t, z) e^{\mathbf{i}(\omega t - \vec{k}\cdot(-\vec{x}))} \\
&\overset{\vec{y} \triangleq -\vec{x}}{\Longrightarrow} \vec{\int} d\vec{y} \int_{-\infty}^{\infty} dt \;\; \phi(-\vec{y}, t, z) e^{\mathbf{i}(\omega t - \vec{k}\cdot\vec{y})} = \vec{\int} d\vec{y} \int_{-\infty}^{\infty} dt \;\; \phi(\vec{y}, t, z) e^{\mathbf{i}(\omega t - \vec{k}\cdot\vec{y})} \\
&= \tilde{\tilde{\phi}}(\vec{k}, \omega, z).
\end{aligned} \tag{10}$$

[4]For example, in equation (33), the expression inside the square-root is always positive

[5]Being real means that its imaginary part is zero.

From equation (10), our Green's operator is an even function of $\vec{k}$. On the other hand, if the signs of $\vec{k}$ and ω are simultaneously flipped, we have,

$$\begin{aligned}\widetilde{\widetilde{\phi}}(-\vec{k},-\omega,z) &= \vec{\int} d\vec{x} \int_{-\infty}^{\infty} dt \;\; \phi(\vec{x},t,z) e^{\mathbf{i}(-\omega t-(-\vec{k})\cdot\vec{x})} = \vec{\int} d\vec{x} \int_{-\infty}^{\infty} dt \;\; \phi(\vec{x},t,z) e^{-\mathbf{i}(\omega t-\vec{k}\cdot\vec{x})} \\ &= \left[\vec{\int} d\vec{x} \int_{-\infty}^{\infty} dt \;\; \phi(\vec{x},t,z) e^{\mathbf{i}(\omega t-\vec{k}\cdot\vec{x})}\right]^* = \left[\widetilde{\widetilde{\phi}}(\vec{k},\omega,z)\right]^*.\end{aligned} \tag{11}$$

Combining equation (10) and equation (11), we have the following symmetry relation,

$$\widetilde{\widetilde{\phi}}(\vec{k},-\omega,z) = \widetilde{\widetilde{\phi}}(-\vec{k},-\omega,z) = \left[\widetilde{\widetilde{\phi}}(\vec{k},\omega,z)\right]^*. \tag{12}$$

In summary, equation (12) states that, when ω is replaced by $-\omega$, the spectrum become the conjugate of the original, i.e, the real part of the spectrum stays the same, but its imaginary part changes sign.

Equation (12) has a clear mandate over choice for the sign of $q = \sqrt[?]{(\omega/c_0)^2 - k^2}$:

- Case I: $\frac{\omega^2}{c_0^2} - k^2 > 0$. In this case $q = \sqrt[?]{\frac{\omega^2}{c_0^2} - k^2}$ is a purely real number, no matter what square-root sign convention we choose. Both $2\mathbf{i}q$ and $e^{\mathbf{i}q|z|}$ have a non-zero imaginary part. How can we define q such that the real part of Green's function stays the same, but the imaginary part flips sign when ω is replaced by $-\omega$? Our choice is to let $q = \omega\sqrt{c_0^{-2} - (k/\omega)^2}$, the same as equation (19) of Clayton and Stolt (1981)[6].
- Case II: $\frac{\omega^2}{c_0^2} - k^2 < 0$. In this case $q = \sqrt[?]{\frac{\omega^2}{c_0^2} - k^2}$ is a purely imaginary number, no matter what square-root sign convention we choose. Both $2\mathbf{i}q$ and $e^{\mathbf{i}q|z|}$ are purely real numbers and have no imaginary part. How can we define q such that the real part of Green's function stays the same, but the imaginary part flips sign when ω is replaced by $-\omega$? Our choice is to let $q = \mathbf{i}\sqrt{k^2 - (\omega/c_0)^2}$, where the positive sign is taken on the square-root[7].

In summary, the square-root's sign in $q = \sqrt[?]{(\omega/c_0)^2 - k^2}$ follows that of ω when its argument is positive. In other situations, i.e, when it has negative argument, the imaginary part of the answer

[6]There is only one other choice to satisfy this symmetry, that is, to let $q = -\omega\sqrt{c_0^{-2} - (k/\omega)^2}$. This choice, however, will cause the result of equation (15) to flip sign after an inverse Fourier transform back into space. Therefore, this choice is not correct in our convention of Fourier transforms, and the symmetry of Green's function unambiguously provides us with the correct sign choice defined in equation (19) of Clayton and Stolt (1981).

[7]There is only one other choice of sign to satisfy the symmetry of Green's function: $q = -\mathbf{i}\sqrt{k^2 - (\omega/c_0)^2}$. This choice, however, will be demonstrated as totally unreasonable since it violates the benchmark equation (18).

must be chosen as "always positive" or "always negative". We choose it as "always positive", because in this case, $e^{\mathbf{i}q|z|}$ always enjoys an exponentially decay[8], as expressed below,

$$q = \overset{?}{\sqrt{(\omega/c_0)^2 - k^2}} \overset{\triangle}{=} \begin{cases} \mathtt{sgn}(\omega)\sqrt{(\omega/c_0)^2 - k^2} & \mathtt{if}\ (\omega/c_0)^2 - k^2 \geq 0 \\ \mathbf{i}\sqrt{k^2 - (\omega/c_0)^2} & \mathtt{if}\ (\omega/c_0)^2 - k^2 < 0 \end{cases} \tag{13}$$

As a verification, we will demonstrate that: (1) our sign choice will lead to 2D Green's function from Morse and Feshbach (1953); Arfken and Weber (1985); and (2) other choices, for example, allowing exponential growth of $e^{\mathbf{i}q|z|}$, cannot lead to our desired Green's function.

For 2D Green's function with fixed $\omega > 0$, using our choice for the sign of square-root in the definition of q, and denote $k_0 = \frac{\omega}{c_0}$, we transform Green's operator back into space (but still in the frequency domain),

$$\begin{aligned} &\frac{1}{2\pi}\int_{-\infty}^{\infty} \frac{e^{\mathbf{i}q|z|}}{2\mathbf{i}q} e^{\mathbf{i}kx} dk \overset{G_0(-k)=G_0(k)}{\Longrightarrow\Longrightarrow\Longrightarrow} \frac{1}{\pi}\int_0^{\infty} \frac{e^{\mathbf{i}q|z|}}{2\mathbf{i}q}\cos[kx]\, dk = \frac{1}{\pi}\left(\int_0^{\omega/c_0} + \int_{\omega/c_0}^{\infty}\right) \\ &= \frac{1}{\pi}\int_0^{k_0} \frac{e^{\mathbf{i}\sqrt{k_0^2-k^2}|z|}}{2\mathbf{i}\sqrt{k_0^2-k^2}}\cos[kx]\, dk + \frac{1}{\pi}\int_{k_0}^{\infty} \frac{\exp\left(-\sqrt{k^2-k_0^2}|z|\right)}{-2\sqrt{k^2-k_0^2}}\cos[kx]\, dk. \end{aligned} \tag{14}$$

In the case of $|z| = 0$, the first integral of equation (14) contains one purely imaginary piece. According to equation (9.1.18) from Abramowitz and Stegun (1965), it reduces to the Bessel function of the $0^{\mathtt{th}}$-order,

$$\begin{aligned} &\frac{1}{\pi}\int_0^{k_0} \frac{e^{\mathbf{i}\sqrt{k_0^2-k^2}|z|}}{2\mathbf{i}\sqrt{k_0^2-k^2}}\cos[kx]\, dk \overset{|z|=0}{\Longrightarrow} \frac{-\mathbf{i}}{2\pi}\int_0^{k_0} \frac{\cos[kx]}{\sqrt{k_0^2-k^2}} dk \\ &\overset{u\overset{\triangle}{=}\arcsin[k/k_0]}{\Longrightarrow\Longrightarrow} \frac{-\mathbf{i}}{2\pi}\int_0^{\pi/2} \cos\left(k_0 x \sin[u]\right) du = \frac{-\mathbf{i}}{4\pi}\int_0^{\pi} \cos\left(k_0 x \sin[u]\right) du = \frac{-\mathbf{i}}{4}\mathbf{J_0}\left(k_0 x\right). \end{aligned} \tag{15}$$

If $|z| \neq 0$, the first integral of equation (14) contains real and imaginary parts, both of which are very complicated,

$$\begin{aligned} \frac{1}{\pi}\int_0^{k_0} \frac{e^{\mathbf{i}\sqrt{k_0^2-k^2}|z|}}{2\mathbf{i}\sqrt{k_0^2-k^2}}\cos[kx]\, dk =& \frac{1}{2\pi}\int_0^{k_0} \frac{\sin\left(\sqrt{k_0^2-k^2}|z|\right)}{\sqrt{k_0^2-k^2}}\cos[kx] dk \\ &-\frac{\mathbf{i}}{2\pi}\int_0^{k_0} \frac{\cos\left(\sqrt{k_0^2-k^2}|z|\right)}{\sqrt{k_0^2-k^2}}\cos[kx] dk. \end{aligned} \tag{16}$$

[8]Due to the absolute sign in Green's function, it requires $|z|$ instead of z itself. Hence its argument $\mathbf{i}q|z|$ is always a negative number.

In some special cases, for example, when $z = 0$, the first integral of equation (16) vanishes and the second one is simple and can be expressed as the Neumann function of the $0^{\mathtt{th}}$-order, according to equation (9.1.24) from Abramowitz and Stegun (1965),

$$\begin{aligned}&\frac{-1}{2\pi}\int_{k_0}^{\infty}\frac{\exp\left(-\sqrt{k^2-k_0^2}|z|\right)}{\sqrt{k^2-k_0^2}}\cos\left[kx\right]dk \overset{|z|=0}{\Longrightarrow} \frac{-1}{2\pi}\int_{k_0}^{\infty}\frac{\cos\left[kx\right]}{\sqrt{k^2-k_0^2}}dk \overset{u\triangleq k/k_0}{\Longrightarrow} \frac{-1}{2\pi}\int_{1}^{\infty}\frac{\cos\left[k_0xu\right]}{\sqrt{u^2-1}}du \\ &=\frac{1}{4}\mathbf{Y_0}(|k_0x|)=\frac{1}{4}\mathbf{Y_0}\left(\left|\frac{\omega x}{c_0}\right|\right)\end{aligned} \tag{17}$$

As a benchmark, a 2D Green's function, for example, equation (7.2.18) from Morse and Feshbach (1953)[9] or Table 8.5 from Arfken and Weber (1985)[10] is,

$$\frac{1}{4}\left[\mathbf{Y_0}\left(\frac{\omega\sqrt{x^2+z^2}}{c_0}\right)-\mathbf{iJ_0}\left(\frac{\omega\sqrt{x^2+z^2}}{c_0}\right)\right].$$

When $z = 0$, we have $|x| = \sqrt{x^2 + z^2}$, and it is clear that equation (15) and equation (17) replicate the real and imaginary part of 2D Green's function, respectively. In summary, our choice for the sign leads to the correct Green's function in the special case of $z = 0$.

Since for any x and z, the sum of both integrals in equation (14) will be the 2D Green's function in the (x, ω)-domain, we must have,

$$\begin{aligned}\frac{1}{4}\mathbf{Y_0}\left(k_0\sqrt{x^2+z^2}\right)=&\frac{1}{2\pi}\int_{0}^{k_0}\frac{\sin\left(\sqrt{k_0^2-k^2}|z|\right)}{\sqrt{k_0^2-k^2}}\cos[kx]dk \\ &+\frac{-1}{2\pi}\int_{k_0}^{\infty}\frac{\exp\left(-\sqrt{k^2-k_0^2}|z|\right)}{\sqrt{k^2-k_0^2}}\cos\left[kx\right]dk,\end{aligned} \tag{18}$$

and,

$$\frac{1}{4}\mathbf{J_0}\left(k_0\sqrt{x^2+z^2}\right)=\frac{1}{2\pi}\int_{0}^{k_0}\frac{\cos\left(\sqrt{k_0^2-k^2}|z|\right)}{\sqrt{k_0^2-k^2}}\cos[kx]dk. \tag{19}$$

Equation (18) and (19) will serve as the benchmark for our choice of sign. First let's demonstrate that, when $k_0^2 - k^2 > 0$, our sign choice satisfies equation (19) for any x and z. In equation (19), it is hard to imagine how the tangled (x, z)-relation on the right-hand-side collapsed into the neat

[9] In Morse and Feshbach (1953), the definition of Green's function differs from our convention by an extra factor -4π.

[10] In equation (8.159) from Arfken and Weber (1985), its definition of Green's function differs from ours by a negative sign.

sum of squares on the left-hand-side. It can actually be proven as follows: defining $u \overset{\triangle}{=} \arcsin[k/k_0]$, the right-hand-side of equation (19) can be written as,

$$\frac{1}{2\pi}\int_0^{\pi/2}\cos\left(k_0|z|\cos[u]\right)\cos\left(k_0 x\sin[u]\right)du = \frac{1}{2\pi}\int_0^{\pi/2}du\left\{\begin{array}{l}\cos\left(k_0|z|\cos[u]-k_0 x\sin[u]\right)+\\ \cos\left(k_0|z|\cos[u]+k_0 x\sin[u]\right)\end{array}\right\}. \quad (20)$$

Since the result is an even function of x, we can assume x is positive and later trivially extend the result for positive x to negative x. We define $r=\sqrt{(k_0x)^2+(k_0z)^2}$, $0\le\theta=\arctan(x/|z|)\le\pi/2$. Equation (20) can be further simplified as,

$$\frac{1}{4\pi}\int_0^{\pi/2}du\left\{\begin{array}{l}\cos\left(r\cos[u+\theta]\right)+\\ \cos\left(r\cos[u-\theta]\right)\end{array}\right\} = \frac{1}{4\pi}\left(\int_\theta^{\pi/2+\theta} + \int_{-\theta}^{\pi/2-\theta}\right)\cos\left(r\cos[u]\right)du \quad (21)$$

In the equation above, both integrals on the right-hand-side can be expressed as adding a slightlylittle bit to, and subtract another little bit from, a much easier integral with fixed limits: $\int_0^{\pi/2}$,

$$\left.\begin{array}{rcl}\int_\theta^{\pi/2+\theta} &=& \int_0^{\pi/2}+\int_{\pi/2}^{\pi/2+\theta}-\int_0^{\theta}\\ \int_{-\theta}^{\pi/2-\theta} &=& \int_0^{\pi/2}+\int_{-\theta}^{0}-\int_{\pi/2-\theta}^{\pi/2}\end{array}\right\} \Longrightarrow \int_\theta^{\pi/2+\theta}+\int_{-\theta}^{\pi/2-\theta} = 2\int_0^{\pi/2}+\int_{-\theta}^{0}-\int_0^{\theta}+\int_{\pi/2}^{\pi/2+\theta}-\int_{\pi/2-\theta}^{\pi/2}. \quad (22)$$

The final result of equation (22) contains five integrals, and it is easy to show that the second integral cancels with the third,

$$\int_{-\theta}^{0} = \int_{-\theta}^{0}\cos[r\cos(u)]du \overset{v\overset{\triangle}{=}-u}{\Longrightarrow} \int_{\theta}^{0}\cos[r\cos(-v)]d(-v) = \int_0^{\theta}\cos[r\cos(v)]dv = \int_0^{\theta},$$

and that the fourth integral cancels with the fifth,

$$\int_{\pi/2}^{\pi+\theta} = \int_{\pi/2}^{\pi+\theta}\cos[r\cos(u)]du \overset{v\overset{\triangle}{=}\pi-u}{\Longrightarrow} \int_{\pi/2}^{\pi/2-\theta}\cos[r\cos(\pi-v)]d(\pi-v) = \int_{\pi/2-\theta}^{\pi/2}\cos[-r\cos(v)]dv$$
$$= \int_{\pi/2-\theta}^{\pi}\cos[r\cos(v)]dv = \int_{\pi/2-\theta}^{\pi/2}.$$

Consequently, using equation 9.1.18 from Abramowitz and Stegun (1965), equation (21) can simply be written as,

$$\frac{2}{4\pi}\int_0^{\pi/2} = \frac{1}{2\pi}\int_0^{\pi/2}\cos(r\cos[u]) = \frac{1}{4\pi}\int_0^{\pi}\cos(r\cos[u])du = \frac{\pi}{4\pi}\mathbf{J_0}(r) = \frac{1}{4}\mathbf{J_0}\left(k_0\sqrt{x^2+z^2}\right). \quad (23)$$

In conclusion, the benchmark result in equation (19) is satisfied by any x and z.

Next we will demonstrate that, when $k_0^2 - k^2 < 0$, our choice of sign do obtain the benchmark Green's function in the special case of $x = 0$. If $x = 0$, equation (18) can also be straightforwardly proven. Its first portion is,

$$\begin{aligned}&\frac{1}{2\pi}\int_0^{k_0}\frac{\sin\left(\sqrt{k_0^2-k^2}|z|\right)}{\sqrt{k_0^2-k^2}}dk \overset{u\triangleq \arccos(k/k_0)}{\Longrightarrow\Longrightarrow} \frac{1}{2\pi}\int_{\pi/2}^{0}\frac{\sin\left(|k_0 z|\sin[u]\right)}{k_0\sin[u]}d(k_0\cos[u])\\ =&\frac{1}{2\pi}\int_0^{\pi/2}\sin\left(|k_0 z|\sin[u]\right) = \frac{1}{4\pi}\int_0^{\pi}\sin\left(k_0|z|\sin[u]\right) = -\frac{1}{4}\mathbf{E_0}(|k_0 z|).\end{aligned} \tag{24}$$

In the last step of the equation above, we applied equation (8.580.2) of Gradshteyn and Ryzhik (1994). In the last part of equation (24), the symbol $\mathbf{E_0}$ is called Weber's function, following the notation of Gradshteyn and Ryzhik (1994). And the second portion of equation (18) is,

$$\begin{aligned}&\frac{-1}{2\pi}\int_{k_0}^{\infty}\frac{\exp\left(-\sqrt{k^2-k_0^2}|z|\right)}{\sqrt{k^2-k_0^2}}dk \overset{u\triangleq k/k_0}{\Longrightarrow} \frac{-1}{2\pi}\int_1^{\infty}\frac{e^{-\sqrt{u^2-1}|k_0 z|}}{\sqrt{u^2-1}}\\ =&\frac{-1}{2\pi}\int_1^{\infty}e^{-\sqrt{u^2-1}|k_0 z|}d\ln\left(u+\sqrt{u^2-1}\right) \overset{v\triangleq \ln\left(u+\sqrt{u^2-1}\right)}{\Longrightarrow\Longrightarrow\Longrightarrow\Longrightarrow} \int_0^{\infty}e^{-|k_0 z|\sinh[v]}dv\\ =&\left(\frac{-1}{2\pi}\right)\left(\frac{-\pi}{2}\right)\left(\mathbf{E_0}(|k_0 z|)+\mathbf{Y_0}(|k_0 z|)\right) = \frac{1}{4}\left(\mathbf{E_0}(|k_0 z|)+\mathbf{Y_0}(|k_0 z|)\right).\end{aligned} \tag{25}$$

In equation (25), we applied formula (3.335) from Gradshteyn and Ryzhik (1994). Adding equation (24) and equation (25) together, we have,

$$\begin{aligned}&\frac{1}{2\pi}\int_0^{k_0}\frac{\sin\left(\sqrt{k_0^2-k^2}|z|\right)}{\sqrt{k_0^2-k^2}}\cos[kx]dk + \frac{-1}{2\pi}\int_{k_0}^{\infty}\frac{\exp\left(-\sqrt{k^2-k_0^2}|z|\right)}{\sqrt{k^2-k_0^2}}\cos[kx]dk\\ \overset{x=0}{\Longrightarrow}&\frac{\mathbf{E_0}(|k_0 z|)+\mathbf{Y_0}(|k_0 z|)}{4}+\frac{-\mathbf{E_0}(|k_0 z|)}{4} = \frac{\mathbf{Y_0}(|k_0 z|)}{4}.\end{aligned} \tag{26}$$

In the second integral of equation (14), if we change our mind, i.e, we choose $\sqrt[?]{k_0^2-k^2} = -\mathbf{i}\sqrt{k^2-k_0^2}$ when $k_0^2 - k^2 < 0$, then, in the special case of $x = 0$,

$$\frac{1}{2\pi}\int_{k_0}^{\infty}\frac{\exp\left(\sqrt{k^2-k_0^2}|z|\right)}{\sqrt{k^2-k_0^2}}\cos\left[kx\right]dk \overset{x=0}{\Longrightarrow} \frac{1}{2\pi}\int_{k_0}^{\infty}\frac{\exp\left(\sqrt{k^2-k_0^2}|z|\right)}{\sqrt{k^2-k_0^2}}dk,$$

will diverge for any z. Consequently, whatever value "the first integral of equation (18)" will converge to, their sum will not result in the desired Neumann function, which is finite for any $z > 0$. This will cause equation (18) to be violated, and this choice for the sign will not lead to the correct Green's function.

2.2 The surprising behavior of and lessons learned from seismic imaging operators for a target without lateral variation

Although the concept of a seismic imaging operator is not explicitly used in Shaw et al. (2003), we can easily derive its result with the seismic imaging operator, and in this process, we demonstrate the behavior of a seismic imaging operator in the simplest scenario. Here is an alternative derivation of equation (B-5) from equation (B-4). After defining: $k_z = -2k_0$, we can rewrite equation (B-4) of Shaw et al. (2003) as,

$$\begin{aligned}\tilde{\alpha}_2(k_z) &= \int_{-\infty}^{\infty} dz'' \alpha_1(z'') \int_{-\infty}^{\infty} dz' \; \frac{-\mathbf{i}k_z}{2} H(z'-z'')\alpha_1(z') e^{-\mathbf{i}k_z z'} \\ &= \int_{-\infty}^{\infty} dz' \alpha_1(z') \int_{-\infty}^{\infty} dz'' \; H(z'-z'')\alpha_1(z'') \frac{-\mathbf{i}k_z}{2} e^{-\mathbf{i}k_z z'}\end{aligned} \tag{27}$$

Applying the Fourier transform[11] $\frac{1}{2\pi} \int_{-\infty}^{\infty} dk_z \; e^{\mathbf{i}k_z z}$ on both sides of equation (27), we have,

$$\begin{aligned}\alpha_2(z) &= \frac{1}{2\pi} \int_{-\infty}^{\infty} dk_z \; e^{\mathbf{i}k_z z} \tilde{\alpha}_2(k_z) \\ &= \frac{1}{2\pi} \int_{-\infty}^{\infty} dk_z \; e^{\mathbf{i}k_z z} \int_{-\infty}^{\infty} dz' \alpha_1(z') \int_{-\infty}^{\infty} dz'' \; H(z'-z'')\alpha_1(z'') \frac{-\mathbf{i}k_z}{2} e^{-\mathbf{i}k'_z}.\end{aligned} \tag{28}$$

If the $\int_{-\infty}^{\infty} dk_z$ is switched to be the inner-most integral and applied first, we have,

$$\int_{-\infty}^{\infty} dz' \alpha_1(z') \int_{-\infty}^{\infty} dz'' \; H(z'-z'')\alpha_1(z'') \frac{1}{2\pi} \int_{-\infty}^{\infty} dk_z \; \frac{-\mathbf{i}k_z}{2} e^{\mathbf{i}k_z z} e^{-\mathbf{i}k_z z'}. \tag{29}$$

Focus on the inner-most integral of equation (29) and carry out the Fourier transform analytically,

$$\frac{1}{2\pi} \int_{-\infty}^{\infty} dk_z \; \frac{-\mathbf{i}k_z}{2} e^{\mathbf{i}k_z z} e^{-\mathbf{i}k_z z'} = \frac{1}{2\pi} \int_{-\infty}^{\infty} dk_z \; \frac{-\mathbf{i}k_z}{2} e^{\mathbf{i}k_z (z-z')} = -\frac{\delta'(z-z')}{2}. \tag{30}$$

[11] Here we use the Fourier transform convention of Shaw et al. (2003).

Equation (30) can simplify the original result in equation (29),

$$\begin{aligned}
&\int_{-\infty}^{\infty} dz' \alpha_1(z') \int_{-\infty}^{\infty} dz''\ H(z'-z'')\alpha_1(z'')\frac{1}{2\pi}\int_{-\infty}^{\infty} dk_z\ \frac{-\mathbf{i}}{2} e^{\mathbf{i}k_z z} e^{-\mathbf{i}k_z z'} \\
=&\frac{-1}{2}\int_{-\infty}^{\infty} dz' \alpha_1(z') \int_{-\infty}^{\infty} dz''\ H(z'-z'')\alpha_1(z'')\delta'(z-z') \\
=&\frac{-1}{2}\int_{-\infty}^{\infty} dz' \alpha_1(z')\delta'(z-z') \int_{-\infty}^{\infty} dz''\ H(z'-z'')\alpha_1(z'') \\
=&\frac{-1}{2}\int_{-\infty}^{\infty} dz' \delta'(z-z')\alpha_1(z') \int_{-\infty}^{z'} dz''\ \alpha_1(z'').
\end{aligned} \tag{31}$$

Let's have a brief look at the integration involving $\delta'(u)$: a given smooth function $f(u)$ (with continuous derivatives), its integral with $\delta'(u-u_0)$ is done by first integrating by parts to manage a $\delta(u-u_0)$ in the integral, then applying the sifting property of $\delta(u-u_0)$ as follows,

$$\int_{-\infty}^{\infty} f(u)\delta'(u-u_0)dx = [f(u)\delta(u-u_0)]_{-\infty}^{\infty} - \int_{-\infty}^{\infty} f'(u)\delta(u-u_0)dx = -f'(u_0).$$

Using the method in the equation above to integrate over δ', we can simplify equation (31) further,

$$\begin{aligned}
&\frac{-1}{2}\int_{-\infty}^{\infty} dz' \delta'(z-z')\alpha_1(z') \int_{-\infty}^{z'} dz''\ \alpha_1(z'') \\
=&\frac{-1}{2}\left[\frac{\partial}{\partial z'}\left(\alpha_1(z')\int_{-\infty}^{z'} dz''\ \alpha_1(z'')\right)\right]_{z'=z} = -\frac{1}{2}\left[\alpha_1^2(z') + \alpha_1'(z')\int_{-\infty}^{z'} \alpha_1(z'')dz''\right]_{z'=z} \\
=&-\frac{1}{2}\left[\alpha_1^2(z) + \alpha_1'(z)\int_{-\infty}^{z} \alpha_1(z')dz'\right].
\end{aligned} \tag{32}$$

Note that equation (32) is exactly the same as equation (B-5) from Shaw et al. (2003). So far we have demonstrated that the seismic imaging operator can be used to duplicate M-OSRP's previous imaging results: i.e, the separation of imaging and inversion terms through integration by parts. Several lessons can be gleaned from this 1D example,

- $\int_{-\infty}^{\infty} dk_z$ is necessary to obtain a clean result above the integration over the entire frequency spectrum[12]. In a more complicated lateral world, this integration over the entire k_z spec-

[12]Although when we actually implement the final formula in digital computers, we never have access to the full spectrum of the data; using them in the derivation process when we calculate the seismic imaging operator, on the other hand, greatly simplifies the final result.

trum should also be necessary, although it will be extremely difficult for target depths up to thousands of meters and will incur expansions with millions of terms.

- The imaging result is initially expressed as an integral, for example, equation (27). But after applying the Fourier transform, partial derivatives appear in the final formula. Extra attention should be paid to the seismic imaging operator.
- Even for simple models without lateral variation, the integral which initially requires $\alpha_1(z)$ may end up asking for $\alpha_1'(z)$ in the final result; in other situations it may want $\alpha_1''(z)$, $\cdots$. It is natural to imagine that, in a more complicated laterally varying world, we may need a unified formalism wanting $\alpha_1(z)$, $\alpha_1'(z)$, $\alpha_1''(z)$ $\cdots$ simultaneously. This structure is indeed verified in this article since the rapid variation of the seismic imaging operator associated with a multi-D earth explicitly asks for variation detail in the data, which is best encapsulated in various derivatives.
- It gives us a remarkably frugal integration scheme: only the sampling at the grid is required, there is no need for anything else from the neighborhood. For example, as demonstrated in equation (32), the seemingly double integral (with n^2 or quadratic complexity) in the beginning ends up with a simple evaluation (with n^0 or constant complexity).

2.3 The seismic imaging operator for laterally varying α_1

In the (k_m, z) domain, with the constraint of $k_h = 0$, α_1 in 2D and 3D seismic can be uniformly expressed as[13],

$$\begin{aligned}
&\widetilde{\alpha}_1(\vec{k}_m, z) = -\frac{8}{c_0}\int_{-\infty}^{\infty} \widetilde{D}\left(\vec{k}_m, \frac{2z'}{c_0}\right)\widetilde{\gamma}_1(k_m, z, z')dz', \\
&\texttt{where} \quad : \quad \widetilde{\gamma}_1(k_m, z, z') = \frac{1}{2\pi}\int_{-\infty}^{\infty} dk_z \frac{k_z^2}{k_z^2 + k_m^2} e^{\mathbf{i}(z'\sqrt{k_z^2+k_m^2} - zk_z)}, \\
&\texttt{and} \quad : \quad \widetilde{D}(\vec{k}_m, \tau) = \vec{\int} d\vec{x}_m e^{-\mathbf{i}\vec{k}_m \bullet \vec{x}_m} \vec{\int} d\vec{x}_h D\left(\vec{x}_m + \frac{\vec{x}_h}{2}, \vec{x}_m - \frac{\vec{x}_h}{2}, \tau\right).
\end{aligned} \tag{33}$$

In equation (33), D is the data in the space and time domain: $D = D(\vec{x}_g, \vec{x}_s, t)$. Changing the integration variable to $\kappa \stackrel{\triangle}{=} k_z/k_m$ and using equation (76), the distribution $\widetilde{\gamma}_1$ can be further

[13] This is a unified formula for equation (2.22) of Liu (2006) and equation (32) of Liu and Weglein (2007).

expressed as,

$$\widetilde{\gamma}_1(k_m,z,z') = \frac{1}{2\pi}\int_{-\infty}^{\infty} dk_z \frac{k_z^2}{k_z^2+k_m^2} e^{\mathbf{i}(z'\sqrt{k_z^2+k_m^2}-zk_z)}$$
$$= \frac{|k_m|}{2\pi}\int_{-\infty}^{\infty} d\kappa \frac{\kappa^2}{\kappa^2+1} e^{\mathbf{i}(k_m z'\sqrt{\kappa^2+1}-k_m z\kappa)} = |k_m|\mathbf{F}_{\mathbf{-2,2}}(k_m z', k_m z).$$

Note that,

1. Although $\widetilde{\gamma}_1$ has three arguments, it can be expressed by the distribution $\mathbf{F}_{\mathbf{-2,2}}$ which has only two degrees of freedom.
2. Due to the fact that in seismic exploration both z and z' can reach several kilometers, the seismic imaging algorithm in equation (33) needs the value of the distribution $\mathbf{F}_{\mathbf{-2,2}}$ at very large depths.
3. For a fixed k_m, the larger the depth, the bigger the argument required in $\mathbf{F}_{\mathbf{-2,2}}$.
4. For a fixed pair of depths (z,z'), the higher the k_m (horizontal wavenumber), the more demanding the algorithm becomes in terms of information from $\mathbf{F}_{\mathbf{-2,2}}$.

2.4 The Seismic imaging operator for laterally varying α_2

In 2D, α_2 can be rewritten in the (k_m,z) domain as[14],

$$\widetilde{\alpha}_2(k_m,z) = \frac{1}{4\pi}\int_{-\infty}^{\infty} dk_1 \int_{-\infty}^{\infty} dz' \widetilde{\alpha}_1(0.5k_m-k_1,z') \int_{-\infty}^{z'} dz'' \widetilde{\alpha}_1(0.5k_m+k_1,z'') \widetilde{\gamma}_2\left(k_m,k_1,z-\frac{z'+z''}{2},\frac{z'-z''}{2}\right). \tag{34}$$

Similarly, in 3D, α_2 can be rewritten in the $\vec{k}_m$ (wavenumber) domain as,

$$\widetilde{\alpha}_2(\vec{k}_m,z) = \frac{1}{8\pi^2}\vec{\int}\vec{k}_1 \int_{-\infty}^{\infty} dz' \widetilde{\alpha}_1(0.5\vec{k}_m-\vec{k}_1,z') \int_{-\infty}^{z'} dz'' \widetilde{\alpha}_1(0.5\vec{k}_m+\vec{k}_1,z'') \widetilde{\gamma}_2\left(k_m,k_1,z-\frac{z'+z''}{2},\frac{z'-z''}{2}\right). \tag{35}$$

[14]Please notice that in equation (36), the definition of $\widetilde{\gamma}_2$ is different from the $\widetilde{\gamma}_2$ of equation (A.29) in Liu (2006), they differ by $\frac{1}{2\pi}$. Currently we feel it is better to put the $\frac{1}{2\pi}$ factor in the definition of $\widetilde{\gamma}_2$ since it belongs to the inverse Fourier transform over k_z. In equation (34), the upper limit of the dz'' integral is changed to be z', which will introduce another factor of 2.

In both equation (34) and (35), the function $\widetilde{\gamma}_2$ is defined with the sign convention for square-root specified in equation (13),

$$\begin{aligned}
&\widetilde{\gamma}_2\left(k_m,k_1,\varepsilon_0,\varepsilon_1\right)=\frac{1}{2\pi}\int\limits_{-\infty}^{\infty}dk_z\mathbf{i}\frac{k_z^2+k_m^2}{u_1}e^{\mathbf{i}(\varepsilon_1u_1-\varepsilon_0k_z)},\\
&\texttt{where}:\quad u_1=\begin{cases}\texttt{sgn}(k_z)\sqrt{k_z^2+k_m^2-4k_1^2} & (\texttt{if } k_z^2+k_m^2-4k_1^2\geq 0)\\ \mathbf{i}\sqrt{4k_1^2-k_m^2-k_z^2} & (\texttt{if } k_z^2+k_m^2-4k_1^2<0)\end{cases}.
\end{aligned}\tag{36}$$

Given that k_z ranges from $-\infty$ to ∞, equation (36) will have very different behavior if the sign of $k_m^2-4k_1^2$ is different. If $k_m^2-4k_1^2\geq 0$, $k_z^2+k_m^2-4k_1^2$ will always be positive for every $k_z\in(-\infty,\infty)$; otherwise $k_z^2+k_m^2-4k_1^2$ may become negative for some small k_z.

1. First case: $k_m^2-4k_1^2\geq 0$, we define $a\triangleq\sqrt{k_m^2-4k_1^2}$, and consequently $u_1=\sqrt{k_z^2+k_m^2-4k_1^2}=\sqrt{k_z^2+a^2}$. Changing the integration variable to $\kappa\triangleq k_z/a$, and using the function defined in equation (76), we can convert equation (36) to,

$$\begin{aligned}
&\widetilde{\gamma}_2\left(k_m,k_1,\varepsilon_0,\varepsilon_1\right)=\frac{1}{2\pi}\int\limits_{-\infty}^{\infty}dk_z\mathbf{i}\frac{k_z^2+k_m^2}{\texttt{sgn}(k_z)\sqrt{k_z^2+a^2}}e^{\mathbf{i}(\varepsilon_1\texttt{sgn}(k_z)\sqrt{k_z^2+a^2}-\varepsilon_0k_z)}\\
=&\frac{a^2}{2\pi}\int\limits_{-\infty}^{\infty}d\kappa\mathbf{i}\frac{\kappa^2e^{\mathbf{i}(a\varepsilon_1\texttt{sgn}(\kappa)\sqrt{\kappa^2+1}-a\varepsilon_0k_z)}}{\texttt{sgn}(\kappa)\sqrt{\kappa^2+1}}+\frac{k_m^2}{2\pi}\int\limits_{-\infty}^{\infty}d\kappa\mathbf{i}\frac{e^{\mathbf{i}(a\varepsilon_1\texttt{sgn}(\kappa)\sqrt{\kappa^2+1}-a\varepsilon_0k_z)}}{\texttt{sgn}(\kappa)\sqrt{\kappa^2+1}}\\
=&a^2\mathbf{F}_{\mathbf{-1,2}}(a\varepsilon_1,a\varepsilon_0)-k_m^2\mathbf{F}_{\mathbf{-1,0}}(a\varepsilon_1,a\varepsilon_0)
\end{aligned}$$

2. Second case: $k_m^2-4k_1^2<0$, we define $a\triangleq\sqrt{4k_1^2-k_m^2}$, and consequently $u_1=\sqrt{k_z^2+k_m^2-4k_1^2}=\sqrt[?]{k_z^2-a^2}$. Please notice that in this case $k_z^2-a^2$ will change sign as k_z varies from $-\infty$ to ∞. In this situation, the integral can be more conveniently written in two partions, each with its own form of $\sqrt[?]{k_z^2-a^2}$,

$$\widetilde{\gamma}_2\left(k_m,k_1,\varepsilon_0,\varepsilon_1\right)=\int\limits_{|k_z|\geq a}+\int\limits_{|k_z|<a}.\tag{37}$$

On the right-hand-side of equation (37), the first integral is the major contribution. Changing the integration variable to $\kappa\triangleq k_z/a$, and using the function relation in equation (77), this

integral can be expressed as,

$$\begin{aligned}
\int\limits_{|k_z|\geq a} &= \frac{1}{2\pi}\int\limits_{|k_z|\geq a} dk_z \mathbf{i}\frac{k_z^2+k_m^2}{\mathtt{sgn}(k_z)\sqrt{k_z^2-a^2}} e^{\mathbf{i}(\varepsilon_1 \mathtt{sgn}(k_z)\sqrt{k_z^2-a^2}-\varepsilon_0 k_z)} \\
=&\frac{a^2}{2\pi}\int\limits_{|\kappa|\geq 1} d\kappa \mathbf{i}\frac{\kappa^2 e^{\mathbf{i}(a\varepsilon_1 \mathtt{sgn}(\kappa)\sqrt{\kappa^2-1}-a\varepsilon_0\kappa)}}{\mathtt{sgn}(\kappa)\sqrt{\kappa^2-1}} + \frac{k_m^2}{2\pi}\int\limits_{|\kappa|\geq 1} d\kappa \mathbf{i}\frac{e^{\mathbf{i}(a\varepsilon_1 \mathtt{sgn}(\kappa)\sqrt{\kappa^2-1}-a\varepsilon_0\kappa)}}{\mathtt{sgn}(\kappa)\sqrt{\kappa^2-1}} \\
=&(-1)^{2-1-1}a^2\mathbf{F}_{\mathbf{1},\mathbf{0}}(-a\varepsilon_0,-a\varepsilon_1) - (-1)^{0-1-1}k_m^2\mathbf{F}_{-\mathbf{1},\mathbf{0}}(-a\varepsilon_0,-a\varepsilon_1) \\
=&a^2\mathbf{F}_{\mathbf{1},\mathbf{0}}(-a\varepsilon_0,-a\varepsilon_1) - k_m^2\mathbf{F}_{-\mathbf{1},\mathbf{0}}(-a\varepsilon_0,-a\varepsilon_1).
\end{aligned} \tag{38}$$

On the other hand, the second integral on the right-hand-side of equation (37) is the minor contribution. Changing the integration variable to $\kappa \stackrel{\triangle}{=} k_z/a$, it can be simplified,

$$\begin{aligned}
\int\limits_{|k_z|\leq a} &= \frac{1}{2\pi}\int\limits_{|k_z|\leq a} dk_z \frac{(k_z^2+k_m^2)e^{-\varepsilon_1\sqrt{a^2-k_z^2}}}{\sqrt{a^2-k_z^2}} e^{-\mathbf{i}\varepsilon_0 k_z} \\
&= \frac{a^2}{2\pi}\int\limits_{|\kappa|\leq 1} d\kappa \frac{\kappa^2 e^{-a\varepsilon_1\sqrt{1-\kappa^2}} e^{-\mathbf{i}a\varepsilon_0\kappa}}{\sqrt{1-\kappa^2}} + \frac{k_m^2}{2\pi}\int\limits_{|\kappa|\leq 1} d\kappa \frac{e^{-a\varepsilon_1\sqrt{1-\kappa^2}} e^{-\mathbf{i}a\varepsilon_0\kappa}}{\sqrt{1-\kappa^2}} \\
&= \frac{a^2}{\pi}\int\limits_0^1 d\kappa \frac{\kappa^2 e^{-a\varepsilon_1\sqrt{1-\kappa^2}}\cos\left[a\varepsilon_0\kappa\right]}{\sqrt{1-\kappa^2}} + \frac{k_m^2}{\pi}\int\limits_0^1 d\kappa \frac{e^{-a\varepsilon_1\sqrt{1-\kappa^2}}\cos\left[a\varepsilon_0\kappa\right]}{\sqrt{1-\kappa^2}}.
\end{aligned} \tag{39}$$

Note that as the value of $\varepsilon_1 = \left|\frac{z'-z''}{2}\right|$ increases, the exponential decay in $e^{-a\varepsilon_1\sqrt{1-x^2}}$ will cause equation (39) to quickly taper to zero. In other words, this term is negligible for large depths.

2.5 Reduced behavior of the seismic imaging operator for earth without lateral variation

It is illuminating to look at the behavior of the seismic imaging operator $\widetilde{\gamma}_2$ if the earth has no lateral variation. In this case, the seismic data's Fourier transform over x will produce a Dirac δ function since the data is a constant with respect to x, that is[15],

$$\widetilde{\alpha}_1(k_m,z) = \int\limits_{-\infty}^{\infty} \alpha_1(z) e^{-\mathbf{i}k_m x} dx = 2\pi\alpha_1(z)\delta(k_m) \tag{40}$$

[15] According to our Fourier convention, i.e, equation (4), there will be a 2π factor in the data

We then substitute the form of data in equation (40) into the α_2 result in equation (34), and then transform it back into x domain,

$$\alpha_2(x,z) = \frac{1}{2\pi}\int_{-\infty}^{\infty} \widetilde{\alpha}_2(k_m,z)e^{-\mathbf{i}k_m x}dk_m = \int_{-\infty}^{\infty} dz'\alpha_1(z')\int_{-\infty}^{z'} dz''\alpha_1(z'') \\ \times \int_{-\infty}^{\infty} dk_m \int_{-\infty}^{\infty} dk_1 e^{-\mathbf{i}k_m x}\delta(0.5k_m - k_1)\delta(0.5k_m + k_1)\frac{\widetilde{\gamma}_2\left(k_m, k_1, z - \frac{z'-z''}{2}, \frac{z'-z''}{2}\right)}{2} \tag{41}$$

Note that the two inner-most integrals in equation (41) do not depend on data and can be immediately evaluated using the sifting properties of the two δ functions. Consequently, it results in the straightforward evaluation of $\widetilde{\gamma}_2\left(k_m, k_1, z - \frac{z'-z''}{2}, \frac{z'-z''}{2}\right)$ at $0.5k_m - k_1 = 0.5k_m + k_1 = 0$, or equivalently $k_m = k_1 = 0$, that is $\widetilde{\gamma}_2\left(0, 0, z - \frac{z'-z''}{2}, \frac{z'-z''}{2}\right)$.

Substituting $k_m = 0$ and $k_1 = 0$ into equation (36), we have,

$$u_1 = 0.5\sqrt[?]{(\omega/c_0)^2 - 4k_1^2} = \sqrt[?]{k_z^2 + k_m^2 - k_1^2} = \sqrt[?]{k_z^2} \equiv k_z \tag{42}$$

and consequently,

$$\frac{\widetilde{\gamma}_2\left(0, 0, z - \frac{z'-z''}{2}, \frac{z'-z''}{2}\right)}{2} = \frac{1}{4\pi}\int_{-\infty}^{\infty} dk_z \mathbf{i}k_z e^{\mathbf{i}(z'-z)} = \frac{1}{2}\delta'(z'-z) = -\frac{1}{2}\delta'(z-z') \tag{43}$$

Note that the final distribution in equation (43) is the same as equation (30), the seismic imaging operator for earth without lateral variations.

3 Matrix formulation of interpolation and integration

Digital computers are designed to finish a task in a finite number of steps, while a typical integral requires we sample the infinite number of points in the integration interval. How can we formulate the integration scheme to arbitrary accuracy in such a way that it is tractable by digital computers in a finite number of steps? The key is interpolation with the help of various derivatives.

Our approach is fundamentally different from the popular polynomial (or rational) interpolation methods, for example, Chapter 3 of Press et al. (1992). The major reason is that: Due to the unique (and one of the best) advantages of the inverse scattering series, i.e, all the details of the integrand are clearly defined, we are able to extract all aspects of variation, for example, the derivatives of Green's function, to arbitrary order.

Note that only by repeatedly using the homogeneous migration velocity, we always have access to every variation detail of the analytic Green's function and hence of the seismic imaging operator. If the reference velocity is updated in every iteration, as proposed in iterative linear inversion, Green's

function will no longer be analytic, and consequently its partial derivatives will no longer be readily available.

Let's consider the interpolation problem of a function $g(y)$,

$$g(y) \qquad , \qquad (y_1 \le y \le y_2). \tag{44}$$

The geometry information, e.g, y_1 and y_2, are not essential to the problem since if we translate y_1 and y_2 by the same constant, the interpolation problem is essentially the same and the new interpolation result is simply the translation of the old one. We can isolate the interval's geometric information with a linear transform below.

3.1 A linear transformation to encapsulate the geometric information of the interpolation interval

Let's define a linear transform $\mathbf{T}$,

$$u = \mathbf{T}[y] \stackrel{\triangle}{=} \frac{y - y_1}{y_2 - y_1}, \tag{45}$$

and define a function $f(u)$ by,

$$f(u) \stackrel{\triangle}{=} g(\mathbf{T}[y]) = g\left(\frac{y - y_1}{y_2 - y_1}\right). \tag{46}$$

It is clear that the transform $\mathbf{T}$ in equation (45) maps the interval (y_1, y_2) uniformly to the interval $(0, 1)$, and using the chain rule we can calculate the corresponding derivatives of $f(u)$ at the ends of the interval $0 \le u \le 1$,

$$\begin{array}{ll}
f(0) = g(y_1), & f(1) = g(y_2), \\
f'(0) = g'(y_1)\mathbf{T}'[y_1] = g'(y_1)(y_2 - y_1), & f'(1) = g'(y_2)\mathbf{T}'[y_2] = g'(y_2)(y_2 - y_1), \\
f''(0) = g''(y_1)(y_2 - y_1)^2, & f''(1) = g''(y_2)(y_2 - y_1)^2, \\
f'''(0) = g'''(y_1)(y_2 - y_1)^3, & f'''(1) = g'''(y_2)(y_2 - y_1)^3, \\
\multicolumn{2}{c}{\cdots}
\end{array} \tag{47}$$

Since $f(u)$ is simply the translated and rescaled form of the original function $g(y)$, we have essentially solved the interpolation in equation (44) if we solve the interpolation problem of $f(u)$ between 0 and 1,

$$f(u) \qquad , \qquad \texttt{where} \quad 0 \le u \le 1. \tag{48}$$

In equation (48), u is defined in equation (45), and its various derivatives at the ends can be obtained via equation (47).

From now on in this section, we focus on an interpolation problem in the normalized interval $(0, 1)$.

3.2 Polynomial approximation and its derivatives

For the interpolation problem in equation (48), we can approximate the function $f(u)$ with a polynomial,

$$f(u) \approx P(u) \stackrel{\triangle}{=} \sum_{n=0}^{N} a_n u^n = a_0 + a_1 u + a_2 u^2 + a_3 u^3 + \cdots + a_N u^N, \tag{49}$$

where the unknown coefficients a_0, a_1, $\cdots$, a_N need to be determined. We can evaluate $P(u)$ and its various derivatives at the end points: $u = 0$ and $u = 1$,

$$\begin{aligned}
&P(0) = a_0, && P(1) = \sum_{n=0}^{N} a_n, \\
&P'(0) = a_1, && P'(1) = \sum_{n=1}^{N} n a_n, \\
&P''(0) = 2! a_2, && P''(1) = \sum_{n=2}^{N} n(n-1) a_n, \\
&P'''(0) = 3! a_3, && P'''(1) = \sum_{n=3}^{N} n(n-1)(n-2) a_n, \\
&\cdots
\end{aligned} \tag{50}$$

If all coefficients in an equation have a common factor, it is often reasonable to move it to the other side through a simple division. This is indeed our case: in equation (50), if the fourth row (associated with the $3^{\mathtt{rd}}$-order derivative) is scaled by $\frac{1}{3!}$, the coefficients on the right hand side become the binomial coefficients $\frac{n(n-1)(n-2)}{3!}$ (Abramowitz and Stegun, 1965, equation 3.1.2) and hence are still integers. Similarly, if the third row (associated with the $2^{\mathtt{nd}}$-order derivative) is scaled by $\frac{1}{2!}$, the coefficients on the right-hand side are again integers $\frac{n(n-1)}{2!}$. Rescaling all of the equations with the same logic, i.e, dividing each equation by the greatest common divisor (**gcd**) of all coefficients, we have,

$$\begin{aligned}
&P(0) = a_0, && P(1) = \sum_{n=0}^{N} a_n, \\
&P'(0)/1! = a_1, && P'(1) = \sum_{n=1}^{N} n a_n, \\
&P''(0)/2! = a_2, && P''(1)/2! = \sum_{n=2}^{N} \frac{n(n-1)}{2!} a_n, \\
&P'''(0)/3! = a_3, && P'''(1)/3! = \sum_{n=3}^{N} \frac{n(n-1)(n-2)}{3!} a_n, \\
&\cdots
\end{aligned} \tag{51}$$

3.3 Solving the polynomial interpolation problem

For the purpose of explanation, let's say we have sampled (at both end points) $f(u)$ and its derivatives up to the third-order[16], then we have 8 pieces of known items: $f(0)$, $f'(0)$, $f''(0)$, $f'''(0)$, $f(1)$,

[16]This formulism is very general, and here the interpolation order $\bar{\wp}$ can be any non-negative integers.

$f'(1)$, $f''(1)$, $f'''(1)$. In this, case, we define the interpolation order as $\bar{\wp} = 3$. The aforementioned 8 known items will be sufficient to determine 8 unknown coefficients: a_0, a_1, $\cdots$, a_7. Grouping the first 8 identities in equation (51) into a matrix problem, we have,

$$\begin{pmatrix} 1 & 0 & 0 & 0 & 0 & 0 & 0 & 0 \\ 0 & 1 & 0 & 0 & 0 & 0 & 0 & 0 \\ 0 & 0 & 1 & 0 & 0 & 0 & 0 & 0 \\ 0 & 0 & 0 & 1 & 0 & 0 & 0 & 0 \\ 1 & 1 & 1 & 1 & 1 & 1 & 1 & 1 \\ 0 & 1 & 2 & 3 & 4 & 5 & 6 & 7 \\ 0 & 0 & 1 & 3 & 6 & 10 & 15 & 21 \\ 0 & 0 & 0 & 1 & 4 & 10 & 20 & 35 \end{pmatrix} \begin{pmatrix} a_0 \\ a_1 \\ a_2 \\ a_3 \\ a_4 \\ a_5 \\ a_6 \\ a_7 \end{pmatrix} = \begin{pmatrix} f(0) \\ f'(0) \\ \frac{f''(0)}{2!} \\ \frac{f'''(0)}{3!} \\ f(1) \\ f'(1) \\ \frac{f''(1)}{2!} \\ \frac{f'''(1)}{3!} \end{pmatrix}. \tag{52}$$

Equation (52) can be easily solved by inverting the matrix on the left-hand-side,

$$\begin{pmatrix} a_0 \\ a_1 \\ a_2 \\ a_3 \\ a_4 \\ a_5 \\ a_6 \\ a_7 \end{pmatrix} = \begin{pmatrix} 1 & 0 & 0 & 0 & 0 & 0 & 0 & 0 \\ 0 & 1 & 0 & 0 & 0 & 0 & 0 & 0 \\ 0 & 0 & 1 & 0 & 0 & 0 & 0 & 0 \\ 0 & 0 & 0 & 1 & 0 & 0 & 0 & 0 \\ -35 & -20 & -10 & -4 & 35 & -15 & 5 & -1 \\ 84 & 45 & 20 & 6 & -84 & 39 & -14 & 3 \\ -70 & -36 & -15 & -4 & 70 & -34 & 13 & -3 \\ 20 & 10 & 4 & 1 & -20 & 10 & -4 & 1 \end{pmatrix} \begin{pmatrix} f(0) \\ f'(0) \\ \frac{f''(0)}{2!} \\ \frac{f'''(0)}{3!} \\ f(1) \\ f'(1) \\ \frac{f''(1)}{2!} \\ \frac{f'''(1)}{3!} \end{pmatrix}. \tag{53}$$

For the purpose of easy explanation, we name the matrix in equation (52) the "**Basic matrix**"[17] and denote it as **B**. On the other hand, the matrix in equation (53) is named the "**Manifest matrix**"[18] and is denoted as **M**.

It is clear that the **Basic matrix** and **Manifest matrix** are mutually inverse to each other,

$$\mathbf{M} = \mathbf{B}^{-1} \qquad , \qquad \mathbf{B} = \mathbf{M}^{-1},$$

and in this case, where the interpolation order is $\bar{\wp} = 3$, the values of **B** and **M** are,

$$\mathbf{B} = \begin{pmatrix} 1 & 0 & 0 & 0 & 0 & 0 & 0 & 0 \\ 0 & 1 & 0 & 0 & 0 & 0 & 0 & 0 \\ 0 & 0 & 1 & 0 & 0 & 0 & 0 & 0 \\ 0 & 0 & 0 & 1 & 0 & 0 & 0 & 0 \\ 1 & 1 & 1 & 1 & 1 & 1 & 1 & 1 \\ 0 & 1 & 2 & 3 & 4 & 5 & 6 & 7 \\ 0 & 0 & 1 & 3 & 6 & 10 & 15 & 21 \\ 0 & 0 & 0 & 1 & 4 & 10 & 20 & 35 \end{pmatrix},$$

[17] This matrix provides the basic formulization of the interpolation problem.

[18] This matrix offers the solution for interpolation problem, or equivalently speaking, makes the solution clear.

$$\mathbf{M} = \begin{pmatrix} 1 & 0 & 0 & 0 & 0 & 0 & 0 & 0 \\ 0 & 1 & 0 & 0 & 0 & 0 & 0 & 0 \\ 0 & 0 & 1 & 0 & 0 & 0 & 0 & 0 \\ 0 & 0 & 0 & 1 & 0 & 0 & 0 & 0 \\ -35 & -20 & -10 & -4 & 35 & -15 & 5 & -1 \\ 84 & 45 & 20 & 6 & -84 & 39 & -14 & 3 \\ -70 & -36 & -15 & -4 & 70 & -34 & 13 & -3 \\ 20 & 10 & 4 & 1 & -20 & 10 & -4 & 1 \end{pmatrix}.$$

So far we have covered the solution of the interpolation problem assuming we know the information of $f(u)$ up to the $3^{\mathtt{rd}}$-order derivatives. Here we list several other simple scenarios that the readers may find useful.

The first case is the simplest, where we know only $f(0)$ and $f(1)$, i.e, have at our disposal the derivatives of $f(u)$ up to the $0^{\mathtt{th}}$-order, in other words $\bar{\wp} = 0$. In this case our interpolation scheme is just the popular linear interpolation. Its application into integration will produce the well-known "Trapezoidal rule", i.e, equation 4.1.3 from Press et al. (1992). In this case the **Basic matrix** and the **Manifest matrix** are,

$$\mathbf{B} = \begin{pmatrix} 1 & 0 \\ 1 & 1 \end{pmatrix} \quad , \quad \mathbf{M} = \begin{pmatrix} 1 & 0 \\ -1 & 1 \end{pmatrix}.$$

If we have knowledge of $f(0)$, $f'(0)$, $f(1)$, and $f'(1)$, i.e, with interpolation order $\bar{\wp} = 1$, we have a scheme that is essentially cubic spline interpolation[19]. Its application into integration will result in cubic spline quadrature. In this case the **Basic matrix** and **Manifest matrix** are,

$$\mathbf{B} = \begin{pmatrix} 1 & 0 & 0 & 0 \\ 0 & 1 & 0 & 0 \\ 1 & 1 & 1 & 1 \\ 0 & 1 & 2 & 3 \end{pmatrix} \quad , \quad \mathbf{M} = \begin{pmatrix} 1 & 0 & 0 & 0 \\ 0 & 1 & 0 & 0 \\ -3 & -2 & 3 & -1 \\ 2 & 1 & -2 & 1 \end{pmatrix}.$$

Although a matrix of integers will generally have non-integer elements, in all cases we have encountered, i.e, maximal interpolation order from $\bar{\wp} = 0$ all the way to $\bar{\wp} = 15$, $\mathbf{M} = \mathbf{B}^{-1}$ are all matrices of only integers. Our operation to re-scale equation (50) into equation (51) surely simplifies solutions.

3.4 Integration over interpolation results

Let's assume we have two functions, $f(u)$ (where $0 \leq u \leq 1$) and $g(u)$ (where $0 \leq u \leq 1$), and we know their derivatives up to the $\bar{\wp}^{\mathtt{th}}$ order at the end points. With the technology before, we can approximate both $f(u)$ and $g(u)$ with polynomials. First let we group the known derivatives into

[19] The difference between our spline interpolation and popular spline interpolation, for example Section 3.3 of Press et al. (1992), is that we use the accurate derivatives rather than evaluating using neighbor grids.

two vectors,

$$\vec{f}\overset{\triangle}{=}\begin{pmatrix} f(0) \\ f'(0) \\ \frac{f''(0)}{2!} \\ \vdots \\ \frac{f^{(\bar{\wp})}(0)}{\bar{\wp}!} \\ f(1) \\ f'(1) \\ \frac{f''(1)}{2!} \\ \vdots \\ \frac{f^{(\bar{\wp})}(1)}{\bar{\wp}!} \end{pmatrix} \quad , \quad \vec{g}\overset{\triangle}{=}\begin{pmatrix} g(0) \\ g'(0) \\ \frac{g''(0)}{2!} \\ \\ \vdots \\ \frac{g^{(\bar{\wp})}(0)}{\bar{\wp}!} \\ g(1) \\ g'(1) \\ \frac{g''(1)}{2!} \\ \vdots \\ \frac{g^{(\bar{\wp})}(1)}{\bar{\wp}!} \end{pmatrix}. \tag{54}$$

Similarly, the coefficients of both polynomials can also be grouped into their corresponding vectors,

$$\vec{a}\overset{\triangle}{=}\begin{pmatrix} a_0 \\ a_1 \\ a_2 \\ \vdots \\ a_{2\bar{\wp}+1} \end{pmatrix} \quad \vec{b}\overset{\triangle}{=}\begin{pmatrix} b_0 \\ b_1 \\ b_2 \\ \vdots \\ b_{2\bar{\wp}+1} \end{pmatrix}, \tag{55}$$

where the functions $f(u)$ and $g(u)$ can be approximated as[20],

$$\begin{aligned} f(u) &\approx P(u) = a_0 + a_1 x + a_2 u^2 + \cdots + a_{2\bar{\wp}+1} u^{2\bar{\wp}+1}, \\ g(u) &\approx Q(u) = b_0 + b_1 x + b_2 u^2 + \cdots + b_{2\bar{\wp}+1} u^{2\bar{\wp}+1}. \end{aligned} \tag{56}$$

From the above derivation of the interpolation procedure, we have,

$$\begin{aligned} \mathbf{B}\vec{a} = \vec{f} \quad &, \quad \vec{a} = \mathbf{M}\vec{f}, \\ \mathbf{B}\vec{b} = \vec{g} \quad &, \quad \vec{b} = \mathbf{M}\vec{g}. \end{aligned} \tag{57}$$

We can approximate the integral of $f(u)g(u)$ from 0 to 1 by integrating over the product of their corresponding approximate polynomials,

$$\begin{aligned} &\int_0^1 f(u)g(u)du \approx \int_0^1 P(u)Q(u)du = \int_0^1 (a_0 + a_1 u + \cdots)\cdot(b_0 + b_1 u + \cdots)\, du \\ &= \int_0^1 \sum_{m=0}^{2\bar{\wp}+1}\sum_{n=0}^{2\bar{\wp}+1} a_m b_n u^{m+n} du = \sum_{m=0}^{2\bar{\wp}+1}\sum_{n=0}^{2\bar{\wp}+1} a_m b_n \int_0^1 u^{m+n} du = \sum_{m=0}^{2\bar{\wp}+1}\sum_{n=0}^{2\bar{\wp}+1} \frac{a_m b_n}{m+n+1}. \end{aligned} \tag{58}$$

[20]Here we assume the interpolation orders for $f(u)$ and $g(u)$ are the same, so their corresponding **Manifest matrices** are identical. It is easy to assume they have different interpolation orders, and the formalism is only slightly more complicated.

The integration result in equation (58) can be expressed as the following bilinear form,

$$\int_0^1 f(u)g(u)du \approx \vec{a}^{\mathtt{T}}\mathbf{H}\vec{b}, \tag{59}$$

where the matrix $\mathbf{H}$'s element in $m^{\mathtt{th}}$-row and $n^{\mathtt{th}}$-column is $\frac{1}{m+n+1}$ ($m = 0, 1, 2, \cdots 2\bar{\wp}+1, n = 0, 1, 2, \cdots, 2\bar{\wp}+1$). It is denoted as $\mathbf{H}$ since it is actually the well-known Hilbert matrix.

Substitute the value of $\vec{a}$ and $\vec{b}$ from equation (57) into equation (59), we have,

$$\int_0^1 f(u)g(u)du \approx \vec{a}^{\mathtt{T}}\mathbf{H}\vec{b} = \left[\mathbf{M}\vec{f}\right]^{\mathtt{T}}\mathbf{H}\mathbf{M}\vec{g} = \vec{f}^{\mathtt{T}}\mathbf{M}^{\mathtt{T}}\mathbf{H}\mathbf{M}\vec{g}. \tag{60}$$

If we define the "**Nexus matrix**"[21] (denoted by $\mathbf{N}$) as,

$$\mathbf{N} = \mathbf{M}^{\mathtt{T}}\mathbf{H}\mathbf{M}, \tag{61}$$

equation (60) can be rewritten as,

$$\int_0^1 f(u)g(u)du \approx \vec{f}^{\mathtt{T}}\mathbf{N}\vec{g}. \tag{62}$$

Equation (62) has three disadvantages:

1. Its vectors contains derivatives of functions divided by a factorial, e.g., it contains $f''/2!$ instead of f'' itself.
2. Each derivatives must be scaled by the power of the original interval, e.g., f'' is scaled by the square of the sampling interval, as exemplified in equation (47).
3. The integration interval is rigidly fixed between 0 and 1.

All three disadvantages can be easily fixed by defining a diagonal matrix,

$$\Lambda(h) = \mathbf{diag}\left(1, \frac{h}{1!}, \frac{h^2}{2!}, \cdots, \frac{h^{\bar{\wp}}}{\bar{\wp}!}, 1, \frac{h}{1!}, \frac{h^2}{2!}, \cdots, \frac{h^{\bar{\wp}}}{\bar{\wp}!}\right), \tag{63}$$

where $h = u_2 - u_1$ is the length of the sampling interval. With the help of $\Lambda(h)$, equation (62) can be extended to general case,

$$\int_{u_1}^{u_2} f(u)g(u)du \approx h\ \vec{f}^{\mathtt{T}}\mathbf{N}\vec{g}, \tag{64}$$

[21] Due to the fact that in calculating the integration result, e.g, equation (62), it serves as a connection between the derivatives of function $f(u)$ and the derivatives of function $g(u)$, and was hence named as Nexus matrix.

where in equation (64), $\vec{f}$ and $\vec{g}$ can be constructed from derivatives of various orders as follows,

$$\vec{f} = \Lambda(h) \begin{pmatrix} f(u_1) \\ f'(u_1) \\ f''(u_1) \\ \vdots \\ f(u_2) \\ f'(u_2) \\ f''(u_2) \\ \vdots \end{pmatrix} = \begin{pmatrix} f(u_1) \\ f'(u_1) * h/1! \\ f''(u_1) * h^2/2! \\ \vdots \\ f(u_2) \\ f'(u_2) * h/1! \\ f''(u_2) * h^2/2! \\ \vdots \end{pmatrix}, \tag{65}$$

$$\vec{g} = \Lambda(h) \begin{pmatrix} g(u_1) \\ g'(u_1) \\ g''(u_1) \\ \vdots \\ g(u_2) \\ g'(u_2) \\ g''(u_2) \\ \vdots \end{pmatrix} = \begin{pmatrix} g(u_1) \\ g'(u_1) * h/1! \\ g''(u_1) * h^2/2! \\ \vdots \\ g(u_2) \\ g'(u_2) * h/1! \\ g''(u_2) * h^2/2! \\ \vdots \end{pmatrix}. \tag{66}$$

4 Fast implementation of the Fourier integral $\int_0^{\Xi}$

The Fourier transform is widely used in science and engineering. Its straightforward implementation over a uniformly sampled grids: discrete Fourier transform (**DFT**) and its corresponding fast implementation: fast Fourier transform (**FFT**) are among the best-known tools in scientific computation (Press et al., 1992, Chapter 12).

We demonstrate that the high-accuracy interpolated Fourier integration can also be expressed as a discrete sum, and hence can be implemented with the $n \log(n)$ efficiency of **FFT**.

4.1 Fourier integral formulated as interpolated integration

Let's assume we need to calculate the integral $\int_0^{\aleph h} f(u)g(u)du$ by dividing it into $\aleph$ uniformly sampled sub-intervals,

$$\int_0^{\aleph h} f(u)g(u)du = \sum_{\ell=0}^{\aleph-1} \int_{\ell}^{(\ell+1)h} f(u)g(u)du = \sum_{\ell=0}^{\aleph-1} h \left(\vec{f}_{\ell}^{\intercal}, \vec{f}_{\ell+1}^{\intercal} \right) \mathbf{N} \begin{pmatrix} \vec{g}_{\ell} \\ \vec{g}_{\ell+1} \end{pmatrix}. \tag{67}$$

In equation (67), h is the length of the sampling interval, ℓ is the index for u, $\aleph$ is the number of intervals[22], and the last step is the direct application of the integration scheme in equation (64). The vectors in equation (64) were rewritten in two pieces:

1. The first piece includes derivatives from the lower-limit of the interval. In equation (67), this part is denoted with index ℓ: for example, $\vec{f}_\ell$ and $\vec{g}_\ell$.
2. On the other hand, the second piece encapsulates the derivatives from the upper-limit of the interval. In equation (67), this part is denoted with index $\ell+1$: for example, $\vec{f}_{\ell+1}$ and $\vec{g}_{\ell+1}$.

According to equation (65) and (66), their explicit values are,

$$\begin{aligned}\vec{f}_\ell^{\,\mathtt{T}} &= \left(f(\ell h), \cdots, \frac{(h)^{\wp}}{\wp!} f^{(\wp)}(\ell h), \cdots, \frac{(h)^{\bar{\wp}}}{\bar{\wp}!} f^{(\bar{\wp})}(\ell h) \right), \\ \vec{g}_\ell^{\,\mathtt{T}} &= \left(g(\ell h), \cdots, \frac{(h)^{\wp}}{\wp!} g^{(\wp)}(\ell h), \cdots, \frac{(h)^{\bar{\wp}}}{\bar{\wp}!} g^{(\bar{\wp})}(\ell h) \right).\end{aligned} \tag{68}$$

In equation (68), $\wp$ is the order of derivatives. $\bar{\wp}$ is the maximal order of derivatives.

4.2 Reformulation into discrete Fourier transform

We want to Fourier transform, hence we define the kernel as $f(u) = e^{\mathbf{i}ku}$, where k is the Fourier conjugate of u. If we use $\hat{\ell}$ to denote the index for k, and $\hat{h}$ denotes the sampling interval of k, we have $k = \hat{\ell}\hat{h}$ and $f(u) = e^{\mathbf{i}ku} = e^{\mathbf{i}\hat{\ell}\hat{h}*\ell h}$. Following the Nyquist frequency defined in equation 12.1.2 from Press et al. (1992), we choose $\hat{h}$ (the sampling interval of k) as follows,

$$\hat{h} = \frac{2\pi}{\aleph h} \Longrightarrow \hat{h}h = \frac{2\pi}{\aleph},$$

and consequently,

$$\begin{aligned} f^{(\wp)}(\mathbf{i}ku) &= \frac{\partial^{\wp}}{\partial x^{\wp}} e^{\mathbf{i}ku} = (\mathbf{i}k)^{\wp} e^{\mathbf{i}ku} = \left(\mathbf{i}\hat{\ell}\hat{h}\right)^{\wp} e^{\mathbf{i}\hat{\ell}\hat{h}u}, \\ \frac{(h)^{\wp}}{\wp!} f^{(\wp)}(\ell h) &= \frac{\left(\mathbf{i}\hat{\ell}\hat{h}h\right)^{\wp}}{\wp!} e^{\mathbf{i}\hat{\ell}\hat{h}*\ell h} = \frac{\left(\mathbf{i}\hat{\ell}\hat{h}h\right)^{\wp}}{\wp!} e^{\mathbf{i}2\pi\hat{\ell}\ell/\aleph}. \end{aligned}$$

It is convenient to define:

$$\vec{\mathtt{F}}(\hat{\ell}) \triangleq \left(1, \frac{\mathbf{i}\hat{\ell}\hat{h}h}{1!}, \cdots, \frac{\left(\mathbf{i}\hat{\ell}\hat{h}h\right)^{\bar{\wp}}}{\bar{\wp}!} \right)^{\mathtt{T}} = \left(1, \frac{\mathbf{i}2\pi\hat{\ell}/\aleph}{1!}, \cdots, \frac{\left(\mathbf{i}2\pi\hat{\ell}/\aleph\right)^{\bar{\wp}}}{\bar{\wp}!} \right)^{\mathtt{T}}. \tag{69}$$

[22]Following section 12.2 of Press et al. (1992), in order to accommodate the future cast into **FFT**, we choose $\aleph$ as an integer power of 2.

From equation (69), it's easy to obtain the following symmetry relation:

$$\vec{\mathrm{F}}(-\hat{\ell}) = \left[\vec{\mathrm{F}}(\hat{\ell})\right]^{*}, \tag{70}$$

and the expression for $\vec{f}_\ell$ and $\vec{f}_{\ell+1}$:

$$\vec{f}_\ell = e^{\mathbf{i}\hat{\ell}\hat{h}*\ell h}\vec{\mathrm{F}}(\hat{\ell}) \qquad , \qquad \vec{f}_{\ell+1} = e^{\mathbf{i}\hat{\ell}\hat{h}*h}\vec{f}_\ell = e^{\mathbf{i}2\pi\hat{\ell}/\aleph}\vec{f}_\ell.$$

In fact $\vec{f}_{\ell+1} = e^{\mathbf{i}2\pi\hat{\ell}/\aleph}\vec{f}_\ell$ has a critical importance: $\vec{f}_\ell$ and $\vec{f}_{\ell+1}$ differ by a constant $e^{\mathbf{i}2\pi\hat{\ell}/\aleph}$ independent of u, any one of them can be easily expressed using the other.

For ease of derivation we divide $\mathbf{N}$ into 4 submatrices with the same size,

$$\mathbf{N} = \begin{pmatrix} \mathbf{N_{LU}} & , & \mathbf{N_{RU}} \\ \mathbf{N_{LD}} & , & \mathbf{N_{RD}} \end{pmatrix}. \tag{71}$$

Consequently, the original integral can be expressed as :

$$\begin{aligned}
&\int_0^{\aleph h} f(u)g(u)du = \sum_{\ell=0}^{\aleph-1} h\left(\vec{f}_\ell^{\mathsf{T}}, \vec{f}_{\ell+1}^{\mathsf{T}}\right)\mathbf{N}\begin{pmatrix}\vec{g}_\ell \\ \vec{g}_{\ell+1}\end{pmatrix} \\
&= h\sum_{\ell=0}^{\aleph-1}\left(e^{\mathbf{i}2\pi\ell\hat{\ell}/\aleph}\left[\vec{\mathrm{F}}(\hat{\ell})\right]^{\mathsf{T}}, e^{\mathbf{i}2\pi(\ell+1)\hat{\ell}/\aleph}\left[\vec{\mathrm{F}}(\hat{\ell})\right]^{\mathsf{T}}\right)\begin{pmatrix}\mathbf{N_{LU}} & \mathbf{N_{RU}} \\ \mathbf{N_{LD}} & \mathbf{N_{RD}}\end{pmatrix}\begin{pmatrix}\vec{g}_\ell \\ \vec{g}_{\ell+1}\end{pmatrix} \\
&= h\sum_{\ell=0}^{\aleph-1} e^{\mathbf{i}2\pi\ell\hat{\ell}/\aleph}\left[\vec{\mathrm{F}}(\hat{\ell})\right]^{\mathsf{T}}\mathbf{N_{LU}}\vec{g}_\ell + e^{\mathbf{i}2\pi(\ell+1)\hat{\ell}/\aleph}\left[\vec{\mathrm{F}}(\hat{\ell})\right]^{\mathsf{T}}\mathbf{N_{LD}}\vec{g}_\ell \\
&+ h\sum_{\ell=0}^{\aleph-1} e^{\mathbf{i}2\pi\ell\hat{\ell}/\aleph}\left[\vec{\mathrm{F}}(\hat{\ell})\right]^{\mathsf{T}}\mathbf{N_{RU}}\vec{g}_{\ell+1} + e^{\mathbf{i}2\pi(\ell+1)\hat{\ell}/\aleph}\left[\vec{\mathrm{F}}(\hat{\ell})\right]^{\mathsf{T}}\mathbf{N_{RD}}\vec{g}_{\ell+1}.
\end{aligned}$$

In a discrete Fourier transform, for example, equation 12.1.6 from Press et al. (1992), typically $\vec{g}_\ell$ multiplies with $e^{\mathbf{i}2\pi\ell\hat{\ell}/\aleph}$ and $\vec{g}_{\ell+1}$ multiplies with $e^{\mathbf{i}2\pi(\ell+1)\hat{\ell}/\aleph}$. This behavior can be easily managed in the equation above since $\vec{f}_\ell = e^{\mathbf{i}2\pi\ell\hat{\ell}/\aleph}\vec{\mathrm{F}}(\hat{\ell})$ and $\vec{f}_{\ell+1} = e^{\mathbf{i}2\pi(\ell+1)\hat{\ell}/\aleph}\vec{\mathrm{F}}(\hat{\ell})$ differ from each other by a constant independent of u, and consequently, the equation above can be rewritten as,

$$\begin{aligned}
&= h\left[\vec{\mathrm{F}}(\hat{\ell})\right]^{\mathsf{T}}\left(\sum_{\ell=0}^{\aleph-1}\left[e^{\mathbf{i}2\pi\ell\hat{\ell}/\aleph}\mathbf{N_{LU}}\vec{g}_\ell + e^{\mathbf{i}2\pi(\ell+1)\hat{\ell}/\aleph}\mathbf{N_{LD}}\vec{g}_\ell\right] + \sum_{\ell=0}^{\aleph-1}\left[e^{\mathbf{i}2\pi\ell\hat{\ell}/\aleph}\mathbf{N_{RU}}\vec{g}_{\ell+1} + e^{\mathbf{i}2\pi(\ell+1)\hat{\ell}/\aleph}\mathbf{N_{RD}}\vec{g}_{\ell+1}\right]\right) \\
&= h\left[\vec{\mathrm{F}}(\hat{\ell})\right]^{\mathsf{T}}\sum_{\ell=0}^{\aleph-1}\begin{pmatrix} e^{\mathbf{i}2\pi\ell\hat{\ell}/\aleph}\left\{\mathbf{N_{LU}} + e^{\mathbf{i}2\pi\hat{\ell}/\aleph}\mathbf{N_{LD}}\right\}\vec{g}_\ell \\ + \\ e^{\mathbf{i}2\pi(\ell+1)\hat{\ell}/\aleph}\left\{e^{-\mathbf{i}2\pi\hat{\ell}/\aleph}\mathbf{N_{RU}} + \mathbf{N_{RD}}\right\}\vec{g}_{\ell+1}\end{pmatrix} = h\begin{Bmatrix}\left[\vec{w}_L(\hat{\ell})\right]^{\mathsf{T}}\sum_{\ell=0}^{\aleph-1} e^{\mathbf{i}2\pi\ell\hat{\ell}/\aleph}\vec{g}_\ell \\ \left[\vec{w}_R(\hat{\ell})\right]^{\mathsf{T}}\sum_{\ell=0}^{\aleph-1} e^{\mathbf{i}2\pi(\ell+1)\hat{\ell}/\aleph}\vec{g}_{\ell+1}\end{Bmatrix},
\end{aligned}$$

where:

$$\begin{aligned}
\left[\vec{w}_L(\hat{\ell})\right]^{\mathsf{T}} &= \left[\vec{\mathrm{F}}(\hat{\ell})\right]^{\mathsf{T}}\left\{\mathbf{N_{LU}} + e^{\mathbf{i}2\pi\hat{\ell}/\aleph}\mathbf{N_{LD}}\right\}, \\
\left[\vec{w}_R(\hat{\ell})\right]^{\mathsf{T}} &= \left[\vec{\mathrm{F}}(\hat{\ell})\right]^{\mathsf{T}}\left\{e^{-\mathbf{i}2\pi\hat{\ell}/\aleph}\mathbf{N_{RU}} + \mathbf{N_{RD}}\right\}.
\end{aligned} \tag{72}$$

Consequently the original integral can be expressed as,

$$h\left\{\begin{array}{l}\left[\vec{w}_L(\hat{\ell})\right]^{\mathtt{T}}\sum_{\ell=0}^{\aleph-1}e^{\mathbf{i}2\pi\ell\hat{\ell}/\aleph}\vec{g}_\ell\\ \left[\vec{w}_R(\hat{\ell})\right]^{\mathtt{T}}\sum_{\ell=0}^{\aleph-1}e^{\mathbf{i}2\pi(\ell+1)\hat{\ell}/\aleph}\vec{g}_{\ell+1}\end{array}\right\}=h\left\{\begin{array}{l}\left[\vec{w}_L(\hat{\ell})\right]^{\mathtt{T}}\sum_{\ell=0}^{\aleph-1}e^{\mathbf{i}2\pi\ell\hat{\ell}/\aleph}\vec{g}_\ell\\ \left[\vec{w}_R(\hat{\ell})\right]^{\mathtt{T}}\sum_{\ell=1}^{\aleph}e^{\mathbf{i}2\pi\ell\hat{\ell}/\aleph}\vec{g}_\ell\end{array}\right\}$$

$$=h\left\{\left[\vec{w}_L(\hat{\ell})+\vec{w}_R(\hat{\ell})\right]^{\mathtt{T}}\left(\sum_{\ell=0}^{\aleph-1}e^{\mathbf{i}2\pi\ell\hat{\ell}/\aleph}\vec{g}_\ell\right)-e^{\mathbf{i}2\pi 0\hat{\ell}/\aleph}\left[\vec{w}_R(\hat{\ell})\right]^{\mathtt{T}}\vec{g}_{\ell=0}+e^{\mathbf{i}2\pi\aleph\hat{\ell}/\aleph}\left[\vec{w}_R(\hat{\ell})\right]^{\mathtt{T}}\vec{g}_{\ell=\aleph}\right\}.$$

Taking advantage of the identity $e^{\mathbf{i}2\pi\hat{\ell}\aleph/\aleph}=e^{2\pi\mathbf{i}}\equiv 1$, the equation above can be further simplified,

$$\int_0^{\aleph h}f(u)g(u)du=h\left\{\left[\vec{w}_L(\hat{\ell})+\vec{w}_R(\hat{\ell})\right]^{\mathtt{T}}\left(\sum_{\ell=0}^{\aleph-1}e^{\mathbf{i}2\pi\ell\hat{\ell}/\aleph}\vec{g}_\ell\right)+\left[\vec{w}_R(\hat{\ell})\right]^{\mathtt{T}}\left[\vec{g}_{\ell=\aleph}-\vec{g}_{\ell=0}\right]\right\}. \tag{73}$$

In the equation above $\sum_{\ell=0}^{\aleph-1}e^{\mathbf{i}2\pi\ell\hat{\ell}/\aleph}\vec{g}_\ell$ is a vector with $\bar{\wp}+1$ components, each of which is of the form $\sum_{\ell=0}^{\aleph-1}e^{\mathbf{i}2\pi\ell\hat{\ell}/\aleph}g^{(\wp)}(\ell h)$ where $\wp=0,1,\cdots,\bar{\wp}$. Note that every sum $\sum_{\ell=0}^{\aleph-1}e^{\mathbf{i}2\pi\ell\hat{\ell}/\aleph}g^{(\wp)}(\ell h)$ shares the same form as equation 12.1.6 from Press et al. (1992) and is actually a discrete Fourier transform. Consequently, $\aleph$ transforms can be efficiently implemented by the Fast Fourier transform with $\aleph\log\aleph$ steps computation.

After the calculation of $\sum_{\ell=0}^{\aleph-1}e^{\mathbf{i}2\pi\ell\hat{\ell}/\aleph}\vec{g}_\ell$, we can calculate its inner-product with the vector $\left[\vec{w}_L(\hat{\ell})+\vec{w}_R(\hat{\ell})\right]^{\mathtt{T}}$ to obtain the integration value with high accuracy.

4.3 Trivial extension for Fourier transform with different sign convention

Note that in the derivation we assume the Fourier transform has the form $\int_0^{\Xi}f(u)e^{\mathbf{i}ku}$, i.e, the sign of the exponential is positive. In many situations a negative sign is used in the exponential $\int_0^{\Xi}f(u)e^{-\mathbf{i}ku}$. For this case we can simply use $-z$ instead of z in the construction of $\vec{\mathtt{F}}$ and $e^{\mathbf{i}kh}=e^{\mathbf{i}2\pi\hat{\ell}/\aleph}$, i.e, use $-\hat{\ell}$ instead of $\hat{\ell}$. All other variables can be kept the same.

From equation (72) and equation (70) and the fact that all the submatrices $\mathbf{N_{LU}}$, $\mathbf{N_{RU}}$, $\mathbf{N_{LD}}$, and $\mathbf{N_{RD}}$ must be real since $\mathbf{N}$ is real, it is easy to verify the symmetry relation

$$\vec{w}_L(-\hat{\ell})=\left[\vec{w}_L(\hat{\ell})\right]^*\qquad\qquad\vec{w}_R(-\hat{\ell})=\left[\vec{w}_R(\hat{\ell})\right]^*. \tag{74}$$

Equation (74) provides the equation to access the weights for $-\hat{\ell}$.

5 Transcendental seismic imaging operator $\mathbf{F}_{\lambda,\mu}$

The seismic imaging operators for α_1 and α_2, and their various derivatives with respect to depth can generally be expressed as the Fourier transform of the function,

$$\mathbf{i}^{\lambda}(-\mathbf{i})^{\mu}k_z^{\mu}\left[\mathtt{sgn}(k_z)\sqrt{1+k_z^2}\right]^{\lambda}e^{\mathbf{i}\breve{z}_0\mathtt{sgn}(k_z)\sqrt{1+k_z^2}}, \tag{75}$$

where $\mu > -1$ and λ are two integers[23].

Use the symbol $\breve{z}$ to denote the Fourier conjugate of k_z and define the transform as,

$$\mathbf{F}_{\lambda,\mu}(\breve{z}_0,\breve{z})\stackrel{\triangle}{=}\frac{1}{2\pi}\int\limits_{-\infty}^{\infty}\mathbf{i}^{\lambda}(-\mathbf{i})^{\mu}k_z^{\mu}\left[\mathtt{sgn}(k_z)\sqrt{1+k_z^2}\right]^{\lambda}e^{\mathbf{i}(\breve{z}_0\mathtt{sgn}(k_z)\sqrt{1+k_z^2}-\breve{z}k_z)}dk_z. \tag{76}$$

Changing the integration variables to $u = \mathtt{sgn}(k_z)\sqrt{k_z^2+1}$, we can use $\mathbf{F}_{\lambda,\mu}(\breve{z}_0,\breve{z})$ to calculate another important class of integrals,

$$\begin{aligned}
&\frac{1}{2\pi}\int\limits_{|k_z|\geq 1}\mathbf{i}^{\lambda}(-\mathbf{i})^{\mu}k_z^{\mu}\left[\mathtt{sgn}(k_z)\sqrt{k_z^2-1}\right]^{\lambda}e^{\mathbf{i}(\breve{z}_0\mathtt{sgn}(k_z)\sqrt{k_z^2-1}-\breve{z}k_z)}dk_z\\
&=\int\limits_{-\infty}^{\infty}\mathbf{i}^{\lambda}(-\mathbf{i})^{\mu}\left[\mathtt{sgn}(u)\sqrt{u^2+1}\right]^{\mu}u^{\lambda}e^{\mathbf{i}(\breve{z}_0u-\breve{z}\mathtt{sgn}(u)\sqrt{u^2+1})}\frac{u}{\mathtt{sgn}(u)\sqrt{u^2+1}}du\\
&=\int\limits_{-\infty}^{\infty}\mathbf{i}^{\lambda}(-\mathbf{i})^{\mu}\left[\mathtt{sgn}(u)\sqrt{u^2+1}\right]^{(\mu-1)}u^{\lambda+1}e^{\mathbf{i}(\breve{z}_0u-\breve{z}\mathtt{sgn}(u)\sqrt{u^2+1})}du\\
&=(-1)^{\lambda+\mu-1}\int\limits_{|u|\geq 1}\mathbf{i}^{\mu-1}(-\mathbf{i})^{\lambda+1}\left[\mathtt{sgn}(u)\sqrt{u^2+1}\right]^{\mu-1}u^{\lambda+1}e^{\mathbf{i}(\breve{z}_0u-\breve{z}\mathtt{sgn}(u)\sqrt{u^2+1})}du\\
&=(-1)^{\lambda+\mu-1}\mathbf{F}_{\lambda,\mu}(-\breve{z}_0,-\breve{z})
\end{aligned} \tag{77}$$

The physics behind this type of Fourier transform is very critical for the structure of the seismic imaging algorithms associated with lateral variations. Several difficulties can be identified immediately,

1. If $\mu+\lambda \geq 0$, the integrand in equation (76) will not converge to zero as $k_z \to \infty$. Consequently, the corresponding integral is not Riemann integrable. How can we calculate it?
2. There are square-root variations in the amplitude term $\mathbf{i}^{\lambda}(-\mathbf{i})^{\mu}k_z^{\mu}\left[\mathtt{sgn}(k_z)\sqrt{1+k_z^2}\right]^{\lambda}$,
3. When $\breve{z}_0 \neq 0$, there are additional, much more daunting complexities caused by square-root complexities in the exponential term, $e^{\mathbf{i}\breve{z}_0\mathtt{sgn}(k_z)\sqrt{1+k_z^2}}$.

[23]We require $\mu > -1$ to make sure the integrand is Riemann integrable in the neighborhood of $k_z = 0$.

A typical Fourier transform in the form of equation (76) normally is rapidly varying (or even discontinuous) with respect to $\check{z}_0$ and $\check{z}$, but those rapid variations and discontinuities are caused by large k_z values in the transform[24]. For the purposes of obtaining the most significant rapid variations, and to study the region where Riemann integrability is violated[25], we only need to study the behavior of the integrand for large k_z, for example: $k_z \geq 1$. If $k_z \geq 1$, k_z^{-2} is well defined and the exponential term in equation (76) can be rewritten as,

$$e^{\mathbf{i}(\check{z}_0 \mathtt{sgn}(k_z)\sqrt{1+k_z^2}-\check{z}k_z)} = e^{\mathbf{i}\check{z}_0(\mathtt{sgn}(k_z)\sqrt{1+k_z^2}-k_z)}e^{\mathbf{i}(\check{z}_0-\check{z})k_z} = e^{\mathbf{i}\check{z}_0(k_z\sqrt{1+k_z^{-2}}-k_z)}e^{\mathbf{i}(\check{z}_0-\check{z})k_z}. \tag{78}$$

If we define: $\tau = k_z\sqrt{1+k_z^{-2}} - k_z$, the phase term in equation (78) can be expressed as,

$$e^{\mathbf{i}\check{z}_0(k_z\sqrt{1+k_z^{-2}}-k_z)}e^{\mathbf{i}(\check{z}_0-\check{z})k_z} = e^{\mathbf{i}\check{z}_0\tau}e^{\mathbf{i}(\check{z}_0-\check{z})k_z} = e^{\mathbf{i}(\check{z}_0-\check{z})k_z} * \sum_{n=0}^{\infty}\frac{(\mathbf{i}\check{z}_0\tau)^n}{n!}. \tag{79}$$

Since $k_z \geq 1$ implies $k_z^{-2} \leq 1$, using the Taylor formula for a single variable, i.e, equation (3.6.9) from Abramowitz and Stegun (1965), we can expand the amplitude term $\mathbf{i}^\lambda(-\mathbf{i})^\mu k_z^\mu\left[\mathtt{sgn}(k_z)\sqrt{1+k_z^2}\right]^\lambda$ as follows,

$$\begin{aligned}
&\mathbf{i}^\lambda(-\mathbf{i})^\mu k_z^\mu\left[\mathtt{sgn}(k_z)\sqrt{1+k_z^2}\right]^\lambda = \mathbf{i}^\lambda(-\mathbf{i})^\mu k_z^\mu\left[k_z\sqrt{1+k_z^{-2}}\right]^\lambda = \mathbf{i}^\lambda(-\mathbf{i})^\mu k_z^{\mu+\lambda}\left(1+k_z^{-2}\right)^{0.5\lambda}\\
&= \mathbf{i}^\lambda(-\mathbf{i})^\mu k_z^{\mu+\lambda}\left(1+\frac{0.5\lambda}{1!}k_z^{-2}+\frac{(0.5\lambda)(0.5\lambda-1)}{2!}k_z^{-4}+\cdots\right)\\
&= \mathbf{i}^\lambda(-\mathbf{i})^\mu k_z^{\mu+\lambda}\left(1+\sum_{n=1}^{\infty}\frac{(0.5\lambda)(0.5\lambda-1)\cdots(0.5\lambda-n+1)}{n!}k_z^{-2n}\right).
\end{aligned} \tag{80}$$

With the amplitude term expressed in equation (80) and the phase term evaluated in equation (79), the integrand in equation (76) can be written as,

$$\begin{aligned}
&\mathbf{i}^\lambda(-\mathbf{i})^\mu k_z^\mu\left[\mathtt{sgn}(k_z)\sqrt{1+k_z^2}\right]^\lambda e^{\mathbf{i}(\check{z}_0\mathtt{sgn}(k_z)\sqrt{1+k_z^2}-\check{z}k_z)}\\
&= \mathbf{i}^\lambda(-\mathbf{i})^\mu k_z^{\mu+\lambda}\left(1+\sum_{n=1}^{\infty}\frac{(0.5\lambda)(0.5\lambda-1)\cdots(0.5\lambda-n+1)}{n!}k_z^{-2n}\right)\left(\sum_{n=0}^{\infty}\frac{(\mathbf{i}\check{z}_0\tau)^n}{n!}\right)e^{\mathbf{i}(\check{z}_0-\check{z})k_z}.
\end{aligned} \tag{81}$$

Now let's have a closer look at the integrand rewritten in equation (81). It is the product of two parts, the first part is the re-constructed phase term and is a simple harmonic sinusoidal function[26],

$$e^{\mathbf{i}(\check{z}_0-\check{z})k_z}. \tag{82}$$

[24] Just like a function in the time domain, the rapid variation, or detail of the change, comes from the high-frequency part of the spectrum. The low-frequency part provides the overall trend, but not the fine detail.

[25] Actually our integral in equation (76) is Riemann integrable for any finite interval since $\mu > -1$.

[26] Note that, for large k_z, the complicated square-root $\mathtt{sgn}(k_z)\sqrt{1+k_z^2}$ can be very well approximated by the linear expression k_z, and the larger the k_z, the better the approximation. Consequently, this new phase term: $e^{\mathbf{i}(\check{z}_0-\check{z})k_z}$ is a very good approximation for the original phase term $e^{\mathbf{i}(\check{z}_0\mathtt{sgn}(k_z)\sqrt{1+k_z^2}-\check{z}k_z)}$.

The second part is the re-constructed amplitude term and is much more complicated,

$$\mathbf{A}\overset{\triangle}{=}\mathbf{i}^{\lambda}(-\mathbf{i})^{\mu}k_z^{\mu+\lambda}\left(1+\sum_{n=1}^{\infty}\frac{(0.5\lambda)(0.5\lambda-1)\cdots(0.5\lambda-n+1)}{n!}k_z^{-2n}\right)\left(\sum_{n=0}^{\infty}\frac{(\mathbf{i}\breve{z}_0\tau)^n}{n!}\right). \tag{83}$$

Note that, if $\mu+\lambda\geq 0$, $\mathbf{A}$ will not converge to zero as $k_z\rightarrow\infty$. Consequently, our Fourier transform,

$$\int_{-\infty}^{\infty}\mathbf{A}e^{\mathbf{i}(\breve{z}_0-\breve{z})k_z}dk_z, \tag{84}$$

is not a Riemann integral. How can we calculate it? Our approach is to expand the amplitude term $\mathbf{A}$ specified in equation (83) to sufficient accuracy. First we need the expression for τ^n $(n=1,2,\cdots)$.

5.1 Expansion of $\left(k_z\sqrt{1+k_z^{-2}}-k_z\right)^n$ $(n=1,2,3,\cdots)$ when $|k_z|>1$

Since $|k_z|\geq 1$ implies $k_z^{-2}\leq 1$, it is straightforward to calculate τ using equation (3.6.9) from Abramowitz and Stegun (1965),

$$\begin{aligned}\sqrt{k_z^{-2}+1}=\left(1+k_z^{-2}\right)^{1/2}&=1+\frac{0.5}{1!}k_z^{-2}+\frac{0.5\,(0.5-1)}{2!}k_z^{-4}+\frac{0.5\,(0.5-1)\,(0.5-2)}{3!}k_z^{-6}+\cdots\\&=1+\sum_{n=1}^{\infty}\frac{0.5\,(0.5-1)\,(0.5-2)\cdots(0.5-n+1)}{n!}k_z^{-2n}.\end{aligned} \tag{85}$$

Consequently, $k_z\sqrt{k_z^{-2}+1}$ can be straightforwardly calculated as follows,

$$k_z\sqrt{k_z^{-2}+1}=k_z+\sum_{n=1}^{\infty}\frac{0.5\,(0.5-1)\,(0.5-2)\cdots(0.5-n+1)}{n!}k_z^{1-2n}. \tag{86}$$

Using equations (85) and (86), we can iteratively calculate τ^n from $n=1$ to whatever order we need. Here are a few examples:

$$\begin{aligned}\left(k_z\sqrt{k_z^{-2}+1}-k_z\right)&=\frac{1}{2}k_z^{-1}-\frac{1}{8}k_z^{-3}+\frac{1}{16}k_z^{-5}-\frac{5}{128}k_z^{-7}+\frac{7}{256}k_z^{-9}-\frac{21}{1024}k_z^{-11}\\&\quad+\frac{33}{2048}k_z^{-13}-\frac{429}{32768}k_z^{-15}+\frac{715}{65536}k_z^{-17}-\frac{2431}{262144}k_z^{-19}+\cdots,\\\left(k_z\sqrt{k_z^{-2}+1}-k_z\right)^2&=\frac{1}{4}k_z^{-2}-\frac{1}{8}k_z^{-4}+\frac{5}{64}k_z^{-6}-\frac{7}{128}k_z^{-8}+\frac{21}{512}k_z^{-10}-\frac{33}{1024}k_z^{-12}\\&\quad+\frac{429}{16384}k_z^{-14}-\frac{715}{32768}k_z^{-16}+\frac{2431}{131072}k_z^{-18}-\frac{4199}{262144}k_z^{-20}+\cdots,\\\left(k_z\sqrt{k_z^{-2}+1}-k_z\right)^3&=\frac{1}{8}k_z^{-3}-\frac{3}{32}k_z^{-5}+\frac{9}{128}k_z^{-7}-\frac{7}{128}k_z^{-9}+\frac{45}{1024}k_z^{-11}-\frac{297}{8192}k_z^{-13}\\&\quad+\frac{1001}{32768}k_z^{-15}-\frac{429}{16384}k_z^{-17}+\frac{5967}{262144}k_z^{-19}-\frac{20995}{1048576}k_z^{-21}+\cdots,\end{aligned}$$

$$\left(k_z\sqrt{k_z^{-2}+1}-k_z\right)^4 = \frac{1}{16}k_z^{-4} - \frac{1}{16}k_z^{-6} + \frac{7}{128}k_z^{-8} - \frac{3}{64}k_z^{-10} + \frac{165}{4096}k_z^{-12} - \frac{143}{4096}k_z^{-14} + \frac{1001}{32768}k_z^{-16} - \frac{221}{8192}k_z^{-18} + \frac{12597}{524288}k_z^{-20} - \frac{11305}{524288}k_z^{-22} + \cdots .$$

In summary, τ^n is of the form,

$$\left(k_z\sqrt{k_z^{-2}+1}-k_z\right)^n = \frac{1}{2^n k_z^n} - \frac{n}{2^{n+2}k_z^{n+2}} + \frac{n(n+3)}{2^{n+5}k_z^{n+4}} - \frac{n(n+4)(n+5)}{2^{n+7}k_z^{n+6}} + \cdots . \tag{87}$$

5.2 Expansion of $\mathbf{i}^\lambda(-\mathbf{i})^\mu k_z^\mu \left[\mathtt{sgn}(k_z)\sqrt{1+k_z^2}\right]^\lambda e^{\mathbf{i}\breve{z}_0\left(\mathtt{sgn}(k_z)\sqrt{1+k_z^2}-k_z\right)}$

After the expansion for τ^n $(n = 1, 2, \cdots)$ is obtained, we can plug it into equation (83) to derive an infinite expansion of the form[27],

$$\mathbf{A} = \sum_{n=0}^{\infty} a_n(\mathbf{i}k_z)^{\mu+\lambda-n} \qquad , \qquad (\textbf{where } |k_z| > 1), \tag{88}$$

where a_n $(n = 0, 1, 2, \cdots)$ are constants[28] independent of k_z and can be computed directly from expanding equation (83). Note that equation (88) is a one-sided expansion: (1) the highest power in the expansion is $(\mathbf{i}k_z)^{\mu+\lambda}$; (2) there is no lowest power. $\mathbf{A}$ is expanded this way so that the total number of positive powers of k_z is finite, therefore we can group them into a polynomial of k_z. This polynomial is called the tapering polynomial and is denoted as $\mathbf{P}^+(\breve{z}_0, k_z)$. The purpose of introducing the tapering polynomial is to make sure the integrand converges to zero as $k_z \to 0$, thus remaining Riemann integrable. The tapering polynomial can be calculated via collecting the non-negative powers of equation (88),

$$\mathbf{P}^+(\breve{z}_0, k_z) = \sum_{n=0}^{n\le\mu+\lambda} a_n(\mathbf{i}k_z)^{\mu+\lambda-n}. \tag{89}$$

Note that each term in equation (89) results in a Dirac δ-function (or its derivatives to a certain order).

[27] This expansion is convergent for any $\breve{z}_0$ and $\breve{z}$, although it may contains millions of terms for the range we are interested in, for example, when $\breve{z}_0$ and $\breve{z}$ reach several kilometers, typical for the seismic exploration.

[28] Due to clear physical meaning of $\mathbf{i}k_z$, $(\mathbf{i}k_z)^2$, $\cdots$, we preferred the powers of $\mathbf{i}k_z$ to k_z itself. There is no difficulty to achieve this since any difference can be assimilated into the constant a_n.

In summary, the Fourier transform of the tapering polynomial is very straightforward,

$$\begin{aligned}
\frac{1}{2\pi}\int_{-\infty}^{\infty}\mathbf{P}^{+}(\breve{z}_0,k_z)dk_z &= \frac{1}{2\pi}\int_{-\infty}^{\infty}\sum_{n=0}^{n\leq\mu+\lambda}a_n(\mathbf{i}k_z)^{\mu+\lambda-n}e^{\mathbf{i}k_z(\breve{z}_0-\breve{z})}dk_z \\
&= \sum_{n=0}^{n\leq\mu+\lambda}a_n\frac{1}{2\pi}\int_{-\infty}^{\infty}(\mathbf{i}k_z)^{\mu+\lambda-n}e^{\mathbf{i}k_z(\breve{z}_0-\breve{z})}dk_z \\
&= \sum_{n=0}^{n\leq\mu+\lambda}a_n\frac{\partial^{\mu+\lambda-n}}{\partial(\breve{z}_0-\breve{z})^{\mu+\lambda-n}}\left[\frac{1}{2\pi}\int_{-\infty}^{\infty}e^{\mathbf{i}k_z(\breve{z}_0-\breve{z})}dk_z\right] = \sum_{n=0}^{n\leq\mu+\lambda}a_n\delta^{(\mu+\lambda-n)}(\breve{z}_0-\breve{z}).
\end{aligned} \tag{90}$$

The remaining terms in equation (88) are grouped in an infinite asymptotic expansion denoted as $\mathbf{P}^{-}(\breve{z}_0,k_z)$,

$$\mathbf{P}^{-}(\breve{z}_0,k_z) = \sum_{n=\mu+\lambda+1}^{\infty}a_n(\mathbf{i}k_z)^{\mu+\lambda-n} \qquad (|k_z|\geq 1). \tag{91}$$

Since the tapering polynomial will produce clean and well-understood distributions like the Dirac δ-function (and/or its derivatives), and the application of the aforementioned δ-functions into the seismic imaging subseries will lead to fast algorithms like that of Shaw et al. (2003) or the terms which is "1D generalizable" or "with clean partial derivatives with respect to x" presented in Liu (2006); Liu and Weglein (2007). The introduction of computational overhead is negligible.

5.3 Well-defined discontinuities

After subtracting the tapering polynomial, our original Fourier transform in equation (76) become,

$$\mathbf{F}_{\lambda,\mu}(\breve{z}_0,\breve{z}) = \sum_{n=0}^{n\leq\mu+\lambda}a_n\delta^{(\mu+\lambda-n)}(\breve{z}_0-\breve{z}) + \mathbf{F}^{\mathbf{Reg}}_{\lambda,\mu}(\breve{z}_0,\breve{z}), \tag{92}$$

where in the right-hand-side of the equation (92), the first part is the linear combination of $\delta(\breve{z}_0-\breve{z})$, $\delta'(\breve{z}_0-\breve{z})$, $\delta''(\breve{z}_0-\breve{z})$, $\cdots$, the second part is a Riemann integral which is finite at every depth, denoted as[29] $\mathbf{F}^{\mathbf{Reg}}_{\lambda,\mu}(\breve{z}_0,\breve{z})$, which can be calculated via,

$$\mathbf{F}^{\mathbf{Reg}}_{\lambda,\mu}(\breve{z}_0,\breve{z}) = \frac{1}{2\pi}\int_{-\infty}^{\infty}\left\{\begin{array}{l}\mathbf{i}^{\lambda}(-\mathbf{i})^{\mu}k_z^{\mu}\left[\mathtt{sgn}(k_z)\sqrt{1+k_z^2}\right]^{\lambda}e^{\mathbf{i}(\breve{z}_0\mathtt{sgn}(k_z)\sqrt{1+k_z^2}-\breve{z}k_z)} \\ -\mathbf{P}^{+}(\breve{z}_0,k_z)e^{\mathbf{i}(\breve{z}_0-\breve{z})k_z}\end{array}\right\}dk_z. \tag{93}$$

Although the $\mathbf{F}^{\mathbf{Reg}}_{\lambda,\mu}(\breve{z}_0,\breve{z})$ is finite, it is also discontinuous when $\breve{z}_0=\breve{z}$, where the δ-function clicks.

Since we have covered the δ-function singularities produced by $(\mathbf{i}k_z)^0$, $(\mathbf{i}k_z)^1$, $(\mathbf{i}k_z)^2$, $\cdots$, it is natural to look at the highest power among the remaining expansion: $(\mathbf{i}k_z)^{-1}$. Indeed this term produces

[29] Due to the fact that is the regularized version of the original integral. It is denoted with a superscript $^{\mathbf{Reg}}$.

discontinuities. The proof is as follows, for an arbitrarily chosen $\boldsymbol{\Xi} \geq 1$, the integral below,

$$\int\limits_{|k_z|\geq\boldsymbol{\Xi}} \frac{e^{\mathbf{i}(\breve{z}_0-\breve{z})k_z}}{\mathbf{i}k_z}dk_z = 2\int\limits_{\boldsymbol{\Xi}}^{\infty} \frac{\sin\left[(\breve{z}_0-\breve{z})k_z\right]}{k_z}dk_z$$

is an odd function of $(\breve{z}_0-\breve{z})$. We only need to study its behavior for positive $(\breve{z}_0-\breve{z})$ to understand its properties everywhere. If we assume $\breve{z}_0-\breve{z}>0$, and change the integration variable to $y\overset{\triangle}{=}k_z*(\breve{z}_0-\breve{z})$, the expression above reduces to the sine integral defined in equation (5.2.1) of Abramowitz and Stegun (1965),

$$\begin{aligned}&\int\limits_{\boldsymbol{\Xi}}^{\infty} \frac{\sin\left[(\breve{z}_0-\breve{z})k_z\right]}{k_z}dk_z = 2\int\limits_{(\breve{z}_0-\breve{z})\boldsymbol{\Xi}}^{\infty} \frac{\sin[y]}{y}dy\\ =&2\left(\frac{\pi}{2}-\int\limits_{0}^{(\breve{z}_0-\breve{z})\boldsymbol{\Xi}}\frac{\sin[y]}{y}dy\right) = 2*\left(\frac{\pi}{2}-\mathtt{Si}([\breve{z}_0-\breve{z}]\boldsymbol{\Xi})\right).\end{aligned}$$

Obviously, according to Figure (5.6) from Abramowitz and Stegun (1965), we have,

$$\lim_{(\breve{z}_0-\breve{z})\to 0^+}\mathtt{Si}([\breve{z}_0-\breve{z}]\boldsymbol{\Xi}) = 0 \qquad (\texttt{For any finite } \boldsymbol{\Xi}).$$

Consequently,

$$\lim_{(\breve{z}_0-\breve{z})\to 0^+}\int\limits_{\boldsymbol{\Xi}}^{\infty} \frac{\sin\left[(\breve{z}_0-\breve{z})k_z\right]}{k_z}dk_z = 2*\left(\frac{\pi}{2}-0\right) = \pi \qquad (\texttt{For any finite } \boldsymbol{\Xi}).$$

The function converges to π from the right $(\breve{z}_0-\breve{z}=0^+)$. Since the function above is an odd function of $(\breve{z}_0-\breve{z})$, it will converge to $-\pi$ from the left $(\breve{z}_0-\breve{z}=0^-)$,

$$\lim_{(\breve{z}_0-\breve{z})\to 0^-}\int\limits_{\boldsymbol{\Xi}}^{\infty} \frac{\sin\left[(\breve{z}_0-\breve{z})k_z\right]}{k_z}dk_z = -2*\left(\frac{\pi}{2}-0\right) = -\pi \qquad (\texttt{For any finite } \boldsymbol{\Xi}).$$

Since this expansion converges to different limits from the left and right. It is discontinuous when $\breve{z}_0-\breve{z}=0$. This is the only discontinuity in the entire expansion[30]. Note that if we change the value of $\boldsymbol{\Xi}$, the size of the discontinuity will not change since it is not a function of $\boldsymbol{\Xi}$. This independency with $\boldsymbol{\Xi}$ is reasonable since $\boldsymbol{\Xi}$ is only artificially chosen and shouldn't affect the size of the discontinuities. In summary, the discontinuity at $\breve{z}_0=\breve{z}$ is,

$$\lim_{\breve{z}_0=\breve{z}+0^+}\mathbf{F}^{\mathbf{Reg}}_{\lambda,\mu}(\breve{z}_0,\breve{z}) - \lim_{\breve{z}_0=\breve{z}+0^-}\mathbf{F}^{\mathbf{Reg}}_{\lambda,\mu}(\breve{z}_0,\breve{z}) = a_{\lambda+\mu+1}\frac{\pi-(-\pi)}{2\pi} = a_{\lambda+\mu+1} \tag{94}$$

[30]First of all, the integral in the finite range $\int\limits_{-\boldsymbol{\Xi}}^{\boldsymbol{\Xi}} dk_z$ will be continuous. And secondly, the $\int\limits_{|k_z|\geq\boldsymbol{\Xi}} dk_z$ integral for $(\mathbf{i}k_z)^{-2}$, $(\mathbf{i}k_z)^{-3}$, $\cdots$ are all well-defined exponential integrals and will all be continuous.

5.4 Interpolated integration of the Fourier integral $\int\limits_{|k_z|\le\Xi} dk_z$

After choosing a constant $\Xi > 1$, we calculate the $\mathbf{F}^{\mathbf{Reg}}_{\lambda,\mu}$ integral in equation (93) with two steps. First calculate the $(-\Xi, \Xi)$ portion of integral,

$$\mathbf{F}^{\mathbf{Reg}}_{\lambda,\mu}(\breve{z}_0, \breve{z}) = \frac{1}{2\pi} \int\limits_{|k_z|<\Xi} \left\{ \begin{array}{l} \mathbf{i}^\lambda (-\mathbf{i})^\mu k_z^\mu \left[\mathtt{sgn}(k_z)\sqrt{1+k_z^2}\right]^\lambda e^{\mathbf{i}(\breve{z}_0 \mathtt{sgn}(k_z)\sqrt{1+k_z^2} - \breve{z}k_z)} \\ -\mathbf{P}^+(\breve{z}_0, k_z) e^{\mathbf{i}(\breve{z}_0 - \breve{z})k_z} \end{array} \right\} dk_z, \tag{95}$$

with the interpolated integration method documented in §3 and §4 since it is essentially a Fourier transform from k_z to $\breve{z}$. The computational overhead caused by the presence of $\mathbf{P}^+(\breve{z}_0, k_z)$ is of n^0 (or constant) complexity since it can be analytically evaluated. Currently in our efforts to calculate $\widetilde{\gamma}_1$ and its partial derivatives to the $7^{\mathtt{th}}$ (totally 64 of them) and to the depth of 3 kilometers, the interpolation order $\bar{\wp} = 15$ is sufficient.

The next step is documented in the next subsection.

5.5 Asymptotic expansion of the Fourier integral $\int\limits_{\Xi}^{\infty} dk_z$

In order to calculate the $\int\limits_{\Xi}^{\infty} dk_z$ integral, we need only to consider the k_z-values that satisfy $|k_z| \ge \Xi$, and within this range, according to the definition of $\mathbf{P}^-(\breve{z}_0,k_z)$, the integrand in equation (76) can be expressed by the asymptotic expansion of equation (91),

$$\mathbf{i}^\lambda (-\mathbf{i})^\mu k_z^\mu \left[\mathtt{sgn}(k_z)\sqrt{1+k_z^2}\right]^\lambda e^{\mathbf{i}(\breve{z}_0 \mathtt{sgn}(k_z)\sqrt{1+k_z^2} - \breve{z}k_z)} - \mathbf{P}^+(\breve{z}_0, k_z) = \mathbf{P}^-(\breve{z}_0,k_z) e^{\mathbf{i}(\breve{z}_0 - \breve{z})k_z}. \tag{96}$$

Consequently, its integral can be calculated via,

$$\begin{aligned} &\frac{1}{2\pi} \int\limits_{|k_z|\ge\Xi} \mathbf{i}^\lambda (-\mathbf{i})^\mu k_z^\mu \left[\mathtt{sgn}(k_z)\sqrt{1+k_z^2}\right]^\lambda e^{\mathbf{i}(\breve{z}_0 \mathtt{sgn}(k_z)\sqrt{1+k_z^2} - \breve{z}k_z)} - \mathbf{P}^+(\breve{z}_0, k_z) dk_z \\ &= \frac{1}{2\pi} \int\limits_{|k_z|\ge\Xi} \mathbf{P}^-(\breve{z}_0,k_z) e^{\mathbf{i}(\breve{z}_0 - \breve{z})k_z} = \frac{1}{2\pi} \sum_{n=\mu+\lambda+1}^{\infty} a_n \int\limits_{|k_z|\ge\Xi} (\mathbf{i}k_z)^{\mu+\lambda-n} e^{\mathbf{i}(\breve{z}_0 - \breve{z})k_z} dk_z. \end{aligned} \tag{97}$$

Each integral in equation (97) can be calculated via the well-known exponential integral. Exponential integrals, e.g., equation (5.1.4) from Abramowitz and Stegun (1965), when their arguments are chosen as $\mathbf{i}(\breve{z}_0 - \breve{z})$, are of the form,

$$\mathtt{E_n}(\mathbf{i}(\breve{z}_0 - \breve{z})) = \int\limits_1^{\infty} \frac{\cos[(\breve{z}_0 - \breve{z})k_z] - \mathbf{i}\sin[(\breve{z}_0 - \breve{z})k_z]}{k_z^n} dk_z. \tag{98}$$

For $|\breve{z}_0 - \breve{z}| \le 2$, the analytic integration can be quickly implemented with a power series, e.g., equation (5.1.12) in Abramowitz and Stegun (1965). Otherwise, it can be quickly implemented with a continued fraction, e.g., equation (5.1.22) in Abramowitz and Stegun (1965).

5.6 Quality control of the seismic imaging operator

1. Values in $\breve{z}_0 = 0$.

   When $\breve{z}_0 = 0$, the square-root complexities in equation (76) vanish and the normally very complicated integral can be found in cosine and sine transforms from Arthur Erdélyi and Bateman (1954). This is the first quality control procedure.

2. Tunnel digging test.

   When we dig a long tunnel through a mountain, it will be much faster if two teams work simultaneously from opposite sides of the mountain. In the end, two teams must reach the same location. We use this idea as a quality control procedure, i.e., our integral is calculated in two parts: $\int\limits_{|k_z|\geq \Xi}$ and $\int\limits_{|k_z|<\Xi}$, where Ξ is an artificial dividing line. Obviously, the final results should agree with each other. So far, the error for this quality control check is within 10^{-20}.

3. Verification of the derivatives from interpolation.

   Our procedure can be used to calculate $\mathbf{F}_{\lambda,\mu}$ and its various derivatives. One quality control procedure is to verify that the derivatives do agree with the actual variation of $\mathbf{F}_{\lambda,\mu}$ with small amount of variation, both in terms of $\breve{z}_0$ and $\breve{z}$.

5.7 Properties of the seismic imaging operator and its impact on the structure of our imaging algorithm

1. Well defined discontinuity.

   As demonstrated in §5.3, the function $\mathbf{F}_{\lambda,\mu}$ is discontinuous. This discontinuity always happens at $\breve{z}_0 = \breve{z}$ where the Dirac δ function clicks. And it can be derived by simply collecting the highest power $(\mathbf{i}k_z)^{-1}$; its final result is listed in equation (94).

2. Flat ocean half, violent mountain half, easily predicted beachhead and mountaintop.

   The distribution $\mathbf{F}_{\lambda,\mu}$ behaves very different in the region where $\breve{z}_0 < \breve{z}$ and the region $\breve{z}_0 > \breve{z}$. We call the first region "ocean half" because with the increase of $\breve{z}_0$ and $\breve{z}$, our distribution becomes more flat and smooth and much closer to zero. We call the second region the "mountain half" because the distribution shows more and more violent oscillations with increase in $\breve{z}_0$ and $\breve{z}$. For a fixed $\breve{z}_0$, the most violent variation always occurs at the limit $\breve{z} = \breve{z}_0$. We define the "beachhead" and "mountaintop" in the $(\breve{z}_0, \breve{z})$ plane as the lines that satisfy $\breve{z}_0 = \breve{z} + 0^-$, and $\breve{z}_0 = \breve{z} + 0^+$, respectively because of the fact that the beachhead is as flat and smooth as the ocean half. For large $\breve{z}_0$, we can safely predict the value at this location as 0 (to be exact, the prediction error will decrease dramatically with the increase of $\breve{z}_0$). Consequently, we can predict the mountaintop using the well-defined discontinuity in equation (94).

3. Mountaintop expansion and possible closed forms.

Although $\mathbf{F}_{\lambda,\mu}$ and $\mathbf{F}^{\mathbf{Reg}}_{\lambda,\mu}$ are highly transcendental functions with daunting complexities far beyond the functions well studied in the literature, their behavior at the diagonal region $\breve{z}_0 = \breve{z}$ is highly predictable, and the bigger the $\breve{z}_0$, the better the predictability.

A Taylor expansion of a 2D function gives,

$$f(u,v) = f(u_0,v_0) + \sum_{n=1}^{\infty} \frac{1}{n!} \left[\left(\frac{\partial}{\partial u}\Delta u + \frac{\partial}{\partial v}\Delta v \right)^n f(u,v) \right]_{u=u_0, v=v_0}. \tag{99}$$

In our case, for an arbitrary location $(\breve{z}_0, \breve{z})$, the closest location with good approximation[31] of f (and its derivatives) happens at the beachhead location (r,r) where $r = \frac{z'+z}{2}$. Using equation (99) with u replaced by $\breve{z}_0$ and v replaced by $\breve{z}$, we have the closest point to start the expansion: $u_0 = v_0 = r = \frac{\breve{z}_0+\breve{z}}{2}$, $\Delta u = \Delta v = \frac{1}{\sqrt{2}}\frac{\breve{z}_0-\breve{z}}{2} = \frac{a}{\sqrt{2}}$, where $a = \frac{\breve{z}_0-\breve{z}}{2}$. We have the mountaintop expansion:

$$\begin{aligned}
\mathbf{F}^{\mathbf{Reg}}_{\mathbf{-2,2}}(\breve{z}_0,\breve{z}) = &-\frac{1}{2}(r) + \frac{1}{2\sqrt{2}}\left(3+\frac{1}{2}r^2\right)a - \frac{1}{4}\left(\frac{3}{2}r+\frac{1}{12}r^3\right)a^2 + \frac{1}{4\sqrt{2}}\left(\frac{2}{3}+\frac{1}{4}r^2+\frac{1}{144}r^4\right)a^3 \\
&- \frac{1}{8}\left(\frac{1}{6}r+\frac{1}{48}r^3+\frac{1}{2880}r^5\right)a^4 + \frac{1}{8\sqrt{2}}\left(\frac{1}{30}+\frac{1}{60}r^2+\frac{1}{960}r^4+\frac{1}{86400}r^6\right)a^5 \\
&- \frac{1}{16}\left(\frac{1}{180}r+\frac{1}{1080}r^3+\frac{1}{28800}r^5+\frac{1}{3628800}r^7\right)a^6 + \cdots
\end{aligned} \tag{100}$$

$$\begin{aligned}
&\cdots + \frac{1}{16\sqrt{2}}\left(\frac{1}{1260}+\frac{r^2}{2520}+\frac{r^4}{30240}+\frac{r^6}{1209600}+\frac{r^8}{203212800}\right)a^7 \\
&- \frac{1}{32}\left(\frac{r}{10080}+\frac{r^3}{60480}+\frac{r^5}{1209600}+\frac{r^7}{67737600}+\frac{r^9}{14631321600}\right)a^8 \\
&+ \frac{1}{32\sqrt{2}}\left(\frac{1}{90720}+\frac{r^2}{181440}+\frac{r^4}{2177280}+\frac{r^6}{65318400}+\frac{r^8}{4877107200}+\frac{r^{10}}{1316818944000}\right)a^9 \\
&- \frac{1}{64}\left(\frac{r}{907200}+\frac{r^3}{5443200}+\frac{r^5}{108864000}+\frac{r^7}{4572288000}+\frac{r^9}{438939648000}+\frac{r^{11}}{144850083840000}\right)a^{10} \\
&+ \cdots
\end{aligned} \tag{101}$$

This is a polynomial approximation for the most critical region in the imaging operator, where the δ-function clicks and the rapidest variation occurs.

First let's look at the highest-order term (in terms of r) in each expansion the ratio between the coefficients of consecutive terms are $2{=}1\times 2$, $6{=}2\times 3$, $12{=}3\times 4$, $20{=}4\times 5$, $30{=}5\times 6$, $42{=}6\times 7$, $56{=}7\times 8$, $72{=}8\times 9$, $90{=}9\times 10$, $110{=}10\times 11$, $\cdots$.

Collecting the highest power in each term, we can guess the following closed-form,

$$-\frac{1}{2}r\sum_{n=0}^{\infty}\frac{(-ra/\sqrt{2})^n}{(n!)^2\,(n+1)}. \tag{102}$$

It is obvious that the second highest term in each expansion follows the same ratio rule. And we can similarly guess the closed-form for the second highest term,

$$\frac{3}{2\sqrt{2}}a\sum_{n=0}^{\infty}\frac{(-ra/\sqrt{2})^n}{(n!)^2\,(n+1)}. \tag{103}$$

[31] The approximation is reached by three steps: (1) approximate the beachhead value of $f(r,r)$ as zero; (2) calculate the discontinuity by equation (94); (3) add the discontinuity to the beachhead value to get the value of mountaintop.

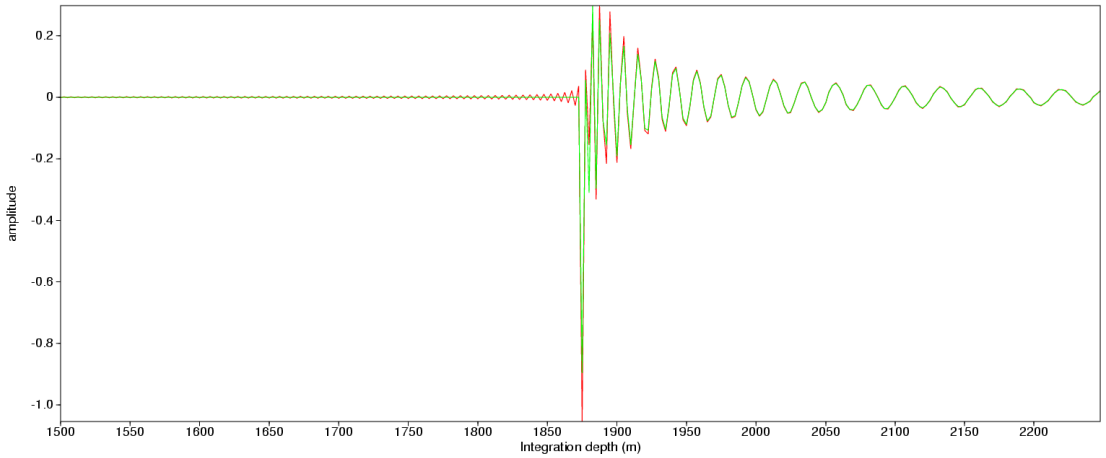

Figure 1: The accurate (in green) and approximate (in red) seismic imaging operator $\widetilde{\gamma}_1$ when the horizontal wavenumber ($k_m = 0.1104$ and the target depth $z = 1875.0m$), the horizontal axis is the integration depth z'.

6 Numerical examples

We had tested the accurate seismic imging operator $\widetilde{\gamma}_1$ against our previously straightforward implementation, which can be regarded as using an approximate seismic imaging operator calculated by a truncated discrete Fourier transform over k_z. The corresponding seismic imaging operators are illustrated in Figure (1), and their difference is shown in Figure (2). From Figure (1), it is obvious that the accurate operator is flat and smooth when $z' < z = 1875.0m$ and discontinuous at $z' = z = 1875.0m$. The approximate operator shows typical Gibbs oscillation at the discontinuity. It is obvious that the accurate seismic imging operators, although has a much more frequency (k_z) content, are much simplier than and smoother than their approximation by a truncated Fourier integral. As an example, we test our accurate seismic imaging operator on a 2D salt model in Figure (3). For this model, we use a homogeneous migration velocity $c_0 = 1500m/s$. Two typical shot gathers with $x_s = \pm 2000m$ are shown in Figure (4). In Figure (5) is the α_1 we previously calculated in the (k_m, k_z) domain with an upper limit for both k_m and k_z values, which is equivalent to using the aforementioned approximate seismic imaging operator. After obtaining the accurate seismic imaging operator $\widetilde{\gamma}_1$ we obtained an improved α_1 image in Figure (7).

After the calculation it is nature to apply equation (2.34) of Liu (2006) to calculate the higher-order imaging subseries (HOIS). The corresponding HOIS results, obtained from approximate $\widetilde{\gamma}_1$ operator and accurate $\widetilde{\gamma}_1$ are shown in Figure (9) and Figure (10), respectively.

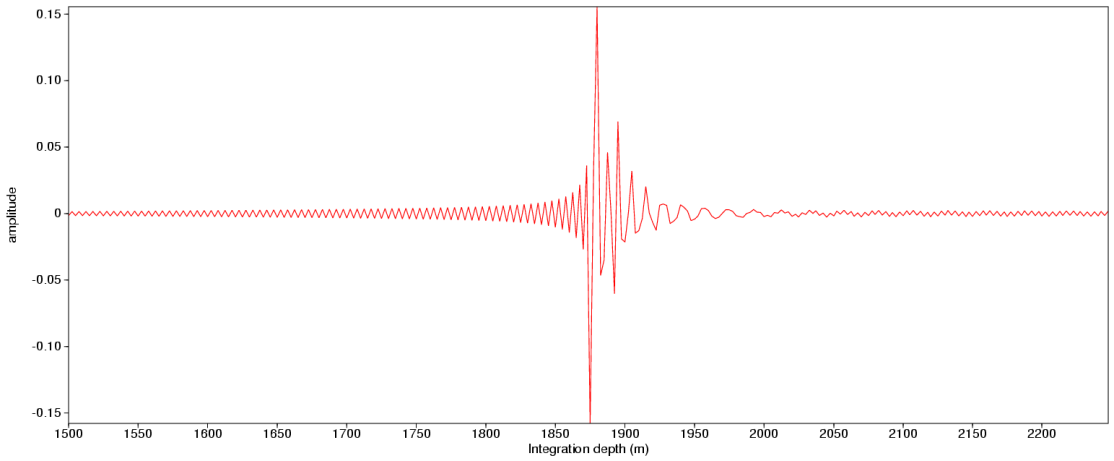

Figure 2: The difference between the accurate and approximate seismic imaging operator when the horizontal wavenumber $k_m = 0.1104$ and the target depth $z = 1875.0m$, the horizontal axis is the integration depth z'

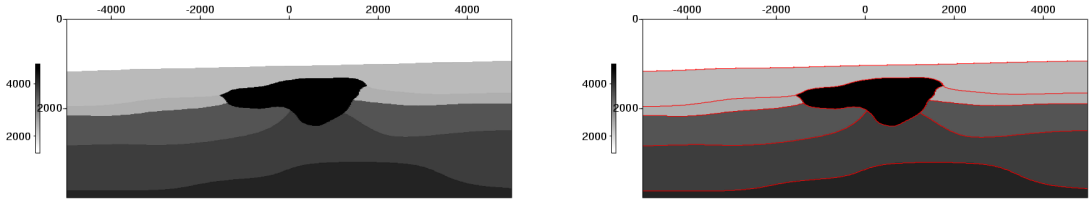

Figure 3: Left: the salt model. Right: salt model with geological boubdaries (red lines). As a benchmark, the geological boundaries will be used in Figure (6), (8), (11), and (12) to demonstrate the effectiveness of the imaging algorithm.

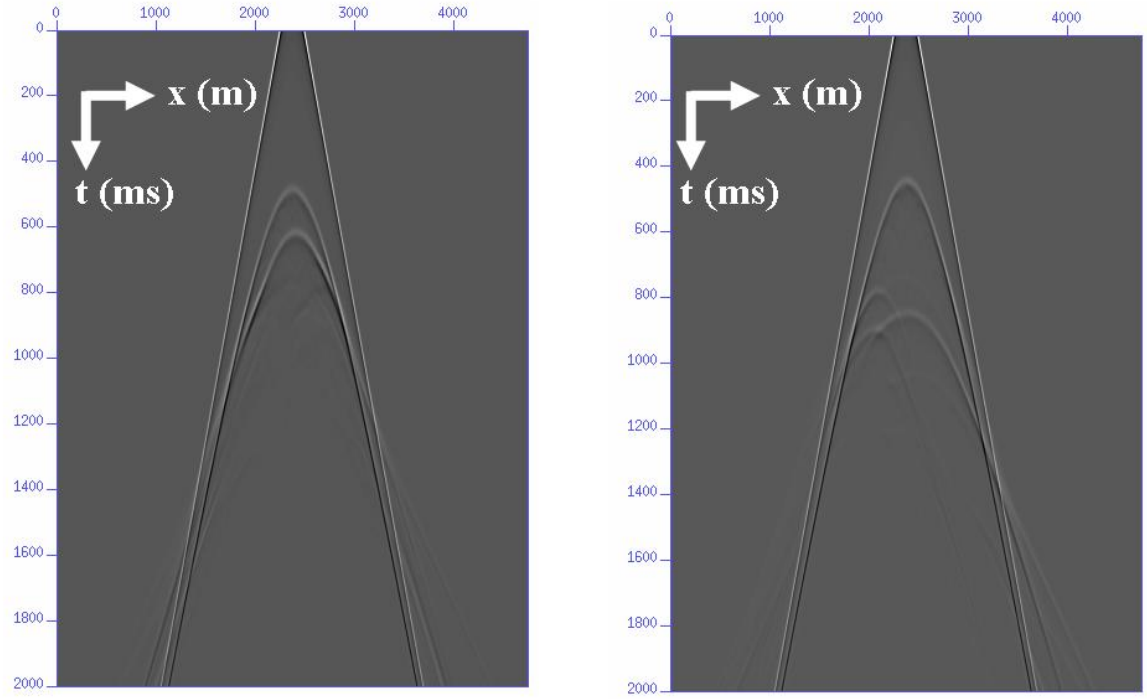

Figure 4: Left: shot gather with $x_s = -2000(m)$. Right: shot gather with $x_s = 2000(m)$. In both shot gathers, conflicting hyperbolas are present which will cause ambiguities in velocity analysis.

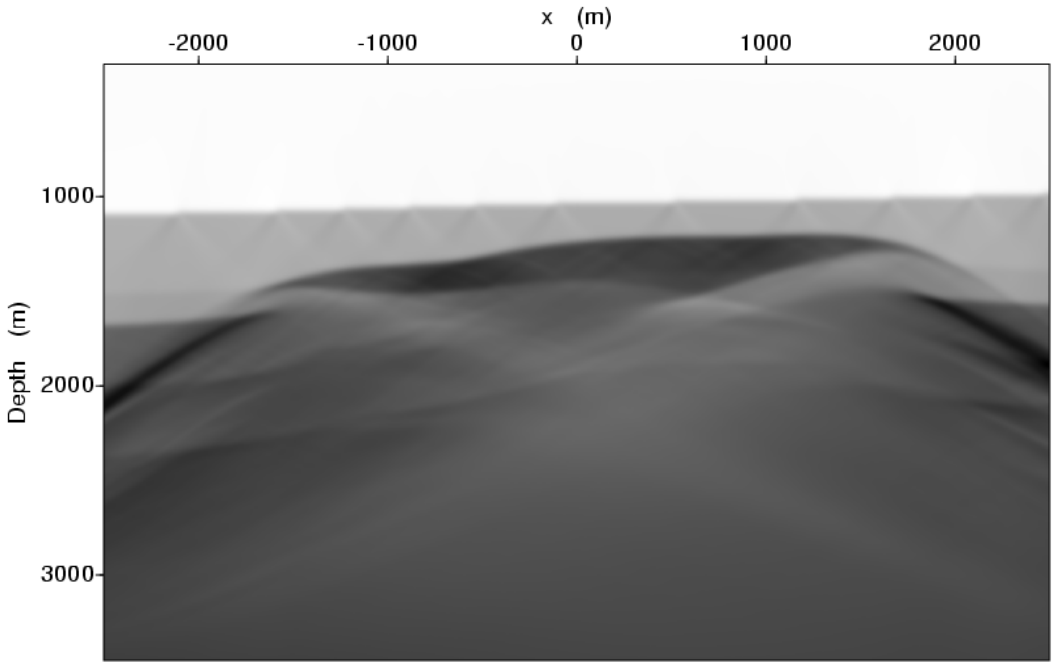

Figure 5: α_1 obtained from approximate seismic imaging operator $\widetilde{\gamma}_1$.

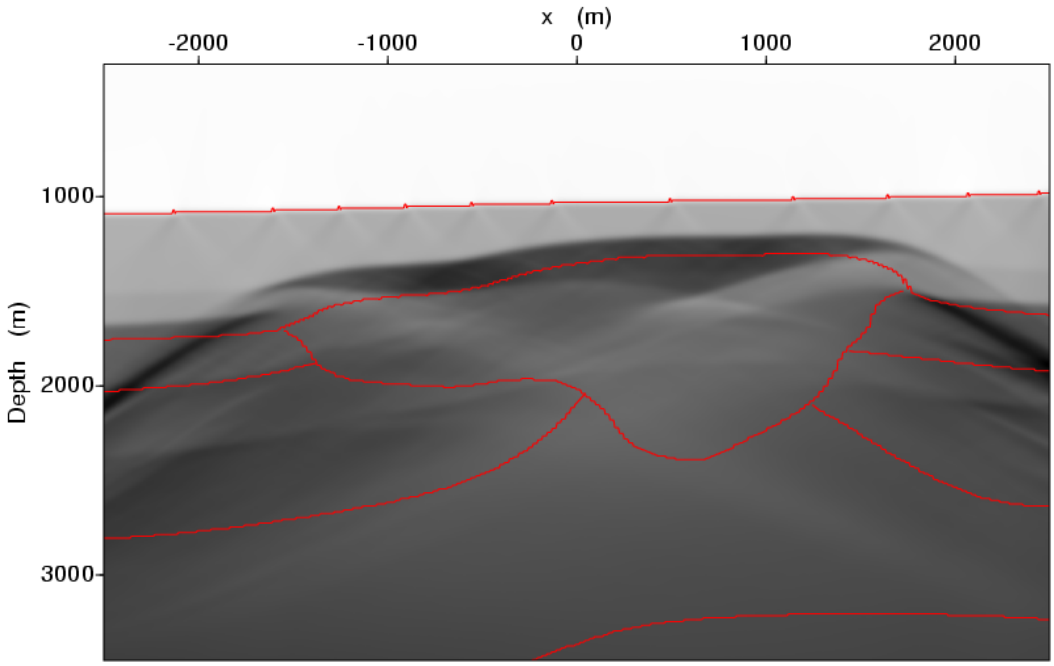

Figure 6: α_1 obtained from approximate $\widetilde{\gamma}_1$ operator with benchmark geological boundaries (in red).

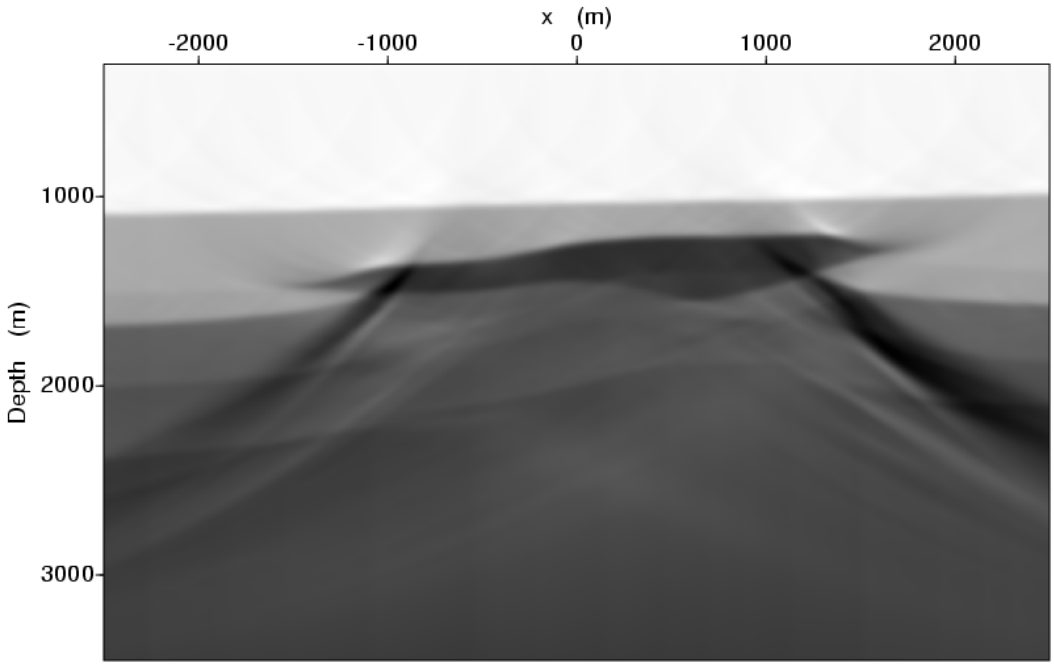

Figure 7: α_1 obtained with accurate seismic imaging operator $\widetilde{\gamma}_1$.

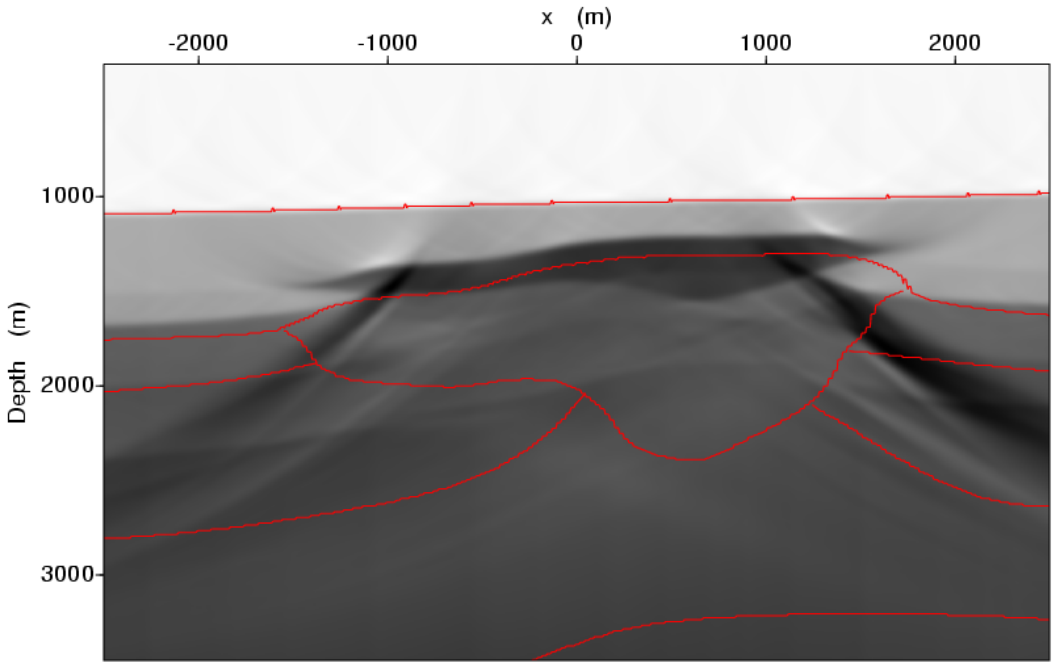

Figure 8: α_1 obtained from accurate $\widetilde{\gamma}_1$ operator with benchmark geological boundaries (in red).

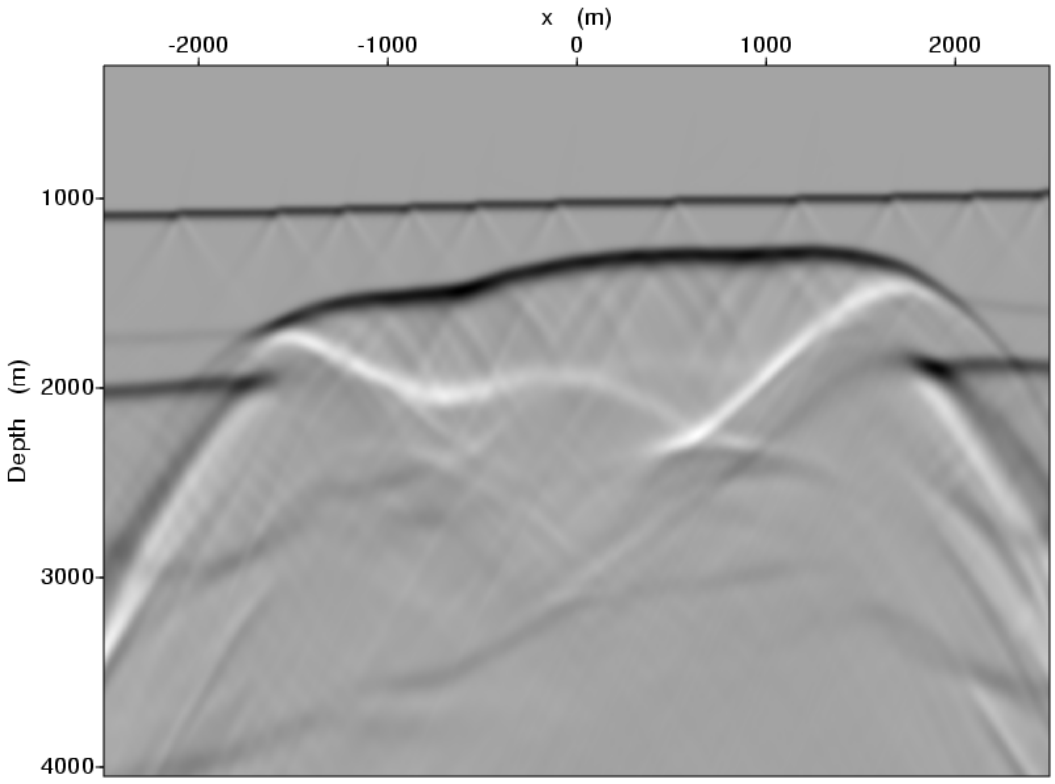

Figure 9: The higher-order imaging result obtained from approximate $\widetilde{\gamma}_1$ operator, the $\frac{\partial}{\partial z}$ operation was taken to emphasize the geological boundary.

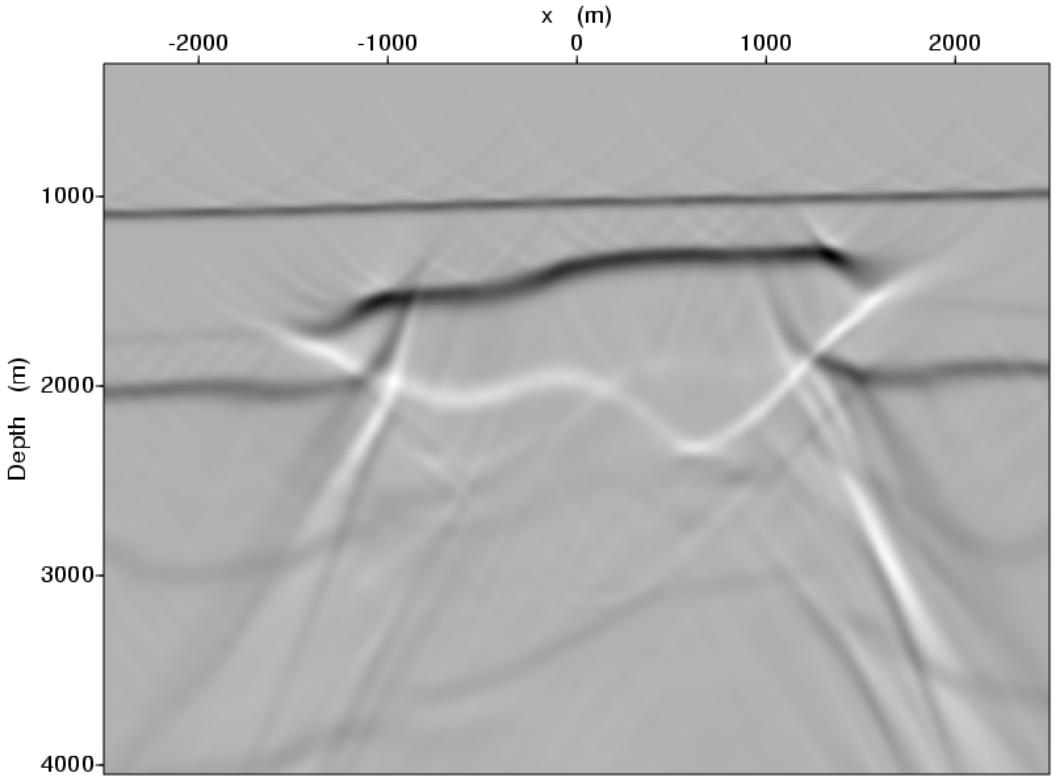

Figure 10: The higher-order imaging result obtained from accurate $\widetilde{\gamma}_1$ operator, the $\frac{\partial}{\partial z}$ operation was taken to emphasize the geological boundary.

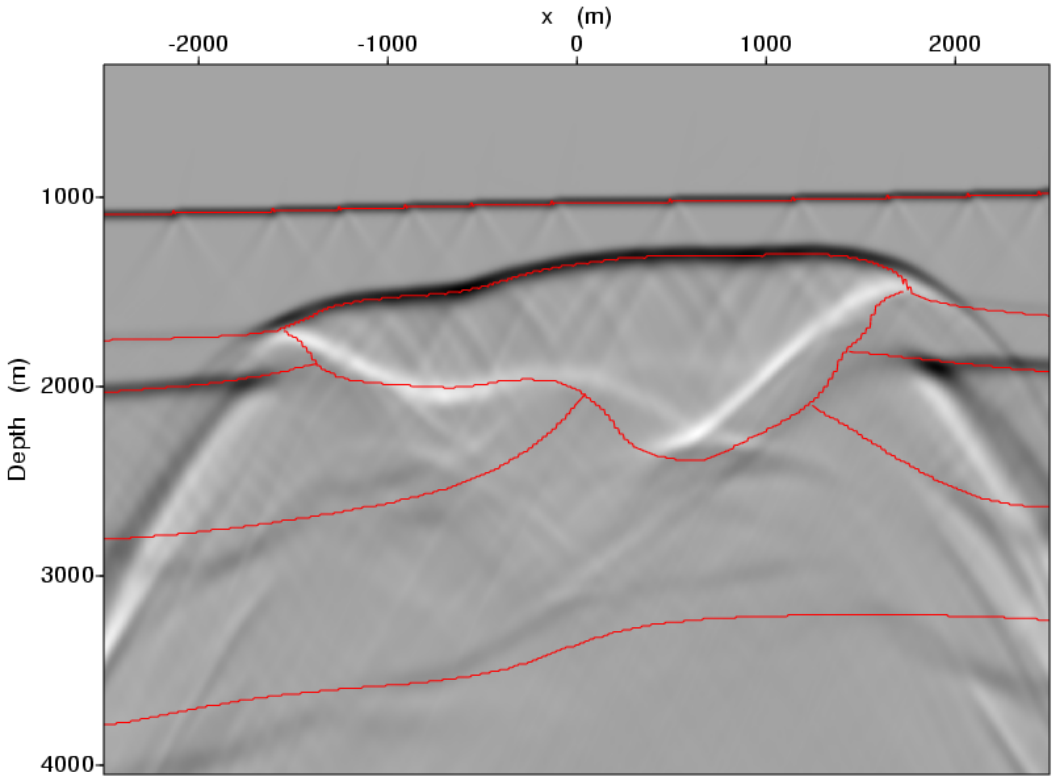

Figure 11: The image in Figure (9) overlayed with benchmark geological boundaries (in red).

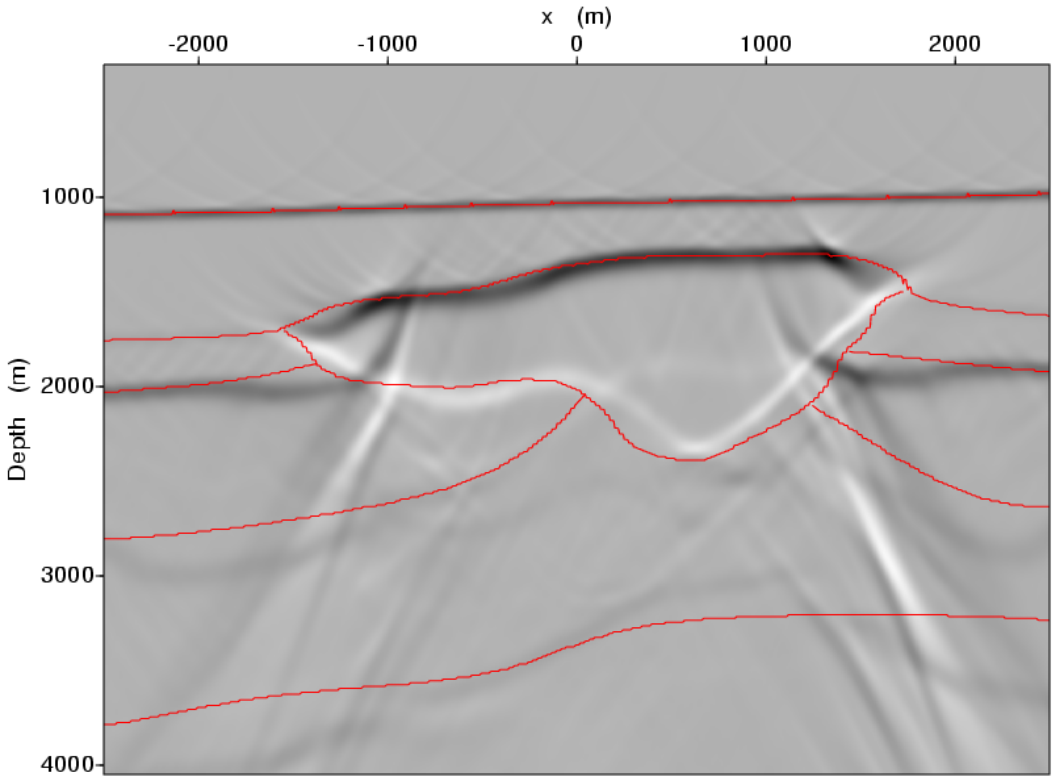

Figure 12: The image in Figure (10) overlayed with benchmark geological boundaries (in red).

7 Conclusions and discussions

Accurate application of the seismic imaging operators for a laterally varying earth has been studied and developed for α_1 and α_2. The seismic imaging operators obtained through full bandwidth integration has been domonstrated to be much simpler and smoother than its band-limited approximation. Polynomial approximations have been identified in the most critical region of the seismic imaging operators, which will help the future effort to obtain more economical closed-form solutions. Encouraging numerical examples with α_1 demonstrated the benefits of the accurate application of seismic imaging operators in better deal with phenomena associated with rapid lateral variations, for example, diffractions.

Acknowledgements

The authors would like to thank all M-OSRP members and sponsors. This work has been partially funded by NSFCMG award DMS-0327778 and DOE Basic Energy Sciences award DE-FG02-05ER15697.

References

Abramowitz, Milton and Irene A. Stegun. *Handbook of Mathematical Functions*. New York: Dover, 1965.

Arfken, George B. and Hans J. Weber. *Mathematical Methods for Physicists*. 5th edition. New York: Harcourt Academic Press, 1985.

Arthur Erdélyi, editor and Harry Bateman. *Tables of integral transforms*. Volume 1 . New York: McGraw-Hill, 1954.

Clayton, R. W. and R. H. Stolt. "A Born-WKBJ inversion method for acoustic reflection data." *Geophysics* 46 (1981): 1559–1567.

Gradshteyn, I. S. and I. M. Ryzhik. *Tables of Integrals, Series, and Products*. 5th edition. San Diego: Academic Press, 1994.

Innanen, Kristopher. A. *Methods for the treatment of acoustic and absorptive/dispersive wave field measurements*. PhD thesis, University of British Columbia, 2003.

Liu, Fang. *Multi-dimensional depth imaging without an adequate velocity model*. PhD thesis, University of Houston, 2006.

Liu, Fang and Arthur B. Weglein. "Inverse scattering series with lateral variations in 3D." *M-OSRP Annual Report* 6 (2007).

Morse, Philip M. and Herman Feshbach. *Methods of theoretical physics*. McGraw-Hill Book Co., 1953.

Press, William, Saul Teukolsky, William Vetterling, and Brian Flannery. *Numerical Recipes in C*. 2nd edition. Cambridge, UK: Cambridge University Press, 1992.

Shaw, S. A., A. B. Weglein, D. J. Foster, K. H. Matson, and R. G. Keys. "Isolation of a leading order depth imaging series and analysis of its convergence properties." *M-OSRP Annual Report* 2 (2003): 157–195.

Shaw, Simon. A. *An inverse scattering series algorithm for depth imaging of reflection data fro m a layered acoustic medium with an unknown velocity model*. PhD thesis, University of Houston, 2005.

Weglein, A. B., F. V. Araújo, P. M. Carvalho, R. H. Stolt, K. H. Matson, R. T. Coates, D. Corrigan, D. J. Foster, S. A. Shaw, and H. Zhang. "Inverse scattering series and seismic exploration." *Inverse Problems* 19 (2003): R27–R83.

Weglein, A. B., D. J. Foster, K. H. Matson, S. A. Shaw, P. M. Carvalho, and D. Corr igan. "Predicting the correct spatial location of reflectors without knowing or determining the precise medium and wave velocity: initial concept, algorithm and analytic and numerical e xample." *Journal of Seismic Exploration* 10 (2002): 367–382.

Weglein, A. B., K. H. Matson, D. J. Foster, P. M. Carvalho, D. Corrigan, and S. A. Shaw. "Imaging and inversion at depth without a velocity model: Theory, concepts a nd initial evaluation." *70th Annual Internat. Mtg., Soc. Expl. Geophys., Expanded Abstracts*. . Soc. Expl. Geophys., 2000. 1016–1019.

Direct non-linear Q compensation of primaries reflecting from a stratified, 2-parameter absorptive medium

K. A. Innanen and J. E. Lira, M-OSRP, University of Houston

Abstract

Q compensation of primaries that have reflected from a stratified, absorptive-dispersive medium may be cast as a direct, non-linear inverse scattering problem. If the reference medium is chosen to be non-attenuating and homogeneous, a candidate Q compensation procedure of this type may be derived which is highly non-linear in the data, but which operates in the absence of prior knowledge of the properties of the subsurface, including its Q structure. It is arrived at by, first, performing an order-by-order inversion of a chosen subset of the Born series, second, isolating and extracting a component of the resulting non-linear inversion equations here argued to enact Q compensation, and third, trivially mapping the result back to data space. Once derived, the procedure can be understood in terms of the non-linear interaction of the input primary reflection data: the attenuation of deeper primaries is corrected by an operator built (automatically) using the angle- and frequency-variations of all shallower absorptive-dispersive primaries. A simple synthetic example demonstrates the viability of the procedure in the presence of densely sampled, broad-band reflection data.

1 Introduction

In this paper we continue to progress and examine candidate algorithms for direct non-linear Q compensation of primaries propagating through, and reflecting from, unknown absorptive structures. The following paper in this volume (Lira et al.) includes an analytic example of an earlier form of the Q compensation algorithm; the current paper focuses on the theoretical development and numerical examples.

We begin with a particular definition of the problem. This is a necessary step, since the state-of-the-art and precise goals of deterministic Q compensation are difficult to neatly pin down; recovery from the resolution-compromising effects of absorption is cast within many otherwise distinct procedures, such as full waveform inversion (e.g., Dahl and Ursin, 1992; Ribodetti and Virieux, 1998; Causse et al., 1999; Hicks and Pratt, 2001; Dasios et al., 2004), downward continuation/imaging (e.g., Mittet et al., 1995; Song and Innanen, 2002; Wang, 2003; Mittet, 2007), and deterministic deconvolution (e.g., Bickel and Natarajan, 1985; Hargreaves and Calvert, 1991; Wang, 2006; Zhang and Ulrych, 2007). We define Q compensation as: *the estimation of the primary reflection data set that would have been measured in the absence of the absorptive component of wave propagation*; i.e., we will pose it such that it is maximally isolated from the other tasks of seismic inversion, as recommended by Hargreaves and Calvert (1991).

Building on earlier studies (Innanen and Weglein, 2003, 2005; Innanen and Lira, 2008), we seek such an algorithm by making use of inverse scattering, a framework with a history of providing

procedures that trade non-linearity for accurate input medium property information, for processing both multiples (as mentioned above) and primaries (Weglein et al., 2001, 2003; Shaw et al., 2004; Shaw, 2005; Zhang and Weglein, 2005; Liu et al., 2006; Liu, 2006; Zhang, 2006). The end goal is to define a processing procedure, which, absent an input Q estimate, returns a Q compensated, pre-stack primary data set due to waves reflecting from an an-elastic medium with arbitrary variability in three dimensions. Here we derive and numerically test a candidate algorithm which is appropriate for primaries reflecting from a simpler medium, a 2-parameter absorptive medium with arbitrary variability in depth. Since we do not take any steps during the derivation which could not—at least in principle—also be taken under conditions of more complex heterogeneity or model-type, this result may be regarded as a potentially useful way-point towards the end goal.

The inverse scattering series, absent manipulation, takes as its input measurements of a scattered field, and creates as its output the perturbation that gave rise to the field. This runs counter to the goals of Q-compensation as we define it, because:

1. The scattered field in general contains all reflected events, including primaries and multiples, whereas (since there exist reliable methods for multiple removal which are not sensitive to the elasticity/anelasticity of the subsurface) we will perform inverse operations on primaries only;
2. Of all the processing steps enacted upon primaries within the full inverse problem, we wish one only, the correction for absorptive propagation, to actually be carried out; and
3. We wish to estimate not the perturbation, a model-like quantity, but, rather, a data-like quantity, a set of reflected primaries that have been Q-compensated.

After posing the scattering problem to accommodate absorptive media, most of the strategy in the algorithm development we present is geared towards managing these three issues. Our route is as follows.

We begin by creating a forward modeling procedure for absorptive-dispersive primaries based on the Born series. The result is a non-linear scattering-based series calculation of *primaries only* in a layered absorptive-dispersive medium, which is accurate for large, extended perturbations. This is useful for our current purposes, because such partial series may be inverted, order-by-order, in exactly the same fashion as the full inverse scattering series, to generate non-linear direct inversion procedures that take as their input data reflected primaries. We continue, then, by carrying out this inversion upon the absorptive-dispersive primary series above. The resulting non-linear inverse scattering equations, which construct approximations of the actual wavespeed and Q perturbations in the medium, are therefore of a form that addresses item (1.) above.

We next note that, because of the direct, analytic nature of these inverse equations, it is possible to make informed conjectures regarding where and how in the mathematics the correction for Q takes place, and by extension how to suppress all of the other non-linear operations. Doing so, we argue, amounts to an extraction and separate execution of the Q-compensation part of the full inversion of primary data; this addresses item (2.) above.

Finally, we point out that given a homogeneous reference medium, the relationship between the linear components of the parameter perturbations and the data is very simple: essentially a Fourier transform. In the second step above, all non-linear aspects of the processing, apart from those that we argue are concerned with Q-compensation, have been suppressed. It follows that in all respects apart from absorption, the output maintains a simple, linear relationship with the data. We map this output trivially back to data-space with a change of variables and an inverse Fourier transform. The final result, which has addressed item (3.) above, is deemed to be the Q-compensated data set.

Direct non-linear Q compensation

We define the reference medium such that the Green's functions for a source at $\mathbf{x_s}$ and a receiver at $\mathbf{x}$ at angular frequency ω obey the scalar (non-absorptive) equation

$$\left[\nabla^2 + \frac{\omega^2}{c_0^2}\right] G_0(\mathbf{x}|\mathbf{x_s};\omega) = \delta(\mathbf{x}-\mathbf{x_s}). \tag{1}$$

The solution to equation (1) in 2D for a line source at (x_s, z_s) and a line receiver at (x_g, z_g), is expressible analytically, as, e.g.,

$$G_0(x_g,z_g,x_s,z_s,\omega) = \frac{1}{2\pi}\int_{-\infty}^{\infty} dk'_x e^{ik'_x(x_g-x_s)}\frac{e^{iq'|z_g-z_s|}}{i2q'}, \tag{2}$$

where $q' = \omega/c_0(1-c_0^2k_x'^2/\omega^2)^{1/2}$. We define the wave field in the actual medium as satisfying a two parameter (nearly-constant Q) absorptive wave equation:

$$\left[\nabla^2 + K^2\right] G(\mathbf{x}|\mathbf{x_s};K) = \delta(\mathbf{x}-\mathbf{x_s}), \tag{3}$$

where, following, e.g., Aki and Richards (2002),

$$K \equiv \frac{\omega}{c(\mathbf{x})}\left[1+\frac{F(\omega)}{Q(\mathbf{x})}\right], \tag{4}$$

and

$$F(\omega) = \frac{i}{2} - \frac{1}{\pi}\ln\left(\frac{\omega}{\omega_r}\right). \tag{5}$$

In the inverse developments to follow, F is assumed known, and Q as assumed unknown. Treating the quantities in square brackets in equations (1) and (3) as the operators $\mathbf{L_0}$ and $\mathbf{L}$ respectively (see, e.g., Weglein et al., 2003), and defining two dimensionless perturbation quantities (Innanen and Weglein, 2007):

$$\alpha(\mathbf{x}) = 1 - \frac{c_0^2(\mathbf{x})}{c^2(\mathbf{x})}, \quad \beta(\mathbf{x}) = \frac{1}{Q(\mathbf{x})}, \tag{6}$$

we arrive at a perturbation operator appropriate for this Q problem:

$$\mathbf{V} = \mathbf{L_0} - \mathbf{L} \approx \frac{\omega^2}{c_0^2} \left[\alpha(\mathbf{x}) - 2F(\omega)\beta(\mathbf{x})\right]. \tag{7}$$

We next restrict the medium such that α and β vary in depth only, and use the above quantities to form a partial Born series:

$$\psi_P = \psi_1 + \psi_2 + \psi_3..., \tag{8}$$

whose terms are judged, via arguments based on relative scattering geometry to construct reflected primaries that have been distorted by Q. This is a 2-parameter extension of the scalar acoustic construction discussed by Innanen (2008). At first order, for instance, after Fourier transforming over x_s, we have

$$\begin{aligned}\psi_1(k_s,\omega) &= \int dx' \int dz' G_0(x_g, z_g, x', z', \omega) k^2 \gamma(z') G_0(x', z', k_s, z_s, \omega) \\ &= -\frac{1}{4\cos^2\theta} \int dz' e^{i2q_s z'} \gamma(z'),\end{aligned}$$

where

$$\gamma(z) = \alpha(z) - 2F(\omega)\beta(z),$$

k_s is the Fourier conjugate of x_s, $q_s = \omega/c_0(1 - c_0^2 k_s^2/\omega^2)^{1/2}$, and $\theta = \sin^{-1}\frac{k_s c_0}{\omega}$, and for convenience we have set $x_g = z_g = z_s = 0$. For another instance, at second order, we have

$$\psi_2(k_s,\omega) = -\frac{(-i2q_s)}{8\cos^4\theta} \int dz' e^{i2q_s z'} \gamma(z') \left(\int^{z'} dz'' \gamma(z'') \right).$$

Continuing with this program of retention and rejection at all orders, the details of which are included in Appendix A, we produce a series for attenuated primaries, ψ_P, which we associate with the measured data $D \equiv \psi_P$:

$$D(k_s,\omega) = \frac{-1}{4\cos^2\theta} \int dz' e^{i2q_s z'} \gamma(z') \sum_{n=0}^{\infty} \frac{1}{n!} \left(\frac{-iq_s}{\cos^2\theta} \int^{z'} dz'' \gamma(z'') \right)^n. \tag{9}$$

Computing and combining a large number of these terms through equation (9) generates an analytic expression for the primary data.

We next form an inverse series for the perturbations α and β, in which the n'th term is defined to be n'th order in the *primary* data modeled above. Let this series be $\gamma = \gamma_1 + \gamma_2 + ...$, that is

$$[\alpha(z) - 2F(\omega)\beta(z)] = [\alpha_1(z) - 2F(\omega)\beta_1(z)] + [\alpha_2(z) - 2F(\omega)\beta_2(z)] + ... \ .$$

This is substituted into equation (9), and like orders are equated (Innanen, 2008), similarly to Carvalho's derivation of the full inverse scattering series (Carvalho, 1992; Weglein et al., 1997).

The inverse solution is generated by sequentially solving for and summing contributions to the perturbation over many orders. At first order, we have

$$D(k_s,\omega) = \frac{-1}{4\cos^2\theta}\int dz' e^{i2q_s z'}[\alpha_1(z') - 2F(\omega)\beta_1(z')]. \tag{10}$$

Innanen and Weglein (2007) describe in detail how this equation may be used to separately determine α_1 and β_1 as functions of pseudo-depth. The process of linear separation requires the data to be combined across sets of incidence angles $\vartheta = \{\theta_1, \theta_2, ...\}$, and may if desired also involve a weighting scheme W, hence in general the outputs must be considered functions of these variables also:

$$\begin{aligned}\alpha_1 &= \alpha_1(z|\vartheta, W),\\ \beta_1 &= \beta_1(z|\vartheta, W).\end{aligned} \tag{11}$$

The quantities α_1 and β_1 have qualitative interpretations that depend on the size and extent of the actual perturbations α and β. If the actual perturbations are small and transient, and some scheme of averaging (e.g., Clayton and Stolt, 1981) is invoked to manage the over-determinedness of the problem, these quantities can be considered model-like, and, if interpreted as inverse Born-approximate model parameter estimates, represent an end-point of the procedure. Alternatively, if the perturbation is large and extended, which in this paper we assume is the case, the quantities α_1 and β_1 bear scant resemblance to the actual perturbations α and β. In fact, they are data-like: they depend on experimental variables, and they have amplitudes and discontinuities that are only distantly and non-linearly related to those of α and β, while being closely and linearly related to those of the reflected primary events. For this reason, in this paper we refer to the α_1, β_1 quantities as being essentially linearly transformed and weighted versions of the input primary data.

With these things in mind, continuing next with the direct non-linear inversion, at second order, we find a relationship between α_1, β_1 and α_2, β_2:

$$\begin{aligned}&\frac{1}{4\cos^2\theta}\int dz' e^{i2q_s z'}[\alpha_2(z'|\vartheta, W) - 2F(\omega)\beta_2(z'|\vartheta, W)]\\ =&-\frac{[-i2q_s]}{8\cos^4\theta}\int dz' e^{i2q_s z'}[\alpha_1(z'|\vartheta, W) - 2F(\omega)\beta_1(z'|\vartheta, W)]\\ &\times\left(\int_0^{z'} dz''[\alpha_1(z''|\vartheta, W) - 2F(\omega)\beta_1(z''|\vartheta, W)]\right).\end{aligned}$$

This continues at third order, wherein a relationship between α_1, β_1 an α_3, β_3 is determined, and beyond. By the third or fourth order, a pattern is discernable in the mathematics that allows the n'th order inverse equation to be straightforwardly predicted. Summing the equations over all orders (by assuming the continuation of this pattern), and defining

$$\begin{aligned}\alpha_P(z|\vartheta, W) &\equiv \sum_{n=0}^{\infty}\alpha_{n+1}(z|\vartheta, W),\\ \beta_P(z|\vartheta, W) &\equiv \sum_{n=0}^{\infty}\beta_{n+1}(z|\vartheta, W),\end{aligned}$$

there results a closed form set of non-linear equations

$$\alpha_P(k_z,\theta|\vartheta,W) - 2F(k_z,\theta)\beta_P(k_z,\theta|\vartheta,W) = \int dz' e^{-ik_z\left[z' + \frac{1}{2\cos^2\theta}\int_0^{z'} dz''[\alpha_1(z''|\vartheta,W) - 2F(k_z,\theta)\beta_1(z''|\vartheta,W)]\right]}[\alpha_1(z'|\vartheta,W) - 2F(k_z,\theta)\beta_1(z'|\vartheta,W)], \tag{12}$$

where $k_z \equiv -2q_s$ is the Fourier conjugate of depth z. This represents a direct inversion of the primary data, exact to within the accuracy of the primary approximation series in equation (9), and appropriate for a layered, 2-parameter, absorptive-dispersive medium. Further details of the derivation of equation (12) are included in Appendix B. The quantities α_P and β_P are the non-linearly determined profiles associated with $c(z)$ and $Q(z)$; each can in principle be independently determined via equation (12) if desired, which may itself be of independent interest. This is shown in Appendix C.

However, our current goal is to carry out a single inverse task, that of compensating for Q, and to ultimately recover a data set, not a set of parameter perturbations. To accomplish these things, we examine equation (12) more closely. We note that the outputs, α_P and β_P, *would* be related linearly to the inputs, α_1 and β_1, except that α_1 and β_1 also appear in the argument of the exponential function in the integrand. Here all of the non-linearity of the inversion resides. We then make the following statements. The principal role of α_1 in the argument of the exponential is to non-linearly accomplish aspects of the inversion associated with wavespeed deviations between the reference and actual media (e.g., to correctly locate linearly misplaced reflectors at depth). And, the principal role of β_1 in the argument is to accomplish aspects of the inversion associated with deviations between reference and actual Q values, meaning, predominantly, compensation. The arguments for these statements are twofold. First, equation (12) is a 2-parameter version of a scheme derived elsewhere for a 1-parameter acoustic medium, i.e., involving α only (Innanen, 2008). Those 1-parameter equations include an exponential function with an argument identical to the first (α_1) term in the exponential of equation (12). Since the β_1 component of the exponential function appears only when absorptive inverse issues appear, we ascribe to it the role of managing these issues. And second, this component of the exponential function, by virtue of the complex nature of the coefficient F, is the only part of the function that grows exponentially, and therefore alone has the numerical capability to perform the (ill-conditioned) boosting of high frequencies characteristic of Q compensation. We will now permit these two statements to lead us to a proposed form of a Q compensation algorithm, and discuss the possibility that they are only approximately true (and the consequences of this) in the discussion section of this paper.

We peremptorily set α_1 in the argument of the exponential to zero, and suggest that as a consequence: (1) the (now altered) outputs α_P and β_P undergo non-linear correction for the attenuation and dispersion associated with propagation in an absorptive medium, but (2) they undergo linear treatment in all other respects.

Calling the partially treated outputs α_Q and β_Q, we have instead

$$\alpha_Q(k_z,\theta|\vartheta,W) - 2F(k_z,\theta)\beta_Q(k_z,\theta|\vartheta,W) = \int dz' e^{-ik_z\left[z' - \frac{F(k_z,\theta)}{\cos^2\theta}\int_0^{z'} dz''\beta_1(z''|\vartheta,W)\right]}[\alpha_1(z'|\vartheta,W) - 2F(k_z,\theta)\beta_1(z'|\vartheta,W)]. \tag{13}$$

By assumption, the form of these equations ensures that only Q-compensation (and not, say, any re-positioning of reflectors away from their linearly-determined depths) takes place as the data (through α_1 and β_1) is processed.

Finally, we will argue for an approach to make the output of this processing a data-like quantity. Equation (13) follows the basic template

$$A = \int e^B C. \tag{14}$$

We proceed by comparing this template, and the associated elements of equation (13), to equation (10). Evidently if β_1 in the exponential function were set to zero we would exactly recover the data by carrying out the integral in equation (13). If our previous suggestion is correct, i.e., that $\beta_1 \neq 0$ in the exponential is responsible solely for Q compensation, then it would appear that the left hand side is already a data-like quantity, different only from the input data set in that its amplitudes have been corrected for absorption and dispersion.

Hence, after constructing the input C and the operator B by linearly transforming and weighting the data, and computing the right-hand side of equation (13), we use the linear relationship defined in equation (10) to map, not α_1 and β_1, but rather the left-hand side of equation (13), back to the (k_s, ω) domain, through, in essence, a change of variables. Our suggestion is that this mapped quantity is a Q-compensated data set in the Fourier domain. That is, we define

$$D_{\text{comp}}(k_z, \theta|\vartheta, W) \equiv -\frac{1}{4\cos^2\theta}[\alpha_Q(k_z, \theta|\vartheta, W) - 2F(k_z, \theta)\beta_Q(k_z, \theta|\vartheta, W)], \tag{15}$$

where $\vartheta = \vartheta(\theta, k_z)$, $W = W(\theta, k_z)$. Changing variables back to k_s, ω and inverse Fourier transforming, the Q compensated data set is estimated as

$$D_{\text{comp}}(x_s, t) = \left(\frac{1}{2\pi}\right)^2 \int\int dk_s d\omega e^{ik_s x_s} e^{i\omega t} D_{\text{comp}}(k_s, \omega). \tag{16}$$

Synthetic example

To exemplify this procedure, we construct a simple synthetic primary data set corresponding to the two-interface absorptive-dispersive model in Figure 1. The resulting primary data (Figure 2, upper panel) are used as input to the linear inverse scattering equations, which involves a transformation and weighting thereof. These data-like quantities are then used to construct both the operator e^B and the operand C as in equation (14). The Q-compensated data set (Figure 2, lower panel) is formed by transforming the result, A in equation (14), to the (k_s, ω) domain, and then performing straightforward inverse Fourier transforms. The Q-compensated results are compared in detail with the input in Figure 3 for three offsets, 0m, 170m, and 335m. For illustration purposes, *after* all processing is complete we convolve the input and output with a Ricker wavelet, which is a cosmetic step; the procedure assumes the source wavelet has been deconvolved from the input data. The dispersion correction, and the clear similarity of the output to the idealized, non-attenuated test

trace, indicate that the algorithm is largely achieving its stated goal. We note a slight under-correction at large angle.

In equations (13) and (15), there are two sets of angles: an input set (ϑ) used to separate α_1 and β_1, and to construct the correction operator, and an output angle θ, which is varied to recover the full, corrected pre-stack data set. Neither inverse scattering theory nor our manipulations of it specifically impose any relationship between the two. For the full inverse scattering parameter estimation problem (Appendix C), this freedom might be exploited for purposes of regularization, or to incorporate prior information. However, for the problem at hand, empirical study suggests that input angles ϑ which "cluster" around the output angle θ be used. We have decided, that is, to correct particular angle and wavenumber components of the data using the data at those same components and their immediate neighbors. In the example above, the input set $\vartheta = \{\theta, \theta + \Delta\theta\}$ (where $\Delta\theta$ is the smallest provided by the synthetic data after the change of variables) was used for each θ of corrected data. The angle pairs were weighted equally ($W = 1$); little of the additional freedom W provides to precondition the data has been explored as yet.

Noisy examples have not been included at this proof-of-concept stage; we have found our approach to share the basic response to noise of all standard Q compensation schemes. We point out that (as is often done in standard Q compensation) with a quick alteration to the function F as it appears in the argument of the exponential in equation (12), this algorithm may be transformed immediately into a "dispersion compensation" procedure, which is well-conditioned and largely unaffected by noise.

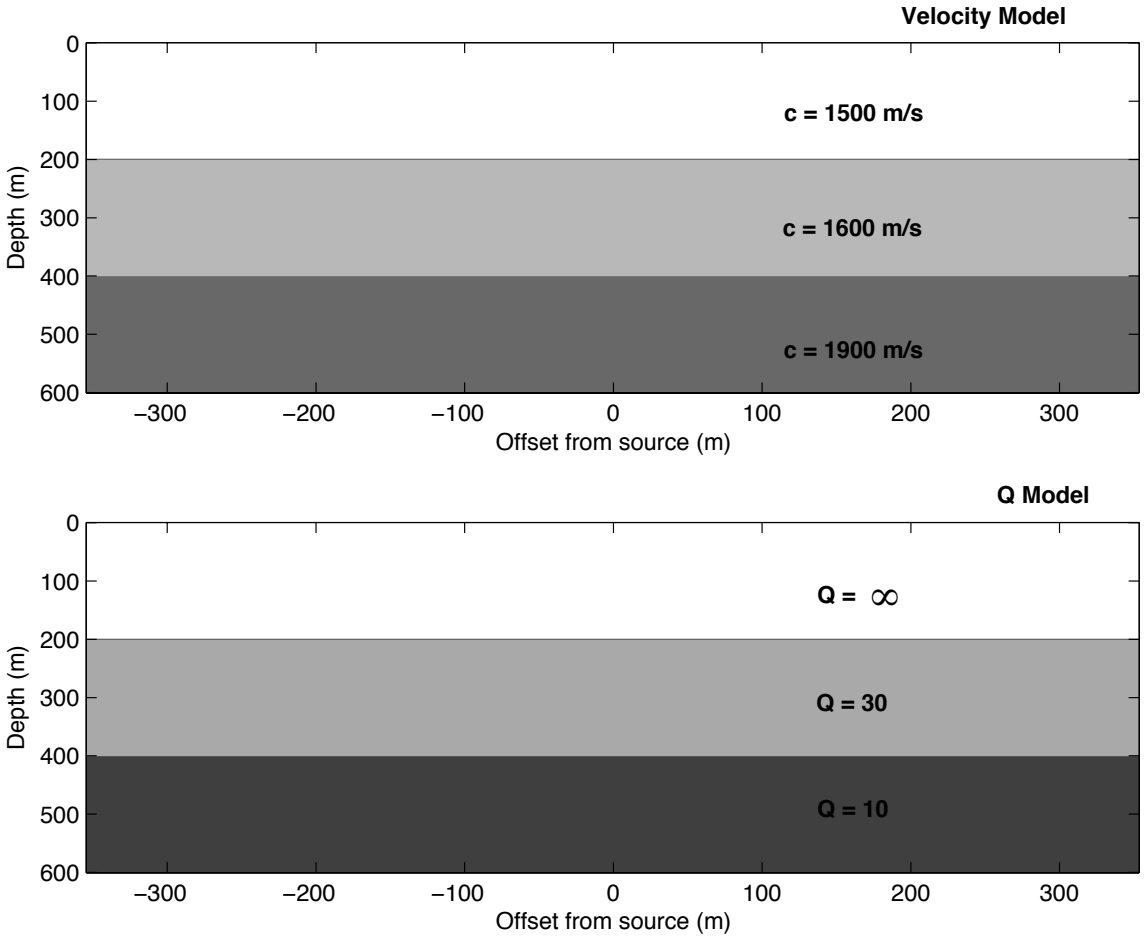

Figure 1: *Two interface absorptive-dispersive model.*

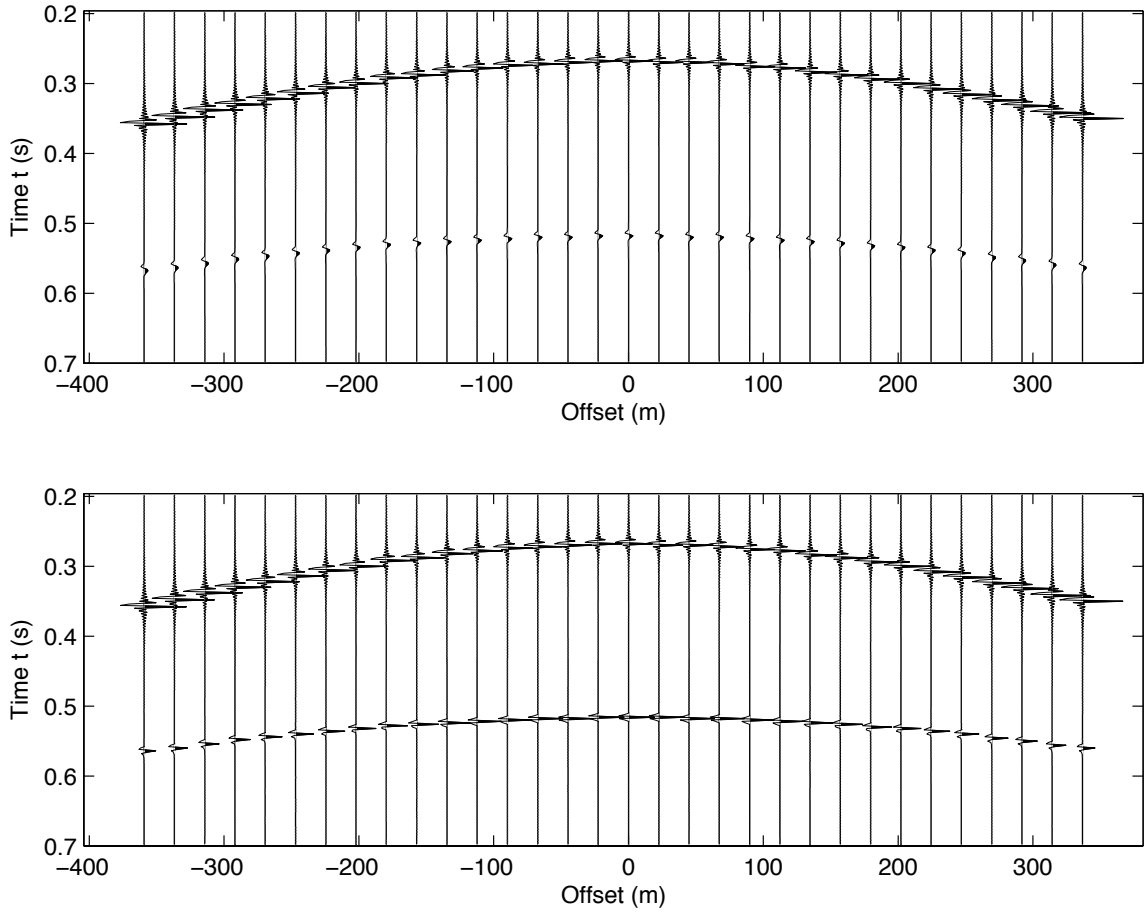

Figure 2: *Top panel: synthetic pre-stack input primary data from the model in Figure 1 (decimated for purposes of display); bottom panel: Q-compensated output data (likewise decimated). The phase rotation of the shallower primary is caused by the strong absorptive reflection coefficient associated with the top interface.*

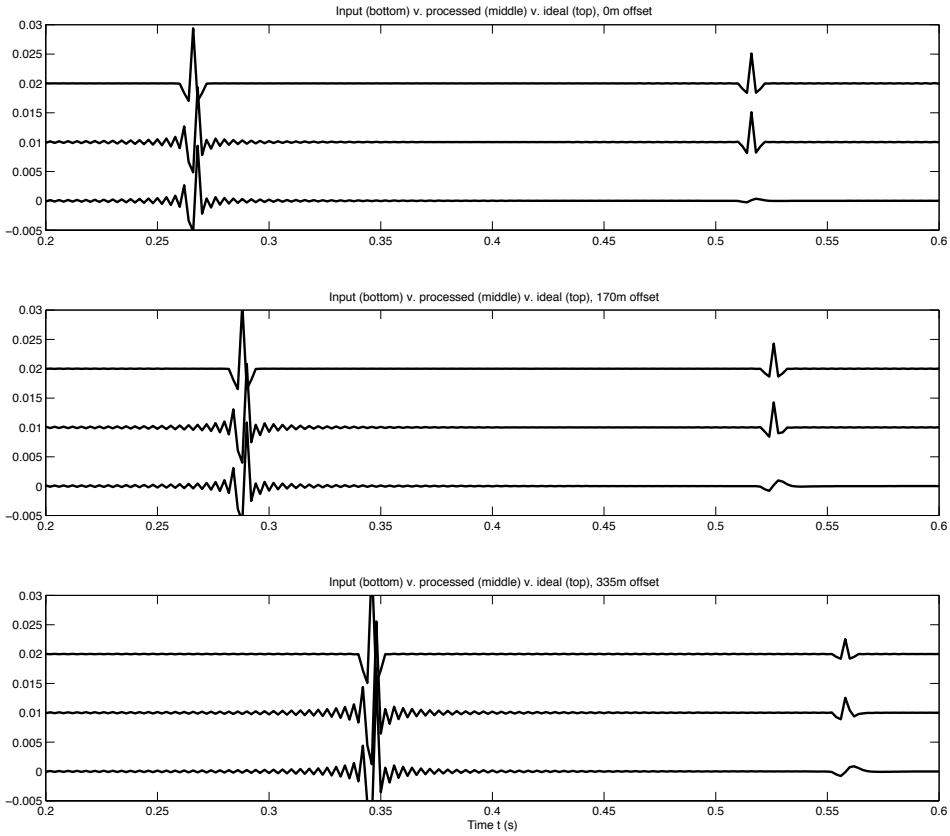

Figure 3: *Detail of Q compensation for three offsets of pre-stack data. Bottom trace in each panel is input, the middle trace is the output, and the top trace, for benchmarking, is an idealized trace constructed without Q, and normalized to the maximum value of the output traces.*

Discussion and conclusions

We choose as the definition of Q compensation, *the estimation of an output data set that is identical to the input, except that all absorptive propagation effects are absent.* We present a candidate scheme, based on non-linear inverse scattering, whose output, we argue, fits this definition. In applying it, a correction operator is automatically constructed from the data themselves, with no requirement for an input estimate of subsurface medium parameters, including its Q structure. Synthetic examples illustrate the scheme in action, and provide proof-of-concept level evidence of the validity of the approach.

The behavior of this algorithm can be interpreted in terms of data events interacting non-linearly. Consider again the schematic form

$$A = \int e^B C, \tag{17}$$

where

$$\begin{aligned} A &= \alpha_Q(k_z, \theta|\vartheta, W) - 2F(k_z, \theta)\beta_Q(k_z, \theta|\vartheta, W), \\ B &= -ik_z \left[z' - \frac{F(k_z, \theta)}{\cos^2\theta} \int_0^{z'} dz'' \beta_1(z''|\vartheta, W) \right], \\ C &= \alpha_1(z'|\vartheta, W) - 2F(k_z, \theta)\beta_1(z'|\vartheta, W), \end{aligned} \tag{18}$$

and recall that α_1 and β_1 are effectively linearly transformed, weighted forms of the data in the pseudo-depth domain (i.e., vertical two-way travel-time scaled with the constant reference wavespeed c_0). The quantity C is being operated on by $\int e^B$ to produce A. One frequency-wavenumber component of the output data (ω and k_s, via k_z and θ), A, comes from contributions from the input data C at all pseudo-depths. For each contributing depth, the C component is boosted by e^B, which from equation (18) can be seen to be the cumulative influence of the values of β_1 that are shallower than the contributing depth. The quantities β_1 and B are constructed from the angle and frequency dependence of the primaries in the input data. Therefore, this Q compensation operator, acting on a given primary, may be understood to have been constructed from the cumulative angle and frequency variations (i.e., the generalized AVO/AVA behavior) of all shallower primaries.

We have made two major assumptions in deriving the scheme:

1. That, by suppressing certain components of the full non-linear inversion equations derived from inverse scattering, we isolate the Q compensation activity inherent to the inversion;
2. That, with trivial linear transformation and changes of variable, the output of this isolated inverse step can be treated as an equivalent data set, different only from the input in the lack of absorption in the primary events.

The soundness of these assumptions is likely best argued for with success in testing, some of which we have provided with our proof-of-concept example. But, we might already anticipate that slightly

more sophisticated choices could ultimately lead to more accurate results, in particular with respect to (1.) above. Part of the argument for isolating and extracting the Q compensation component of the inverse equations lay in comparing the 2-parameter absorptive system of inverse equations with its 1-parameter acoustic counterpart. But the 2-parameter linear inverse problem, by which we determine the correction operator, is subject to phenomena not shared by 1-parameter problems, for instance, leakage, or the tendency for one parameter's *actual* variations to be accounted for with variations in multiple *linearly estimated* parameters (discussed for the absorptive problem by Innanen and Weglein, 2007). Study of this issue may in the future lead to a more sophisticated program for isolation of the absorption compensation component of the non-linear equations.

Direct, non-linear methods bring a greatly reduced requirement for prior information as compared to their linear counterparts. But they demand broadband, densely sampled, wide-aperture, deghosted, deconvolved (of the *source* wavelet), and demultipled data in return. Data fidelity, bandwidth and coverage are the first requirements in considering methods such as this one. The data set used in the synthetic example is broad-band, and includes low (sub-Hz) frequencies (although not close to zero frequency–the nearly constant Q model we are using in fact diverges at and near that limit). The requirement for this kind of data is typical of non-linear, wave theoretic inverse methods. The best outcome will result from actual acquisition of maximally low frequency data, of course; however, various assumptions, for instance that of a piecewise-constant overburden, can additionally be made, removing the sensitivity to cut-off of low frequencies.

Two other issues are at the forefront when it comes to contemplating field data application of an algorithm of this kind. The first has to do with the way in which the data are interrogated for information in constructing the operator (B in equation (14)), which is described in detail by Innanen and Weglein (2007). Briefly, it is the frequency- and angle-dependence of the transmission-altered reflection coefficients of the primaries (as we have stated above, loosely a brand of AVO/AVA behaviour specific to absorptive-dispersive media) that drives the construction of the operator. That this behavior exists is a straightforward prediction of wave theory. However, it may appear as subtle variations in field data. Detecting it is critical to the procedure.

The second is a consequence of the algorithm's interest in amplitude variations in the data. As it stands, the algorithm considers data to be due to a layered, 2-parameter ("an-acoustic"), absorptive-dispersive medium. When that is true, as in our synthetic examples, the results are of high quality. When that is (at best) only approximately true, as in a seismic field data application, the results will presumably suffer. The basic framework and arguments underlying this candidate direct non-linear Q compensation procedure have been purposefully chosen never to *fundamentally* restrict the results to either an-acoustic or layered (1D) media. However, some specific aspects of the procedure, for instance the availability of closed forms, are a consequence of these simplifications. A clear next step is to alter the construction of the corrective operator to be in accordance with a more suitable anelastic, and heterogeneous medium model, although we anticipate a greater degree of algorithm complexity as a result.

Acknowledgements

The sponsors and personnel of M-OSRP are thanked, especially Art Weglein. K. Innanen was also supported by U.S. D.O.E. Grant No. DOE-De-FG02-05ER15697. J. Lira was also supported by Petrobras.

References

Aki, K. and P. G. Richards. *Quantitative Seismology.* 2nd edition. University Science Books, 2002.

Bickel, S. H. and R. R. Natarajan. "Plane-wave Q deconvolution." *Geophysics* 50 (1985): 1426–1439.

Carvalho, P. M. *Free-surface multiple reflection elimination method based on nonlinear inversion of seismic data.* PhD thesis, Universidade Federal da Bahia, 1992.

Causse, E., R. Mittet, and B. Ursin. "Preconditioning of full-waveform inversion in viscoacoustic media." *Geophysics* 64 (1999): 130–145.

Clayton, R. W. and R. H. Stolt. "A Born-WKBJ inversion method for acoustic reflection data." *Geophysics* 46 (1981): 1559–1567.

Dahl, T. and B. Ursin. "Non-linear AVO inversion for a stack of anelastic layers." *Geophysical Prospecting* 40 (1992): 243.

Dasios, A., C. McCann, and T. Astin. "Least-squares inversion of in-situ sonic Q measurements: stability and resolution." *Geophysics* 69 (2004): 378–385.

Hargreaves, N. D. and A. J. Calvert. "Inverse Q-filtering by Fourier transform." *Geophysics* 56 (1991): 519–527.

Hicks, G. and R. G. Pratt. "Reflection waveform inversion using local descent methods: estimating attenuation and velocity over a gas-sand deposit." *Geophysics* 66 (2001): 598–612.

Innanen, K. A. "A direct non-linear inversion of primary wave data reflecting from extended, heterogeneous media." *Inverse Problems* 24 (2008): 035021.

Innanen, K. A. and J. E. Lira. "Direct non-linear Q compensation of primaries in layered media: theory and synthetic examples." *Proceedings of the 78th Annual Meeting of the Society of Exploration Geophysicists, Las Vegas, NV.* . Soc. Expl. Geophys., 2008.

Innanen, K. A. and A. B. Weglein. "Construction of absorptive/dispersive wave fields with the forward scattering series." *Journal of Seismic Exploration* 12 (2003): 259–282.

Innanen, K. A. and A. B. Weglein. "Towards non-linear construction of a Q-compensation operator directly from reflection seismic data." *Proceedings of the 75th Annual Meeting of the Society of Exploration Geophysicists, Houston, TX.* . Soc. Expl. Geophys., 2005.

Innanen, K. A. and A. B. Weglein. "On the construction of an absorptive-dispersive medium model via direct linear inversion of reflected seismic primaries." *Inverse Problems* (2007): 2289–2310.

Liu, F., A. B. Weglein, K. A. Innanen, and B. G. Nita. "Multi-dimensional seismic imaging using the inverse scattering series." *Proceedings of the 76th Annual Meeting of the Society of Exploration Geophysicists, New Orleans, LA.* . Soc. Expl. Geophys., 2006.

Liu, Fang. *Multi-dimensional depth imaging without an adequate velocity model*. PhD thesis, University of Houston, 2006.

Mittet, R. "A simple design procedure for depth extrapolation operators that compensate for absorption and dispersion." *Geophysics* 72 (2007): S105–S112.

Mittet, R., R. Sollie, and K. Hostad. "Prestack depth migration with compensation for absorption and dispersion." *Geophysics* 60 (1995): 1485–1494.

Ribodetti, A. and J. Virieux. "Asymptotic theory for imaging the attenuation factor Q." *Geophysics* 63 (1998): 1767–1778.

Shaw, S. A. *An inverse scattering series algorithm for depth imaging of reflection data from a layered acoustic medium with an unknown velocity model*. PhD thesis, University of Houston, 2005.

Shaw, S. A., A. B. Weglein, D. J. Foster, K. H. Matson, and R. G. Keys. "Isolation of a leading order depth imaging series and analysis of its convergence properties." *Journal of Seismic Exploration* 2 (November 2004): 157–195.

Song, S. and K. A. Innanen. "Multiresolution modelling and wavefield reconstruction in attenuating media." *Geophysics* 67 (2002): 1192–1201.

Verschuur, D. J. and A. J. Berkhout. "Estimation of multiple scattering by iterative inversion, part II: practical aspects and examples." *Geophysics* 62 (1997): 1596–1611.

Verschuur, D. J., A. J. Berkhout, and C. P. A. Wapenaar. "Adaptive surface-related multiple elimination." *Geophysics* 57 (1992): 1166–1177.

Wang, Y. "Quantifying the effectiveness of stabilized inverse Q filtering." *Geophysics* 68 (2003): 337–345.

Wang, Y. "Inverse Q-filter for seismic resolution enhancement." *Geophysics* 71 (2006): V51–V60.

Weglein, A. B., F. V. Araújo, P. M. Carvalho, R. H. Stolt, K. H. Matson, R. T. Coates, D. Corrigan, D. J. Foster, S. A. Shaw, and H. Zhang. "Inverse Scattering Series and Seismic Exploration." *Inverse Problems* (2003): R27–R83.

Weglein, A. B., D. J. Foster, K. H. Matson, S. A. Shaw, P. M. Carvalho, and D. Corrigan. "An inverse-scattering sub-series for predicting the spatial location of reflectors without the precise reference medium and wave velocity." *71st Annual Internat. Mtg., Soc. Expl. Geophys., Expanded Abstracts.* . Soc. Expl. Geophys., 2001. 2108–2111.

Weglein, A. B., F. A. Gasparotto, P. M. Carvalho, and R. H. Stolt. "An Inverse-Scattering Series Method for Attenuating Multiples in Seismic Reflection Data." *Geophysics* 62 (November-December 1997): 1975–1989.

Weglein, A.B. and W.H. Dragoset. *Multiple Attenuation.* Geophysics reprint series. Soc. Expl. Geophys., 2005.

Zhang, C. and T. J. Ulrych. "Seismic absorption compensation: a least squares inverse scheme." *Geophysics* 72 (2007): R109–R114.

Zhang, H. *Direct non-linear acoustic and elastic inversion: towards fundamentally new comprehensive and realistic target identification.* PhD thesis, University of Houston, 2006.

Zhang, H. and A.B. Weglein. "The inverse scattering series for tasks associated with primaries: depth imaging and direct non-linear inversion of 1D variable velocity and density acoustic media." *SEG Technical Program Expanded Abstracts.* 2005, 1705–1708.

Appendix A: Primaries in a layered absorptive medium

In this appendix we take the scattering quantities defined in the body of the paper, and use them to construct the first three terms in the absorptive-dispersive Born series. Arguments from relative scattering geometry are used to extract a subset of terms from this series, which are adjudged to construct only the absorptive-dispersive primaries. Patterns in these terms are used to deduce a full non-linear absorptive-dispersive primary approximation.

We proceed assuming a non-absorptive reference medium. For waves at oblique incidence (i.e., a non-zero source plane wave angle θ) above a layered absorptive medium, with reflected waves detected at a lateral line receiver location x_g, the first order term of the Born series is

$$\begin{aligned}\psi_1(x_g,z_g,k_s,z_s,\omega) &= \int dx' \int dz' G_0(x_g,z_g,x',z',\omega)k^2\gamma(z')G_0(x',z',k_s,z_s,\omega) \\ &= -\frac{1}{4}\frac{k^2}{q_s^2}e^{-iq_s(z_g+z_s)}e^{ik_sx_g}\int dz' e^{i2q_sz'}\gamma(z'),\end{aligned} \tag{19}$$

where

$$\gamma(z) = \alpha(z) - 2F(\omega)\beta(z). \tag{20}$$

This term constructs only primaries, and as such is kept in full as the first order term in the primary series also. For convenience we set $x_g = z_g = z_s = 0$, and rename the linear term ψ_{1P}:

$$\psi_{1P}(k_s,\omega) = -\frac{1}{4\cos^2\theta}\int dz' e^{i2q_sz'}\gamma(z'). \tag{21}$$

The second order term of the Born series is also needed in its entirety in the primary approximation. We have, again with $x_g = z_g = z_s = 0$,

$$\begin{aligned}\psi_{2P}(k_s,\omega) &= -\frac{(-i2q_s)}{16\cos^4\theta}\int dz' e^{iq_s z'}\gamma(z')\int dz'' e^{iq_s|z'-z''|}\gamma(z'')e^{iq_s z''} \\ &= -\frac{1}{8\cos^4\theta}(-i2q_s)\int dz' e^{i2q_s z'}\gamma(z')\left(\int^{z'} dz''\gamma(z'')\right).\end{aligned} \tag{22}$$

At third order, we begin with the full Born series term

$$\begin{aligned}&\psi_3(k_s,\omega) = \\ &\quad -\frac{(-i2q_s)^2}{64\cos^6\theta}\int dz' e^{iq_s z'}\gamma(z')\int dz'' e^{iq_s|z'-z''|}\gamma(z'')\int dz''' e^{iq_s|z''-z'''|}\gamma(z''')e^{iq_s z'''},\end{aligned} \tag{23}$$

but reject the component for which the "middle" scattering location z'' is shallower than both z' and z''', which begins the construction of multiples (Weglein et al., 1997). This means rejecting one of the four components of equation (23) that arise when the absolute value bars are evaluated case-wise. Retaining the other three components, we have

$$\begin{aligned}\psi_{3P}(k_s,\omega) &= -\frac{(-i2q_s)^2}{64\cos^6\theta}\int dz' e^{i2q_s z'}\gamma(z')\int^{z'} dz''\gamma(z'')\int^{z''} dz'''\gamma(z''') \\ &= -\frac{(-i2q_s)^2}{32\cos^6\theta}\int dz' e^{i2q_s z'}\gamma(z')\left(\int^{z'} dz''\gamma(z'')\right)^2,\end{aligned} \tag{24}$$

where again for convenience $x_g = z_g = z_s = 0$ (for cases involving non-zero source receiver depths, or several x_g values, the simple exponential factors outside the integrals may be easily re-instated). The pattern visible from orders 1–3 persists at higher order. Collecting all of terms that fit the same pattern creates an approximation of primaries appropriate for large, extended absorptive-dispersive perturbations. The approximation is a straightforward extension of the scalar (acoustic) approximation discussed by Innanen (2008). Calling the approximation ψ_P, we have

$$\begin{aligned}\psi_P(k_s,\omega) &= \sum_{n=0}^{\infty}\psi_{nP}(k_s,\omega) \\ &= -\frac{1}{4\cos^2\theta}\int dz' e^{i2q_s z'}\gamma(z')\sum_{n=0}^{\infty}\frac{1}{n!}\left(-\frac{iq_s}{\cos^2\theta}\int^{z'} dz''\gamma(z'')\right)^n.\end{aligned} \tag{25}$$

This may be summed to closed form, as was done in direct non-linear imaging by Shaw et al. (2004):

$$\psi_P(k_s,\omega) = -\frac{1}{4\cos^2\theta}\int dz' e^{i2q_s\left[z'-(1/2)\cos^{-2}\theta\int^{z'} dz''\gamma(z'')\right]}\gamma(z'). \tag{26}$$

In this paper, the summed form is of less significance, since our aim will be to perform an order by order inversion. As the key result of this appendix, then, we have the series in equation (25),

expressed explicitly in terms of the wavespeed and Q perturbations α and β:

$$\begin{aligned}\psi_P(k_s,\omega) = &- \int dz' \frac{e^{i2q_s z'}}{4\cos^2\theta}[\alpha(z') - 2F(\omega)\beta(z')] \\ &\times \sum_{n=0}^{\infty} \frac{1}{n!}\left(\frac{-iq_s}{\cos^2\theta}\int^{z'} dz''[\alpha(z'') - 2F(\omega)\beta(z'')]\right)^n .\end{aligned} \tag{27}$$

Appendix B: Direct non-linear absorptive inversion

In this appendix we perform a direct, order-by-order inversion of the absorptive-dispersive primary approximation derived in Appendix A. We assume that the data (1) contain only primaries, (2) have been deconvolved of the source wavelet, and (3) have been deghosted. These assumptions are typical for direct non-linear primary algorithms based on the inverse scattering series (Weglein et al., 2003). If this is the case, and if the perturbations α and β are of such a size and extent that equation (27) is accurate, we may write

$$\begin{aligned} & D(k_s,\omega) \\ = &- \frac{1}{4\cos^2\theta}\int dz' e^{i2q_s z'}[\alpha(z') - 2F(\omega)\beta(z')] \\ &- \frac{[-i2q_s]}{8\cos^4\theta}\int dz' e^{i2q_s z'}[\alpha(z') - 2F(\omega)\beta(z')]\left(\int_0^{z'} dz''[\alpha(z'') - 2F(\omega)\beta(z'')]\right) \\ &- \frac{[-i2q_s]^2}{32\cos^6\theta}\int dz' e^{i2q_s z'}[\alpha(z') - 2F(\omega)\beta(z')]\left(\int_0^{z'} dz''[\alpha(z'') - 2F(\omega)\beta(z'')]\right)^2 \\ &+ ..., \end{aligned} \tag{28}$$

where θ and q_s are particular arrangements of experimental variables k_s and ω:

$$\begin{aligned} \theta &= \sin^{-1}\frac{k_s c_0}{\omega}, \\ q_s &= \frac{\omega}{c_0}\sqrt{1 - \frac{k_s^2 c_0^2}{\omega^2}}. \end{aligned} \tag{29}$$

The aim in the remainder of this appendix will be to directly invert equation (28).

An inverse series for absorptive primaries

We form an inverse series for the perturbations α and β, in which the n'th term is defined to be n'th order in the *primary* data modeled in equation (27). Let this series be

$$[\alpha(z) - 2F(\omega)\beta(z)] = [\alpha_1(z) - 2F(\omega)\beta_1(z)] + [\alpha_2(z) - 2F(\omega)\beta_2(z)] + ... \tag{30}$$

This is substituted into equation (28), and like orders are equated (Innanen, 2008), in a manner similar to Carvalho's derivation of the full inverse scattering series (Carvalho, 1992). At first order we have

$$D(k_s,\omega) = -\frac{1}{4\cos^2\theta}\int dz' e^{i2q_s z'}[\alpha_1(z') - 2F(\omega)\beta_1(z')]. \tag{31}$$

At second order, we have

$$\begin{aligned}&\frac{1}{4\cos^2\theta}\int dz' e^{i2q_s z'}[\alpha_2(z') - 2F(\omega)\beta_2(z')]\\ =&-\frac{[-i2q_s]}{8\cos^4\theta}\int dz' e^{i2q_s z'}[\alpha_1(z') - 2F(\omega)\beta_1(z')]\left(\int_0^{z'} dz''[\alpha_1(z'') - 2F(\omega)\beta_1(z'')]\right).\end{aligned} \tag{32}$$

At third order, we have

$$\begin{aligned}&\frac{1}{4\cos^2\theta}\int dz' e^{i2q_s z'}[\alpha_3(z') - 2F(\omega)\beta_3(z')]\\ =&-\frac{[-i2q_s]}{8\cos^4\theta}\int dz' e^{i2q_s z'}[\alpha_1(z') - 2F(\omega)\beta_1(z')]\left(\int_0^{z'} dz''[\alpha_2(z'') - 2F(\omega)\beta_2(z'')]\right)\\ &-\frac{[-i2q_s]}{8\cos^4\theta}\int dz' e^{i2q_s z'}[\alpha_2(z') - 2F(\omega)\beta_2(z')]\left(\int_0^{z'} dz''[\alpha_1(z'') - 2F(\omega)\beta_1(z'')]\right)\\ &-\frac{[-i2q_s]^2}{32\cos^6\theta}\int dz' e^{i2q_s z'}[\alpha_1(z') - 2F(\omega)\beta_1(z')]\left(\int_0^{z'} dz''[\alpha_1(z'') - 2F(\omega)\beta_1(z'')]\right)^2.\end{aligned} \tag{33}$$

This continues. Just as in the full inverse scattering series, the sequential direct solution for perturbation components at each order, followed by their summation, produces the desired solution. Our approach will be to carry out the inversion explicitly on the first three orders only, thereafter deducing a pattern that holds over all orders.

First order

The construction of the first order components of the absorptive-dispersive perturbations α_1 and β_1 from the data (i.e., the solution of equation (31)), and the resulting issues of conditioning, detectability, and relationships with the actual medium perturbations, have been described in detail by Innanen and Weglein (2007), and will not be extensively reviewed here. Briefly put, two profiles, $\alpha_1(z|\vartheta, W)$ and $\beta_1(z|\vartheta, W)$, over layered absorptive media, may be constructed given a single shot-record or receiver record of reflected primary data and the acoustic reference wavespeed c_0, which is assumed to agree with the actual medium at and above the sources and receivers. Since two or more plane wave incidence angles are required to separately construct the profiles, but many varied sets of these angles may do so, we define the quantity $\vartheta = \{\theta_1, \theta_2, ...\}$ to represent the particular set of angles used. In addition, since the freedom also exists to weight the data at each angle, we define W to represent the particular weighting scheme (if any) chosen. The profiles

are then functions of these quantities also. Summarizing, we establish a mapping between $D(k_s, \omega)$ and $\alpha_1(z|\vartheta, W)$, $\beta_1(z|\vartheta, W)$. The mapping is simple, generally a linear combination of Fourier components of the data.

Second order

The second order term in equation (32) is close to a form suitable for the direct non-linear inverse equations. Since the relationships in equations (31)–(33) hold for all k_s and ω, by comparing integrands in equation (32), we see that instances of $\alpha_2 - 2F\beta_2$ occurring under Fourier integrals may be replaced by

$$\begin{aligned}&\alpha_2(z) - 2F(\omega)\beta_2(z)\\ &= -\frac{[-i2q_s]}{2\cos^2\theta}[\alpha_1(z) - 2F(\omega)\beta_1(z)]\left(\int_0^z dz'[\alpha_1(z') - 2F(\omega)\beta_1(z')]\right).\end{aligned} \tag{34}$$

This will be useful for manipulations at third order. We further change variables to θ and $k_z = -2q_s$:

$$\begin{aligned}&\int dz' e^{-ik_z z'}[\alpha_2(z'|\vartheta, W) - 2F(k_z, \theta)\beta_2(z'|\vartheta, W)]\\ &= \frac{-ik_z}{2\cos^2\theta}\int dz' e^{-ik_z z'}[\alpha_1(z'|\vartheta, W) - 2F(k_z, \theta)\beta_1(z'|\vartheta, W)]\\ &\quad\times\left(\int_0^{z'} dz''[\alpha_1(z''|\vartheta, W) - 2F(k_z, \theta)\beta_1(z''|\vartheta, W)]\right),\end{aligned} \tag{35}$$

where we have employed the specific forms for α_1 and β_1 derived above, including the set of angles ϑ and weights W. Since the first order input to the second order term has these dependences, so also must the second order perturbations $\alpha_2 = \alpha_2(z|\vartheta, W)$, $\beta_2 = \beta_2(z|\vartheta, W)$.

Third order

The third order problem requires a greater level of manipulation. The middle two terms in equation (33) may be written alternatively as the sum of

$$\frac{[-i2q_s]^2}{32\cos^4\theta)}\int dz' e^{i2q_s z'}[\alpha_1(z') - 2F(\omega)\beta_1(z')]\left(\int_0^{z'} dz''[\alpha_1(z'') - 2F(\omega)\beta_1(z'')]\right)^2 \tag{36}$$

and

$$\frac{[-i2q_s]^2}{16\cos^4\theta}\int dz' e^{i2q_s z'}[\alpha_1(z') - 2F(\omega)\beta_1(z')]\left(\int_0^{z'} dz''[\alpha_1(z'') - 2F(\omega)\beta_1(z'')]\right)^2. \tag{37}$$

The second of these re-written forms is immediate; to derive the first, we have used the fact that for any integrable function f,

$$\int_{-\infty}^{z} f(z')\int_{-\infty}^{z'} f(z'')dz''dz' = \frac{1}{2}\left(\int_{-\infty}^{z} f(z')dz'\right)^2. \tag{38}$$

The two terms in equation (33) are, then, of the same form, and sum to produce

$$\frac{3[-i2q_s]^2}{32\cos^6\theta}\int dz' e^{i2q_s z'}[\alpha_1(z') - 2F(\omega)\beta_1(z')]\left(\int_0^{z'} dz''[\alpha_1(z'') - 2F(\omega)\beta_1(z'')]\right)^2.$$

This quantity is, in turn, of the same form as that of the last term in equation (33), and so the third order inverse equation may be re-expressed in full as

$$\begin{aligned}&\frac{1}{4\cos^2\theta(k_s,\omega)}\int dz' e^{i2q_s(k_s,\omega)z'}[\alpha_3(z') - 2F(\omega)\beta_3(z')]\\ =&\frac{[-i2q_s(k_s,\omega)]^2}{16\cos^6\theta(k_s,\omega)}\int dz' e^{i2q_s(k_s,\omega)z'}[\alpha_1(z') - 2F(\omega)\beta_1(z')]\\ &\times\left(\int_0^{z'} dz''[\alpha_1(z'') - 2F(\omega)\beta_1(z'')]\right)^2.\end{aligned} \tag{39}$$

Simplifying, and changing variables to k_z and θ, we have

$$\begin{aligned}&\int dz' e^{-ik_z z'}[\alpha_3(z'|\vartheta,W) - 2F(k_z,\theta)\beta_3(z'|\vartheta,W)]\\ =&\frac{[-ik_z]^2}{4\cos^4\theta}\int dz' e^{-ik_z z'}[\alpha_1(z'|\vartheta,W) - 2F(k_z,\theta)\beta_1(z'|\vartheta,W)]\\ &\times\left(\int_0^{z'} dz''[\alpha_1(z''|\vartheta,W) - 2F(k_z,\theta)\beta_1(z''|\vartheta,W)]\right)^2.\end{aligned} \tag{40}$$

Again, since at first and second orders the outputs are functions of the set of angles and weights used in the first order procedure, so must the third order terms, i.e., $\alpha_3 = \alpha_3(z'|\vartheta,W)$ and $\beta_3 = \beta_3(z'|\vartheta,W)$.

Direct non-linear absorptive inversion equations

A pattern is discernible in equations (35) and (40), whose form, like in the forward case, persists at higher order. In fact, α_{n+1} and β_{n+1} are related to α_1 and β_1 via

$$\begin{aligned}&\int dz' e^{-ik_z z'}[\alpha_{n+1}(z'|\vartheta,W) - 2F(k_z,\theta)\beta_{n+1}(z'|\vartheta,W)]\\ &=\frac{1}{n!}\left(\frac{-ik_z}{2\cos^2\theta}\right)^n\\ &\times\int dz' e^{-ik_z z'}[\alpha_1(z'|\vartheta,W) - 2F(k_z,\theta)\beta_1(z'|\vartheta,W)]\\ &\times\left(\int_0^{z'} dz''[\alpha_1(z''|\vartheta,W) - 2F(k_z,\theta)\beta_1(z''|\vartheta,W)]\right)^n.\end{aligned} \tag{41}$$

Defining

$$\begin{aligned}\alpha_P(z|\vartheta,W) &\equiv \sum_{n=0}^{\infty}\alpha_{n+1}(z'|\vartheta,W),\\ \beta_P(z|\vartheta,W) &\equiv \sum_{n=0}^{\infty}\beta_{n+1}(z'|\vartheta,W),\end{aligned} \tag{42}$$

creating an instance of equation (41) for every value of $n \geq 0$, and adding them together, the left-hand side becomes

$$\begin{aligned}&\sum_{n=0}^{\infty}\int dz' e^{-ik_z z'}[\alpha_{n+1}(z'|\vartheta,W) - 2F(k_z,\theta)\beta_{n+1}(z'|\vartheta,W)]\\ =&\int dz' e^{-ik_z z'}[\alpha_P(z'|\vartheta,W) - 2F(k_z,\theta)\beta_P(z'|\vartheta,W)],\end{aligned} \tag{43}$$

and the right-hand side becomes

$$\begin{aligned}&\sum_{n=0}^{\infty}\frac{1}{n!}\left(\frac{-ik_z}{2\cos^2\theta}\right)^n\\ &\times\int dz' e^{-ik_z z'}[\alpha_1(z'|\vartheta,W) - 2F(k_z,\theta)\beta_1(z'|\vartheta,W)]\\ &\times\left(\int_0^{z'} dz''[\alpha_1(z''|\vartheta,W) - 2F(k_z,\theta)\beta_1(z''|\vartheta,W)]\right)^n\\ =&\int dz' e^{-ik_z z'}[\alpha_1(z'|\vartheta,W) - 2F(k_z,\theta)\beta_1(z'|\vartheta,W)]\times\\ &\sum_{n=0}^{\infty}\frac{1}{n!}\left(\frac{-ik_z}{2\cos^2\theta}\int_0^{z'} dz''[\alpha_1(z''|\vartheta,W) - 2F(k_z,\theta)\beta_1(z''|\vartheta,W)]\right)^n\\ =&\int dz' e^{-ik_z\left[z'+\frac{1}{2\cos^2\theta}\int_0^{z'} dz''[\alpha_1(z''|\vartheta,W)-2F(k_z,\theta)\beta_1(z''|\vartheta,W)]\right]}\\ &\times[\alpha_1(z'|\vartheta,W) - 2F(k_z,\theta)\beta_1(z'|\vartheta,W)],\end{aligned} \tag{44}$$

where in the last step we have performed the same collapsing step (devised by Shaw et al. (2004)) that occurred in the forward problem. Equating these two expressions:

$$\begin{aligned}&\int dz' e^{-ik_z z'}[\alpha_P(z'|\vartheta,W) - 2F(k_z,\theta)\beta_P(z'|\vartheta,W)]\\ =&\int dz' e^{-ik_z\left[z'+\frac{1}{2\cos^2\theta}\int_0^{z'} dz''[\alpha_1(z''|\vartheta,W)-2F(k_z,\theta)\beta_1(z''|\vartheta,W)]\right]}\\ &\times[\alpha_1(z'|\vartheta,W) - 2F(k_z,\theta)\beta_1(z'|\vartheta,W)],\end{aligned} \tag{45}$$

we form the basic equations of direct non-linear inversion for absorptive-dispersive primaries.

Appendix C: Absorptive model construction via non-linear direct inversion

The aim of inverse scattering procedures varies from the construction of spatial distributions of perturbation quantities to the construction of processed data sets. The direct non-linear primary inversion quantities derived in Appendix B lend themselves to either goal. In this appendix we will address the former of these aims for layered, 2-parameter absorptive-dispersive media.

We begin with a straightforward manipulation of equation (45). Recognizing the left-hand side as a Fourier transform, we have

$$\alpha_P(k_z|\vartheta,W) - 2F(k_z,\theta)\beta_P(k_z|\vartheta,W) = \Delta(k_z,\theta|\vartheta,W), \tag{46}$$

where we define

$$\begin{aligned}\Delta(k_z,\theta|\vartheta,W) \equiv \\ \int dz' e^{-ik_z\left[z' + \frac{1}{2\cos^2\theta}\int_0^{z'} dz''[\alpha_1(z''|\vartheta,W) - 2F(k_z,\theta)\beta_1(z''|\vartheta,W)]\right]} \\ \times [\alpha_1(z'|\vartheta,W) - 2F(k_z,\theta)\beta_1(z'|\vartheta,W)].\end{aligned} \tag{47}$$

We wish to separately calculate α_P and β_P at each relevant depth wavenumber k_z; given at least two angles per depth wavenumber k_z, and, if desired, an additional weighting scheme, this is an over-determined problem. Some notational care will be required, because, as we see in equations (46)-(47), an earlier set of angles and weights, $\vartheta = \{\theta_1, \theta_2, ...\}$ and W, is already in play.

We proceed by defining a new set of angles $\widetilde{\vartheta} = \{\widetilde{\theta}_1, \widetilde{\theta}_2, ...\} \neq \vartheta$ and weights $\widetilde{W} \neq W$. There is no formal requirement that $\widetilde{\vartheta}$ and $\widetilde{W}$ be related in any way to ϑ and W. During the numerical application of the direct Q compensation algorithms in this paper we have argued towards a relationship for that specific situation, but in general they are distinct and un-related. Consequently, the results in this appendix are considered a function of both.

Given the $N > 2$ angles $\widetilde{\vartheta}$, the N resulting instances of equation (46) may be written in matrix form:

$$\mathbf{F}(k_z,\widetilde{\vartheta}) \begin{bmatrix} \alpha_P(k_z|\vartheta,W) \\ \beta_P(k_z|\vartheta,W) \end{bmatrix} = \mathbf{\Delta}(k_z,\widetilde{\vartheta}|\vartheta,W), \tag{48}$$

where

$$\mathbf{F}(k_z,\widetilde{\vartheta}) = \begin{bmatrix} 1 & -2F(k_z,\widetilde{\theta}_1) \\ 1 & -2F(k_z,\widetilde{\theta}_2) \\ \vdots & \vdots \\ 1 & -2F(k_z,\widetilde{\theta}_N) \end{bmatrix}, \tag{49}$$

and

$$\mathbf{\Delta}(k_z,\widetilde{\vartheta}|\vartheta,W) = \begin{bmatrix} \Delta(k_z,\widetilde{\theta}_1|\vartheta,W) \\ \Delta(k_z,\widetilde{\theta}_2|\vartheta,W) \\ \vdots \\ \Delta(k_z,\widetilde{\theta}_N|\vartheta,W) \end{bmatrix}. \tag{50}$$

A new weighting scheme $\widetilde{W}$ may be brought in via whatever choices are made in inverting $\mathbf{F}(k_z, \widetilde{\vartheta})$. That is, $\mathbf{F}^{-1} = \mathbf{F}^{-1}(k_z, \widetilde{\vartheta}, \widetilde{W})$. Now, this means that the outputs α_P and β_P are dependent on k_z, but also on (1) the weights and angles used to create the linear output, ϑ and W, and on (2) the weights and angles used above to create the non-linear output, $\widetilde{\vartheta}$ and $\widetilde{W}$. That is,

$$\left[\begin{array}{c} \alpha_P(k_z|\widetilde{\vartheta}, \widetilde{W}, \vartheta, W) \\ \beta_P(k_z|\widetilde{\vartheta}, \widetilde{W}, \vartheta, W) \end{array} \right] = \mathbf{F}^{-1}(k_z, \widetilde{\vartheta}, \widetilde{W}) \mathbf{\Delta}(k_z, \widetilde{\vartheta}|\vartheta, W). \tag{51}$$

Finally, profiles may be generated through inverse Fourier transforms:

$$\begin{aligned} \alpha_P(z|\widetilde{\vartheta}, \widetilde{W}, \vartheta, W) &= \frac{1}{2\pi} \int dk_z e^{ik_z z} \alpha_P(k_z|\widetilde{\vartheta}, \widetilde{W}, \vartheta, W), \\ \beta_P(z|\widetilde{\vartheta}, \widetilde{W}, \vartheta, W) &= \frac{1}{2\pi} \int dk_z e^{ik_z z} \beta_P(k_z|\widetilde{\vartheta}, \widetilde{W}, \vartheta, W). \end{aligned} \tag{52}$$

The freedom to *twice* choose both the subsets of the data we use, and their weights, during the calculation of the profiles in equation (52), suggests a large range of types of inverse result is possible.

An analytic example of direct non-linear Q compensation

J. E. Lira and K. A. Innanen, M-OSRP, University of Houston

Abstract

Q compensation signifies processing of a seismic data set such that its events are corrected for the decaying and broadening influence of absorptive wave propagation. Qualitatively, the process "sharpens" these events, and enhances resolution. The inverse scattering series has been investigated for its potential to permit Q-compensation to occur directly and nonlinearly in terms of data, absent of an accurate input Q model. Several candidate procedures have been suggested, all acting more or less consistently on the data. In this paper we create an analytic data set, input it into one of these prototype algorithms, and analyze the resulting mathematics. We clarify the influence of the integral over shallow data events on the "sharpening" of deeper events. This represents the first analytic study of inverse scattering-based Q-compensation.

1 Introduction

In this second of two papers on the subject in the current M-OSRP volume, we provide an analytic example of direct non-linear Q compensation. In previous research, linear and non-linear inverse scattering have been analyzed (Innanen and Weglein, 2003a,b, 2005, 2007; Innanen and Lira, 2008) with an aim to extract and separately pose algorithms for Q compensation of reflected seismic primaries. Several distinct proto-type algorithms have been produced and considered with respect to their basic behavior and their potential for practical use. One important early example, derived in close analogy to the direct non-linear imaging research that was progressing at that time (Weglein et al., 2001; Shaw et al., 2004), is particularly well-suited to analysis, although it involves the use of a drastically oversimplified Earth model. Numerical testing of this version of direct non-linear Q compensation (Innanen and Weglein, 2005) was sufficiently encouraging to lead to continued development of the theory to more complex cases; however, much of that algorithm's potential for analytical investigation has so far remained un-exploited.

We investigate this prototype algorithm using analytic data. Because the analysis takes place in time, frequency, wavenumber, and pseudo-depth domains, we use a simple, non-dispersive model of attenuation which has simple, analytic forms in each of these domains. Other methods deriving from non-linear inverse scattering have been understandable in terms of the multiplicative action of data sets on themselves: e.g., free-surface multiples are predicted via the combination of primary sub-events when the data traces are convolved with themselves. The potential value of the current study is to begin to provide the inverse scattering Q compensation machinery a similar description. In short, to provide intuitive as well as formal explanations for how a data-driven Q compensation algorithm behaves.

1.1 Inverse scattering series and absorption

Inverse scattering admits a wide range of linear/convolutional wave propagation models, including many anelastic types (Weglein et al., 2003), which include linear viscoelastic and other anelastic models. The literature contains a limited set of studies on linearized inversion of attenuated seismic data, generally constrained, for instance with an assumed velocity model, for Q profiles (Carrion and VerWest, 1987). These studies, while not precisely useful for our non-linear purposes, have however generated the important result that an anelastic medium with unknown variation in both space and frequency cannot be determined.

1.2 Direct linear inversion

The linear component of the inverse scattering series relates the measured data to the first-order estimate of the perturbation. If the perturbation is small, this component may form the basis for the linear Born inverse approximation; however, if it is large and extended, this construction may be viewed as essentially a linear transformation and weighting of the data, in preparation for use as input to the higher order terms.

To derive direct non-linear Q compensation operators from high order parts of the inverse scattering series requires a well-posed linear inverse procedure designed to accommodate perturbations in absorptive parameters (e.g., Q) as well as any other relevant elastic/acoustic parameters (e.g., wavespeed, or bulk modulus). A 2-parameter multidimensional procedure of this kind for use with pre-stack reflection seismic data has been described by Innanen and Weglein (2007). We will make use of essentially that theory, reduced to the case of variations in a single parameter (Q) and data from a normally-incident wave.

1.3 A prototype direct non-linear Q compensation procedure

Weglein et al. (2001) proposed using the inverse scattering series to process primaries in a task-separated way, in particular to accomplish imaging of reflectors. Shaw et al. (2004) and Shaw (2005) presented a closed-form for a task specific sub-series for imaging primaries, the *leading order imaging series*, which for moderate perturbations locates the medium's reflectors at depth and without *a priori* information about the medium. On the assumption that the wave attenuation is corrected-for by similar inverse scattering terms to those which correct for the phase issues in imaging, Innanen and Weglein (2005) presented an analogous prototype algorithm, a *leading order Q compensation* subseries, a task specific sub-series for correcting the effect of absorption in the seismic data. The formula is:

$$D_C(z) = \int_{-\infty}^{\infty} e^{ik_z\left[z - \frac{1}{2}\int_0^z \beta_1(z')dz'\right]} D(k_z)dk_z, \tag{1}$$

where β_1 is a weighted integral of the data:

$$\beta_1(z) = 4\int_0^z D(z')dz', \tag{2}$$

D (the input data) and D_C (the output, Q compensated data) are expressed in the pseudo-depth domain[1], and $k_z = \frac{2\omega}{c_0}$ is a wavenumber conjugate to pseudo-depth. Innanen and Weglein (2005) presented encouraging numerical tests with the algorithm in equation (1), showing a significant level of Q-compensation in their results. Equation (1) does not form the basis for the current multi-parameter form of direct non-linear Q compensation (Innanen and Lira, 2008), i.e., the latter does not reduce to equation (1). However, the two approaches are qualitatively similar, and the insight we gain from studying this carries over to all current candidate algorithms.

2 Direct non-linear Q compensation: the algorithm

In equation (1), it is true that:

- β_1 and data are the only input, and the latter is computed directly from smoothed and attenuated data;
- Since, by construction β_1 is complex, equation (1) amounts to the application of an operator that contains the cumulative effect of Q down to a given z, magnifying the large wavenumber components of the data $D(k_z)$.

In this paper, we analyze the same equation, but instead of computing it numerically we define an analytic expression for the input data in an absorptive medium. The analytic data are used as input for the computation of D_C, which is the Q-compensated data.

3 Analytic data

In this section we provide an analytic data set, using a simple expression for a non-dispersive pulse propagating in an absorptive medium discussed by Aki and Richards (2002):

$$p(x,t) = \frac{1}{\pi}\left[\frac{\frac{x}{2cQ}}{\left(\frac{x}{2cQ}\right)^2 + \left(\frac{x}{c} - t\right)^2}\right]. \tag{3}$$

The pulse shape of equation (3) for an arrival time of 1.37 s is illustrated in Figure 1.

[1] A scaled version of time based on the homogeneous reference wavespeed c_0.

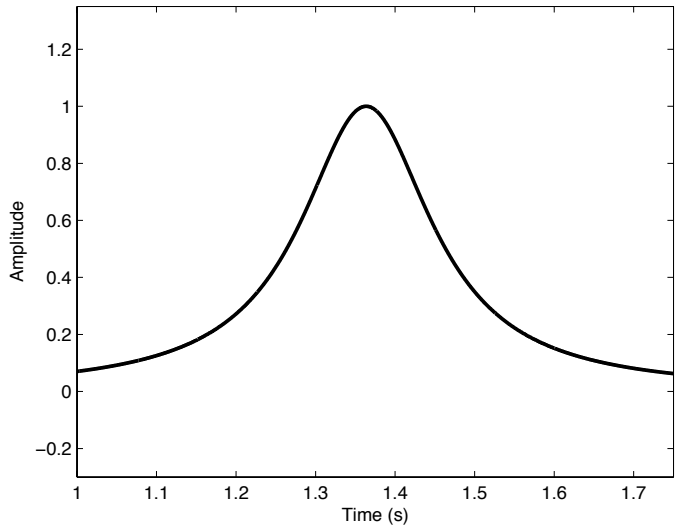

Figure 1: An illustration showing a pulse based on the model of a pulse propagating in an absorptive medium (Aki and Richards, 2002)

Aki and Richards (2002) point out that this wave is non-causal and it is symmetric, neither of which agrees with physics or experiment. However, it is analytically expressible in time, frequency and wavenumber domains, a requirement for this study.

3.1 A qualitative view of the sharpness of the pulse

The goal in this paper is to observe in the mathematics the sharpening of attenuated events. We begin therefore with a discussion of what "more" vs. "less" attenuated means in the context of events whose amplitudes and arrival times are described by equation (3). An observation: the lower the value of Q, the greater must be the attenuation. In equation (3) this effect is produced by the numerator and the first term in the denominator. The second term in the denominator fixes the arrival time. Notice that if a further quantity Δ was formally introduced to p:

$$p(x,t) = \frac{1}{\pi}\left[\frac{\frac{x}{2cQ} - \Delta}{\left(\frac{x}{2cQ} - \Delta\right)^2 + \left(\frac{x}{c} - t\right)^2}\right], \tag{4}$$

it would tend to act to alter the width, or sharpness, of the pulse. We see from Figures 1 and 2 that by changing Δ in the term $\left[\frac{x}{2cQ} - \Delta\right]$, we change the shape of the pulse, sharpening or broadening it as we increase or decrease Δ respectively. We will return to this qualitative observation in the following to interpret the non-linear operation of inverse scattering Q compensation machinery.

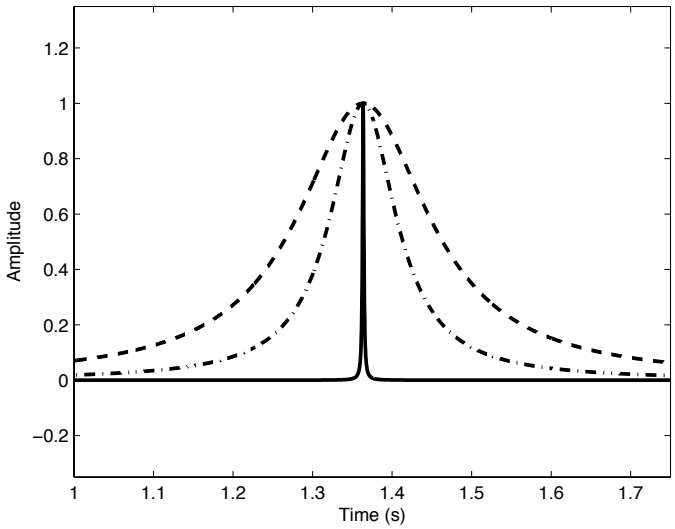

Figure 2: An illustration showing the same pulse of Figure 1 for the three different values of the term $\left(\frac{x}{2cQ} - \Delta\right)$ in equation (4). The values are: 0.1 for the outermost curve, 0.05 for the intermediate curve and 0.001 for the innermost curve.

3.2 Modeling two primaries reflecting at normal incidence from an absorptive layer

We next use the above results to forward model two primaries reflecting from the layer illustrated in Figure 3. To keep the data aligned with the assumptions within equation (1), the reflections are due to contrasts in Q only.

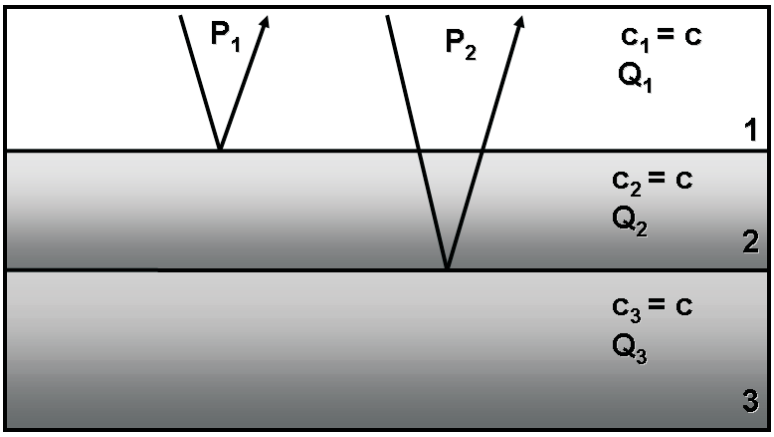

Figure 3: The constant velocity absorptive 1-D model assumed for the generation of the analytical data, where the only parameter permitted to change was the absorption parameter Q and with a non-absorptive layer 1. The synthetic data-set is comprised by the two primaries P_1 and P_2.

The parameter Q for layer 1 is chosen to be essentially infinity, hence no absorption takes place in that layer, i.e., we assume an acoustic reference medium. The data with two primaries may be expressed analytically as:

$$P(t) = P_1(t) + P_2(t), \tag{5}$$

where

$$P_1(t) = \frac{R_1}{\pi}\delta(t - t_1) \tag{6}$$

$$P_2(t) = \frac{T_{12}R_2T_{21}}{\pi}\frac{\left(\frac{z_2-z_1}{cQ_2}\right)}{\left(\frac{z_2-z_1}{cQ_2}\right)^2 + (t_2 - t)^2}, \tag{7}$$

where $t_1 = \frac{2z_1}{c}$, $t_2 = t_1 + \frac{2(z_2-z_1)}{c}$, $R_1 = \frac{k_1-k_2}{k_1+k_2}$, $R_2 = \frac{k_2-k_3}{k_2+k_3}$, $T_{12} = \frac{2k_1}{k_1+k_2}$, $T_{21} = \frac{2k_2}{k_1+k_2}$ and $k_i = \frac{\omega}{c}\left(1 + \frac{i}{2Q_i}\right)$.

4 Analytic example of direct non-linear Q-compensation

In order to use the attenuated data set in equation (5) as input into the processing formula in equation (1), it first needs to be linearly manipulated to correspond with the two appearances of data on the right-hand side of equation (1). To generate $D(k_z)$, we Fourier transform equation (5) and change variables from ω to k_z:

$$\begin{aligned} D(k_z) &= P_1(k_z) + P_2(k_z) \\ &= \frac{R_1}{2\pi}e^{-ik_zz_1}e^{-\frac{z_1}{2Q_1}k_z} + \frac{T_{12}R_2T_{21}}{2\pi}e^{-ik_zz_2}e^{-k_z\left(\frac{z_1}{2Q_1}+\frac{(z_2-z_1)}{2Q_2}\right)}. \end{aligned} \tag{8}$$

Next we use equations (5) and (2) to determine $\beta_1(z)$:

$$\begin{aligned}\beta_1(z) &= 4\int_0^z [P_1(z') + P_2(z')]dz' = \\ &= 4\int_0^z \left[\frac{R_1}{2\pi^2}\frac{\left(\frac{z_1}{2Q_1}\right)}{\left(\frac{z_1}{2Q_1}\right)^2 + (z'-z_1)^2} + \frac{T_{12}R_2T_{21}}{2\pi^2}\frac{\left(\frac{z_1}{2Q_1} + \frac{(z_2-z_1)}{2Q_2}\right)}{\left(\frac{z_1}{2Q_1} + \frac{(z_2-z_1)}{2Q_2}\right)^2 + (z'-z_2)^2}\right] dz'. \quad (9)\end{aligned}$$

For details of this mathematics see Appendix A.

The deeper of the two primaries, $P_2(t)$, is the event that will be corrected in this example (since no reflected wave arrives before $P_1(t)$, the non-linear operator will, correctly, have no influence on P_1). To simplify the analysis, we therefore retain only $P_2(k_z)$ as data to be operated on. Equation (1) is used in the form:

$$P_{2C}(z) = \int_{-\infty}^{\infty} e^{ik_z\left[z - \frac{1}{2}\int_0^z \beta_1(z')dz'\right]} P_2(k_z)dk_z. \quad (10)$$

Evaluating equation (10) results in:

$$P_{2_C}(z) = 2\frac{T_{12}R_2T_{21}}{\pi}\frac{\left(\frac{(z_2-z_1)}{2Q_2} - \Gamma_q(z)\right)}{\left(\frac{(z_2-z_1)}{2Q_2} - \Gamma_q(z)\right)^2 + (z-z_2)^2}, \quad (11)$$

where

$$\begin{aligned}\Gamma_q(z) &= 2\left(\frac{T_{12}R_2T_{21}}{\pi^2}\right)\left[\left(\frac{(z_2-z_1)}{2Q_2}\right)\left(\arctan\left(\frac{z-z_2}{\frac{(z_2-z_1)}{2Q_2}}\right)\left(\frac{z-z_2}{\frac{(z_2-z_1)}{2Q_2}}\right)\right.\right. \\ &\quad + \ln\left(\frac{\frac{(z_2-z_1)}{2Q_2}}{\sqrt{\left(\frac{(z_2-z_1)}{2Q_2}\right)^2 + (z-z_2)^2}}\right) - \arctan\left(\frac{-z_2}{\frac{(z_2-z_1)}{2Q_2}}\right)\left(\frac{-z_2}{\frac{(z_2-z_1)}{2Q_2}}\right) \\ &\quad \left.\left. - \ln\left(\frac{\frac{(z_2-z_1)}{2Q_2}}{\sqrt{\left(\frac{(z_2-z_1)}{2Q_2}\right)^2 + (-z_2)^2}}\right)\right) - \arctan\left(\frac{-z_2}{\frac{(z_2-z_1)}{2Q_2}}\right) z\right]. \quad (12)\end{aligned}$$

The full mathematics of this derivation is in Appendix A.

The interest is to compare the attenuated event before compensation and after compensation. We re-write equations (7) and (11) together to make the comparison easier. Before compensation, the attenuated event in the pseudo-depth domain has the form

$$P_2(z) = \frac{T_{12}R_2T_{21}}{\pi}\frac{\left(\frac{(z_2-z_1)}{2Q_2}\right)}{\left(\frac{(z_2-z_1)}{2Q_2}\right)^2 + (z-z_2)^2}, \quad (13)$$

and after compensation, it has the form

$$P_{2_C}(z) = 2\frac{T_{12}R_2T_{21}}{\pi}\frac{\left(\frac{(z_2-z_1)}{2Q_2} - \Gamma_q(z)\right)}{\left(\frac{(z_2-z_1)}{2Q_2} - \Gamma_q(z)\right)^2 + (z-z_2)^2}. \tag{14}$$

They are equal, except for the term $\Gamma_q(z)$ in equation (13). Notice that this term, which is a function only of the input data and reference velocity, plays a role similar to that of Δ in equation (4).

Evidently the mathematical activity of direct non-linear Q compensation involves a conferring, on a given primary, of accumulated amplitudes from shallower primaries precisely into the parts of the data phase and amplitude in which the breadth of the pulse is determined.

5 Plots of the analytic results

In this section we present synthetic examples showing three cases representing media with the Q profile representing low attenuation, large Q, to high attenuation, small Q. Table 1 contains the parameter values of each data set:

Depth (m)	c (m/s)	1	2	3	Q_i
000-1500	2200	∞	∞	∞	Q_1
1500-2500	2200	200	150	100	Q_2
2500-∞	2200	50	50	50	Q_3

Table 1. *Absorptive Earth models.*

Since the absorptive effects are present only in P_2, as in the analytic results we plot only this primary. Figure 4 illustrates P_2 for each model.

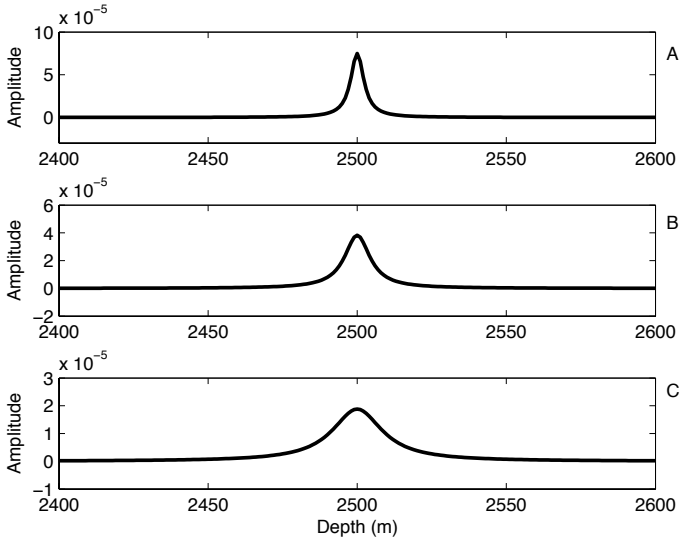

Figure 4: The attenuated primary P_2 for each Q-profiles in table 1. (A) The low attenuation Q-profile, (B) the intermediate attenuation Q-profile, and (C) the high attenuation Q-profile.

We next plot the correction of these P_2 events, *i.e*, the left-hand side of equation (13). We plot in Figure 6, the actual primaries for each one of the Q-profiles of Table 1, and the corresponding corrected one, normalizing both at their maximum amplitudes.

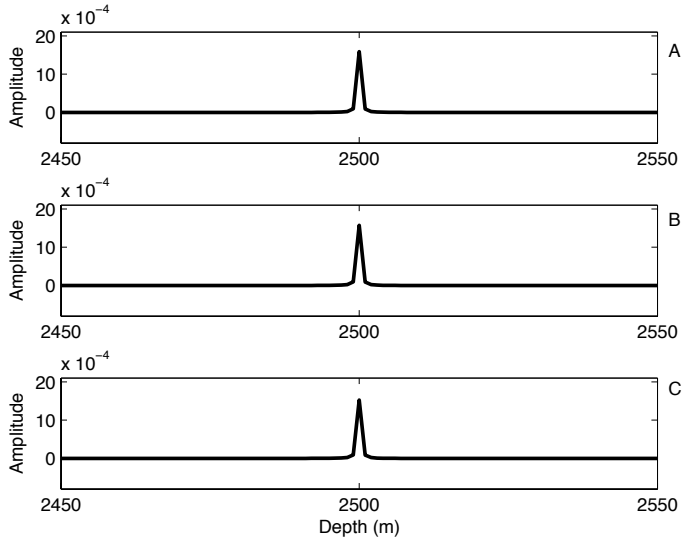

Figure 5: An illustration showing the corrected primary $P_{2C}(z)$ in equation (13) generated by the solution of the leading order Q-compensation sub-series represented by equation (1) for all the three Q-profiles listed in table 1. (A) The low attenuation Q-profile, (B) the intermediate attenuation Q-profile, and (C) the high attenuation Q-profile.

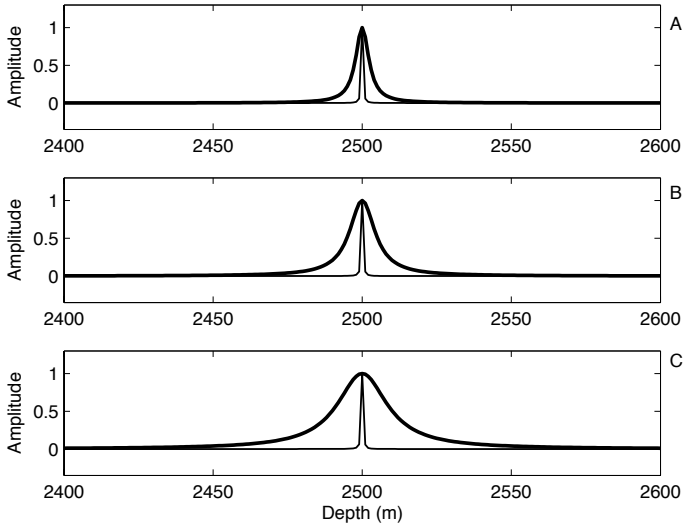

Figure 6: An illustration showing the original primary P_2 (solid line) and the corrected primary P_{2C} (bold solid line) for all the three Q-profiles listed in table 1. (A) The low attenuation Q-profile, (B) the intermediate attenuation Q-profile, and (C) the high attenuation Q-profile.

References

Aki, K. and P. G. Richards. *Quantitative Seismology*. 2nd edition. University Science Books, 2002.

Carrion, P. M. and B. VerWest. "A procedure for inverting seismic data to obtain Q-profiles." *Inverse Problems* (1987): 65–71.

Innanen, K. A. and J. E. Lira. "Direct non-linear Q compensation of primaries in layered media: Theory and synthetic examples." *Proceedings of the 78th Annual Meeting of the Society of Exploration Geophysicists, Las Vegas, Nevada.* . Soc. Expl. Geophys., 2008.

Innanen, K. A. and A. B. Weglein. "Construction of absorptive/dispersive wave fields with the forward scattering series." *Journal of Seismic Exploration* 12 (2003): 259–282.

Innanen, K. A. and A. B. Weglein. "Simultaneous Imaging and Inversion with the Inverse Scattering Series." *Proceedings of the Eighth International Congress of the SBGf and Fifth Latin American Geophysical Conference.* . SBGf, 2003.

Innanen, K. A. and A. B. Weglein. "Non-linear construction of a Q-compensation operator directly from measured reflection data." *2004 Mission Oriented Seismic Research Program Annual Report* (2005): 282–293.

Innanen, K. A. and A. B. Weglein. "On the construction of an absorptive-dispersive medium model via direct linear inversion of reflected seismic primaries." *Inverse Problems* (2007): 2289–2310.

Shaw, S. A. *An inverse scattering series algorithm for depth imaging of reflection data from a layered acoustic medium with an unknown velocity model*. PhD thesis, University of Houston, 2005.

Shaw, S. A., A. B. Weglein, D. J. Foster, K. H. Matson, and R. G. Keys. "Isolation of a leading order depth imaging series and analysis of its convergence properties." *Journal of Seismic Exploration* 2 (November 2004): 157–195.

Weglein, A. B., D. J. Foster, K. H. Matson, S. A. Shaw, P. M. Carvalho, and D. Corrigan. "An inverse-scattering sub-series for predicting the spatial location of reflectors without the precise reference medium and wave velocity." *71st Annual Internat. Mtg., Soc. Expl. Geophys., Expanded Abstracts.* . Soc. Expl. Geophys., 2001. 2108–2111.

Weglein, Arthur B., Fernanda V. Araújo, Paulo M. Carvalho, Robert H. Stolt, Kenneth H. Matson, Richard T. Coats, Dennis Corrigan, Douglas J. Foster, Simon A. Shaw, and Haiyan Zhang. "Inverse Scattering Series and Seismic Exploration." *Inverse Problems* (2003): R27–R83.

Appendix A. The mathematics of the analytic Q compensation example

In this section we derive the mathematical forms for $\beta_1(z)$ seen in equation (9) and $\Gamma_q(z)$ seen in equation (12). First we calculate $\beta_1(z)$ in the pseudo-depth domain. We start by Fourier

transforming the shallower primary in equation (6). We have

$$P_1(\omega) = \int_{-\infty}^{\infty} \frac{R_1}{\pi} \frac{\left(\frac{z_1}{c_1 Q_1}\right) e^{-i\omega t} dt}{\left(\frac{z_1}{c_1 Q_1}\right)^2 + \left(\frac{2z_1}{c_1} - t\right)^2}, \tag{15}$$

hence, letting $\tau = \frac{2z_1}{c_1 Q_1} - t$ and $d\tau = -dt$,

$$\begin{aligned} P_1(\omega) &= \frac{-R_1}{\pi} \int_{\infty}^{-\infty} \frac{\left(\frac{z_1}{c_1 Q_1}\right) e^{-i\omega\left(\frac{2z_1}{c_1} - \tau\right)} d\tau}{\left(\frac{z_1}{c_1 Q_1}\right)^2 + \tau^2} \\ &= \frac{R_1}{\pi} e^{-i\omega \frac{2z_1}{c_1}} \int_{-\infty}^{\infty} \frac{\left(\frac{z_1}{c_1 Q}\right) e^{-i\omega\tau} d\tau}{\left(\frac{z_1}{c_1 Q}\right)^2 + \tau^2}, \end{aligned} \tag{16}$$

which can be immediately evaluated:

$$P_1(\omega) = \frac{R_1}{2\pi} e^{-i\omega \frac{2z_1}{c_1}} e^{-\frac{z_1}{c_1 Q_1}|\omega|}. \tag{17}$$

Then we similarly transform the deeper primary in equation (7):

$$\begin{aligned} P_2(\omega) &= \frac{T_{12} R_2 T_{21}}{\pi} \int_{-\infty}^{\infty} \frac{\left(\frac{z_1}{c_1 Q_1} + \frac{z_2 - z_1}{c_1 Q_2}\right) e^{-i\omega t} dt}{\left(\frac{z_1}{c_1 Q_1} + \frac{z_2 - z_1}{c_1 Q_2}\right)^2 + \left(\frac{2z_1}{c_1} + \frac{2(z_2 - z_1)}{c_1} - t\right)^2} \\ &= \frac{T_{12} R_2 T_{21}}{2\pi} \left[e^{-i\omega\left(\frac{2z_2}{c_1}\right)} e^{-\left(\frac{z_1}{c_1 Q_1} + \frac{(z_2 - z_1)}{c_1 Q_2}\right)} \right]. \end{aligned} \tag{18}$$

We next change variables from ω to $k_z = 2\omega / c_0$:

$$P_1(k_z) = \frac{R_1}{2\pi} e^{-ik_z z_1} e^{-\frac{z_1}{2Q_1} k_z} \tag{19}$$

$$P_2(k_z) = \frac{T_{12} R_2 T_{21}}{2\pi} e^{-ik_z z_2} e^{-k_z\left(\frac{z_1}{2Q_1} + \frac{(z_2 - z_1)}{2Q_2}\right)}. \tag{20}$$

Finally, we inverse Fourier transform over k_z to the pseudo-depth domain. For the first primary we obtain

$$P_1(z) = \frac{1}{2\pi} \int_{-\infty}^{\infty} \left(\frac{R_1}{2\pi}\right) e^{-ik_z z_1} e^{-k_z \frac{z_1}{2Q_1}} e^{ik_z} dk_z \tag{21}$$

$$= \frac{R_1}{2\pi} \left[\frac{1}{2\pi} \int_{-\infty}^{\infty} e^{-k_z \frac{z_1}{2Q_1}} e^{ik_z (z - z_1)} dk_z \right], \tag{22}$$

or, evaluating the integral,

$$P_1(z) = \frac{R_1}{2\pi^2} \frac{\left(\frac{z_1}{2Q_1}\right)}{\left(\frac{z_1}{2Q_1}\right)^2 + (z - z_1)^2}. \tag{23}$$

Following the same procedure for $P_2(z)$ we have:

$$P_2(z) = \frac{T_{12}R_2T_{21}}{2\pi^2} \frac{\left(\frac{z_1}{2Q_1} + \frac{(z_2-z_1)}{2Q_2}\right)}{\left(\frac{z_1}{2Q_1} + \frac{(z_2-z_1)}{2Q_2}\right)^2 + (z-z_2)^2}. \tag{24}$$

To calculate $\beta_1(z)$ we need to weight and integrate the data in z domain, $[P_1(z) + P_2(z)]$ as in equation (2):

$$\begin{aligned}
\beta_1(z) &= 4\int_0^z [P_1(z') + P_2(z')]dz' \\
&= 4\int_0^z \left[\underbrace{\frac{R_1}{2\pi^2} \frac{\left(\frac{z_1}{2Q_1}\right)}{\left(\frac{z_1}{2Q_1}\right)^2 + (z'-z_1)^2}}_{A} + \underbrace{\frac{T_{12}R_2T_{21}}{2\pi^2} \frac{\left(\frac{z_1}{2Q_1} + \frac{(z_2-z_1)}{2Q_2}\right)}{\left(\frac{z_1}{2Q_1} + \frac{(z_2-z_1)}{2Q_2}\right)^2 + (z'-z_2)^2}}_{B} \right] dz'.
\end{aligned}$$

Integrating A and B separately, we have:

$$\begin{aligned}
A &= \int_0^z \left(\frac{R_1}{2\pi^2} \frac{\left(\frac{z_1}{2Q_1}\right)}{\left(\frac{z_1}{2Q_1}\right)^2 + (z'-z_1)^2} \right) dz' && (25) \\
&= \frac{R_1}{2\pi^2} \left(\arctan\left(\frac{z-z_1}{z_1/2Q_1}\right) - \arctan(-2Q_1) \right), && (26)
\end{aligned}$$

and

$$\begin{aligned}
B &= \int_0^z \left(\frac{T_{12}R_2T_{21}}{2\pi^2}\right) \frac{\frac{z_1}{2Q_1} + \frac{(z_2-z_1)}{2Q_2}}{\left(\frac{(z_2-z_1)}{2Q_2}\right)^2 + (z'-z_2)^2} && (27) \\
&= \left(\frac{T_{12}R_2T_{21}}{2\pi^2}\right) \left(\arctan\left[\frac{(z-z_2)}{\frac{z_1}{2Q_1} + \frac{(z_2-z_1)}{2Q_2}}\right] - \arctan\left[\frac{-z_2}{\frac{z_1}{2Q_1} + \frac{(z_2-z_1)}{2c_2Q_2}}\right] \right),
\end{aligned}$$

hence

$$\begin{aligned}
\beta_1(z) = \; 4 \; & \left(\left[\frac{R_1}{2\pi^2} \left(\arctan\left(\frac{z-z_1}{z_1/2Q_1}\right) - \arctan(-2Q_1) \right) \right] \right. && (28) \\
& \left. + \left(\frac{T_{12}R_2T_{21}}{2\pi^2}\right) \left(\arctan\left[\frac{(z-z_2)}{\frac{z_1}{2Q_1} + \frac{(z_2-z_1)}{2Q_2}}\right] - \arctan\left[\frac{-z_2}{\frac{z_1}{2Q_1} + \frac{(z_2-z_1)}{2Q_2}}\right] \right) \right).
\end{aligned}$$

To enact the direct non-linear Q compensation in equation (1), we next must use this result to calculate $\int_0^z \beta_1(z')dz'$:

$$\begin{aligned}
&\int_0^z \beta_1(z')dz' \\
&=4\left[\left(\frac{R_1}{2\pi^2}\right)\left(\left(\frac{z_1}{2Q_1}\right)\left(\arctan\left(\frac{z-z_1}{z_1/2Q_1}\right)\left(\frac{z-z_1}{z_1/2Q_1}\right)+\ln\left(\frac{z_1/2Q_1}{\sqrt{(z-z_1)^2+(z_1/2Q_1)^2}}\right)\right.\right.\right. \\
&\quad\left.\left.\left.-\ \arctan(-2Q_1)(-2Q_1)-\ln\left(\frac{z_1/2Q_1}{\sqrt{z_1^2+(z_1/2Q_1)^2}}\right)\right)-\arctan(-2Q_1)z\right)\right. \\
&\quad+\left(\frac{T_{12}R_2T_{21}}{2\pi^2}\right)\left(\left(\frac{z_1}{2Q_1}+\frac{(z_2-z_1)}{2Q_2}\right)\left(\arctan\left(\frac{z-z_2}{\frac{z_1}{2Q_1}+\frac{(z_2-z_1)}{2Q_2}}\right)\left(\frac{z-z_2}{\frac{z_1}{2Q_1}+\frac{(z_2-z_1)}{2Q_2}}\right)\right.\right. \\
&\quad+\ln\left(\frac{\frac{z_1}{2Q_1}+\frac{(z_2-z_1)}{2Q_2}}{\sqrt{\left(\frac{z_1}{2Q_1}+\frac{(z_2-z_1)}{2Q_2}\right)^2+(z-z_2)^2}}\right)-\arctan\left(\frac{-z_2}{\frac{z_1}{2Q_1}+\frac{(z_2-z_1)}{2Q_2}}\right)\left(\frac{-(z_1+(z_2-z_1))}{\frac{z_1}{2Q_1}+\frac{(z_2-z_1)}{2Q_2}}\right) \\
&\quad\left.\left.-\ln\left(\frac{\frac{z_1}{2Q_1}+\frac{(z_2-z_1)}{2Q_2}}{\sqrt{\left(\frac{z_1}{2Q_1}+\frac{(z_2-z_1)}{2Q_2}\right)^2+(-z_2))^2}}\right)\right)-\arctan\left(\frac{-(z_2)}{\frac{z_1}{2Q_1}+\frac{(z_2-z_1)}{2Q_2}}\right)(z)\right)\right].
\end{aligned} \tag{29}$$

In calculating equation (1), the above result will be included in the argument of the exponential function, and that exponential will operate on the data in the k_z domain. Innanen and Weglein (2005) presented the algorithm in a slightly different way, involving effectively the anti-derivative of both sides of equation (1). This leads to the use of $\beta_1(k_z)$ rather than $D(k_z)$ under the integral. We will perform our calculation with this β_1 form, and return to the data form afterwards with a derivative operation. In our analytic example, the part of the integrand to be operated on becomes

$$\begin{aligned}
\beta_1(k_z) &= -4\frac{D(\frac{c_1}{2}k_z)}{ik_z} \\
&= -4\frac{P_1(\frac{c_1}{2}k_z)+P_2(\frac{c_1}{2}k_z)}{ik_z} \\
&= -\frac{4}{ik_z}\left[\frac{R_1}{2\pi}\left(e^{-iz_1k_z}e^{-\frac{z_1}{2Q_1}k_z}\right)+\frac{T_{12}R_2T_{21}}{2\pi}\left(e^{-ik_zz_2}e^{-\left(\frac{z_1}{2Q_1}+\frac{(z_2-z_1)}{2Q_2}\right)k_z}\right)\right].
\end{aligned} \tag{30}$$

With equations (29) and (30) in hand, we may finally solve the Q compensation integral

$$\int_{-\infty}^{\infty} e^{ik_z\left(z-\frac{1}{2}\int_0^z \beta_1(z')dz'\right)}\beta_1(k_z)dk_z. \tag{31}$$

To make this process tractable, we point out a critical issue with regards to reflection coefficients from contrasts in Q only. Consider the reflection coefficient R_1 due to the contrast between layers

1 and 2 in Figure 3, in which we assume Q_1 is essentially infinite. It is straightforward to show that

$$R_1 = \frac{i(2Q_2)^{-1}}{2 + i(2Q_2)^{-1}} = \frac{i}{4Q_2} + \frac{1}{16Q_2^2} + ..., \tag{32}$$

i.e., that to a high degree of accuracy R_1 is an imaginary quantity. This means it is possible to regard the right-hand side of equation (29) as i multiplied by a real function of pseudo-depth. To hide the algebraic complexity of the equation, we call this real function $\Gamma_q(z)$, and replace equation (29) with

$$\int_0^z \beta_1(z')dz' = i4\Gamma_q(z), \tag{33}$$

which will simplify the result.

Our final simplification comes from recognizing that the integral of β_1 down to the first event, P_1, will be zero. This is an expected result: since no attenuation occurs to waves propagating in the non-absorptive reference medium, there is no Q compensation to be carried out on P_1. For this reason, we turn our focus entirely to the effect of direct non-linear Q compensation on P_2, leaving P_1 out of the analysis. The analytic direct non-linear Q compensation calculation becomes

$$\begin{aligned}
&\int_{-\infty}^{\infty} e^{ik_z\left(z-\frac{1}{2}\int_0^z \beta_1(z')dz'\right)}\beta_1(k_z)dk_z \\
&\quad = -\frac{4}{ik_z}\int_{-\infty}^{\infty} e^{ik_z(z-i\Gamma_q(z))}\left[\ldots + \frac{T_{12}R_2T_{21}}{2\pi}\left(e^{-ik_z z_2}e^{-\left(\frac{z_1}{2Q_1}+\frac{(z_2-z_1)}{2Q_2}\right)k_z}\right)\right]dk_z.
\end{aligned} \tag{34}$$

Carrying out the integration, we have

$$\begin{aligned}
&-\frac{2}{ik_z\pi}\int_{-\infty}^{\infty} e^{ik_z z}e^{\Gamma_q(z)k_z}\left[\cdots + T_{12}R_2T_{21}\left(e^{-ik_z z_2}e^{-\left(\frac{z_1}{2Q_1}+\frac{(z_2-z_1)}{2Q_2}\right)k_z}\right)\right]dk_z \\
&= -\frac{2}{ik_z}\frac{T_{12}R_2T_{21}}{\pi}\int_{-\infty}^{\infty}\cdots\left(e^{-i(z-z_2)k_z}e^{\left[\Gamma_q(z)-\left(\frac{z_1}{2Q_1}+\frac{(z_2-z_1)}{2Q_2}\right)\right]k_z}\right)\Bigg]dk_z \\
&= -\frac{2}{ik_z}\frac{T_{12}R_2T_{21}}{\pi}\frac{\left(\Gamma_q(z)_z - \frac{z_1}{2Q_1}+\frac{(z_2-z_1)}{2Q_2}\right)}{\left(\Gamma_q(z) - \frac{z_1}{2Q_1}+\frac{(z_2-z_1)}{2Q_2}\right)^2 + (z-z_2)^2} \\
&= \frac{2}{ik_z}\frac{T_{12}R_2T_{21}}{\pi}\frac{\left(\frac{z_1}{2Q_1}+\frac{(z_2-z_1)}{2Q_2} - \Gamma_q(z)\right)}{\left(\frac{z_1}{2Q_1}+\frac{(z_2-z_1)}{2Q_2} - \Gamma_q(z)\right)^2 + (z-z_2)^2},
\end{aligned} \tag{35}$$

which, after the derivative with respect to z is taken (i.e., multiplication by ik_z), produces the desired result.

Clarifying the underlying and fundamental meaning of the approximate linear inversion of seismic data

A. B. Weglein[1], J. Zhang[2], H. Zhang[3], A. C. Ramirez[4] and F. Liu[1]
[1] University of Houston, 617 Science and Research Bldg. 1, Houston, TX 77204-5005
[2] Currently BP America, 501 Westlake Park Blvd., Houston, TX 77079
[3] Currently ConocoPhillips, 600 N. Dairy Ashford, Houston, TX 77079
[4] Currently WesternGeco, 10001 Richmond Ave. Houston, Tx, 77042

Abstract

The inverse scattering series (ISS) is the only fully non-linear and direct multi-dimensional seismic inversion methodology. The directness and fully non-linear character of the ISS method together provide a set of unique benefits and advantages, with tremendous conceptual and practical value and consequence. In previous publications the capability of the inverse scattering series to achieve all processing goals, e.g., multiple removal, depth imaging, Q compensation and non-linear AVO, and without needing or determining traditional subsurface information, and directly in terms of only data, were described and exemplified. In this paper, another unique benefit of the ISS is presented: The very meaning of a linear approximate estimate is for the first time defined as the linear estimate to the actual sought after physical property. The direct non-linear solution for changes in earth mechanical properties at a target provided by the ISS unquestionably and unambiguously requires all multi-components of data, and not only PP data. Hence, the data required for direct non-linear inversion of property changes defines the data set that is required in defining a linear estimate of property changes. The linear estimate of a change in physical properties, to be considered a linear inverse estimate needs to be linear in a data that can actually determine the physical property. The ISS is the only direct non-linear inversion method, and in its prescriptive and explicit directness-it has unambiguously communicated both the data requirement and algorithms for direct non-linear and linear inversion.

1 Background and Introduction

Among the unique qualities of the inverse scattering series, (e.g., Weglein et al., 2003, Weglein et al., 1997) are: (1) a capability to achieve all processing objectives, (e.g., (i) free surface multiple removal, (ii) internal multiple removal, (iii) depth imaging, (iv) Q compensation, and (v) direct non-linear target identification), all achievable directly in terms of measured data, without a need, in principle or practice, to know or to determine, or to even roughly estimate any information, whatsoever, (e.g., no velocity and no density information, nor information concerning Q) related to subsurface properties that govern the propagation of waves in the actual subsurface, and absolutely required by conventional linear migration and migration-inversion to locate and identify targets; (2) distinct direct algorithms input the data and output each of the processing objectives listed in item (1, (i)-(v)) through the introduction of isolated task subseries; (3) among the tasks listed above ((i)-(iii))are each achievable by a distinct earth model-type independent algorithm, whether

the earth is acoustic, elastic, etc; (4) the inverse step is always the same, and is only in terms of water speed Green's functions and is provided by a single water speed FK Stolt migration, without the need for a generalized inverse, model matching or background updating schemes, and their well documented issues and pitfalls of low-frequency data demands and often inadequate earth model types.

In this paper, we present a new and here-to-fore unrecognized and unheralded benefit of the fully non-linear and direct multi-dimensional inversion represented by the inverse scattering series. That new contribution is at the central core of all inversion theory and impacts both how we better understand previously observed and reported results from other groups and researchers, as well as providing a firm and unambiguous platform and guide to researchers and explorationists. It allows us to understand, for the very first time, the data collection mandated and required for a meaningful and consistent linear approximate inverse solution, and, in addition, a direct prescription and determination of the linear estimate and a more realistic and reliable non-linear inverse target identification.

The direct non-linear solution only provided by the ISS provides the first unambiguous and consistent meaning for a direct approximate linear inverse solution. Inverting PP data linearly for approximate changes in earth mechanical properties, is providing a linear approximate solution, to the PP data equation, but not a linear approximate inverse solution for changes in earth mechanical properties. To achieve the higher bar of a linear approximate inverse solution requires a non-approximate inverse solution, as a starting point, as either a closed form or expressed as a series that is going to be reduced and simplified in a linear approximate form. The inverse scattering series represents a non-approximate fully non-linear and direct inverse solution. The direct inversion of earth mechanical properties requires PP, PS, SP and SS data in a 2D world, and PP, PSv, PSh, SvSv, ShSh, ShP, SvP, SvSh, ShSv, in a 3D earth. Hence, the linear approximate inverse solution, must be linear in the data that allows the linear solution to correspond to the linear approximation of the inverse solution. PP data alone can produce a linear approximate solution, but PP, PS, SP and SS can provide a linear approximate inverse solution.

The conclusion is that only multi-component data can produce a linear approximate, that is a linear approximation inversion solution, as a first step towards a complete non-linear and direct solution.

We recognize that the changes in material properties across a single reflector and the corresponding reflection coefficients and reflection data have a non-linear relationship in both a modeling, and, therefore, in an inversion sense. However, the key and salient point is that while changes in earth mechanical properties at an interface can through the Zoeppritz relations directly, non-linearly and exactly and separately determine each of the PP, PS, SS reflection coefficients, it requires all of those reflection coefficients taken together to determine any one, or more, of those changes in mechanical properties. That message is neither obvious, or reasonable or even plausible. However, the message here is that it is all of those difficult and unattractive things, and yet it is also unambiguously and unmistakably true. In general, inversion or processing is not modeling run backwards.

Direct linear and indirect methods (e.g., full wavefield inversion) have not, and cannot, bring that clarity to the meaning and unambiguous prescription of the linear approximate inverse solution. Model matching with global searches of PP data alone has no framework or other reason to suspect the fundamental inadequacy of that PP data to provide a linear inverse let alone non-linear

inverse solution. We have published papers ourselves using PP data to estimate changes in physical properties, and along with the entire petroleum industry have used PP data in AVO analysis. PP data has enough degrees of freedom given enough angles to more than solve for linear estimates in changes in earth material properties. So what is the problem?

We are all fully aware that a single angle of data will not be able to simultaneously invert for several changes in earth mechanical properties. That is called count-conservation between the degrees of freedom in your data and the sought after earth material properties, everywhere recognized and understood in inverse theory. That is a necessary but not a sufficient condition for a linear inverse solution, although necessary and sufficient for a linear solution. The fact that all components of elastic data are absolutely base-line required to provide a meaningful linear inverse or non-linear inverse solution- is a new and much more subtle but no less important message. The fact that the inverse scattering series is the only direct and non-linear inversion method allowed it to stand alone and to provide a framework for the very meaning of linear inverse and a systematic and precise way to directly improve upon those estimates through higher terms in the expansion of those earth mechanical properties directly in terms of the data. That required data is full multi-component data and not only PP.

If you have an expansion for a change in a physical property, call it V, in terms of reflection data, D, then schematically

$$V(D) = V(D=0) + V'(D=0)D + \frac{1}{2}V''(D=0)D^2 + \cdots .$$

Where $V(D=0) = 0$, and $V'(0)D$ is the linear estimate to $V(D)$ where D is the data needed to determine $V(D)$. Only the Inverse Scattering Series provides the precise series for $V(D)$ and, hence, in that process defines both the data necessary to find $V(D)$ and its linear estimate $V_1 = V'(0)D$. You cannot change the expansion variable in a Taylor series, if D determines the series, then each term including the first linear term depends on D, all elements of D. D is multi-component data for the determination of changes in elastic properties. That is the story.

The need for multi-component data is not adding a set of constraints beyond PP data, but providing the base line necessary data needed to satisfy the fundamental non-linear relationship between reflection data and changes in earth mechanical properties. It is a fundamental data need, that stands with data dimensionality and degrees of freedom, that comes in at the ground floor, before subtler and important issues of robustness and stability are examined, and not merely as a practical enhancement or boost to PP data inversion potential and capability. The need for multi-component data is fundamental. As with other things it can be ignored but will rarely be ignorable.

The latter PP data is fundamentally inadequate from a conceptual and math-physics analysis perspective for a consistent and meaningful target identification, and the needed data and the methods for using that data are only provided by the directness and fully non-linear and prescriptive nature of the inverse scattering series. Those unique properties and benefits of the ISS are not provided by either: (1) linear approximate direct inverse methods, behind all current mainstream leading edge migration and migration-inversion algorithms, or (2) non-linear indirect inverse methods such as iterative linear or other indirect model matching inversion methods, or “full-wave field inversion”.

In this paper, we take the reader through the thinking process and deliberation within our group that brought this issue to light. It began in the simpler acoustic world, where the difference between forward and inverse problem needed some attention and clarification. In this paper we will ask and answer the following questions.

1. What does linear in the data mean?
2. Linear in what data?
3. Conservation of dimension (having enough degrees of freedom in your data to "solve" an equation) is not a sufficient condition to define "what data" and being able to solve an equation (in isolation) is not the same as finding a physically meaningful solution or even a linear estimate;
4. Solving an equation without the context and framework within which that equation resides, and ignoring the assumptions that lead to that equation is a dangerous path towards an inverse illusion;
5. Implications for data collection and target identification.

We begin with a review of the inverse scattering series.

Scattering theory relates the perturbation (the difference between the reference and actual medium properties) to the scattered wave field (the difference between the reference medium's and the actual medium's wave field). It is therefore reasonable that in discussing scattering theory, we begin with the basic wave equations governing the wave propagation in the actual and reference medium, respectively,

$$LG = \delta, \tag{1}$$

$$L_0 G_0 = \delta, \tag{2}$$

where L and L_0 are respectively the differential operators that describe wave propagation in the actual and reference medium, and G and G_0 are the corresponding Green's operators. The δ on the right hand side of both equations is a Dirac delta operator and represents an impulsive source.

The perturbation is defined as $V = L_0 - L$. The Lippmann-Schwinger equation,

$$G = G_0 + G_0 V G, \tag{3}$$

relates G, G_0 and V (see, e.g., Taylor, 1972). Iterating this equation back into itself generates the forward scattering series

$$G = G_0 + G_0 V G_0 + G_0 V G_0 V G_0 + \cdots . \tag{4}$$

Then the scattered field $\psi_s \equiv G - G_0$ can be written as

$$\begin{aligned} \psi_s &= G_0 V G_0 + G_0 V G_0 V G_0 + \cdots \\ &= (\psi_s)_1 + (\psi_s)_2 + \cdots , \end{aligned} \tag{5}$$

where $(\psi_s)_n$ is the portion of ψ_s that is n^{th} order in V. The measured values of ψ_s are the data, D, where

$$D = (\psi_s)_{ms} = (\psi_s)_{\text{on the measurement surface}}.$$

In the inverse scattering series, expanding V as a series in orders of D,

$$V = V_1 + V_2 + V_3 + \cdots, \tag{6}$$

then substituting equation 6 into equation 5, and evaluating equation 5 on the measurement surface yields

$$D = [G_0(V_1 + V_2 + \cdots)G_0]_{ms} + [G_0(V_1 + V_2 + \cdots)G_0(V_1 + V_2 + \cdots)G_0]_{ms} + \cdots. \tag{7}$$

Setting terms of equal order in the data equal, leads to the equations that determine V_1, V_2, ... directly from D and G_0.

$$D = [G_0V_1G_0]_{ms}, \tag{8}$$

$$0 = [G_0V_2G_0]_{ms} + [G_0V_1G_0V_1G_0]_{ms}, \tag{9}$$

$$\begin{aligned} 0 =& [G_0V_3G_0]_{ms} + [G_0V_1G_0V_2G_0]_{ms} + [G_0V_2G_0V_1G_0]_{ms} \\ &+ [G_0V_1G_0V_1G_0V_1G_0]_{ms}, \end{aligned} \tag{10}$$

etc. Equations 8 $\sim$ 10 permit the sequential calculation of V_1, V_2, ..., and, hence, achieve full inversion for V (see equation 6) from the recorded data D and the reference wave field (i.e., the Green's operator of the reference medium) G_0. Therefore, the inverse scattering series is a multi-D inversion procedure that directly determines physical properties using only reflection data and reference medium information.

For the parochial purposes of this paper the absolutely critical point to recognize at this juncture is that the equations for V_1, V_2, ... are exact equations for V_1, V_2, ..., where V_1, V_2, ... are linear and quadratic estimates for V, respectively ... but the equations for V_1, V_2 etc are the exact equations for the latter quantities.

2 Acoustic case

In this section, we will consider a 1D acoustic two parameter earth model (e.g. bulk modulus and density or velocity and density). We start with the 3D acoustic wave equations in the actual and reference medium:

$$\left[\frac{\omega^2}{K(\mathbf{r})} + \nabla \cdot \frac{1}{\rho(\mathbf{r})}\nabla\right] G(\mathbf{r}, \mathbf{r}_s; \omega) = \delta(\mathbf{r} - \mathbf{r}_s), \tag{11}$$

$$\left[\frac{\omega^2}{K_0(\mathbf{r})} + \nabla \cdot \frac{1}{\rho_0(\mathbf{r})}\nabla\right] G_0(\mathbf{r}, \mathbf{r}_s; \omega) = \delta(\mathbf{r} - \mathbf{r}_s), \tag{12}$$

where $G(\mathbf{r}, \mathbf{r}_s; \omega)$ and $G_0(\mathbf{r}, \mathbf{r}_s; \omega)$ are respectively the free-space causal Green's functions that describe wave propagation in the actual and reference medium. $K = c^2\rho$, is P-wave bulk modulus,

c is P-wave velocity and ρ is the density. The quantities with subscript "0" are for the reference medium, and those without the subscript are for the actual medium. The perturbation is

$$V = L_0 - L = \frac{\omega^2 \alpha}{K_0} + \nabla \cdot \frac{\beta}{\rho_0} \nabla, \tag{13}$$

where $\alpha = 1 - \frac{K_0}{K}$ and $\beta = 1 - \frac{\rho_0}{\rho}$ are the two parameters we choose to do the inversion. Assuming both ρ_0 and c_0 are constants, equation 12 becomes

$$\left(\frac{\omega^2}{c_0^2} + \nabla^2 \right) G_0(\mathbf{r}, \mathbf{r}_s; \omega) = \rho_0 \delta(\mathbf{r} - \mathbf{r}_s). \tag{14}$$

For the 1-D case, the perturbation V has the following form

$$V(z, \nabla) = \frac{\omega^2 \alpha(z)}{K_0} + \frac{1}{\rho_0} \beta(z) \frac{\partial^2}{\partial x^2} + \frac{1}{\rho_0} \frac{\partial}{\partial z} \beta(z) \frac{\partial}{\partial z}. \tag{15}$$

$V(z, \nabla)$, $\alpha(z)$ and $\beta(z)$ can be expanded respectively as

$$V(z, \nabla) = V_1(z, \nabla) + V_2(z, \nabla) + \cdots, \tag{16}$$

$$\alpha(z) = \alpha_1(z) + \alpha_2(z) + \cdots, \tag{17}$$

$$\beta(z) = \beta_1(z) + \beta_2(z) + \cdots. \tag{18}$$

Then we have

$$V_1(z, \nabla) = \frac{\omega^2 \alpha_1(z)}{K_0} + \frac{1}{\rho_0} \beta_1(z) \frac{\partial^2}{\partial x^2} + \frac{1}{\rho_0} \frac{\partial}{\partial z} \beta_1(z) \frac{\partial}{\partial z}, \tag{19}$$

$$V_2(z, \nabla) = \frac{\omega^2 \alpha_2(z)}{K_0} + \frac{1}{\rho_0} \beta_2(z) \frac{\partial^2}{\partial x^2} + \frac{1}{\rho_0} \frac{\partial}{\partial z} \beta_2(z) \frac{\partial}{\partial z}, \tag{20}$$

$$\vdots$$

Substituting equation 19 into equation 8, we can get the linear solution for α_1 and β_1 in the frequency domain

$$\widetilde{D}(q_g, \theta, z_g, z_s) = -\frac{\rho_0}{4} e^{-iq_g(z_s + z_g)} \left[\frac{1}{\cos^2 \theta} \widetilde{\alpha_1}(-2q_g) + (1 - \tan^2 \theta) \widetilde{\beta}_1(-2q_g) \right]. \tag{21}$$

Let $z_s = z_g = 0$,

$$D(z, \theta) = -\frac{\rho_0}{4} \Big(\frac{1}{\cos^2 \theta} \alpha_1(z) + (1 - \tan^2 \theta) \beta_1(z) \Big) \tag{22}$$

Let's consider the following logic. Equation 22 is an exact equation for the linear estimates $\alpha_1(z)$ and $\beta_1(z)$, and choosing two (or more) values of θ will allow you to solve equation 22 for $\alpha_1(z)$ and $\beta_1(z)$.

For a single reflector model, the left hand side of equation 22 is the migration of the surface recorded data. The migration provides a step-function at the depth of the reflector whose angle dependent amplitude is the reflector's angle dependent reflection coefficient.

The right hand side of equation 22 can be rewritten as

$$-\frac{\rho_0}{4}\Big(\alpha_1(z)+\beta_1(z)+(\alpha_1(z)-\beta_1(z))\tan^2\theta\Big). \tag{23}$$

Separately, we know that the exact plane wave reflection coefficient is (e.g., Keys, 1989)

$$R(\theta)=\frac{(\rho_1/\rho_0)(c_1/c_0)\sqrt{1-\sin^2\theta}-\sqrt{1-(c_1^2/c_0^2)\sin^2\theta}}{(\rho_1/\rho_0)(c_1/c_0)\sqrt{1-\sin^2\theta}+\sqrt{1-(c_1^2/c_0^2)\sin^2\theta}}. \tag{24}$$

and we can find a Taylor series in R as a function of $\sin^2\theta$ or another Taylor series using

$$\sin^2\theta=\frac{\tan^2\theta}{1+\tan^2\theta}.$$

This series is

$$\begin{aligned} R(\theta) =& R(\tan^2\theta) \\ =& R(\tan^2\theta=0)+\Big(\frac{d\,R(\tan^2\theta)}{d(\tan^2\theta)}\Big)\Big|_{\tan^2\theta=0}\cdot\tan^2\theta \\ &+\Big(\frac{d\,R(\tan^2\theta)}{d(\tan^2\theta)}\Big)\Big|_{\tan^2\theta=0}\cdot\tan^4\theta+\cdots \end{aligned} \tag{25}$$

Equation 25 is exact and the amplitude of the step-function in equation 23 is

$$R(\tan^2\theta)=\alpha_1+\beta_1+(\alpha_1-\beta_1)\tan^2\theta. \tag{26}$$

The first term in the inverse scattering series is (claimed to be) an exact equation for the linear estimates of α and β, α_1 and β_1, respectively.

How can you reconcile equation 26 being exact with equation 25 being exact?

Equation 26 would seem to represent a truncated; and, therefore, approximate form of the Zoeppritz exact reflection coefficient (equation 25).

If we don't accept equation 26 as an approximation as being acceptable then we must alter either equation 25 or equation 26, and we are not going to alter Zoeppritz equation 25.

We are forced to conclude that consistency between equation 25 and equation 26 requires that α_1 and β_1 must be functions of θ.

Let's see where that supposition then takes us from equation 26:

$$R(\tan^2\theta)=\alpha_1(\theta)+\beta_1(\theta)+[\alpha_1(\theta)-\beta_1(\theta)]\tan^2\theta; \tag{27}$$

and, if you choose two value of θ, say θ_1 and θ_2, then equation 27 will lead to two equations in four unknowns, $\alpha_1(\theta_1)$, $\alpha_1(\theta_2)$, $\beta_1(\theta_1)$ and $\beta_1(\theta_2)$. Not a positive moment.

The problem here is that we have forgotten the basic meaning and starting point in defining α, β and α_1, β_1.

In an inverse scattering series expansion for a parameter in orders of the data it is critically important to assure that the data in terms of which you are expanding the parameter is sufficient to determine that parameter. The data needed to determine a parameter is dependent upon what other parameters are (or are not) in your model; i.e., it depends on the context within which that parameter resides.

Now consider a two parameter world defined by $\alpha(z)$ and $\beta(z)$, and the expansions of α and β in orders of the data. In this case, if we suppose that α and β are expandable in terms of data at two different plane wave angles assuming that such a relationship between $D(z,\theta_1)$, $D(z,\theta_2)$ and α and β exists and is sufficient to determine α and β (not α_1 and β_1) then we can write the series for $\alpha(z)$ and $\beta(z)$ as follows:

$$\alpha(z) = \alpha_1(z, D(z,\theta_1), D(z,\theta_2)) + \alpha_2(z, D(z,\theta_1), D(z,\theta_2)) + \cdots$$

and in a compact notation

$$\alpha(z) = \alpha_1(z,\theta_1,\theta_2) + \alpha_2(z,\theta_1,\theta_2) + \cdots$$

where α_1 is the portion of α linear in the data set $(D(z,\theta_1), D(z,\theta_2))$. Similarly,

$$\beta(z) = \beta_1(z,\theta_1,\theta_2) + \beta_2(z,\theta_1,\theta_2) + \cdots \tag{28}$$

If the model only allowed bulk modulus changes, but not density variation then the data required for solving for α would only consist of data at a single angle; and in that single parameter world

$$\alpha(z) = \alpha_1(z,\theta_1) + \alpha_2(z,\theta_1) + \ldots. \tag{29}$$

Now in the two parameter inverse problem, the data is

$$\begin{pmatrix} D(z,\theta_1) \\ D(z,\theta_2) \end{pmatrix}$$

and then $D = G_0 V_1 G_0$ is equal to

$$\begin{pmatrix} D(z,\theta_1) \\ D(z,\theta_2) \end{pmatrix} = \begin{pmatrix} (1+\tan^2\theta_1) & (1-\tan^2\theta_1) \\ (1+\tan^2\theta_2) & (1-\tan^2\theta_2) \end{pmatrix} \begin{pmatrix} \alpha_1(z,\theta_1,\theta_2) \\ \beta_1(z,\theta_1,\theta_2) \end{pmatrix} \tag{30}$$

and $\begin{pmatrix} \alpha_1(z,\theta_1,\theta_2) \\ \beta_1(z,\theta_1,\theta_2) \end{pmatrix}$ is linearly related to $\begin{pmatrix} D(z,\theta_1) \\ D(z,\theta_2) \end{pmatrix}$. α_1 and β_1 will depend upon which particular angles θ_1 and θ_2 were chosen, and that is anticipated and perfectly reasonable, since being a linear approximation in the data could(and should) be a different linear estimate depending on the data subset you are considering.

Equation 30, a matrix equation, is the first term in the inverse series and determines α_1 and β_1, the linear estimate of α and β.

THE KEY POINT

The lesson here is that the inverse problem doesn't start with $G_0V_1G_0 = D$, but with $V = V_1+V_2+V_3+\ldots$ and the latter equation is driven by a view of what data set can determine the operator V.

This might seem like a somewhat useless academic exercise, since equation 30 is the equation you would have solved for α_1 and β_1 if you just ignored their θ dependence entirely. It is anything but that. There are at least two problems with that conclusion. The value of the above analysis is: (1) with α_1 and β_1 independent of θ, you have difficulty claiming or satisfying the important requirement that the first equation in the inverse series is exact; and (2) more importantly you can get into serious conceptual and practical problems in the elastic case if you don't have very clear grasp of the underlying inverse issues and relationships in the acoustic case.

3 Elastic case

The scattering theory and the inverse scattering series for the 1-D isotropic elastic earth is developed in Zhang and Weglein (2009b).

3.1 Background for 2D elastic inversion

In this section we consider the inversion problem in two dimensions for an elastic medium. We start with the displacement space, and then, for convenience (e.g., Aki and Richards, 2002, Weglein and Stolt, 1992), we change the basis and transform the equations to PS space. Finally, we do the elastic inversion in the PS domain.

3.2 In the displacement space

We begin with some basic equations in the displacement space (Matson, 1997):

$$L\mathbf{u} = \mathbf{f}, \tag{31}$$

$$L_0\mathbf{u} = \mathbf{f}, \tag{32}$$

$$LG = \delta, \tag{33}$$

$$L_0G_0 = \delta, \tag{34}$$

where L and L_0 are the differential operators that describe the wave propagation in the actual and reference medium, respectively, $\mathbf{u}$ and $\mathbf{f}$ are the corresponding displacement and source terms, respectively, and G and G_0 are the corresponding Green's operators for the actual and reference medium.

Following closely Weglein et al. (1997), Weglein et al. (2002) and Weglein et al. (2003), defining the perturbation $V = L_0 - L$, the Lippmann-Schwinger equation for the elastic media in the displacement space is

$$G = G_0 + G_0 V G. \tag{35}$$

Iterating this equation back into itself generates the Born series

$$G = G_0 + G_0 V G_0 + G_0 V G_0 V G_0 + \cdots . \tag{36}$$

We define the data D as the measured values of the scattered wave field. Then, on the measurement surface, we have

$$D = G_0 V G_0 + G_0 V G_0 V G_0 + \cdots . \tag{37}$$

Expanding V as a series in orders of D we have

$$V = V_1 + V_2 + V_3 + \cdots . \tag{38}$$

Substituting equation 38 into equation 37, evaluating equation 37, and setting terms of equal order in the data equal, the equations that determine V_1, V_2, ... from D and G_0 would be obtained.

$$D = G_0 V_1 G_0, \tag{39}$$

$$0 = G_0 V_2 G_0 + G_0 V_1 G_0 V_1 G_0, \tag{40}$$

$$\vdots$$

In the actual medium, the 2-D elastic wave equation is (Weglein and Stolt, 1992)

$$L\mathbf{u} \equiv \left[\rho\omega^2 \begin{pmatrix} 1 & 0 \\ 0 & 1 \end{pmatrix} + \begin{pmatrix} \partial_1\gamma\partial_1 + \partial_2\mu\partial_2 & \partial_1(\gamma - 2\mu)\partial_2 + \partial_2\mu\partial_1 \\ \partial_2(\gamma - 2\mu)\partial_1 + \partial_1\mu\partial_2 & \partial_2\gamma\partial_2 + \partial_1\mu\partial_1 \end{pmatrix}\right] \begin{bmatrix} u_1 \\ u_2 \end{bmatrix} = \mathbf{f}, \tag{41}$$

where $\mathbf{u} = \begin{bmatrix} u_1 \\ u_2 \end{bmatrix}$ = displacement, ρ = density, γ = bulk modulus ($\equiv \rho\alpha^2$ where α = P-wave velocity), μ = shear modulus ($\equiv \rho\beta^2$ where β = S-wave velocity),

ω = temporal frequency (angular),

∂_1 and ∂_2 denote the derivative over x and z, respectively, and

$\mathbf{f}$ is the source term.

For constant $(\rho, \gamma, \mu) = (\rho_0, \gamma_0, \mu_0)$, $(\alpha, \beta) = (\alpha_0, \beta_0)$, the operator L becomes

$$L_0 \equiv \left[\rho_0\omega^2 \begin{pmatrix} 1 & 0 \\ 0 & 1 \end{pmatrix} + \begin{pmatrix} \gamma_0\partial_1^2 + \mu_0\partial_2^2 & (\gamma_0 - \mu_0)\partial_1\partial_2 \\ (\gamma_0 - \mu_0)\partial_1\partial_2 & \mu_0\partial_1^2 + \gamma_0\partial_2^2 \end{pmatrix}\right]. \tag{42}$$

Then,

$$V \equiv L_0 - L$$

$$= -\rho_0 \begin{bmatrix} a_\rho\omega^2 + \alpha_0^2\partial_1 a_\gamma \partial_1 + \beta_0^2\partial_2 a_\mu \partial_2 & \partial_1(\alpha_0^2 a_\gamma - 2\beta_0^2 a_\mu)\partial_2 + \beta_0^2\partial_2 a_\mu \partial_1 \\ \partial_2(\alpha_0^2 a_\gamma - 2\beta_0^2 a_\mu)\partial_1 + \beta_0^2\partial_1 a_\mu \partial_2 & a_\rho\omega^2 + \alpha_0^2\partial_2 a_\gamma \partial_2 + \beta_0^2\partial_1 a_\mu \partial_1 \end{bmatrix}, \tag{43}$$

where $a_\rho \equiv \frac{\rho}{\rho_0} - 1$, $a_\gamma \equiv \frac{\gamma}{\gamma_0} - 1$ and $a_\mu \equiv \frac{\mu}{\mu_0} - 1$ are the three parameters we choose to do the elastic inversion. For a 1D earth (i.e. a_ρ, a_γ and a_μ are only functions of depth z), the expression above for V becomes

$$V = -\rho_0 \begin{bmatrix} a_\rho\omega^2 + \alpha_0^2 a_\gamma \partial_1^2 + \beta_0^2\partial_2 a_\mu \partial_2 & (\alpha_0^2 a_\gamma - 2\beta_0^2 a_\mu)\partial_1\partial_2 + \beta_0^2\partial_2 a_\mu \partial_1 \\ \partial_2(\alpha_0^2 a_\gamma - 2\beta_0^2 a_\mu)\partial_1 + \beta_0^2 a_\mu \partial_1\partial_2 & a_\rho\omega^2 + \alpha_0^2\partial_2 a_\gamma \partial_2 + \beta_0^2 a_\mu \partial_1^2 \end{bmatrix}. \tag{44}$$

3.3 Transforming to PS space

For convenience, we can change the basis from $\mathbf{u} = \begin{bmatrix} u_1 \\ u_2 \end{bmatrix}$ to $\begin{pmatrix} \phi^P \\ \phi^S \end{pmatrix}$ to allow L_0 to be diagonal,

$$\mathbf{\Phi} = \begin{pmatrix} \phi^P \\ \phi^S \end{pmatrix} = \begin{bmatrix} \gamma_0(\partial_1 u_1 + \partial_2 u_2) \\ \mu_0(\partial_1 u_2 - \partial_2 u_1) \end{bmatrix}, \tag{45}$$

also, we have

$$\begin{pmatrix} \phi^P \\ \phi^S \end{pmatrix} = \Gamma_0 \Pi \mathbf{u} = \begin{bmatrix} \gamma_0(\partial_1 u_1 + \partial_2 u_2) \\ \mu_0(\partial_1 u_2 - \partial_2 u_1) \end{bmatrix}, \tag{46}$$

where $\Pi = \begin{pmatrix} \partial_1 & \partial_2 \\ -\partial_2 & \partial_1 \end{pmatrix}$, $\Gamma_0 = \begin{pmatrix} \gamma_0 & 0 \\ 0 & \mu_0 \end{pmatrix}$.

In the reference medium, the operator L_0 will transform in the new basis via a transformation

$$\hat{L}_0 \equiv \Pi L_0 \Pi^{-1} \Gamma_0^{-1} = \begin{pmatrix} \hat{L}_0^P & 0 \\ 0 & \hat{L}_0^S \end{pmatrix},$$

where $\hat{L}_0$ is L_0 transformed to PS space, $\Pi^{-1} = \begin{pmatrix} \partial_1 & -\partial_2 \\ \partial_2 & \partial_1 \end{pmatrix} \nabla^{-2}$ is the inverse matrix of Π, $\hat{L}_0^P = \omega^2/\alpha_0^2 + \nabla^2$, $\hat{L}_0^S = \omega^2/\beta_0^2 + \nabla^2$, and

$$\mathbf{F} = \Pi \mathbf{f} = \begin{pmatrix} F^P \\ F^S \end{pmatrix}. \tag{47}$$

Then, in PS domain, equation 32 becomes,

$$\begin{pmatrix} \hat{L}_0^P & 0 \\ 0 & \hat{L}_0^S \end{pmatrix} \begin{pmatrix} \phi^P \\ \phi^S \end{pmatrix} = \begin{pmatrix} F^P \\ F^S \end{pmatrix}. \tag{48}$$

Since $G_0 \equiv L_0^{-1}$, let $\hat{G}_0^P = \left(\hat{L}_0^P\right)^{-1}$ and $\hat{G}_0^S = \left(\hat{L}_0^S\right)^{-1}$, then the displacement G_0 in PS domain becomes

$$\hat{G}_0 = \Gamma_0 \Pi G_0 \Pi^{-1} = \begin{pmatrix} \hat{G}_0^P & 0 \\ 0 & \hat{G}_0^S \end{pmatrix}. \tag{49}$$

So, in the reference medium, after transforming from the displacement domain to PS domain, both L_0 and G_0 become diagonal.

Multiplying equation 35 from the left by the operator $\Gamma_0\Pi$ and from the right by the operator Π^{-1}, and using equation 49,

$$\begin{aligned}\Gamma_0\Pi G\Pi^{-1} &= \hat{G}_0 + \hat{G}_0\left(\Pi V\Pi^{-1}\Gamma_0^{-1}\right)\Gamma_0\Pi G\Pi^{-1}\\ &= \hat{G}_0 + \hat{G}_0\hat{V}\hat{G},\end{aligned} \tag{50}$$

where the displacement Green's operator G is transformed to the PS domain as

$$\hat{G} = \Gamma_0\Pi G\Pi^{-1} = \begin{pmatrix}\hat{G}^{PP} & \hat{G}^{PS}\\ \hat{G}^{SP} & \hat{G}^{SS}\end{pmatrix}. \tag{51}$$

The perturbation V in the PS domain becomes

$$\hat{V} = \Pi V\Pi^{-1}\Gamma_0^{-1} = \begin{pmatrix}\hat{V}^{PP} & \hat{V}^{PS}\\ \hat{V}^{SP} & \hat{V}^{SS}\end{pmatrix}, \tag{52}$$

where the left superscripts of the matrix elements represent the type of measurement and the right ones are the source type.

Similarly, applying the PS transformation to the entire inverse series gives

$$\hat{V} = \hat{V}_1 + \hat{V}_2 + \hat{V}_3 + \cdots. \tag{53}$$

It follows, from equations 50 and 53 that

$$\hat{D} = \hat{G}_0\hat{V}_1\hat{G}_0, \tag{54}$$

$$\hat{G}_0\hat{V}_2\hat{G}_0 = -\hat{G}_0\hat{V}_1\hat{G}_0\hat{V}_1\hat{G}_0, \tag{55}$$

$$\vdots$$

where $\hat{D} = \begin{pmatrix}\hat{D}^{PP} & \hat{D}^{PS}\\ \hat{D}^{SP} & \hat{D}^{SS}\end{pmatrix}$ are the data in the PS domain.

In the displacement space we have, for equation 31,

$$\mathbf{u} = G\mathbf{f}. \tag{56}$$

Then, in the PS domain, equation 56 becomes

$$\mathbf{\Phi} = \hat{G}\mathbf{F}. \tag{57}$$

On the measurement surface, we have

$$\hat{G} = \hat{G}_0 + \hat{G}_0\hat{V}_1\hat{G}_0. \tag{58}$$

Substituting equation 58 into equation 57, and rewriting equation 57 in matrix form:

$$\begin{pmatrix}\phi^P\\ \phi^S\end{pmatrix} = \begin{pmatrix}\hat{G}_0^P & 0\\ 0 & \hat{G}_0^S\end{pmatrix}\begin{pmatrix}F^P\\ F^S\end{pmatrix} + \begin{pmatrix}\hat{G}_0^P & 0\\ 0 & \hat{G}_0^S\end{pmatrix}\begin{pmatrix}\hat{V}_1^{PP} & \hat{V}_1^{PS}\\ \hat{V}_1^{SP} & \hat{V}_1^{SS}\end{pmatrix}\begin{pmatrix}\hat{G}_0^P & 0\\ 0 & \hat{G}_0^S\end{pmatrix}\begin{pmatrix}F^P\\ F^S\end{pmatrix}. \tag{59}$$

This can be written as the following two equations

$$\phi^P = \hat{G}_0^P F^P + \hat{G}_0^P \hat{V}_1^{PP}\hat{G}_0^P F^P + \hat{G}_0^P \hat{V}_1^{PS}\hat{G}_0^S F^S, \tag{60}$$

$$\phi^S = \hat{G}_0^S F^S + \hat{G}_0^S \hat{V}_1^{SP}\hat{G}_0^P F^P + \hat{G}_0^S \hat{V}_1^{SS}\hat{G}_0^S F^S. \tag{61}$$

We can see, from the two equations above, that for homogeneous media, (no perturbation, $\hat{V}_1 = 0$), there are only direct P and S waves and that the two kinds of waves are separated. However, for inhomogeneous media, these two kinds of waves will be mixed together. If only the P wave is incident, $F^P = 1$, $F^S = 0$, then the two equations 60 and 61 above are respectively reduced to

$$\phi^P = \hat{G}_0^P + \hat{G}_0^P \hat{V}_1^{PP}\hat{G}_0^P, \tag{62}$$

$$\phi^S = \hat{G}_0^S \hat{V}_1^{SP}\hat{G}_0^P. \tag{63}$$

Hence, in this case, there is only the direct P wave $\hat{G}_0^P$, and no direct wave S. But there are two kinds of scattered waves: one is the P-to-P wave $\hat{G}_0^P \hat{V}_1^{PP}\hat{G}_0^P$, and the other is the P-to-S wave $\hat{G}_0^S \hat{V}_1^{SP}\hat{G}_0^P$. For the acoustic case, only the P wave exists, and hence we only have one equation $\phi^P = \hat{G}_0^P + \hat{G}_0^P \hat{V}_1^{PP}\hat{G}_0^P$.

Similarly, if only the S wave is incident, $F^P = 0$, $F^S = 1$, and the two equations 60 and 61 are, respectively, reduced to

$$\phi^P = \hat{G}_0^P \hat{V}_1^{PS}\hat{G}_0^S, \tag{64}$$

$$\phi^S = \hat{G}_0^S + \hat{G}_0^S \hat{V}_1^{SS}\hat{G}_0^S. \tag{65}$$

In this case, there is only the direct S wave $\hat{G}_0^S$, and no direct P wave. There are also two kinds of scattered waves: one is the S-to-P wave $\hat{G}_0^P \hat{V}_1^{PS}\hat{G}_0^S$, the other is the S-to-S wave $\hat{G}_0^S \hat{V}_1^{SS}\hat{G}_0^S$.

3.4 Linear inversion of a 1D elastic medium

Writing equation 54 in matrix form

$$\begin{pmatrix}\hat{D}^{PP} & \hat{D}^{PS}\\ \hat{D}^{SP} & \hat{D}^{SS}\end{pmatrix} = \begin{pmatrix}\hat{G}_0^P & 0\\ 0 & \hat{G}_0^S\end{pmatrix}\begin{pmatrix}\hat{V}_1^{PP} & \hat{V}_1^{PS}\\ \hat{V}_1^{SP} & \hat{V}_1^{SS}\end{pmatrix}\begin{pmatrix}\hat{G}_0^P & 0\\ 0 & \hat{G}_0^S\end{pmatrix}, \tag{66}$$

leads to four equations

$$\hat{D}^{PP} = \hat{G}_0^P \hat{V}_1^{PP}\hat{G}_0^P, \tag{67}$$

$$\hat{D}^{PS} = \hat{G}_0^P \hat{V}_1^{PS}\hat{G}_0^S, \tag{68}$$

$$\hat{D}^{SP} = \hat{G}_0^S \hat{V}_1^{SP}\hat{G}_0^P, \tag{69}$$

$$\hat{D}^{SS} = \hat{G}_0^S \hat{V}_1^{SS}\hat{G}_0^S. \tag{70}$$

For $z_s = z_g = 0$, in the $(k_s, z_s; k_g, z_g; \omega)$ domain, we get the following four equations relating the linear components of the three elastic parameters and the four data types:

$$\widetilde{D}^{PP}(k_g, 0; -k_g, 0; \omega) = -\frac{1}{4}\left(1 - \frac{k_g^2}{\nu_g^2}\right)\widetilde{a}_\rho^{(1)}(-2\nu_g) - \frac{1}{4}\left(1 + \frac{k_g^2}{\nu_g^2}\right)\widetilde{a}_\gamma^{(1)}(-2\nu_g) + \frac{2k_g^2\beta_0^2}{(\nu_g^2 + k_g^2)\alpha_0^2}\widetilde{a}_\mu^{(1)}(-2\nu_g), \tag{71}$$

$$\widetilde{D}^{PS}(\nu_g, \eta_g) = -\frac{1}{4}\left(\frac{k_g}{\nu_g} + \frac{k_g}{\eta_g}\right)\widetilde{a}_\rho^{(1)}(-\nu_g - \eta_g) - \frac{\beta_0^2}{2\omega^2}k_g(\nu_g + \eta_g)\left(1 - \frac{k_g^2}{\nu_g\eta_g}\right)\widetilde{a}_\mu^{(1)}(-\nu_g - \eta_g), \tag{72}$$

$$\widetilde{D}^{SP}(\nu_g, \eta_g) = \frac{1}{4}\left(\frac{k_g}{\nu_g} + \frac{k_g}{\eta_g}\right)\widetilde{a}_\rho^{(1)}(-\nu_g - \eta_g) + \frac{\beta_0^2}{2\omega^2}k_g(\nu_g + \eta_g)\left(1 - \frac{k_g^2}{\nu_g\eta_g}\right)\widetilde{a}_\mu^{(1)}(-\nu_g - \eta_g), \tag{73}$$

$$\widetilde{D}^{SS}(k_g, \eta_g) = -\frac{1}{4}\left(1 - \frac{k_g^2}{\eta_g^2}\right)\widetilde{a}_\rho^{(1)}(-2\eta_g) - \left[\frac{\eta_g^2 + k_g^2}{4\eta_g^2} - \frac{2k_g^2}{\eta_g^2 + k_g^2}\right]\widetilde{a}_\mu^{(1)}(-2\eta_g), \tag{74}$$

where

$$\nu_g^2 + k_g^2 = \frac{\omega^2}{\alpha_0^2},$$

$$\eta_g^2 + k_g^2 = \frac{\omega^2}{\beta_0^2}.$$

For the P-wave incidence case (see Figure 1), using $k_g^2/\nu_g^2 = \tan^2\theta$ and $k_g^2/(\nu_g^2 + k_g^2) = \sin^2\theta$, where θ is the P-wave incident angle, equation 71 becomes

$$\widetilde{D}^{PP}(\nu_g, \theta) = -\frac{1}{4}(1 - \tan^2\theta)\widetilde{a}_\rho^{(1)}(-2\nu_g) - \frac{1}{4}(1 + \tan^2\theta)\widetilde{a}_\gamma^{(1)}(-2\nu_g) + \frac{2\beta_0^2\sin^2\theta}{\alpha_0^2}\widetilde{a}_\mu^{(1)}(-2\nu_g). \tag{75}$$

In this case, when $\beta_0 = \beta_1 = 0$, equation 75 reduces to the acoustic two parameter case equation 7 in Zhang and Weglein (2005) for $z_g = z_s = 0$.

$$\widetilde{D}(q_g, \theta) = -\frac{\rho_0}{4}\left[\frac{1}{\cos^2\theta}\widetilde{\alpha_1}(-2q_g) + (1 - \tan^2\theta)\widetilde{\beta}_1(-2q_g)\right], \tag{76}$$

3.5 Direct non-linear inversion of 1D elastic medium

Writing equation 55 in matrix form:

$$\begin{pmatrix} \hat{G}_0^P & 0 \\ 0 & \hat{G}_0^S \end{pmatrix}\begin{pmatrix} \hat{V}_2^{PP} & \hat{V}_2^{PS} \\ \hat{V}_2^{SP} & \hat{V}_2^{SS} \end{pmatrix}\begin{pmatrix} \hat{G}_0^P & 0 \\ 0 & \hat{G}_0^S \end{pmatrix}$$

$$= - \begin{pmatrix} \hat{G}_0^P & 0 \\ 0 & \hat{G}_0^S \end{pmatrix} \begin{pmatrix} \hat{V}_1^{PP} & \hat{V}_1^{PS} \\ \hat{V}_1^{SP} & \hat{V}_1^{SS} \end{pmatrix} \begin{pmatrix} \hat{G}_0^P & 0 \\ 0 & \hat{G}_0^S \end{pmatrix} \begin{pmatrix} \hat{V}_1^{PP} & \hat{V}_1^{PS} \\ \hat{V}_1^{SP} & \hat{V}_1^{SS} \end{pmatrix} \begin{pmatrix} \hat{G}_0^P & 0 \\ 0 & \hat{G}_0^S \end{pmatrix}, \tag{77}$$

leads to four equations

$$\hat{G}_0^P \hat{V}_2^{PP} \hat{G}_0^P = -\hat{G}_0^P \hat{V}_1^{PP} \hat{G}_0^P \hat{V}_1^{PP} \hat{G}_0^P - \hat{G}_0^P \hat{V}_1^{PS} \hat{G}_0^S \hat{V}_1^{SP} \hat{G}_0^P, \tag{78}$$

$$\hat{G}_0^P \hat{V}_2^{PS} \hat{G}_0^S = -\hat{G}_0^P \hat{V}_1^{PP} \hat{G}_0^P \hat{V}_1^{PS} \hat{G}_0^S - \hat{G}_0^P \hat{V}_1^{PS} \hat{G}_0^S \hat{V}_1^{SS} \hat{G}_0^S, \tag{79}$$

$$\hat{G}_0^S \hat{V}_2^{SP} \hat{G}_0^P = -\hat{G}_0^S \hat{V}_1^{SP} \hat{G}_0^P \hat{V}_1^{PP} \hat{G}_0^P - \hat{G}_0^S \hat{V}_1^{SS} \hat{G}_0^S \hat{V}_1^{SP} \hat{G}_0^P, \tag{80}$$

$$\hat{G}_0^S \hat{V}_2^{SS} \hat{G}_0^S = -\hat{G}_0^S \hat{V}_1^{SP} \hat{G}_0^P \hat{V}_1^{PS} \hat{G}_0^S - \hat{G}_0^S \hat{V}_1^{SS} \hat{G}_0^S \hat{V}_1^{SS} \hat{G}_0^S. \tag{81}$$

Since $\hat{V}_1^{PP}$ relates to $\hat{D}^{PP}$, $\hat{V}_1^{PS}$ relates to $\hat{D}^{PS}$, and so on, the four components of the data will be coupled in the non-linear elastic inversion. We cannot perform the direct non-linear inversion without knowing all components of the data. As shown in Zhang and Weglein (2005) and this note, when the work on the two parameter acoustic case is extended to the present three parameter elastic case, it is not just simply adding one more parameter, but there are more issues involved. Even for the linear case, the linear solutions found in equations 71 $\sim$ 74 are much more complicated than those of the acoustic case. For instance, four different sets of linear parameter estimates are produced from each component of the data. Also, generally four distinct reflector mislocations arise from the two reference velocities (P-wave velocity and S-wave velocity).

The three parameters we are seeking to determine

- $a_\gamma \rightarrow$ relative change in bulk modulus,
- $a_\rho \rightarrow$ relative change in density,
- $a_\mu \rightarrow$ relative change in shear modulus,

are to be expanded as a series in the data. What data?

The answer is once again the data needed to determine those three quantities.

What H. Zhang's thesis has demonstrated for the first time is not only an explicit and direct set of equations for improving upon linear estimates of the changes in those elastic properties, but perhaps equally and maybe even more important, is for the first time the absolutely clear data requirements for determining a_γ, a_ρ and a_μ.

The data requirements are

$$D = \begin{pmatrix} \hat{D}^{PP} & \hat{D}^{PS} \\ \hat{D}^{SP} & \hat{D}^{SS} \end{pmatrix}, \tag{82}$$

for a $2D$ earth and generalize to a 3×3 matrix for a $3D$ earth with SH and SV shear waves.

The $2D$ message is delivered in equation 77, equations 78-81 that the first non-linear contribution to a_γ, a_μ, a_ρ requires that data; and, hence the exact determination of those elastic quantities also require that data set.

$$\begin{pmatrix} V^{PP} & V^{PS} \\ V^{SP} & V^{SS} \end{pmatrix} = \begin{pmatrix} V_1^{PP} & V_1^{PS} \\ V_1^{SP} & V_1^{SS} \end{pmatrix} + \begin{pmatrix} V_2^{PP} & V_2^{PS} \\ V_2^{SP} & V_2^{SS} \end{pmatrix} + \cdots \tag{83}$$

The logic is as follows:
$\begin{pmatrix} a_\gamma \\ a_\mu \\ a_\rho \end{pmatrix}$ requires $\begin{pmatrix} \hat{D}^{PP} & \hat{D}^{PS} \\ \hat{D}^{SP} & \hat{D}^{SS} \end{pmatrix}$ since $\begin{pmatrix} a_\gamma^{(2)} \\ a_\mu^{(2)} \\ a_\rho^{(2)} \end{pmatrix}$ requires $\begin{pmatrix} \hat{D}^{PP} & \hat{D}^{PS} \\ \hat{D}^{SP} & \hat{D}^{SS} \end{pmatrix}$. Hence $\begin{pmatrix} a_\gamma^{(1)} \\ a_\mu^{(1)} \\ a_\rho^{(1)} \end{pmatrix}$ must mean linear in $\begin{pmatrix} \hat{D}^{PP} & \hat{D}^{PS} \\ \hat{D}^{SP} & \hat{D}^{SS} \end{pmatrix}$, i.e., linear in the data needed to determine $\begin{pmatrix} a_\gamma \\ a_\mu \\ a_\rho \end{pmatrix}$.

Inverting

$$\hat{D}^{PP} = G_0^P V_1^{PP} G_0^P$$

alone for $a_\gamma^{(1)}$, $a_\mu^{(1)}$ and $a_\rho^{(1)}$ while mathematically achievable is a challenged and incorrect linear relationship since what you determine from that procedure doesn't represent the linear estimate of those quantities in terms of a data that can actually determine those quantities.

Solving for $a_\gamma^{(1)}$, $a_\mu^{(1)}$ and $a_\rho^{(1)}$ from $\hat{D}^{PP}$ alone is an injured or challenged linear estimate.

The inverse scattering series and task specific subseries need to : (1) treat the linear term with respect and then (2) the higher order terms can carry out their purpose.

If you injure the linear estimate, the inverse scattering series cannot recover or compensate–it wants the linear estimate to be the linear estimate, and never expects it to be exact or close to exact, but it never expects it to be less than linear, as well. Let linear be linear.

The power and promise of the inverse scattering series derives from its deliberate and physically consistent and explicit nature. It recognizes that when you perturb anything in a medium the associated perturbation in the wavefield is always non-linearly related to that change.

The inverse implies that the medium perturbation is itself non-linearly related to the perturbation in the wavefield; including the change in the wavefield on the measurement surface.

$$\psi_s = (\psi_s)_1 + (\psi_s)_2 + (\psi_s)_3 + \dots \tag{84}$$
$$V = V_1 + V_2 + V_3 + \dots, \tag{85}$$

where $(\psi_s)_n$ is the portion of ψ_s which is the n^{th} order in V and where V_n is the portion of V which is the n^{th} order in the measured values of ψ_s. That's it, equations 84 and 85. That is all you assume, and that is incontrovertible and hard to argue against.

Beyond that point the process and procedure for determining $V_1, V_2, V_3, \dots$ is out of your hands and away from your control. How you find V_1 from D is prescribed and what you do with V_1 to determine V_2 is also prescribed. That non-linear explicit and direct nature, and the steps to determine those terms $V_1, V_2, V_3, \dots$ are not decision-making opportunities for you. If *you* decide what to do with V_1 rather than have the non-linear relationship between data and V decide, then you step away from a single and defined physics into, e.g., the math world of iterative linear inversion or model matching. How do you formulate a multiple removal algorithm concept in iterative linear inverse or model matching scheme? The latter immediately aims to either improve or match the model properties with the subsurface. From the inverse scattering series perspective, the latter

all or nothing strategy is: (1) missing the opportunity to achieve other useful but less daunting tasks, i.e., multiple removal and depth imaging; and (2) moving at the first step straight into the most challenging task: parameter estimation, with all of the pitfalls of insufficient model-types and bandwidth sensitivities.

For the inverse scattering series the decisions are not under your control or influence. It is away from you and it is carrying out its single-minded purpose. It has one physical reference model, the water, and a single *unchanged* separation of the earth into a reference medium and a general perturbation operator that can accommodate a very wide range of earth model types, that need not be specified unless you want the direct non-linear AVO subseries. The ISS provides a set of direct equations to solve, with an analytic unchanged inverse operation.

Only that 100% physics consistent inverse formalism predicted that you required all four components of the data $\begin{pmatrix} \hat{D}^{PP} & \hat{D}^{PS} \\ \hat{D}^{SP} & \hat{D}^{SS} \end{pmatrix}$ to even linearly estimate elastic properties. Iterative linear inversion tries to substitute a set of constantly changed problems with linear updates for a single entirely prescriptive, consistent and explicit non-linear physics. The latter is the inverse scattering series, the former has an attraction to linear inverses (and generalized inverses) which has no single physical theory and consistency. Linear inversion and generalized inverse theory are part of standard graduate training in geophysics; and, hence it's easy to understand trying to recast the actual non-linear problem into a set of iterative linear problems where the tools are familiar. The model matching schemes and iteratively linear inversion are reasonable and sometimes useful but they are more math than physics and have no way to provide the framework for inversion that staying consistent with the physics will provide.

The practical added value that direct ISS non-linear inversion provided beyond linear inversion, is described in Zhang (2006), Zhang and Weglein (2005), Zhang and Weglein (2006), Zhang and Weglein (2009a), and Zhang and Weglein (2009b). There are circumstances where very different target lithologies have very similar changes in mechanical properties. The added-value was demonstrated in 4D application in discriminating between pressure and fluid saturation effects. That distinction results in the difference between a drill and a no-drill decision.

4 Conclusion

There is a unique and unambiguous data requirement message sent out from the inverse scattering series for linear and non-linear direct inversion. Other methods and approaches that look at the inverse problem, e.g., either linear or beyond linear, e.g., iterative linear or model matching indirect inversion methods have never and will never provide that clarity and definition. We can model-match D_{pp} or iteratively invert D_{pp} until the cows come home and you will find *ambiguities* and resolution challenges, and when those methods use more data, they sometimes produce less ambiguity and better resolution, but we don't know why.

As a final remark it is interesting to note that the first and linear term of the elastic inverse problem was not only influenced by the non-linear term, it was in fact defined by that term. That data requirement message, along with the entire inverse series apparatus, results from the

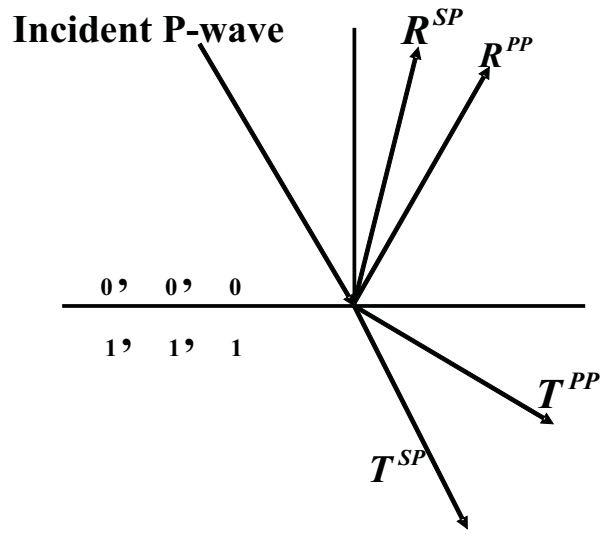

Figure 1: *Response of incident compressional wave on a planar elastic interface. α_0, β_0 and ρ_0 are the compressional wave velocity, shear wave velocity and density of the upper layer, respectively; α_1, β_1 and ρ_1 denote the compressional wave velocity, shear wave velocity and density of the lower layer. R^{PP}, R^{SP}, T^{PP} and T^{SP} denote the coefficients of the reflected compressional wave, the reflected shear wave, the transmitted compressional wave and the transmitted shear wave, respectively (Foster et al., 1997).*

observation that the perturbed wavefield and the perturbation are non-linearly related. Honor and respect that fundamental non-linear relationship and a physics driven set of consistent, deliberate and purposeful algorithms and a clear platform and unambiguous framework (that explains earlier anecdotal experiences) are the dividend and value.

Acknowledgements

We thank all sponsors of M-OSRP for their support and encouragement. We have been partially funded by and are grateful for NSF-CMG award DMS-0327778 and DOE Basic Sciences award DE-FG02-05ER15697. We would like to thank BP America, ConocoPhillips and WesternGeco for permission to publish. A.B. Weglein would like to thank R.H. Stolt, Doug Foster, and Bob Keys for stimulating, interesting and very helpful discussions.

References

Aki, K. and P. G. Richards. *Quantitative Seismology.* 2nd edition. University Science Books, 2002.

Foster, D. J., R. G. Keys, and D. P. Schmitt. *Detecting subsurface hydrocarbons with elastic*

wavefields. Springer-In Inverse Problems in Wave Progagation, Volume 90 of The IMA Volumes in Mathematics and its Applications, 1997.

Keys, R. G. "Polarity reversals in reflections from layered media." *Geophysics* 54 (1989): 900–905.

Matson, K. H. *An inverse-scattering series method for attenuating elastic multiples from multi-component land and ocean bottom seismic data*. PhD thesis, University of British Columbia, 1997.

Taylor, J. R. *Scattering theory: the quantum theory of nonrelativistic collisions*. John Wiley & Sons, Inc., 1972.

Weglein, A. B., F. V. Araújo, P. M. Carvalho, R. H. Stolt, K. H. Matson, R. T. Coates, D. Corrigan, D. J. Foster, S. A. Shaw, and H. Zhang. "Inverse Scattering Series and Seismic Exploration." *Inverse Problems* (2003): R27–R83.

Weglein, A. B., D. J. Foster, K. H. Matson, S. A. Shaw, P. M. Carvalho, and D. Corrigan. "Predicting the correct spatial location of reflectors without knowing or determining the precise medium and wave velocity: initial concept, algorithm and analytic and numerical example." *Journal of Seismic Exploration* 10 (2002): 367–382.

Weglein, A. B., F. A. Gasparotto, P. M. Carvalho, and R. H. Stolt. "An Inverse-Scattering Series Method for Attenuating Multiples in Seismic Reflection Data." *Geophysics* 62 (November-December 1997): 1975–1989.

Weglein, A. B. and R. H. Stolt. "Approaches on linear and non-linear migration-inversion." Personal Communication (1992).

Zhang, H. *Direct non-linear acoustic and elastic inversion: Towards fundamentally new comprehensive and realistic target identification*. PhD thesis, University of Houston, 2006.

Zhang, H. and A. B. Weglein. "The inverse scattering series for tasks associated with primaries: Depth imaging and direct non-linear inversion of 1D variable velocity and density acoustic media." *75th Annual Internat. Mtg., Soc. Expl. Geophys., Expanded Abstracts*. . Soc. Expl. Geophys., 2005. 1705–1708.

Zhang, H. and A. B. Weglein. "The inverse scattering series for tasks associated with primaries: direct non-linear inversion of 1D elastic media." *76th Annual Internat. Mtg., Soc. Expl. Geophys., Expanded Abstracts*. . Soc. Expl. Geophys., 2006. 2062–2066.

Zhang, H. and A. B. Weglein. "Direct non-linear inversion of 1D acoustic media using inverse scattering subseries." *Geophysics* submitted (2009).

Zhang, H. and A. B. Weglein. "Direct non-linear inversion of multi-parameter 1D elastic media using the inverse scattering series." *Geophysics* submitted (2009).

Direct non-linear inversion of 1D acoustic media using inverse scattering subseries

H. Zhang[1] and A. B. Weglein[2]
[1] Previously Department of Physics, University of Houston, currently ConocoPhillips, 600 N. Dairy Ashford Houston, TX 77079
[2] University of Houston, 617 Science and Research Bldg. 1, Houston, TX 77204-5005

Abstract

A task specific multi-parameter (more than one mechanical property changes across a reflector) direct non-linear inversion subseries of the inverse scattering series is derived and tested for a vertically velocity and density varying acoustic medium. Here "task specific" means that the terms in the distinct subseries obtained corresponding to the tasks for imaging-only and inversion-only are identified and separated, and "direct" means that there are formulas that explicitly and straight-away solve for and output the physical properties, without e.g., search algorithms, model matching and optimization schemes, and proxies that typically characterize indirect methods. Numerical test results with analytic data indicate that one term beyond linear provides added value beyond standard linear techniques, and the improved estimates are valid over a larger range of angles. The acoustic direct inverse target identification is non-linear. It serves as an important step for new concepts and methods to guide the much more complicated and minimally realistic elastic inverse for exploration seismology target identification purposes.

1 Introduction

The objective of seismic exploration is to determine the location (imaging) and mechanical properties (inversion) of subsurface targets to identify hydrocarbon resources in the earth using recorded data. Current inversion methods include: (1) the linear approximation (e.g., Clayton and Stolt, 1981) which is often useful, especially in the presence of small earth property changes across the boundary and/or small angle reflections, and (2) indirect model matching methods with global searching (e.g., Tarantola et al., 1984; Sen and Stoffa, 1995; Mora, 1987; C. Bunks and Chavent, 1995; E. Forgues and Pratt, 1998 and Shin and Min, 2006) which define an objective function assumed to be minimized when the best fitting model is obtained. The assumptions of the former methods (like the small contrast assumptions) are often violated in practice and can cause erroneous predictions; the latter category usually involves a significant and often daunting computation effort (especially in multi-D cases) and/or sometimes have reported erroneous or ambiguous results. In order to provide more accurate and reliable target identification especially with large contrast, large angle target geometry, in present paper, a more comprehensive multi-parameter multi-dimensional direct non-linear inversion framework is developed based on the inverse scattering task-specific subseries (see, e.g., Weglein et al., 2003). The inverse scattering series has a tremendous generality and comprehensiveness allowing many distinct traditional processing objectives to be achieved within

a single framework, but without the traditional need to provide information about the properties that govern actual wave propagation in the earth. It begins with scattering theory, which is the relationship between the perturbation or alteration in a medium's properties and the concomitant perturbation or change in the wave field. The relationship between those two changes is always non-linear. Any change in a medium will result in a change in the wave-field that is non-linearly related to that physical property change. Specifically, in thispresent paper we examine the relationship between the perturbation in a medium and the perturbation in a wave field for the case of a 1D variable velocity and variable density acoustic medium. Like other methods, the algorithm presented in the current paper also has its assumptions. We assume the original unperturbed medium is a homogeneous whole-space. We further assume that free surface and internal multiples have been removed from the recorded data (see, e.g., Weglein et al., 2003), and we assume that we are recording primaries. Our objectives are to: (1) locate reflectors and (2) determine medium properties of the actual medium. In thiscurrent paper we present: (1) the first derivation of equations to directly achieve those two distinct objectives for a one dimensional velocity and density varying acoustic medium [1], and (2) we then reduce this general formalism to the special case of a single horizontal reflector, where the acoustic medium above the reflector is known, but the objective is to determine the acoustic properties of the half-space below the reflector.

The original inverse scattering series research aimed at separating imaging and inversion tasks on primaries was developed for a 1D acoustic one parameter case (constant density medium, only velocity variable in depth) and a plane wave at normal incidence (Weglein et al., 2002; Shaw et al., 2003). In thispresent paper we move a step closer to seismic exploration relevance by extending that earlier work to a multi-parameter acoustic model — two parameter case (velocity and density vary vertically in depth) and allowing for point sources and receivers over a 1D acoustic medium. Clayton and Stolt (1981) gave a two parameter *linear* inversion solution for *2D* acoustic media (velocity and density vary both vertically and laterally). In thispresent paper, we use the same parameters but concentrate on *1D* acoustic media to derive the direct *non-linear* inversion solution. The extension of this work to the 1D isotropic elastic medium case using three parameters is presented in another paper Zhang and Weglein (2006) or Zhang and Weglein (2009). In the application of the direct *non-linear* inverse algorithm, we move one step each time (e.g., from one parameter 1D acoustic case to two parameter 1D acoustic case, or to one parameter 2D acoustic case, instead of 'jumping' directly to two parameter 2D acoustic case) so that we can solve the problem step by step and learn lessons from each step which would guide us to step further towards our goal of greater realism and increased reliable prediction. For one parameter 1D and 2D acoustic media, two important references on direct non-linear imaging with reference velocity are presented by Shaw (2005) and Liu et al. (2005), respectively. It has been shown in thiscurrent paper that imaging and inversion for two parameter medium are much more complicated compared to one parameter case, although it seems like just simply adding one parameter. Examples of the new inverse issues that arise in a two parameter world (and needed responses) that have no one parameter analogue are leakage (and the inverse scattering series response for that new challenge) and the identification of the special parameter for inversion that avoids leakage, and the conceptual insights that this understanding provides for our campaign to address pressing imaging and inversion challenges.

[1]For numerical example, please see Shaw (2005) for imaging-only term tests on one parameter acoustic cases and Zhang (2006) for inversion-only term tests on one or multi-parameter cases.

For the direct non-linear inversion solution obtained in thispresent paper, the tasks for imaging-only and inversion-only terms are separated. Tests with analytic data indicate significant added value for parameter predictions, beyond linear estimates, in terms of both the proximity to actual value and the increased range of angles over which the improved estimates are useful.

A closed form of the inversion terms for the one-interface case is also obtained. This closed form might be useful in predicting the precritical data using the postcritical data. [2]

A special parameter Δc ($\Delta c = c - c_0$) (P-wave velocity change across an interface) is also found. Its Born inversion $(\Delta c)_1$ always has the right sign. That is, the sign of $(\Delta c)_1$ is always the same as that of Δc. In practice, it could be very useful to know whether the velocity increases or decreases across the interface. After changing parameters, from α (relative changes in P-wave bulk modulus) and β (relative changes in density) to velocity and β, another form of the non-linear solution is obtained. There is no leakage correction (please see details in the section on three important messages) in this solution. This new form clearly indicates that the imaging terms "care" only about velocity errors, ...and produce the depth image without knowing or requiring the velocity, in principle or practice, neither directly nor indirectly. The second term in the imaging series first determines if the input velocity is adequate. If the velocity is determined to be adequate then the second term and all the terms beyond that term in the imaging series are zero. In that case the imaging series reduces to its first term which is conventional depth imaging. This generalizes to multi-D media, and also points to possible model-type independent imaging which only depends on velocity changes.

The following section is a brief introduction of the inverse scattering subseries. We then gave the one dimensional multi-parameter acoustic derivation in detail, and that is followed by the numerical tests for the single reflector case. We also provided a further discussion about the special physical non-leaking acoustic parameter.

2 Inverse scattering subseries

Scattering theory relates the perturbation (the difference between the reference and actual medium properties) to the scattered wave field (the difference between the reference medium's and the actual medium's wave field). It is therefore reasonable that in discussing scattering theory, we begin with the basic wave equations governing the wave propagation in the actual and reference medium, respectively [3],

$$LG = \delta, \tag{1}$$

$$L_0 G_0 = \delta, \tag{2}$$

where L and L_0 are respectively the differential operators that describe wave propagation in the actual and reference medium, and G and G_0 are the corresponding Green's operators. The δ on the right hand side of both equations is a Dirac delta operator and represents an impulsive source.

[2] Precritical data refers to a plane wave incident upon a reflector, and the emanating reflected wave-field emerges at less than the critical angle from the normal.

[3] In this introductory math development, we follow closely Weglein et al. (1997); Weglein et al. (2002); Weglein et al. (2003).

The perturbation is defined as $V = L_0 - L$. The Lippmann-Schwinger equation,

$$G = G_0 + G_0 V G, \tag{3}$$

relates G, G_0 and V (see, e.g., Taylor, 1972). Iterating this equation back into itself generates the forward scattering series

$$G = G_0 + G_0 V G_0 + G_0 V G_0 V G_0 + \cdots . \tag{4}$$

Then the scattered field $\psi_s \equiv G - G_0$ can be written as

$$\begin{aligned} \psi_s &= G_0 V G_0 + G_0 V G_0 V G_0 + \cdots \\ &= (\psi_s)_1 + (\psi_s)_2 + \cdots , \end{aligned} \tag{5}$$

where $(\psi_s)_n$ is the portion of ψ_s that is n^{th} order in V. The measured values of ψ_s are the data, D, where

$$D = (\psi_s)_{ms} = (\psi_s)_{\text{on the measurement surface}}.$$

In the inverse scattering series, expanding V as a series in orders of D,

$$V = V_1 + V_2 + V_3 + \cdots , \tag{6}$$

where the subscript "i" in V_i (i=1, 2, 3, ...) denotes the portion of V i-th order in the data. Substituting equation 6 into equation 5, and evaluating equation 5 on the measurement surface yields

$$D = [G_0(V_1 + V_2 + \cdots)G_0]_{ms} + [G_0(V_1 + V_2 + \cdots)G_0(V_1 + V_2 + \cdots)G_0]_{ms} + \cdots . \tag{7}$$

Setting terms of equal order in the data equal, leads to the equations that determine V_1, V_2, ... directly from D and G_0.

$$D = [G_0 V_1 G_0]_{ms}, \tag{8}$$

$$0 = [G_0 V_2 G_0]_{ms} + [G_0 V_1 G_0 V_1 G_0]_{ms}, \tag{9}$$

$$\begin{aligned} 0 =& [G_0 V_3 G_0]_{ms} + [G_0 V_1 G_0 V_2 G_0]_{ms} + [G_0 V_2 G_0 V_1 G_0]_{ms} \\ &+ [G_0 V_1 G_0 V_1 G_0 V_1 G_0]_{ms}, \end{aligned} \tag{10}$$

etc. Equations (8) $\sim$ (10) permit the sequential calculation of V_1, V_2, ..., and, hence, achieve full inversion for V (see equation 6 from the recorded data D and the reference wave field (i.e., the Green's operator of the reference medium) G_0. Therefore, the inverse scattering series is a multi-D inversion procedure that directly determines physical properties using only reflection data and reference medium information.

3 Derivation of α_1, β_1 and α_2, β_2

In this section, we will consider a 1D acoustic two parameter earth model (e.g. bulk modulus and density or velocity and density). We start with the 3D (3D earth model and 3D geometrical spreading or wave propagation) acoustic wave equations in the actual and reference medium (Clayton and Stolt, 1981; Weglein et al., 1997)

$$\left[\frac{\omega^2}{K(\mathbf{r})} + \nabla \cdot \frac{1}{\rho(\mathbf{r})}\nabla\right] G(\mathbf{r}, \mathbf{r}_s; \omega) = \delta(\mathbf{r} - \mathbf{r}_s), \tag{11}$$

$$\left[\frac{\omega^2}{K_0(\mathbf{r})} + \nabla \cdot \frac{1}{\rho_0(\mathbf{r})}\nabla\right] G_0(\mathbf{r}, \mathbf{r}_s; \omega) = \delta(\mathbf{r} - \mathbf{r}_s), \tag{12}$$

where $G(\mathbf{r}, \mathbf{r}_s; \omega)$ and $G_0(\mathbf{r}, \mathbf{r}_s; \omega)$ are respectively the free-space causal Green's functions that describe wave propagation in the actual and reference medium. $K = c^2\rho$, is P-wave bulk modulus, c is P-wave velocity and ρ is the density. The quantities with subscript "0" are for the reference medium, and those without the subscript are for the actual medium. The perturbation is

$$V = L_0 - L = \frac{\omega^2\alpha}{K_0} + \nabla \cdot \frac{\beta}{\rho_0}\nabla, \tag{13}$$

where $\alpha = 1 - \frac{K_0}{K}$ and $\beta = 1 - \frac{\rho_0}{\rho}$ are the two parameters we choose to do the inversion. Assuming both ρ_0 and c_0 are constants, equation 12 becomes

$$\left(\frac{\omega^2}{c_0^2} + \nabla^2\right) G_0(\mathbf{r}, \mathbf{r}_s; \omega) = \rho_0\delta(\mathbf{r} - \mathbf{r}_s). \tag{14}$$

For the 1-D1D vertically varying only medium case, the perturbation V has the following form

$$V(z, \nabla) = \frac{\omega^2\alpha(z)}{K_0} + \frac{1}{\rho_0}\beta(z)\frac{\partial^2}{\partial x^2} + \frac{1}{\rho_0}\frac{\partial}{\partial z}\beta(z)\frac{\partial}{\partial z}. \tag{15}$$

$V(z, \nabla)$, $\alpha(z)$ and $\beta(z)$ can be expanded respectively as

$$V(z, \nabla) = V_1(z, \nabla) + V_2(z, \nabla) + \cdots, \tag{16}$$

$$\alpha(z) = \alpha_1(z) + \alpha_2(z) + \cdots, \tag{17}$$

$$\beta(z) = \beta_1(z) + \beta_2(z) + \cdots. \tag{18}$$

Where the subscript "i" in V_i, α_i and β_i (i=1, 2, 3, ...) denote the portion of those quantities i-th order in the data.Then we have

$$V_1(z, \nabla) = \frac{\omega^2\alpha_1(z)}{K_0} + \frac{1}{\rho_0}\beta_1(z)\frac{\partial^2}{\partial x^2} + \frac{1}{\rho_0}\frac{\partial}{\partial z}\beta_1(z)\frac{\partial}{\partial z}, \tag{19}$$

$$V_2(z, \nabla) = \frac{\omega^2\alpha_2(z)}{K_0} + \frac{1}{\rho_0}\beta_2(z)\frac{\partial^2}{\partial x^2} + \frac{1}{\rho_0}\frac{\partial}{\partial z}\beta_2(z)\frac{\partial}{\partial z}, \tag{20}$$

$$\vdots$$

SSpecifically, for the 1D acoustic medium mentioned above and 2D data (2D geometrical spreading) case, substituting equation 19 into equation 8, we can get the linear solution for α_1 and β_1 in the frequency domain (more details about the derivation could be found in Zhang, 2006)

$$\widetilde{D}(q_g,\theta,z_g,z_s)=-\frac{\rho_0}{4}e^{-iq_g(z_s+z_g)}\left[\frac{1}{\cos^2\theta}\widetilde{\alpha_1}(-2q_g)+(1-\tan^2\theta)\widetilde{\beta}_1(-2q_g)\right], \tag{21}$$

where $\widetilde{D}$, $\widetilde{\alpha_1}$ and $\widetilde{\beta}_1$ are in the frequency domain after the Fourier transform over z. The subscripts s and g denote source and receiver quantities respectively, and q_g, θ and $k=\omega/c_0$ shown in Figure 1, have the following relations (Matson, 1997)

$$\begin{aligned} q_g &= q_s = k\cos\theta,\\ k_g &= k_s = k\sin\theta. \end{aligned}$$

Similarly, substituting equation 20 into equation 9, we can get the solution for $\alpha_2(z)$ and $\beta_2(z)$ as a function of $\alpha_1(z)$ and $\beta_1(z)$

$$\begin{aligned} \frac{1}{\cos^2\theta}\alpha_2(z)+(1-\tan^2\theta)\beta_2(z) =& -\frac{1}{2\cos^4\theta}\alpha_1^2(z)-\frac{1}{2}(1+\tan^4\theta)\beta_1^2(z)+\frac{\tan^2\theta}{\cos^2\theta}\alpha_1(z)\beta_1(z)\\ &-\frac{1}{2\cos^4\theta}\alpha_1'(z)\int_0^z dz'[\alpha_1(z')-\beta_1(z')]\\ &+\frac{1}{2}(\tan^4\theta-1)\beta_1'(z)\int_0^z dz'[\alpha_1(z')-\beta_1(z')], \end{aligned} \tag{22}$$

where $\alpha_1'(z)=\frac{\mathrm{d}\alpha_1(\mathrm{z})}{\mathrm{dz}}$, $\beta_1'(z)=\frac{\mathrm{d}\beta_1(\mathrm{z})}{\mathrm{dz}}$.

The first two parameter direct non-linear inversion of 1D acoustic media for a 2D experiment has been obtained. As shown in equations 21 and 22, given two different angles θ, we can determine α_1, β_1 and then α_2, β_2. For a single-interface example, it can be shown that only the first three terms on the right hand side contribute to parameter predictions, while the last two terms perform imaging in depth since they will be zero after the integration across the interface (see the section on three important messages). Therefore, in this solution, the tasks for imaging-only and inversion-only terms are separated.

For the $\theta=0$ and constant density case, equation 22 reduces to the non-linear solution for 1D one parameter normal incidence case (e.g., Shaw, 2005)

$$\alpha_2(z)=-\frac{1}{2}\left[\alpha_1^2(z)+\alpha_1'(z)\int_{-\infty}^z dz'\alpha_1(z')\right]. \tag{23}$$

If another choice of free parameter other than θ (e.g., ω or k_h) is selected, then the functional form between the data and the first order perturbation equation 21 would change. Furthermore,

the relationship between the first and second order perturbation equation 22 would, then, also be different, and new analysis would be required for the purpose of identifying specific task separated terms. Empirically, the choice of θ as free parameter (for a 1D medium) is particularly well suited for allowing a task separated identification of terms in the inverse series.

There are several important messages that exist in equations 21 and 22: (1) purposeful perturbation, (2) leakage, and (3) the special parameter for inversion. These three concepts will be discussed later in thispresent paper. In equation 21, it seems simple and straightforward to use data at two angles in order to obtain α_1 and β_1. This is what we do in thiscurrent paper. However, by doing this, it requires a whole new understanding of the definition of "the data". That is part of the discoveries of on-going research activities by Weglein et al. (2007)Weglein (2007). The imaging algorithm given by Liu et al. (2005) has been generalized to the two parameter case by Weglein et al. (2007)Weglein (2007) based on the understanding of equation 22.

4 A special case: one-interface model

In this section, we derive a closed form for the inversion-only terms. From this closed form, we can easily get the same inversion terms as those in equations 21 and 22. We also show some numerical tests using analytic data. From the numerical results, we see how the corresponding non-linear terms contribute to the parameter predictions such as the relative changes in the P-wave bulk modulus $\left(\alpha = \frac{\Delta K}{K}\right)$, density $\left(\beta = \frac{\Delta \rho}{\rho}\right)$, impedance $\left(\frac{\Delta I}{I}\right)$ and velocity $\left(\frac{\Delta c}{c}\right)$.

4.1 Closed form for the inversion terms

1. Incident angle not greater than critical angle, i.e. $\theta \leq \theta_c$

For a single interface example, the reflection coefficient has the following form (Keys, 1989)

$$R(\theta) = \frac{(\rho_1/\rho_0)(c_1/c_0)\sqrt{1-\sin^2\theta} - \sqrt{1-(c_1^2/c_0^2)\sin^2\theta}}{(\rho_1/\rho_0)(c_1/c_0)\sqrt{1-\sin^2\theta} + \sqrt{1-(c_1^2/c_0^2)\sin^2\theta}}. \tag{24}$$

After adding 1 on both sides of equation 24, we can get

$$1 + R(\theta) = \frac{2\cos\theta}{\cos\theta + (\rho_0/\rho_1)\sqrt{\left(c_0^2/c_1^2\right) - \sin^2\theta}}. \tag{25}$$

Then, using the definitions of $\alpha = 1 - \frac{K_0}{K_1} = 1 - \frac{\rho_0 c_0^2}{\rho_1 c_1^2}$ and $\beta = 1 - \frac{\rho_0}{\rho_1}$, equation 25 becomes

$$\frac{4R(\theta)}{(1+R(\theta))^2} = \frac{\alpha}{\cos^2\theta} + (1-\tan^2\theta)\beta - \frac{\alpha\beta}{\cos^2\theta} + \beta^2\tan^2\theta, \tag{26}$$

which is the closed form we derived for the one interface two parameter acoustic inversion-only terms.

2. Incident angle greater than critical angle, i.e. $\theta > \theta_c$

For the same single interface example as above and looking at the equation 24, if $c_0 < c_1$, then the term $1-(c_1^2/c_0^2)\sin^2\theta$ under the square root would be less than zero as $\theta > \theta_c$, equation 24 becomes

$$R(\theta) = \frac{(\rho_1/\rho_0)(c_1/c_0)\sqrt{1-\sin^2\theta} - i\sqrt{(c_1^2/c_0^2)\sin^2\theta - 1}}{(\rho_1/\rho_0)(c_1/c_0)\sqrt{1-\sin^2\theta} + i\sqrt{(c_1^2/c_0^2)\sin^2\theta - 1}}. \tag{27}$$

Then, equation 25 becomes

$$1 + R(\theta) = \frac{2\cos\theta}{\cos\theta + i\,(\rho_0/\rho_1)\sqrt{\sin^2\theta - \left(c_0^2/c_1^2\right)}}, \tag{28}$$

which leads to the same closed form as equation 26

$$\frac{4R(\theta)}{(1+R(\theta))^2} = \frac{\alpha}{\cos^2\theta} + (1-\tan^2\theta)\beta - \frac{\alpha\beta}{\cos^2\theta} + \beta^2\tan^2\theta.$$

As we see, this closed form is valid for all incident angles.

In addition, for normal incidence ($\theta = 0$) and constant density ($\beta = 0$) media, the closed form equation 26 will be reduced to

$$\alpha = \frac{4R}{(1+R)^2}. \tag{29}$$

This represents the relationship between α and R for the one parameter 1D acoustic constant density medium and 1D normal incidence obtained in Innanen (2003). In this case, α becomes $1 - c_0^2/c_1^2$ and R becomes $(c_1 - c_0)\,/\,(c_1 + c_0)$.

3. Derivation of the inversion terms from the closed form

From the closed form equation 26, using Taylor expansion on the left hand side

$$\frac{1}{(1+R(\theta))^2} = \left[1 - R(\theta) + R^2(\theta) - \ldots\right]^2,$$

and setting the terms of equal order in the data equal, we have

$$\frac{\alpha_1}{\cos^2\theta} + (1-\tan^2\theta)\beta_1 = 4R(\theta), \tag{30}$$

$$\frac{\alpha_2}{\cos^2\theta} + (1-\tan^2\theta)\beta_2 = -\frac{1}{2}\frac{\alpha_1^2}{\cos^4\theta} - \frac{1}{2}(1+\tan^4\theta)\beta_1^2 + \frac{\tan^2\theta}{\cos^2\theta}\alpha_1\beta_1. \tag{31}$$

For a one-interface example (in Figure 2), equations 21 and 22 will respectively reduce to the same form as equations 30 and 31, which is shown below.

Assume the interface surface is at depth $z = a$, and suppose $z_s = z_g = 0$. Using the analytic data (Clayton and Stolt, 1981; Weglein et al., 1986),

$$\widetilde{D}(q_g, \theta) = \rho_0 R(\theta)\frac{e^{2iq_g a}}{4\pi i q_g}, \tag{32}$$

and substituting equation 32 into equation 21, after Fourier transformation over $2q_g$, for $z > a$ and fixed θ, we get

$$\frac{1}{\cos^2\theta}\alpha_1(z) + (1-\tan^2\theta)\beta_1(z) = 4R(\theta)H(z-a). \tag{33}$$

Also, the non-linear solution equation 22 will reduce to

$$\begin{aligned}\frac{1}{\cos^2\theta}\alpha_2(z) + (1-\tan^2\theta)\beta_2(z) = &-\frac{1}{2\cos^4\theta}\alpha_1^2(z) - \frac{1}{2}(1+\tan^4\theta)\beta_1^2(z) \\ &+ \frac{\tan^2\theta}{\cos^2\theta}\alpha_1(z)\beta_1(z),\end{aligned} \tag{34}$$

The two equations 33 and 34 agree with equations 30 and 31, respectively.

4.2 Numerical tests

From equation 33, we choose two different angles to solve for α_1 and β_1

$$\beta_1(\theta_1,\theta_2) = 4\frac{R(\theta_1)\cos^2\theta_1 - R(\theta_2)\cos^2\theta_2}{\cos(2\theta_1)-\cos(2\theta_2)}, \tag{35}$$

$$\alpha_1(\theta_1,\theta_2) = \beta_1(\theta_1,\theta_2) + 4\frac{R(\theta_1)-R(\theta_2)}{\tan^2\theta_1 - \tan^2\theta_2}. \tag{36}$$

Similarly, from equation 34, given two different angles we can solve for α_2 and β_2 in terms of α_1 and β_1

$$\begin{aligned}\beta_2(\theta_1,\theta_2) = \Bigg[&-\frac{1}{2}\alpha_1^2\left(\frac{1}{\cos^2\theta_1} - \frac{1}{\cos^2\theta_2}\right) + \alpha_1\beta_1\left(\tan^2\theta_1 - \tan^2\theta_2\right) - \frac{1}{2}\beta_1^2 \\ &\times\left(\cos^2\theta_1 - \cos^2\theta_2 + \frac{\sin^4\theta_1}{\cos^2\theta_1} - \frac{\sin^4\theta_2}{\cos^2\theta_2}\right)\Bigg] / \left[\cos(2\theta_1)-\cos(2\theta_2)\right],\end{aligned} \tag{37}$$

$$\begin{aligned}\alpha_2(\theta_1,\theta_2) = &\beta_2(\theta_1,\theta_2) + \left[-\frac{1}{2}\alpha_1^2\left(\frac{1}{\cos^4\theta_1} - \frac{1}{\cos^4\theta_2}\right) + \alpha_1\beta_1\left(\frac{\tan^2\theta_1}{\cos^2\theta_1} - \frac{\tan^2\theta_2}{\cos^2\theta_2}\right)\right. \\ &\left.-\frac{1}{2}\beta_1^2\left(\tan^4\theta_1 - \tan^4\theta_2\right)\right] / \left(\tan^2\theta_1 - \tan^2\theta_2\right);\end{aligned} \tag{38}$$

where α_1 and β_1 in equations 37 and 38 denote $\alpha_1(\theta_1,\theta_2)$ and $\beta_1(\theta_1,\theta_2)$, respectively.

For a specific model, $\rho_0 = 1.0g/cm^3$, $\rho_1 = 1.1g/cm^3$, $c_0 = 1500m/s$ and $c_1 = 1700m/s$, in the following figures we give the results for the relative changes in the P-wave bulk modulus $\left(\alpha = \frac{\Delta K}{K}\right)$, density $\left(\beta = \frac{\Delta\rho}{\rho}\right)$, impedance $\left(\frac{\Delta I}{I}\right)$ and velocity $\left(\frac{\Delta c}{c}\right)$ corresponding to different pairs of θ_1 and θ_2.

From Figure 3, we can see that when we add α_2 to α_1, the result is much closer to the exact value of α. Furthermore, the result is better behaved; i.e., the plot surface becomes flatter, over a larger range of precritical angles. Similarly, as shown in Figure 4, the results of $\beta_1 + \beta_2$ are much better

than those of β_1. In addition, the sign of β_1 is wrong at some angles, while, the results for $\beta_1 + \beta_2$ always have the right sign. So after including β_2, the sign of the density is corrected, which is very important in the earth identification, and also the results of $\frac{\Delta I}{I}$ (see Figure 5) and $\frac{\Delta c}{c}$ (see Figure 6) are much closer to their exact values respectively compared to the linear results.

Especially, the values of $\left(\frac{\Delta c}{c}\right)_1$ are always greater than zero, that is, the sign of $(\Delta c)_1$ is always positive, which is the same as that of the exact value Δc. We will further discuss this in the next section.

5 Three important messages

As mentioned before, in general, since the relationship between data and target property changes is non-linear, linear inversion will produce errors in target property prediction. When one actual property change is zero, the linear prediction of the change can be non-zero. For example, considering equation 24 and equation 35, in the case of $\rho_1 = \rho_0$, the actual density change β is zero, but the linear approximation of the change β_1 could be non-zero. Also, when the actual change is positive, the predicted linear approximation can be negative. There is a special parameter for linear inversion of acoustic media, that never suffers the latter problem.

From equation 24 we can see that when $c_0 = c_1$, the reflection coefficient is independent of θ, then from the linear form equation 36, we have

$$\left(\frac{\Delta c}{c}\right)_1 = \frac{1}{2}(\alpha_1 - \beta_1) = 0 \text{ when } \Delta \mathrm{c} = 0,$$

i.e., when $\Delta c = 0$, $(\Delta c)_1 = 0$. This generalizes to $(\Delta c)_1 > 0$ when $\Delta c > 0$, or $(\Delta c)_1 < 0$ when $\Delta c < 0$, as well. This can be shown mathematically (See Appendix B for details).

Therefore, we can, first, get the right sign of the relative change in P-wave velocity from the linear inversion $(\Delta c)_1$, then, get more accurate values by including non-linear terms.

Another interesting point is that the image does not move when the velocity does not change across an interface, i.e., $c_0 = c_1$, since, in this situation, the integrands of imaging terms $\alpha_1 - \beta_1$ in equation 22 are zero. We can see this more explicitly when we change the two parameters α and β to $\frac{\Delta c}{c}$ and β. Using the two relationships below (See details in Appendix A)

$$\left(\frac{\Delta c}{c}\right)_1 = \frac{1}{2}(\alpha_1 - \beta_1),$$

and

$$\left(\frac{\Delta c}{c}\right)_2 = \frac{1}{2}\left[\frac{1}{4}(\alpha_1 + \beta_1)^2 - \beta_1^2 + (\alpha_2 - \beta_2)\right],$$

rewriting equation 22 asequation 22 can be rewritten as

$$\frac{1}{\cos^2\theta}\left(\frac{\Delta c}{c}\right)_2(z) + \beta_2(z) = \frac{\cos^2\theta - 2}{2\cos^4\theta}\left(\frac{\Delta c}{c}\right)_1^2(z) - \frac{1}{2}\beta_1^2(z)$$

$$- \frac{1}{\cos^4\theta}\left(\frac{\Delta c}{c}\right)'_1(z)\int_0^z dz'\left(\frac{\Delta c}{c}\right)_1$$
$$- \frac{1}{\cos^2\theta}\beta_1'(z)\int_0^z dz'\left(\frac{\Delta c}{c}\right)_1. \quad (39)$$

This equation indicates two important concepts. One is leakage: there is no leakage correction at all in this expression. Here the leakage means that, if the actual value of α (relative changes in P-wave bulk modulus) is zero, its linear approximation α_1 could be non-zero since α and β are coupled together (like the coupled term $\alpha_1\beta_1$ in equation 22) and α_1 could get leakage values from β_1. While in equation 39, no such coupled term is present at all and thus, if the actual changes in the velocity are zero, then its linear inversion $\left(\frac{\Delta c}{c}\right)_1$ would be zero and there would be no leakage from β_1. This leakage issue or coupled term has no analogue in the 1D one parameter acoustic case (equation 23) since in this case we only have one parameter and there is no other parameter to leak into. In other words, in the one parameter (velocity) case, each 'jump' in the amplitude of the data (primaries only) corresponds to each wrong location with a wrong amplitude for the parameter predicted in the linear inverse step; while in the two parameter case of thiscurrent paper, each 'jump' in the data no longer has the simple one-to-one relationship with the amplitude and location of the two parameters.

The other concept is purposeful perturbation. The integrand $\left(\frac{\Delta c}{c}\right)_1$ of the imaging terms clearly tells that if we have the right velocity, the imaging terms will automatically be zero even without doing any integration; otherwise, if we do not have the right velocity, these imaging terms would be used to move the interface closer to the right location from the wrong location. The conclusion from this equation is that the depth imaging terms depend only on the velocity errors.

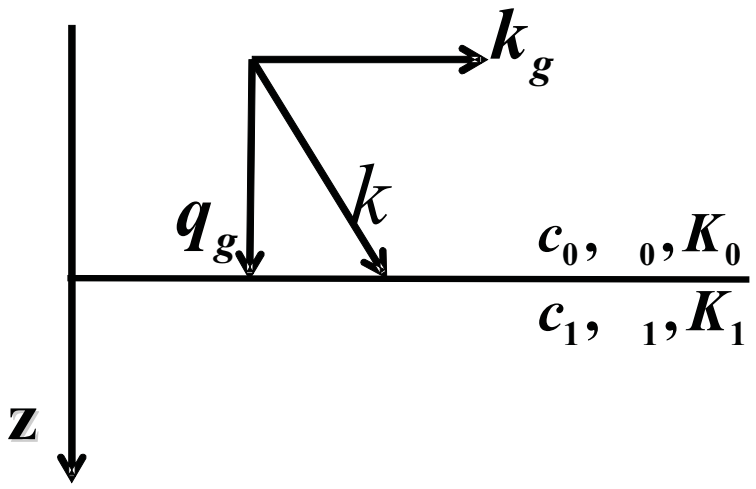

Figure 1: The relationship between q_g, k_g and θ.

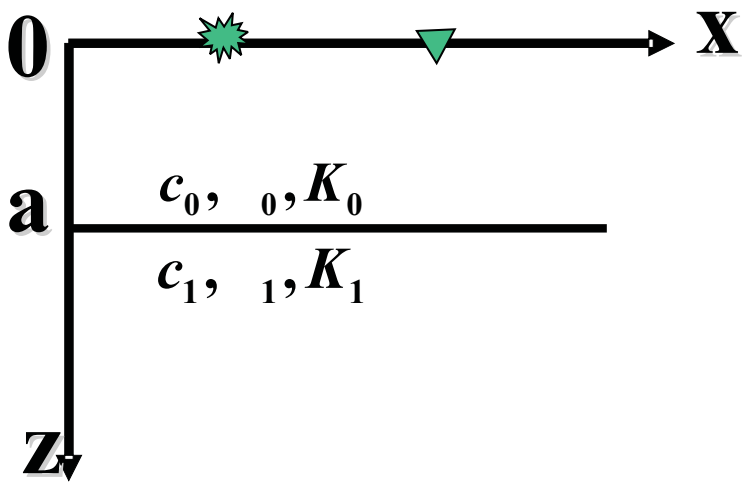

Figure 2: 1D one-interface acoustic model.

6 Conclusion

In thispresent paper, we derive the first two parameter direct non-linear inversion solution for 1D acoustic media with a 2D experiment. Numerical tests show that the terms beyond linearity in earth property identification subseries provide added value. Although the model we used in the numerical tests is simple, the potential within equations 21 and 22 applies to more complex models since the inverse scattering series is a direct inversion procedure which inverts data directly without knowing the specific properties above the target.

As shown above, adding one parameter in the wave equation makes the problem much more complicated in comparison with the one parameter case. Three important concepts (purposeful perturbation, leakage and special parameter for inversion) have been discussed and how they relate to the linear and non-linear results for parameter estimation, addressing leakage, and imaging. Further progress on these issues is being carried out with on-going research.

The work presented in thiscurrent paper is an important step forward for imaging without the velocity model, and target identification for the minimally acceptable elastic isotropic target. In thispresent paper for the first time the general one-dimensional formalism for a depth varying acoustic medium is presented for depth imaging and direct parameter estimation, without needing to determine medium velocity properties that govern actual wave propagation for depth imaging, or what medium is above a target to be identified. The encouraging numerical results motivated us to move one step further — extension of this work to the isotropic elastic case (see, e.g., Boyse and Keller, 1986) using three parameters and elastic wave equation. The companion and sequel paper to this one provides that extension.

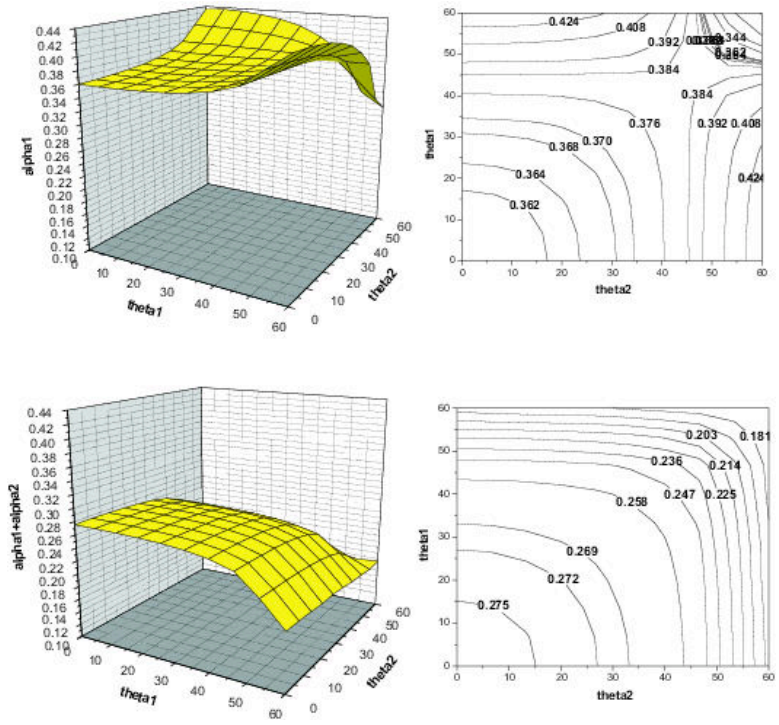

Figure 3: α_1 (top) and $\alpha_1 + \alpha_2$ (bottom) displayed as a function of two different angles. The graphs on the right are the corresponding contour plots of the graphs on the left. In this example, the exact value of α is 0.292.

Acknowledgements

We thank all sponsors of M-OSRP and we are grateful that Robert Keys and Douglas Foster for valuable discussions. The first author would also like to thank ConocoPhillips for permission to publish this work.

References

Boyse, W. E. and J. B. Keller. "Inverse elastic scattering in three dimensions." *J. Acoust. Soc. Am.* 79 (1986): 215–218.

C. Bunks, S. Zaleski,F. M. Saleck and G. Chavent. "Multiscale seismic waveform inversion." *Geophysics* 60 (1995): 1457–1473.

Clayton, R. W. and R. H. Stolt. "A Born-WKBJ inversion method for acoustic reflection data." *Geophysics* 46 (1981): 1559–1567.

E. Forgues, E. Scala and R. G. Pratt. "High resolution velocity model estimation from refraction and reflection data." *68th Annual Internat. Mtg., Soc. Expl. Geophys., Expanded Abstracts.* . Soc. Expl. Geophys., 1998. 1211–1214.

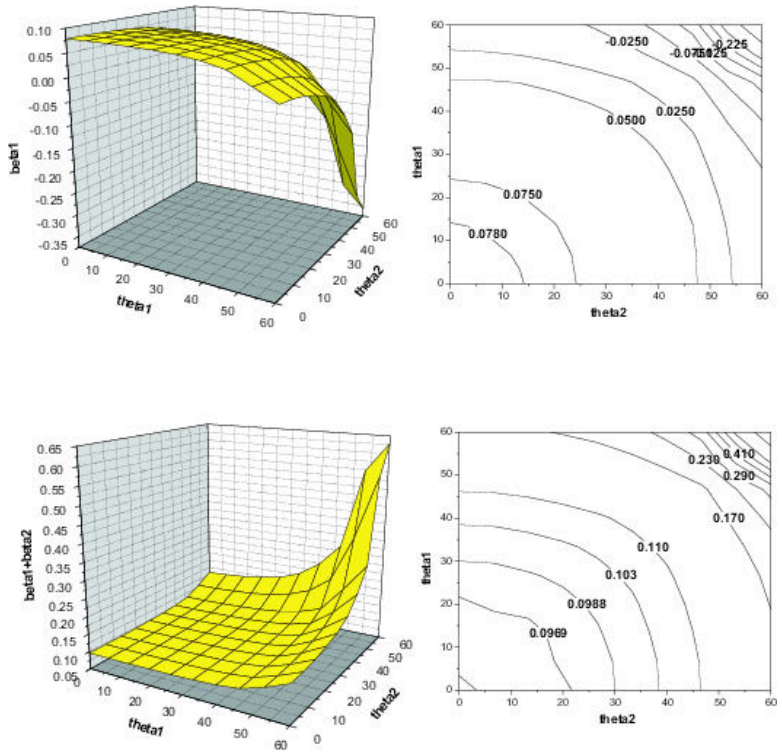

Figure 4: β_1 (top) and $\beta_1 + \beta_2$ (bottom). In this example, the exact value of β is 0.09.

Innanen, Kristopher. A. *Methods for the treatment of acoustic and absorptive/dispersive wave field measurements*. PhD thesis, University of British Columbia, 2003.

Keys, R. G. "Polarity reversals in reflections from layered media." *Geophysics* 54 (1989): 900–905.

Liu, F., A. B. Weglein K. A. Innanen, and B. G. Nita. "Extension of the non-linear depth imaging capability of the inverse scattering series to multidimensional media: strategies and numerical results." *9th Ann. Cong. SBGf, Expanded Abstracts*. . SBGf, 2005.

Matson, K. H. *An inverse-scattering series method for attenuating elastic multiples from multi-component land and ocean bottom seismic data*. PhD thesis, University of British Columbia, 1997.

Mora, P. "Wave equation inversion and diffraction tomography repaired." *57th Annual Internat. Mtg., Soc. Expl. Geophys., Expanded Abstracts*. . Soc. Expl. Geophys., 1987. 755–757.

Sen, M. and P. L. Stoffa. *Global Optimization Methods in Geophysical Inversion*. Amsterdam: Elsevier, 1995.

Shaw, S. A. *An inverse scattering series algorithm for depth imaging of reflection data from a layered acoustic medium with an unknown velocity model*. PhD thesis, University of Houston, 2005.

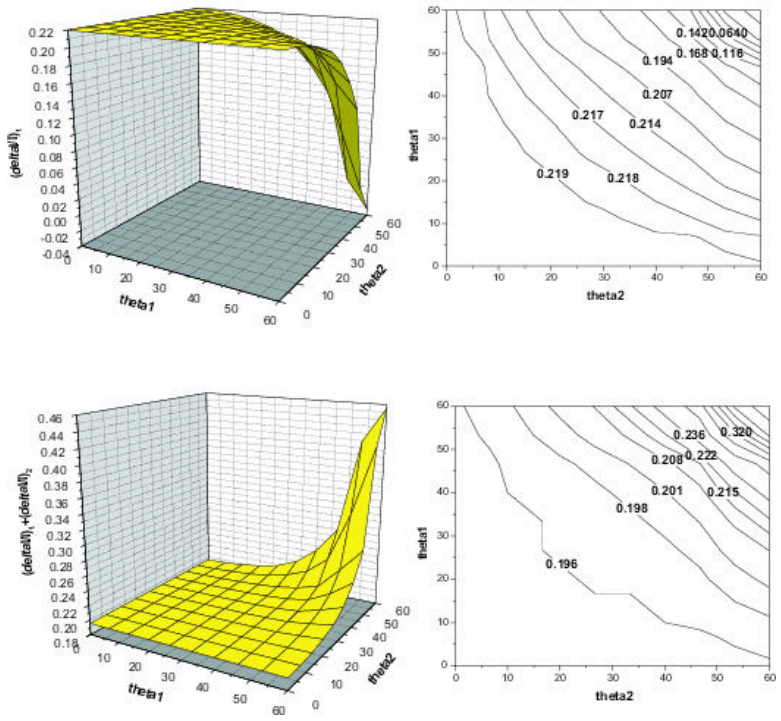

Figure 5: Linear approximation to relative change in impedance (see details in Appendix A) $\left(\frac{\Delta I}{I}\right)_1 = \frac{1}{2}(\alpha_1 + \beta_1)$ (top). Sum of linear and first non-linear terms $\left(\frac{\Delta I}{I}\right)_1 + \left(\frac{\Delta I}{I}\right)_2 = \left(\frac{\Delta I}{I}\right)_1 + \frac{1}{2}\left[\frac{1}{4}(\alpha_1 - \beta_1)^2 + (\alpha_2 + \beta_2)\right]$ (bottom). In this example, the exact value of $\frac{\Delta I}{I}$ is 0.198.

Shaw, S. A., A. B. Weglein, D. J. Foster, K. H. Matson, and R. G. Keys. "Isolation of a leading order depth imaging series and analysis of its convergence properties." *M-OSRP Annual Report* 2 (2003): 157–195.

Shin, C. and D. Min. "Waveform inversion using a logarithmic wavefield." *Geophysics* 71 (2006): R31–R42.

Tarantola, A., A. Nercessian, and O. Gauthier. "Nonlinear Inversion of Seismic Reflection Data." *54rd Annual Internat. Mtg., Soc. Expl. Geophys., Expanded Abstracts.* . Soc. Expl. Geophys., 1984. 645–649.

Taylor, J. R. *Scattering theory: the quantum theory of nonrelativistic collisions.* John Wiley & Sons, Inc., 1972.

Weglein, A. B. "A note: data requirements for inverse theory." *M-OSRP Annual Report* 6 (2007).

Weglein, A. B., F. V. Araújo, P. M. Carvalho, R. H. Stolt, K. H. Matson, R. T. Coates, D. Corrigan, D. J. Foster, S. A. Shaw, and H. Zhang. "Inverse scattering series and seismic exploration." *Inverse Problems* 19 (2003): R27–R83.

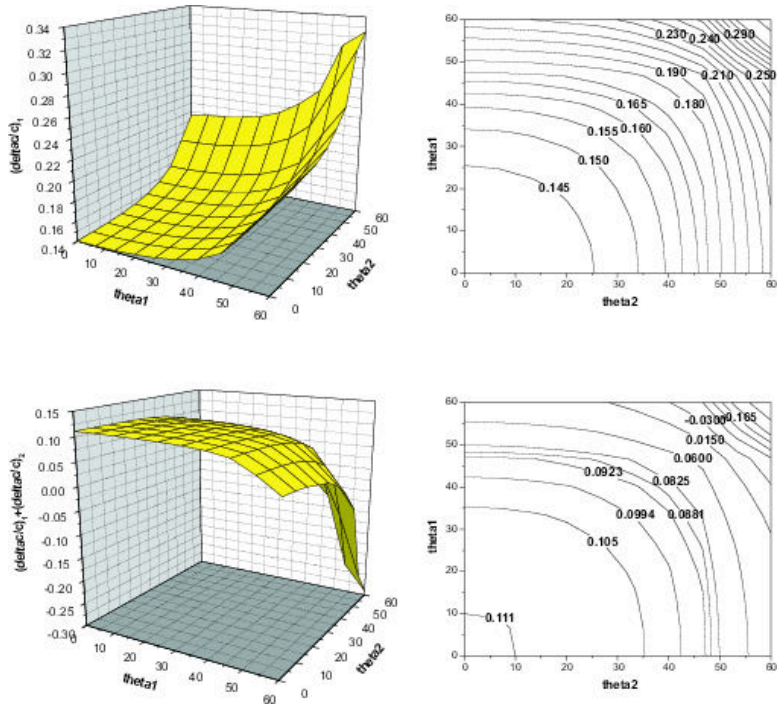

Figure 6: Linear approximation to relative change in velocity (see details in Appendix A) $\left(\frac{\Delta c}{c}\right)_1 = \frac{1}{2}(\alpha_1 - \beta_1)$ (top). Sum of linear and first non-linear terms $\left(\frac{\Delta c}{c}\right)_1 + \left(\frac{\Delta c}{c}\right)_2 = \left(\frac{\Delta c}{c}\right)_1 + \frac{1}{2}\left[\frac{1}{4}(\alpha_1 + \beta_1)^2 - \beta_1^2 + (\alpha_2 - \beta_2)\right]$ (bottom). In this example, the exact value of $\frac{\Delta c}{c}$ is 0.118.

Weglein, A. B., D. J. Foster, K. H. Matson, S. A. Shaw, P. M. Carvalho, and D. Corrigan. "Predicting the correct spatial location of reflectors without knowing or determining the precise medium and wave velocity: initial concept, algorithm and analytic and numerical example." *Journal of Seismic Exploration* 10 (2002): 367–382.

Weglein, A. B., F. A. Gasparotto, P. M. Carvalho, and R. H. Stolt. "An inverse-scattering series method for attenuating multiples in seismic reflection data." *Geophysics* 62 (1997): 1975–1989.

Weglein, A. B., P. B. Violette, and T. H. Keho. "Using multiparameter Born theory to obtain certain exact multiparameter inversion goals." *Geophysics* 51 (1986): 1069–1074.

Zhang, H. *Direct non-linear acoustic and elastic inversion: Towards fundamentally new comprehensive and realistic target identification.* PhD thesis, University of Houston, 2006.

Zhang, H. and A. B. Weglein. "The inverse scattering series for tasks associated with primaries: direct non-linear inversion of 1D elastic media." *76th Annual Internat. Mtg., Soc. Expl. Geophys., Expanded Abstracts.* . Soc. Expl. Geophys., 2006. 2062–2066.

Zhang, H. and A. B. Weglein. "Direct non-linear inversion of multi-parameter 1D elastic media using the inverse scattering series." *Geophysics* (2009): Submitted.

Appendix A

In this appendix, we derive the expressions of $\left(\frac{\Delta c}{c}\right)_1$, $\left(\frac{\Delta c}{c}\right)_2$, $\left(\frac{\Delta I}{I}\right)_1$ and $\left(\frac{\Delta I}{I}\right)_2$ in terms of α_1, β_1 and α_2, β_2. Define $\Delta c = c - c_0$, $\Delta I = I - I_0$, $\Delta K = K - K_0$ and $\Delta\rho = \rho - \rho_0$.

Since $K = c^2\rho$, then we have

$$(c - \Delta c)^2 = \frac{K - \Delta K}{\rho - \Delta\rho}.$$

Divided by c^2, the equation above will become

$$2\left(\frac{\Delta c}{c}\right) - \left(\frac{\Delta c}{c}\right)^2 = \frac{\frac{\Delta K}{K} - \frac{\Delta\rho}{\rho}}{1 - \frac{\Delta\rho}{\rho}}.$$

Remember that $\alpha = \frac{\Delta K}{K}$ and $\beta = \frac{\Delta\rho}{\rho}$, the equation above can be rewritten as

$$2\left(\frac{\Delta c}{c}\right) - \left(\frac{\Delta c}{c}\right)^2 = \frac{\alpha - \beta}{1 - \beta}.$$

Then we have

$$2\left(\frac{\Delta c}{c}\right) - \left(\frac{\Delta c}{c}\right)^2 = (\alpha - \beta)(1 + \beta + \beta^2 + \cdots), \tag{40}$$

where the series expansion is valid for $|\beta| < 1$.

Similar to equations 17 and 18, $\frac{\Delta c}{c}$ can be expanded as

$$\left(\frac{\Delta c}{c}\right) = \left(\frac{\Delta c}{c}\right)_1 + \left(\frac{\Delta c}{c}\right)_2 + \cdots. \tag{41}$$

Then substitute equations 41, 17 and 18 into equation 40, and set those terms of equal order equal on both sides of equation 40, we can get

$$\left(\frac{\Delta c}{c}\right)_1 = \frac{1}{2}(\alpha_1 - \beta_1), \tag{42}$$

and

$$\left(\frac{\Delta c}{c}\right)_2 = \frac{1}{2}\left[\frac{1}{4}(\alpha_1 + \beta_1)^2 - \beta_1^2 + (\alpha_2 - \beta_2)\right]. \tag{43}$$

Similarly, using $I = c\rho$, we have

$$(I - \Delta I)^2 = (K - \Delta K)(\rho - \Delta\rho).$$

Divided by I^2, the equation above will become

$$2\left(\frac{\Delta I}{I}\right) - \left(\frac{\Delta I}{I}\right)^2 = \alpha + \beta - \alpha\beta. \tag{44}$$

Expanding $\frac{\Delta I}{I}$ as

$$\left(\frac{\Delta I}{I}\right) = \left(\frac{\Delta I}{I}\right)_1 + \left(\frac{\Delta I}{I}\right)_2 + \cdots, \tag{45}$$

and substitute equations 45, 17 and 18 into equation 44, setting those terms of equal order equal on both sides of equation 44), we can get

$$\left(\frac{\Delta I}{I}\right)_1 = \frac{1}{2}(\alpha_1 + \beta_1), \tag{46}$$

and

$$\left(\frac{\Delta I}{I}\right)_2 = \frac{1}{2}\left[\frac{1}{4}(\alpha_1 - \beta_1)^2 + (\alpha_2 + \beta_2)\right]. \tag{47}$$

Appendix B

In this appendix, we show that $\left(\frac{\Delta c}{c}\right)_1$ has the same sign as Δc. For the single interface example, from equations 36 and 42, we have

$$\left(\frac{\Delta c}{c}\right)_1 = 2\frac{R(\theta_1) - R(\theta_2)}{\tan^2\theta_1 - \tan^2\theta_2}.$$

The reflection coefficient is

$$R(\theta) = \frac{(\rho_1/\rho_0)(c_1/c_0)\sqrt{1-\sin^2\theta} - \sqrt{1-(c_1^2/c_0^2)\sin^2\theta}}{(\rho_1/\rho_0)(c_1/c_0)\sqrt{1-\sin^2\theta} + \sqrt{1-(c_1^2/c_0^2)\sin^2\theta}}.$$

Let

$$A(\theta) = (\rho_1/\rho_0)(c_1/c_0)\sqrt{1-\sin^2\theta},$$
$$B(\theta) = \sqrt{1-(c_1^2/c_0^2)\sin^2\theta}.$$

Then

$$R(\theta_1) - R(\theta_2) = 2\frac{A(\theta_1)B(\theta_2) - B(\theta_1)A(\theta_2)}{[A(\theta_1) + B(\theta_1)]\,[A(\theta_2) + B(\theta_2)]},$$

where the denominator is greater than zero. The numerator is

$$\begin{aligned} 2\left[A(\theta_1)B(\theta_2) - B(\theta_1)A(\theta_2)\right] =& 2(\rho_1/\rho_0)(c_1/c_0)\left[\sqrt{1-\sin^2\theta_1}\sqrt{1-(c_1^2/c_0^2)\sin^2\theta_2}\right. \\ & \left. -\sqrt{1-\sin^2\theta_2}\sqrt{1-(c_1^2/c_0^2)\sin^2\theta_1}\right]. \end{aligned}$$

Let

$$C = \sqrt{1-\sin^2\theta_1}\sqrt{1-(c_1^2/c_0^2)\sin^2\theta_2},$$
$$D = \sqrt{1-\sin^2\theta_2}\sqrt{1-(c_1^2/c_0^2)\sin^2\theta_1}.$$

Then,

$$C^2 - D^2 = \left(\frac{c_1^2}{c_0^2} - 1\right)(sin^2\theta_1 - sin^2\theta_2).$$

When $c_1 > c_0$ and $\theta_1 > \theta_2$, we have (Noticing that both C and D are positive.)

$$\left(\frac{c_1^2}{c_0^2} - 1\right)(sin^2\theta_1 - sin^2\theta_2) > 0,$$

so

$$R(\theta_1) - R(\theta_2) > 0;$$

Similarly, when $c_1 < c_0$ and $\theta_1 > \theta_2$, we have

$$\left(\frac{c_1^2}{c_0^2} - 1\right)(sin^2\theta_1 - sin^2\theta_2) < 0,$$

so

$$R(\theta_1) - R(\theta_2) < 0.$$

Remembering that $\left(\frac{\Delta c}{c}\right)_1 = 2\frac{R(\theta_1)-R(\theta_2)}{\tan^2\theta_1 - \tan^2\theta_2}$. So for $c_1 > c_0$, $(\Delta c)_1 > 0$ and for $c_1 < c_0$, $(\Delta c)_1 < 0$.

Direct non-linear inversion of multi-parameter 1D elastic media using the inverse scattering series

H. Zhang[1] and A. B. Weglein[2]
[1] Previously Department of Physics, University of Houston, currently ConocoPhillips, 600 N. Dairy Ashford Houston, TX 77079
[2] University of Houston, 617 Science and Research Bldg. 1, Houston, TX 77204-5005

Abstract

In this paper, we present the first direct non-linear target identification method and algorithms for 1D elastic media (that is P velocity, shear velocity and density are depth dependent). Direct non-linear means that we provide explicit formulas that: (1) input data and directly output changes in material properties, without the use or need for any indirect procedures such as model matching, searching, optimization or other assumed aligned objectives or proxies, and (2) the algorithms recognize and directly invert the intrinsic non-linear relationship between changes in material properties and changes in the reflected measured wave-field. The results clearly demonstrate that, in order to achieve full elastic inversion, all four components of data ($\hat{D}^{PP}$, $\hat{D}^{PS}$, $\hat{D}^{SP}$ and $\hat{D}^{SS}$) are needed. The method assumes that only data and reference medium properties are input, and terms in the inverse series for moving mislocated reflectors resulting from the linear inverse term, are separated from amplitude correction terms. Although in principle this direct inversion approach requires all four components of elastic data, synthetic tests indicate that a consistent value-added result may be achieved given only $\hat{D}^{PP}$ measurements, as long as the $\hat{D}^{PP}$ were used to approximately synthesize the $\hat{D}^{PS}$, $\hat{D}^{SP}$ and $\hat{D}^{SS}$ components. We can reasonably infer that further value would derive from actually measuring $\hat{D}^{PP}$, $\hat{D}^{PS}$, $\hat{D}^{SP}$ and $\hat{D}^{SS}$ as the method requires. For the case that all four components of data are available, we give one consistent method to solve for all of the second terms (the first terms beyond linear). The method's direct and explicit non-linear inversion solution provides for the very first time -this unambiguous data requirement message, and that unique and prescriptive clarity, and the explicit non-linear formulas distinguish themselves and provide conceptual and practical added value beyond both linear approaches and all indirect methods.

1 Introduction

The ultimate objective of inverse problems is to determine medium and target properties from measurements external to the object under investigation. At the very first moment of problem definition, there is an immediate requirement and unavoidable expectation, that the model type of the medium be specified. In that step of model type specification, the number and type of parameters and dimension of spatial variation of those parameters are given, and carefully prescribed, and in that way you provide the inverse problem with clarity and meaning. Among the different model types used in exploration seismology are, e.g., acoustic, elastic, heterogeneous, anisotropic, and anelastic, and perhaps most important, the dimension of variability of the properties associated

with these model types. One would reasonably expect that the details of methods and algorithms for inversion objectives, and any tasks associated with achieving those ultimate objectives, would overall and each separately depend upon that starting assumption on model type. However, the ultimate objective of seismic inversion has never been achieved in a straight ahead single step manner directly from the seismic data, and that lack of success has not been due to a lack of computer power. The indirect model matching procedures have that computer power problem, especially in the applications to a multi-dimensional complex earth, where it is rare to have a reasonable proximal starting model. Those complex ill-defined geologic circumstances are the biggest impediments and challenges to current exploration and production seismic effectiveness.

The only direct multi-dimensional inversion procedure for seismic application, the inverse scattering series, does not require a proximal starting model and only assumes reference medium information. Of course, the whole inverse series has very limited application (Carvalho et al., 1992). What makes the inverse scattering series powerful is the so-called task isolated subseries which is a subset of the whole series that acts like only one task is performed for that subset (Weglein et al., 2003). All of these subseries act in a certain sequence so that the total seismic data can be processed accordingly. The order of processing is : (1) free-surface multiple removal, (2) internal multiple removal, (3) depth imaging without velocity, and (4) inversion or target identification. Since the entire process requires only reflection data and reference medium information, it is reasonable to assume that these intermediate steps, i.e., all of the derived subseries which are associated with achieving that objective, would also be attainable with only the reference medium and reflection data and no subsurface medium information is required.

The free surface multiple removal and internal multiple attenuation subseries have been presented by (Carvalho, 1992; Araújo, 1994; Weglein et al., 1997; Matson, 1997). Those two multiple procedures are model type independent, i.e., they work for acoustic, elastic and anelastic medium. Taking internal multiples from attenuation to elimination is being studied (Ramírez and Weglein, 2005). The task specific subseries associated with primaries (i.e., for imaging and inversion) have been progressed too: (1) imaging without the velocity for one parameter 1D and then 2D acoustic media (Weglein et al., 2002; Shaw and Weglein, 2003; Shaw et al., 2003a; Shaw et al., 2003b; Shaw et al., 2004; Shaw and Weglein, 2004; Liu and Weglein, 2003; Liu et al., 2004; Liu et al., 2005), and (2) direct non-linear inversion for multi-parameter 1D acoustic and then elastic media (Zhang and Weglein, 2005). Furthermore, recent work (Innanen and Weglein, 2004; Innanen and Weglein, 2005) suggests that some well-known seismic processing tasks associated with resolution enhancement (i.e., "Q-compensation") can be accomplished within the task-separated inverse scattering series framework. In this paper, we focus on item (2) above.

Compared with model type independent multiple removal procedures, there is a full expectation that tasks and algorithms associated with primaries will have a closer interest in model type. For example, there is no way to even imagine that medium property identification can take place without reference to a specific model type. Tasks and issues associated with structural determination, without knowing the medium, are also vastly different depending on the dimension of variation number of velocities that are required for imaging. Hence, a staged approach and isolation of tasks philosophy is essential in this yet tougher neighborhood, and even more in demand for seeking insights and then practical algorithms for these more complicated and daunting objectives. We

adopt the staged and isolation of issues approach for primaries. The isolated task achievement plan can often spin-off incomplete but useful intermediate objectives. The test and standard is not necessarily how complete the method is but rather how does it compare to, and improve upon, current best practice.

The stages within the strategy for primaries are as follows: (1) 1D earth, with one parameter, velocity as a function of depth, and a normal incidence wave, (2) 1D earth with one parameter subsurface and offset data, one shot record; (3) 2D earth with one parameter, velocity, varying in x and z, and a suite of shot records; (4) 1D acoustic earth with two parameters varying, velocity and density, one propagation velocity, and one shot record of PP data, and (5) 1D elastic earth, two elastic isotropic parameters and density, and two wave speeds, for P and S waves, and PP, PS, SP, and SS shot records data collected. This paper takes another step of direct non-linear inversion methodology, and task isolation and specifically for tasks associated with primaries, to the 1D elastic case, stage (5). The model is elastic and another paper in acoustic has been presented in Zhang and Weglein (2005). We take these steps and learn to navigate through this complexity and steer it towards useful and powerful algorithms.

However, more realism is more complicated with more issues involved. Following the task separation strategy, we ask the question what kind of tasks should we expect in this more complex, elastic, setting? In the acoustic case, for example, the acoustic medium only supports P-waves, and hence only one reference velocity (P-wave velocity) is involved. Therefore, when only one velocity is incorrect (i.e., poorly estimated), there exists only one "mislocation" for each parameter, and the imaging terms only need to correct this one mislocation. When we extend our previous work on the two parameter acoustic case to the present three parameter elastic case, there will be four mislocations because of the two reference velocities (P wave velocity and S velocity). Our reasoning is that the elastic medium supports both P- and S-wave propagation, and hence two reference velocities (P-wave velocity and S-wave velocity) are involved. When both of these velocities are incorrect, generally, there exist four mislocations due to each of four different combinations[1] of the two wrong velocities. Therefore, in non-linear elastic imaging-inversion, the imaging terms need to correct the four mislocations arising from linear inversion of any single mechanical property, such that a single correct location for the corresponding actual change in that property is determined.

In this paper, the first non-linear inversion term for three parameter 1D elastic medium is presented. It is demonstrated that under the inverse scattering series inversion framework, all four components of the data are needed in order to perform full elastic inversion. For the case that we don't have all four components data and only PP data are available, encouraging inversion results have been obtained by constructing other components of data from PP data. This means that we could perform elastic inversion only using pressure measurements, i.e. towed streamer data. For the case that all four components of data are available, a consistent method is provided. Further tests and evaluation of the four components of data.

The paper has the following structure: the next section is a brief introduction to the inverse

[1]The "four combinations" refers to PP, PS, SP and SS, where, for instance, PP means P-wave incidence, and P-wave reflection. Since P-waves non-normal incidence on an elastic interface can produce S-waves, or vice versa, which in those cases are known as converted waves (Aki and Richards, 2002), the elastic data generally contain four components: PP, PS, SP and SS.

scattering series and then presents, respectively, the derivations and numerical tests for elastic non-linear inversion when only PP data is available. A full non-linear elastic inversion method is also provided. Finally we will present some concluding remarks.

2 Background for 2D elastic inversion

In this section we consider the inversion problem in two dimensions for an elastic medium. We start with the displacement space, and then, for convenience (see e.g., Weglein and Stolt, 1992; Aki and Richards, 2002), we change the basis and transform the equations to PS space. Finally, we do the elastic inversion in the PS domain.

2.1 In the displacement space

We begin with some basic equations in the displacement space (Matson, 1997):

$$L\mathbf{u} = \mathbf{f}, \tag{1}$$

$$L_0\mathbf{u} = \mathbf{f}, \tag{2}$$

$$LG = \delta, \tag{3}$$

$$L_0G_0 = \delta, \tag{4}$$

where L and L_0 are the differential operators that describe the wave propagation in the actual and reference medium, respectively, $\mathbf{u}$ and $\mathbf{f}$ are the corresponding displacement and source terms, respectively, and G and G_0 are the corresponding Green's operators for the actual and reference medium. In the following, the quantities with subscript "0" are for the reference medium, and those without the subscript are for the actual medium.

Following closely Weglein et al. (1997); Weglein et al. (2002) and Weglein et al. (2003), defining the perturbation $V = L_0 - L$, the Lippmann- Schwinger equation for the elastic media in the displacement space is

$$G = G_0 + G_0VG. \tag{5}$$

Iterating this equation back into itself generates the Born series

$$G = G_0 + G_0VG_0 + G_0VG_0VG_0 + \cdots . \tag{6}$$

We define the data D as the measured values of the scattered wave field. Then, on the measurement surface, we have

$$D = G_0VG_0 + G_0VG_0VG_0 + \cdots . \tag{7}$$

Expanding V as a series in orders of D we have

$$V = V_1 + V_2 + V_3 + \cdots . \tag{8}$$

Where the subscript "i" in V_i (i=1, 2, 3, ...) denotes the portion of V i-th order in the data. Substituting equation 8 into equation 7, evaluating equation 7, and setting terms of equal order in the data equal, the equations that determine V_1, V_2, ... from D and G_0 would be obtained.

$$D = G_0 V_1 G_0, \tag{9}$$

$$0 = G_0 V_2 G_0 + G_0 V_1 G_0 V_1 G_0, \tag{10}$$

$$\vdots$$

In the actual medium, the 2-D elastic wave equation is (Weglein and Stolt, 1992)

$$L\mathbf{u} \equiv \left[\rho\omega^2 \begin{pmatrix} 1 & 0 \\ 0 & 1 \end{pmatrix} + \begin{pmatrix} \partial_1\gamma\partial_1 + \partial_2\mu\partial_2 & \partial_1(\gamma - 2\mu)\partial_2 + \partial_2\mu\partial_1 \\ \partial_2(\gamma - 2\mu)\partial_1 + \partial_1\mu\partial_2 & \partial_2\gamma\partial_2 + \partial_1\mu\partial_1 \end{pmatrix}\right] \begin{bmatrix} u_1 \\ u_2 \end{bmatrix} = \mathbf{f}, \tag{11}$$

where

$\mathbf{u} = \begin{bmatrix} u_1 \\ u_2 \end{bmatrix}$ = displacement,

ρ = density,

γ = bulk modulus ($\equiv \rho\alpha^2$ where α = P-wave velocity),

μ = shear modulus ($\equiv \rho\beta^2$ where β = S-wave velocity),

ω = temporal frequency (angular), ∂_1 and ∂_2 denote the derivative over x and z, respectively, and $\mathbf{f}$ is the source term.

For constant $(\rho, \gamma, \mu) = (\rho_0, \gamma_0, \mu_0)$, $(\alpha, \beta) = (\alpha_0, \beta_0)$, the operator L becomes

$$L_0 \equiv \left[\rho_0\omega^2 \begin{pmatrix} 1 & 0 \\ 0 & 1 \end{pmatrix} + \begin{pmatrix} \gamma_0\partial_1^2 + \mu_0\partial_2^2 & (\gamma_0 - \mu_0)\partial_1\partial_2 \\ (\gamma_0 - \mu_0)\partial_1\partial_2 & \mu_0\partial_1^2 + \gamma_0\partial_2^2 \end{pmatrix}\right]. \tag{12}$$

Then,

$$\begin{aligned} V \equiv & L_0 - L \\ = & -\rho_0 \begin{bmatrix} a_\rho\omega^2 + \alpha_0^2\partial_1 a_\gamma\partial_1 + \beta_0^2\partial_2 a_\mu\partial_2 & \partial_1(\alpha_0^2 a_\gamma - 2\beta_0^2 a_\mu)\partial_2 + \beta_0^2\partial_2 a_\mu\partial_1 \\ \partial_2(\alpha_0^2 a_\gamma - 2\beta_0^2 a_\mu)\partial_1 + \beta_0^2\partial_1 a_\mu\partial_2 & a_\rho\omega^2 + \alpha_0^2\partial_2 a_\gamma\partial_2 + \beta_0^2\partial_1 a_\mu\partial_1 \end{bmatrix}, \end{aligned} \tag{13}$$

where $a_\rho \equiv \frac{\rho}{\rho_0} - 1$, $a_\gamma \equiv \frac{\gamma}{\gamma_0} - 1$ and $a_\mu \equiv \frac{\mu}{\mu_0} - 1$ are the three parameters we choose to do the elastic inversion. For a 1D earth (i.e. a_ρ, a_γ and a_μ are only functions of depth z), the expression above for V becomes

$$V = -\rho_0 \begin{bmatrix} a_\rho\omega^2 + \alpha_0^2 a_\gamma\partial_1^2 + \beta_0^2\partial_2 a_\mu\partial_2 & (\alpha_0^2 a_\gamma - 2\beta_0^2 a_\mu)\partial_1\partial_2 + \beta_0^2\partial_2 a_\mu\partial_1 \\ \partial_2(\alpha_0^2 a_\gamma - 2\beta_0^2 a_\mu)\partial_1 + \beta_0^2 a_\mu\partial_1\partial_2 & a_\rho\omega^2 + \alpha_0^2\partial_2 a_\gamma\partial_2 + \beta_0^2 a_\mu\partial_1^2 \end{bmatrix}. \tag{14}$$

2.2 Transforming to PS space

For convenience, we can change the basis from $\mathbf{u} = \begin{bmatrix} u_1 \\ u_2 \end{bmatrix}$ to $\begin{pmatrix} \phi^P \\ \phi^S \end{pmatrix}$ to allow L_0 to be diagonal,

$$\mathbf{\Phi} = \begin{pmatrix} \phi^P \\ \phi^S \end{pmatrix} = \begin{bmatrix} \gamma_0(\partial_1 u_1 + \partial_2 u_2) \\ \mu_0(\partial_1 u_2 - \partial_2 u_1) \end{bmatrix}, \tag{15}$$

also, we have

$$\begin{pmatrix} \phi^P \\ \phi^S \end{pmatrix} = \Gamma_0 \Pi \mathbf{u} = \begin{bmatrix} \gamma_0(\partial_1 u_1 + \partial_2 u_2) \\ \mu_0(\partial_1 u_2 - \partial_2 u_1) \end{bmatrix}, \tag{16}$$

where $\Pi = \begin{pmatrix} \partial_1 & \partial_2 \\ -\partial_2 & \partial_1 \end{pmatrix}$, $\Gamma_0 = \begin{pmatrix} \gamma_0 & 0 \\ 0 & \mu_0 \end{pmatrix}$. In the reference medium, the operator L_0 will transform in the new basis via a transformation

$$\hat{L}_0 \equiv \Pi L_0 \Pi^{-1} \Gamma_0^{-1} = \begin{pmatrix} \hat{L}_0^P & 0 \\ 0 & \hat{L}_0^S \end{pmatrix},$$

where $\hat{L}_0$ is L_0 transformed to PS space, $\Pi^{-1} = \begin{pmatrix} \partial_1 & -\partial_2 \\ \partial_2 & \partial_1 \end{pmatrix} \nabla^{-2}$ is the inverse matrix of Π, $\hat{L}_0^P = \omega^2/\alpha_0^2 + \nabla^2$, $\hat{L}_0^S = \omega^2/\beta_0^2 + \nabla^2$, and

$$\mathbf{F} = \Pi \mathbf{f} = \begin{pmatrix} F^P \\ F^S \end{pmatrix}. \tag{17}$$

Then, in PS domain, equation 2 becomes,

$$\begin{pmatrix} \hat{L}_0^P & 0 \\ 0 & \hat{L}_0^S \end{pmatrix} \begin{pmatrix} \phi^P \\ \phi^S \end{pmatrix} = \begin{pmatrix} F^P \\ F^S \end{pmatrix}. \tag{18}$$

Since $G_0 \equiv L_0^{-1}$, let $\hat{G}_0^P = \left(\hat{L}_0^P\right)^{-1}$ and $\hat{G}_0^S = \left(\hat{L}_0^S\right)^{-1}$, then the displacement G_0 in PS domain becomes

$$\hat{G}_0 = \Gamma_0 \Pi G_0 \Pi^{-1} = \begin{pmatrix} \hat{G}_0^P & 0 \\ 0 & \hat{G}_0^S \end{pmatrix}. \tag{19}$$

So, in the reference medium, after transforming from the displacement domain to PS domain, both L_0 and G_0 become diagonal.

Multiplying equation 5 from the left by the operator $\Gamma_0 \Pi$ and from the right by the operator Π^{-1}, and using equation 19,

$$\begin{aligned} \Gamma_0 \Pi G \Pi^{-1} &= \hat{G}_0 + \hat{G}_0 \left(\Pi V \Pi^{-1} \Gamma_0^{-1}\right) \Gamma_0 \Pi G \Pi^{-1} \\ &= \hat{G}_0 + \hat{G}_0 \hat{V} \hat{G}, \end{aligned} \tag{20}$$

where the displacement Green's operator G is transformed to the PS domain as

$$\hat{G} = \Gamma_0 \Pi G \Pi^{-1} = \begin{pmatrix} \hat{G}^{PP} & \hat{G}^{PS} \\ \hat{G}^{SP} & \hat{G}^{SS} \end{pmatrix}. \tag{21}$$

The perturbation V in the PS domain becomes

$$\hat{V} = \Pi V \Pi^{-1} \Gamma_0^{-1} = \begin{pmatrix} \hat{V}^{PP} & \hat{V}^{PS} \\ \hat{V}^{SP} & \hat{V}^{SS} \end{pmatrix}, \tag{22}$$

where the left superscripts of the matrix elements represent the type of measurement and the right ones are the source type.

Similarly, applying the PS transformation to the entire inverse series gives

$$\hat{V} = \hat{V}_1 + \hat{V}_2 + \hat{V}_3 + \cdots . \tag{23}$$

It follows, from equations 20 and 23 that

$$\hat{D} = \hat{G}_0 \hat{V}_1 \hat{G}_0, \tag{24}$$

$$\hat{G}_0 \hat{V}_2 \hat{G}_0 = -\hat{G}_0 \hat{V}_1 \hat{G}_0 \hat{V}_1 \hat{G}_0, \tag{25}$$

$$\vdots$$

where $\hat{D} = \begin{pmatrix} \hat{D}^{PP} & \hat{D}^{PS} \\ \hat{D}^{SP} & \hat{D}^{SS} \end{pmatrix}$ are the data in the PS domain.

In the displacement space we have, for equation 1,

$$\mathbf{u} = G\mathbf{f}. \tag{26}$$

Then, in the PS domain, equation 26 becomes

$$\mathbf{\Phi} = \hat{G}\mathbf{F}. \tag{27}$$

On the measurement surface, we have

$$\hat{G} = \hat{G}_0 + \hat{G}_0 \hat{V}_1 \hat{G}_0. \tag{28}$$

Substituting equation 28 into equation 27, and rewriting equation 27 in matrix form:

$$\begin{pmatrix} \phi^P \\ \phi^S \end{pmatrix} = \begin{pmatrix} \hat{G}_0^P & 0 \\ 0 & \hat{G}_0^S \end{pmatrix} \begin{pmatrix} F^P \\ F^S \end{pmatrix} + \begin{pmatrix} \hat{G}_0^P & 0 \\ 0 & \hat{G}_0^S \end{pmatrix} \begin{pmatrix} \hat{V}_1^{PP} & \hat{V}_1^{PS} \\ \hat{V}_1^{SP} & \hat{V}_1^{SS} \end{pmatrix} \begin{pmatrix} \hat{G}_0^P & 0 \\ 0 & \hat{G}_0^S \end{pmatrix} \begin{pmatrix} F^P \\ F^S \end{pmatrix}. \tag{29}$$

This can be written as the following two equations

$$\phi^P = \hat{G}_0^P F^P + \hat{G}_0^P \hat{V}_1^{PP} \hat{G}_0^P F^P + \hat{G}_0^P \hat{V}_1^{PS} \hat{G}_0^S F^S, \tag{30}$$

$$\phi^S = \hat{G}_0^S F^S + \hat{G}_0^S \hat{V}_1^{SP} \hat{G}_0^P F^P + \hat{G}_0^S \hat{V}_1^{SS} \hat{G}_0^S F^S. \tag{31}$$

We can see, from the two equations above, that for homogeneous media, (no perturbation, $\hat{V}_1 = 0$), there are only direct P and S waves and that the two kind of waves are separated. However, for inhomogeneous media, these two kinds of waves will be mixed together. If only the P wave is incident, $F^P = 1$, $F^S = 0$, then the two equations 30 and 31 above are respectively reduced to

$$\phi^P = \hat{G}_0^P + \hat{G}_0^P \hat{V}_1^{PP} \hat{G}_0^P, \tag{32}$$

$$\phi^S = \hat{G}_0^S \hat{V}_1^{SP} \hat{G}_0^P. \tag{33}$$

Hence, in this case, there is only the direct P wave $\hat{G}_0^P$, and no direct wave S. But there are two kinds of scattered waves: one is the P-to-P wave $\hat{G}_0^P \hat{V}_1^{PP} \hat{G}_0^P$, and the other is the P-to-S wave $\hat{G}_0^S \hat{V}_1^{SP} \hat{G}_0^P$. For the acoustic case, only the P wave exists, and hence we only have one equation $\phi^P = \hat{G}_0^P + \hat{G}_0^P \hat{V}_1^{PP} \hat{G}_0^P$.

Similarly, if only the S wave is incident, $F^P = 0$, $F^S = 1$, and the two equations 30 and 31 are, respectively, reduced to

$$\phi^P = \hat{G}_0^P \hat{V}_1^{PS} \hat{G}_0^S, \tag{34}$$

$$\phi^S = \hat{G}_0^S + \hat{G}_0^S \hat{V}_1^{SS} \hat{G}_0^S. \tag{35}$$

In this case, there is only the direct S wave $\hat{G}_0^S$, and no direct P wave. There are also two kinds of scattered waves: one is the S-to-P wave $\hat{G}_0^P \hat{V}_1^{PS} \hat{G}_0^S$, the other is the S-to-S wave $\hat{G}_0^S \hat{V}_1^{SS} \hat{G}_0^S$.

3 Linear inversion of a 1D elastic medium

Writing equation 24 in matrix form

$$\begin{pmatrix} \hat{D}^{PP} & \hat{D}^{PS} \\ \hat{D}^{SP} & \hat{D}^{SS} \end{pmatrix} = \begin{pmatrix} \hat{G}_0^P & 0 \\ 0 & \hat{G}_0^S \end{pmatrix} \begin{pmatrix} \hat{V}_1^{PP} & \hat{V}_1^{PS} \\ \hat{V}_1^{SP} & \hat{V}_1^{SS} \end{pmatrix} \begin{pmatrix} \hat{G}_0^P & 0 \\ 0 & \hat{G}_0^S \end{pmatrix}, \tag{36}$$

leads to four equations

$$\hat{D}^{PP} = \hat{G}_0^P \hat{V}_1^{PP} \hat{G}_0^P, \tag{37}$$

$$\hat{D}^{PS} = \hat{G}_0^P \hat{V}_1^{PS} \hat{G}_0^S, \tag{38}$$

$$\hat{D}^{SP} = \hat{G}_0^S \hat{V}_1^{SP} \hat{G}_0^P, \tag{39}$$

$$\hat{D}^{SS} = \hat{G}_0^S \hat{V}_1^{SS} \hat{G}_0^S. \tag{40}$$

For $z_s = z_g = 0$, in the $(k_s, z_s; k_g, z_g; \omega)$ domain, we get the following four equations relating the linear components (the "linear" is denoted by adding a superscript "(1)" on the three parameters) of the three elastic parameters and the four data types:

$$\begin{aligned} \widetilde{D}^{PP}(k_g, 0; -k_g, 0; \omega) = &- \frac{1}{4}\left(1 - \frac{k_g^2}{\nu_g^2}\right) \widetilde{a}_\rho^{(1)}(-2\nu_g) - \frac{1}{4}\left(1 + \frac{k_g^2}{\nu_g^2}\right) \widetilde{a}_\gamma^{(1)}(-2\nu_g) \\ &+ \frac{2k_g^2 \beta_0^2}{(\nu_g^2 + k_g^2)\alpha_0^2} \widetilde{a}_\mu^{(1)}(-2\nu_g), \end{aligned} \tag{41}$$

$$\widetilde{D}^{PS}(\nu_g, \eta_g) = -\frac{1}{4}\left(\frac{k_g}{\nu_g} + \frac{k_g}{\eta_g}\right) \widetilde{a}_\rho^{(1)}(-\nu_g - \eta_g) - \frac{\beta_0^2}{2\omega^2} k_g(\nu_g + \eta_g)\left(1 - \frac{k_g^2}{\nu_g \eta_g}\right) \widetilde{a}_\mu^{(1)}(-\nu_g - \eta_g), \tag{42}$$

$$\widetilde{D}^{SP}(\nu_g, \eta_g) = \frac{1}{4}\left(\frac{k_g}{\nu_g} + \frac{k_g}{\eta_g}\right) \widetilde{a}_\rho^{(1)}(-\nu_g - \eta_g) + \frac{\beta_0^2}{2\omega^2} k_g(\nu_g + \eta_g)\left(1 - \frac{k_g^2}{\nu_g \eta_g}\right) \widetilde{a}_\mu^{(1)}(-\nu_g - \eta_g), \tag{43}$$

$$\widetilde{D}^{SS}(k_g,\eta_g) = -\frac{1}{4}\left(1-\frac{k_g^2}{\eta_g^2}\right)\widetilde{a}_\rho^{(1)}(-2\eta_g) - \left[\frac{\eta_g^2+k_g^2}{4\eta_g^2} - \frac{2k_g^2}{\eta_g^2+k_g^2}\right]\widetilde{a}_\mu^{(1)}(-2\eta_g), \tag{44}$$

where

$$\nu_g^2 + k_g^2 = \frac{\omega^2}{\alpha_0^2},$$

$$\eta_g^2 + k_g^2 = \frac{\omega^2}{\beta_0^2},$$

For the P-wave incidence case (see Figure 1), using $k_g^2/\nu_g^2 = \tan^2\theta$ and $k_g^2/(\nu_g^2+k_g^2) = \sin^2\theta$, where θ is the P-wave incident angle, equation 41 becomes

$$\widetilde{D}^{PP}(\nu_g,\theta) = -\frac{1}{4}(1-\tan^2\theta)\widetilde{a}_\rho^{(1)}(-2\nu_g) - \frac{1}{4}(1+\tan^2\theta)\widetilde{a}_\gamma^{(1)}(-2\nu_g) + \frac{2\beta_0^2\sin^2\theta}{\alpha_0^2}\widetilde{a}_\mu^{(1)}(-2\nu_g). \tag{45}$$

In this case, when $\beta_0 = \beta_1 = 0$, equation 45 reduces to the acoustic two parameter case equation 7 in Zhang and Weglein (2005) for $z_g = z_s = 0$.

$$\widetilde{D}(q_g,\theta) = -\frac{\rho_0}{4}\left[\frac{1}{\cos^2\theta}\widetilde{\alpha_1}(-2q_g) + (1-\tan^2\theta)\widetilde{\beta}_1(-2q_g)\right], \tag{46}$$

In equation 45, it seems straightforward that using the data at three angles to obtain the linear inversion of a_ρ, a_γ and a_μ, and this is what we do in this paper. However, by doing this it requires a whole new understanding of the definition of "the data". This point has been discussed by Weglein et al. (2007).

4 Direct non-linear inversion of 1D elastic medium

Writing equation 25 in matrix form:

$$\begin{aligned}
&\begin{pmatrix}\hat{G}_0^P & 0\\ 0 & \hat{G}_0^S\end{pmatrix}\begin{pmatrix}\hat{V}_2^{PP} & \hat{V}_2^{PS}\\ \hat{V}_2^{SP} & \hat{V}_2^{SS}\end{pmatrix}\begin{pmatrix}\hat{G}_0^P & 0\\ 0 & \hat{G}_0^S\end{pmatrix}\\
&= -\begin{pmatrix}\hat{G}_0^P & 0\\ 0 & \hat{G}_0^S\end{pmatrix}\begin{pmatrix}\hat{V}_1^{PP} & \hat{V}_1^{PS}\\ \hat{V}_1^{SP} & \hat{V}_1^{SS}\end{pmatrix}\begin{pmatrix}\hat{G}_0^P & 0\\ 0 & \hat{G}_0^S\end{pmatrix}\begin{pmatrix}\hat{V}_1^{PP} & \hat{V}_1^{PS}\\ \hat{V}_1^{SP} & \hat{V}_1^{SS}\end{pmatrix}\begin{pmatrix}\hat{G}_0^P & 0\\ 0 & \hat{G}_0^S\end{pmatrix},
\end{aligned} \tag{47}$$

leads to four equations

$$\hat{G}_0^P\hat{V}_2^{PP}\hat{G}_0^P = -\hat{G}_0^P\hat{V}_1^{PP}\hat{G}_0^P\hat{V}_1^{PP}\hat{G}_0^P - \hat{G}_0^P\hat{V}_1^{PS}\hat{G}_0^S\hat{V}_1^{SP}\hat{G}_0^P, \tag{48}$$

$$\hat{G}_0^P\hat{V}_2^{PS}\hat{G}_0^S = -\hat{G}_0^P\hat{V}_1^{PP}\hat{G}_0^P\hat{V}_1^{PS}\hat{G}_0^S - \hat{G}_0^P\hat{V}_1^{PS}\hat{G}_0^S\hat{V}_1^{SS}\hat{G}_0^S, \tag{49}$$

$$\hat{G}_0^S\hat{V}_2^{SP}\hat{G}_0^P = -\hat{G}_0^S\hat{V}_1^{SP}\hat{G}_0^P\hat{V}_1^{PP}\hat{G}_0^P - \hat{G}_0^S\hat{V}_1^{SS}\hat{G}_0^S\hat{V}_1^{SP}\hat{G}_0^P, \tag{50}$$

$$\hat{G}_0^S\hat{V}_2^{SS}\hat{G}_0^S = -\hat{G}_0^S\hat{V}_1^{SP}\hat{G}_0^P\hat{V}_1^{PS}\hat{G}_0^S - \hat{G}_0^S\hat{V}_1^{SS}\hat{G}_0^S\hat{V}_1^{SS}\hat{G}_0^S. \tag{51}$$

Since $\hat{V}_1^{PP}$ relates to $\hat{D}^{PP}$, $\hat{V}_1^{PS}$ relates to $\hat{D}^{PS}$, and so on, the four components of the data will be coupled in the non-linear elastic inversion. We cannot perform the direct non-linear inversion without knowing all components of the data. As shown in Zhang and Weglein (2005) and this chapter, when the work on the two parameter acoustic case is extended to the present three parameter elastic case, it is not just simply adding one more parameter, but there are more issues involved. Even for the linear case, the linear solutions found in (41) $\sim$ (44) are much more complicated than those of the acoustic case. For instance, four different sets of linear parameter estimates are produced from each component of the data. Also, generally four distinct reflector mislocations arise from the two reference velocities (P-wave velocity and S-wave velocity).

However, in some situations like the towed streamer case, we do not have all components of data available. A particular non-linear approach to be presented in the next section, has been chosen to side-step a portion of this complexity and address our typical lack of four components of elastic data: using $\hat{D}^{PP}$ as the fundamental data input, and perform a reduced form of non-linear elastic inversion, concurrently asking: what beyond-linear value does this simpler framework add? We will see from the numerical tests presented in the following section.

4.1 Only using $\hat{D}^{PP}$ — a particular non-linear approach and the numerical tests

When assuming only $\hat{D}^{PP}$ are available, first, we compute the linear solution for $a_\rho^{(1)}$, $a_\gamma^{(1)}$ and $a_\mu^{(1)}$ from equation 41. Then, substituting the solution into the other three equations (42), (43) and (44), we synthesize the other components of data — $\hat{D}^{PS}$, $\hat{D}^{SP}$ and $\hat{D}^{SS}$. Finally, using the given $\hat{D}^{PP}$ and the synthesized data, we perform the non-linear elastic inversion, getting the following second order (first term beyond linear) elastic inversion solution from equation 48,

$$
\begin{aligned}
&\left(1-\tan^2\theta\right)a_\rho^{(2)}(z)+\left(1+\tan^2\theta\right)a_\gamma^{(2)}(z)-8b^2\sin^2\theta a_\mu^{(2)}(z)\\
=&-\frac{1}{2}\left(\tan^4\theta-1\right)\left[a_\gamma^{(1)}(z)\right]^2+\frac{\tan^2\theta}{\cos^2\theta}a_\gamma^{(1)}(z)a_\rho^{(1)}(z)\\
&+\frac{1}{2}\left[\left(1-\tan^4\theta\right)-\frac{2}{C+1}\left(\frac{1}{C}\right)\left(\frac{\alpha_0^2}{\beta_0^2}-1\right)\frac{\tan^2\theta}{\cos^2\theta}\right]\left[a_\rho^{(1)}(z)\right]^2\\
&-4b^2\left[\tan^2\theta-\frac{2}{C+1}\left(\frac{1}{2C}\right)\left(\frac{\alpha_0^2}{\beta_0^2}-1\right)\tan^4\theta\right]a_\rho^{(1)}(z)a_\mu^{(1)}(z)\\
&+2b^4\left(\tan^2\theta-\frac{\alpha_0^2}{\beta_0^2}\right)\left[2\sin^2\theta-\frac{2}{C+1}\frac{1}{C}\left(\frac{\alpha_0^2}{\beta_0^2}-1\right)\tan^2\theta\right]\left[a_\mu^{(1)}(z)\right]^2\\
&-\frac{1}{2}\left(\frac{1}{\cos^4\theta}\right)a_\gamma^{(1)\prime}(z)\int_0^z dz'\left[a_\gamma^{(1)}\left(z'\right)-a_\rho^{(1)}\left(z'\right)\right]\\
&-\frac{1}{2}\left(1-\tan^4\theta\right)a_\rho^{(1)\prime}(z)\int_0^z dz'\left[a_\gamma^{(1)}\left(z'\right)-a_\rho^{(1)}\left(z'\right)\right]\\
&+4b^2\tan^2\theta a_\mu^{(1)\prime}(z)\int_0^z dz'\left[a_\gamma^{(1)}\left(z'\right)-a_\rho^{(1)}\left(z'\right)\right]\\
&+\frac{2}{C+1}\frac{1}{C}\left(\frac{\alpha_0^2}{\beta_0^2}-1\right)\tan^2\theta\left(\tan^2\theta-C\right)b^2\int_0^z dz' a_{\mu\ z}^{(1)}\left(\frac{(C-1)z'+2z}{(C+1)}\right)a_\rho^{(1)}\left(z'\right)
\end{aligned}
$$

$$
\begin{aligned}
&- \frac{2}{C+1}\frac{2}{C}\left(\frac{\alpha_0^2}{\beta_0^2}-1\right)\tan^2\theta\left(\tan^2\theta-\frac{\alpha_0^2}{\beta_0^2}\right)b^4\int_0^z dz' a_\mu^{(1)}{}_z\left(\frac{(C-1)\,z'+2z}{(C+1)}\right)a_\mu^{(1)}\left(z'\right)\\
&+ \frac{2}{C+1}\frac{1}{C}\left(\frac{\alpha_0^2}{\beta_0^2}-1\right)\tan^2\theta\left(\tan^2\theta+C\right)b^2\int_0^z dz' a_\mu^{(1)}\left(z'\right)a_\rho^{(1)}{}_z\left(\frac{(C-1)z'+2z}{(C+1)}\right)\\
&- \frac{2}{C+1}\frac{1}{2C}\left(\frac{\alpha_0^2}{\beta_0^2}-1\right)\tan^2\theta\left(\tan^2\theta+1\right)\int_0^z dz' a_\rho^{(1)}\left(z'\right)a_\rho^{(1)}{}_z\left(\frac{(C-1)\,z'+2z}{(C+1)}\right), \qquad (52)
\end{aligned}
$$

where $a_\rho^{(1)}{}_z\left(\frac{(C-1)z'+2z}{(C+1)}\right) = d\left[a_\rho^{(1)}\left(\frac{(C-1)z'+2z}{(C+1)}\right)\right]/dz$, $b=\frac{\beta_0}{\alpha_0}$ and $C=\frac{\eta_g}{\nu_g}=\frac{\sqrt{1-b^2\sin^2\theta}}{b\sqrt{1-\sin^2\theta}}$.

The first five terms on the right side of equation 52 are inversion terms; i.e., they contribute to parameter predictions. The other terms on the right side of the equation are imaging terms. The arguments for the remarks above are the same as in the acoustic case in (Zhang and Weglein, 2005). For one interface model, there is no imaging task. The only task is inversion. In this case, all of the integration terms on the right side of equation 52 are zero, and only the first five terms can be non-zero. Thus, we conclude that the integration terms (which care about duration) are imaging terms, and the first five terms are inversion terms. Both the inversion and imaging terms (especially the imaging terms) become much more complicated after the extension of acoustic case (Zhang and Weglein, 2005) to elastic case. The integrand of the first three integral terms is the first order approximation of the relative change in P-wave velocity. The derivatives $a_\gamma^{(1)\prime}$, $a_\rho^{(1)\prime}$ and $a_\mu^{(1)\prime}$ in front of those integrals are acting to correct the wrong locations caused by the inaccurate reference P-wave velocity. The other four terms with integrals willbe zero as $\beta_0 \to 0$ since in this case $C \to \infty$.

In the following, we test this approach numerically.

For a single interface 1D elastic medium case, as shown in Figure 1, the reflection coefficient R^{PP} has the following form (Foster et al., 1997)

$$R^{PP} = \frac{N}{D}, \qquad (53)$$

where

$$
\begin{aligned}
N = &-(1+2kx^2)^2 b\sqrt{1-c^2x^2}\sqrt{1-d^2x^2} - (1-a+2kx^2)^2 bcdx^2\\
&+(a-2kx^2)^2 cd\sqrt{1-x^2}\sqrt{1-b^2x^2}\\
&+4k^2x^2\sqrt{1-x^2}\sqrt{1-b^2x^2}\sqrt{1-c^2x^2}\sqrt{1-d^2x^2} - ad\sqrt{1-b^2x^2}\sqrt{1-c^2x^2}\\
&+abc\sqrt{1-x^2}\sqrt{1-d^2x^2}, \qquad (54)
\end{aligned}
$$

$$
\begin{aligned}
D = &(1+2kx^2)^2 b\sqrt{1-c^2x^2}\sqrt{1-d^2x^2} + (1-a+2kx^2)^2 bcdx^2\\
&+(a-2kx^2)^2 cd\sqrt{1-x^2}\sqrt{1-b^2x^2}\\
&+4k^2x^2\sqrt{1-x^2}\sqrt{1-b^2x^2}\sqrt{1-c^2x^2}\sqrt{1-d^2x^2} + ad\sqrt{1-b^2x^2}\sqrt{1-c^2x^2}\\
&+abc\sqrt{1-x^2}\sqrt{1-d^2x^2}, \qquad (55)
\end{aligned}
$$

where $a = \rho_1/\rho_0$, $b = \beta_0/\alpha_0$, $c = \alpha_1/\alpha_0$, $d = \beta_1/\alpha_0$, $k = ad^2 - b^2$ and $x = \sin\theta$, and the subscripts "0" and "1" denote the reference medium and actual medium respectively. Similar to the acoustic case, using the analytic data (Clayton and Stolt, 1981; Weglein et al., 1986)

$$\widetilde{D}^{PP}(\nu_g, \theta) = R^{PP}(\theta)\frac{e^{2i\nu_g a}}{4\pi i\nu_g}, \tag{56}$$

where a is the depth of the interface. Substituting equation 56 into equation 45, Fourier transforming equation 45 over $2\nu_g$, and fixing $z > a$ and θ, we have

$$(1 - \tan^2\theta)a_\rho^{(1)}(z) + (1 + \tan^2\theta)a_\gamma^{(1)}(z) - 8\frac{\beta_0^2}{\alpha_0^2}\sin^2\theta a_\mu^{(1)}(z) = 4R^{PP}(\theta)H(z - a). \tag{57}$$

In this section, we numerically test the direct inversion approach on the following four models:

Model 1: shale (0.20 porosity) over oil sand (0.10 porosity). $\rho_0 = 2.32g/cm^3$, $\rho_1 = 2.46g/cm^3$; $\alpha_0 = 2627m/s$, $\alpha_1 = 4423m/s$; $\beta_0 = 1245m/s$, $\beta_1 = 2939m/s$.

Model 2: shale over oil sand, 0.20 porosity. $\rho_0 = 2.32g/cm^3$, $\rho_1 = 2.27g/cm^3$; $\alpha_0 = 2627m/s$, $\alpha_1 = 3251m/s$; $\beta_0 = 1245m/s$, $\beta_1 = 2138m/s$.

Model 3: shale (0.20 porosity) over oil sand (0.30 porosity). $\rho_0 = 2.32g/cm^3$, $\rho_1 = 2.08g/cm^3$; $\alpha_0 = 2627m/s$, $\alpha_1 = 2330m/s$; $\beta_0 = 1245m/s$, $\beta_1 = 1488m/s$.

Model 4: oil sand over wet sand, 0.20 porosity. $\rho_0 = 2.27g/cm^3$, $\rho_1 = 2.32g/cm^3$; $\alpha_0 = 3251m/s$, $\alpha_1 = 3507m/s$; $\beta_0 = 2138m/s$, $\beta_1 = 2116m/s$.

To test and compare methods, the top of sand reflection was modeled for oil sands with porosities of 10, 20, and 30%. The three models used the same shale overburden. An oil/water contact model was also constructed for the 20% porosity sand.

The low porosity model (10%) represents a deep, consolidated reservoir sand. Pore fluids have little effect on the seismic response of the reservoir sand. It is difficult to distinguish oil sands from brine sands on the basis of seismic response. Impedance of the sand is higher than impedance of the shale.

The moderate porosity model (20%) represents deeper, compacted reservoirs. Pore fluids have a large impact on seismic response, but the fluid effect is less than that of the high porosity case. The overlying shale has high density compared to the reservoir sand, but the P-wave velocity of the oil sand exceeds that of the shale. As a result, impedance contrast is reduced, and shear wave information becomes more important for detecting the reservoir.

The high porosity model (30%) is typical of a weakly consolidated, shallow reservoir sand. Pore fluids have a large impact on the seismic response. Density, P-wave velocity, and the α/β ratio of the oil sand are lower than the density, P-wave velocity, and α/β ratio of the overlying shale. Consequently, there is a significant decrease in density and P-wave bulk modulus and an increase in shear modulus at the shale/oil sand interface.

The fourth model denotes an oil/water contact in a 20% porosity sand. At a fluid contact, both density and P-wave velocity increase in going from the oil zone into the wet zone. Because pore fluids have no affect on shear modulus, there is no change in shear modulus.

Using these four models, we can find the corresponding R^{PP} from equation 53. Then, choosing three different angles θ_1, θ_2 and θ_3, we can get the linear solutions for $a_\rho^{(1)}$, $a_\gamma^{(1)}$ and $a_\mu^{(1)}$ from equation 57 , and then get the solutions for $a_\rho^{(2)}$, $a_\gamma^{(2)}$ and $a_\mu^{(2)}$ from equation 52.

There are two plots in each figure. The left ones are the results for the first order, while the right ones are the results for the first order plus the second order. The red lines denote the corresponding actual values. In the figures, we illustrate the results corresponding to different sets of angles θ_1 and θ_2. The third angle θ_3 is fixed at zero.

The numerical results indicate that all the second order solutions provide improvements over the linear solutions for all of the four models. When the second term is added to linear order, the results become much closer to the corresponding exact values and the surfaces become flatter in a larger range of angles. But the degrees of those improvements are different for different models. How accurately $\hat{D}^{PP}$ effectively synthesize $\hat{D}^{PS}$ and $\hat{D}^{SP}$ (as shown in Figures 14 $\sim$ 17) determined the degree of benefit provided by the non-linear elastic approach. All of the "predicted" values in the figures are predicted using the linear results from $\hat{D}^{PP}$. And the "actual" values are calculated from the Zoeppritz' equations.

In principle, the elastic non-linear direct inversion in 2D requires all four components of data. However, in this section we introduce an approach which requires only $\hat{D}^{PP}$ and approximately synthesizes the other required components. Based on this approach, the first direct non-linear elastic inversion solution is derived. Value-added results are obtained from the non-linear inversion terms beyond linear. Although $\hat{D}^{PP}$ can itself provide useful non-linear direct inversion results, the implication of this research is that further value would derive from actually measuring $\hat{D}^{PP}$, $\hat{D}^{PS}$, $\hat{D}^{SP}$ and $\hat{D}^{SS}$, as the method requires. In the following section, we give a consistent method and solve all of the second order equations 48, 49, 50 and 51 with all four components of data available.

4.2 Using all four components of data — full direct non-linear elastic inversion

Using four components of data, one consistent method to solve for the second terms is, first, using the linear solutions as shown in equations 41, 42, 43 and 44, we can get the linear solution for $a_\rho^{(1)}$, $a_\gamma^{(1)}$ and $a_\mu^{(1)}$ in terms of $\hat{D}^{PP}, \hat{D}^{PS}, \hat{D}^{SP}$and $\hat{D}^{SS}$ through the following way

$$\begin{pmatrix} a_\rho^{(1)} \\ a_\gamma^{(1)} \\ a_\mu^{(1)} \end{pmatrix} = (O^T O)^{-1} O^T \begin{pmatrix} \hat{D}^{PP} \\ \hat{D}^{PS} \\ \hat{D}^{SP} \\ \hat{D}^{SS} \end{pmatrix}, \tag{58}$$

where the matrix O is

$$\begin{pmatrix} -\frac{1}{4}\left(1-\frac{k_g^{PP^2}}{\nu_g^{PP^2}}\right) & -\frac{1}{4}\left(1+\frac{k_g^{PP^2}}{\nu_g^{PP^2}}\right) & \frac{2\beta_0^2 k_g^{PP^2}}{\alpha_0^2\left(\nu_g^{PP^2}+k_g^{PP^2}\right)} \\ -\frac{1}{4}\left(\frac{k_g^{PS}}{\nu_g^{PS}}+\frac{k_g^{PS}}{\eta_g^{PS}}\right) & 0 & -\frac{\beta_0^2}{2\omega^2}k_g^{PS}\left(\nu_g^{PS}+\eta_g^{PS}\right)\left(1-\frac{k_g^{PS^2}}{\nu_g^{PS}\eta_g^{PS}}\right) \\ \frac{1}{4}\left(\frac{k_g^{SP}}{\nu_g^{SP}}+\frac{k_g^{SP}}{\eta_g^{SP}}\right) & 0 & \frac{\beta_0^2}{2\omega^2}k_g^{SP}\left(\nu_g^{SP}+\eta_g^{SP}\right)\left(1-\frac{k_g^{SP^2}}{\nu_g^{SP}\eta_g^{SP}}\right) \\ -\frac{1}{4}\left(1-\frac{k_g^{SS^2}}{\eta_g^{SS^2}}\right) & 0 & -\left[\frac{k_g^{SS^2}+\eta_g^{SS^2}}{4\eta_g^{SS^2}}-\frac{2k_g^{SS^2}}{k_g^{SS^2}+\eta_g^{SS^2}}\right] \end{pmatrix}, \tag{59}$$

and O^T is the transpose of matrix O, the superscript -1 denotes the inverse of the matrix O^TO.

Let the arguments of $a_\rho^{(1)}$ and $a_\mu^{(1)}$ in equations 41, 42, 43 and 44 equal, we need

$$-2\nu_g^{PP} = -\nu_g^{PS} - \eta_g^{PS} = -\nu_g^{SP} - \eta_g^{SP} = -2\eta_g^{SS},$$

which leads to (please see details in Appendix A)

$$\begin{aligned} 2\frac{\omega}{\alpha_0}\cos\theta^{PP} &= \frac{\omega}{\alpha_0}\sqrt{1-\frac{\alpha_0^2}{\beta_0^2}\sin^2\theta^{PS}} + \frac{\omega}{\beta_0}\cos\theta^{PS} = \frac{\omega}{\alpha_0}\cos\theta^{SP} + \frac{\omega}{\beta_0}\sqrt{1-\frac{\beta_0^2}{\alpha_0^2}\sin^2\theta^{SP}} \\ &= 2\frac{\omega}{\beta_0}\cos\theta^{SS}. \end{aligned}$$

From the expression above, given θ^{PP}, as shown in Figure 18, we can find the corresponding angles θ^{PS}, θ^{SP} and θ^{SS} which appear in matrix O

$$\begin{aligned} \theta^{PS} &= \cos^{-1}\left[\frac{4b^2\cos^2\theta^{PP}+1-b^2}{4b\cos\theta^{PP}}\right], \\ \theta^{SP} &= \cos^{-1}\left[\frac{4b^2\cos^2\theta^{PP}-1+b^2}{4b^2\cos\theta^{PP}}\right], \\ \theta^{SS} &= \cos^{-1}\left(b\cos\theta^{PP}\right), \end{aligned}$$

where $b = \frac{\beta_0}{\alpha_0}$.

Then, through the similar way, we can get the solution for $a_\rho^{(2)}$, $a_\gamma^{(2)}$ and $a_\mu^{(2)}$ in terms of $a_\rho^{(1)}$, $a_\gamma^{(1)}$ and $a_\mu^{(1)}$

$$\begin{pmatrix} a_\rho^{(2)} \\ a_\gamma^{(2)} \\ a_\mu^{(2)} \end{pmatrix} = (O^TO)^{-1}O^TQ, \tag{60}$$

where the matrix Q is in terms of $a_\rho^{(1)}$, $a_\gamma^{(1)}$ and $a_\mu^{(1)}$.

Based on this idea, we get the following non-linear solutions for equations 48, 49, 50 and 51 respectively.

The form of the solution for equation 48, i.e.,

$$\hat{G}_0^P \hat{V}_2^{PP} \hat{G}_0^P = -\hat{G}_0^P \hat{V}_1^{PP} \hat{G}_0^P \hat{V}_1^{PP} \hat{G}_0^P - \hat{G}_0^P \hat{V}_1^{PS} \hat{G}_0^S \hat{V}_1^{SP} \hat{G}_0^P ,$$

is the same as equation 52. In the $(k_s, z_s; k_g, z_g; \omega)$ domain, we get the the other three solutions respectively, for equations 49, 50 and 51.

The solution for equation 49, i.e.,

$$\hat{G}_0^P \hat{V}_2^{PS} \hat{G}_0^S = -\hat{G}_0^P \hat{V}_1^{PP} \hat{G}_0^P \hat{V}_1^{PS} \hat{G}_0^S - \hat{G}_0^P \hat{V}_1^{PS} \hat{G}_0^S \hat{V}_1^{SS} \hat{G}_0^S,$$

is

$$\begin{aligned}
&-\frac{1}{4}\left(\frac{k_g}{\nu_g}+\frac{k_g}{\eta_g}\right) a_\rho^{(2)}(z) - \frac{\beta_0^2}{2\omega^2} k_g \left(\nu_g+\eta_g\right)\left(1-\frac{k_g^2}{\nu_g\eta_g}\right) a_\mu^{(2)}(z) \\
=&-\left[\left(\frac{1}{2}+\frac{1}{C+1}\right)\frac{1}{\eta_g\nu_g^2}\left(\frac{\beta_0^4}{\alpha_0^4}Ck_g^3 - 3\frac{\beta_0^2}{\alpha_0^2}Ck_g^5\frac{\beta_0^2}{\omega^2} - k_g^3\nu_g^2\frac{\beta_0^2}{\omega^2} + 2k_g^5\nu_g^2\frac{\beta_0^4}{\omega^4} + 2Ck_g^7\frac{\beta_0^4}{\omega^4}\right)\right. \\
&+\left(\frac{1}{2}-\frac{1}{C+1}\right)\frac{1}{\eta_g\nu_g^2}\left(\frac{\beta_0^2}{\alpha_0^2}Ck_g^3\nu_g^2\frac{\beta_0^2}{\omega^2} + 2\frac{\beta_0^2}{\alpha_0^2}k_g^5\frac{\beta_0^2}{\omega^2} - 2Ck_g^5\nu_g^2\frac{\beta_0^4}{\omega^4} - \frac{\beta_0^2}{\alpha_0^2}k_g^3 + k_g^5\frac{\beta_0^2}{\omega^2} - 2k_g^7\frac{\beta_0^4}{\omega^4}\right) \\
&+\left(\frac{1}{2C}+\frac{1}{C+1}\right)\frac{1}{4\eta_g^2\nu_g}\left(6k_g^3 - 12k_g^5\frac{\beta_0^2}{\omega^2} - k_g\frac{\omega^2}{\beta_0^2} + 8k_g^7\frac{\beta_0^4}{\omega^4} + 8C^3\nu_g^2k_g^5\frac{\beta_0^4}{\omega^4}\right. \\
&\left.-4\frac{\beta_0^2}{\alpha_0^2}C^3\nu_g^2k_g^3\frac{\beta_0^2}{\omega^2}\right) \\
&-\left(\frac{1}{2C}-\frac{1}{C+1}\right)\frac{1}{4\eta_g\nu_g^2}\left(4\frac{\beta_0^2}{\alpha_0^2}k_g^3 - 8k_g^5\frac{\beta_0^2}{\omega^2} - k_g\frac{\omega^2}{\alpha_0^2} + 2k_g^3 - 4C\nu_g^2k_g^3\frac{\beta_0^2}{\omega^2} + 8C\nu_g^2k_g^5\frac{\beta_0^4}{\omega^4}\right. \\
&\left.\left.-4\frac{\beta_0^2}{\alpha_0^2}k_g^5\frac{\beta_0^2}{\omega^2} + 8k_g^7\frac{\beta_0^4}{\omega^4}\right) - \frac{\beta_0^2}{\alpha_0^2}\frac{k_g^3}{\nu_g}\frac{\beta_0^2}{\omega^2} + \frac{k_g}{2\eta_g}\left(2k_g^2\frac{\beta_0^2}{\omega^2}-1\right)\right] a_\mu^{(1)}(z)a_\mu^{(1)}(z) \\
&-\left[\left(\frac{1}{2}+\frac{1}{C+1}\right)\frac{k_g}{8\eta_g\nu_g^2}\left(Ck_g^2+\nu_g^2\right) - \left(\frac{1}{2}-\frac{1}{C+1}\right)\frac{k_g}{8\eta_g\nu_g^2}\left(k_g^2+C\nu_g^2\right)\right. \\
&\left.+\left(\frac{1}{2C}+\frac{1}{C+1}\right)\frac{k_g}{8\eta_g^2\nu_g}\left(C^3\nu_g^2+k_g^2\right) - \left(\frac{1}{2C}-\frac{1}{C+1}\right)\frac{k_g}{8\eta_g\nu_g^2}\left(k_g^2+C\nu_g^2\right)\right] a_\rho^{(1)}(z)a_\rho^{(1)}(z) \\
&-\left[\left(\frac{1}{2}+\frac{1}{C+1}\right)\frac{\beta_0^2}{\alpha_0^2}\frac{1}{4\nu_g^3}k_g\left(k_g^2-\nu_g^2\right) + \left(\frac{1}{2}-\frac{1}{C+1}\right)\frac{1}{4\eta_g\nu_g^2}\left(k_g\frac{\omega^2}{\alpha_0^2} - 2\frac{\beta_0^2}{\alpha_0^2}k_g^3\right) + \frac{\beta_0^2}{\alpha_0^2}\frac{k_g}{2\nu_g}\right] \\
&\times a_\mu^{(1)}(z)a_\gamma^{(1)}(z) \\
&+\left[\left(\frac{1}{2}+\frac{1}{C+1}\right)\frac{k_g\left(k_g^2+\nu_g^2\right)}{8\nu_g^3} - \left(\frac{1}{2}-\frac{1}{C+1}\right)\frac{k_g\left(k_g^2+\nu_g^2\right)}{8\eta_g\nu_g^2}\right] a_\rho^{(1)}(z)a_\gamma^{(1)}(z) \\
&-\left[\left(\frac{1}{2}+\frac{1}{C+1}\right)\frac{1}{4\eta_g\nu_g^2}\left(3\frac{\beta_0^2}{\alpha_0^2}Ck_g^3 + \nu_g^2k_g - 4Ck_g^5\frac{\beta_0^2}{\omega^2} - 4k_g^3\nu_g^2\frac{\beta_0^2}{\omega^2}\right)\right. \\
&\left.-\left(\frac{1}{2}-\frac{1}{C+1}\right)\frac{1}{4\eta_g\nu_g^2}\left(\frac{\beta_0^2}{\alpha_0^2}C\nu_g^2k_g + k_g^3 - 4k_g^5\frac{\beta_0^2}{\omega^2} - 4Ck_g^3\nu_g^2\frac{\beta_0^2}{\omega^2} + 2\frac{\beta_0^2}{\alpha_0^2}k_g^3\right)\right.
\end{aligned}$$

$$
\begin{aligned}
&+\left(\frac{1}{2C}+\frac{1}{C+1}\right)\frac{1}{4\eta_g^2\nu_g}\left(k_g^3-2k_g^5\frac{\beta_0^2}{\omega^2}+\frac{\beta_0^2}{\alpha_0^2}C^3\nu_g^2k_g-4C^3\nu_g^2k_g^3\frac{\beta_0^2}{\omega^2}-\frac{1}{2}k_g\frac{\omega^2}{\beta_0^2}\right.\\
&\left.+2C^2\nu_g^2k_g^3\frac{\beta_0^2}{\omega^2}\right)\\
&-\left(\frac{1}{2C}-\frac{1}{C+1}\right)\frac{1}{4\eta_g\nu_g^2}\left(C\nu_g^2k_g-2C\nu_g^2k_g^3\frac{\beta_0^2}{\omega^2}+\frac{\beta_0^2}{\alpha_0^2}k_g^3-2k_g^5\frac{\beta_0^2}{\omega^2}+2C^2\nu_g^2k_g^3\frac{\beta_0^2}{\omega^2}\right.\\
&\left.-2C\nu_g^2k_g^3\frac{\beta_0^2}{\omega^2}-\frac{1}{2}k_g\frac{\omega^2}{\beta_0^2}\right)\Bigg]\times a_\rho^{(1)}(z)a_\mu^{(1)}(z)\\
&-\frac{1}{\eta_g\nu_g^2}\left(\frac{\beta_0^4}{\alpha_0^4}Ck_g^3-3\frac{\beta_0^2}{\alpha_0^2}Ck_g^5\frac{\beta_0^2}{\omega^2}-k_g^3\nu_g^2\frac{\beta_0^2}{\omega^2}+2k_g^5\nu_g^2\frac{\beta_0^4}{\omega^4}+2Ck_g^7\frac{\beta_0^4}{\omega^4}\right)\\
&\times\left[\frac{1}{2}\int_0^z dz' {a_\mu^{(1)}}_z\left(\frac{(C+1)z-(C-1)\,z'}{2}\right)a_\mu^{(1)}\left(z'\right)+\frac{1}{C+1}a_\mu^{(1)'}(z)\int_0^z dz' a_\mu^{(1)}(z')\right]\\
&-\frac{1}{\eta_g\nu_g^2}\left(\frac{\beta_0^2}{\alpha_0^2}Ck_g^3\nu_g^2\frac{\beta_0^2}{\omega^2}+2\frac{\beta_0^2}{\alpha_0^2}k_g^5\frac{\beta_0^2}{\omega^2}-2Ck_g^5\nu_g^2\frac{\beta_0^4}{\omega^4}-\frac{\beta_0^2}{\alpha_0^2}k_g^3+k_g^5\frac{\beta_0^2}{\omega^2}-2k_g^7\frac{\beta_0^4}{\omega^4}\right)\\
&\times\left[\frac{1}{2}\int_0^z dz' {a_\mu^{(1)}}_z\left(\frac{(C+1)z-(C-1)\,z'}{2}\right)a_\mu^{(1)}\left(z'\right)-\frac{1}{C+1}a_\mu^{(1)'}(z)\int_0^z dz' a_\mu^{(1)}(z')\right]\\
&-\frac{1}{4\eta_g^2\nu_g}\left(6k_g^3-12k_g^5\frac{\beta_0^2}{\omega^2}-k_g\frac{\omega^2}{\beta_0^2}+8k_g^7\frac{\beta_0^4}{\omega^4}+8C^3\nu_g^2k_g^5\frac{\beta_0^4}{\omega^4}-4\frac{\beta_0^2}{\alpha_0^2}C^3\nu_g^2k_g^3\frac{\beta_0^2}{\omega^2}\right)\\
&\times\left[\frac{1}{2C}\int_0^z dz' {a_\mu^{(1)}}_z\left(\frac{(C+1)z+(C-1)\,z'}{2C}\right)a_\mu^{(1)}\left(z'\right)+\frac{1}{C+1}a_\mu^{(1)'}(z)\int_0^z dz' a_\mu^{(1)}(z')\right]\\
&+\frac{1}{4\eta_g\nu_g^2}\left(4\frac{\beta_0^2}{\alpha_0^2}k_g^3-8k_g^5\frac{\beta_0^2}{\omega^2}-k_g\frac{\omega^2}{\alpha_0^2}+2k_g^3-4C\nu_g^2k_g^3\frac{\beta_0^2}{\omega^2}+8C\nu_g^2k_g^5\frac{\beta_0^4}{\omega^4}-4\frac{\beta_0^2}{\alpha_0^2}k_g^5\frac{\beta_0^2}{\omega^2}+8k_g^7\frac{\beta_0^4}{\omega^4}\right)\\
&\times\left[\frac{1}{2C}\int_0^z dz' {a_\mu^{(1)}}_z\left(\frac{(C+1)z+(C-1)\,z'}{2C}\right)a_\mu^{(1)}\left(z'\right)-\frac{1}{C+1}a_\mu^{(1)'}(z)\int_0^z dz' a_\mu^{(1)}(z')\right]\\
&-\frac{k_g\left(Ck_g^2+\nu_g^2\right)}{8\eta_g\nu_g^2}\left[\frac{1}{2}\int_0^z dz' {a_\rho^{(1)}}_z\left(\frac{(C+1)z-(C-1)\,z'}{2}\right)a_\rho^{(1)}\left(z'\right)\right.\\
&\left.+\frac{1}{C+1}a_\rho^{(1)'}(z)\int_0^z dz' a_\rho^{(1)}(z')\right]\\
&+\frac{k_g\left(k_g^2+C\nu_g^2\right)}{8\eta_g\nu_g^2}\left[\frac{1}{2}\int_0^z dz' {a_\rho^{(1)}}_z\left(\frac{(C+1)z-(C-1)\,z'}{2}\right)a_\rho^{(1)}\left(z'\right)\right.\\
&\left.-\frac{1}{C+1}a_\rho^{(1)'}(z)\int_0^z dz' a_\rho^{(1)}(z')\right]\\
&-\frac{C^3k_g\nu_g^2+k_g^3}{8\eta_g^2\nu_g}\left[\frac{1}{2C}\int_0^z dz' {a_\rho^{(1)}}_z\left(\frac{(C+1)z+(C-1)\,z'}{2C}\right)a_\rho^{(1)}\left(z'\right)\right.\\
&\left.+\frac{1}{C+1}a_\rho^{(1)'}(z)\int_0^z dz' a_\rho^{(1)}(z')\right]\\
&+\frac{k_g\left(k_g^2+C\nu_g^2\right)}{8\eta_g\nu_g^2}\left[\frac{1}{2C}\int_0^z dz' {a_\rho^{(1)}}_z\left(\frac{(C+1)z+(C-1)\,z'}{2C}\right)a_\rho^{(1)}\left(z'\right)\right.
\end{aligned}
$$

$$
\begin{aligned}
&-\frac{1}{C+1}a_{\rho}^{(1)'}(z)\int_0^z dz' a_{\rho}^{(1)}(z')\Bigg] \\
&-\frac{\beta_0^2}{\alpha_0^2}\frac{k_g\left(k_g^2-\nu_g^2\right)}{4\nu_g^3}\left[\frac{1}{2}\int_0^z dz' a_{\gamma}^{(1)}{}_z\left(\frac{(C+1)z-(C-1)\,z'}{2}\right)a_{\mu}^{(1)}\left(z'\right)\right. \\
&\left.+\frac{1}{C+1}a_{\mu}^{(1)'}(z)\int_0^z dz' a_{\gamma}^{(1)}(z')\right] \\
&-\frac{1}{4\eta_g\nu_g^2}\left(k_g\frac{\omega^2}{\alpha_0^2}-2\frac{\beta_0^2}{\alpha_0^2}k_g^3\right)\left[\frac{1}{2}\int_0^z dz' a_{\gamma}^{(1)}{}_z\left(\frac{(C+1)z-(C-1)\,z'}{2}\right)a_{\mu}^{(1)}\left(z'\right)\right. \\
&\left.-\frac{1}{C+1}a_{\mu}^{(1)'}(z)\int_0^z dz' a_{\gamma}^{(1)}(z')\right] \\
&+\frac{k_g\left(k_g^2+\nu_g^2\right)}{8\nu_g^3}\left[\frac{1}{2}\int_0^z dz' a_{\gamma}^{(1)}{}_z\left(\frac{(C+1)z-(C-1)\,z'}{2}\right)a_{\rho}^{(1)}\left(z'\right)\right. \\
&\left.+\frac{1}{C+1}a_{\rho}^{(1)'}(z)\int_0^z dz' a_{\gamma}^{(1)}(z')\right] \\
&-\frac{k_g\left(k_g^2+\nu_g^2\right)}{8\eta_g\nu_g^2}\left[\frac{1}{2}\int_0^z dz' a_{\gamma}^{(1)}{}_z\left(\frac{(C+1)z-(C-1)\,z'}{2}\right)a_{\rho}^{(1)}\left(z'\right)\right. \\
&\left.-\frac{1}{C+1}a_{\rho}^{(1)'}(z)\int_0^z dz' a_{\gamma}^{(1)}(z')\right] \\
&-\frac{1}{4\eta_g\nu_g^2}\left(\frac{\beta_0^2}{\alpha_0^2}Ck_g^3+\nu_g^2k_g-2Ck_g^5\frac{\beta_0^2}{\omega^2}-2k_g^3\nu_g^2\frac{\beta_0^2}{\omega^2}\right) \\
&\times\left[\frac{1}{2}\int_0^z dz' a_{\rho}^{(1)}{}_z\left(\frac{(C+1)z-(C-1)\,z'}{2}\right)a_{\mu}^{(1)}\left(z'\right)+\frac{1}{C+1}a_{\mu}^{(1)'}(z)\int_0^z dz' a_{\rho}^{(1)}(z')\right] \\
&-\frac{1}{4\eta_g\nu_g^2}\left(2\frac{\beta_0^2}{\alpha_0^2}Ck_g^3-2Ck_g^5\frac{\beta_0^2}{\omega^2}-2k_g^3\nu_g^2\frac{\beta_0^2}{\omega^2}\right) \\
&\times\left[\frac{1}{2}\int_0^z dz' a_{\mu}^{(1)}{}_z\left(\frac{(C+1)z-(C-1)\,z'}{2}\right)a_{\rho}^{(1)}\left(z'\right)+\frac{1}{C+1}a_{\rho}^{(1)'}(z)\int_0^z dz' a_{\mu}^{(1)}(z')\right] \\
&+\frac{1}{4\eta_g\nu_g^2}\left(\frac{\beta_0^2}{\alpha_0^2}C\nu_g^2k_g+k_g^3-2k_g^5\frac{\beta_0^2}{\omega^2}-2Ck_g^3\nu_g^2\frac{\beta_0^2}{\omega^2}\right) \\
&\times\left[\frac{1}{2}\int_0^z dz' a_{\rho}^{(1)}{}_z\left(\frac{(C+1)z-(C-1)\,z'}{2}\right)a_{\mu}^{(1)}\left(z'\right)-\frac{1}{C+1}a_{\mu}^{(1)'}(z)\int_0^z dz' a_{\rho}^{(1)}(z')\right] \\
&+\frac{1}{4\eta_g\nu_g^2}\left(2\frac{\beta_0^2}{\alpha_0^2}k_g^3-2k_g^5\frac{\beta_0^2}{\omega^2}-2Ck_g^3\nu_g^2\frac{\beta_0^2}{\omega^2}\right) \\
&\times\left[\frac{1}{2}\int_0^z dz' a_{\mu}^{(1)}{}_z\left(\frac{(C+1)z-(C-1)\,z'}{2}\right)a_{\rho}^{(1)}\left(z'\right)-\frac{1}{C+1}a_{\rho}^{(1)'}(z)\int_0^z dz' a_{\mu}^{(1)}(z')\right] \\
&-\frac{1}{4\eta_g^2\nu_g}\left(k_g^3-2k_g^5\frac{\beta_0^2}{\omega^2}+\frac{\beta_0^2}{\alpha_0^2}C^3\nu_g^2k_g-2C^3\nu_g^2k_g^3\frac{\beta_0^2}{\omega^2}\right) \\
&\times\left[\frac{1}{2C}\int_0^z dz' a_{\rho}^{(1)}{}_z\left(\frac{(C+1)z+(C-1)\,z'}{2C}\right)a_{\mu}^{(1)}\left(z'\right)+\frac{1}{C+1}a_{\mu}^{(1)'}(z)\int_0^z dz' a_{\rho}^{(1)}(z')\right]
\end{aligned}
$$

$$
\begin{aligned}
&- \frac{1}{4\eta_g^2\nu_g}\left(-2C^3\nu_g^2k_g^3\frac{\beta_0^2}{\omega^2} - \frac{1}{2}k_g\frac{\omega^2}{\beta_0^2} + 2C^2\nu_g^2k_g^3\frac{\beta_0^2}{\omega^2}\right)\\
&\times\left[\frac{1}{2C}\int_0^z dz' a_\mu^{(1)}{}_z\left(\frac{(C+1)z+(C-1)\,z'}{2C}\right)a_\rho^{(1)}\left(z'\right) + \frac{1}{C+1}a_\rho^{(1)'}(z)\int_0^z dz' a_\mu^{(1)}(z')\right]\\
&+ \frac{1}{4\eta_g\nu_g^2}\left(C\nu_g^2k_g - 2C\nu_g^2k_g^3\frac{\beta_0^2}{\omega^2} + \frac{\beta_0^2}{\alpha_0^2}k_g^3 - 2k_g^5\frac{\beta_0^2}{\omega^2}\right)\\
&\times\left[\frac{1}{2C}\int_0^z dz' a_\rho^{(1)}{}_z\left(\frac{(C+1)z+(C-1)\,z'}{2C}\right)a_\mu^{(1)}\left(z'\right) - \frac{1}{C+1}a_\mu^{(1)'}(z)\int_0^z dz' a_\rho^{(1)}(z')\right]\\
&+ \frac{1}{4\eta_g\nu_g^2}\left(2C^2\nu_g^2k_g^3\frac{\beta_0^2}{\omega^2} - 2C\nu_g^2k_g^3\frac{\beta_0^2}{\omega^2} - \frac{1}{2}k_g\frac{\omega^2}{\beta_0^2}\right)\\
&\times\left[\frac{1}{2C}\int_0^z dz' a_\mu^{(1)}{}_z\left(\frac{(C+1)z+(C-1)\,z'}{2C}\right)a_\rho^{(1)}\left(z'\right) - \frac{1}{C+1}a_\rho^{(1)'}(z)\int_0^z dz' a_\mu^{(1)}(z')\right],
\end{aligned}
$$

the solution for equation 50, i.e.,

$$\hat{G}_0^S\hat{V}_2^{SP}\hat{G}_0^P = -\hat{G}_0^S\hat{V}_1^{SP}\hat{G}_0^P\hat{V}_1^{PP}\hat{G}_0^P - \hat{G}_0^S\hat{V}_1^{SS}\hat{G}_0^S\hat{V}_1^{SP}\hat{G}_0^P,$$

is

$$
\begin{aligned}
&\frac{1}{4}\left(\frac{k_g}{\nu_g}+\frac{k_g}{\eta_g}\right)a_\rho^{(2)}(z) + \frac{\beta_0^2}{2\omega^2}k_g\left(\nu_g+\eta_g\right)\left(1-\frac{k_g^2}{\nu_g\eta_g}\right)a_\mu^{(2)}(z)\\
=&\Bigg\{-\frac{1}{2\eta_g\nu_g^2}\left[2(C-1)\nu_g^2k_g^5\frac{\beta_0^4}{\omega^4} + \left(1-\frac{\beta_0^2}{\alpha_0^2}C\right)\nu_g^2k_g^3\frac{\beta_0^2}{\omega^2}\right] - \frac{\beta_0^2}{\alpha_0^2}\frac{k_g^3}{\nu_g}\frac{\beta_0^2}{\omega^2} + \frac{k_g}{2\eta_g}\left(2k_g^2\frac{\beta_0^2}{\omega^2}-1\right)\\
&+\left(\frac{1}{2C}+\frac{1}{C+1}\right)\frac{1}{4\eta_g^2\nu_g}\left(6k_g^3 - 12k_g^5\frac{\beta_0^2}{\omega^2} - k_g\frac{\omega^2}{\beta_0^2} + 8k_g^7\frac{\beta_0^4}{\omega^4} + 8C^3\nu_g^2k_g^5\frac{\beta_0^4}{\omega^4}\right.\\
&\left.-4\frac{\beta_0^2}{\alpha_0^2}C^3\nu_g^2k_g^3\frac{\beta_0^2}{\omega^2}\right)\\
&-\left(\frac{1}{2C}-\frac{1}{C+1}\right)\frac{1}{4\eta_g\nu_g^2}\left(4\frac{\beta_0^2}{\alpha_0^2}k_g^3 - 8k_g^5\frac{\beta_0^2}{\omega^2} - k_g\frac{\omega^2}{\alpha_0^2} + 2k_g^3 - 4C\nu_g^2k_g^3\frac{\beta_0^2}{\omega^2} + 8C\nu_g^2k_g^5\frac{\beta_0^4}{\omega^4}\right.\\
&\left.-4\frac{\beta_0^2}{\alpha_0^2}k_g^5\frac{\beta_0^2}{\omega^2} + 8k_g^7\frac{\beta_0^4}{\omega^4}\right)\Bigg\}a_\mu^{(1)}(z)a_\mu^{(1)}(z)\\
&+\left[\left(\frac{1}{2}+\frac{1}{C+1}\right)\frac{k_g}{8\eta_g\nu_g^2}\left(Ck_g^2+\nu_g^2\right) - \left(\frac{1}{2}-\frac{1}{C+1}\right)\frac{k_g}{8\eta_g\nu_g^2}\left(k_g^2+C\nu_g^2\right)\right.\\
&\left.+\left(\frac{1}{2C}+\frac{1}{C+1}\right)\frac{k_g}{8\eta_g^2\nu_g}\left(C^3\nu_g^2+k_g^2\right) - \left(\frac{1}{2C}-\frac{1}{C+1}\right)\frac{k_g}{8\eta_g\nu_g^2}\left(k_g^2+C\nu_g^2\right)\right]a_\rho^{(1)}(z)a_\rho^{(1)}(z)\\
&+\left[\left(\frac{1}{2}+\frac{1}{C+1}\right)\frac{\beta_0^2}{\alpha_0^2}\frac{1}{4\nu_g^3}k_g\left(k_g^2-\nu_g^2\right) + \left(\frac{1}{2}-\frac{1}{C+1}\right)\frac{1}{4\eta_g\nu_g^2}\left(k_g\frac{\omega^2}{\alpha_0^2} - 2\frac{\beta_0^2}{\alpha_0^2}k_g^3\right)\right.\\
&\left.+\frac{\beta_0^2}{\alpha_0^2}\frac{k_g}{2\nu_g}\right]a_\mu^{(1)}(z)a_\gamma^{(1)}(z)\\
&-\left[\left(\frac{1}{2}+\frac{1}{C+1}\right)\frac{k_g\left(k_g^2+\nu_g^2\right)}{8\nu_g^3} - \left(\frac{1}{2}-\frac{1}{C+1}\right)\frac{k_g\left(k_g^2+\nu_g^2\right)}{8\eta_g\nu_g^2}\right]a_\rho^{(1)}(z)a_\gamma^{(1)}(z)
\end{aligned}
$$

$$
\begin{aligned}
&- \left[\left(\frac{1}{2} + \frac{1}{C+1} \right) \frac{1}{4\eta_g \nu_g^2} \left(2\nu_g^2 k_g^3 \frac{\beta_0^2}{\omega^2} - \nu_g^2 k_g + 2Ck_g^5 \frac{\beta_0^2}{\omega^2} - \frac{\beta_0^2}{\alpha_0^2} Ck_g^3 \right) \right. \\
&- \left(\frac{1}{2} - \frac{1}{C+1} \right) \frac{1}{4\eta_g \nu_g^2} \left(2C\nu_g^2 k_g^3 \frac{\beta_0^2}{\omega^2} - \frac{\beta_0^2}{\alpha_0^2} C\nu_g^2 k_g + 2k_g^5 \frac{\beta_0^2}{\omega^2} - k_g^3 \right) \\
&- \left(\frac{1}{2C} + \frac{1}{C+1} \right) \frac{1}{4\eta_g^2 \nu_g} \left(3k_g^3 + \frac{\beta_0^2}{\alpha_0^2} C^3 \nu_g^2 k_g - 4C^3 \nu_g^2 k_g^3 \frac{\beta_0^2}{\omega^2} - 4k_g^5 \frac{\beta_0^2}{\omega^2} - \frac{1}{2} k_g \frac{\omega^2}{\beta_0^2} \right) \\
&+ \left(\frac{1}{2C} - \frac{1}{C+1} \right) \frac{1}{4\eta_g \nu_g^2} \left(C\nu_g^2 k_g + 2k_g^3 + \frac{\beta_0^2}{\alpha_0^2} k_g^3 - 4k_g^5 \frac{\beta_0^2}{\omega^2} - 4C\nu_g^2 k_g^3 \frac{\beta_0^2}{\omega^2} - \frac{1}{2} k_g \frac{\omega^2}{\beta_0^2} \right) \\
&\left. -(C-1) \frac{k_g^3}{2\eta_g} \frac{\beta_0^2}{\omega^2} \right] a_\rho^{(1)}(z) a_\mu^{(1)}(z) \\
&- \frac{1}{2\eta_g \nu_g^2} \left[2(C-1)\nu_g^2 k_g^5 \frac{\beta_0^4}{\omega^4} + \left(1 - \frac{\beta_0^2}{\alpha_0^2} C \right) \nu_g^2 k_g^3 \frac{\beta_0^2}{\omega^2} \right] \\
&\times \int_0^z dz' a_\mu^{(1)}{}_z \left(\frac{(C+1)z - (C-1)\, z'}{2} \right) a_\mu^{(1)}\left(z' \right) \\
&+ \frac{1}{4\eta_g^2 \nu_g} \left(6k_g^3 - 12k_g^5 \frac{\beta_0^2}{\omega^2} - k_g \frac{\omega^2}{\beta_0^2} + 8k_g^7 \frac{\beta_0^4}{\omega^4} + 8C^3 \nu_g^2 k_g^5 \frac{\beta_0^4}{\omega^4} - 4\frac{\beta_0^2}{\alpha_0^2} C^3 \nu_g^2 k_g^3 \frac{\beta_0^2}{\omega^2} \right) \\
&\times \left[\frac{1}{2C} \int_0^z dz' a_\mu^{(1)}{}_z \left(\frac{(C+1)z + (C-1)\, z'}{2C} \right) a_\mu^{(1)}\left(z' \right) + \frac{1}{C+1} a_\mu^{(1)'}(z) \int_0^z dz' a_\mu^{(1)}(z') \right] \\
&- \frac{1}{4\eta_g \nu_g^2} \left(4\frac{\beta_0^2}{\alpha_0^2} k_g^3 - 8k_g^5 \frac{\beta_0^2}{\omega^2} - k_g \frac{\omega^2}{\alpha_0^2} + 2k_g^3 - 4C\nu_g^2 k_g^3 \frac{\beta_0^2}{\omega^2} + 8C\nu_g^2 k_g^5 \frac{\beta_0^4}{\omega^4} - 4\frac{\beta_0^2}{\alpha_0^2} k_g^5 \frac{\beta_0^2}{\omega^2} + 8k_g^7 \frac{\beta_0^4}{\omega^4} \right) \\
&\times \left[\frac{1}{2C} \int_0^z dz' a_\mu^{(1)}{}_z \left(\frac{(C+1)z + (C-1)\, z'}{2C} \right) a_\mu^{(1)}\left(z' \right) - \frac{1}{C+1} a_\mu^{(1)'}(z) \int_0^z dz' a_\mu^{(1)}(z') \right] \\
&+ \frac{k_g \left(Ck_g^2 + \nu_g^2 \right)}{8\eta_g \nu_g^2} \left[\frac{1}{2} \int_0^z dz' a_\rho^{(1)}{}_z \left(\frac{(C+1)z - (C-1)\, z'}{2} \right) a_\rho^{(1)}\left(z' \right) \right. \\
&\left. + \frac{1}{C+1} a_\rho^{(1)'}(z) \int_0^z dz' a_\rho^{(1)}(z') \right] \\
&- \frac{k_g \left(k_g^2 + C\nu_g^2 \right)}{8\eta_g \nu_g^2} \left[\frac{1}{2} \int_0^z dz' a_\rho^{(1)}{}_z \left(\frac{(C+1)z - (C-1)\, z'}{2} \right) a_\rho^{(1)}\left(z' \right) \right. \\
&\left. - \frac{1}{C+1} a_\rho^{(1)'}(z) \int_0^z dz' a_\rho^{(1)}(z') \right] \\
&+ \frac{C^3 k_g \nu_g^2 + k_g^3}{8\eta_g^2 \nu_g} \left[\frac{1}{2C} \int_0^z dz' a_\rho^{(1)}{}_z \left(\frac{(C+1)z + (C-1)\, z'}{2C} \right) a_\rho^{(1)}\left(z' \right) \right. \\
&\left. + \frac{1}{C+1} a_\rho^{(1)'}(z) \int_0^z dz' a_\rho^{(1)}(z') \right] \\
&- \frac{k_g \left(k_g^2 + C\nu_g^2 \right)}{8\eta_g \nu_g^2} \left[\frac{1}{2C} \int_0^z dz' a_\rho^{(1)}{}_z \left(\frac{(C+1)z + (C-1)\, z'}{2C} \right) a_\rho^{(1)}\left(z' \right) \right.
\end{aligned}
$$

$$
\begin{aligned}
&-\frac{1}{C+1}a_{\rho}^{(1)'}(z)\int_0^z dz' a_{\rho}^{(1)}(z')\Bigg] \\
&+\frac{\beta_0^2}{\alpha_0^2}\frac{k_g\left(k_g^2-\nu_g^2\right)}{4\nu_g^3}\left[\frac{1}{2}\int_0^z dz' a_{\gamma}^{(1)}{}_z\left(\frac{(C+1)z-(C-1)\,z'}{2}\right)a_{\mu}^{(1)}\left(z'\right)\right. \\
&\left.+\frac{1}{C+1}a_{\mu}^{(1)'}(z)\int_0^z dz' a_{\gamma}^{(1)}(z')\right] \\
&+\frac{1}{4\eta_g\nu_g^2}\left(k_g\frac{\omega^2}{\alpha_0^2}-2\frac{\beta_0^2}{\alpha_0^2}k_g^3\right)\left[\frac{1}{2}\int_0^z dz' a_{\gamma}^{(1)}{}_z\left(\frac{(C+1)z-(C-1)\,z'}{2}\right)a_{\mu}^{(1)}\left(z'\right)\right. \\
&\left.-\frac{1}{C+1}a_{\mu}^{(1)'}(z)\int_0^z dz' a_{\gamma}^{(1)}(z')\right] \\
&-\frac{k_g\left(k_g^2+\nu_g^2\right)}{8\nu_g^3}\left[\frac{1}{2}\int_0^z dz' a_{\gamma}^{(1)}{}_z\left(\frac{(C+1)z-(C-1)\,z'}{2}\right)a_{\rho}^{(1)}\left(z'\right)\right. \\
&\left.+\frac{1}{C+1}a_{\rho}^{(1)'}(z)\int_0^z dz' a_{\gamma}^{(1)}(z')\right] \\
&+\frac{k_g\left(k_g^2+\nu_g^2\right)}{8\eta_g\nu_g^2}\left[\frac{1}{2}\int_0^z dz' a_{\gamma}^{(1)}{}_z\left(\frac{(C+1)z-(C-1)\,z'}{2}\right)a_{\rho}^{(1)}\left(z'\right)\right. \\
&\left.-\frac{1}{C+1}a_{\rho}^{(1)'}(z)\int_0^z dz' a_{\gamma}^{(1)}(z')\right] \\
&-\frac{1}{4\eta_g\nu_g^2}\left(2\nu_g^2k_g^3\frac{\beta_0^2}{\omega^2}-\nu_g^2k_g+2Ck_g^5\frac{\beta_0^2}{\omega^2}-\frac{\beta_0^2}{\alpha_0^2}Ck_g^3\right) \\
&\times\left[\frac{1}{2}\int_0^z dz' a_{\rho}^{(1)}{}_z\left(\frac{(C+1)z-(C-1)\,z'}{2}\right)a_{\mu}^{(1)}\left(z'\right)+\frac{1}{C+1}a_{\mu}^{(1)'}(z)\int_0^z dz' a_{\rho}^{(1)}(z')\right] \\
&+\frac{1}{4\eta_g\nu_g^2}\left(2C\nu_g^2k_g^3\frac{\beta_0^2}{\omega^2}-\frac{\beta_0^2}{\alpha_0^2}C\nu_g^2k_g+2k_g^5\frac{\beta_0^2}{\omega^2}-k_g^3\right) \\
&\times\left[\frac{1}{2}\int_0^z dz' a_{\rho}^{(1)}{}_z\left(\frac{(C+1)z-(C-1)\,z'}{2}\right)a_{\mu}^{(1)}\left(z'\right)-\frac{1}{C+1}a_{\mu}^{(1)'}(z)\int_0^z dz' a_{\rho}^{(1)}(z')\right] \\
&+(C-1)\frac{k_g^3}{2\eta_g}\frac{\beta_0^2}{\omega^2}\int_0^z dz' a_{\mu}^{(1)}{}_z\left(\frac{(C+1)z-(C-1)\,z'}{2}\right)a_{\rho}^{(1)}\left(z'\right) \\
&-\frac{1}{4\eta_g^2\nu_g}\left(-2k_g^3+2C^3\nu_g^2k_g^3\frac{\beta_0^2}{\omega^2}+2k_g^5\frac{\beta_0^2}{\omega^2}+\frac{1}{2}k_g\frac{\omega^2}{\beta_0^2}\right) \\
&\times\left[\frac{1}{2C}\int_0^z dz' a_{\mu}^{(1)}{}_z\left(\frac{(C+1)z+(C-1)\,z'}{2C}\right)a_{\rho}^{(1)}\left(z'\right)+\frac{1}{C+1}a_{\rho}^{(1)'}(z)\int_0^z dz' a_{\mu}^{(1)}(z')\right] \\
&-\frac{1}{4\eta_g^2\nu_g}\left(-k_g^3-\frac{\beta_0^2}{\alpha_0^2}C^3\nu_g^2k_g+2C^3\nu_g^2k_g^3\frac{\beta_0^2}{\omega^2}+2k_g^5\frac{\beta_0^2}{\omega^2}\right) \\
&\times\left[\frac{1}{2C}\int_0^z dz' a_{\rho}^{(1)}{}_z\left(\frac{(C+1)z+(C-1)\,z'}{2C}\right)a_{\mu}^{(1)}\left(z'\right)+\frac{1}{C+1}a_{\mu}^{(1)'}(z)\int_0^z dz' a_{\rho}^{(1)}(z')\right] \\
&-\frac{1}{4\eta_g\nu_g^2}\left(2k_g^3-2k_g^5\frac{\beta_0^2}{\omega^2}-2C\nu_g^2k_g^3\frac{\beta_0^2}{\omega^2}-\frac{1}{2}k_g\frac{\omega^2}{\beta_0^2}\right)
\end{aligned}
$$

$$\times \left[\frac{1}{2C}\int_0^z dz' a_\mu^{(1)}{}_z \left(\frac{(C+1)z+(C-1)\,z'}{2C}\right) a_\rho^{(1)}\left(z'\right) - \frac{1}{C+1}a_\rho^{(1)'}(z)\int_0^z dz' a_\mu^{(1)}(z')\right]$$
$$-\frac{1}{4\eta_g\nu_g^2}\left(C\nu_g^2 k_g + \frac{\beta_0^2}{\alpha_0^2}k_g^3 - 2k_g^5\frac{\beta_0^2}{\omega^2} - 2C\nu_g^2 k_g^3\frac{\beta_0^2}{\omega^2}\right)$$
$$\times \left[\frac{1}{2C}\int_0^z dz' a_\rho^{(1)}{}_z \left(\frac{(C+1)z+(C-1)\,z'}{2C}\right) a_\mu^{(1)}\left(z'\right) - \frac{1}{C+1}a_\mu^{(1)'}(z)\int_0^z dz' a_\rho^{(1)}(z')\right],$$

and the solution for equation 51, i.e.,

$$\hat{G}_0^S\hat{V}_2^{SS}\hat{G}_0^S = -\hat{G}_0^S\hat{V}_1^{SP}\hat{G}_0^P\hat{V}_1^{PS}\hat{G}_0^S - \hat{G}_0^S\hat{V}_1^{SS}\hat{G}_0^S\hat{V}_1^{SS}\hat{G}_0^S,$$

is

$$-\frac{1}{4}\left(1-\frac{k_g^2}{\eta_g^2}\right)a_\rho^{(2)}(z) - \left[\frac{k_g^2+\eta_g^2}{4\eta_g^2} - \frac{2k_g^2}{k_g^2+\eta_g^2}\right]a_\mu^{(2)}(z)$$
$$= -\left\{\frac{1}{8\eta_g^4}\left(8k_g^2\eta_g^2 - \frac{\omega^4}{\beta_0^4}\right) - \frac{1}{4\eta_g^2}\left(\frac{\omega^2}{\beta_0^2} - 4\frac{\beta_0^2}{\omega^2}\eta_g^2 k_g^2\right) - \frac{\beta_0^2}{\alpha_0^2}k_g^2\frac{\beta_0^2}{\omega^2}\right.$$
$$\left. + \frac{1}{\eta_g^2(C+1)}\left[k_g^2\left(\frac{\beta_0^4}{\alpha_0^4}C^2-1\right) - 4k_g^4\frac{\beta_0^2}{\omega^2}\left(\frac{\beta_0^2}{\alpha_0^2}C^2-1\right) + 4k_g^6\frac{\beta_0^4}{\omega^4}(C^2-1)\right]\right\}a_\mu^{(1)}(z)a_\mu^{(1)}(z)$$
$$-\left[\frac{1}{8\eta_g^4}\left(\eta_g^4-k_g^4\right) + \frac{1}{4\eta_g^2}k_g^2(C-1)\right]a_\rho^{(1)}(z)a_\rho^{(1)}(z)$$
$$+\left\{\frac{k_g^2}{\eta_g^2} - \frac{1}{\eta_g^2(C+1)}\left[k_g^2\left(\frac{\beta_0^2}{\alpha_0^2}C^2-1\right) - 2\frac{\beta_0^2}{\omega^2}k_g^4\left(C^2-1\right)\right]\right\}a_\mu^{(1)}(z)a_\rho^{(1)}(z)$$
$$-\frac{1}{8\eta_g^4}\left(8k_g^2\eta_g^2 - \frac{\omega^4}{\beta_0^4}\right)a_\mu^{(1)'}(z)\int_0^z dz' a_\mu^{(1)}(z')$$
$$-\frac{1}{8\eta_g^4}\left(\eta_g^4-k_g^4\right)a_\rho^{(1)'}(z)\int_0^z dz' a_\rho^{(1)}(z')$$
$$+\frac{k_g^2}{2\eta_g^2}\left[a_\mu^{(1)'}(z)\int_0^z dz' a_\rho^{(1)}(z') + a_\rho^{(1)'}(z)\int_0^z dz' a_\mu^{(1)}(z')\right]$$
$$-\frac{1}{8\eta_g^2}\left(\eta_g^2-3k_g^2\right)\left[a_\mu^{(1)'}(z)\int_0^z dz' a_\rho^{(1)}(z') - a_\rho^{(1)'}(z)\int_0^z dz' a_\mu^{(1)}(z')\right]$$
$$-\frac{1}{\eta_g^2(C+1)}\left[k_g^2\left(\frac{\beta_0^4}{\alpha_0^4}C^2-1\right) - 4k_g^4\frac{\beta_0^2}{\omega^2}\left(\frac{\beta_0^2}{\alpha_0^2}C^2-1\right) + 4k_g^6\frac{\beta_0^4}{\omega^4}(C^2-1)\right]$$
$$\times \int_0^z dz' a_\mu^{(1)}{}_z \left(\frac{2Cz-(C-1)\,z'}{(C+1)}\right)a_\mu^{(1)}\left(z'\right)$$
$$-\frac{1}{4\eta_g^2}k_g^2(C-1)\int_0^z dz' a_\rho^{(1)}{}_z \left(\frac{2Cz-(C-1)\,z'}{(C+1)}\right)a_\rho^{(1)}\left(z'\right)$$
$$-\frac{1}{2\eta_g^2(C+1)}\left[k_g^2\left(\frac{\beta_0^2}{\alpha_0^2}C^2-1\right) - 2\frac{\beta_0^2}{\omega^2}k_g^4\left(C^2-1\right)\right]$$
$$\times \left[\int_0^z dz' a_\mu^{(1)}{}_z \left(\frac{2Cz-(C-1)\,z'}{(C+1)}\right)a_\rho^{(1)}\left(z'\right) + \int_0^z dz' a_\rho^{(1)}{}_z \left(\frac{2Cz-(C-1)\,z'}{(C+1)}\right)a_\mu^{(1)}\left(z'\right)\right]$$

$$+\frac{Ck_g^2}{2(C+1)\eta_g^2}\left(\frac{\beta_0^2}{\alpha_0^2}-1\right)$$
$$\times\left[\int_0^z dz' a_\mu^{(1)}{}_z\left(\frac{2Cz-(C-1)\,z'}{(C+1)}\right)a_\rho^{(1)}\left(z'\right)-\int_0^z dz' a_\rho^{(1)}{}_z\left(\frac{2Cz-(C-1)\,z'}{(C+1)}\right)a_\mu^{(1)}\left(z'\right)\right],$$

where $\eta_g = C\nu_g, k_g^2+\nu_g^2=\omega^2/\alpha_0^2$ and $k_g^2+\eta_g^2=\omega^2/\beta_0^2$.

After we solve all (four) of the second order equations, future research is to perform numerical tests with all four components of data available.

5 Conclusion

In this paper, a framework and algorithm have been developed for more accurate target identification. The elastic non-linear inversion requires all four components of data. In this paper we analyzed an algorithm which inputs only $\hat{D}^{PP}$. Although $\hat{D}^{PP}$ can itself provide useful non-linear direct inversion results, when we use $\hat{D}^{PP}$ to synthesize the other components, the implication of this research is that further value would derive from actually measuring $\hat{D}^{PP}$, $\hat{D}^{PS}$, $\hat{D}^{SP}$ and $\hat{D}^{SS}$, as the method requires. Pitfalls of indirect methods that use assumed aligned objectives, while sounding eminently persuasive and reasonable, can have a serious flaw in violating the fundamental physics behind non-linear inversion, and can never sense its problem, in any clear and definitive manner. There are very serious conceptual and practical consequences to that disconnect. For the case that all four components of data available, we also provided a consistent method to solve for all of the second terms. Further tests with the actual four components of data (in a 2-D world) are underway, to compare with $\hat{D}^{PP}$ and synthesized data components.

Acknowledgements

The M-OSRP sponsors are thanked for supporting this research. We are grateful to Robert Keys and Douglas Foster for useful comments and suggestions. We have been partially funded by and are grateful for NSF-CMG award DMS-0327778 and DOE Basic Sciences award DE-FG02-05ER15697. The first author would also like to thank ConocoPhillips for permission to publish this work.

References

Aki, K. and P. G. Richards. *Quantitative Seismology.* 2nd edition. University Science Books, 2002.

Araújo, F. V. *Linear and non-linear methods derived from scattering theory: backscattered tomography and internal multiple attenuation.* PhD thesis, Universidade Federal da Bahia, 1994.

Carvalho, P. M. *Free-surface multiple reflection elimination method based on nonlinear inversion of seismic data.* PhD thesis, Universidade Federal da Bahia, 1992.

Carvalho, P. M., A. B. Weglein, and R. H. Stolt. "Nonlinear inverse scattering for multiple suppression: Application to real data. part I." *62nd Ann. Internat. Mtg: Soc. of Expl. Geophys., Expanded Abstracts*. . Soc. Expl. Geophys., 1992. 1093–1095.

Clayton, R. W. and R. H. Stolt. "A Born-WKBJ inversion method for acoustic reflection data." *Geophysics* 46 (1981): 1559–1567.

Foster, D. J., R. G. Keys, and D. P. Schmitt. *Detecting subsurface hydrocarbons with elastic wavefields*. Springer-In Inverse Problems in Wave Progagation, Volume 90 of The IMA Volumes in Mathematics and its Applications, 1997.

Innanen, K. A. and A. B. Weglein. "Linear inversion for absorptive/dispersive medium parameters." *74th Annual Internat. Mtg., Soc. Expl. Geophys., Expanded Abstracts*. . Soc. Expl. Geophys., 2004. 1834–1837.

Innanen, K. A. and A. B. Weglein. "Towards non-linear construction of a Q-compensation operator directly from measured seismic reflection data." *75th Annual Internat. Mtg., Soc. Expl. Geophys., Expanded Abstracts*. . Soc. Expl. Geophys., 2005. 1693–1696.

Liu, F., A. B. Weglein K. A. Innanen, and B. G. Nita. "Extension of the non-linear depth imaging capability of the inverse scattering series to multidimensional media: strategies and numerical results." *9th Ann. Cong. SBGf, Expanded Abstracts*. . SBGf, 2005.

Liu, F., B. G. Nita, A. B. Weglein, and K. A. Innanen. "Inverse Scattering Series in the presence of lateral variations." *M-OSRP Annual Report* 3 (2004).

Liu, F. and A. B. Weglein. "Initial analysis of the inverse scattering series for a variable background." *M-OSRP Annual Report* 2 (2003): 210–225.

Matson, K. H. *An inverse-scattering series method for attenuating elastic multiples from multicomponent land and ocean bottom seismic data*. PhD thesis, University of British Columbia, 1997.

Ramírez, Adriana C. and Arthur B. Weglein. "An inverse scattering internal multiple elimination method: Beyond attenuation, a new algorithm and initial tests." *75th Annual Internat. Mtg., Soc. Expl. Geophys., Expanded Abstracts*. . Soc. Expl. Geophys., 2005. 2115–2118.

Shaw, S. A. and A. B. Weglein. "Imaging seismic reflection data at the correct depth without specifying an accurate velocity model: Initial examples of an inverse scattering subseries." *Frontiers of remote sensing information processing*. Ed. C. H. Chen. World Scientific Publishing Company, 2003. chapter 21, 469–484.

Shaw, S. A. and A. B. Weglein. "A leading order imaging series for prestack data acquired over a laterally invariant acoustic medium. Part II: Analysis for data missing low frequencies." *M-OSRP Annual Report* 3 (2004).

Shaw, S. A., A. B. Weglein, D. J. Foster, K. H. Matson, and R. G. Keys. "Convergence properties of a leading order depth imaging series." *73rd Annual Internat. Mtg., Soc. Expl. Geophys., Expanded Abstracts*. . Soc. Expl. Geophys., 2003. 937–940.

Shaw, S. A., A. B. Weglein, D. J. Foster, K. H. Matson, and R. G. Keys. "Isolation of a leading order depth imaging series and analysis of its convergence properties." *M-OSRP Annual Report* 2 (2003): 157–195.

Shaw, S. A., A. B. Weglein, D. J. Foster, K. H. Matson, and R. G. Keys. "Isolation of a leading order depth imaging series and analysis of its convergence properties." *Journal of Seismic Exploration* 2 (November 2004): 157–195.

Weglein, A. B., F. V. Araújo, P. M. Carvalho, R. H. Stolt, K. H. Matson, R. T. Coates, D. Corrigan, D. J. Foster, S. A. Shaw, and H. Zhang. "Inverse scattering series and seismic exploration." *Inverse Problems* 19 (2003): R27–R83.

Weglein, A. B., D. J. Foster, K. H. Matson, S. A. Shaw, P. M. Carvalho, and D. Corrigan. "Predicting the correct spatial location of reflectors without knowing or determining the precise medium and wave velocity: initial concept, algorithm and analytic and numerical example." *Journal of Seismic Exploration* 10 (2002): 367–382.

Weglein, A. B., F. A. Gasparotto, P. M. Carvalho, and R. H. Stolt. "An inverse-scattering series method for attenuating multiples in seismic reflection data." *Geophysics* 62 (1997): 1975–1989.

Weglein, A. B. and R. H. Stolt. "Approaches on linear and non-linear migration-inversion." Personal Communication (1992).

Weglein, A. B., P. B. Violette, and T. H. Keho. "Using multiparameter Born theory to obtain certain exact multiparameter inversion goals." *Geophysics* 51 (1986): 1069–1074.

Zhang, H. and A. B. Weglein. "The inverse scattering series for tasks associated with primaries: Depth imaging and direct non-linear inversion of 1D variable velocity and density acoustic media." *75th Annual Internat. Mtg., Soc. Expl. Geophys., Expanded Abstracts.* . Soc. Expl. Geophys., 2005. 1705–1708.

Appendix A

In this Appendix, we give the different coefficients before every linear quantity $(a_\gamma^{(1)}, a_\rho^{(1)}, a_\mu^{(1)})$ — different incidence angle θ. For P to P case, we have

$$k_g^{PP} = \frac{\omega}{\alpha_0}\sin\theta^{PP},$$
$$\nu_g^{PP} = \frac{\omega}{\alpha_0}\cos\theta^{PP},$$

For S to P case,

$$k_g^{PS} = \frac{\omega}{\beta_0}\sin\theta^{PS},$$

$$\nu_g^{PS} = \frac{\omega}{\alpha_0}\sqrt{1 - \frac{\alpha_0^2}{\beta_0^2}\sin^2\theta^{PS}}$$
$$\eta_g^{PS} = \frac{\omega}{\beta_0}\cos\theta^{PS},$$

For P to S case,

$$k_g^{SP} = \frac{\omega}{\alpha_0}\sin\theta^{SP},$$
$$\nu_g^{SP} = \frac{\omega}{\alpha_0}\cos\theta^{SP}$$
$$\eta_g^{SP} = \frac{\omega}{\beta_0}\sqrt{1 - \frac{\beta_0^2}{\alpha_0^2}\sin^2\theta^{SP}},$$

For S to S case,

$$k_g^{SS} = \frac{\omega}{\beta_0}\sin\theta^{SS},$$
$$\eta_g^{SS} = \frac{\omega}{\beta_0}\cos\theta^{SS},$$

Let the arguments of $a_\rho^{(1)}$ and $a_\mu^{(1)}$ in equations 41, 42, 43 and 44 equal, we need

$$-2\nu_g^{PP} = -\nu_g^{PS} - \eta_g^{PS} = -\nu_g^{SP} - \eta_g^{SP} = -2\eta_g^{SS},$$

which leads to

$$2\frac{\omega}{\alpha_0}\cos\theta^{PP} = \frac{\omega}{\alpha_0}\sqrt{1 - \frac{\alpha_0^2}{\beta_0^2}\sin^2\theta^{PS}} + \frac{\omega}{\beta_0}\cos\theta^{PS}$$
$$= \frac{\omega}{\alpha_0}\cos\theta^{SP} + \frac{\omega}{\beta_0}\sqrt{1 - \frac{\beta_0^2}{\alpha_0^2}\sin^2\theta^{SP}} = 2\frac{\omega}{\beta_0}\cos\theta^{SS},$$

From the expression above, given θ^{PP}, we can find the corresponding θ^{PS}, θ^{SP} and θ^{SS}.

$$\theta^{PS} = \cos^{-1}\left[\frac{4b^2\cos^2\theta^{PP} + 1 - b^2}{4b\cos\theta^{PP}}\right],$$
$$\theta^{SP} = \cos^{-1}\left[\frac{4b^2\cos^2\theta^{PP} - 1 + b^2}{4b^2\cos\theta^{PP}}\right],$$
$$\theta^{SS} = \cos^{-1}\left(b\cos\theta^{PP}\right),$$

where $b = \frac{\beta_0}{\alpha_0}$.

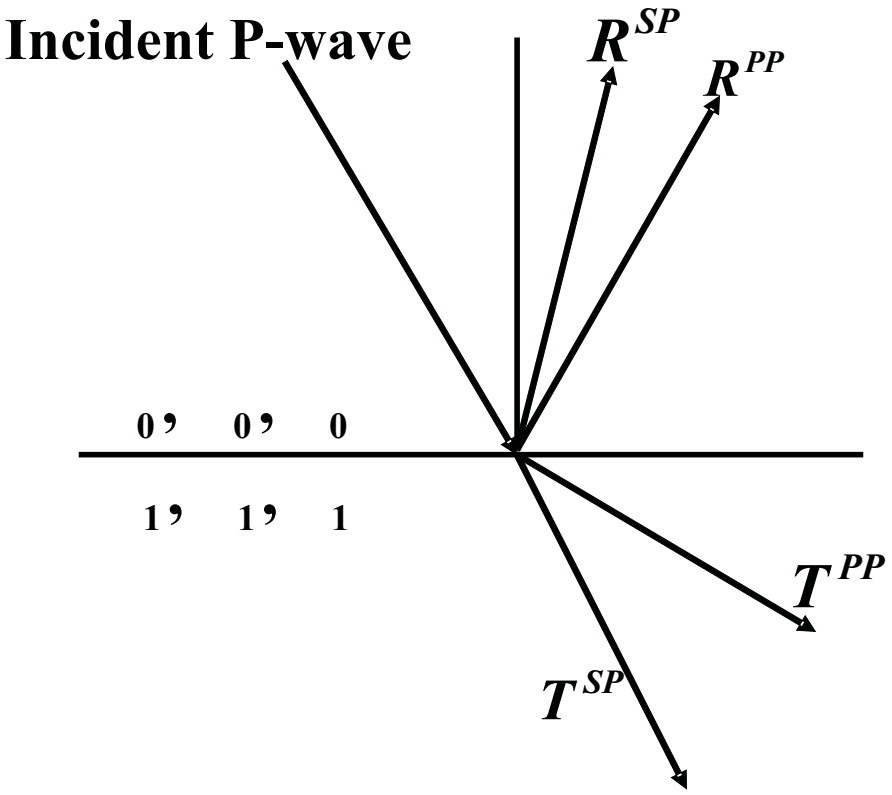

Figure 1: Response of incident compressional wave on a planar elastic interface. α_0, β_0 and ρ_0 are the compressional wave velocity, shear wave velocity and density of the upper layer, respectively; α_1, β_1 and ρ_1 denote the compressional wave velocity, shear wave velocity and density of the lower layer. R^{PP}, R^{SP}, T^{PP} and T^{SP} denote the coefficients of the reflected compressional wave, the reflected shear wave, the transmitted compressional wave and the transmitted shear wave, respectively. (Foster et al., 1997)

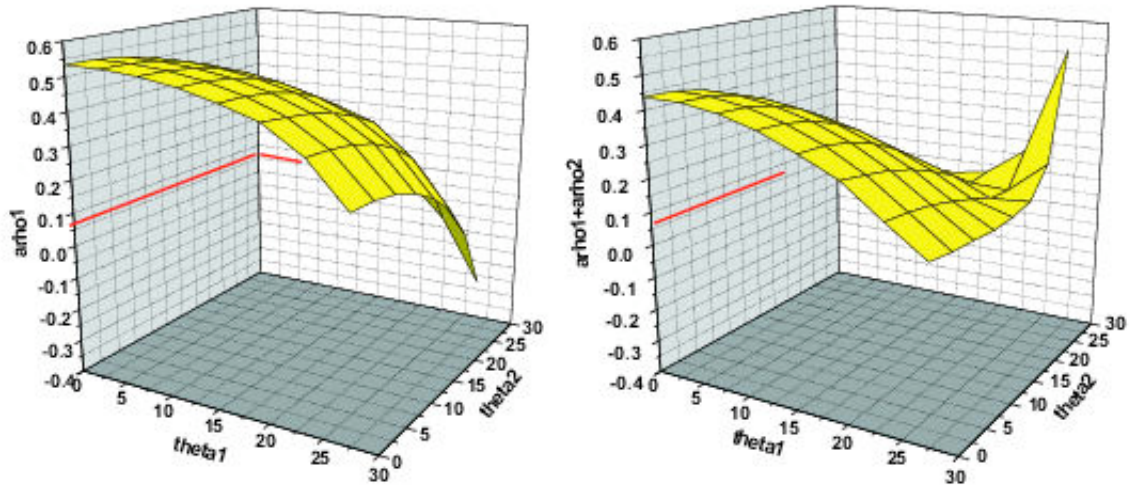

Figure 2: Model 1: shale (0.20 porosity) over oil sand (0.10 porosity). $\rho_0 = 2.32g/cm^3, \rho_1 = 2.46g/cm^3; \alpha_0 = 2627m/s, \alpha_1 = 4423m/s; \beta_0 = 1245m/s, \beta_1 = 2939m/s$. For this model, the exact value of a_ρ is 0.06. The linear approximation $a_\rho^{(1)}$ (left) and the sum of linear and first non-linear $a_\rho^{(1)} + a_\rho^{(2)}$ (right).

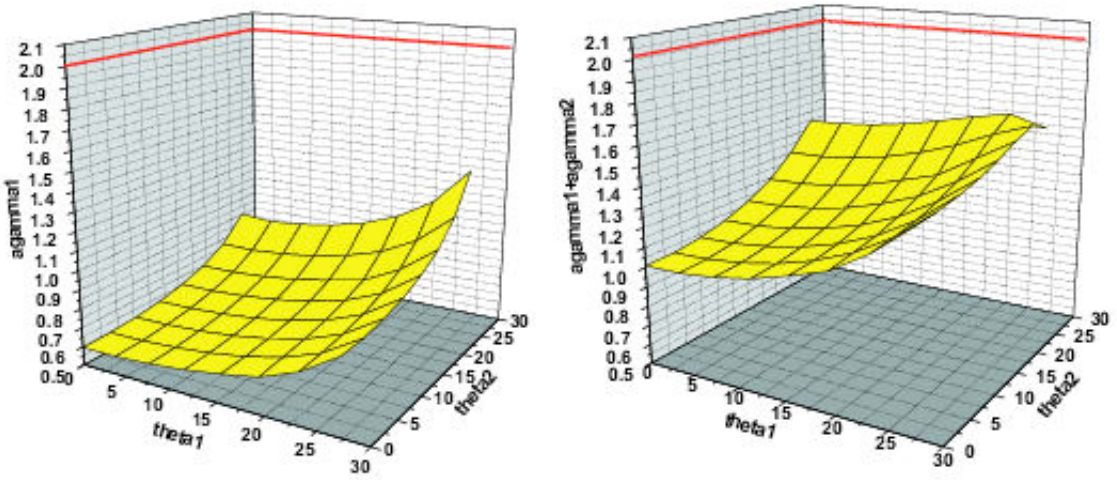

Figure 3: Model 1: shale (0.20 porosity) over oil sand (0.10 porosity). $\rho_0 = 2.32g/cm^3, \rho_1 = 2.46g/cm^3; \alpha_0 = 2627m/s, \alpha_1 = 4423m/s; \beta_0 = 1245m/s, \beta_1 = 2939m/s$. For this model, the exact value of a_γ is 2.01. The linear approximation $a_\gamma^{(1)}$ (left) and the sum of linear and first non-linear $a_\gamma^{(1)} + a_\gamma^{(2)}$ (right).

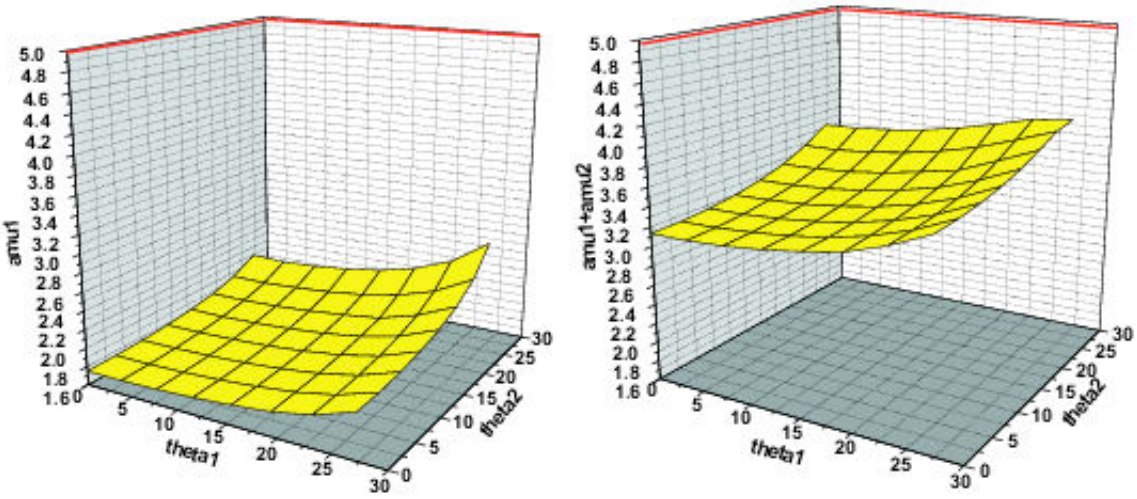

Figure 4: Model 1: shale (0.20 porosity) over oil sand (0.10 porosity). $\rho_0 = 2.32g/cm^3, \rho_1 = 2.46g/cm^3; \alpha_0 = 2627m/s, \alpha_1 = 4423m/s; \beta_0 = 1245m/s, \beta_1 = 2939m/s$. For this model, the exact value of a_μ is 4.91. The linear approximation $a_\mu^{(1)}$ (left) and the sum of linear and first non-linear $a_\mu^{(1)} + a_\mu^{(2)}$ (right).

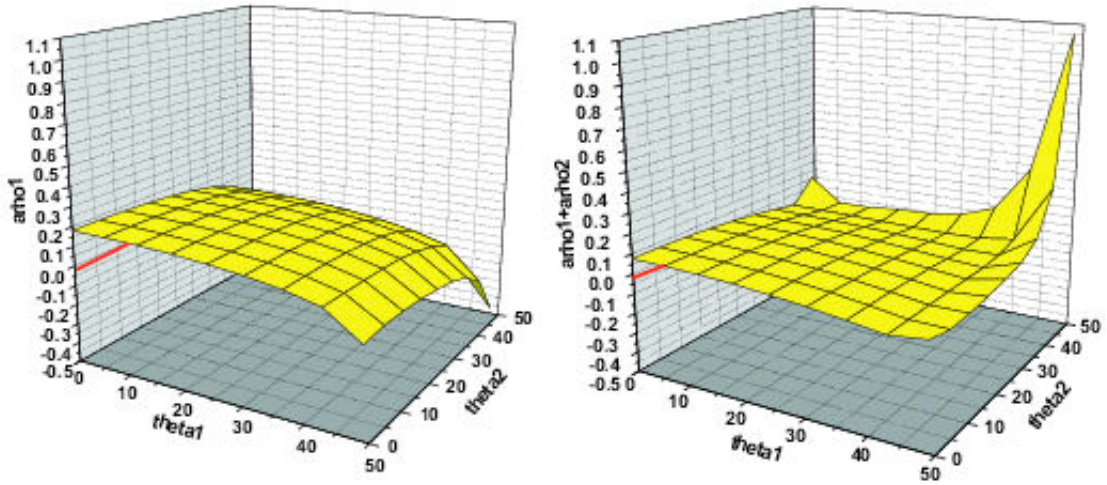

Figure 5: Model 2: shale over oil sand, 0.20 porosity. $\rho_0 = 2.32g/cm^3, \rho_1 = 2.27g/cm^3; \alpha_0 = 2627m/s, \alpha_1 = 3251m/s; \beta_0 = 1245m/s, \beta_1 = 2138m/s$. For this model, the exact value of a_ρ is -0.022. The linear approximation $a_\rho^{(1)}$ (left) and the sum of linear and first non-linear $a_\rho^{(1)} + a_\rho^{(2)}$ (right).

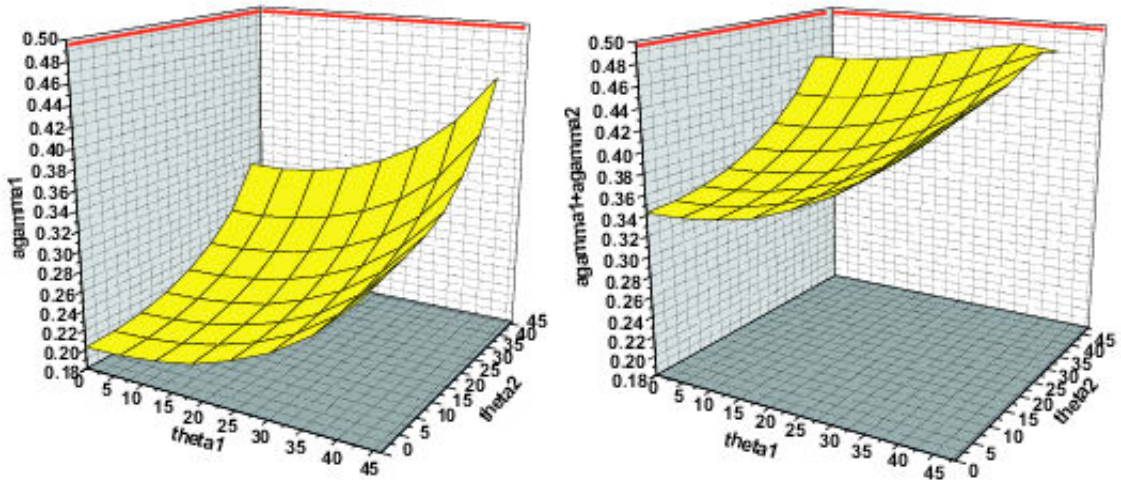

Figure 6: Model 2: shale over oil sand, 0.20 porosity. $\rho_0 = 2.32g/cm^3, \rho_1 = 2.27g/cm^3; \alpha_0 = 2627m/s, \alpha_1 = 3251m/s; \beta_0 = 1245m/s, \beta_1 = 2138m/s$. For this model, the exact value of a_γ is 0.498. The linear approximation $a_\gamma^{(1)}$ (left) and the sum of linear and first non-linear $a_\gamma^{(1)} + a_\gamma^{(2)}$ (right).

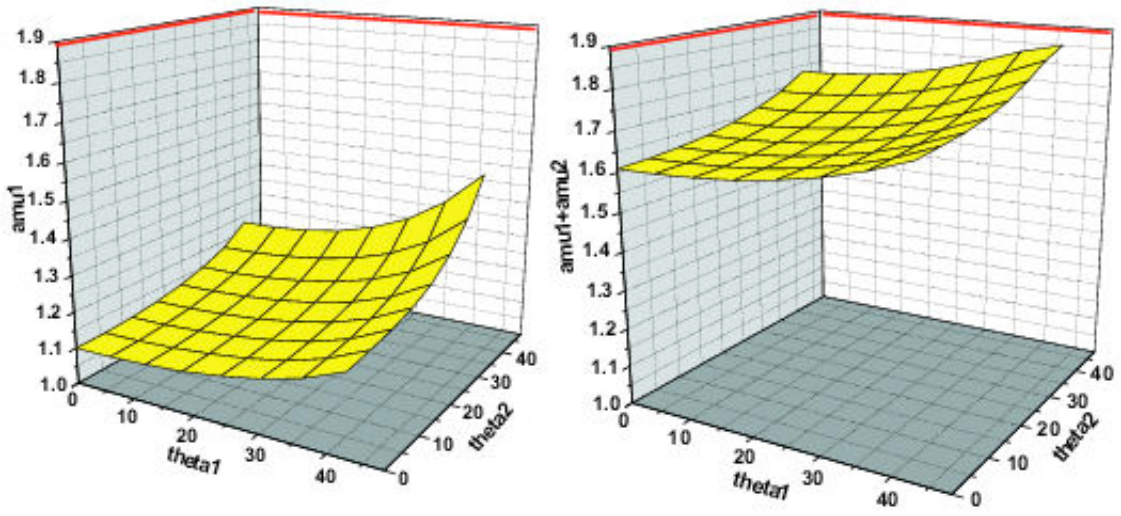

Figure 7: Model 2: shale over oil sand, 0.20 porosity. $\rho_0 = 2.32g/cm^3, \rho_1 = 2.27g/cm^3; \alpha_0 = 2627m/s, \alpha_1 = 3251m/s; \beta_0 = 1245m/s, \beta_1 = 2138m/s$. For this model, the exact value of a_μ is 1.89. The linear approximation $a_\mu^{(1)}$ (left) and the sum of linear and first non-linear $a_\mu^{(1)} + a_\mu^{(2)}$ (right).

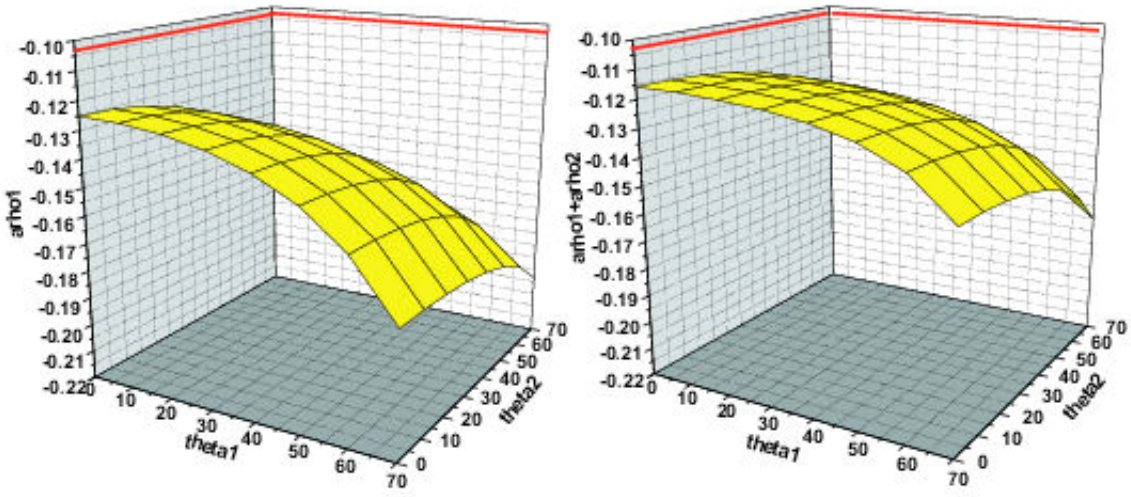

Figure 8: Model 3: shale (0.20 porosity) over oil sand (0.30 porosity). $\rho_0 = 2.32g/cm^3, \rho_1 = 2.08g/cm^3; \alpha_0 = 2627m/s, \alpha_1 = 2330m/s; \beta_0 = 1245m/s, \beta_1 = 1488m/s$. For this model, the exact value of a_ρ is -0.103. The linear approximation $a_\rho^{(1)}$ (left) and the sum of linear and first non-linear $a_\rho^{(1)} + a_\rho^{(2)}$ (right).

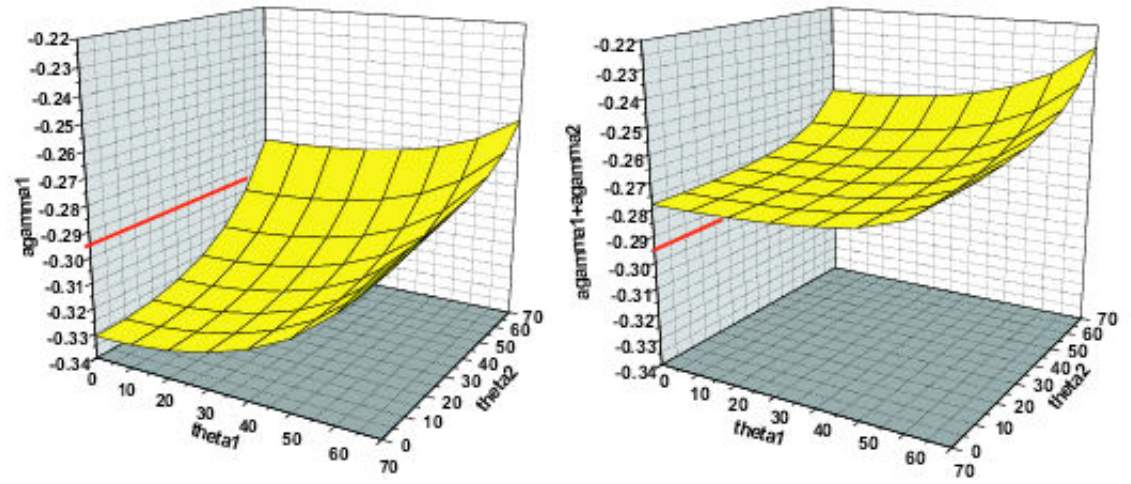

Figure 9: Model 3: shale (0.20 porosity) over oil sand (0.30 porosity). $\rho_0 = 2.32g/cm^3, \rho_1 = 2.08g/cm^3; \alpha_0 = 2627m/s, \alpha_1 = 2330m/s; \beta_0 = 1245m/s, \beta_1 = 1488m/s$. For this model, the exact value of a_γ is -0.295. The linear approximation $a_\gamma^{(1)}$ (left) and the sum of linear and first non-linear $a_\gamma^{(1)} + a_\gamma^{(2)}$ (right).

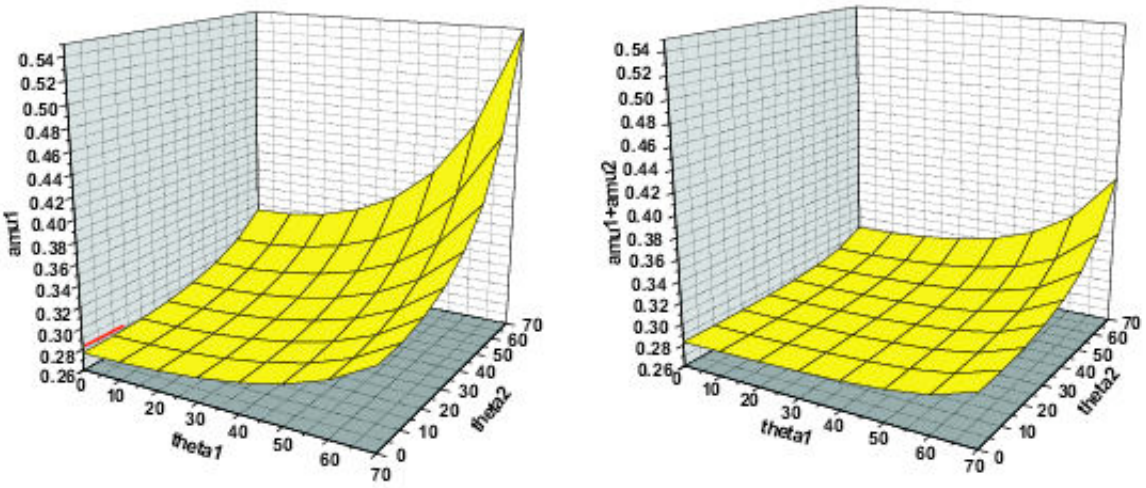

Figure 10: Model 3: shale (0.20 porosity) over oil sand (0.30 porosity). $\rho_0 = 2.32g/cm^3, \rho_1 = 2.08g/cm^3; \alpha_0 = 2627m/s, \alpha_1 = 2330m/s; \beta_0 = 1245m/s, \beta_1 = 1488m/s$. For this model, the exact value of a_μ is 0.281. The linear approximation $a_\mu^{(1)}$ (left) and the sum of linear and first non-linear $a_\mu^{(1)} + a_\mu^{(2)}$ (right).

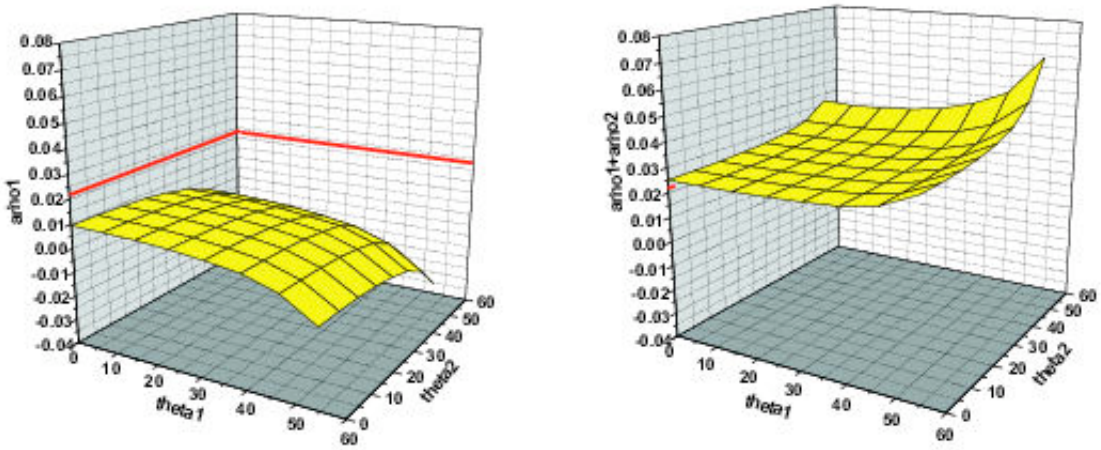

Figure 11: Model 4: oil sand over wet sand, 0.20 porosity. $\rho_0 = 2.27g/cm^3, \rho_1 = 2.32g/cm^3; \alpha_0 = 3251m/s, \alpha_1 = 3507m/s; \beta_0 = 2138m/s, \beta_1 = 2116m/s$. For this model, the exact value of a_ρ is 0.022. The linear approximation $a_\rho^{(1)}$ (left) and the sum of linear and first non-linear $a_\rho^{(1)} + a_\rho^{(2)}$ (right).

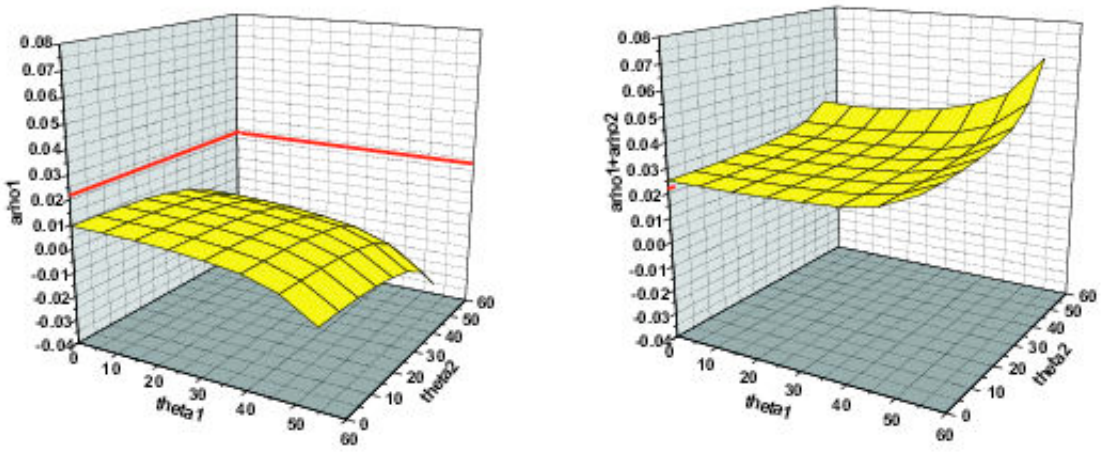

Figure 12: Model 4: oil sand over wet sand, 0.20 porosity. $\rho_0 = 2.27g/cm^3, \rho_1 = 2.32g/cm^3; \alpha_0 = 3251m/s, \alpha_1 = 3507m/s; \beta_0 = 2138m/s, \beta_1 = 2116m/s$. For this model, the exact value of a_γ is 0.19. The linear approximation $a_\gamma^{(1)}$ (left) and the sum of linear and first non-linear $a_\gamma^{(1)} + a_\gamma^{(2)}$ (right).

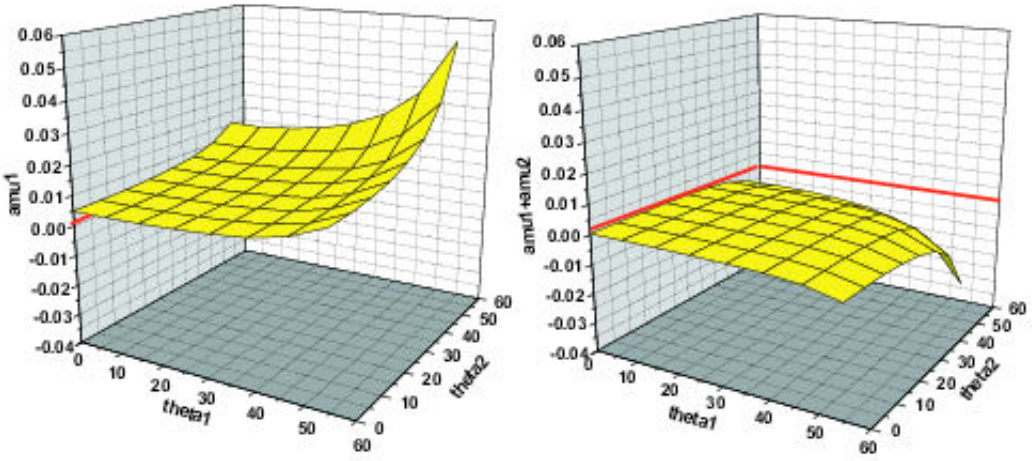

Figure 13: Model 4: oil sand over wet sand, 0.20 porosity. $\rho_0 = 2.27g/cm^3, \rho_1 = 2.32g/cm^3; \alpha_0 = 3251m/s, \alpha_1 = 3507m/s; \beta_0 = 2138m/s, \beta_1 = 2116m/s$. For this model, the exact value of a_μ is 0.001. The linear approximation $a_\mu^{(1)}$ (left) and the sum of linear and first non-linear $a_\mu^{(1)} + a_\mu^{(2)}$ (right).

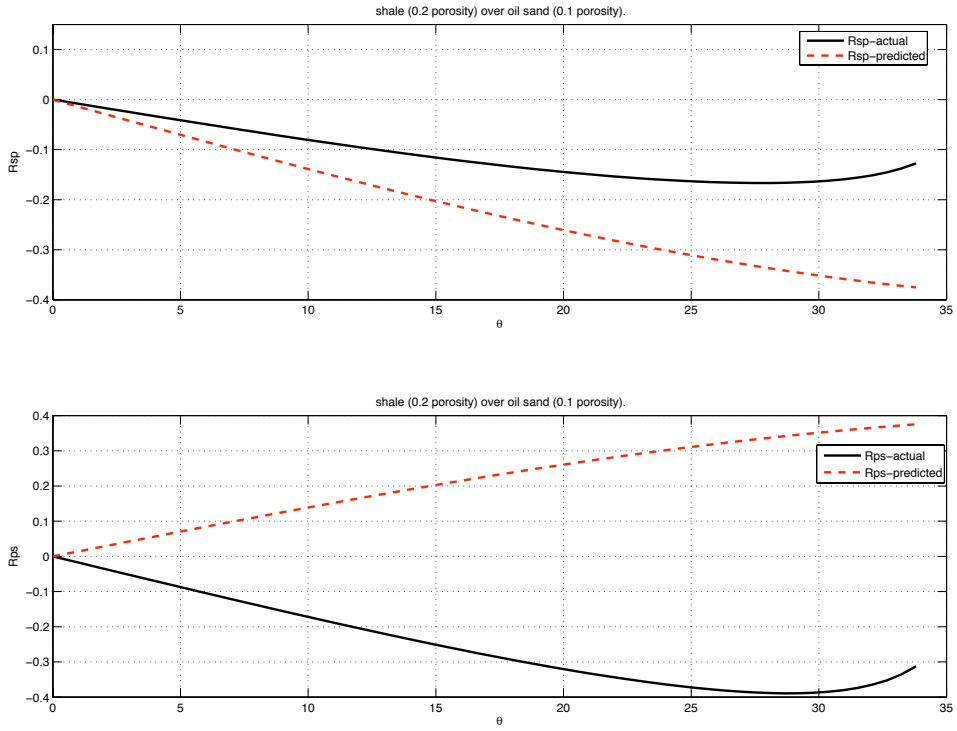

Figure 14: The comparison between the synthesized values and the actual values of Rsp (top) and Rps (bottom) for Model 1: shale (0.20 porosity) over oil sand (0.10 porosity). $\rho_0 = 2.32g/cm^3, \rho_1 = 2.46g/cm^3; \alpha_0 = 2627m/s, \alpha_1 = 4423m/s; \beta_0 = 1245m/s, \beta_1 = 2939m/s.$

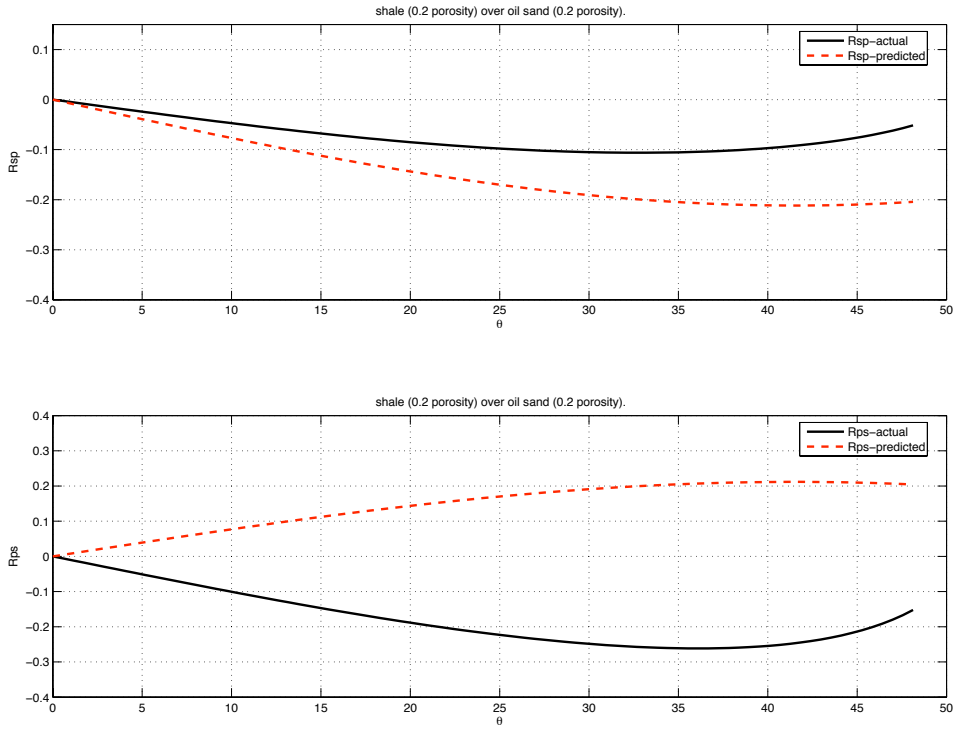

Figure 15: The comparison between the synthesized values and the actual values of Rsp (top) and Rps (bottom) for Model 2: shale over oil sand, 0.20 porosity. $\rho_0 = 2.32g/cm^3, \rho_1 = 2.27g/cm^3; \alpha_0 = 2627m/s, \alpha_1 = 3251m/s; \beta_0 = 1245m/s, \beta_1 = 2138m/s$.

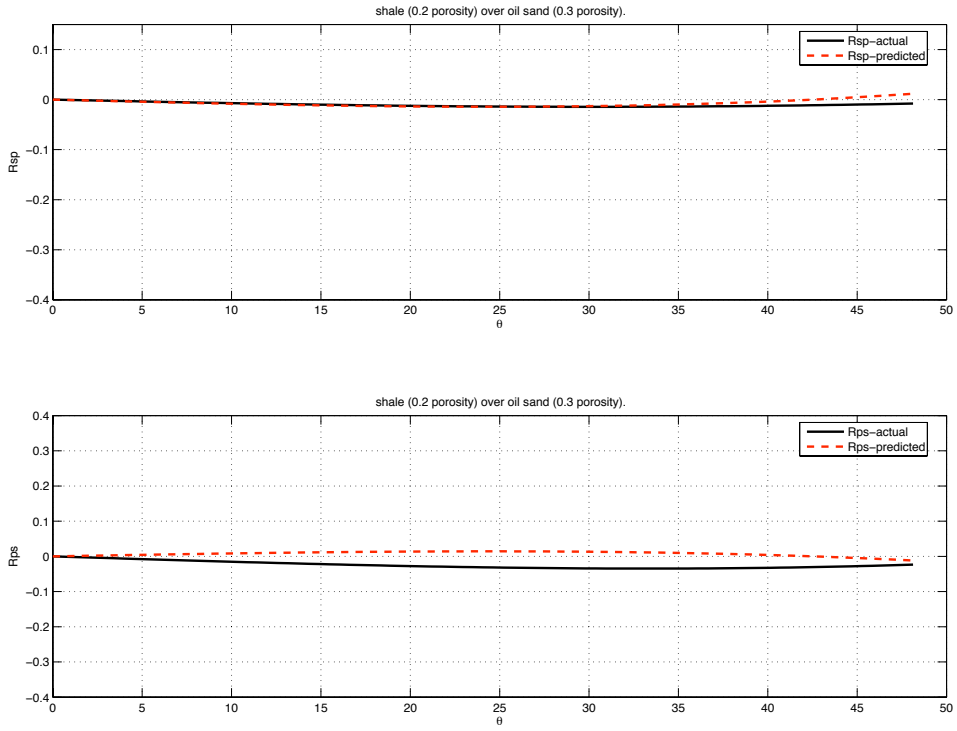

Figure 16: The comparison between the synthesized values and the actual values of Rsp (top) and Rps (bottom) for Model 3: shale (0.20 porosity) over oil sand (0.30 porosity). $\rho_0 = 2.32g/cm^3, \rho_1 = 2.08g/cm^3; \alpha_0 = 2627m/s, \alpha_1 = 2330m/s; \beta_0 = 1245m/s, \beta_1 = 1488m/s.$

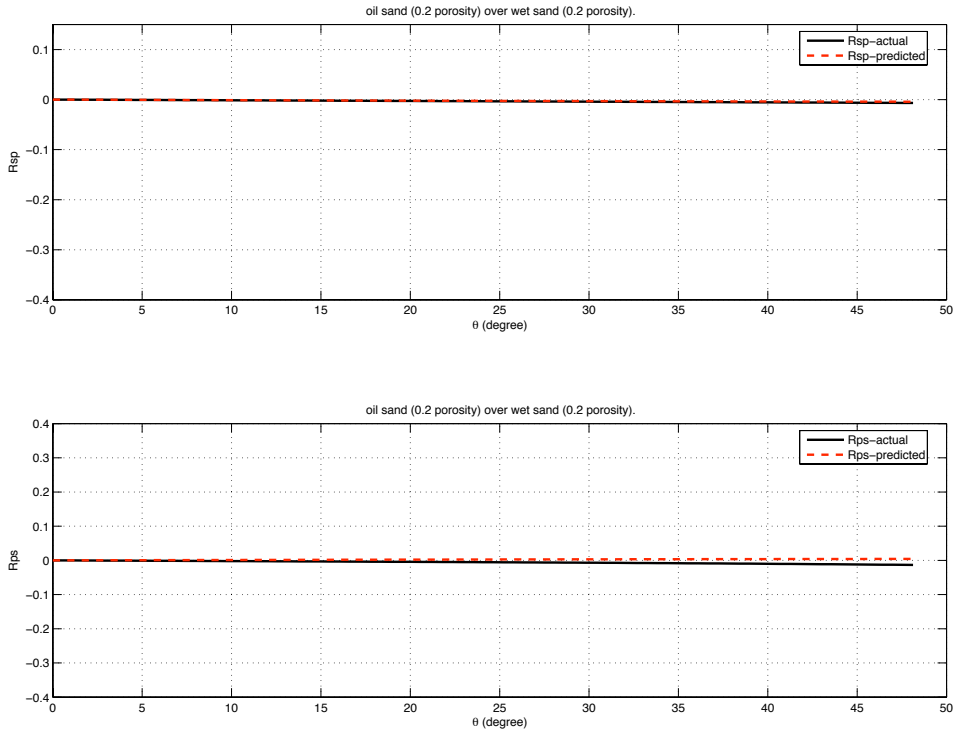

Figure 17: The comparison between the synthesized values and the actual values of Rsp (top) and Rps (bottom) for Model 4: oil sand over wet sand, 0.20 porosity. $\rho_0 = 2.27g/cm^3, \rho_1 = 2.32g/cm^3; \alpha_0 = 3251m/s, \alpha_1 = 3507m/s; \beta_0 = 2138m/s, \beta_1 = 2116m/s$.

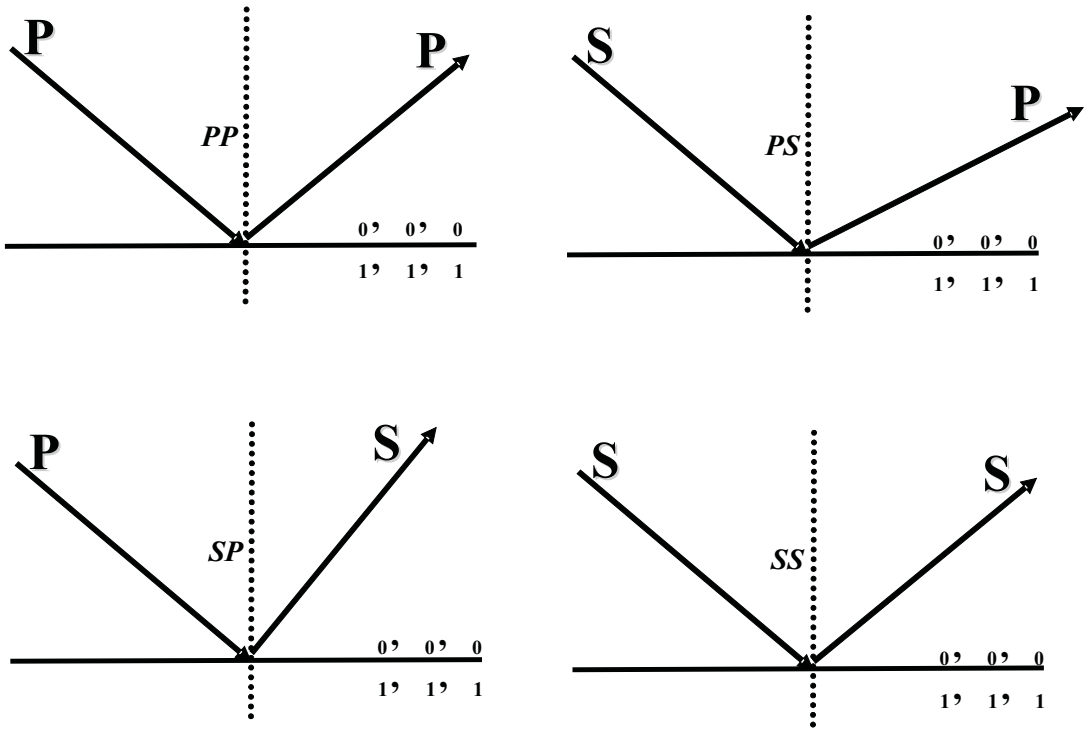

Figure 18: Different incident angles.